frontiers | Research Topics

Updates on epigenetic regulation of endocrine disorders with polygenic traits: What is new?

Edited by
Ahmet Uçar, Baris Binay and Bibekanand Mallick

Published in
Frontiers in Endocrinology

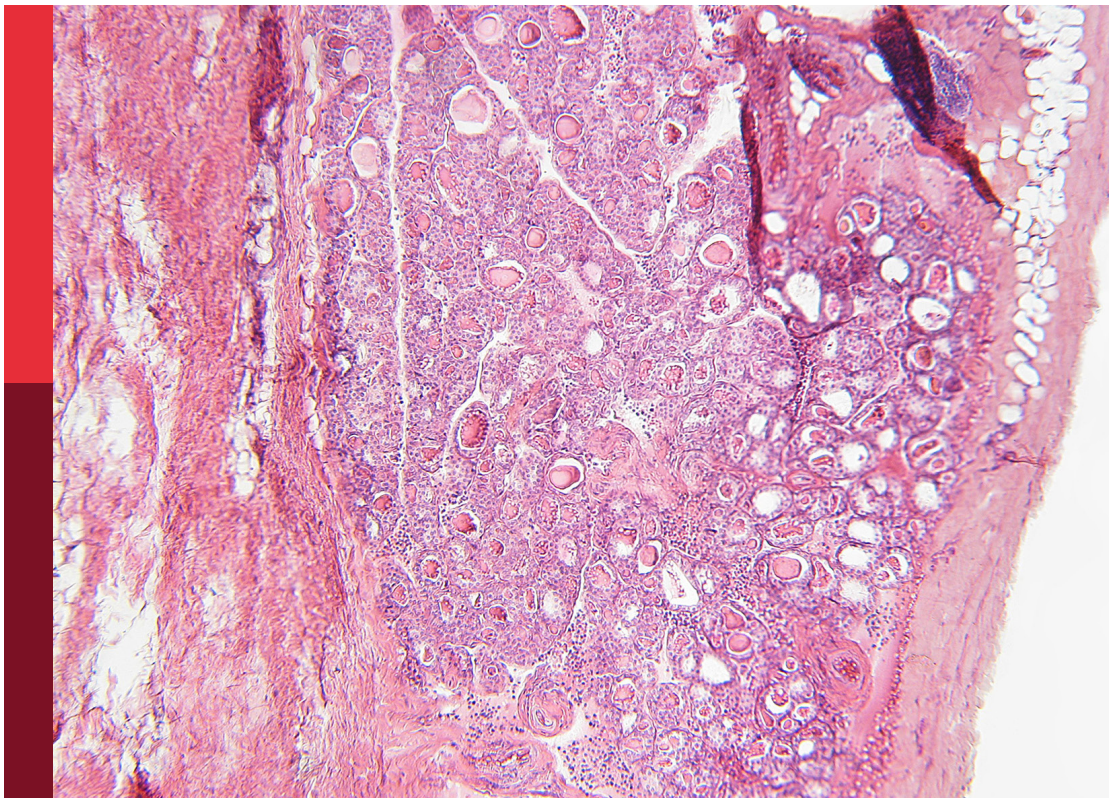

ISSN 1664-8714
ISBN 978-2-83250-768-1
DOI 10.3389/978-2-83250-768-1

About Frontiers

Frontiers is more than just an open access publisher of scholarly articles: it is a pioneering approach to the world of academia, radically improving the way scholarly research is managed. The grand vision of Frontiers is a world where all people have an equal opportunity to seek, share and generate knowledge. Frontiers provides immediate and permanent online open access to all its publications, but this alone is not enough to realize our grand goals.

Frontiers journal series

The Frontiers journal series is a multi-tier and interdisciplinary set of open-access, online journals, promising a paradigm shift from the current review, selection and dissemination processes in academic publishing. All Frontiers journals are driven by researchers for researchers; therefore, they constitute a service to the scholarly community. At the same time, the *Frontiers journal series* operates on a revolutionary invention, the tiered publishing system, initially addressing specific communities of scholars, and gradually climbing up to broader public understanding, thus serving the interests of the lay society, too.

Dedication to quality

Each Frontiers article is a landmark of the highest quality, thanks to genuinely collaborative interactions between authors and review editors, who include some of the world's best academicians. Research must be certified by peers before entering a stream of knowledge that may eventually reach the public - and shape society; therefore, Frontiers only applies the most rigorous and unbiased reviews. Frontiers revolutionizes research publishing by freely delivering the most outstanding research, evaluated with no bias from both the academic and social point of view. By applying the most advanced information technologies, Frontiers is catapulting scholarly publishing into a new generation.

What are Frontiers Research Topics?

Frontiers Research Topics are very popular trademarks of the *Frontiers journals series*: they are collections of at least ten articles, all centered on a particular subject. With their unique mix of varied contributions from Original Research to Review Articles, Frontiers Research Topics unify the most influential researchers, the latest key findings and historical advances in a hot research area.

Find out more on how to host your own Frontiers Research Topic or contribute to one as an author by contacting the Frontiers editorial office: frontiersin.org/about/contact

Updates on epigenetic regulation of endocrine disorders with polygenic traits: What is new?

Topic editors

Ahmet Uçar — Şişli Hamidiye Etfal Education and Research Hospital, Türkiye

Baris Binay — Gebze Technical University, Türkiye

Bibekanand Mallick — National Institute of Technology Rourkela, India

Citation

Uçar, A., Binay, B., Mallick, B., eds. (2023). *Updates on epigenetic regulation of endocrine disorders with polygenic traits: What is new?*

Lausanne: Frontiers Media SA. doi: 10.3389/978-2-83250-768-1

Table of contents

frontiers | Frontiers in Endocrinology

TYPE Editorial
PUBLISHED 17 November 2022
DOI 10.3389/fendo.2022.1073226

OPEN ACCESS

EDITED AND REVIEWED BY
James M Olcese,
Florida State University, United States

*CORRESPONDENCE
Ahmet Uçar
aucar76@yahoo.com

SPECIALTY SECTION
This article was submitted to Translational Endocrinology, a section of the journal Frontiers in Endocrinology

RECEIVED 18 October 2022
ACCEPTED 07 November 2022
PUBLISHED 17 November 2022

CITATION
Uçar A, Binay B and Mallick B (2022) Editorial: Updates on epigenetic regulation of endocrine disorders with polygenic traits: What is new? *Front. Endocrinol.* 13:1073226. doi: 10.3389/fendo.2022.1073226

Editorial: Updates on epigenetic regulation of endocrine disorders with polygenic traits: What is new?

Ahmet Uçar[1]*, Barış Binay[2] and Bibekanand Mallick[3]

[1]Department of Pediatric Endocrinology and Diabetes, University of Health Sciences, Şişli Hamidiye Etfal Education and Research Hospital, Istanbul, Turkey, [2]Department of Bioengineering, Gebze Technical University, Kocaeli, Turkey, [3]RNAi and Functional Genomics Laboratory, Department of Life Science, National Institute of Technology, Rourkela, India

KEYWORDS

epigenetic, non-coding RNAs (ncRNA), methylation, obesity, diabetes, Graves disease, metabolomics, endocrine disruptors

Editorial on the Research Topic
Updates on epigenetic regulation of endocrine disorders with polygenic traits: What is new?

A major impetus for a change in paradigm on the genetic approach to endocrine disorders with oligogenic/polygenic traits (influenced by two or more genes) has been the significant lack of available data regarding the frequency of pathogenic variants in coding regions of human genome (1). The common molecular changes that underlie epigenetic control are DNA methylation, chromatin remodeling, covalent histone modification, the localization of histone variants, and feedback loops (2). Epigenetic changes may be targeted to specific genes by either transcription factors (TFs) or non-coding RNAs (ncRNAs). Non-coding RNAs may be classified as small ncRNAs (including microRNAs (miRNAs), small interfering RNAs (siRNAs), small nucleolar RNAs (snoRNAs), PIWI interacting RNAs (piRNAs)) and long ncRNAs (lncRNAs) (3). It is not surprising that during the past two decades, researchers have discovered aberrations in the expression of ncRNAs associated with many human diseases such as cancer (4), cardiovascular diseases (5) and neurodegenerative disorders (6). Understanding the causal link between ncRNAs and human diseases have paved the path for novel strategies, such as the use of anti-ncRNA oligonucleotides to inhibit ncRNA for treating some types of cancer (7) and use of ncRNAs to enhance the sensitivity or reduce the resistance of the chemotherapeutic drugs (8–10).

This Research Topic is dedicated to exploring the most recent advances in evaluation of ncRNAs and the current knowledge on the putative influence of epigenetics with the evolution and phenotypic severity of endocrine disorders with oligogenic/polygenic traits. The contents of this Research Topic may serve to identify critical research gaps, and pave the path for future studies.

Obesity, metabolic syndrome (metS) and T2D are well-established to be the most common endocrine disorders with polygenic traits. Nevertheless, the available treatment options may not be successful in the long term as discussed elsewhere (11). Differential expressions of numerous genes are observed in obesity and T2D and miRNAs are involved in transcriptional regulation of target mRNAs (12). Zhang et al. identified upregulation of miR-342-3p as a positive regulator of appetite *via* reduced expression of snap25 gene, which leads to functional impairment of hypothalamic neurons and excess of food intake in a mouse model with fructose induced obesity. A similar study by Yamaguchi et al. identified overexpression of miR-222-3p as a positive regulator of obesity *via* increased adipogenesis. Inhibition of specific miRNAs may serve to address obesity and its complications by promoting novel treatments. Moreover, another novel suggestion to prevent and treat diabetes *via* mesenchymal stromal cells-derived small extracellular vesicles (MSC-sEVs) was reviewed by Li et al. These vesicles contain ncRNA, protein and DNA (13), and the authors report that MSC-sEVs repair or prevent damage from the complications of diabetes through several mechanisms, such as anti-inflammatory effects and reduction of endoplasmic reticulum-related protein stress.

Non-alcoholic fatty liver disease (NAFLD) is a complication of obesity associated with T2D. Several trials have been performed to treat NALFD with variable success (14). A major reason for lack of absolute success with the available treatment is that the cellular and molecular mechanisms leading to NAFLD are still unclear. Xu et al. examined the impact of a lncRNA growth arrest specific 5 (GAS5) on hepatic lipid metabolism in fatty liver in high fat diet-fed obese mice and showed that downregulation of GAS5 led to a series of intracellular events mitigating hepatic lipid metabolism. Therefore, downregulation of GAS5 may be a promising therapeutic option for NAFLD.

Owing to the well-established increase in prevalence of obesity, the distinction between Type 1 Diabetes (T1D) and T2D may be challenging. This is particularly of relevance in some circumstances, especially in Far East countries such as China, where the "thin-phenotype" T2D is more common than the usually expected obese phenotype (15). Lv et al. examined the differential expression of lncRNAs in in peripheral blood leukocytes from patients with T1D, T2D and healthy controls and found four lncRNAs that could be of importance to distinguish T1D and T2D since the treatment differs between the two entities. Further contributing to the diagnostic value of lncRNAs in hyperglycemic states, Yan et al. identified three lncRNAs in patients with hypertriglyceridemia, which could distinguish those with T2D and prediabetes or normoglycemia. The clinical use of these lncRNAs as biomarkers remains to be determined.

In an effort to provide a biologically plausible explanation to the "thin-phenotype" T2D in Far East (15) and South East Asia (16), Sletner et al. examined the association of placental leptin gene DNA methylation with maternal ethnicity, elevated low density lipoprotein-cholesterol and maternal hyperglycemia and found that South Asian ethnicity and gestational diabetes were associated with higher placental leptin gene methylation.

Mir et al. examined the association of miRNAs with dysglycemia in obese patients and found that they were associated with at least one trait of metS. Nevertheless, owing to the relatively low number of the patients enrolled in the study, and the cross sectional nature of the study, further studies are needed to confirm the validity of the differentially expressed miRNAs as biomarkers of metabolically unhealthy obesity.

The utility of miRNAs as biomarkers is not limited to mets components but they can also be of use as a diagnostic marker in microvascular complications of diabetes such as diabetic retinopathy (DR) (17). To this end, Ma et al. performed a meta-analysis investigating the validity of miRNAs as biomarkers of DR, and reported that they can be used with high diagnostic accuracy.

In addition to their potential role as biomarkers, miRNAs may also have a role in adaptive responses to stressors such as hypoglycemia. Ramanjaneya et al. documented that expression levels of miRNAs significantly differed in patients with T2D subjected to insulin induced hypoglycemia versus healthy controls. They showed that blunting of the response to hypoglycemia in patients with T2D with disease of short duration was associated with loss of counter-regulatory response in parallel with the lack of miRNA response.

Exposure to endocrine disruptors at critical times/stages of metabolic programming may also lead to epigenetic changes that may affect phenotype (2). Tawar et al. showed that organochlorine pesticides were associated with endoplasmic reticulum stress markers on adipose tissue samples of patients with T2D *versus* normoglycemic subjects, which further reinforced the concept that endocrine disruptors may be important as contributors to T2D, revealing the persistence of the gene-environment interaction in the etiology of T2D.

The use of miRNAs as biomarkers and/or surrogates of metabolism is not limited to obesity, metS and its complications. Four articles in the current Research Topic describe potential utility of miRNAs as either diagnostic biomarker or follow-up variable in other endocrine disorders: Baloun et al. reported associations of circulating miRNAs with estrogen status and bone metabolism in postmenopausal osteoporosis. Catellani et al. reported changes in circulating levels of miRNAs in patients with growth hormone(GH) deficiency after onset of GH treatment and indicated that the changes in several serum miRNA levels at three months of treatment were associated with the treatment response to GH at one year. Using knock-down or overexpression of the miRNA let-7e-5p in the muscle tissue of orchiectomized(ORX) and androgen treated ORX mice, Okamura et al. suggested that let-7e-5p could be a potential diagnostic marker for muscle atrophy. Galuppini et al. reported potential associations of microRNAs in papillary thyroid cancer with histological variants, which is of clinical significance owing

to prognostic implications on follow-up. The available data suggest that miRNAs may be of use in clinical practice in the new era.

Metabolomics is an emerging approach in a systems biology field. Metabolome's measurement is nowadays frequently implemented to understand pathophysiological processes involved in disease progression as well as to search for new diagnostic or prognostic biomarkers of various organism's disorders (18). Xia et al. assessed patients with Graves disease and found significant alterations in transfer RNA biosynthesis, amino acids,purine and primidine metabolism. The impact of these changes on the outcome of hyperthyroidism remain to be determined.

In conclusion, we hope that this Research Topic will serve as a point of reference and source of inspiration for researchers and clinicians interested in epigenetic regulation of endocrine disorders. While there has been a massive increase in studies assessing the interrelation of miRNAs, DNA methylation changes and endocrine disruptors with endocrine disorders with polygenic inheritance and/or autoimmune nature, there is a call for further in-depth evaluation of the putatively influential associations of these disorders with ncRNAs other than miRNAs.

Author contributions

AU drafted the manuscript and agreed to be accountable for all aspects of the work in ensuring that questions related to the accuracy or integrity of any part of the work are appropriately investigated and resolved. All co-authors revised the manuscript for important intellectual content, and approved the final version to be published.

Acknowledgments

We would like to thank all the contributors to the Research Topic.

Conflict of interest

The authors declare that the research was conducted in the absence of any commercial or financial relationships that could be construed as a potential conflict of interest.

Publisher's note

References

1. Zhang F, Lupski JR. Non-coding genetic variants in human disease. *Hum Mol Genet* (2015) 24(R1):R102–10. doi: 10.1093/hmg/ddv259

2. Fitz-James MH, Cavalli G. Molecular mechanisms of transgenerational epigenetic inheritance. *Nat Rev Genet* (2022) 23(6):325–41. doi: 10.1038/s41576-021-00438-5

3. Hombach S, Kretz M. Non-coding RNAs: Classification, biology and functioning. *Adv Exp Med Biol* (2016) 937:3–17. doi: 10.1007/978-3-319-42059-2_1

4. Saw PE, Xu X, Chen J, Song EW. Non-coding RNAs: the new central dogma of cancer biology. *Sci China Life Sci* (2021) 64(1):22–50. doi: 10.1007/s11427-020-1700-9

5. Poller W, Dimmeler S, Heymans S, Zeller T, Haas J, Karakas M, et al. Non-coding RNAs in cardiovascular diseases: diagnostic and therapeutic perspectives. *Eur Heart J* (2018) 39(29):2704–16. doi: 10.1093/eurheartj/ehx165

6. Wu YY, Kuo HC. Functional roles and networks of non-coding RNAs in the pathogenesis of neurodegenerative diseases. *J BioMed Sci* (2020) 27(1):49. doi: 10.1186/s12929-020-00636-z

7. Kara G, Calin GA, Ozpolat B. RNAi-based therapeutics and tumor targeted delivery in cancer. *Adv Drug Delivery Rev* (2022) 182:114113. doi: 10.1016/j.addr.2022.114113

8. Jain N, Das B, Mallick B. miR-197-5p increases doxorubicin-mediated anticancer cytotoxicity of HT1080 fibrosarcoma cells by decreasing drug efflux. *DNA Repair (Amst)* (2022) 109:103259. doi: 10.1016/j.dnarep.2021.103259

9. Das B, Jain N, Mallick B. piR-39980 mediates doxorubicin resistance in fibrosarcoma by regulating drug accumulation and DNA repair. *Commun Biol* (2021) 4(1):1312. doi: 10.1038/s42003-021-02844-1

10. Roy J, Das B, Jain N, Mallick B. PIWI-interacting RNA 39980 promotes tumor progression and reduces drug sensitivity in neuroblastoma cells. *J Cell Physiol* (2020) 235(3):2286–99. doi: 10.1002/jcp.29136

11. Raman V, Gupta A, Ashraf AP, Breidbart E, Gourgari E, Kamboj M, et al. Pharmacologic weight management in the era of adolescent obesity. *J Clin Endocrinol Metab* (2022) 107(10):2716–28. doi: 10.1210/clinem/dgac418

12. Wendt A, Esguerra JL, Eliasson L. Islet microRNAs in health and type-2 diabetes. *Curr Opin Pharmacol* (2018) 43:46–52. doi: 10.1016/j.coph.2018.08.003

13. Fang SB, Zhang HY, Wang C, He BX, Liu XQ, Meng XC, et al. Small extracellular vesicles derived from human mesenchymal stromal cells prevent group 2 innate lymphoid cell-dominant allergic airway inflammation through delivery of miR-146a-5p. *J Extracell Vesicles* (2020) 9(1):1723260. doi: 10.1080/20013078.2020.1723260

14. Makri E, Goulas A, Polyzos SA. Epidemiology, pathogenesis, diagnosis and emerging treatment of nonalcoholic fatty liver disease. *Arch Med Res* (2021) 52 (1):25–37. doi: 10.1016/j.arcmed.2020.11.010

15. Hu C, Jia W. Diabetes in China: Epidemiology and genetic risk factors and their clinical utility in personalized medication. *Diabetes* (2018) 67(1):3–11. doi: 10.2337/dbi17-0013

16. Venkataraman H, Ram U, Craik S, Arungunasekaran A, Seshadri S, Saravanan P. Increased fetal adiposity prior to diagnosis of gestational diabetes in south asians: more evidence for the 'thin-fat' baby. *Diabetologia* (2016) 60 (3):399–405. doi: 10.1007/s00125-016-4166-2

17. Gong Q, Su G. Roles of miRNAs and long noncoding RNAs in the progression of diabetic retinopathy. *Biosci Rep* (2017) 37(6):BSR20171157. doi: 10.1042/BSR20171157

18. Bujak R, Struck-Lewicka W, Markuszewski MJ, Kaliszan R. Metabolomics for laboratory diagnostics. *J Pharm BioMed Anal* (2015) 113:108–20. doi: 10.1016/j.jpba.2014.12.017

frontiers in Endocrinology

ORIGINAL RESEARCH
published: 30 August 2021
doi: 10.3389/fendo.2021.727915

Upregulation of *Mir342* in Diet-Induced Obesity Mouse and the Hypothalamic Appetite Control

Dongxiao Zhang[1], *Satoshi Yamaguchi*[1], *Xinhao Zhang*[1], *Boxuan Yang*[1], *Naoko Kurooka*[1], *Ryosuke Sugawara*[1], *Haya Hamed H. Albuayjan*[1], *Atsuko Nakatsuka*[1], *Jun Eguchi*[1], *Takeshi Y. Hiyama*[2], *Atsunori Kamiya*[2] *and Jun Wada*[1]*

[1] *Department of Nephrology, Rheumatology, Endocrinology and Metabolism, Okayama University Graduate School of Medicine, Dentistry and Pharmaceutical Sciences, Okayama, Japan,* [2] *Department of Cellular Physiology, Okayama University Graduate School of Medicine, Dentistry and Pharmaceutical Sciences, Okayama, Japan*

In obesity and type 2 diabetes, numerous genes are differentially expressed, and microRNAs are involved in transcriptional regulation of target mRNAs, but miRNAs critically involved in the appetite control are not known. Here, we identified upregulation of miR-342-3p and its host gene *Evl* in brain and adipose tissues in C57BL/6 mice fed with high fat-high sucrose (HFHS) chow by RNA sequencing. *Mir342* (-/-) mice fed with HFHS chow were protected from obesity and diabetes. The hypothalamic arcuate nucleus neurons co-express *Mir342* and EVL. The percentage of activated $NPY^{+}pSTAT3^{+}$ neurons were reduced, while $POMC^{+}pSTAT3^{+}$ neurons increased in *Mir342* (-/-) mice, and they demonstrated the reduction of food intake and amelioration of metabolic phenotypes. *Snap25* was identified as a major target gene of miR-342-3p and the reduced expression of *Snap25* may link to functional impairment hypothalamic neurons and excess of food intake. The inhibition of miR-342-3p may be a potential candidate for miRNA-based therapy.

Keywords: abdominal obesity, non-coding RNAs, adipose tissues, appetite regulation, hypothalamus

OPEN ACCESS

Edited by:
Marc Thibonnier, AptamiR Therapeutics Inc., United States

Reviewed by:
Yuko Maejima, Fukushima Medical University, Japan
Denise D. Belsham, University of Toronto, Canada

***Correspondence:**
Jun Wada
junwada@okayama-u.ac.jp

Specialty section:
This article was submitted to Obesity, a section of the journal Frontiers in Endocrinology

Received: *20 June 2021*
Accepted: *10 August 2021*
Published: *30 August 2021*

Citation:
Zhang D, Yamaguchi S, Zhang X, Yang B, Kurooka N, Sugawara R, Albuayjan HHH, Nakatsuka A, Eguchi J, Hiyama TY, Kamiya A and Wada J (2021) Upregulation of Mir342 in Diet-Induced Obesity Mouse and the Hypothalamic Appetite Control. Front. Endocrinol. 12:727915. doi: 10.3389/fendo.2021.727915

INTRODUCTION

microRNAs are non-coding RNAs with the length of 21-25 nucleic acids and repress the expression of hundreds of target mRNAs by the binding to complete or 1- or 2-bp mismatched complementary sequences on 3'-untranslated regions (UTR), mRNA cleavage, mRNA deadenylation, and subsequent translational repression (1). Numerous studies demonstrated that miRNAs play critical roles in fine-tuning of gene expression in various physiological and pathological states (2). Furthermore, miRNAs themselves are transcriptionally regulated, however, little is known about the structural features of miRNA promoters (3) and the accurate miRNA promotor identification is underway (2). In the disease states of obesity and diabetes, differential expression of miRNAs associated with regulation of target mRNAs would be critically involved in the pathogenesis and they are candidates for biomarkers and therapeutic targets. In fact, initial attempts were made to survey miRNA expression profile in pancreatic β cells caused by obesity, hyperglycemia, and dyslipidemia. In the islets of healthy and type 2 diabetes (T2D) organ donors, miR-7a, miR-130a/b, miR-152, and miR-184 were differentially expressed (4). The expression of

microRNA is regulated by environmental, genetic, and epigenetic factors and their disturbance is critically involved in the pathogenesis of diabetes and its complications (5, 6). The promoter CpG islands of maternally expressed *MEG3* and miRNA cluster was hypomethylated in T2D organ donors, and reduction of miRNAs caused upregulation of their target genes such as *TP53INP1*, which induced the apoptosis of pancreatic β cells (7). T2D loci were recently identified at clusters of miRNAs maternally expressed *MEG3* and paternally expressed *DLK1* (8). *DLK1* is known to inhibit adipocyte differentiation and protect against obesity (9).

The further attempts were made to identify the miRNAs related to insulin resistance in obesity and T2D, and miRNAs profiling studies were extensively performed in adipose tissues, liver and muscle (6). Notably, miRNAs can be packaged in the extracellular vesicle such as exosomes, which transfer miRNAs between cells and mediate the interorgan crosstalk. Thus, the profile of circulating miRNAs was also vigorously performed (10). In our attempts to identify new therapeutic target of miRNAs, we surveyed expression profile in liver, muscle, white adipose tissues, and sera of C57BL/6JJcl mice fed with standard (STD) and high fat-high sucrose (HFHS) chow by RNA sequencing (GSE61959) (11). We identified unique miRNA gene, *Mir342*, and it is highly upregulated in brain and white adipose tissues by the feeding of HFHS chow in C57BL/6JJcl mice. Here, we report the benefits of the deletion of *Mir342* gene in C57BL/6JJcl mice fed with HFHS chow, *i.e.*, amelioration of obesity and T2D. *Mir342* (-/-) mice fed with HFHS chow were characterized with reduced chow intake and reduced activation of neuropeptide Y (NPY) neurons in arcuate nuclei. We also investigated the expression of *Evl*, host gene of *Mir342*, and identified *Snap25* as a target gene of miR-342-3p.

MATERIALS AND METHODS

Animal Models

We obtained Sanger MirKO ES cell line *Mir342* (*Mir342*^{tm1Wtsi}) from MMRRC (Mutant Mouse Resource & Research Centers, University of California, Davis, USA). The insertion of the PGK_EM7_PuDtk_bGHpA cassette created a deletion of size 196 bp (109,896,794–109,896,990 of Chromosome 12 in NC_000078.5 Chromosome 12 Reference MGSCv37 C57BL/6J; 108,624,843-108,624,915 in NC_000078.7 Chromosome 12 Reference GRCm39 C57BL/6J). This deletion eliminates the DNA sequence for this microRNA. The cassette is composed of a loxP site followed by an F3 site followed by a PGK-puromycin-delta-tk cassette, a loxP site and finally an FRT site (12). The germline chimeric mice were prepared under the background of C57BL/6N. Targeted *Mir342* was confirmed by 2 sets of primer pairs, 5' common rev 5′-ATAGCATACATTATACGAAGTTATCACTGG-3′ and 5' gene specific fwd (LR1) 5′-AGCTCACTTACATTTTATTTATTTTCTCCT-3′ (5,739 bp); 3' common fwd 5′-TCTAGAAAGTATAGGAACTTCCATGGTC-3′ and 3' gene specific rev (LR4) 5′-GTAGGCAAGAAGACATAATACAGAAAAG-3′ (3,232 bp). Wild-type *Mir342* was detected by primers, LR1 and LR4 (8,789 bp). The male chimeric mice were mated with C57BL/6JJcl (CLEA Japan, Tokyo, Japan) to generate heterozygous *Mir342* (+/-). By crossing *Mir342* (+/-) C57BL/6JJcl mice, we generated male homozygous *Mir342* (-/-) and wild-type *Mir342* (+/+) littermates. Five-week-old mice were randomly assigned to standard diet (STD) group (MF, Oriental Yeast, Japan) or high fat high sucrose diet (HFHS) group (D12331, Research Diets, New Brunswick, NJ). At 24 weeks of age, we obtained various organs and they were subjected to following experiments.

Human Serum Samples

Human serum samples were collected from 65 patients with type 2 diabetes (T2D) in Okayama University Hospital and 45 subjects with normal fasting glucose (NFG, fasting glucose < 110 mg/dL). The patients with malignancies, treatment with steroids and immunosuppressants, and total pancreas resection were excluded. It was approved by Okayama University Graduate School of Medicine, Dentistry and Pharmaceutical Sciences and Okayama University Hospital, Ethics Committee (#1708-045).

3T3-L1 Cell Cultures

3T3-L1 pre-adipocytes were cultured in Dulbecco's modified eagle's medium (DMEM, 124951, Gibco). On day 0, the media were changed to the differentiation media of the DMEM supplemented with 10% FBS, 10 μg/ml insulin (I1882, Sigma), 1 μM DEX (D2915, Sigma) and 0.5 mM IBMX (I5879, Sigma). On day 2, the media were changed to DMEM supplemented with 10 μg/ml insulin and 10% FBS. The media were changed every day. Total RNA was isolated from 3T3-L1 cells during differentiation from day 1 to day 10 using RNeasy Mini kit (74106, Qiagen) and subjected to RT-qPCR.

Insulin Tolerance Test and Glucose Tolerance Test (ITT and GTT)

The 20-week-old mice (n=4 in each experimental group) were fasted for 16 hours in GTT and for 3 hours in ITT. They were then intraperitoneally injected with glucose solution (1 mg/g body weight) and human insulin (1 unit/kg in HFHS groups and 0.75 unit/kg in STD groups) for GTT and ITT, respectively. Serum Insulin and leptin levels were measured (Skylight Biotech, Tokyo, Japan).

Food Intake, Locomotor Activity, and Basal Metabolic Rate

At 16 weeks of age, daily food intake was measured and calculated; daily food intake [g/day/body weight (BW)] = [initial food weight (g) – leftover food weight (g)]/measurement period (days)/BW (g). The locomotor activity was recorded for 24 hours by the frequency of interrupting an infrared sensor (ACTIMO-100, Shinfactory, Fukuoka, Japan). O_2/CO_2 metabolism measuring system (MK-5000, Muromachi Kikai, Tokyo, Japan) were used to quantify oxygen consumption rate and carbon dioxide production for the estimation of $\dot{V}O2$ and respiratory quotient (RQ). Four mice in each experimental group were examined.

Pair-Feeding Study

Mir342 (+/+) and *Mir342* (-/-) mice (n=3 for free-feeding and n=5 for pair-feeding) were individually housed and fed with HFHS chow, body weight was measured every week. Food intake of free-fed mice were measured every 3 days. The equal amount of chow consumed by free-fed *Mir342* (-/-) mice for 3 days was given to the pair-fed *Mir342* (+/+) and *Mir342* (-/-) mice.

Reverse Transcription-Quantitative Polymerase Chain Reaction

RNAs were extracted from frozen tissues and cultured 3T3-L1 cells with RNeasy Mini Kit (Qiagen). For brain tissues, the hypothalamus and ventral midbrain region were removed by free-hand dissection. The QIAamp Circulating Nucleic Acid Kit and the exoRNeasy Serum/Plasma Midi Kit (Qiagen) were used for the isolation of total RNAs from serum and exosomes. For gene expression analyses, cDNAs were prepared with High-Capacity RNA-to-cDNA Kit (Thermo Fisher Scientific). TaqMan gene expression primers, *Evl* (Mm00468405_m1), *Snap25* (Mm01276449_m1), *Cidea* (Mm00432554_m1), *Cox7a1* (Mm00438297_g1), *Pparg* (Mm00440940_m1), *Il6* (Mm00446190_m1), *Il1b* (Mm00434228_m1), *Tnf* (Mm00443258_m1), *Ifng* (Mm01168134_m1), *Lpl* (Mm00434764_m1), *Adipoq* (Mm00456425_m1), *Nhlh2* (Mm01959164_u1), *Msi1* (Mm01203522_m1), *Fat2* (Mm01295775_m1), *Rplp0* (Mm00725448_s1), and *Rn18s* (Mm03928990_g1) were employed. For miRNA expression studies, cDNAs were prepared from total RNAs by TaqMan MicroRNA Reverse Transcription Kit (Life Technologies). MicroRNA primers, hsa-miR-342p (002260), snoRNA202 (001232), snoRNA234 (001234), and cel-miR-39 (000200) were used. *Rplp0*, *Rn18s*, snoRNA202, snoRNA234, and cel-miR-39 were served as the invariant controls. The RT-qPCR was performed using TaqMan Universal PCR Master mix II (no UNG) at a StepOne Plus Real-Time PCR system. The quantification was performed by the $2^{-\Delta\Delta CT}$ analysis method.

Western Blot Analysis

The brain and hypothalamic tissues from 24-week-old mice (n=3-4 in each experimental group) were homogenized in RIPA lysis buffer (radioimmunoprecipitation buffer) plus protease inhibitors. The samples were boiled in SDS-PAGE loading buffer, separated on 12% Mini-PROTEAN TGX Precast Protein Gels (Bio-Rad), and transferred to a PVDF Blotting Membrane (cytiva). After blocking with 5% nonfat milk for 1 hour at room temperature (RT), the blots were incubated with rabbit Anti-SNAP25 antibody (ab5666, Abcam, 1:1000), rabbit Anti-EVL antibody (ab204835, Abcam, 1:1000) overnight at 4°C. Rabbit anti-β-Actin antibody (4967S, Cell Signaling Technology) was used as a loading control. After washing three times with Tris-buffered saline (TBS), the blots were incubated with ECL Donkey Anti-Rabbit IgG, HRP-Conjugated Antibodies (NA934V, GE healthcare Life science, 1:10000) at RT for 1 hour. The blots were developed with Pierce ECL Western Blotting Substrate (TE261327, Thermo Fisher Scientific). The chemiluminescence was analyzed using ImageQuant LAS-4000 mini (FUJIFILM).

Morphometric Analysis for Adipocyte Size

Epididymal and subdermal adipose tissues were fixed by 10% formalin, embedded with paraffin. The 5-μm paraffin sections were prepared and stained with PAS. The images were captured using an Olympus BX51 microscope. The size of the adipocytes was analyzed by the ImageJ software (National Institutes of Health). Epididymal and subdermal adipose tissue were taken from 4 individual animals from each experimental group.

In Situ Hybridization

In situ hybridization for miRNA was performed using miRCURY LNA miRNA ISH Optimization Kit (FFPE) 4 (Qiagen) on formalin-fixed paraffin embedded (FFPE) tissue samples. The sections were deparaffinized in xylene, hydrated in a series of graded alcohols until water at RT, and followed by washing three times with phosphate-buffered saline (PBS). The slides were incubated for 30 minutes with 3 μg/ml of proteinase K at 37° C. After washing twice with PBS and dehydrated, the sections were hybridized for 2 hours with a gene specific probe (40 nM for double-DIG LNA *Mir342* probe) and LNA *Scramble-miR* probe (double DIG labeled) at 55°C. LNA *U6* snRNA probe (5' DIG labeled) and LNA *Scramble-miR* probe was used for endogenous control. The sections were washed in stringent condition with 5×SSC, 1×SSC and 0.2× SSC for 10 minutes at 55°C. After the wash with PBS, the sections were blocked with Antibody blocking solution (PBS, 0.1% Tween, 2% Sheep serum, and 1% BSA) and incubated with Anti-Digoxigenin-AP Fab fragments (11093274910, Roche, 1:800) in Antibody Dilutant solution (PBS, 0.05% Tween, 1% Sheep serum, and 1% BSA) for 1 hour at RT. After washing by PBS, the sections were incubated with AP substrate, *i.e.* NBT/BCIP ready-to-use tablet (ROCHE) in 10 ml Milli-Q water and 0.2 mM Levamisole for 2 hours at 30°C. They were then incubated in KTBT buffer (50 mM Tris-Cl, 150 mM NaCl, 10 mM KCl, and 1% Triton X-100) twice for 5 min each to stop the reaction. Finally, the slides were counterstained, dehydrated, and mounted. The processed sections were visualized using an Olympus BX51 microscope.

Immunofluorescence

The mice (n=4-5 in each experimental group) were fasted for 16 hours and euthanized. The whole brain was taken after systemic perfusion with 4% paraformaldehyde (PFA). For STAT3 activation study, the intraperitoneal injection of mouse recombinant leptin (181030-10-4, FUJIFILM) (1 mg/kg body weight) was given 1 hour before euthanasia. The frozen coronal brain sections (-1.10 mm to -1.90 mm from bregma) were cut at 20-μm thick and fixed in 4% PFA for 15 min. For adipose tissues, 5-μm paraffin sections were first deparaffinized in xylene and hydrated in a series of graded alcohols until water. After antigen retrieval in HistoVT One (nacalai tesque) at 90°C for 15 min, the sections were first incubated in the avidin-biotin blocking kit and incubated with primary antibodies, rabbit Anti-EVL antibody (ab204835, Abcam, 1:250), rabbit Anti-pSTAT3

Antibody (9131, Cell Signaling Technology, 1:500), mouse Anti-NPY antibody (GTX60971, Gene Tex, 1:2000), goat Anti-POMC antibody (ab32893, Abcam, 1:4000), mouse Anti-Neun antibody (ab104224, Abcam,1:500), chicken Anti-GFAP antibody (ab4674, Abcam, 1:500), mouse Anti-IBA1 antibody (sc-32725, Santa Cruz, 1:500), mouse Anti-Myelin Basic Protein antibody (ab62631, Abcam, 1:500), chicken Anti-Tyrosine Hydroxylase antibody (ab76442, Abcam, 1:500) and rat Anti-F4/80 Antibody (ab6640, Abcam, 1:100) for 3 days at 4°C. After 3 times washing by PBS, the tissue sections were then incubated with secondary antibodies, Alexa 647-conjugated goat Anti-Rabbit IgG (ab150083, Abcam, 1:500), Alexa 488-conjugated goat Anti-Rat (ab150165, Abcam, 1:500), Alexa 488-conjugated goat Anti-Mouse (ab150117, Abcam, 1:500), Alexa 488-conjugated donkey Anti-Goat IgG (ab150129, Abcam, 1:500), Alexa 488-conjugated goat Anti-Chicken IgY (ab150173, Abcam, 1:500), Biotin-conjugated donkey Anti-Rabbit/Goat IgG (711-065-152, 705-065-147, Jackson ImmunoResearch, 1:500) for 1 hour at RT. Next, the sections were incubated with fluorescent streptavidin (SA-1200, Vector) for 1 hour at RT. Finally, the sections were mounted using ProLong Gold Antifade Mountant with DAPI (P36931, Thermo Fisher) and observed by an Olympus BX51 microscope. Images covering the whole arcuate nucleus of brain sections (438.6 μm x 330.2 μm = 0.14 mm^2) were subjected to count cell numbers using Image J software. For quantification, the average cell count from 3 sections per animal was obtained.

Isolation of Stromal Vascular Fraction From White Adipose Tissues

SVF was isolated from epididymal adipose tissue of 24-week-old mice. Briefly, fresh mouse epididymal fat pads were minced and digested with collagenase type 1 (CLSS1, Worthington) in HBSS containing 10% FBS for 45 minutes at 37°C. The mixture was filtered through a nylon mesh (100 μm), then centrifuged at 400 g for 1 minute. The adipocyte fraction was obtained from the supernatant and the SVF from the pellet.

Identification of *Mir342* Target mRNAs

The mRNA microarray was performed by GeneChip Mouse Gene 2.0 array using total RNA of epidydimal fat obtained from 16-week-old mice (3 individual animals from each group) and analyzed by Filgen (Nagoya, Japan). The raw data are available in Gene Expression Omnibus (GEO; https://www.ncbi.nlm.nih.gov/geo/) (GSE163880). TargetScan (http://www.targetscan.org/vert_72/), miRDB (http://www.mirdb.org/), Pictar (https://pictar.mdc-berlin.de/) and DIANA-microT v5.0 (https://bio.tools/DIANA-microT) and were used to identify potential target genes for *Mir342*.

Luciferase Reporter Assay

To quantitatively evaluate miRNA activity on cloned miRNA target sequence from 3'-untranslated region (3'-UTR) of *Snap25*, pmirGLO dual luciferase miRNA Target expression vector (E1330, Promega) was used. Firstly, the pmirGLO plasmid was linearized by double digestion with *Xho*I and *Sac*I. The cDNAs of *Snap25* wild type (WT) 3′-UTR and *Snap25* mutant (MT) 3'-UTR were amplified by PCR and ligated with CIP treated pmirGLO Vector. The primers are Forward *Xho*I *Snap25*: 5'-GGGGGGCTCGAGACAAAGATGCTGGGAAGTGG-3′, Reverse *Sac*I *Snap25*: 5'-GGGGGGGAGCTCCAAACCAACAGAGGAGACAG-3′, Reverse *Sac*I mutant *Snap25*: 5'-GGGGGGGAGCTCCATGCTGTAATGATATTTAGCGCACAGTTTATC-3′. The seed sequence "TCTCACA" was mutated to "GCGCACA". After transformation to *E. coli* JM109 cells, pmirGLO-*Snap25* WT 3'-UTR, pmirGLO-*Snap25* MT 3'-UTR, and pmirGLO no-insert control plasmids were isolated with EndoFree Plasmid Maxi Kit (12362, Qiagen). HEK293T cells were seeded at a density of 120,000 cells/mL, then co-transfected with *Mir342* mimic (MSY0000590, Qiagen), *Mir342* inhibitor (MIN0000590, Qiagen), negative control *siRNA* (1027280, Qiagen), inhibitor negative control (1027271, Qiagen), pmirGLO-*Snap25* WT 3'-UTR, pmirGLO-*Snap25* MT 3'-UTR, and pmirGLO no-insert control plasmids. Twenty-four hours after transfection, the cells were analyzed to measure luciferase activities using the Dual-Glo Luciferase Assay System and a GloMax 20/20 luminometer (Promega).

DNA Methylation Analysis

The methylation status of *Evl* and *Mir342* genes was investigated (EpigenDx, http://www.epigendx.com/). NGS (next-generation sequencing) methylation assays were designed to interrogate the DNA methylation status of 103 CpG sites in the 5' upstream to 3'UTR regions of the Mouse *Evl* gene. The CpG loci location or coordinates are based on Ensembl Gene ID ENSMUSG00000021262 and GRCm39 genomic build. Genomic DNA extracted from brain tissues of *Mir342* (+/+) mice fed with HFHS or STD chow (n=3) were subjected to NGS methylation analysis. Bisulfite modification was carried out using EZ DNA Methylation-Direct Kit (D5020) according to the manufacturer's protocol (Zymo Research). PCRs included 0.5 units of HotStarTaq (203205, Qiagen), 0.2 μM primers, and 3 μL of bisulfite-treated 200-500 ng DNA in a 20 μL reaction. All PCR products were verified using the Qiagen QIAxcel Advanced System (v1.0.6). Prior to library preparation, PCR products from the same sample were pooled and then purified using the QIAquick PCR Purification Kit columns or plates (28106, Qiagen). Libraries were prepared using a custom Library Preparation method created by EpigenDX. Next, libraries were purified using Agencourt AMPure XP beads (A63882, Beckman Coulter). Barcoded samples were then pooled in an equimolar fashion before template preparation and enrichment were performed in the Ion Chef system using Ion 520 & Ion 530 ExT Chef reagents (A30670, Thermo Fisher). Following this, enriched, template-positive libraries were sequenced on the Ion S5 sequencer using an Ion 530 sequencing chip (A27764). FASTQ files from the Ion Torrent S5 server were aligned to the local reference database using open-source Bismark Bisulfite Read Mapper with the Bowtie2 alignment algorithm. Methylation levels were calculated in Bismark by dividing the number of methylated reads by the total number of reads.

Statistical Analysis

All values were represented as the mean ± standard deviation (SD). Statistical analyses were conducted using IBM SPSS Statistics 23 and GraphPad Prism (version 8.0). Independent *t*-test, one-way ANOVA with Tukey test and two-way ANOVA with Bonferroni

tests were used to determine the differences. For DNA methylation analysis, Fisher's exact test was applied at each CpG site, and Mann–Whitney *U* test was used by NGS methylation assay. For correlation, non-parametric Spearman r coefficient was used. $p<0.05$ was considered statistically significant.

RESULTS

Mir342 (-/-) Mice Are Resistant to Diet-Induced Obesity and Diabetes

To identify miRNAs which are critically involved in the disease process of metabolic syndrome and type 2 diabetes (T2D), we performed miRNA profiling of serum, liver and epididymal fat tissues in C57BL/6JJcl mice fed with standard (STD) and high fat-high sucrose (HFHS) chow (11). The Illumina RNA sequencing data are available in the Gene Expression Omnibus (GEO) under the accession number GSE61959. The miRNA genes with read number more than 2,000 were sorted by HFHS/STD ratios and we identified that *Mir342* was ranked second with 9.5-fold up-regulation in epididymal adipose tissues of HFHS group (**Figure 1A** and **Supplementary Table 1**). In the patients with T2D (n=65), we found that serum concentrations of miR-342-3p showed positive and significant correlation with body weight (**Figure 2**). However, in NFG (n=45) and NFG + T2D (n=110), there were no significant correlations between miR-342-3p and body weight (**Supplementary Figure 1**). There were no significant differences of miR-342-3p levels in T2D with and without metformin (**Supplementary Table 2**). To further give a new insight and investigate the role of *Mir342* in obesity and diabetes, we obtained Sanger MirKO ES cell line *Mir342* (*Mir342*^{tm1Wtsi}) from MMRRC (Mutant Mouse Resource & Research Centers) and generated *Mir342* knockout mice [*Mir342* (-/-)].

Body weight of *Mir342* (-/-) mice fed with HFHS chow was significantly reduced compared with *Mir342* (+/+) mice. The weight of epididymal, subdermal and brown fat was also reduced in *Mir342* (-/-) mice. The *Mir342* (-/-) and *Mir342* (+/+) mice fed with STD chow demonstrated no significant differences in their body and tissue weight (**Figure 1B**). The size of adipocytes in epididymal and subdermal adipose tissues derived from *Mir342* (-/-) mice fed with HFHS chow was smaller compared with *Mir342* (+/+) mice (**Figure 1C**). To investigate glucose homeostasis, we performed insulin tolerance test (ITT) and glucose tolerance test (GTT). The blood glucose levels of *Mir342* (-/-) mice fed with HFHS chow were significantly reduced both in ITT and GTT (**Figure 1D**). In GTT, *Mir342* (-/-) mice exhibited significantly lower serum insulin level at 30 and 60 minutes after the peritoneal injection of glucose solution (**Figure 1E**), indicating that insulin sensitivity was significantly improved in *Mir342* (-/-) mice fed with HFHS chow. The levels of fasting serum leptin were also decreased in *Mir342* (-/-) mice, suggesting improved leptin sensitivity (**Figure 1F**). To investigate whether reduced adiposity in *Mir342* (-/-) mice was due to changes in energy intake or energy expenditure, we measured food intake, locomotor activity, and basal metabolic rates. *Mir342* (-/-) mice at 16 weeks of age demonstrated reduced daily food intake under HFHS chow whereas no changes in STD chow (**Figures 3A, B**). To prove that increased food intake is the main cause of obesity, we performed pair-feeding experiments in mice fed with HFHS chow. The pair-fed *Mir342* (+/+) mice demonstrated similar body weight with *Mir342* (-/-) mice whereas significantly higher body weight and food consumption were demonstrated in free-fed *Mir342* (+/+) mice after 12 weeks old (**Figure 3C**). The locomotor activity was recorded for over 24 hours, most of the activities were observed during the dark phase in all groups. The significantly increased activity was observed in *Mir342* (-/-) mice under HFHS chow during 23:00-24:00; however, there were no significant differences during whole dark period (**Supplementary Figures 2A, B**). Dark-period oxygen consumption rate, $\dot{V}O2$, was increased, while daily respiratory quotient (RQ) was reduced in *Mir342* (-/-) mice fed with HFHS chow compared with *Mir342* (+/+) mice (**Supplementary Figures 2C, D**). Since the changes in $\dot{V}O2$ and RQ were rather mild, the data suggested that the reduction of food intake mainly contributed to the resistance to diet-induced obesity and diabetes in *Mir342* (-/-) mice. There was no difference in the concentrations of miR-342-3p in both isolated exosome and total serum between *Mir342* (+/+) fed with HFHS and STD chow (**Supplementary Figure 3A**). The gene expression of *Cidea*, *Cox7a1*, and *Pparg* was down regulated in brown adipose tissue of *Mir342* (-/-) mice fed compared with *Mir342* (+/+) mice fed with HFHS chow, while they were not altered in epididymal adipose tissue (**Supplementary Figure 3B**).

Mir342 and Its Host Gene *Evl* Are Highly Expressed in Neurons Under HFHS Chow

Mir342 is located within an intron of the *Evl* (Enabled/vasodilator-stimulated phosphoprotein-like) gene, thus *Evl* is regarded as a host gene of *Mir342* (**Figure 4A**). We further investigated *Mir342* and *Evl* expression in various organs. miR-342-3p was abundantly expressed in spleen, brain and white adipose tissues and they were significantly upregulated in *Mir342* (+/+) fed with HFHS compared with STD chow (**Figure 4B**). We further investigated the distribution of miR-342-3p in hypothalamus and ventral midbrain region, including ventral tegmental area and substantial nigra (**Supplementary Figure 3C**). miR-342-3p was upregulated by HFHS chow in both brain areas, and it was highly expressed in hypothalamus compared with midbrain region. The similar tissue distributions of *Evl* were observed and it was also significantly upregulated in brain and white adipose tissues in *Mir342* (+/+) mice fed with HFHS chow (**Figure 4C**). Both expressions of *Mir342* and *Evl* were regulated in parallel and rather accentuated in brain tissues compared with adipose tissues. In *Mir342* (-/-) mice, the expression of miR-342-3p was absent in all tissues and mRNA expression of *Evl* was reduced in brain and adipose tissues compared with *Mir342* (+/+) mice fed with HFHS chow without statistical significance (**Figures 4B, C**). The reduction of protein levels of EVL were confirmed by Western blot analyses using brain samples in *Mir342* (-/-) mice fed with HFHS chow (**Figure 4D** and **Supplementary Figure 4**).

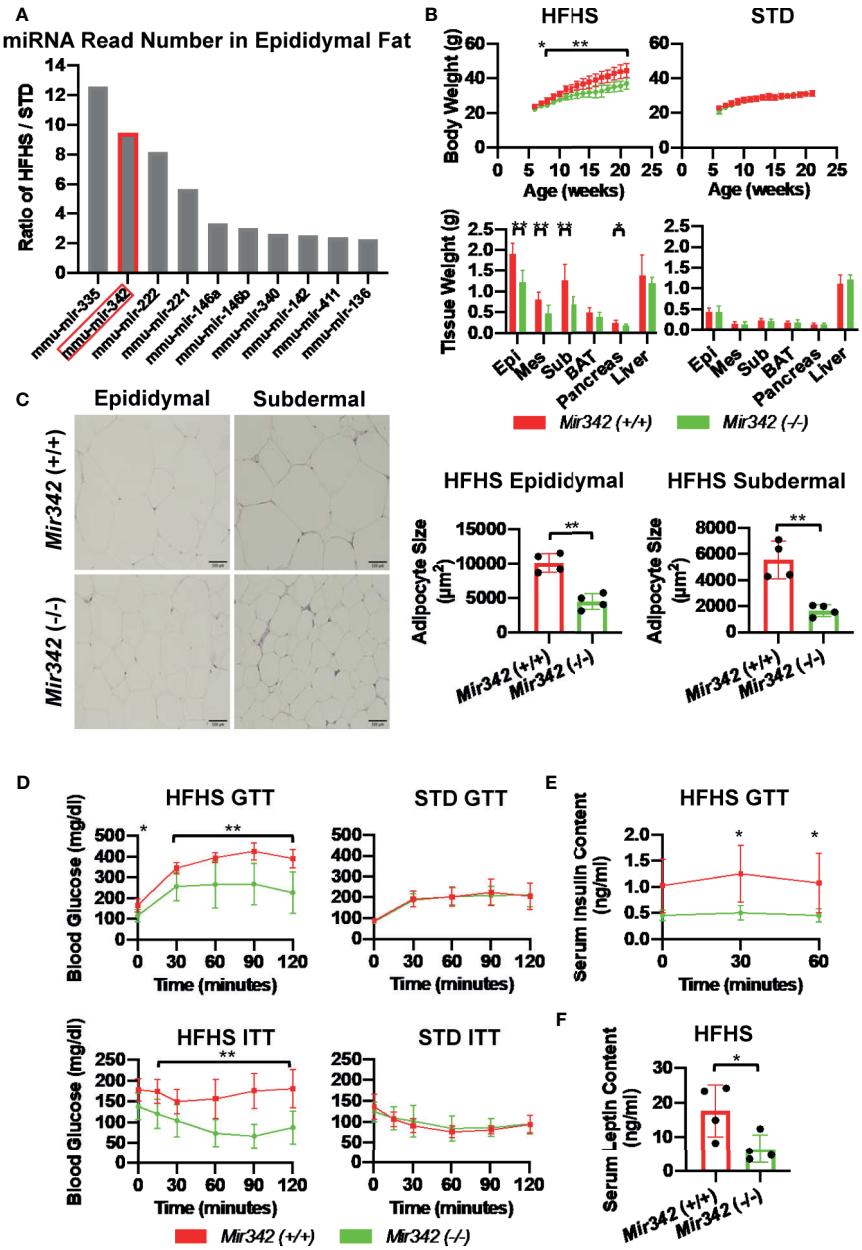

FIGURE 1 | The metabolic phenotypes of *Mir342* (-/-) and *Mir342* (+/+) mice fed with high fat-high sucrose (HFHS) or standard (STD) chow. **(A)** The HFHS/STD ratio of miRNA read numbers in epididymal fat tissues. **(B)** Body and tissue weight of *Mir342* (+/+) and *Mir342* (-/-) mice fed with HFHS (n=7) or STD chow (n=8). **(C)** Adipocyte area in epididymal and subdermal adipose tissues (n=4). Quantitative analyses were carried out on PAS-stained paraffin sections. **(D)** Glucose tolerance test (GTT) and insulin tolerance test (ITT) of mice fed with HFHS (n=7) or STD chow (n=8). **(E)** Serum insulin levels in *Mir342* (+/+) and *Mir342* (-/-) mice fed with HFHS chow during GTT (n=4). **(F)** Fasting serum leptin levels in *Mir342* (+/+) and *Mir342* (-/-) mice fed with HFHS mice (n=4). Data shown as mean ± SD and analyzed by independent *t*-test or two-way ANOVA with Bonferroni tests (*p < 0.05; **p < 0.01).

The expression of *Evl* is mainly regulated by the methylation status of CpG islands (13) and miRNA biogenesis is enhanced by DNA methylation in the regions flanking the miRNA coding sequence (14), we examined the DNA methylation status of 103 CpG sites ranging from the 5' upstream to 3'UTR regions of the mouse *Evl* gene. The flanking regions of *Mir342* (103,758-103,874 and 115,467-115,543 from TTS of *Evl* gene) were highly methylated. The immediate upstream (103,758-103,874 from TTS) of *Mir342* demonstrated slightly increased methylation by HFHS chow (**Supplementary Figure 5** and **Supplementary Data**) and it may be responsible for the upregulation of *Mir342* by HFHS chow. In contrast, all

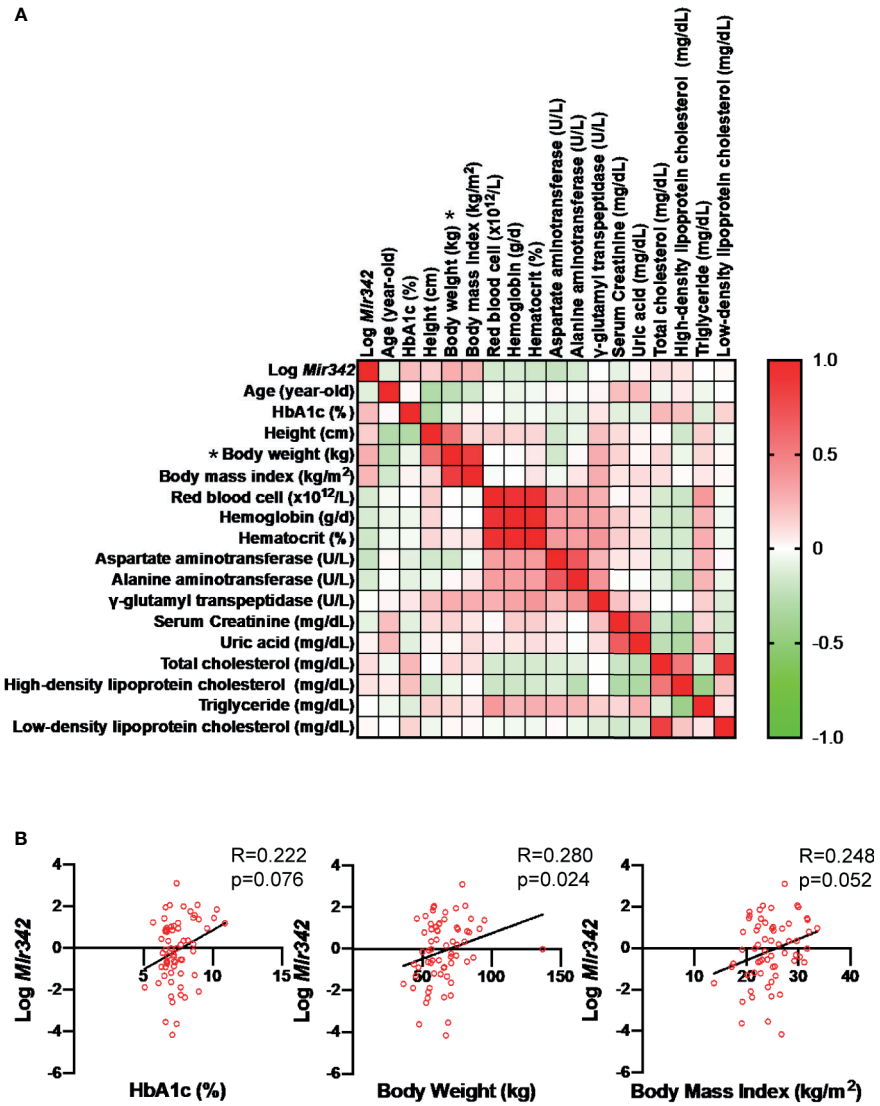

FIGURE 2 | Correlation of serum mmu-mir-342-3p levels (*Log Mir342*) with various clinical parameters in the patients with type 2 diabetes (n=65). **(A)** In correlation matrix, Spearman's rank correlation coefficient is shown. *P < 0.05. **(B)** The correlations between Log miR-342-3p (Log *Mir342*) with HbA1c (R=0.222, p=0.076), body weight (R=0.280, p=0.024) and body mass index (R=0.248, p=0.052).

samples of both STD and HFHS groups were demethylated throughout the CpG island located at 293-585 from TTS of *Evl* gene. The methylation status of CpG island was not responsible for the upregulation of *Evl* gene by HFHS chow.

Next, we investigated the localization of *Mir342* in the cell fractions of epididymal adipose tissues. miR-342-3p was predominantly expressed in stromal vascular fraction (SVF), but lower in mature adipocytes (**Supplementary Figure 6A**). 3T3-L1 pre-adipocytes were induced to differentiate for 10 days, while *Mir342* expression was continuously declined during differentiation (**Supplementary Figure 6B**). Double immunostaining demonstrated that EVL was colocalized with F4/80, indicating that adipose tissue macrophages express EVL (**Supplementary Figures 6C–F**). In cerebral cortex, EVL was colocalized with neuron marker (NeuN, neuronal nuclei), but EVL-positive cells were negative for the markers of dopaminergic neurons (TH, tyrosine hydroxylase), astrocytes (GFAP, glial fibrillary acidic protein), microglia (IBA1, ionized calcium binding adaptor molecule 1), and oligodendrocytes (MBP, myeline basic protein) (**Supplementary Figure 7**). *In situ* hybridization of *Mir342* and immunostaining of EVL demonstrated that they showed similar distribution and their expressions were accentuated in arcuate nuclei in hypothalamus (**Figures 4E–J**). The data indicated that EVL and its intronic miRNA, *Mir342*, colocalized in cells and tissues, especially neurons in central nervous system, and their transcriptional activities were coregulated in a parallel manner.

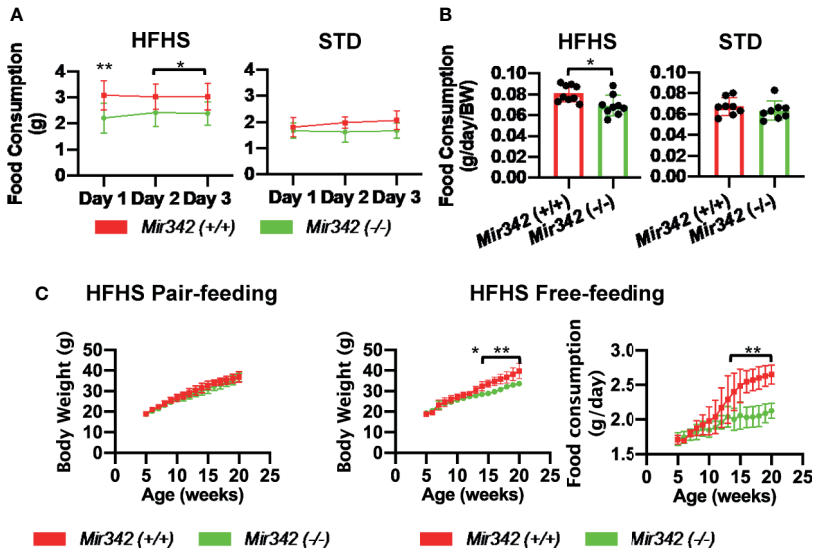

FIGURE 3 | Food intake of *Mir342* (-/-) and *Mir342* (+/+) mice fed with high fat-high sucrose (HFHS) or standard (STD) chow. **(A)** Daily food intake over 3 consecutive days of mice fed with HFHS (n=9) or STD chow (n=8) at 18 weeks of age. **(B)** Average food intake over 3 days per g body weight of mice fed with HFHS (n=9) or STD chow (n=8). **(C)** Pair-feeding studies in *Mir342* (+/+) and *Mir342* (-/-) mice fed with HFHS chow (n=5). Free-feeding mice (n=3 in each group) were used as controls to match the food intake. Data shown as mean ± SD and analyzed by independent *t*-test or two-way ANOVA with Bonferroni tests (*p < 0.05; **p < 0.01).

NPY$^+$EVL$^+$ and NPY$^+$pSTAT3$^+$ Neurons Are Reduced in *Mir342 (-/-)* Mice

An important function of the hypothalamus is to control appetite and satiety. Neuropeptide Y (NPY) and proopiomelanocortin (POMC) neurons are main target of leptin and distribute in hypothalamus. The activation of POMC neurons decreases food intake whereas the activation of NPY neurons increases food intake. The activation of NPY and POMC neurons was investigated after the injection of leptin by double immunostainings of NPY, POMC and phosphorylated signal transducer and activator of transcription 3 (pSTAT3). We identified EVL-positive and EVL-negative NPY and POMC neuron populations in hypothalamus. The percentage of NPY$^+$EVL$^+$ cells in NPY$^+$ neurons were significantly reduced in *Mir342* (-/-) mice compared with *Mir342* (+/+) mice in both STD and HFHS chow (**Figure 5A** and **Supplementary Figures 8A, 9A**). The total number of NPY$^+$EVL$^+$ neurons were significantly reduced in *Mir342* (-/-) mice fed with HFHS chow (**Figure 5A**). Both percentage and number of activated NPY$^+$pSTAT3$^+$ neurons were significantly reduced in *Mir342* (-/-) mice fed with HFHS chow (**Figure 5B** and **Supplementary Figure 8B**). No significant difference was obtained in the group of STD chow (**Supplementary Figure 9B**). In contrast, both percentage and total number of POMC$^+$EVL$^+$ were comparable in the two genotypes, and slight elevation was detected in percentage of POMC$^+$pSTAT3$^+$ neurons in *Mir342* (-/-) mice (**Figures 5C, D** and **Supplementary Figures 8C, D**). However, there were no significant differences in POMC$^+$EVL$^+$ and POMC$^+$pSTAT3$^+$ neurons under STD chow (**Supplementary Figures 9C, D**). In *Mir342* (-/-) mice fed with both STD and HFHS chow, total NPY$^+$ neurons were reduced compared with *Mir342* (+/+) mice, while POMC$^+$ neurons were increased in HFHS chow (**Figure 5E** and **Supplementary Figure 9E**). Similar to the results of Western blot, EVL-positive cells were reduced in STD and HFHS chow, total pSTAT3$^+$ cells were increased in *Mir342* (-/-) mice in HFHS chow (**Figure 5F** and **Supplementary Figure 9F**). The results suggested that deficiency of *Mir342* links to the reduced population and blunted activation of NPY orexigenic neurons, which result in reduced food intake and amelioration of obesity and diabetes under HFHS chow.

Snap25 Is a Target of miR-342-3p

We further performed mRNA profiling by DNA microarray using total RNAs derived from epididymal fat tissues to identify the target genes (GSE163880). We compared 4 groups of *Mir342* (+/+) and *Mir342* (-/-) mice fed with STD and HFHS chow (**Supplementary Tables 3–5**). We selected the predicted target genes of miR-342-3p from TargetScan, miRDB, Pictar and DIANA-microT v5.0 (**Supplementary Table 6**). The results of gene chip demonstrated that *Snap25* (synaptosomal-associated protein, 25kDa) was ranked as top among the genes upregulated in *Mir342* (-/-) mice fed with both STD and HFHS chow (**Supplementary Table 7**). We performed RT-qPCR of top-ranked 3 mRNAs including *Snap25*, *Fat2*, and *Msi1*. In addition, we also check the expression of *Nhlh2*, since it was reported as hypothalamic basic helix-loop-helix transcription factor and the deletion of *Nhlh2* in mice displays adult-onset obesity (15) (**Figure 6**). We confirmed that *Snap25* mRNA increased in both brain and epididymal adipose tissues in *Mir342 (-/-)* mice fed with STD and HFHS chow (**Figure 6A**), while other 3 genes were not altered by the deletion of *Mir342* in brain tissues (**Figure 6D**). Western blot analyses further confirmed that protein expression of SNAP25 was reduced in hypothalamus (**Figure 6B** and **Supplementary Figure 4**).

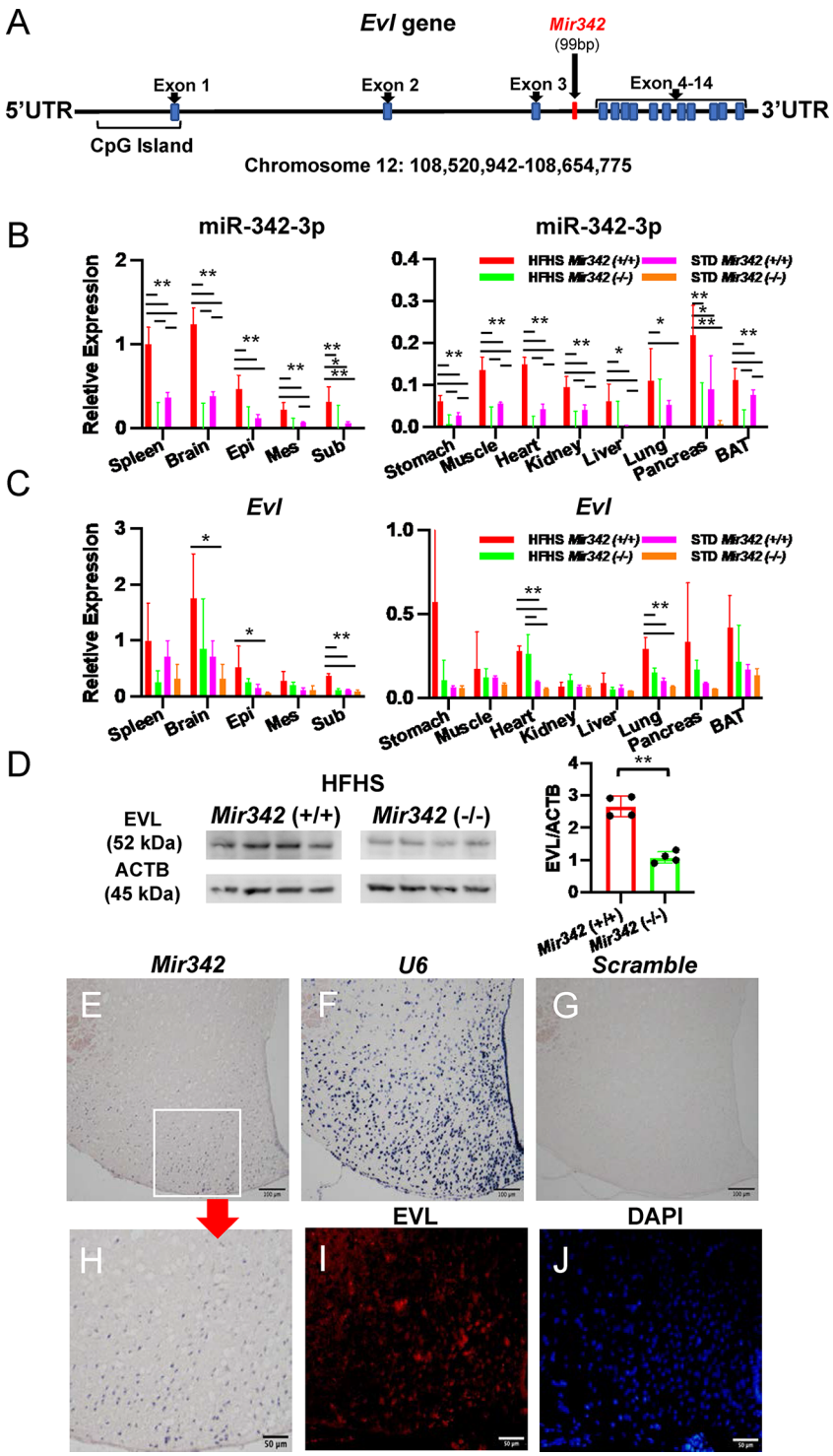

FIGURE 4 | Expression of *Mir342* and its host gene *Evl*. **(A)** *Mir342* is an intronic miRNA in *Evl* (Enabled/Vasodilator-stimulated phosphoprotein) gene. **(B, C)** In various tissues, the expression of miR-342-3p is normalized by snoRNA202 and snoRNA234, while *Evl* is normalized by *Rplp0* and *Rn18s*. HFHS *Mir342* (+/+) (n=4), HFHS *Mir342* (-/-) (n=3), STD *Mir342* (+/+) (n=4) and STD *Mir342* (-/-) mice (n=4). Bar=100 μm. Data are analyzed by one-way ANOVA with a Tukey test. **(D)** Western blot analyses and quantification of EVL protein levels of brain tissue normalized by β-actin (ACTB). Data are analyzed by independent *t*-test. **(E–H)** In *in situ* hybridization, the sections of hypothalamus from *Mir342* (+/+) mice were hybridized with *Mir342* probe (**E**; *Mir342*), *U6* snRNA probe (**F**; *U6*), and *Scramble-miR* probe (**G**; *Scramble*). The inset in **(E)** is shown in panel **(H)**. Immunostaining of EVL (red) in hypothalamus of *Mir342* (+/+) mice **(I)** and nuclear staining of DAPI (blue) **(J)** are shown. Bars are 100 and 50 μm in panels **(E, H)**, respectively. Data presented as means ± SD (*p < 0.05; **p < 0.01).

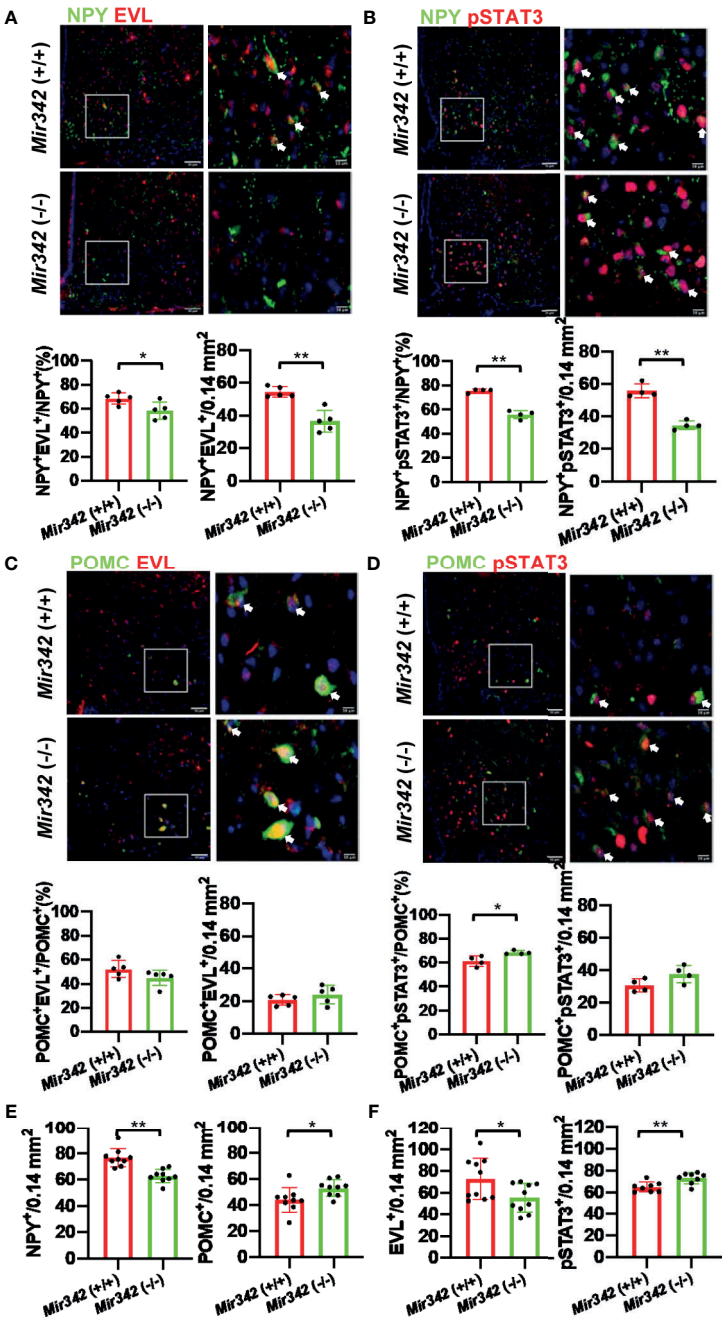

FIGURE 5 | The activation of neuropeptide Y (NPY) and proopiomelanocortin (POMC) neurons by leptin injection. **(A)** Representative photographs of NPY (Green) and EVL (Red) double staining in arcuate nuclei from *Mir342* (+/+) and *Mir342* (-/-) mice fed with HFHS chow (n=5 each). The arrows indicate double-positive cells. The percentage and total numbers of NPY^+EVL^+ cells are shown. **(B)** NPY (Green) and pSTAT3 (Red) double staining in the mice fed with HFHS (n=4) after intraperitoneal injection of leptin (1 mg/kg body weight). The percentage and total numbers of $NPY^+pSTAT3^+$ cells are shown. **(C)** Double staining with POMC (Green) and EVL (Red) in *Mir342* (+/+) and *Mir342* (-/-) mice fed with HFHS chow (n=5). The percentage and total numbers of $POMC^+EVL^+$ cells are shown. **(D)** POMC (Green) and pSTAT3 (Red) double staining in the mice fed with HFHS (n=4) after intraperitoneal injection of leptin (1 mg/kg body weight). The percentage and total numbers of $POMC^+pSTAT3^+$ cells are shown. **(E)** Average cell numbers of NPY^+ (n=9) and $POMC^+$ (n=9) cells detected in hypothalamus of the mice fed with HFHS. **(F)** Average cell numbers of EVL^+ (n=10) and $pSTAT3^+$ (n=8) cells detected in hypothalamus of the mice fed with HFHS. Data shown as mean ± SD and analyzed by independent *t*-test (*$p < 0.05$; **$p < 0.01$).

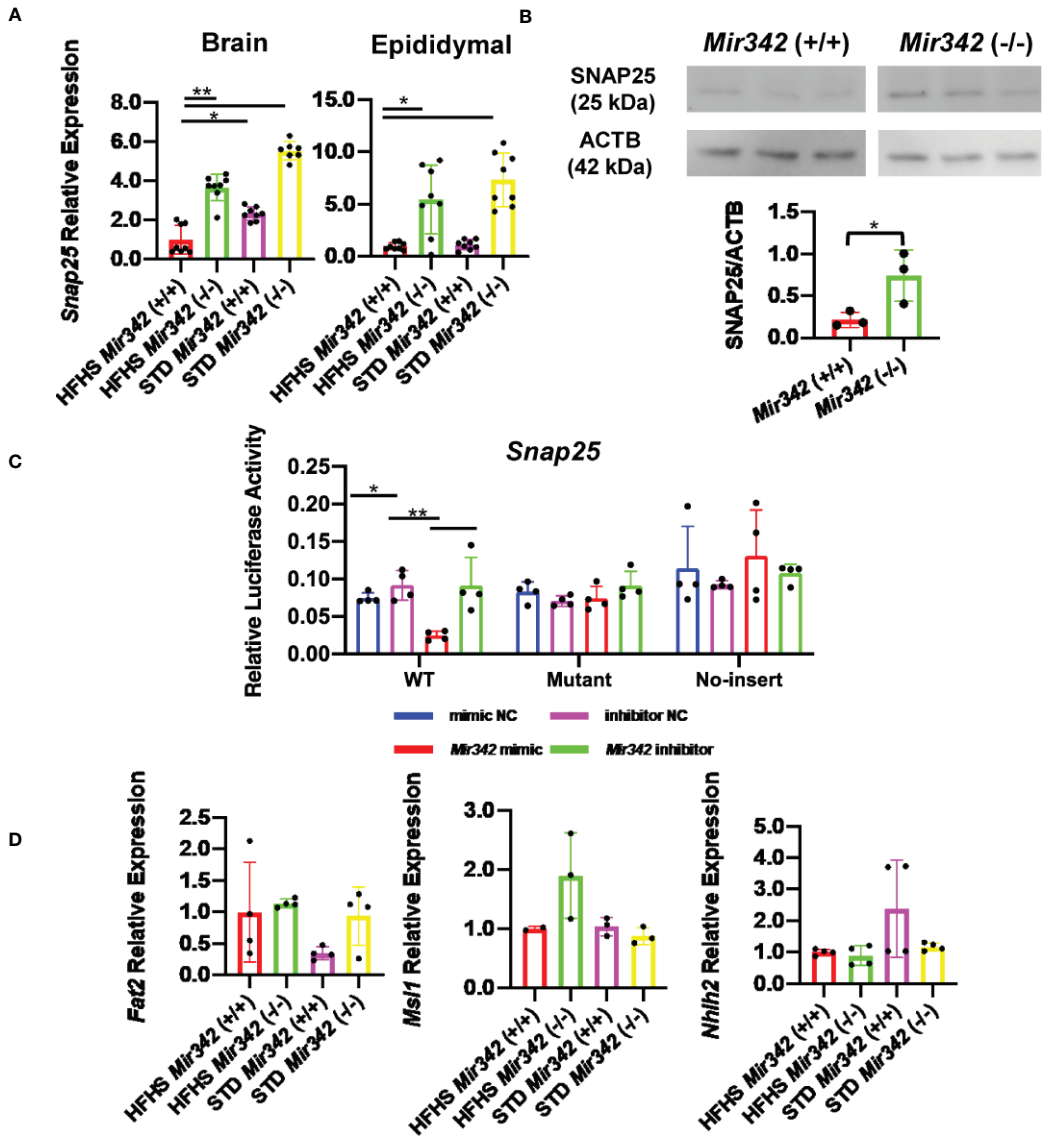

FIGURE 6 | The expression and reporter assay of Snap25 (synaptosomal-associated protein, 25kDa). **(A)** Relative mRNA expression of Snap25 normalized by Rplp0 and Rn18s in brain and epididymal fat tissues detected by RT-qPCR. **(B)** Western blot analyses and quantification of SNAP25 protein levels in hypothalamus. **(C)** Dual-luciferase reporter assay. pmirGLO-Snap25 WT 3'-UTR, pmirGLO-Snap25 MT 3'-UTR, and pmirGLO no-insert control plasmids were cotransfected with Mir342 mimic, Mir342 inhibitor, negative control siRNA (mimic NC), inhibitor negative control (inhibitor NC) into HEK293T cells, respectively. **(D)** The expression of predicted target genes (Fat2, Msi1 and Nhlh2) in brain. Data are analyzed by independent t-test or one-way ANOVA with a Tukey test. All data are presented as mean ± SD (*$p < 0.05$; **$p < 0.01$).

Finally, luciferase reporter assay demonstrated that the transfection of *Mir342* mimic reduced the luciferase activity of pmirGLO-*Snap25* WT 3'-UTR. The luciferase activity of pmirGLO-*Snap25* MT 3'-UTR was not altered by the co-transfection of *Mir342* mimic (**Figure 6C**).

DISCUSSION

Mir342 was highly upregulated by HFHS chow in brain in mice, and the striking feature of *Mir342* (-/-) mice fed with HFHS is that they were resistant to development of obesity and T2D. The food intake was reduced in *Mir342* (-/-) mice fed with HFHS and the STAT3 activation of NPY orexigenic neurons was suppressed. By high throughput sequencing, arcuate and paraventricular nuclei were defined by abundant expression of *Mirlet7*, *Mir7*, *Mir9*, and *Mir30* gene families (16), while *Mirlet7a*, *Mir9*, *Mir30b*, *Mir100a*, and *Mir145* were altered by caloric restriction and high-fat diet in hypothalamus (17). The specific knockdown of *Mir7* and knockout of *Mir17-Mir92* in POMC neurons aggravated diet-induced obesity in females and males, respectively (18). In current investigation, we firstly

demonstrate the expression of *Mir342* in neurons in arcuate nucleus by *in situ* hybridization and functional relevance in control of appetite and satiety. Intriguingly, STD chow intake was not altered, while HFHS chow intake was reduced by the genetic deletion of *Mir342*. It suggested the roles of *Mir342* and *Evl* in the appetite control for the lipid and sugar rich diet by the alter the development and activation of NPY/POMC progenitors (**Supplementary Figure 10**). We performed RT-qPCR for miR-342-3p in hypothalamus and ventral midbrain region including ventral tegmental area and substantial nigra; however, we did not check the status of dopaminergic neurons in ventral midbrain region in *Mir342* (-/-) mice fed with HFHS. To further confirm whether the inhibition of miR-342-3p is a new therapeutic modality to control appetite and satiety in obesity, the experiments with neuron specific *Mir342* knockout and transgenic mice, and direct injection of miR-342-3p mimic and antagomir are required.

Another major site of *Mir342* expression is adipose tissue. The upregulated expression of *Mir342* in white adipose tissue was reported in diet-induced obese mice (19) and ob/ob mice (20) and also in the patients with HIV-induced lipodystrophy (21). miR-342-3p promotes the adipogenesis in mesenchymal stem cells by suppressing CtBP2 and releasing C/EBPα from CtBP2 binding (22). In the female patients with T2D and impaired fasting glucose (IFG), miRNAs including miR-342-3p were upregulated and *in silico* enrichment analyses suggested the 11 top differentially expressed miRNAs possibly involved in oxidative stress, inflammation and insulin signaling (23). In our study, miR-342-3p was prominently expressed in SVF of epididymal adipose tissue and we were interested in the status of inflammation. However, the gene expression of *Il6*, *Il1b* and *Tnf* were not altered in epididymal adipose tissues.

Epigenetic silencing of *MIR342* and its host gene *EVL* by DNA methylation was reported in colorectal cancer (13, 24, 25), multiple myeloma (26), and B cell lymphoma (27) from the patients. CpG island is located at the promotor region of *EVL* gene, while the expression of *EVL* and intronic miR-342-3p is coregulated in parallel. The DNA methylation of CpG island causes the reduction of miR-342-3p, which is resulted in failure to operate tumor suppressor function by inhibiting pro-survival autophagy by targeting *MAP1LC3B* and *DNMT1* in B cell lymphoma (27). In various tissues of *Mir342* (+/+) mice fed with HFHS chow, the expression of *Evl* and miR-342-3p upregulated in parallel and both genes demonstrated tight co-expression. *EVL* gene is suppressed in colon cancer cells and associated with a dense methylation of CpG island in the 5'-UTR region of *EVL*, which is known as tumor suppressor gene (13). In contrast to previous studies, genomic DNAs in *Mir342* (+/+) mice fed with STD and HFHS were demethylated throughout the CpG island located at 293-585 from TTS of *Evl* gene. However, the flanking regions of *Mir342* were highly methylated. It has been reported that miRNA biogenesis is enhanced by DNA methylation in the regions flanking the miRNA coding sequence (14). It suggested that transcriptional activity of *Evl* and *Mir342* under HFHS chow are differentially regulated by site-specific DNA methylation in the brain. EVL also involves in the actin cytoskeleton formation and multiple actin-dependent process such as axonal morphogenesis and neurites formation (28). One can speculate that the upregulation of *Evl* in neurons and adipose tissue macrophages may alter the neuronal function and motility of macrophages by facilitating the actin cytoskeletal formation, respectively. However, in current investigation, the *Evl* expression was maintained in brain and adipose tissues from *Mir342* (-/-) mice fed with HFHS chow, the roles of *Evl* in obesity and T2D remains unexplored.

In current investigation, we identified *Snap25* as one of the major target genes of miR-342-3p. *Snap25* is an important component of the soluble N-ethylmaleimide-sensitive factor attachment protein (SNARE) complex, contributes formation of 2 out of 4 α helices of the complex, and regulates the membrane fusion during the process of exocytosis (29). The SNARE-mediated fusion such as exocytic fusion and synaptic transmission involved vesicle-associated membrane protein-2 (VAMP2), SNAP25, and syntaxin-1, which are sufficient to fuse membranes *in vitro* experiments (30). *Snap25* is developmentally regulated in neuroendocrine cells and SNAP25a precedes SNAP25b in the development of mouse brain, and SNAP25b becomes major splicing variant at the 2nd postnatal week (31). SNAP25b containing SNARE complexes demonstrate a higher degree of stability associated with increased numbers of pooled and primed vesicles (32). *Snap25b* deficient mice fed with HFHS diet demonstrated exacerbated hyperglycemia, liver steatosis, adipocyte hypertrophy, and reduced expression of pSTAT3 in hypothalamic samples (33), suggesting reduction of SNARE complex stability tightly linked to the obesity and diabetes phenotypes (29). In human studies, *SNAP25* gene single nucleotide polymorphism (SNP, rs362551) associated with severity of metabolic syndrome and type 2 diabetes (34). In addition, SNAP25 interacting protein such as syntaxin-1 SNPs were also associated with obesity (35) and type 2 diabetes (36). Prominent upregulation of miR-342-3p and subsequent reduction of *Snap25* expression in neurons in hypothalamus may link to the instability of SNARE complexes and impairment of neurotransmission.

Taken together, upregulation of *Mir342* and its host gene *Evl* in brain and adipose tissues tightly links to the metabolic syndrome phenotype of HFHS chow induced obesity mice. Percentage activated $NPY^{+}pSTAT3^{+}$ neurons were reduced while $POMC^{+}pSTAT3^{+}$ neurons increased in *Mir342* (-/-) mice, and they demonstrated the reduction of food intake and amelioration of metabolic phenotypes. We also identified that the major target gene of miR-342-3p is *Snap25* and the functional impairment of SNARE complexes in arcuate nucleus neurons may link to the excess of food intake under HFHS chow. The future studies are necessary to validate the beneficial effects of miR-342-3p antagomir by proof of concept (POC) study using the disease animal models.

Limitation of Study

In this study, we demonstrated *Mir342* and *Evl* are co-expressed in the central nervous system and adipose tissues, and they were highly upregulated by HFHS chow in C57BL/6JJcl mice. The functional roles of *Mir342* in obesity were demonstrated in the study by investigating *Mir342* (-/-) mice, however, the expression of *Evl* was maintained in *Mir342* (-/-) mice and role of *Evl* in obesity and T2D remains elusive. We examined the expression of miR-342-3p in the sera, exosomes, and various tissues, however, inter-organ communication was not clearly demonstrated, since we did not inject the labeled miR-342-3p

into the animal model. The transcriptional regulation of miRNAs is not fully understood, and we did not find out the transcription factors which regulated the expression of *Mir342* and *Evl*. We mainly investigated the major mature form of *Mir342*, *i.e.*, miR-342-3p, however, minor mature form of miR-342-5p may have a role in obesity and T2D.

DATA AVAILABILITY STATEMENT

The raw data supporting the conclusions of this article will be made available by the authors, without undue reservation. RNA sequencing and mRNA microarray data generated in this study is available at GEO: GSE61959 and GSE163880.

ETHICS STATEMENT

The observational clinical study was approved by Okayama University Graduate School of Medicine, Dentistry and Pharmaceutical Sciences and Okayama University Hospital, Ethics Committee (#1708-045). The patients/participants provided their written informed consent to participate in this study. All animal experiments were approved by the Animal Care and Use Committee of the Department of Animal Resources, Advanced Science Research Center, Okayama University (OKU-2015547, 2016030, 2016203, 2018477, and 2018480).

AUTHOR CONTRIBUTIONS

DZ, SY, TH, AK, and JW designed the project and experiments and wrote the manuscript. DZ, SY, XZ, BY, NK, RS, and HA performed animal experiments and analyzed and interpreted data. AN and JE performed culture experiments and molecular biology experiments. TH and AK performed immunohistochemistry of brain tissue. SY, NK, AN, JE, and JW designed clinical study using human serum samples. All authors contributed to the article and approved the submitted version.

FUNDING

This work was supported by a Grant-in-Aid for Scientific Research (B) 19H03675, Japan Agency for Medical Research and Development (AMED, grant no: 17ek0210095h0001, 20ek0109445h0001).

ACKNOWLEDGMENTS

We greatly appreciate Prof. Masato Asanuma, Dr. Ikuko Miyazaki, and Nami Isooka at Department of Medical Neurobiology, Okayama University Graduate School of Medicine, Dentistry and Pharmaceutical Sciences for the valuable discussion. We also thank Nami Isooka for excellent technical support. We acknowledge support from Central Research Laboratory, Okayama University Medical School; usage of BECKMAN COULTER XL 80, ABI PRISM3130, and producing paraffin blocks and sections.

SUPPLEMENTARY MATERIAL

The Supplementary Material for this article can be found online at: https://www.frontiersin.org/articles/10.3389/fendo.2021.727915/full#supplementary-material

REFERENCES

1. Winter J, Jung S, Keller S, Gregory RI, Diederichs S. Many Roads to Maturity: microRNA Biogenesis Pathways and Their Regulation. *Nat Cell Biol* (2009) 11:228–34. doi: 10.1038/ncb0309-228
2. Perdikopanis N, Georgakilas GK, Grigoriadis D, Pierros V, Kavakiotis I, Alexiou P, et al. DIANA-Mirgen V4: Indexing Promoters and Regulators for More Than 1500 microRNAs. *Nucleic Acids Res* (2021) 49:D151–D9. doi: 10.1093/nar/gkaa1060
3. Schanen BC, Li X. Transcriptional Regulation of Mammalian miRNA Genes. *Genomics* (2011) 97:1–6. doi: 10.1016/j.ygeno.2010.10.005
4. Eliasson L, Regazzi R. Micro(RNA) Management and Mismanagement of the Islet. *J Mol Biol* (2020) 432:1419–28. doi: 10.1016/j.jmb.2019.09.017
5. La Sala L, Micheloni S, De Nigris V, Prattichizzo F, Ceriello A. Novel Insights Into the Regulation of miRNA Transcriptional Control: Implications for T2D and Related Complications. *Acta Diabetol* (2018) 55:989–98. doi: 10.1007/s00592-018-1149-4
6. Hashimoto N, Tanaka T. Role of miRNAs in the Pathogenesis and Susceptibility of Diabetes Mellitus. *J Hum Genet* (2017) 62:141–50. doi: 10.1038/jhg.2016.150
7. Kameswaran V, Bramswig NC, McKenna LB, Penn M, Schug J, Hand NJ, et al. Epigenetic Regulation of the DLK1-MEG3 microRNA Cluster in Human Type 2 Diabetic Islets. *Cell Metab* (2014) 19:135–45. doi: 10.1016/j.cmet.2013.11.016
8. Spracklen CN, Horikoshi M, Kim YJ, Lin K, Bragg F, Moon S, et al. Identification of Type 2 Diabetes Loci in 433,540 East Asian Individuals. *Nature* (2020) 582:240–5. doi: 10.1038/s41586-020-2263-3
9. Moon YS, Smas CM, Lee K, Villena JA, Kim KH, Yun EJ, et al. Mice Lacking Paternally Expressed Pref-1/Dlk1 Display Growth Retardation and Accelerated Adiposity. *Mol Cell Biol* (2002) 22:5585–92. doi: 10.1128/mcb.22.15.5585-5592.2002
10. Ji C, Guo X. The Clinical Potential of Circulating microRNAs in Obesity. *Nat Rev Endocrinol* (2019) 15:731–43. doi: 10.1038/s41574-019-0260-0
11. Higuchi C, Nakatsuka A, Eguchi J, Teshigawara S, Kanzaki M, Katayama A, et al. Identification of Circulating miR-101, miR-375 and miR-802 as Biomarkers for Type 2 Diabetes. *Metabolism* (2015) 64:489–97. doi: 10.1016/j.metabol.2014.12.003
12. Prosser HM, Koike-Yusa H, Cooper JD, Law FC. Bradley A. A Resource of Vectors and ES Cells for Targeted Deletion of microRNAs in Mice. *Nat Biotechnol* (2011) 29:840–5. doi: 10.1038/nbt.1929
13. Grady WM, Parkin RK, Mitchell PS, Lee JH, Kim YH, Tsuchiya KD, et al. Epigenetic Silencing of the Intronic microRNA hsa-miR-342 and Its Host Gene EVL in Colorectal Cancer. *Oncogene* (2008) 27:3880–8. doi: 10.1038/onc.2008.10
14. Glaich O, Parikh S, Bell RE, Mekahel K, Donyo M, Leader Y, et al. DNA Methylation Directs microRNA Biogenesis in Mammalian Cells. *Nat Commun* (2019) 10:5657. doi: 10.1038/s41467-019-13527-1
15. Good DJ, Porter FD, Mahon KA, Parlow AF, Westphal H, Kirsch IR. Hypogonadism and Obesity in Mice With a Targeted Deletion of the Nhlh2 Gene. *Nat Genet* (1997) 15:397–401. doi: 10.1038/ng0497-397
16. Amar L, Benoit C, Beaumont G, Vacher CM, Crepin D, Taouis M, et al. MicroRNA Expression Profiling of Hypothalamic Arcuate and Paraventricular Nuclei From Single Rats Using Illumina Sequencing

Technology. *J Neurosci Methods* (2012) 209:134–43. doi: 10.1016/j.jneumeth.2012.05.033
17. Sangiao-Alvarellos S, Pena-Bello L, Manfredi-Lozano M, Tena-Sempere M, Cordido F. Perturbation of Hypothalamic microRNA Expression Patterns in Male Rats After Metabolic Distress: Impact of Obesity and Conditions of Negative Energy Balance. *Endocrinol* (2014) 155:1838–50. doi: 10.1210/en.2013-1770
18. Gao Y, Li J, Zhang Z, Zhang R, Pollock A, Sun T. MicroRNA miR-7 and miR-17-92 in the Arcuate Nucleus of Mouse Hypothalamus Regulate Sex-Specific Diet-Induced Obesity. *Mol Neurobiol* (2019) 56:7508–21. doi: 10.1007/s12035-019-1618-y
19. Chartoumpekis DV, Zaravinos A, Ziros PG, Iskrenova RP, Psyrogiannis AI, Kyriazopoulou VE, et al. Differential Expression of microRNAs in Adipose Tissue After Long-Term High-Fat Diet-Induced Obesity in Mice. *PloS One* (2012) 7:e34872. doi: 10.1371/journal.pone.0034872
20. Oger F, Gheeraert C, Mogilenko D, Benomar Y, Molendi-Coste O, Bouchaert E, et al. Cell-Specific Dysregulation of microRNA Expression in Obese White Adipose Tissue. *J Clin Endocrinol Metab* (2014) 99:2821–33. doi: 10.1210/jc.2013-4259
21. Squillace N, Bresciani E, Torsello A, Bandera A, Sabbatini F, Giovannetti C, et al. Changes in Subcutaneous Adipose Tissue microRNA Expression in HIV-Infected Patients. *J Antimicrob Chemother* (2014) 69:3067–75. doi: 10.1093/jac/dku264
22. Wang L, Xu L, Xu M, Liu G, Xing J, Sun C, et al. Obesity-Associated MiR-342-3p Promotes Adipogenesis of Mesenchymal Stem Cells by Suppressing CtBP2 and Releasing C/EBPalpha From CtBP2 Binding. *Cell Physiol Biochem* (2015) 35:2285–98. doi: 10.1159/000374032
23. Strycharz J, Wroblewski A, Zieleniak A, Swiderska E, Matyjas T, Rucinska M, et al. Visceral Adipose Tissue of Prediabetic and Diabetic Females Shares a Set of Similarly Upregulated microRNAs Functionally Annotated to Inflammation, Oxidative Stress and Insulin Signaling. *Antioxidants (Basel)* (2021) 10(1):101. doi: 10.3390/antiox10010101
24. Mokarram P, Kumar K, Brim H, Naghibalhossaini F, Saberi-firoozi M, Nouraie M, et al. Distinct High-Profile Methylated Genes in Colorectal Cancer. *PloS One* (2009) 4:e7012. doi: 10.1371/journal.pone.0007012
25. Yi JM, Dhir M, Van Neste L, Downing SR, Jeschke J, Glockner SC, et al. Genomic and Epigenomic Integration Identifies a Prognostic Signature in Colon Cancer. *Clin Cancer Res* (2011) 17:1535–45. doi: 10.1158/1078-0432.CCR-10-2509
26. Li Z, Wong KY, Chan GC, Chng WJ, Chim CS. Epigenetic Silencing of EVL/miR-342 in Multiple Myeloma. *Transl Res* (2018) 192:46–53. doi: 10.1016/j.trsl.2017.11.005
27. Zhang MY, Calin GA, Yuen KS, Jin DY, Chim CS. Epigenetic Silencing of miR-342-3p in B Cell Lymphoma and Its Impact on Autophagy. *Clin Epigenetics* (2020) 12:150. doi: 10.1186/s13148-020-00926-1
28. Menzies AS, Aszodi A, Williams SE, Pfeifer A, Wehman AM, Goh KL, et al. Mena and Vasodilator-Stimulated Phosphoprotein are Required for Multiple Actin-Dependent Processes That Shape the Vertebrate Nervous System. *J Neurosci* (2004) 24:8029–38. doi: 10.1523/JNEUROSCI.1057-04.2004
29. Irfan M, Daraio T, Bark C. SNAP-25 Puts SNAREs at Center Stage in Metabolic Disease. *Neuroscience* (2019) 420:86–96. doi: 10.1016/j.neuroscience.2018.07.035
30. Urbina FL, Gupton SL. SNARE-Mediated Exocytosis in Neuronal Development. *Front Mol Neurosci* (2020) 13:133. doi: 10.3389/fnmol.2020.00133
31. Bark IC, Hahn KM, Ryabinin AE, Wilson MC. Differential Expression of SNAP-25 Protein Isoforms During Divergent Vesicle Fusion Events of Neural Development. *Proc Natl Acad Sci U S A* (1995) 92:1510–4. doi: 10.1073/pnas.92.5.1510
32. Johansson JU, Ericsson J, Janson J, Beraki S, Stanic D, Mandic SA, et al. An Ancient Duplication of Exon 5 in the Snap25 Gene is Required for Complex Neuronal Development/Function. *PloS Genet* (2008) 4:e1000278. doi: 10.1371/journal.pgen.1000278
33. Valladolid-Acebes I, Daraio T, Brismar K, Harkany T, Ogren SO, Hokfelt TG, et al. Replacing SNAP-25b With SNAP-25a Expression Results in Metabolic Disease. *Proc Natl Acad Sci U S A* (2015) 112:E4326–35. doi: 10.1073/pnas.1511951112
34. Chen YL, Pei D, Hung YJ, Lee CH, Hsiao FC, Wu CZ, et al. Associations Between Genetic Variants and the Severity of Metabolic Syndrome in Subjects With Type 2 Diabetes. *Genet Mol Res* (2015) 14:2518–26. doi: 10.4238/2015.March.30.10
35. Romeo S, Sentinelli F, Cavallo MG, Leonetti F, Fallarino M, Mariotti S, et al. Search for Genetic Variants of the SYNTAXIN 1a (STX1A) Gene: The -352 a>T Variant in the STX1A Promoter Associates With Impaired Glucose Metabolism in an Italian Obese Population. *Int J Obes (Lond)* (2008) 32:413–20. doi: 10.1038/sj.ijo.0803743
36. Tsunoda K, Sanke T, Nakagawa T, Furuta H, Nanjo K. Single Nucleotide Polymorphism (D68D, T to C) in the Syntaxin 1A Gene Correlates to Age at Onset and Insulin Requirement in Type II Diabetic Patients. *Diabetologia* (2001) 44:2092–7. doi: 10.1007/s001250100015

Conflict of Interest: JW receives speaker honoraria from Astra Zeneca, Daiichi Sankyo, MSD, Novartis, Tanabe Mitsubishi, Taisho Toyama and receives grant support from Baxter, Chugai, Dainippon Sumitomo, Ono, Teijin.

The remaining authors declare that the research was conducted in the absence of any commercial or financial relationships that could be construed as a potential conflict of interest.

Publisher's Note: All claims expressed in this article are solely those of the authors and do not necessarily represent those of their affiliated organizations, or those of the publisher, the editors and the reviewers. Any product that may be evaluated in this article, or claim that may be made by its manufacturer, is not guaranteed or endorsed by the publisher.

frontiers in Endocrinology

ORIGINAL RESEARCH
published: 16 November 2021
doi: 10.3389/fendo.2021.752496

Comprehensive Metabolomics Study in Children With Graves' Disease

Qin Xia[1†], Weifeng Qian[2†], Linqi Chen[1], Xiuli Chen[1], Rongrong Xie[1], Dandan Zhang[1], Haiying Wu[1], Hui Sun[1], Fengyun Wang[1], Jingjing Liu[3] and Ting Chen[1]*

[1] Department of Endocrinology, Genetics and Metabolism, Children's Hospital of Soochow University, Suzhou, China, [2] Department of Thyroid and Breast Surgery, The Affiliated Suzhou Hospital of Nanjing Medical University, Suzhou, China, [3] Department of Biochemistry and Molecular Biology, School of Medical and Biological Sciences, Soochow University, Suzhou, China

Objective: Graves' disease (GD) related hyperthyroidism (HT) has profound effects on metabolic activity and metabolism of macromolecules affecting energy homeostasis. In this study, we aimed to get a comprehensive understanding of the metabolic changes and their clinical relevance in GD children.

Methods: We investigated serum substances from 30 newly diagnosed GD children and 30 age- and gender-matched healthy controls. We explored the metabolomics using ultra-high-performance liquid chromatography–quadrupole time-of-flight mass spectrometry (UHPLC-QTOF/MS) analysis, and then analyzed the metabolomic data *via* multivariate statistical analysis.

Results: By untargeted metabolomic analysis, a total of 730 metabolites were identified in all participants, among which 48 differential metabolites between GD and control groups were filtered out, including amino acids, dipeptides, lipids, purines, etc. Among these metabolites, 33 were detected with higher levels, while 15 with lower levels in GD group compared to controls. Pathway analysis showed that HT had a significant impact on aminoacyl-transfer ribonucleic acid (tRNA) biosynthesis, several amino acids metabolism, purine metabolism, and pyrimidine metabolism.

Conclusion: In this study, *via* untargeted metabolomics analysis, significant variations of serum metabolomic patterns were detected in GD children.

Keywords: Graves' disease, children, serum metabolomics, untargeted metabolomics, metabolic pathway

OPEN ACCESS

Edited by:
Sally Radovick, The State University of New Jersey, United States

Reviewed by:
Maurizio Delvecchio, Giovanni XXIII Children's Hospital, Italy
Nicolas C. Nicolaides, National and Kapodistrian University of Athens, Greece

***Correspondence:**
Ting Chen
chenting888@suda.edu.cn

†These authors have contributed equally to this work

Specialty section:
This article was submitted to Pediatric Endocrinology, a section of the journal Frontiers in Endocrinology

Received: *03 August 2021*
Accepted: *28 October 2021*
Published: *16 November 2021*

Citation:
Xia Q, Qian W, Chen L, Chen X, Xie R, Zhang D, Wu H, Sun H, Wang F, Liu J and Chen T (2021) Comprehensive Metabolomics Study in Children With Graves' Disease. Front. Endocrinol. 12:752496. doi: 10.3389/fendo.2021.752496

INTRODUCTION

Graves' disease (GD) is the most common cause of hyperthyroidism (HT) with an autoimmune origin in children and adults (1–3). The incidence of GD in children is about 0.9-14.1/100,000, peaking in adolescent females (4–6). A trend of surging incidence of juvenile thyrotoxicosis was observed worldwide, with two to three times higher incidence in the Chinese pediatric population compared to the Caucasians (4–6).

It is well known that thyroid hormone regulates metabolic processes essential for normal growth and development in children (7). With excessive thyroid hormone, HT facilitates the metabolism

process *via* elevated resting energy expenditure, weight loss, upregulated lipolysis, and gluconeogenesis, as well as decreased cholesterol levels (8).

Metabolomics is the study of specific small molecule metabolites or their profiles. Untargeted metabolomics provides a global fingerprint of information through the simultaneous identification of as many metabolites as possible within a tissue, biological fluid, or even cell sample (9, 10). Different instrumental platforms, including nuclear magnetic resonance (NMR) spectroscopy, gas chromatography (GC), and liquid chromatography (LC) coupled with mass spectrometry (MS), are used to cover different features of the human metabolome (9, 10). Metabolomics has been used to explore new biomarkers of disease risk in large-scale studies. In smaller studies, metabolomics has been designed to investigate the underlying mechanisms and progression of certain diseases, or to reveal the potential roles of dietary and environmental exposures, as well as gut flora activity in chronic diseases (11, 12). Multiple studies on metabolomic changes in GD adult patients have been reported, which showed that acylcarnitine and polyamine profiles were different between GD patients and healthy controls (13, 14). Metabolic pathways, such as arginine and proline metabolism and aminoacyl-transfer ribonucleic acid (tRNA) biosynthesis have also been altered in GD patients (15). However, the metabolomic alterations of GD in pediatric population have not been fully explored.

In the present study, we used an ultra-high-performance liquid chromatography coupled with the quadruple time-of-fight mass spectrometry (UHPLC-QTOF/MS)-based untargeted metabolomics approach to explore the perturbation of metabolic process in GD children compared to age- and gender- matched healthy normal controls. We aim to extend the current knowledge beyond previously reported targeted metabolite changes by examining the global serum metabolomics profiles of GD, and propose new dietary suggestions which may improve the treatment of GD.

MATERIALS AND METHODS

Study Design and Participants

Blood samples of 30 newly diagnosed drug-naïve GD patients at Children's Hospital of Soochow University from March 2017 to May 2018 were collected for our study. Meanwhile, 30 age- and sex-matched healthy controls were enrolled from their annual physical examination. GD was diagnosed according to guidelines (16) and as previously described (17).

All patients and control subjects underwent general physical examination and laboratory evaluation before enrollment. We excluded subjects with liver dysfunction, cardiovascular complications, or other endocrine disorders and immune diseases. Moreover, to avoid the impact of sex hormones on metabolites, we only included prepubertal children in this study, which means only boys and girls at Tanner stage I were recruited in the study.

Sample Collection

Serum levels of thyroid-related hormones, including total thyroxine (TT4), total triiodothyronine (TT3), free thyroxine (FT4), free triiodothyronine (FT3), and thyroid stimulating hormone (TSH), as well as thyroid autoantibodies, containing thyroid peroxidase antibody (TPOAb), thyroglobulin antibody (TGAb), and thyroid stimulating hormone receptor antibodies (TRAb) were measured by electrochemiluminescence immunoassay at the laboratories of our hospital. Serum samples for untargeted metabolomics were taken after 10-12h night fasting from an antecubital venous catheter. Samples were placed on ice, separated within 20min, and stored at -80°C until analysis.

Untargeted Metabolomics Analyzed by UHPLC-QTOF/MS

Samples were thawed at 4°C on ice. Then a 100μL sample was extracted by adding 400μL of extraction solvent (V methanol: V acetonitrile= 1:1, containing internal standard 2 μg/mL), vortexing for 30s, sonicating for 10min at 4°C, and then incubating for 1h at -20°C. The precipitated protein was then centrifuged at 4°C and 12000rpm for 15 min. Subsequently, the 425μL supernatant was dried in a vacuum concentrator without heating, resolved by 100μL extraction solvent (V acetonitrile: V water= 1:1), vortexed for 30s, sonicated for 10min at 4°C, and centrifuged for 15min at 12000rpm, 4°C. Then the supernatant (60μL) was transferred into a LC/MS vial for UHPLC-QTOF/MS analysis. To ensure data quality, 10μL supernatant from different individual serum samples were pooled as a quality control sample.

Metabolomics performed were described in a previous study (14). In brief, LC-MS/MS analyses were performed using a 1290 UHPLC system (Agilent Technologies, Santa Clara, CA, USA) with a UPLC BEH Amide column (1.7μm, 2.1*100mm, Waters) coupled to Triple time-of-flight 6600 (Q-TOF, AB Sciex, Framingham, MA, USA). The injection volume for each sample was 1μL. The mass spectroscopy (MS) data were collected from m/z 50-1200 Da. The MS spectra acquisition was performed using Analyst TF 1.7 software (AB Sciex) based on the information-dependent basis (IDA) mode. In each cycle, 12 precursor ions whose intensity greater than 100 were chosen for fragmentation at collision energy (CE) of 30 eV (15 MS/MS events per 50 ms of product ion accumulation time). The electrospray ionization (ESI) source conditions were set as following: nebulizer pressure, 60 Psi; auxiliary pressure, 60 Psi; curtain gas, 35 Psi; source temperature 650°C; ion spray voltage floating (ISVF) 5000 V or - 4000 V in positive or negative modes, respectively.

Statistical Analysis

The UHPLC-QTOF/MS data analysis was performed as previously described (18).Briefly, MS raw data (.wiff) files were converted to the mzXML format using Proteo Wizard, and processed by R package XCMS (version 3.2). The preprocessing results generated a data matrix that consisted of the retention time (RT), massto-charge ratio (m/z) values, and peak intensity. R package CAMERA was used for peak annotation after XCMS data processing. In-house MS2 database was applied in metabolite identification. The SIMCA

14.1 software package (Unetrics, Umea, Sweden) was used to analyze the metabolites. Both principal component analysis (PCA) and orthogonal partial least squared-discriminant analysis (OPLS-DA) were used for the multivariate data analysis (MVDA). The SPSS 25.0 software (SPSS Inc., Chicago, IL, USA) was used to determine significant differences between GD and normal control groups. The metabolic features with both variable importance in projection (VIP) value > 1.5 and fold change (FC) >1.2 or <0.83 in the OPLA-DA model and values $P<0.05$ were considered significantly different. The correlations between substances and thyroid function, as well as autoantibodies, were analyzed *via* Spearman rank correlation and $P<0.05$ was considered as statistically significant.

When comparing quantitative variables between 2 groups, for normally distributed data, Student's t-test was used and the results were expressed as means ± standard deviations. For data not normally distributed, Mann-Whitney *U*-test was used, and the results were expressed as medians (25th-75th percentiles).

RESULTS

Demographics of the Study Population

The baseline clinical and biochemical characteristics of 30 GD patients and 30 age- and gender-matched healthy controls were shown in **Table 1**. As expected, girls (83.3%) are more susceptible to GD than boys (16.7%). Although all in normal ranges, GD patients had higher alanine aminotransferase (ALT), aspartate aminotranspherase (AST), gamma-glutamyl transpeptidase (GGT), alkaline phosphatase (ALP), direct bilirubin (DBIL), triglyceride (TG), and lower total cholesterol (TCHOL) levels than normal controls.

Differential Metabolites Between the GD and Control Groups

A total of 730 metabolites were identified in all participants. PCA score plots showed clustering of the control and HT groups with the cumulative fitness (R2 value) of the PCA model being 0.52 and 0.53, respectively, for positive and negative ion models (**Supplemental Figure 1**). The OPLS-DA analysis indicated clear separations between the HT and control groups both in positive (R2X=0.178, R2Y=0.895, Q2 = 0.727) and negative (R2X=0.152, R2Y=0.86, Q2 = 0.669) ion models (**Supplemental Figure 2**).

Based on the selection criteria including VIP > 1.5, $P < 0.05$, and FC > 1.2 or FC < 0.83, a total of 48 differential metabolites between GD and control groups were filtered out. Among these metabolites, 33 were detected with higher levels, while 15 with lower levels in GD group compared to controls (**Table 2**).

Differential Pathways Between the GD and Control Groups

By comparing with the KEGG PATHWAY database (https://www.genome.jp/kegg/), the differentially abundant metabolites were cross-referenced with the related pathways. After enrichment and topology analysis, the impact values of each pathway were obtained. Essential pathways with large impacts were labeled in each comparison, with the detailed results of pathway analyses listed in **Figure 1** and **Table 3**. In GD group, the most significant changes were found in aminoacyl-tRNA biosynthesis, nitrogen metabolism,

TABLE 1 | Clinical and biochemical characteristics of the GD and control groups.

	Normal range	GD group (n = 30)	Control group (n = 30)	*p* Value
Age (months)[a]	NA	78.80 ± 20.50	72 ± 20.42	NS
Girls/Boys	NA	25/5	25/5	—
Wt (Kg)[b]	NA	24.86 (20.38~28.25)	26.48 (22.73~29.16)	NS
FT3 (pg/ml)[a]	2.71-4.69	11.41 ± 6.0	3.91 ± 0.32	<0.01
FT4 (ng/dl)[a]	1.04-1.83	4.33 ± 2.41	1.37 ± 0.16	<0.01
TSH(μIU/ml)[a]	0.91-4.63	0.0067 ± 0.0039	2.61 ± 1.31	<0.01
TT3 (ng/ml)[a]	0.81-2.43	3.18 ± 1.45	1.12 ± 0.23	<0.01
TT4 (ng/ml)[a]	55.33-124.22	157.92 ± 71.58	80.12 ± 13.33	<0.01
TPOAb (IU/ml)[a]	0.00-60.00	172.19 ± 39.16	44.57 ± 9.01	<0.01
TGAb (IU/ml)[a]	0.00-60.00	760.45 ± 1125.21	23.85 ± 9.72	<0.01
TRAb (IU/L)[a]	0.00-1.50	20.11 ± 11.06	0.51 ± 0.24	<0.01
ALT (U/L)[b]	5-35	26.70 (20.30~35.78)	12.70 (11.45~14.40)	<0.01
AST (U/L)[b]	10-67	28.50 (23.10~33.48)	24.50 (21.85~28.25)	<0.05
GGT (U/L)[b]	7-32	20.95 (14.10~33.73)	10.40 (8.80~11.60)	<0.01
ALP (U/L)[b]	0-500	295 (253~333)	209 (180~234)	<0.01
TBIL (μmol/l)[b]	3.40-17.10	8.80 (6.78~13.58)	8.40 (6.40~11.65)	NS
DBIL (μmol/l)[b]	0.00-10.00	3.61 (2.63~5.28)	2.70 (2.40~3.59)	<0.05
IBIL (μmol/l)[b]	0.00-17.00	5.15 (4.02~7.70)	5.90 (3.95~8.44)	NS
TP (g/l)[a]	60.0-83.0	66.03 ± 4.55	70.17 ± 4.02	NS
TG (mmol/l)[b]	0.00-1.70	0.83 (0.58~1.23)	0.65 (0.49~0.85)	<0.05
TCHOL (mmol/l)[a]	0.00-5.20	3.17 ± 0.52	4.54 ± 0.89	<0.05

GD, Graves' disease; Wt, weight; FT3, free triiodothyronine; FT4, free thyroxine; TSH, thyroid stimulating hormone; TT3, total triiodothyronine;TT4, total thyroxine; TPOAb, thyroid peroxidase antibody; TGAb, thyroglobulin antibody; TRAb,thyroid stimulating hormone receptor antibodies; ALT, alanine aminotransferase; AST, aspartate aminotransferase; GGT, gamma-glutamyl transpeptidase; ALP, alkaline phosphatase; TBIL, total bilirubin; DBIL, direct bilirubin; IBIL, indirect bilirubin; TP, total protein; Tg, thyroglobulin; TCHOL, total cholesterol.

[a]*The data were normally distributed.*

[b]*The data were not normally distributed.*

NA, Not available; NS, No significance.

TABLE 2 | Significantly changed metabolites of GD children compared to controls.

	Metabolites	VIP	P	FC
Amino acid metabolism	Isovalerylglycine	2.08	0	1.65
	L-Pipecolic acid	1.63	0	1.52
	L-Tyrosine	1.76	0	1.4
	L-Tryptophan	2.23	0	1.4
	L-Methionine	2.28	0	1.29
	L-Phenylalanine	2.48	0	1.3
	L-Threonine	1.8	0	1.28
	L-Glutamate	1.51	0	1.26
	Tyramine	2.46	0	1.24
	Creatinine	2.61	0	0.76
	Indoxyl sulfate	1.73	0.01	0.61
	Guanidinosuccinic acid	2.66	0	0.59
Dipeptides	gamma-L-Glutamyl-L-valine	2.8	0	1.73
	Gly-Glu	2.77	0	1.54
	Val-Met	3.08	0	1.48
	Ile-Ala	1.87	0	1.47
	Met-Tyr	1.61	0	1.45
	Pro-Glu	2.61	0	1.39
	His-Glu	1.72	0	1.35
	Phe-Glu	1.63	0.04	1.29
	Trp-Ile	1.97	0	1.22
	Ile-Val	2.41	0	0.57
Lipid metabolism	pregnenolone sulfate	2.21	0	2.71
	1-Palmitoyl Lysophosphatidic Acid	2.66	0	2.38
	Decanoyl-L-carnitine	2.13	0	1.87
	5-Oxo-ETE	1.57	0.01	1.45
	7-Oxocholesterol	1.73	0.02	1.44
	D-erythro-Sphingosine-1-phosphate	2.26	0	1.32
	Cortisone	1.32	0.03	1.22
	1-Palmitoyllysophosphatidylcholine	1.6	0.01	0.82
	Pristanic acid	1.58	0.01	0.81
	all cis-(6,9,12)-Linolenic acid	1.69	0.01	0.73
	Linoleic acid	2.02	0	0.73
	Pentadecanoic Acid	1.8	0	0.73
	Tridecanoic acid (Tridecylic acid)	1.55	0.02	0.72
	Sphinganine	2.22	0	0.69
	Myristic acid	2.12	0	0.64
	3b-Hydroxy-5-cholenoic acid	1.58	0.04	0.56
Tricarboxylic acid cycle	Isocitrate	1.66	0	1.77
	Succinate	1.59	0	1.47
Nucleotide metabolism	Hypoxanthine	1.56	0	1.41
	Xanthine	2	0	1.34
	S-Methyl-5'-thioadenosine	1.96	0	1.35
	5,2'-O-dimethyluridine	2.09	0	1.34
	2'-Deoxycytidine 5'-monophosphate (dCMP)	2.31	0	1.27
	5,10-methylene-THF	1.7	0.04	1.25
Others	Phenylacetic acid	1.51	0.04	0.8
	Protoporphyrin IX	1.89	0	0.55

purine metabolism, alanine, aspartate and glutamate metabolism and phenylalanine metabolism.

Relationship Between Thyroid Indices and Metabolites in GD Children

The correlations between thyroid indices and differential metabolite levels in GD patients were analyzed *via* Spearman's correlation analysis. Correlations with Spearman rank correlation coefficient > 0.4 and $P < 0.05$ were filtered out and listed in **Table 4**. We found that three metabolites were associated with TT3, four with TT4, two with FT3, and three with FT4. Among the differential metabolites, three were associated with TPOAb, one with TRAb, two with TGAb, and one with TSH.

DISCUSSION

The present study showed that serum metabolic patterns were significantly different between GD children and healthy controls. A total of 730 metabolites were identified in all participants, among which 48 differential metabolites between GD and control groups were filtered out. To our knowledge, this is the

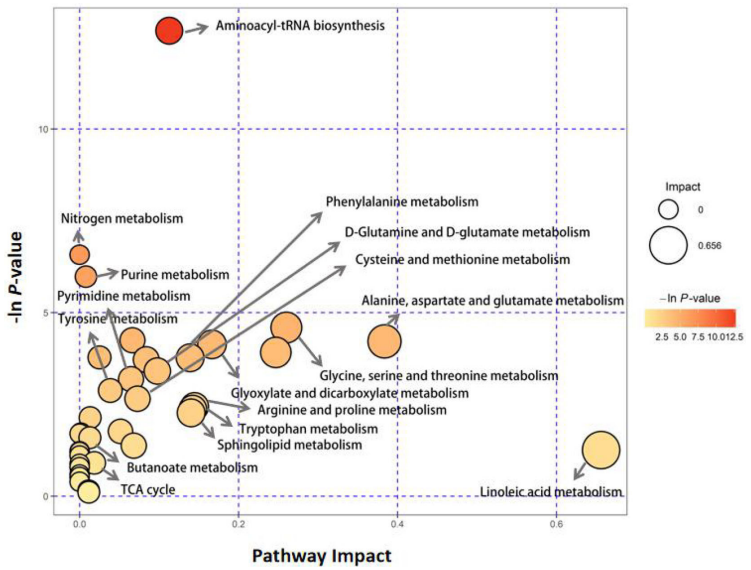

FIGURE 1 | Pathway analysis of serum metabolite profiles of the hyperthyroidism group compared to the control group.

first study analyzing the metabolic changes in GD children *via* an untargeted metabolomic method.

Amino acids are organic compounds that contain amine (-NH2) and carboxyl (-COOH) functional groups, along with a side chain (R group) specific to each amino acid (19). Amino acids are the monomers that make up human proteins and the second largest component of human muscle and other tissues. Besides, amino acids also actively participate in numerous biological processes, including biosynthesis and neurotransmitter transport (19). In the present study, we found that GD children had more active protein digestion/absorption and nitrogen metabolism. Quite a few amino acids, mostly essential amino acids, had much higher levels in GD children compared with controls. Interestingly, the amino acid pattern changes in GD children are quite different from those of adult patients. For example, significant changes of arginine and proline metabolism pathways were observed in GD adult patients (20), but not the children. This may be explained by the different amino acid metabolism among various age groups (20). Additionally, significantly elevated levels of phenylalanine and tyrosine were observed in GD children, but not in GD adults (20). Most phenylalanine is converted to tyrosine, a key component of thyroxine, through phenylalanine hydroxylase (21). Thus, reduction of phenylalanine intake in GD children, but not adults, may be a potential way to decrease their thyroxine production.

Tryptophan (Trp) is an essential amino acid that serves several important purposes and a precursor of the neurotransmitter serotonin. The tri-iodothyronine (T3) and thyroxine (T4) entry into different cell types depends on the aromatic amino acid transport system T, and there is a counter transportation between T3 and Trp. Thus, Trp supplementation may reduce the T3 uptake of cells (22, 23). Normal Trp metabolism has two main branches: 3-10% of Trp keeps the indole ring intact while producing chemical messengers such as serotonin, while the majority (90%) breaks the indole ring generating the kynurenine path, kynurenine, nicotinic acid, and the nicotinamide adenine dinucleotide (NAD^+) (24). Previous studies have reported that thyroxine elevated the conversion ratio of Trp to nicotinamide, not through the kynurenine pathway but *via* aminocarboxymuconate semialdehyde decarboxylase (25). Our results were consistent with previous studies since no elevation of substrates in the kynurenine pathway was observed. Moreover, elevated 5-hydroy-indoleacetate were detected in the serum of GD children, indicating an intensified conversion of Trp to serotonin. Similar findings have been reported in the brain of adult GD patients, and the elevation of serotonin may contribute to the mood change of GD patients (26). Besides, we found that Trp levels in GD children were negatively correlated with TGAb levels, which may suggest a regulation role of Trp in the autoimmune process of GD. Indeed, previous studies have points to Trp degradation as a potent immunosuppressive mechanism involved in the maintenance of immunological tolerance. Therefore, Trp metabolism is quite important in the pathogenesis of GD, further studies are needed to explore the impact of supplementation and/or deprivation of Trp on GD pathogenesis.

Sphingosine 1-phosphate (S1P), a sphingolipid mediator, regulates various cellular functions *via* high-affinity G protein-coupled receptors, S1P1-5, and plays an important regulatory role in congenital and adaptive immune responses (27). Sphk1/S1P/S1PR signaling pathway can be used as a target for the treatment of autoimmune diseases (28). For example, the immunosuppressant Fingolimod (FTY720), a sphingosine analogue, is used as an S1PR antagonist in the treatment of multiple sclerosis (29). In addition, S1P lyase inhibitors can alleviate joint inflammation and destruction in rheumatoid arthritis mice (30). In recent years, Cheng Han et al. found

TABLE 3 | Differential pathways between the GD and control groups.

Pathway	Hits	-ln(p)	FDR	Impact
Aminoacyl-tRNA biosynthesis	10	12.68	0.00	0.11
Nitrogen metabolism	5	6.58	0.06	0.00
Purine metabolism	6	4.25	0.18	0.07
Alanine, aspartate and glutamate metabolism	3	4.22	0.18	0.38
Phenylalanine metabolism	4	4.13	0.18	0.17
Glycine, serine and threonine metabolism	4	3.92	0.18	0.25
Glyoxylate and dicarboxylate metabolism	4	3.78	0.18	0.02
D-Glutamine and D-glutamate metabolism	2	3.77	0.18	0.14
Tyrosine metabolism	5	3.72	0.18	0.08
Cysteine and methionine metabolism	4	3.41	0.22	0.10
Pyrimidine metabolism	4	3.19	0.25	0.06
Butanoate metabolism	3	2.88	0.32	0.04
Citrate cycle (TCA cycle)	2	2.66	0.37	0.07
Arginine and proline metabolism	4	2.44	0.44	0.14
Tryptophan metabolism	4	2.37	0.44	0.14
Sphingolipid metabolism	2	2.27	0.46	0.14
Linoleic acid metabolism	1	1.26	0.89	0.66

FDR, P value adjusted by false discovery rate; Hits, the matched number of metabolites in a pathway; Impact value, value calculated from pathway topography analysis.

TABLE 4 | Relationship between thyroid indices and metabolites levels in GD children.

Metabolites	Thyroid indices	Spearman rank correlation coefficient	*P* Value
L-Tryptophan	TGAb (IU/ml)	-0.770	0.009
L-Glutamate	FT4 (ng/dl)	0.424	0.027
S-Methyl-5'-thioadenosine	TSH (uIU/ml)	-0.464	0.046
S-Methyl-5'-thioadenosine	TPOAb (IU/ml)	-0.720	0.006
Guanidinosuccinic acid	TPOAb (IU/ml)	-0.687	0.01
Creatinine	TT4 (ng/ml)	-0.576	0.008
Creatinine	TT3 (ng/ml)	-0.596	0.006
Succinate	TPOAb (IU/ml)	-0.593	0.033
Succinate	TT3 (ng/ml)	-0.449	0.047
Succinate	FT4 (ng/dl)	0.434	0.024
D-erythro-Sphingosine-1-phosphate	TT4 (ng/ml)	0.544	0.013
Decanoyl-L-carnitine	TT4 (ng/ml)	0.484	0.031
Acetylvalerenolic acid	FT3 (pg/ml)	-0.578	0.015
3b-Hydroxy-5-cholenoic acid	FT3 (pg/ml)	0.502	0.04
1-Palmitoyl Lysophosphatidic Acid	FT4 (ng/dl)	0.522	0.005
Phe-Glu	TRAb (IU/L)	0.405	0.049
Met-Tyr	TGAb (IU/ml)	0.721	0.019
Indoxyl sulfate	TT3 (ng/ml)	-0.547	0.013
Indoxyl sulfate	TT4 (ng/ml)	-0.469	0.037

that Sphk1/S1P/S1PR1 signal transduction is involved in the development of mice autoimmune thyroiditis (AIT). In AIT mice, the proportions of inflammation-related cell subtypes (such as Th1, Th17 and Tfh) are elevated, while FTY720 administration can decrease the their levels, suggesting that suppression of Sphk1/S1P/S1PR1 signaling pathway may be a potential therapeutic target of AIT (31). In this study, we found that sphinganine decreased, while S1P levels increased in the GD group. Besides, S1P levels positively correlate with TT4 levels. Thus, we suppose that FTY720 is also promising in the treatment of GD.

We detected much higher levels of pregnenolone sulfate in GD patients, which is consistent with previous studies (32). Pregnenolone sulfate is the source of steroid synthesis pathway. More importantly, pregnenolone sulfate regulates the release of multiple neurotransmitters and is crucial to multiple brain functions (33). The elevated pregnenolone sulfate levels may exert important effects on the neurodevelopment of GD children, but further studies are still needed to elucidate the consequences.

Protoporphyrin IX levels were significantly lower in GD children compared to those of controls. This can be easily explained by the fact that protoporphyrin IX is a crucial constituent of thyroid peroxidase (TPO), and more protoporphyrin IX is transported into the thyroid gland in GD patients. Interestingly, exacerbation of erythropoietic protoporphyria and acute intermittent porphyria has been reported in a few patients with HT patients (34, 35). Since these situations are quite rare and a decrease of protoporphyrin IX is observed in otherwise normal GD children, the correlation of HT and porphyria needs further investigation.

Our study has several limitations. Firstly, the sample size was relatively small, and further studies with larger sample size are needed to confirm our findings. Secondly, the main findings need

to be validated by a second method. Thirdly, because this study included only local Chinese children, our results may not apply to other populations.

In conclusion, GD children have highly different serum metabolomic patterns compared to healthy controls, which may be induced either by HT or by autoimmunity. Our study is the first study addressing metabolic changes in GD children *via* untargeted metabolomic analysis. More importantly, our study provides comprehensive insights into the changes of metabolic processes, which is beneficial in improving the understanding and treatment of GD children.

DATA AVAILABILITY STATEMENT

The original contributions presented in the study are included in the article/**Supplementary Material**. Further inquiries can be directed to the corresponding author.

ETHICS STATEMENT

The studies involving human participants were reviewed and approved by Ethics Committee of Children's Hospital affiliated to Suzhou University. Written informed consent to participate in this study was provided by the participants' legal guardian/next of kin.

AUTHOR CONTRIBUTIONS

Conceived and designed the experiments: TC; Performed the experiments: QX, WQ, LC, XC, RX, DZ, HW, HS, FW, JL; Analyzed the data: QX, WQ and TC; Wrote the paper: TC, QX, and WQ. All authors contributed to the article and approved the submitted version.

FUNDING

This study was supported by Suzhou Personnel Planning Project (project code GSWS2019051 and GSWS2020046), and Suzhou Science and Technology Development Project (SS22064) awarded to TC; a National Natural Science Foundation of China (project code 31701251) awarded to JL. This study was also supported by the Department of Pediatrics Clinical Center of Suzhou (Szzx201504).

SUPPLEMENTARY MATERIAL

The Supplementary Material for this article can be found online at: https://www.frontiersin.org/articles/10.3389/fendo.2021.752496/full#supplementary-material

REFERENCES

1. Talbot NB, Sobel EH, McArthur JW, Crawford JD. *Functional Endocrinology: From Birth to Adolescence*. Cambridge: Harvard University Press (1952). p. 472.
2. Wilkins L. *The Diagnosis and Treatment of Endocrine Disorders in Childhood and Adolescence*. Oxford: Blackwell Scientific Publications (1957). p. 184.
3. Léger J, Carel JC. Hyperthyroidism in Childhood: Causes, When and How to Treat. *J Clin Res Pediatr Endocrinol* (2013) 5:50. doi: 10.4274/jcrpe.854
4. Williamson S, Greene SA. Incidence of Thyrotoxicosis in Childhood: A National Population Based Study in the UK and Ireland. *Clin Endocrinol (Oxf)* (2010) 72:358–63. doi: 10.1111/j.1365-2265.2009.03717.x
5. Kjær RH, Andersen MS, Hansen D. Increasing Incidence of Juvenile Thyrotoxicosis in Denmark: A Nationwide Study, 1998-2012. *Horm Res Paediatr* (2015) 84:102–7. doi: 10.1159/000430985
6. Wong GWK, Cheng PS. Increasing Incidence of Childhood Graves' Disease in Hong Kong: A Follow-Up Study. *Clin Endocrinol (Oxf)* (2001) 54:547–50. doi: 10.1046/j.1365-2265.2001.01252.x
7. Mullur R, Liu Y-Y, Brent GA. Thyroid Hormone Regulation of Metabolism. *Physiol Rev* (2014) 94:355–82. doi: 10.1152/physrev.00030.2013
8. Brent GA. Graves' Disease. *N Engl J Med* (2008) 358:2594–605. doi: 10.1056/NEJMcp0801880
9. Brunius C, Shi L, Landberg R. Metabolomics for Improved Understanding and Prediction of Cardiometabolic Diseases—Recent Findings From Human Studies. *Curr Nutr Rep* (2015) 4:348–64. doi: 10.1007/s13668-015-0144-4
10. Denoroy L, Zimmer L, Renaud B, Parrot S. Ultra High Performance Liquid Chromatography as a Tool for the Discovery and the Analysis of Biomarkers of Diseases: A Review. *J Chromatogr B* (2013) 927:37–53. doi: 10.1016/j.jchromb.2012.12.005
11. Rappaport SM, Barupal DK, Wishart D, Vineis P, Scalbert A. The Blood Exposome and its Role in Discovering Causes of Disease. *Environ Health Perspect* (2014) 122:769–74. doi: 10.1289/ehp.1308015
12. Wientzek A, Tormo Díaz M-J, Castaño JMH, Amiano P, Arriola L, Overvad K, et al. Cross-Sectional Associations of Objectively Measured Physical Activity, Cardiorespiratory Fitness and Anthropometry in European Adults. *Obesity* (2014) 22:E127–34. doi: 10.1002/oby.20530
13. Al-Majdoub M, Lantz M, Spegel P. Treatment of Swedish Patients With Graves' Hyperthyroidism Is Associated With Changes in Acylcarnitine Levels. *Thyroid* (2017) 27(9):1109–17. doi: 10.1089/thy.2017.0218
14. Song J, Shan Z, Mao J, Teng W. Serum Polyamine Metabolic Profile in Autoimmune Thyroid Disease Patients. *Clin Endocrinol (Oxf)* (2019) 90 (5):727–36. doi: 10.1111/cen.13946
15. Liu J, Fu J, Jia Y, Yang N, Li J, Wang G. Serum Metabolomic Patterns in Patients With Autoimmune Thyroid Disease. *Endocr Pract* (2020) 26:82–96. doi: 10.4158/EP-2019-0162
16. Ross DS, Burch HB, Cooper DS, Greenlee MC, Laurberg P, Maia AL, et al. 2016 American Thyroid Association Guidelines for Diagnosis and Management of Hyperthyroidism and Other Causes of Thyrotoxicosis. *Thyroid* (2016) 26(10):1343–421. doi: 10.1089/thy.2016.0229
17. Chen T, Chen L, Song H, Chen X, Xie R, Xia Q, et al. Clinical Relevance of T Lymphocyte Subsets in Pediatric Graves' Disease. *J Pediatr Endocrinol Metab* (2020) 33(11):1425–30. doi: 10.1515/jpem-2020-0158
18. Wang W, Zhao L, He Z, Wu N, Li Q, Qiu X, et al. Metabolomics-Based Evidence of the Hypoglycemic Effect of Ge-Gen-Jiao-Tai-Wan in Type 2 Diabetic Rats *via* UHPLC-QTOF/MS Analysis. *J Ethnopharmacol* (2018) 219:299–318. doi: 10.1016/j.jep.2018.03.026
19. Boyle J. "Lehninger Principles of Biochemistry". In: D Nelson, M Cox, editors. *Biochem Mol Biol Educ*, *4th ed*, vol. 33. New York: W.H. Freeman (2005). p. 74–5. doi: 10.1002/bmb.2005.494033010419
20. Timmerman KL, Volpi E. Amino Acid Metabolism and Regulatory Effects in Aging. *Curr Opin Clin Nutr Metab Care* (2008) 11:45–9. doi: 10.1097/MCO.0b013e3282f2a592
21. Furman BL. *Thyroid Agents*. SJ Enna, DBBTTCPR Bylund, editors. New York: Elsevier (2007). p. 1. doi: 10.1016/B978-008055232-3.61060-8
22. Zhou Y, Samson M, Francon J, Blondeau JP. Thyroid Hormone Concentrative Uptake in Rat Erythrocytes. Involvement of the Tryptophan Transport System T in Countertransport of Tri-Iodothyronine and Aromatic Amino Acids. *Biochem J* (1992) 281(Pt 1):81–6. doi: 10.1042/bj2810081

23. Centanni M, Canettieri G, Viceconti N, Sibilla R, Bei A, Andreoli M. Effect of Tryptophan on the Early Tri-Iodothyronine Uptake in Mouse Thymocytes. *Eur J Endocrinol* (2000) 143:119–23. doi: 10.1530/eje.0.1430119
24. Palego L, Betti L, Rossi A, Giannaccini G. Tryptophan Biochemistry: Structural, Nutritional, Metabolic, and Medical Aspects in Humans. *J Amino Acids* (2016) 2016:8952520. doi: 10.1155/2016/8952520
25. Shibata K, Toda S. Effects of Thyroxine on the Conversion Ratio of Tryptophan to Nicotinamide in Rats. *Biosci Biotechnol Biochem* (1994) 58:1757–62. doi: 10.1271/bbb.58.1757
26. Bauer M, Heinz A, Whybrow PC. Thyroid Hormones, Serotonin and Mood: Of Synergy and Significance in the Adult Brain. *Mol Psychiatry* (2002) 7:140–56. doi: 10.1038/sj.mp.4000963
27. Spiegel S, Milstien S. The Outs and the Ins of Sphingosine-1-Phosphate in Immunity. *Nat Rev Immunol* (2011) 11(6):403–15. doi: 10.1038/nri2974
28. Tsai HC, Han MH. Sphingosine-1-Phosphate (S1P) and S1P Signaling Pathway: Therapeutic Targets in Autoimmunity and Inflammation. *Drugs* (2016) 76(11):1067–79. doi: 10.1007/s40265-016-0603-2
29. Chaudhry BZ, Cohen JA, Conway. Sphingosine 1-Phosphate Receptor Modulators for the Treatment of Multiple Sclerosis. *Neurotherapeutics* (2017) 14(4):859–73. doi: 10.1007/s13311-017-0565-4
30. Bagdanoff JT, Donoviel MS, Nouraldeen A, Carlsen M, Jessop TC, Tarver J, et al. Inhibition of Sphingosine 1-Phosphate Lyase for the Treatment of Rheumatoid Arthritis. *J Med Chem* (2010) 53(24):8650–62. doi: 10.1021/jm101183p
31. Han C, He X, Xia X, Guo J, Liu A, Liu X, et al. Sphk1_S1P_S1PR1 Signaling is Involved in the Development of Autoimmune Thyroiditis in Patients and NOD.H-2h4 Mice. *Thyroid* (2019) 29(5):700–13. doi: 10.1089/thy.2018.0065
32. Tagawa N, Takano T, Fukata S, Kuma K, Tada H, Izumi Y, et al. Serum Concentration of Androstenediol and Androstenediol Sulfate in Patients With Hyperthyroidism and Hypothyroidism. *Endocr J* (2001) 48(3):345–54. doi: 10.1507/endocrj.48.345
33. Harteneck C. Pregnenolone Sulfate: From Steroid Metabolite to TRP Channel Ligand. *Molecules* (2013) 18:12012–28. doi: 10.3390/molecules181012012
34. Minder EI, Karlaganis G, Paumgartner G. Radioimmunological Determination of Serum 3 Beta-Hydroxy-5-Cholenoic Acid in Normal Subjects and Patients With Liver Disease. *J Lipid Res* (1979) 20:986–93. doi: 10.1016/S0022-2275(20)40000-8
35. Vithian K, Samat A, Jones MK. Acute Intermittent Porphyria Associated With Hyperthyroidism. *Ann Clin Biochem* (2006) 43:414–5. doi: 10.1258/000456306778520061

Conflict of Interest: The authors declare that the research was conducted in the absence of any commercial or financial relationships that could be construed as a potential conflict of interest.

frontiers in Endocrinology

REVIEW
published: 20 December 2021
doi: 10.3389/fendo.2021.780974

The Role of Mesenchymal Stromal Cells-Derived Small Extracellular Vesicles in Diabetes and Its Chronic Complications

*Fu-Xing-Zi Li[1], Xiao Lin[2], Feng Xu[1], Su-Kang Shan[1], Bei Guo[1], Li-Min Lei[1], Ming-Hui Zheng[1], Yi Wang[1], Qiu-Shuang Xu[1] and Ling-Qing Yuan[1]**

[1] National Clinical Research Center for Metabolic Disease, Department of Endocrinology and Metabolism, The Second Xiangya Hospital, Central South University, Changsha, China, [2] Department of Radiology, The Second Xiangya Hospital, Central South University, Changsha, China

Mesenchymal stromal cells (MSCs) are applied in regenerative medicine of several tissues and organs nowadays by virtue of their self-renewal capabilities, multiple differentiation capacity, potent immunomodulatory properties, and their ability to be favourably cultured and manipulated. With the continuous development of "cell-free therapy" research, MSC-derived small extracellular vesicles (MSC-sEVs) have increasingly become a research hotspot in the treatment of various diseases. Small extracellular vesicles (SEVs) are membrane vesicles with diameters of 30 to 150 nm that mediate signal transduction between adjacent or distal cells or organs by delivering non-coding RNA, protein, and DNA. The contents and effects of sEVs vary depending on the properties of the originating cell. In recent years, MSC-sEVs have been found to play an important role in the occurrence and development of diabetes mellitus as a new way of communication between cells. Diabetes mellitus is a common metabolic disease in clinic. Its complications of the heart, brain, kidney, eyes, and peripheral nerves are a serious threat to human health and has been a hot issue for clinicians. MSC-sEVs could be applied to repair or prevent damage from the complications of diabetes mellitus through anti-inflammatory effects, reduction of endoplasmic reticulum-related protein stress, polarization of M2 macrophages, and increasing autophagy. Therefore, we highly recommend that MSC-sEVs-based therapies to treat diabetes mellitus and its chronic complication be further explored. The analysis of the role and molecular mechanisms of MSC-sEVs in diabetes and its related complications will provide new idea and insights for the prevention and treatment of diabetes.

Keywords: diabetic complication, extracellular vesicles, insulin resistance, mesenchymal stromal cells, microRNAs

OPEN ACCESS

Edited by:
Jean-François Tanti, U1065 Centre Méditerranéen de Médecine Moléculaire (INSERM), France

Reviewed by:
Babak Arjmand, Tehran University of Medical Sciences, Iran
Soazig Le Lay, Institut National de la Santé et de la Recherche Médicale (INSERM), France

***Correspondence:**
Ling-Qing Yuan
allenylq@csu.edu.cn

Specialty section:
This article was submitted to Diabetes: Molecular Mechanisms, a section of the journal Frontiers in Endocrinology

Received: *22 September 2021*
Accepted: *29 November 2021*
Published: *20 December 2021*

Citation:
Li F-X-Z, Lin X, Xu F, Shan S-K, Guo B, Lei L-M, Zheng M-H, Wang Y, Xu Q-S and Yuan L-Q (2021) The Role of Mesenchymal Stromal Cells-Derived Small Extracellular Vesicles in Diabetes and Its Chronic Complications. Front. Endocrinol. 12:780974. doi: 10.3389/fendo.2021.780974

INTRODUCTION

Diabetes is a group of metabolic diseases characterized by chronic hyperglycemia caused by multiple causes. It is caused by defects in insulin secretion and/or function. By 2045, the number of diabetic patients is predicted to rise to 693 million (1). Diabetes is mainly manifested by absolute or relative deficiency of insulin and decreased sensitivity of target cells to insulin (2). Persistent high blood sugar can cause extensive vascular damage to the cardiovascular system, retina, kidneys, and nerves, which can lead to various complications (3–5). At present, the application of therapeutic insulin and oral hypoglycemic agents is one of the methods to effectively control the blood glucose level of diabetic

patients (6, 7). However, the long-term use of insulin and hypoglycemic drugs causes side effects of varying degrees, and exogenous insulin is still not enough to mimic the natural activity of endogenous insulin. There is also a risk of hypoglycaemia (8). In addition, transplantation of pancreatic or islet cells has been widely restricted in clinical applications due to the lack of pancreatic donors, the number and activity of pancreatic cells, allogeneic immune rejection, surgery and post-operation and many other complex factors (9).

Mesenchymal stromal cells (MSCs) have been established as promising candidate sources for cell therapy due to their contributions to tissue and organ homeostasis, repair and support by self-renewal and multi-differentiation, as well as by their anti-inflammatory, anti-proliferative, immunomodulatory, trophic and pro-angiogenic properties (10). Various diseases have been successfully treated by MSCs in animal models and hundreds of clinical trials related to the potential benefits of MSCs are in progress or have concluded satisfactorily (11). MSCs are commonly used in hematopoietic stem cell transplantation, repair of tissue injuries (bone, cartilage, joint, heart, liver, spinal cord, and nervous system diseases), autoimmune diseases, and as vectors for gene therapy (12). MSCs can promote the regeneration of pancreatic β-cells, protect endogenous pancreatic β-cells from apoptosis, and improve the insulin resistance (IR) of peripheral tissues by providing a supportive microenvironment driven by the secretion of paracrine factors or the deposition of extracellular matrix (13, 14). Numerous studies have shown that the therapeutic effects of MSCs are mediated in a paracrine manner, mainly through extracellular vesicles such as small extracellular vesicles (sEVs) (15). Therefore, cell-free therapy technology based on MSC-derived small extracellular vesicles (MSC-sEVs) has gradually become a research direction. Existing studies have shown that MSC-sEVs have a therapeutic effect on diabetes (16, 17). MSC-sEVs also show great potential in the tissue repair of diabetes complications. Therefore, the regenerative and immunomodulatory properties of MSC-sEVs have the potential to treat diabetes and related complications, such as diabetic nephropathy (DN) (18) and central nervous system damage (19). Information has emerged regarding the roles of specific miRNAs and other MSC-sEVs components as mediators of the protective effects of MSCs administration in preclinical diabetes disease models but many remains unknown. Currently, the role of MSC-sEVs in the treatment of diabetes diseases is an area of active preclinical study. This review mainly introduces the research progress of MSC-sEVs in the treatment and pathogenesis of diabetic central and peripheral neuropathy, diabetic vascular disease, diabetic skin disease, and DN in recent years.

DIABETES

Diabetes describes a group of conditions in which blood glucose is not properly regulated. Diabetes mellitus occurs when β-cells fail to secrete the insulin necessary to maintain the homeostasis of glucose in the blood. The most common forms of diabetes are type 1 (T1DM) and type 2 diabetes mellitus (T2DM). T1DM results from a cell-mediated autoimmune destruction of β-cells, whereas in T2DM, IR from peripheral organs is coupled with insulin deficiency resulting from an insufficient β-cell mass or function. Other forms of diabetes include gestational diabetes, latent autoimmune diabetes of adulthood (LADA), and neonatal diabetes mellitus (NMD) and maturity onset diabetes of the young (MODY) in which mutations in key pancreatic genes are found (e.g. Glucokinase, Pdx1, etc.). Over time, diabetes can lead to the development of different long-term complications such as diabetic retinopathy, neuropathy, nephropathy, critical ischemia of the limbs and so on. The pathogenesis of related diabetes complications was shown in **Table 1**. Currently, diabetes cannot be cured, and the treatment of diabetes consists of handling hyperglycemia by providing an exogenous insulin and medications supply or by islet cell transplantation. However, the inability to achieve tight control of glucose regulation has motivated more efforts to develop other approaches to address diabetes and reduce the burden of existing diabetes complications. Moreover, the diabetes-based existence of a chronic inflammatory state, impaired immune response, impaired coagulation and other related complications could be among the underlying pathophysiological mechanisms contributing to the increased morbidity and mortality of people with diabetes.

MESENCHYMAL STROMAL CELL DERIVED SMALL EXTRACELLULAR VESICLES

Extracellular vesicles (EVs) refer to vesicle-like bodies with a double-layer membrane structure that fall off the cell membrane or are secreted by cells. They are widely present in various body fluids and cell supernatants, and stably carry some important signal molecules (46). According to MISEV 2018, they can be divided into 3 subgroups: small EVs (< 100 nm or < 200 nm), medium/large EVs (> 200 nm) (47). EVs are involved in cell communication, cell migration, angiogenesis, tumor cell growth and other processes. They act as new mediators of long-distance cell-to-cell communication and can transfer various biologically active molecules (such as encapsulated cytokines and genetic information) from their parental cells to distant target cells (47).

Exosomes, the smallest EVs with the size range of 30 - 150 nm in diameter,have a bilayer structure and saucer-like morphology (48). In the full text of this article, we all use the exosomes command as sEVs. After fusion with the cell membrane, the contents of the sEVs are released into the extracellular matrix (49) as depicted in **Figure 1**. Almost all types of cells can secrete sEVs, mainly from body fluids, such as blood (19), urine (39), cerebrospinal fluid (52), saliva (53), and breast milk (54). sEVs apply their effects through targeting their cargos, such as nucleic acids (DNA, mRNA, miRNA, lncRNA and so on), lipids and proteins at the host cells, which leads to a shift in the behaviour of the recipient cells (55, 56). sEVs play an important role in various physiological and pathological processes, such as adipose metabolism, angiogenesis,

TABLE 1 | Application of MSC-sEVs in diabete diseases.

Types of diabetes complications	Pathogenesis of diabetic complications	MSC-sEVs source	MSC-sEVs dose used	MSC-sEVs delivery	MSC-sEVs Isolation	Mechanisms	Reference
Diabetic autonomic neuropathy	Ischemia, hypoxia, activation of polyol metabolic pathways, reduced inositol synthesis, genetic factors, and autoimmune impairment	Rat AD-MSCs	200 μg/0.1 mL PBS *in vivo*	IV	ExoQuick	Delivering corin, anti-inflammatory	(20)
		Rat AD-MSCs	10-100 μg *in vivo*	IV	ExoQuick	Exosomal miRNA transfer	(21)
		Rat BM-MSCs	100 μg/0.2 mL PBS *in vivo*	IV	UCF	Exosomal miR-21-5p transfer, inhibiting the expression ofPDCD4	(22)
Diabetic retinopathy	Oxidative stress, susceptibility genes, activation of polyol metabolic pathways, role of cytokines, non-enzymatic glycosylation of proteins, activation of protein kinase C	Human BM-MSCs	4 μL of 1 x 10^6 particle/mL	vitreous humor	ExoQuick	Enhancing functional recovery, reducing neuroinflammation and cell apoptosis	(23)
		Rabbit AD-MSCs	100 mg p/mL	IV	UCF	Exosomal miR-222 transfer	(24)
		Human UC-MSCs	250 μg/mL	*ex vivo*	UCF	Exosomal miR-1 26 transfer, suppressing the HMGBI signaling pathway	(25)
Macrovascular disease	Injury of endothelial cells, proliferation of smooth muscle cells, enhancement of platelet aggregation and adhesion	Rat BM-MSCs	5-20 μg/mL	*ex vivo*	UCF	Exosomal miR-146a transfer to VSMCs	(26)
Diabetic nephropathy	Genetic factors, abnormal renal hemodynamics, metabolic abnormalities caused by hyperglycemia, hypertension, abnormal metabolism of vasoactive substances	Mouse BM-MSCs	100 μg/kg *in vivo*	IV	UCF	Enhancing autophagy through the mTOR signaling pathway	(11)
		Mouse AD-MSCs	25 μg/mL *in vitro*	IV	ExoQuick	Exosomal miR-146a transfer inhibition of Smad1/mTOR signaling pathway in podocyte	(27)
		Rat BM-MSCs	5.3 × 10^7/0.2 mL PBS *in vivo*	RSI	ExoQuick	Anti-apoptotic effect and protecting tight junction structure in tubular epithelial cells	(28)
		Human USCs	not reported	*ex vivo*	UCF	Exosomal miRNA transfer, mainly miR-145	(29)
		Human USCs	100 μg/0.2 mL PBS *in vivo*	IV	UCF	Reducing the urine volume and urinary microalbumin excretion, preventing podocyte cell apoptosis	(18)
		Human USCs	10 μg /0.2 mL PBS *in vivo*	IV	ExoQu ick	Exosomal miR-16-5p transfer to podocytes	(30)
		Mouse AD-MSCs	not reported	*ex vivo*	ExoQuick	Exosomal miR-215-Sp transfer to podocytes	(31)
		Human UC-MSCs	25, 50, 100 μg/mL *in vitro*	*ex vivo*	Not reported	Depressing cytokine expression	(32)
Diabetic foot ulcer, diabetic skin damage	Neurological and vascular lesions and traumatic infections. Glycoprotein deposition on the basement membrane of capillaries thickens the tube wall and causes hypoxia in tissues, resulting in microvascular lesions	Human BM-MSCs	not reported	SUB	ExoQuick	Anti-inflammatory, increasing ratio ofM2/M1 polarization	(33)
		Human MB-MSCs	10 μg/0.1 mL PBS *in vivo*	SUB	UCF	Inducing Ml/M2 polarization, enhancing neoangiogenesis, activating of the NF-κβ	(34)

(Continued)

TABLE 1 | Continued

Types of diabetes complications	Pathogenesis of diabetic complications	MSC-sEVs source	MSC-sEVs dose used	MSC-sEVs delivery	MSC-sEVs Isolation	Mechanisms	Reference
		Human GG-MSCs	150 μg/0.1 mL in PBS *in vivo*	hydrogel	UCF	Promoting re-epithelialization, enhancing angiogenesis and neuronal ingrowth.	(35)
		Human UC-MSCs	60 μg/0.5 mL in PBS *in vivo*	SUB	UCF	let-7b, regulating macrophage plasticity through activating TLR4/NF- κβ /STAT3/ AKT signaling	(36)
		Human AD-MSCs	not repotted	not repotted	ExoQuick	Overexpressing Nrf2, decreasing ROS, anti-inflammatory	(37)
		Human UC-MSCs	200 μg/0.1 mL PBS *in vivo*	SUB	UCF	Exosomal miR-2 l-3p transfer, inhibit PTEN and SPRY l	(38)
		Human USCs	200 μg/0.1 mL PBS *in vivo*	SUB	ExoQuick	Promoting angiogenesis and activating PI3K-Akt signaling pathway via transferring DMBT1 protein	(39)
		Human AD-MSCs	200 μg/0.1 mL PBS *in vivo*	SUB	UCF	mmu_circ_0000250/ miR-128-3p/SIRT1 axis	(40)
		Rat AD-MSCs	100 μg/0.2mL PBS *in vivo*	SUB	UCF	Targeting on miR124, stimulating the Wnt/β-catenin pathway	(41)
Diabetic peripheral neuropathy	Metabolic abnormalities, vascular disorders theory, protein glycosylation, immune factors, vitamin deficiency theory	Mouse BM-MSCs	1×10^9 particle	IV	UCF	Abundant miRNAs, targeting the Toll-like receptor (TLR)4/NF-κβ signaling pathway	(42)
		Rat BM-MSCs	not reported	not reported	UCF	Exosomal miR-133b transfer	(44)
		Rat BM-MSCs	0.5 μg/2 μL	ICV	UCF	Enhancing oxidative stress, enhancing remover glutamate from the brain and maintain K^+ balance	(43)
		Rat BM-MSCs	3×10^{11} particle	IV	ExoQuick	miR-9/ABCA1 pathway, anti-inflammatory	(19)
		Rat BM-MSCs	not reported	*ex vivo*	UCF	miR-146a-expressing exosome transfer, anti-inflammatory	(45)

BM, bone matTow; UC, umbilical cord; USC, urine-derived stem cells; AD, adipose tissue; MSC, mesenchymal stem cell; MB, menstrual blood; GG, gingival; IV, intravenous; RSI, renal subcapsular injection; SUB, subcutaneous; ICY, intracerebroventricularly; UCF, ultracentrifugation.

inflammatory response, tissue regeneration, tumorigenesis, nerve regeneration, islet resistance, and immune regulation (57, 58). The current gold standard for isolating sEVs is ultracentrifugation (59, 60). The main molecular markers of exosomes include tetraspanin (CD9, CD63, CD81) and ESCRT proteins (TSG101, ALIX) (61–64). The methods for identifying sEVs mainly include the use of protein immunoassays. Western blot (WB) is used to detect molecular markers (65). Ultrastructure and particle size are measured by transmission electron microscopy (TEM) (66). Dynamic light scattering (DLS) or nanometer particle tracking analysis (NTA) detects particle size distribution (67).

MSCs can be isolated from various adult tissues such as bone marrow, umbilical cord, adipose, peripheral blood, liver, and gums (68). It is also favored for its advantages, such as easy collection, low immune rejection, and less ethical controversy (69). It has been used in the repair and regeneration treatment of various tissues and organs. Previous studies have shown that by MSCs being transplanted into damaged tissues and differentiated to replace damaged cells, systemic administration of MSCs can

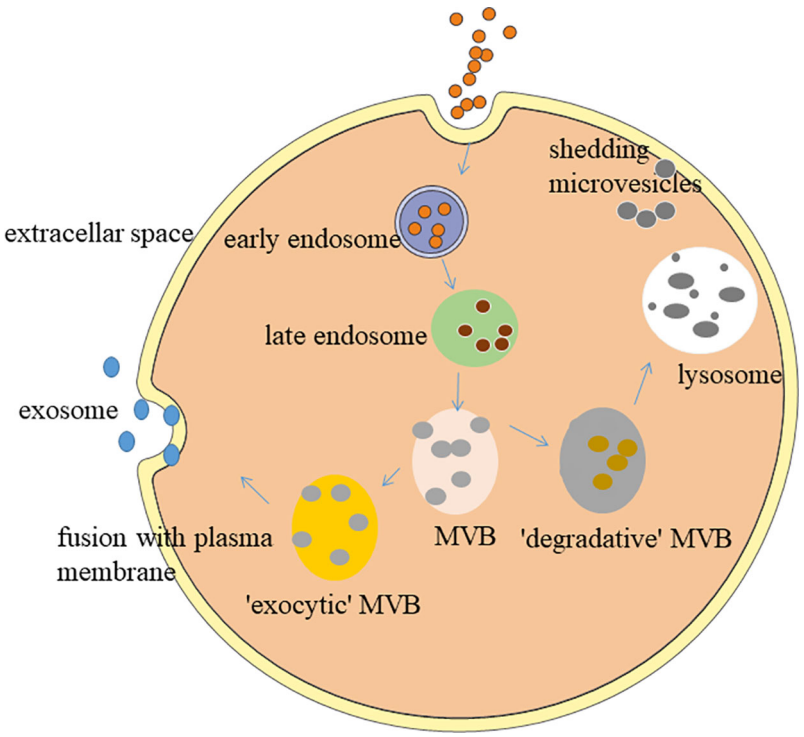

FIGURE 1 | Biogenesis of small extracellular vesicles. The formation of sEVs originates from a series of regulation processes of "endocytosis-fusion-efflux"; that is, early endosomes formed after the plasma membrane of the cell is recessed. The envelope of early endosomes keeps invading and selectively accepts biologically active components, such as proteins, nucleic acids, and lipids in the cells, and eventually forms late endosomes. Late endosomes produce multiple intraluminal vesicles in the form of internal budding, which selectively receive cytosolic proteins, nucleic acids, or lipids to form multivesicular bodies (MVB). MVB are divided into exocytic-MVB and degradative-MVB. Exocytic-MVB release the vesicles in the MVB to the outside of the cell in the form of exocytosis through the plasma membrane fusion mediated by Rab27, and the released membranous vesicles are the sEVs. Degradative-MVB are degraded by fusion with lysosomes (50, 51).

prevent the occurrence of T1DM. However, the proportion of transplanted MSCs reaching the damaged tissue was less than 1%, and most of them were trapped in organs such as liver and lung (70). Even if the transplanted MSCs had tissue repair effects, the transplantation and differentiation of MSCs in the damaged parts was low and short-lived (71), suggesting that MSCs exert the greatest effect through the secretion media. Simple MSCs transplantation may also have the risk of embolism, abnormal differentiation and tumor formation, these factors limit the use of MSCs (72). MSCs are recruited to the damaged tissue and secretes cytokines through paracrine action to change the microenvironment and induce the repair of the tissue structure and function of the damaged organ. In addition to several common modes (endocrine, paracrine, chemical synapse communication between neuron and target cell, autocrine, contact dependent communication between cells), there are other modes of information communication between cells through exosomes. Due to the vesicle structure of sEVs, the way of information exchange between cells is different from the typical mode mentioned above. There are three main ways for sEVs to participate in information exchange between cells, including the direct action of signal molecules on the membrane surface, intracellular regulation of content during membrane fusion and regulation of release of bioactive components. The discovery of sEVs makes the information exchange between cells more precise and comprehensive. The discovery of sEVs reveals the RNA intercellular transfer pathway existing in the body itself, which is expected to become an ideal gene therapy vector in the field of gene therapy due to its safe and effective targeted transport capacity. (73). MSCs are prolific sEVs secretors that shed a higher dose of sEVs compared to other cell types (74, 75). Indeed, most *in vitro* studies have directed their focus on sEVs derived from MSC subtypes, including adipose-derived stem cells (ADSCs), umbilical cord mesenchymal stem cells (UC-MSCs), bone marrow-derived mesenchymal stem cells (BM-MSCs), and others. The amount of sEVs released from MSCs is strongly associated with their proliferation rate (75). MSC-sEVs seem to be particularly beneficial in enhancing the recovery of various disease models. A recent study found that MSC-sEVs have tissue repair and reconstruction functions similar to MSCs. MSC-sEVs act on target cells such as β-cells, adipose cells, liver cells, macrophages, and skeletal muscle cells, by carrying specific miRNAs, proteins and other substances, thereby participating in the occurrence and development of IR and diabetes. As a new research hotspot, compared with MSCs, MSC-sEVs have the following advantages (76–78): (1) MSC-sEVs do not have the same issues as human cell transplantation, so the risk of immune rejection and aneuploidy is lower, and the

safety is higher. There are also no ethical issues. (2) MSC-sEVs is stable in nature, can be stored for a long time at -20 °C, are easy to manage and control, and the type and quantity of its contents can be changed artificially. Also, its contents are not easily degraded (79, 80). (3) MSC-sEVs are small in size and will not block capillaries as easily as MSCs. The dosage of MSC-sEVs can be adjusted as needed. Many of the proteins found in MSC-sEVs are enzymes, which are milder than drugs and may reduce the risk of overdose or under-dose (81, 82). (4) MSC-sEVs have a more direct effect and can target specific organs and damaged parts. MSC-sEVs can cross the blood-brain barrier due to its own structural characteristics and have higher histocompatibility. (5) The production cost of MSC-sEVs is controllable, and MSC-sEVs can be conveniently transported and stored.

STUDY ON THE APPLICATION OF SMALL EXTRACELLULAR VESICLES IN THE DIAGNOSIS OF DIABETES

Small Extracellular Vesicles -Related miRNAs

Increasing blood glucose is the main criterion for diagnosing diabetes. Although the detection method is simple and cost-effective, it cannot provide relevant information about the patient's pathogenesis or disease progression. During the onset and development of diabetes, the morphology and number of circulating sEVs change with the individual's physiological or pathological conditions, suggesting that it may be used as a new marker (83). Studies have shown that sEVs can be used as carriers to transport miRNAs or other RNAs to neighbouring cells through the binding of receptors and ligands, and as biomarkers to indicate physiological or pathological changes in tissues or organs. miRNA is a type of small single-stranded RNA with a length of 18-25 nucleotides. It can mediate post-transcriptional gene silencing by binding to the 3'-untranslated region or open reading frame region of the target mRNA (84). It plays an important regulatory role in the process of differentiation, migration, and disease occurrence and development. Exosomal miRNA is protected from RNase degradation by the phosphatidic acid molecular layer, which is conducive to the isolation, extraction and storage of exosomal miRNA (85). Garcia-Contreras et al. (86) performed exosomal miRNA chip detection on plasma samples of 12 patients in the T1DM group and 12 healthy person in the control group, and the results demonstrated that there were significant differences between the two groups of 7 miRNAs, and the up-regulated miR-16- 5p, miR-302d-3p, miR-378e, miR-570-3p, miR-574-5p, and miR-579; miR-25-3p were down-regulated. It was verified by RT-qPCR that miR-16-5p and miR-574-5p in the control group were significantly higher than in the T1DM group. This study revealed for the first time that miRNA isolated from patient plasma sEVs was expected to be a potential biomarker for the diagnosis of T1DM. Glutamate decarboxylase-65 antibody, insulin antigen-512 and insulin antibody are the main autoantibodies in patients with T1DM. The sEVs containing autoantibody-positive miRNAs or proteins secreted by pancreatic β-cells can be used for the diagnosis of T1DM potential markers (86, 87). In addition, circulating sEVs in the body fluids of diabetic patients show higher procoagulant activity (88). Compared with the normal healthy group, whether they have microvascular complications or uncomplicated, all patients with T1DM have a significantly higher sEVs level. It can be used as one of the diagnostic basis (89). Meanwhile, Katayama et al. found that exosome-derived extracellular miR-20b-5p, a highly abundant exoRNA in patients with T2DM, is a circulating biomarker associated with T2DM that plays an intracellular role in modulating insulin-stimulated glucose metabolism *via* AKT signalling (90). Moreover, in peripheral blood microvesicles, among 104 miRNAs in EVs, miR-320-3p is highly expressed in microvesicles of plasma (2.637-fold more than in blood cells), as well as, miR-320-3p has also been associated with the regulation of Glucose-Induced Gene expression in T2DM (91). During the occurrence and development of diabetes, the content or number of sEVs will change abnormally, which suggests the possibility for using sEVs as new markers. In addition, quantitative and stoichiometric analyses of miRNAs content in sEVs highlight the lack of reliable natural sources for miRNA-loaded particles, which necessitates the need for custom sEVs or nanoparticles to efficiently deliver miRNAs closely related to immunity, metabolism, and epigenetics in target cells. However, loading extracellular mature miRNAs into recipient cells comes at a cost, as it at least blocks the dynamic localization of miRNAs in the nucleoli, or leads to inefficient miRNAs delivery due to rapid exonuclease recovery. All of this work requires the design of new bionic vectors and *in vivo* assessment of miRNA function when delivered by natural or bionic nanoparticles to control metabolic diseases from infancy to adulthood.

Small Extracellular Vesicles-Related Protein

The latest research shows that C-megalin in urinary sEVs is positively correlated with the severity of DN (92). With the increase in urinary albumin, the level of C-megalin in urinary sEVs also increases, which is expected to become a diagnostic marker for DN. Aquaporins (AQPs) are a class of transmembrane proteins that are highly selective to water and have important physiological functions in regulating water metabolism. Polyuria is an early clinical symptom of diabetes. The levels of AQP2 and AQP5 in the urinary sEVs of DN patients are positively correlated with the histological grade of DN (93), indicating that AQPs of sEVs may become biomarkers for early diagnosis and monitoring of DN.

THE ROLE OF MSC-SEVS IN DIABETES

The Improvement of Pancreatic β-Cell Function

MSC-sEVs improve the function of pancreatic β-cells, which may be one of its mechanisms of treatment of diabetes. After transplantation, MSC-sEVs can specifically chemoattract and

migrate to the damaged islets to promote the proliferation of β-cells in the damaged islets, so as to repair and regenerate β-cells and inhibit β-cell apoptosis. Sabry et al. (94) found that injecting MSC-sEVs into streptozotocin (STZ) -induced diabetic rats had a better hypoglycaemic effect and faster effect than MSCs themselves. In the MSC-sEVs group, blood glucose levels decreased, plasma insulin levels increased, islet cell regeneration was enhanced, the number and size of islets increased, fibrosis and inflammation decreased, and the islet regeneration genes insulin, Pdx1, Smad2, Smad3, and Tgf-b were all significantly up-regulated. Another study found that sEVs isolation from menstrual blood-derived-MSCs through homing to the pancreas and pancreatic and duodenal homeobox 1 pathway enhanced the STZ-induced wistar rat β-cell quality and insulin production (95). Chen et al. (96) used the mouse β-cell line βTC-6 and found that the expression of apoptosis-related proteins cleaved caspase 3 and poly ADP-ribose polymerase (PARP) were up-regulated under hypoxia. MSC-sEVs with miRNA-21 reduced endoplasmic reticulum stress-related protein (GRP78, GRP94, p-eIF2α and CHOP) expression and inhibited of p38/MAPK phosphorylation, thereby protecting β-cells from hypoxia-induced apoptosis. MSC-sEVs are as effective as parental MSCs in improving the survival rate and function of islet cells (97). This cytoprotective effect may be mediated by vascular endothelial growth factor (VEGF) in MSC-sEVs (97). Another study by Kordelas et al. (98) demonstrated that MSC-sEVs can also help the angiogenesis and survival of transplanted pancreatic islets, improving the efficiency and success rate of the treatment. Overall, MSC-sEVs can improve the survival and function of the coated islets and benefit diabetic patients.

Amelioration of Insulin Resistance in Peripheral Target Tissues

Regulation of Autophagy

Autophagy is an important regulatory pathway for maintaining cell homeostasis, and maintains normal cell function by affecting the degradation of intracellular substances. The dysregulation of autophagy-related mechanisms after diabetes can lead to a decrease in the number of pancreatic β-cells and dysfunction, resulting in a decrease in insulin secretion (99). The latest study found that MSC-sEVs can promote liver glycolysis, glycogen storage and lipolysis of 0.25mM palmitic acid (PA)-treated LO2 cells and reduce gluconeogenesis (100). They found that the AMPK signaling pathway was activated and induced autophagy in T2DM rats and PA-treated LO2 cells. The formation of autophagosomes in the MSC-sEVs group increased, and the autophagy marker proteins BECN1 and MAP 1LC3B increased. Furthermore, the autophagy inhibitor 3-methyladenine significantly reduced the effect of MSC-sEVs on glucose and lipid metabolism in T2DM rats.

Mechanism of Insulin Resistance in Peripheral Target Tissues

Sun et al. (101) established a T2DM rat model with high-fat diet (HFD) and STZ induction. Through the results of oral glucose tolerance tests (OGTTs), peritoneal insulin tolerance tests (IPITTs), IR index (HOMA-IR) and serum insulin tests, they found that intravenous injection of sEVs from MSCs (hucMSC-sEVs) can effectively alleviate hyperglycemia in T2DM rats. In T2DM rats, hucMSC-sEVs restored the phosphorylation of insulin receptor substrate 1 (IRS-1) and protein kinase B (Akt), and promoted the expression and membrane translocation of glucose transporter 4 (GLUT4) in muscles. The expression level of glycogen synthesis related protein p-GSK3β and glycogen synthase rises, increasing the storage of liver glycogen to maintain glucose homeostasis. At the same time, hucMSC-sEVs inhibited STZ-induced β-cell apoptosis and restored the insulin secretion function of T2DM. The study of Su et al. (102) effectively explained a clinical phenomenon, which is "Why do the elderly often develop IR?" They extracted the sEVs released by BM-MSCs from young and aged mice. They found that the highly enriched miR-29b-3p sEVs released by BM-MSCs can be absorbed by adipocytes, cardiomyocytes and hepatocytes, thereby producing IR *in vivo* and *in vitro*. Their research further found that miR-29b-3p could directly target SIRT1. Interestingly, they utilized an aptamer-mediated nanocomplex delivery system, which can specifically target BM-MSCs. Down-regulating/up-regulating the level of miR-29b-3p in BM-MSCs-derived sEVs could significantly ameliorate/increase IR in elderly mice.

Anti-Inflammatory and Immune Regulation Mechanism

Immunity imbalance is one of the key factors in the pathogenesis of diabetes. Generally, inflammatory cells secrete pro-inflammatory cytokines, such as tumor necrosis factor-α (TNF-α) and interleukin 6 (lL-6) (101, 103), which are the main causes of IR in chronic inflammatory tissues. Therefore, timely and effective ameliorate the body's microenvironment and regulation of immune response through MSC-sEVs is one of the important directions and strategies for diabetes treatment. As we all know, T1DM is an autoimmune disease characterized by permanent destruction of pancreatic β-cells mediated by T cells (104). Recent studies found that the autoimmune response or immune imbalance was closely related to IR and the progressive decline of pancreatic β-cell function during the pathogenesis of T2DM (105). In addition, the incidence of diabetes-related complications is also affected by autoimmune reactions (106). Sun et al. (101) found that, in the STZ-induced rat diabetes model, hucMSC-sEVs injected *via* the tail vein inhibited the secretion of pro-inflammatory cytokine TNF-α to reverse T2DM IR and indirectly increased the insulin/AKT signaling pathway activation. Zhao et al. (107) introduced ADSCsEVs into mice fed with HFD-Fed, which can significantly reduce systemic IR caused by obesity, attenuation of dsylipiemia, inhibit fat cell hypertrophy. By measuring the area under the glucose tolerance test curve, it was observed that ADSCsEVs can increase the effect of insulin by 27.8%. The transfer of ADSC-sEVs carrying active STAT3 to activate arginase-1 from adipose-derived mesenchymal stem cells to macrophages induces polarization of M2 macrophages and attenuation of WAT inflammation in

HFD-Fed Mice. M2 macrophages induced by ADSC–sEVs can express high levels of tyrosine hydroxylase. Also ADSC–sEVs can drive the expression of Arg-1 by transporting STAT3 to promote ADSCs proliferation and lactate production. The Fas/FasL pathway plays an important role in β-cell apoptosis in T1DM, especially under high glucose conditions (108). Human BM-MSCs and their sEVs can deliver siFas and anti-miR-375 together to inhibit the early apoptosis of transplanted human islets (109). Under inflammatory cytokine treatment, after simultaneously silencing Fas and miR-375, pancreatic islet cell apoptosis was markedly inhibited, and insulin release was enhanced. In the humanized NOD scid gamma mouse model, intravenous injection of BM-MSCs and peripheral blood mononuclear cells (PBMC) co-cultured sEVs can further suppress the immune response by inhibiting the proliferation of PBMC and enhancing the function of regulatory T cells (Treg). BM-MSCs and derived sEVs may be an effective method to improve islet function under inflammation as showed in **Figure 2**.

THE ROLE OF MSC-SEVS IN THE COMPLICATIONS OF DIABETES

Microvascular Disease

Microvessels refer to capillaries and microvessels between tiny arteries and tiny veins with a lumen diameter of less than 100 μm. Microangiopathy is a specific complication of diabetes. Its typical changes are microcirculation disorder and thickening of the microvascular basement membrane. The main risk factors include long duration of diabetes, poor blood sugar control, high blood pressure, dyslipidemia, smoking, and IR. Microvascular disease mainly manifests in the retina, kidney, nerve, and myocardial tissue, among which DN and diabetic retinopathy (DR) are particularly important. Fortunately, MSC-sEVs has been found to have a positive therapeutic effect in these microvascular diseases.

Repair Function of MSC-sEVs in Diabetic Nephropathy

DN occurs in 20% to 40% of diabetic patients (110). DN has become one of the main causes of end-stage renal disease. Diabetes with long-term hyperglycemia infiltration and micro-inflammatory environment can cause substantial kidney damage. Its clinical feature is proteinuria, and its final pathological manifestation is renal fibrosis. Studies have pointed out that sEVs not only participate in the early diagnosis of DN, but also have the ability to repair kidney tissue. Ebrahim et al. (11) found that STZ-induced diabetes rat after tail vein injection of MSC-sEVs can ameliorate kidney injury. A kidney biopsy showed that glomerular and tubular collagen fibre deposition was reduced, glomerular basement membrane thickened and foot process fusion was reduced. Many autophagosomes can be seen in the cytoplasm. RT-qPCR and WB showed that the expression of mTOR was reduced, and the expression of autophagy-related proteins LC3II and Beclin-1 increased. It may be possible to up-regulate the expression of LC3II and Beclin-1 by inhibiting the mTOR signalling pathway to enhance autophagy. In turn, it reduced podocyte apoptosis and collagen fibre deposition and exerted renal protection. In addition, ADSC-sEVs also have a renal protective effect (27). After the tail vein injection of ADSC-sEVs in mice, blood urea nitrogen, serum creatinine, and urine protein decreased, and podocyte apoptosis decreased. The addition of ADSC-sEVs co-cultivation can effectively alleviate the limitation of high glucose culture on the proliferation rate of MPC5 cells. The exosomal miR-486 reduced the expression of Smad1, inhibited the activation of p62/mTOR signalling pathway and caspase3, up-regulated the expression of LC3 and Beclin-1, enhanced autophagy, and reduced podocyte apoptosis to

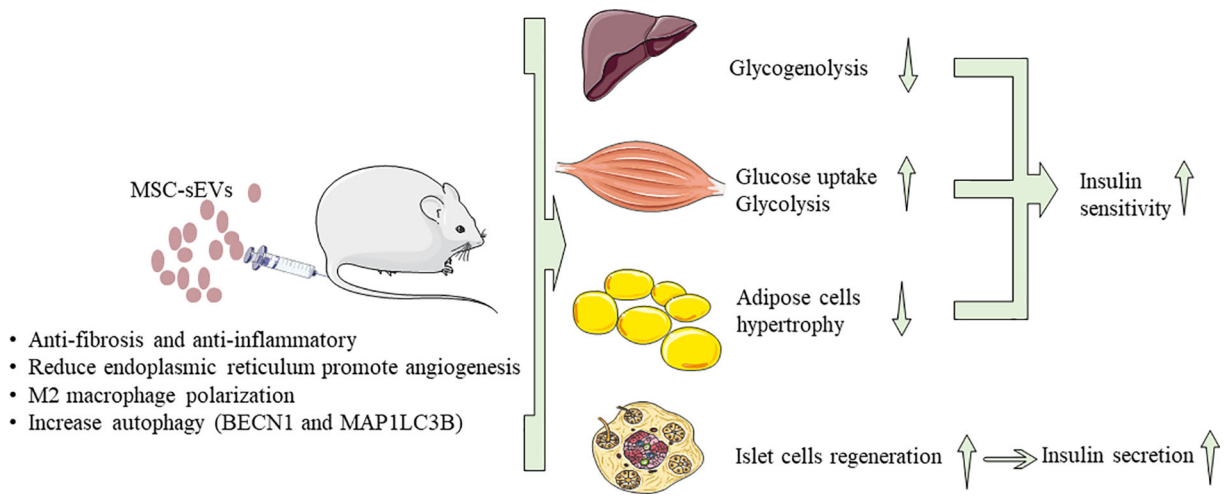

FIGURE 2 | The approach of MSC-sEVs to treat diabetes. MSC-sEVs down regulate blood glucose through reverse insulin resistance in insulin target tissues (liver, muscle, adipose tissue) and relieve islet β cells destruction.

improve kidney injury in db/db mice. Exosomal miR-486 may be a key factor for stem cells to improve DN. MSC-sEVs protect the kidney by regulating autophagy-related factors, providing a new direction for the treatment of DN. Nagaishi et al. (28) found that the treatment of MSCs and MSCs sEVs can inhibit the abnormal infiltration and interstitial fibrosis of BMSCs in the kidney and inhibited inflammatory signals by inhibiting the p38-MAPK pathway and the overexpression of TGF-β. It reversed the severe damage to renal tubular epithelial cells (TECs) caused by high glucose stimulation, inhibited epithelial–mesenchymal transition (EMT), and reduced the damage caused by DN. In addition, in the diabetic rat model induced by STZ, the tail vein injection of human urine stem cell-derived small extracellular vesicles (USC-sEVs) can promote angiogenesis and cell survival by inhibiting the overexpression of caspase-3 protease and reduce podocyte apoptosis (29). Another study by Jiang et al. (18) demonstrated that USCs-sEVs could potentially reduce the urine volume and urinary microalbumin excretion, prevent podocyte and tubular epithelial cell apoptosis, suppress the caspase-3 overexpression, and increase glomerular endothelial cell proliferation in diabetic rats. Other related studies have also found that MSCs and its sEVs also delay the EMT of podocytes and renal tubular interstitial cells induced by high glucose and have anti-fibrotic effects on DN (31, 32). Overall, these findings provide the basis for the future application of MSC-sEVs as a new biological treatment of DN. However, its therapeutic value is currently limited to animal models. If MSC-sEVs treatment is to be applied into the clinic, further clinical trials are needed.

Repair Function of MSC-sEVs in Diabetic Retinopathy

Hyperglycemia can damage the basement membrane, endothelial cells and retinal perivascular cells of the retinal vascular system (111). Early treatment is to strictly control blood sugar and blood pressure to control disease risk factors, and later can be treated by laser photocoagulation, intraocular anti-VEGF, or glucocorticoid drugs (112). However, these treatments have certain complications and related problems, such as unstable efficacy. Therefore, the treatment of MSC-sEVs has become an alternative solution. At present, scholars generally believe that the occurrence of DR is related to retinal cell degeneration (including retinal cell apoptosis, glial cell dysfunction) and retinal microvascular dysfunction (retina no perfusion, changes in vascular permeability, and retinal neovascularization) (113). The results of Zhang et al. (25) showed that MSC-sEVs injection can alleviate the inflammatory response of diabetic rats or human retinal endothelial cells exposed to high glucose by down-regulating the levels of caspase-1, IL-1b, and IL-18. Compared with control MSC-sEVs, overexpression of miR-126 in MSC-sEVs significantly inhibited the HMGB1 signalling pathway in diabetic rats and inhibited inflammation. *In vitro*, miR-126 overexpression in MSC-sEVs significantly reduced HMGB1 expression and NLRP3 inflammasome activity induced by high glucose. Safwat et al. (24) showed that ADSC-sEVs reduce STZ-induced DR degeneration in rabbits by delivering micRNA-222 to retinal cells. Mathew et al. (23) explained that in the rat model, MSC-sEVs injected into the vitreous humor 24 h after retinal ischemia can significantly enhance functional recovery and reduce neuroinflammation and cell apoptosis. Generally speaking, MSC-sEVs have great potential as a biomaterial for neuroprotection and regeneration therapy of retinal diseases.

Macrovascular Disease

The predisposing factors of atherosclerosis such as obesity, hypertension and dyslipidemia, often occur in people with diabetes (mainly T2DM) (114). The prevalence of atherosclerosis in diabetic patients is higher, and the onset is earlier. The progress is faster. Atherosclerosis mainly invades the aorta, coronary arteries, cerebral arteries, renal arteries and limb arteries, causing coronary heart disease, ischemic cerebrovascular disease, renal arteriosclerosis, and other diseases. Studies have pointed out that sEVs derived from BM-MSCs can treat brain cognitive dysfunction caused by diabetes. Diabetic vascular calcification (VC) is a common pathological basis in diabetic vascular disease, which is characterized by the deposition of calcium phosphate in the cardiovascular structure (115–118). Advanced glycation end products (AGEs) are the main cause of diabetes-related vascular complications, including diabetic vascular smooth muscle cells (VSMCs) calcification, which can cause VSMCs to calcify (119). The thioredoxin-interacting protein (TXNIP) is a member of the α-arrestin family of inhibitory proteins. In a high glucose state, TXNIP can bind to thioredoxin (Trx) and cause its inactivation and activity. The increase in oxygen species and the production of vascular inflammation are closely related to the production of AGEs (120). Wang et al. (26) found that MSC-sEVs contained high levels of miR-146a. When it was co-cultured with VSMCs pretreated AGE modified bovine serum albumin (AGE-BSA), it could be transferred into cells, by targeting to inhibit the production of TXNIP to protect Trx activity, and inhibit reactive oxygen species (ROS) to prevent AGE-BSA-induced calcification. Therefore, MSC-sEVs may be a potential therapeutic target for VC and play an important role in diabetic vascular disease.

Repair Function of MSC-sEVs in Diabetic Central Nervous System Damage

Diabetic neuropathy is divided into central nervous system disease and peripheral nervous system disease. Central nervous system diseases include brain diseases and spinal cord diseases (121). The abnormal glucose metabolism caused by hyperglycemia damages nerve cells and slows down the conduction speed of brain cells, which can be measured by neuroelectrophysiological equipment. Many people with diabetes have worse memory, reaction speed, and thinking and cognitive abilities than people without diabetes (122). The conduction velocity of the spinal nerve is slowed down, and the patient has symmetry deep paresthesias in the lower limbs, such as loss of position sense, unstable walking, and dysuria. The main cause of cognitive impairment in diabetic patients may be damage to hippocampal neurons and astrocytes. In a study

published by Nakano et al. (43) intravenous injection of MSC-sEVs easily spreads from blood vessels to the brain parenchyma. It was internalized by astrocytes and neurons, enhancing the ability of astrocytes to resist oxidative stress. At the same time, MSC-sEVs enhanced the ability of astrocytes to remove glutamate from the brain and maintain K+ balance, thereby promoting neuronal function, brain balance and synapse formation and improving cognitive impairment caused by diabetes. Local injection of BM-MSC-sEVs may be an effective drug for the treatment of cognitive impairment caused by diabetes. Xin et al. (44) found that MiR-133b in sEVs released after stroke by MSCs can transfer to astrocytes and regulate the gene expression of middle cerebral artery occlusion (MCAo) rats. miR-133b regulates the expression of Ras homolog gene family member A (RhoA) and connective tissue growth factor (CTGF), thereby promoting neurite remodelling and growth, and promoting the functional recovery of nerve cells. Venkat et al. (19) found that MSC-sEVs treatment of T2DM stroke can increase the expression of tight junction protein ZO-1, reduce blood-brain barrier leakage and bleeding, reduce body weight and reduce the expression of inflammatory factors (MMP-9 and MCP-1). At the same time, it promotes the remodelling of white matter marked by the increase in axon and myelin density to produce the therapeutic effect of nerve function recovery. The therapeutic effect induced by MSC-sEVs may be partly mediated by reducing the expression of miR-9 and up-regulating the ABCA1-IGFR1 pathway. Kubota et al. (45) further found that an enriched environment promoted the up-regulation of miR-146a secreted by endogenous BM-MSC-sEVs and down-regulation of IL-1 receptor-associated kinase 1 (IRAK1) expression, thereby inhibiting the NF-κB pathway and reducing the production of TNF-α, thereby exerting an anti-inflammatory effect on damaged astrocytes and preventing diabetes-induced cognitive impairment. In addition, some scholars have extracted sEVs derived from BM-MSCs of TIDM rats and BM-MSCs of normal rats and injected them into the brains of TIDM stroke rats (123). They found that the former has the ability to remodel the cerebral blood vessels and white matter. The test results showed that the former serum miR-145 expression decreased, while the miR-145 target gene adenosine triphosphate binding cassette transporter 1 and insulin-like long factor 1 receptor expression increased. Studies have further confirmed that the sEVs transfected and knocked out miR-145 affect the degree of nerve growth, indicating that miR-145 plays an important regulatory role in neuroprotection. MSC-sEVs carry a large number of proteins and nucleic acids that protect nerves and nutrient nerves, can regulate related molecular pathways, protect myelin sheath, reshape synapses, repair damaged neurons, and so on to promote neuron growth and functional recovery. The above research results proved that MSC-sEVs treatment was a powerful tool for central nervous system damage in diabetic patients.

The Role of MSC-sEVs in Diabetic Peripheral Neuropathy and Autonomic Neuropathy

Diabetic peripheral neuropathy (DPN) is one of the main complications of diabetes and one of the important causes of the incidence and death of diabetes (124, 125). There is currently no effective treatment for this disease. Fan et al. (42) applied BM-MSC-sEVs to a DPN mouse model. The results showed that, after treatment with sEVs, the expression of TNF-α in nerve tissues was reduced, and the levels of TGF-β, IL-10, and Arg1 increased, indicating that exosome treatment reversed the increase in M1 type macrophages and the decrease in M2 type macrophages caused by diabetes, which is achieved by the polarization of macrophages M2 to reduce inflammation and improve neurovascular function. From these results we know that MSC-sEVs can reduce neurovascular dysfunction and improve the functional recovery of DPN mice by inhibiting the expression of pro-inflammatory genes.

Erectile dysfunction (ED) is a common comorbidity of male diabetes, and its pathogenesis may be caused by dysregulation of corpus cavernosum smooth muscle cells (CCSMCs). According to epidemiological data, about 50% of diabetic male patients develop erectile dysfunction within 10 years after diagnosis (126). Considering the low efficacy of oral phosphodiesterase type 5 inhibitors (PDE5i) in these patients (127, 128), MSC-sEVs therapy is an attractive tool for the treatment of diabetic ED (DED). Zhu et al. (21) showed that ADSC-sEVs contains some pro-angiogenic microRNA (miR-126, miR-130a, and miR-132) and an anti-fibrotic microRNA family (miR-let7b and miR-let7c). ADSC-sEVs have pro-angiogenic properties *in vitro*. *In vivo* ADSC-SEVs can induce endothelial cell proliferation, reduce cavernous fibrosis, and restore erectile function. Wang et al. (20) also found that ADSC-sEVs promoted neurovascular function by delivering corin and inhibited the expression of inflammatory factors to restore erectile function in diabetic rats. Huo et al. (22) explained that miR-21-5p delivered by MSC-sEVs can inhibit the expression of PDCD4 in T1DM rats, thereby stimulating the proliferation of corpus caverno-sum smooth muscle cells (CCSMCs), inhibiting CCSMCs apoptosis, and improving DED. These findings may provide new insights into the role of MSC-sEVs in the innovative treatment of DED.

The Role of MSC-sEVs in Diabetic Foot Ulcers and Diabetic Skin Damage

Diabetic foot ulcers (DFU) is a serious complication of diabetes. Although people are increasingly aware of its pathophysiology and cellular and molecular responses, the reason for this pessimistic situation is the lack of effective treatments. DFU is mainly caused by ischemic, neurological, or combined neuroischemic abnormalities (129). It is a slow-healing deep chronic wound and microvascular obstruction. In recent years, multiple studies have reported the potential of MSC-sEVs to treat lower extremity ischemia and ulcers caused by diabetes. MSC-sEVs show stupendous therapeutic potential in the immune regulation and angiogenesis stage of DFU. In the immune regulation stage, MSC-sEVs could secrete miR124a/125b (130) to reduce inflammation, produce leb-7b (36) to regulates macrophage polarization, and secrete miR21 (38, 131, 132) to modulate dendritic cell differentiation. In the angiogenesis stage, MSC-sEVs have the ability to produce NRF2 (37), mmu_circ_0000250 (40), DMBT1 (39), lncRNA

H19 (133), OxOband (41), miR126 (134, 135), miR23 (136), and miR21 (38, 131, 132) to promote the process of angiogenesis, granulation tissue formation, and re-epithelialization. The detailed summary of this part can be found in the review by An et al. (137). The exosome-derived miRNA and protein can be better protected by the exosomal membrane structure to avoid degradation, which not only helps to open up new targets for the early treatment of DFU, but also delays or even reverses the disease caused by the DFU process.

Poor healing of diabetic wounds can increase the risk of gangrene, amputation and even death. The main reasons for this complication include hypoxia, impaired angiogenesis, reactive oxygen species injury, and neuropathy (37, 138). At present, the main methods for treating diabetic chronic skin damage are debridement and dressing, but these treatment methods do not bring satisfactory results (139). Studies have shown that MSC-sEVs can carry a variety of anti-inflammatory factors and growth factors, which can regulate the immune response and inflammation (140, 141), promote wound angiogenesis (142, 143), accelerate the proliferation and regeneration of skin cells (142), and activate the collagen secretion of fibroblasts (144), eventually promoting the re-epithelialization of the skin wound. ADSC-sEVs exert an immunosuppressive effect by reducing the secretion of IFN-α, thereby inhibiting the activation of T cells (145). Li et al. (37) found that ADSC-sEVs inhibited the production of ROS and inflammatory factors through the overexpression of Nrf2 in a high glucose environment and prevented the senescence of endothelial cells. In addition, a new method to promote the healing of diabetic wounds has emerged: Shi et al.'s study in diabetic rat skin defect models showed that the combination of sEVs derived from gingival MSCs and chitosan/silk hydrogel can promote the regeneration of extracellular matrix (35). Epithelialization, deposition and remodelling promote angiogenesis and inward growth of neurons, thereby effectively promoting the healing of ulcer wounds in diabetic rats. ADSC-sEVs riched in miRNA-125a and miRNA-31, which can be transferred to vascular endothelial cells to stimulate proliferation, and promote angiogenesis (142, 143). At the same time, ADSC-sEVs can inhibit the expression of angiogenesis inhibitor (DLL4) and the anti-angiogenesis gene HIF1 in vascular endothelial cells, thereby promoting the migration of vascular endothelial cells and enhancing angiogenesis. In the early stage, ADSC-sEVs promote collagen remodelling by synthesizing type I and III collagen and, in the late stage reduce scar formation by inhibiting collagen formation (144). In addition, ADSC-sEVs stimulate the reconstruction of the extracellular matrix by regulating the differentiation and gene expression of fibroblasts, thereby promoting wound healing. Wang et al. (146) found that ADSC-sEVs increased the ratio of transforming growth factor-β3 (TGF-β3) to TGF-β1 *in vivo*. ADSC-sEVs also increased the expression of MMP3 in skin dermal fibroblasts, which was beneficial to the remodelling of the extracellular matrix (ECM) to reduce scar formation. These evidences prove that MSC-sEVs or its combination with new materials have strong therapeutic potential as depicted in **Figure 3**.

PHARMACEUTICAL DEVELOPMENT OF MSC-SEVS-BASED THERAPEUTICS FOR DIABETES DISEASES

With such promising preclinical findings in various types of disease models, investigators are now tasked with developing safe, feasible and reproducible MSC-sEVs-based therapies. Currently, 93 clinical trials involving exosomes are listed in www.clinicaltrials.gov. The majority of these trials focus on the use of sEVs from several body fluids as early diagnostic tools to predict the outcome of various treatments. MSC-sEVs have been shown in preclinical studies to be safe and scalable to large, clinically relevant doses (147).To date, several clinical applications of MSC-sEVs have been reported (148). A published study demonstrated that increasing dosages of MSC-sEVs in a patient with severe therapy-refractory acute graft versus-host disease (GVHD), was well tolerated and led to a significant and sustainable improvement of symptoms, which remained stable for five months (98). Globally, at least one clinical trial of MSC-derived sEVs for the improvement of β-cell mass in T1DM patients has been reported (https://clinicaltrials.gov/ct2/show/NCT02138331?term=MSC+exosomes&draw=1&rank=1). The first phase I clinical trial was initiated in 2014 with the aim of evaluating the safety of UC-MSC-sEVs in 20 patients with type 1 diabetes. Patients received a systemic injection of sEVs (ranging between 40-180 nm, in a dose of the supernatant produced from (1.22-1.51) × 106/kg/IV) at day 0 and of microvesicles (ranging between 180-1000 nm, in a dose of the supernatant produced from (1.22-1.51) × 106/kg/IV) at day 7. At the end of study (3 months) the following parameters are being evaluated: liver functions tests, kidney functions tests, HbA1c, glucose tolerance test, fasting and 2 h postprandial blood glucose levels, C-peptide chain level, and calculated total daily insulin dose. However, the status of the trial is unknown. More studies of MSC-sEVs-based therapeutics will be initiated in the near future (https://www.clinicaltrials.gov; unique identifier: NCT02138331, NCT03437759, NCT03384433) (98, 149). However, there remain significant challenges to translating this therapy into the clinic.

NEW STRATEGY FOR MSC-sEVs TREATMENT

The treatment of diabetes and its related complications is a huge economic burden for all countries in the world. At present, the most common way to diagnose diabetes is to measure blood glucose levels. However, before the blood sugar rises, there are potential vascular damage and decreased insulin sensitivity, so it is particularly important to find new alternative treatments. Numerous studies have shown that MSC-sEVs can mimic the biological functions of MSCs. But, MSCs mostly reside in the liver, spleen, and lungs, reaching less than 1% of the injured site. Most of the MSCs that reach the target tissue disappear after a few days, and the fate of most MSCs is anoikis or phagocytosis. Only a small amount of MSCs stayed at the injury site for a long

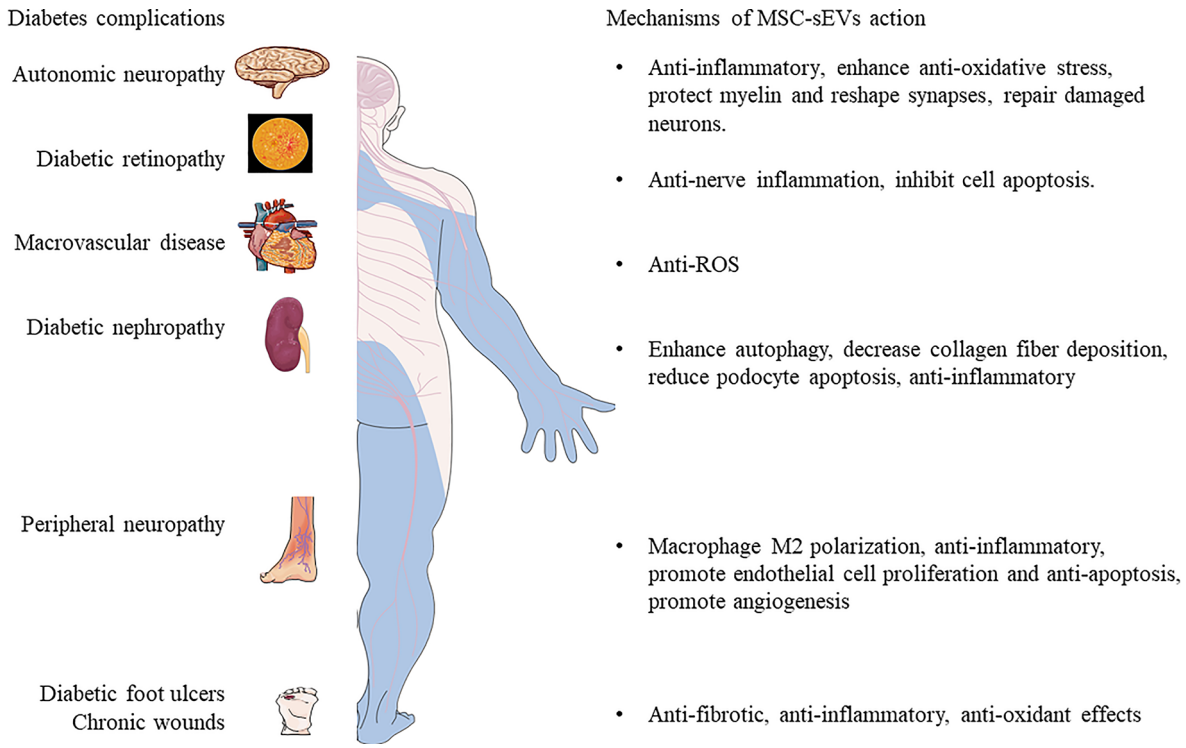

FIGURE 3 | The mechanisms of MSC-sEVs in the treatment of complex diabetic complications.

time. In recent years, with the deepening of sEVs research, scholars have proposed sEVs as a new biomarker for early diagnosis of diabetes. Studies have confirmed that injection of therapeutic sEVs can maintain a lasting biological effect within 6 weeks, suggesting that sEVs can transmit lasting signal information between cells (150). Whether or not it is advisable to develop MSC-sEVs therapy since it seems that the miRNAs on their own have a therapeutic effect rather than the MSC-sEVs? Our answer is that it is necessary to develop the treatment of MSC-sEVs. Although current studies on the mechanism of MSC-sEVs have reported that miRNAs play a major role (151), miRNAs will eventually need a vector for gene therapy involving miRNAs (152). Loading of extracellular mature miRNA into recipient cells comes with a cost by at least impeding dynamic localization of miRNAs in nucleoli or inefficient miRNA delivery due to rapid recycling by exonucleases. All these works are calling for the design of new biomimetic vehicles. There have been some reports of genetic drugs/carrier, but they can be eaten up by the immune system and they're not very stable, they have some immunogenicity (153). SEVs have a transport function and can increase the potency of miRNAs or drugs by modifying aptamer to specifically target tissues (67) and *in vivo* assessment of miRNA functionality when delivered by natural or biomimetic nanoparticles in order to control metabolic diseases. MSC-sEVs have great potential in cell-free therapy. This therapy is safer and easier to operate than cell therapy. It can circumvent potential tumorigenicity (154–156), untargeted tissue differentiation, undesired immune response in stem cell transplantation (157), low survival rate of transplanted cells (158), heterogeneity of clinical donors, *in vitro* expansion, cryopreservation methods, poor safety. Moreover, small-size EV preparations that are isolated using protocols including a filtration step through 0.22 μm membranes can be considered as sterile and do not require an additional sterilization step. These advantages make sEVs a safer and more effective alternative to traditional viral vectors (159), and sEVs can be designed as carriers for targeted delivery of molecular therapy (160). Because sEVs can transmit bioactive molecules between cells to affect the insulin sensitivity of target cells, using sEVs as therapeutic agents and carriers to enhance β-cell proliferation and repair also provides a new direction for the treatment of diabetes. With the development of targeted therapy technology, MSC-sEVs have shown great potential as a biomarker for the diagnosis and prognosis of diabetes and related complications (77). MSC-sEVs mediate a variety of signaling pathways in diabetes and its complications, transmit different messages between cells, and regulate pathological activities and physiological functions. Due to different physiological or pathological conditions, sEVs and their contents will undergo corresponding differential changes. If biomarkers are found in them, the detection of body fluid sEVs may become an effective early diagnosis and treatment

method for diabetes and its complications. SEVs contain a variety of proteins and biological genetic materials, and sEVs can travel throughout the whole body and even penetrate the blood-brain barrier, so proteins and macromolecular genetic materials can be loaded in the sEVs. If the corresponding drugs are wrapped into the sEVs, and then targeted and absorbed by cells, they will become an effective means of precision treatment. MSC-sEVs will become an ideal solution for cell-free therapy in the field of regenerative medicine. Proteins and miRNAs that help tissue regeneration can be packaged into specially designed MSC-sEVs. The ligands expressed by these packaged MSC-sEVs help to attach to therapeutic targets. Theoretically, injection of these sEVs will allow the drug to be delivered directly to specific target cells. This therapy can be used in patients with diabetic nephropathy or central nervous system damage to stimulate cell regeneration. What's more, it can also be used as a supportive treatment for islet transplant recipients, prolonging insulin independence and reducing patients' dependence on immunosuppressive drugs. All the advantages for MSC-sEVs treatment by comparison to MSCs donor cells as showed in **Table 2**. But the long-term effectiveness and safety of this treatment must first be evaluated. Research on sEVs is still in its early stages. There is no comprehensive clinical trial using MSC-sEVs-based regenerative therapy. Research progress depends on a deeper understanding of sEVs formation and signal transduction mechanisms.

CHALLENGES

Unfortunately, few experimental studies have compared the efficacy of MSCs and MSC-sEVs in diabetes and its chronic complications. MSC-sEVs therapy prevents abnormal renal function in HFD- and STZ-diabetic mice, similar to MSCs therapy (28). However, MSC-sEVs in HFD-diabetic mice conferred anti-inflammatory and renoprotective effects exceeding those of their parent MSCs (28). The combination of MSCs and MSC-sEVs was more effective to either one alone inhibit further immune response of transplanted islets, suggesting additive effects (109). Both strategies supported the notion that MSC-sEVs recapitulate the salutary effects of MSCs.

Although MSC-sEVs are a good natural carrier, uncertainty remains regarding sEVs fate, safety, isolation, characterization and long-term effects, which might impose important limitations on their path to clinical translation. In translational clinical studies, people have not yet reached a consensus on the dose of sEVs, the quantification of MSC-sEVs is essential to understanding the basic biological relationship between MSC-sEVs and its parent cells and the underlying interpretation of MSC-sEVs signals. Currently, researchers use several different methods to quantify the dose of sEVs, protein concentration and NTA, tunable resistance pulse sensing (TRPS) and flow cytometry, which make it difficult to compare studies with each other (161). Therefore, to help inter-study comparison,

TABLE 2 | The advantages for MSC-sEVs treatment by comparison to MSCs donor cells.

1. SEVs as drug carriers.
• As a nanocarrier, sEVs have the advantages of being similar to cell membranes, small in size, negatively charged, avoiding phagocytosis, generating immune escape, long circulation time, and being able to penetrate deep tissues.
• High biocompatibility and low immunogenicity.
• More significant safety. SEVs have no adverse effects on the kidney and liver.
• Concentration, dosage and route are easier to control.
• SEVs have cell targeting ability.
• SEVs have the ability to cross biological barriers: sEVs can cross the body's thick tissue barriers, such as the blood-brain barrier.
2. SEVs are used for disease diagnosis.
• Richer sample formats: Almost all body fluid samples contain sEVs.
• Thanks to the protection of the phospholipid bilayer, the contents of the sEVs have better stability.
• Circumvent potential ethical issues and tumorigenicity.
• "Cell-free therapy" therapy is safer and easier to operate than cell therapy.
3. SEVs are used for treatment.
• Low immunogenicity.
• Easy to store, no need to proliferate, easy to use quantitatively and to recruit from the damage. sEVs are stored at -20°C for 6 months, and stored at -80°C for a long time without losing their biochemical activity. It avoids the inconvenience of cryopreservation and recovery of MSCs, and can be used after dissolution, and the use time is easy to grasp.
• Mass production: sEVs can be enriched in a large amount in the culture medium.
• Controllable: The function of sEVs can be changed by changing the cell environment.
4. Problems to be solved with sEVs.
• Efficient extraction technology (the extraction method and its complicated classification system hinder its application).
• The concentration of sEVs in the injured area after local injection of MSC-sEVs in animal experiments is unknown.
• The optimal concentration to promote tissue regeneration or immune regulation, and the half-life of sEVs also needs more in-depth research.
• The sEVs secreted by different cells or the same cell under different physiological conditions may be different, and the contents and mechanisms of sEVs need to be further studied.
• SEVs transport a variety of biomolecules, and how to regulate recipient cells in the body and change the state and fate of cells is still unknown.
• Separation schemes suitable for large-scale preparation, purification and storage.
• Standardization schemes for quantification, molecular and physical characterization.
• Clear quality control (QC) standards for clinical use: to ensure that the quality, safety and effectiveness of the sEVs products produced are guaranteed. For example, sEVs should be stored in isotonic buffer to prevent pH changes during storage and freeze-thaw cycles.

we need multiple quantifications using various quantification tools. Next, the route of administration still requires further clarification. Therefore, it is necessary to further research and establish a uniform administration procedure for sEVs.

The storability of MSC-sEVs is an important aspect, both for basic research and for clinical applications. Currently, there is no standardized procedure for the storage of MSC-sEVs. Whether MSC-sEVs is suitable for storage at 4°C, -80°C, -196°C or other temperatures is no standardized procedure (162). It's still impractical to always use fresh MSC-sEVs preparations. In addition, storage vials can also affect the quality of MSC-sEVs, because MSC-sEVs may accidentally and irreversibly combine with certain materials (163). Due to the lack of data to address the impact of storage time and drugs on the stability and effectiveness of MSC-sEVs, it is necessary to develop a customized agreement for MSC-sEVs.

At present, there are still a series of problems, such as complicated sEVs extraction processes, low purity, expensive reagent supplies and so on (77). It is essential to expand the production of MSC-sEVs to meet the needs of clinical research (164, 165). A standardized sEVs detection platform should be established as soon as possible to accelerate the clinical transformation of large sEVs and big data, and provide a new direction for the diagnosis and treatment of diabetes. Based on the complexity of the biological substances contained in sEVs, the specific mechanisms and signaling pathways of sEVs involved in diabetes coupling still need to be further explored. Therefore, it is necessary to further research and establish a uniform administration procedure for sEVs.

CONCLUSION AND FUTURE PERSPECTIVE

With a more complete understanding of the mechanisms driving sEVs formation, sEVs could be engineered as vectors for the targeted delivery of molecular therapies injection of these sEVs would, in theory, allow for the discriminate delivery of medicine directly into specific target cells. It could also be of benefit as a supportive treatment for pancreatic islet transplant recipients, lengthening insulin independence and reducing the patients' dependence on immunosuppressive medication. With great perspective, MSC-sEVs therapy brings a bright future for diabetes treatment. Besides, sEVs from MSCs as well as pre-treatment of MSC-sEVs can be regarded as a key breakthrough to improve therapeutic efficiency.

In conclusion, MSC-sEVs is a therapeutic option for diabetes and its chronic complications in the future. However, long term studies are required to evaluate the efficacy and safety of sEVs therapy to find new and novel strategies for the treatment of diabetes; and further studies in humans are necessary to investigate the results on animal models. In the future, one can hope that sEVs therapy can be used in reduce the blood glucose, restore insulin sensitivity along with other complications treatments and promises a new therapeutic approach in clinical applications. In addition, with rapid advances in bioengineering and cell modification technologies, the next step in the field of sEVs will be the engineering or modification of exosome surfaces and contents, which may be more specific, extending its application to more complex medical fields.

AUTHOR CONTRIBUTIONS

L-QY: manuscript writing and approving final version of manuscript. F-X-ZL: study conduct, data analysis, and manuscript writing. XL, FX, S-KS, BG, L-ML, M-HZ, YW and Q-SX: data analysis. All authors: reviewed the manuscript. All authors contributed to the article and approved the submitted version.

FUNDING

This work was supported by funding from the National Natural Science Foundation of China (Nos. 81770881 and 82070910). Key R &; D plan of Hunan Province (2020SK2078).

REFERENCES

1. Cho NH, Shaw JE, Karuranga S, Huang Y, Da, Rocha Fernandez ,JD, Ohlrogge AW, et al. IDF Diabetes Atlas: Global Estimates of Diabetes Prevalence for 2017 and Projections for 2045. *Diabetes Res Clin Pract* (2018) 138:271–81. doi: 10.1016/j.diabres.2018.02.023
2. Saeedi Borujeni MJ, Esfandiary E, Taheripak G, Codoñer-Franch P, Alonso-Iglesias E, Mirzaei H. Molecular Aspects of Diabetes Mellitus: Resistin, microRNA, and Exosome. *J Cell Biochem* (2018) 119:1257–72. doi: 10.1002/jcb.26271
3. Yazdanpanah L, Nasiri M, Adarvishi S. Literature Review on the Management of Diabetic Foot Ulcer. *World J Diabetes* (2015) 6:37–53. doi: 10.4239/wjd.v6.i1.37
4. Wu T, Qiao S, Shi C, Wang S, Ji G. Metabolomics Window Into Diabetic Complications. *J Diabetes Investig* (2018) 9:244–55. doi: 10.1111/jdi.12723
5. Wang C, Zhang W, Wang Y, Wan H, Chen Y, Xia F, et al. Novel Associations Between Sex Hormones and Diabetic Vascular Complications in Men and Postmenopausal Women: A Cross-Sectional Study. *Cardiovasc Diabetol* (2019) 18:97. doi: 10.1186/s12933-019-0901-6
6. Atkinson MA, Eisenbarth GS, Michels AW. Type 1 Diabetes. *Lancet* (2014) 383:69–82. doi: 10.1016/S0140-6736(13)60591-7
7. Miller KM, Foster NC, Beck RW, Bergenstal RM, Dubose SN, Dimeglio LA, et al. Current State of Type 1 Diabetes Treatment in the U.S.: Updated Data From the T1D Exchange Clinic Registry. *Diabetes Care* (2015) 38:971–8. doi: 10.2337/dc15-0078
8. Lilly MA, Davis MF, Fabie JE, Terhune EB, Gallicano GI. Current Stem Cell Based Therapies in Diabetes. *Am J Stem Cells* (2016) 5:87–98.
9. Pokrywczynska M, Lanzoni G, Ricordi C. From Adult Pancreatic Islets to Stem Cells. *Principles Regenerative Med* (2019), 335–49. doi: 10.1016/B978-0-12-809880-6.00021-7
10. Dominici M, Le Blanc K, Mueller I, Slaper-Cortenbach I, Marini F, Krause D, et al. Minimal Criteria for Defining Multipotent Mesenchymal Stromal Cells. The International Society for Cellular Therapy Position Statement. *Cytotherapy* (2006) 8:315–7. doi: 10.1080/14653240600855905

11. Ebrahim N, Ahmed IA, Hussien NI, Dessouky AA, Farid AS. Mesenchymal Stem Cell-Derived Exosomes Ameliorated Diabetic Nephropathy by Autophagy Induction Through the mTOR Signaling Pathway. *Cells* (2018) 7:226. doi: 10.3390/cells7120226
12. Peng BY, Dubey NK, Mishra VK, Tsai FC, Dubey R, Deng WP. Addressing Stem Cell Therapeutic Approaches in Pathobiology of Diabetes and Its Complications. *J Diabetes Res* (2018) 2018:7806435. doi: 10.1155/2018/7806435
13. Labusca L, Herea DD, Mashayekhi K. Stem Cells as Delivery Vehicles for Regenerative Medicine-Challenges and Perspectives. *World J Stem Cells* (2018) 10:43–56. doi: 10.4252/wjsc.v10.i5.43
14. Lei LM, Lin X, Xu F, Shan SK, Guo B, Li FX, et al. Exosomes and Obesity-Related Insulin Resistance. *Front Cell Dev Biol* (2021) 9:651996. doi: 10.3389/fcell.2021.651996
15. Squillaro T, Peluso G, Galderisi U. Clinical Trials With Mesenchymal Stem Cells: An Update. *Cell Transplant* (2016) 25:829–48. doi: 10.3727/096368915X689622
16. Cantaluppi V, Biancone L, Figliolini F, Beltramo S, Medica D, Deregibus MC, et al. Microvesicles Derived From Endothelial Progenitor Cells Enhance Neoangiogenesis of Human Pancreatic Islets. *Cell Transplant* (2012) 21:1305–20. doi: 10.3727/096368911X627534
17. Zhang S, Chuah SJ, Lai RC, Hui JHP, Lim SK, Toh WS. MSC Exosomes Mediate Cartilage Repair by Enhancing Proliferation, Attenuating Apoptosis and Modulating Immune Reactivity. *Biomaterials* (2018) 156:16–27. doi: 10.1016/j.biomaterials.2017.11.028
18. Jiang ZZ, Liu YM, Niu X, Yin JY, Hu B, Guo SC, et al. Exosomes Secreted by Human Urine-Derived Stem Cells Could Prevent Kidney Complications From Type I Diabetes in Rats. *Stem Cell Res Ther* (2016) 7:24. doi: 10.1186/s13287-016-0287-2
19. Venkat P, Zacharek A, Landschoot-Ward J, Wang F, Culmone L, Chen Z, et al. Exosomes Derived From Bone Marrow Mesenchymal Stem Cells Harvested From Type Two Diabetes Rats Promotes Neurorestorative Effects After Stroke in Type Two Diabetes Rats. *Exp Neurol* (2020) 334:113456. doi: 10.1016/j.expneurol.2020.113456
20. Wang J, Mi Y, Wu S, You X, Huang Y, Zhu J, et al. Exosomes From Adipose-Derived Stem Cells Protect Against High Glucose-Induced Erectile Dysfunction by Delivery of Corin in a Streptozotocin-Induced Diabetic Rat Model. *Regener Ther* (2020) 14:227–33. doi: 10.1016/j.reth.2020.03.002
21. Zhu LL, Huang X, Yu W, Chen H, Chen Y, Dai YT. Transplantation of Adipose Tissue-Derived Stem Cell-Derived Exosomes Ameliorates Erectile Function in Diabetic Rats. *Andrologia* (2018) 50. doi: 10.1111/and.12871
22. Huo W, Li Y, Zhang Y, Li H. Mesenchymal Stem Cells-Derived Exosomal microRNA-21-5p Downregulates PDCD4 and Ameliorates Erectile Dysfunction in a Rat Model of Diabetes Mellitus. *FASEB J* (2020) 34:13345–60. doi: 10.1096/fj.202000102RR
23. Mathew B, Ravindran S, Liu X, Torres L, Chennakesavalu M, Huang CC, et al. Mesenchymal Stem Cell-Derived Extracellular Vesicles and Retinal Ischemia-Reperfusion. *Biomaterials* (2019) 197:146–60. doi: 10.1016/j.biomaterials.2019.01.016
24. Safwat A, Sabry D, Ragiae A, Amer E, Mahmoud RH, Shamardan RM. Adipose Mesenchymal Stem Cells-Derived Exosomes Attenuate Retina Degeneration of Streptozotocin-Induced Diabetes in Rabbits. *J Circ Biomark* (2018) 7:1849454418807827. doi: 10.1177/1849454418807827
25. Zhang W, Wang Y, Kong Y. Exosomes Derived From Mesenchymal Stem Cells Modulate miR-126 to Ameliorate Hyperglycemia-Induced Retinal Inflammation *Via* Targeting Hmgb1. *Invest Ophthalmol Vis Sci* (2019) 60:294–303. doi: 10.1167/iovs.18-25617
26. Wang Y, Ma WQ, Zhu Y, Han XQ, Liu N. Exosomes Derived From Mesenchymal Stromal Cells Pretreated With Advanced Glycation End Product-Bovine Serum Albumin Inhibit Calcification of Vascular Smooth Muscle Cells. *Front Endocrinol (Lausanne)* (2018) 9:524. doi: 10.3389/fendo.2018.00524
27. Jin J, Shi Y, Gong J, Zhao L, Li Y, He Q. Exosome Secreted From Adipose-Derived Stem Cells Attenuates Diabetic Nephropathy by Promoting Autophagy Flux and Inhibiting Apoptosis in Podocyte. *Stem Cell Res Ther* (2019) 10:95. doi: 10.1186/s13287-019-1177-1
28. Nagaishi K, Mizue Y, Chikenji T, Otani M, Nakano M, Konari N, et al. Mesenchymal Stem Cell Therapy Ameliorates Diabetic Nephropathy *via* the Paracrine Effect of Renal Trophic Factors Including Exosomes. *Sci Rep* (2016) 6:34842. doi: 10.1038/srep34842
29. Barutta F, Tricarico M, Corbelli A, Annaratone L, Pinach S, Grimaldi S, et al. Urinary Exosomal microRNAs in Incipient Diabetic Nephropathy. *PloS One* (2013) 8:e73798. doi: 10.1371/journal.pone.0073798
30. Duan YR, Chen BP, Chen F, Yang SX, Zhu CY, Ma YL, et al. Exosomal microRNA-16-5p From Human Urine-Derived Stem Cells Ameliorates Diabetic Nephropathy Through Protection of Podocyte. *J Cell Mol Med* (2019) 25:10798–813. doi: 10.1111/jcmm.14558
31. Jin J, Wang Y. Exosomal miRNA-215-5p Derived From Adipose-Derived Stem Cells Attenuates Epithelial-Mesenchymal Transition of Podocytes by Inhibiting Zeb2. *BioMed Res Int* (2020) 2020:2685305. doi: 10.1155/2020/2685305
32. Xiang E, Han B, Zhang Q, Rao W, Wang Z, Chang C, et al. Human Umbilical Cord-Derived Mesenchymal Stem Cells Prevent the Progression of Early Diabetic Nephropathy Through Inhibiting Inflammation and Fibrosis. *Stem Cell Res Ther* (2020) 11:336. doi: 10.1186/s13287-020-01852-y
33. Liu W, Yu M, Xie D, Wang L, Ye C, Zhu Q, et al. Melatonin-Stimulated MSC-Derived Exosomes Improve Diabetic Wound Healing Through Regulating Macrophage M1 and M2 Polarization by Targeting the PTEN/AKT Pathway. *Stem Cell Res Ther* (2020) 11:259. doi: 10.1186/s13287-020-01756-x
34. Dalirfardouei R, Jamialahmadi K, Jafarian AH, Mahdipour E. Promising Effects of Exosomes Isolated From Menstrual Blood-Derived Mesenchymal Stem Cell on Wound-Healing Process in Diabetic Mouse Model. *J Tissue Eng Regener Med* (2019) 13:555–68. doi: 10.1002/term.2799
35. Shi Q, Qian Z, Liu D, Sun J, Wang X, Liu H, et al. GMSC-Derived Exosomes Combined With a Chitosan/Silk Hydrogel Sponge Accelerates Wound Healing in a Diabetic Rat Skin Defect Model. *Front Physiol* (2017) 8:904. doi: 10.3389/fphys.2017.00904
36. Ti D, Hao H, Tong C, Liu J, Dong L, Zheng J, et al. LPS-Preconditioned Mesenchymal Stromal Cells Modify Macrophage Polarization for Resolution of Chronic Inflammation *via* exosome-shuttled let-7b. *J Transl Med* (2015) 13:308. doi: 10.1186/s12967-015-0642-6
37. Li X, Xie X, Lian W, Shi R, Han S, Zhang H, et al. Exosomes From Adipose-Derived Stem Cells Overexpressing Nrf2 Accelerate Cutaneous Wound Healing by Promoting Vascularization in a Diabetic Foot Ulcer Rat Model. *Exp Mol Med* (2018) 50:1–14. doi: 10.1038/s12276-018-0058-5
38. Hu Y, Rao SS, Wang ZX, Cao J, Tan YJ, Luo J, et al. Exosomes From Human Umbilical Cord Blood Accelerate Cutaneous Wound Healing Through miR-21-3p-Mediated Promotion of Angiogenesis and Fibroblast Function. *Theranostics* (2018) 8:169–84. doi: 10.7150/thno.21234
39. Chen CY, Rao SS, Ren L, Hu XK, Tan YJ, Hu Y, et al. Exosomal DMBT1 From Human Urine-Derived Stem Cells Facilitates Diabetic Wound Repair by Promoting Angiogenesis. *Theranostics* (2018) 8:1607–23. doi: 10.7150/thno.22958
40. Shi R, Jin Y, Hu W, Lian W, Cao C, Han S, et al. Exosomes Derived From Mmu_Circ_0000250-Modified Adipose-Derived Mesenchymal Stem Cells Promote Wound Healing in Diabetic Mice by Inducing miR-128-3p/SIRT1-Mediated Autophagy. *Am J Physiol Cell Physiol* (2020) 318:C848–c856. doi: 10.1152/ajpcell.00041.2020
41. Shiekh PA, Singh A, Kumar A. Exosome Laden Oxygen Releasing Antioxidant and Antibacterial Cryogel Wound Dressing OxOBand Alleviate Diabetic and Infectious Wound Healing. *Biomaterials* (2020) 249:120020. doi: 10.1016/j.biomaterials.2020.120020
42. Fan B, Li C, Szalad A, Wang L, Pan W, Zhang R, et al. Mesenchymal Stromal Cell-Derived Exosomes Ameliorate Peripheral Neuropathy in a Mouse Model of Diabetes. *Diabetologia* (2020) 63:431–43. doi: 10.1007/s00125-019-05043-0
43. Nakano M, Nagaishi K, Konari N, Saito Y, Chikenji T, Mizue Y, et al. Bone Marrow-Derived Mesenchymal Stem Cells Improve Diabetes-Induced Cognitive Impairment by Exosome Transfer Into Damaged Neurons and Astrocytes. *Sci Rep* (2016) 6:24805. doi: 10.1038/srep24805
44. Xin H, Li Y, Liu Z, Wang X, Shang X, Cui Y, et al. MiR-133b Promotes Neural Plasticity and Functional Recovery After Treatment of Stroke With Multipotent Mesenchymal Stromal Cells in Rats *via* Transfer of Exosome-Enriched Extracellular Particles. *Stem Cells* (2013) 31:2737–46. doi: 10.1002/stem.1409

45. Kubota K, Nakano M, Kobayashi E, Mizue Y, Chikenji T, Otani M, et al. An Enriched Environment Prevents Diabetes-Induced Cognitive Impairment in Rats by Enhancing Exosomal miR-146a Secretion From Endogenous Bone Marrow-Derived Mesenchymal Stem Cells. *PloS One* (2018) 13:e0204252. doi: 10.1371/journal.pone.0204252
46. Shaihov-Teper O, Ram E, Ballan N, Brzezinski RY, Naftali-Shani N, Masoud R, et al. Extracellular Vesicles From Epicardial Fat Facilitate Atrial Fibrillation. *Circulation* (2021) 143:2475–93. doi: 10.1161/CIRCULATIONAHA.120.052009
47. Théry C, Witwer KW. Minimal Information for Studies of Extracellular Vesicles 2018 (MISEV2018): A Position Statement of the International Society for Extracellular Vesicles and Update of the MISEV2014 Guidelines. *J Extracell Vesicles* (2018) 7:1535750. doi: 10.1080/20013078.2018.1535750
48. Ahmadi M, Rezaie J. Tumor Cells Derived-Exosomes as Angiogenenic Agents: Possible Therapeutic Implications. *J Transl Med* (2020) 18:249. doi: 10.1186/s12967-020-02426-5
49. He C, Zheng S, Luo Y, Wang B. Exosome Theranostics: Biology and Translational Medicine. *Theranostics* (2018) 8:237–55. doi: 10.7150/thno.21945
50. Pegtel DM, Gould SJ. Exosomes. *Annu Rev Biochem* (2019) 88:487–514. doi: 10.1146/annurev-biochem-013118-111902
51. Zhang D, Lee H, Wang X, Groot M, Sharma L, Dela Cruz CS, et al. A Potential Role of Microvesicle-Containing miR-223/142 in Lung Inflammation. *Thorax* (2019) 74:865–74. doi: 10.1136/thoraxjnl-2018-212994
52. Spaull R, Mcpherson B, Gialeli A, Clayton A, Uney J, Heep A, et al. Exosomes Populate the Cerebrospinal Fluid of Preterm Infants With Post-Haemorrhagic Hydrocephalus. *Int J Dev Neurosci* (2019) 73:59–65. doi: 10.1016/j.ijdevneu.2019.01.004
53. Nawaz M, Malik MI, Zhang H, Hassan IA, Cao J, Zhou Y, et al. Proteomic Analysis of Exosome-Like Vesicles Isolated From Saliva of the Tick Haemaphysalis Longicornis. *Front Cell Infect Microbiol* (2020) 10:542319. doi: 10.3389/fcimb.2020.542319
54. Grossen P, Portmann M, Koller E, Duschmalé M, Minz T, Sewing S, et al. Evaluation of Bovine Milk Extracellular Vesicles for the Delivery of Locked Nucleic Acid Antisense Oligonucleotides. *Eur J Pharm Biopharm* (2021) 158:198–210. doi: 10.1016/j.ejpb.2020.11.012
55. Li FX, Liu JJ, Xu F, Lin X, Zhong JY, Wu F, et al. Role of Tumor-Derived Exosomes in Bone Metastasis. *Oncol Lett* (2019) 18:3935–45. doi: 10.3892/ol.2019.10776
56. Rezaie J, Aslan C, Ahmadi M, Zolbanin NM, Kashanchi F, Jafari R. The Versatile Role of Exosomes in Human Retroviral Infections: From Immunopathogenesis to Clinical Application. *Cell Biosci* (2021) 11:19. doi: 10.1186/s13578-021-00537-0
57. Shan SK, Lin X, Li F, Xu F, Zhong JY, Guo B, et al. Exosomes and Bone Disease. *Curr Pharm Des* (2019) 25:4536–49. doi: 10.2174/1381612825666191127114054
58. Wu F, Li F, Lin X, Xu F, Cui RR, Zhong JY, et al. Exosomes Increased Angiogenesis in Papillary Thyroid Cancer Microenvironment. *Endocr Relat Cancer* (2019) 26:525–38. doi: 10.1530/ERC-19-0008
59. Li P, Kaslan M, Lee SH, Yao J, Gao Z. Progress in Exosome Isolation Techniques. *Theranostics* (2017) 7:789–804. doi: 10.7150/thno.18133
60. Nikfarjam S, Rezaie J, Zolbanin NM, Jafari R. Mesenchymal Stem Cell Derived-Exosomes: A Modern Approach in Translational Medicine. *J Trans Med* (2020) 18:449. doi: 10.1186/s12967-020-02622-3
61. Colombo M, Raposo G, Théry C. Biogenesis, Secretion, and Intercellular [interactions of Exosomes and Other Extracellular Vesicles. *Annu Rev Cell Dev Biol* (2014) 30:255–89. doi: 10.1146/annurev-cellbio-101512-122326
62. Rezaie J, Nejati V, Khaksar M, Oryan A, Aghamohamadzadeh N, Shariatzadeh MA, et al. Diabetic Sera Disrupted the Normal Exosome Signaling Pathway in Human Mesenchymal Stem Cells. *Vitro Cell Tissue Res* (2018) 374:555–65. doi: 10.1007/s00441-018-2895-x
63. Lin X, Zhu T, Xu F, Zhong JY, Li F, Shan SK, et al. Plasma Exosomes Derived From Patients With End-Stage Renal Disease and Renal Transplant Recipients Have Different Effects on Vascular Calcification. *Front Cell Dev Biol* (2020) 8:618228. doi: 10.3389/fcell.2020.618228
64. Nikfarjam S, Rezaie J, Kashanchi F, Jafari R. Dexosomes as a Cell-Free Vaccine for Cancer Immunotherapy. *J Exp Clin Cancer Res* (2020) 39:258. doi: 10.1186/s13046-020-01781-x
65. Arima Y, Liu W, Takahashi Y. Effects of Localization of Antigen Proteins in Antigen-Loaded Exosomes on Efficiency of Antigen Presentation. *Mol Pharm* (2019) 16:2309–14. doi: 10.1021/acs.molpharmaceut.8b01093
66. Hardin H, Helein H, Meyer K, Robertson S, Zhang R, Zhong W, et al. Thyroid Cancer Stem-Like Cell Exosomes: Regulation of EMT *via* Transfer of lncRNAs. *Lab Invest* (2018) 98:1133–42. doi: 10.1038/s41374-018-0065-0
67. Luo ZW, Li FX, Liu YW, Rao SS, Yin H, Huang J, et al. Aptamer-Functionalized Exosomes From Bone Marrow Stromal Cells Target Bone to Promote Bone Regeneration. *Nanoscale* (2019) 11:20884–92. doi: 10.1039/C9NR02791B
68. Yu B, Zhang X, Li X. Exosomes Derived From Mesenchymal Stem Cells. *Int J Mol Sci* (2014) 15:4142–57. doi: 10.3390/ijms15034142
69. Torre P, Flores AI. Current Status and Future Prospects of Perinatal Stem Cells. *Genes (Basel)* (2020) 12:6. doi: 10.3390/genes12010006
70. Phinney DG, Prockop DJ. Concise Review: Mesenchymal Stem/Multipotent Stromal Cells: The State of Transdifferentiation and Modes of Tissue Repair–Current Views. *Stem Cells* (2007) 25:2896–902. doi: 10.1634/stemcells.2007-0637
71. Katsha AM, Ohkouchi S, Xin H, Kanehira M, Sun R, Nukiwa T, et al. Paracrine Factors of Multipotent Stromal Cells Ameliorate Lung Injury in an Elastase-Induced Emphysema Model. *Mol Ther* (2011) 19:196–203. doi: 10.1038/mt.2010.192
72. Lai RC, Chen TS, Lim SK. Mesenchymal Stem Cell Exosome: A Novel Stem Cell-Based Therapy for Cardiovascular Disease. *Regener Med* (2011) 6:481–92. doi: 10.2217/rme.11.35
73. Jeppesen DK, Fenix AM, Franklin JL, Higginbotham JN, Zhang Q, Zimmerman LJ, et al. Reassessment of Exosome Composition. *Cell* (2019) 177:428–445.e418. doi: 10.1016/j.cell.2019.02.029
74. Yoo KH, Jang IK, Lee MW, Kim HE, Yang MS, Eom Y, et al. Comparison of Immunomodulatory Properties of Mesenchymal Stem Cells Derived From Adult Human Tissues. *Cell Immunol* (2009) 259:150–6. doi: 10.1016/j.cellimm.2009.06.010
75. Yeo RW, Lai RC, Zhang B, Tan SS, Yin Y, Teh BJ, et al. Mesenchymal Stem Cell: An Efficient Mass Producer of Exosomes for Drug Delivery. *Adv Drug Deliv Rev* (2013) 65:336–41. doi: 10.1016/j.addr.2012.07.001
76. Altaner C, Altanerova U. Mesenchymal Stem Cell Exosome-Mediated Prodrug Gene Therapy for Cancer. *Methods Mol Biol* (2019) 1895:75–85. doi: 10.1007/978-1-4939-8922-5_6
77. Castaño C, Novials A. Exosomes and Diabetes. *Diabetes Metab Res Rev* (2019) 35:e3107. doi: 10.1002/dmrr.3107
78. Zheng M, Huang M, Ma X, Chen H, Gao X. Harnessing Exosomes for the Development of Brain Drug Delivery Systems. *Bioconjug Chem* (2019) 30:994–1005. doi: 10.1021/acs.bioconjchem.9b00085
79. Munoz JL, Bliss SA, Greco SJ, Ramkissoon SH, Ligon KL, Rameshwar P. Delivery of Functional Anti-miR-9 by Mesenchymal Stem Cell-Derived Exosomes to Glioblastoma Multiforme Cells Conferred Chemosensitivity. *Mol Ther Nucleic Acids* (2013) 2:e126. doi: 10.1038/mtna.2013.60
80. Yu B, Gong M, Wang Y, Millard RW, Pasha Z, Yang Y, et al. Cardiomyocyte Protection by GATA-4 Gene Engineered Mesenchymal Stem Cells Is Partially Mediated by Translocation of miR-221 in Microvesicles. *PLoS One* (2013) 8:e73304. doi: 10.1371/journal.pone.0073304
81. Furlani D, Ugurlucan M, Ong L, Bieback K, Pittermann E, Westien I, et al. Is the Intravascular Administration of Mesenchymal Stem Cells Safe? Mesenchymal Stem Cells and Intravital Microscopy. *Microvasc Res* (2009) 77:370–6. doi: 10.1016/j.mvr.2009.02.001
82. Lou G, Chen Z, Zheng M, Liu Y. Mesenchymal Stem Cell-Derived Exosomes as a New Therapeutic Strategy for Liver Diseases. *Exp Mol Med* (2017) 49:e346. doi: 10.1038/emm.2017.63
83. Guay C, Regazzi R. Exosomes as New Players in Metabolic Organ Cross-Talk. *Diabetes Obes Metab* (2017) 19(Suppl 1):137–46. doi: 10.1111/dom.13027
84. Lin X, Li F, Xu F, Cui RR, Xiong D, Zhong JY, et al. Aberration Methylation of miR-34b was Involved in Regulating Vascular Calcification by Targeting Notch1. *Aging (Albany NY)* (2019) 11:3182–97. doi: 10.18632/aging.101973
85. Montecalvo A, Larregina AT, Shufesky WJ, Stolz DB, Sullivan ML, Karlsson JM, et al. Mechanism of Transfer of Functional microRNAs Between Mouse Dendritic Cells *via* Exosomes. *Blood* (2012) 119:756–66. doi: 10.1182/blood-2011-02-338004

86. Garcia-Contreras M, Brooks RW, Boccuzzi L, Robbins PD, Ricordi C. Exosomes as Biomarkers and Therapeutic Tools for Type 1 Diabetes Mellitus. *Eur Rev Med Pharmacol Sci* (2017) 21:2940–56.
87. Cianciaruso C, Phelps EA, Pasquier M, Hamelin R, Demurtas D, Alibashe Ahmed M, et al. Primary Human and Rat β-Cells Release the Intracellular Autoantigens GAD65, IA-2, and Proinsulin in Exosomes Together With Cytokine-Induced Enhancers of Immunity. *Diabetes* (2017) 66:460–73. doi: 10.2337/db16-0671
88. La Marca V, Fierabracci A. Insights Into the Diagnostic Potential of Extracellular Vesicles and Their miRNA Signature From Liquid Biopsy as Early Biomarkers of Diabetic Micro/Macrovascular Complications. *Int J Mol Sci* (2017) 18:1974. doi: 10.3390/ijms18091974
89. Salem MA, Adly AA, Ismail EA, Darwish YW, Kamel HA. Platelets Microparticles as a Link Between Micro- and Macro-Angiopathy in Young Patients With Type 1 Diabetes. *Platelets* (2015) 26:682–8. doi: 10.3109/09537104.2015.1018880
90. Katayama M, Wiklander OPB, Fritz T, Caidahl K, El-Andaloussi S, Zierath JR. Circulating Exosomal miR-20b-5p Is Elevated in Type 2 Diabetes and Could Impair Insulin Action in Human Skeletal Muscle. *Diabetes* (2019) 3:515–26. doi: 10.2337/db18-0470
91. Feng B, Chakrabarti S. miR-320 Regulates Glucose-Induced Gene Expression in Diabetes. *ISRN Endocrinol* (2012) 2012:549875. doi: 10.5402/2012/549875
92. De S, Kuwahara S, Hosojima M, Ishikawa T, Kaseda R, Sarkar P, et al. Exocytosis-Mediated Urinary Full-Length Megalin Excretion Is Linked With the Pathogenesis of Diabetic Nephropathy. *Diabetes* (2017) 66:1391–404. doi: 10.2337/db16-1031
93. Rossi L, Nicoletti MC, Carmosino M. Urinary Excretion of Kidney Aquaporins as Possible Diagnostic Biomarker of Diabetic Nephropathy. *J Diabetes Res* (2017) 2017:4360357. doi: 10.1155/2017/4360357
94. Sabry D, Marzouk S, Zakaria R, Ibrahim HA, Samir M. The Effect of Exosomes Derived From Mesenchymal Stem Cells in the Treatment of Induced Type 1 Diabetes Mellitus in Rats. *Biotechnol Lett* (2020) 42:1597–610. doi: 10.1007/s10529-020-02908-y
95. Mahdipour E, Salmasi Z, Sabeti N. Potential of Stem Cell-Derived Exosomes to Regenerate β Islets Through Pdx-1 Dependent Mechanism in a Rat Model of Type 1 Diabetes. *J Cell Physiol* (2019) 234:20310–21. doi: 10.1002/jcp.28631
96. Chen J, Chen J, Cheng Y, Fu Y, Zhao H, Tang M, et al. Mesenchymal Stem Cell-Derived Exosomes Protect Beta Cells Against Hypoxia-Induced Apoptosis *via* miR-21 by Alleviating ER Stress and Inhibiting P38 MAPK Phosphorylation. *Stem Cell Res Ther* (2020) 11:97. doi: 10.1186/s13287-020-01610-0
97. Keshtkar S, Kaviani M, Sarvestani FS, Ghahremani MH, Aghdaei MH, Al-Abdullah IH, et al. Exosomes Derived From Human Mesenchymal Stem Cells Preserve Mouse Islet Survival and Insulin Secretion Function. *Excli J* (2020) 19:1064–80. doi: 10.17179/excli2020-2451
98. Kordelas L, Rebmann V, Ludwig AK, Radtke S, Ruesing J, Doeppner TR, et al. MSC-Derived Exosomes: A Novel Tool to Treat Therapy-Refractory Graft-Versus-Host Disease. *Leukemia* (2014) 28:970–3. doi: 10.1038/leu.2014.41
99. Lee YH, Kim J, Park K, Lee MS. β-Cell Autophagy: Mechanism and Role in β-Cell Dysfunction. *Mol Metab* (2019) 27s:S92–s103. doi: 10.1016/j.molmet.2019.06.014
100. He Q, Wang L, Zhao R, Yan F, Sha S, Cui C, et al. Mesenchymal Stem Cell-Derived Exosomes Exert Ameliorative Effects in Type 2 Diabetes by Improving Hepatic Glucose and Lipid Metabolism *via* Enhancing Autophagy. *Stem Cell Res Ther* (2020) 11:223. doi: 10.1186/s13287-020-01731-6
101. Sun Y, Shi H, Yin S, Ji C, Zhang X, Zhang B, et al. Human Mesenchymal Stem Cell Derived Exosomes Alleviate Type 2 Diabetes Mellitus by Reversing Peripheral Insulin Resistance and Relieving β-Cell Destruction. *ACS Nano* (2018) 12:7613–28. doi: 10.1021/acsnano.7b07643
102. Su T, Xiao Y, Xiao Y, Guo Q, Li C, Huang Y, et al. Bone Marrow Mesenchymal Stem Cells-Derived Exosomal MiR-29b-3p Regulates Aging-Associated Insulin Resistance. *ACS Nano* (2019) 13:2450–62. doi: 10.1021/acsnano.8b09375
103. Kawano Y, Nakae J, Watanabe N, Kikuchi T, Tateya S, Tamori Y, et al. Colonic Pro-Inflammatory Macrophages Cause Insulin Resistance in an Intestinal Ccl2/Ccr2-Dependent Manner. *Cell Metab* (2016) 24:295–310. doi: 10.1016/j.cmet.2016.07.009
104. Zaccardi F, Webb DR, Yates T, Davies MJ. Pathophysiology of Type 1 and Type 2 Diabetes Mellitus: A 90-Year Perspective. *Postgrad Med J* (2016) 92:63–9. doi: 10.1136/postgradmedj-2015-133281
105. Xie Z, Hao H, Tong C, Cheng Y, Liu J, Pang Y, et al. Human Umbilical Cord-Derived Mesenchymal Stem Cells Elicit Macrophages Into an Anti-Inflammatory Phenotype to Alleviate Insulin Resistance in Type 2 Diabetic Rats. *Stem Cells* (2016) 34:627–39. doi: 10.1002/stem.2238
106. Esser N, Legrand-Poels S, Piette J, Scheen AJ, Paquot N. Inflammation as a Link Between Obesity, Metabolic Syndrome and Type 2 Diabetes. *Diabetes Res Clin Pract* (2014) 105:141–50. doi: 10.1016/j.diabres.2014.04.006
107. Zhao H, Shang Q, Pan Z, Bai Y, Li Z, Zhang H, et al. Exosomes From Adipose-Derived Stem Cells Attenuate Adipose Inflammation and Obesity Through Polarizing M2 Macrophages and Beiging in White Adipose Tissue. *Diabetes* (2018) 67:235–47. doi: 10.2337/db17-0356
108. Silva DG, Petrovsky N, Socha L, Slattery R, Gatenby P, Charlton B. Mechanisms of Accelerated Immune-Mediated Diabetes Resulting From Islet Beta Cell Expression of a Fas Ligand Transgene. *J Immunol* (2003) 170:4996–5002. doi: 10.4049/jimmunol.170.10.4996
109. Wen D, Peng Y, Liu D, Weizmann Y, Mahato RI. Mesenchymal Stem Cell and Derived Exosome as Small RNA Carrier and Immunomodulator to Improve Islet Transplantation. *J Control Release* (2016) 238:166–75. doi: 10.1016/j.jconrel.2016.07.044
110. Kim SS, Kim JH, Kim IJ. Current Challenges in Diabetic Nephropathy: Early Diagnosis and Ways to Improve Outcomes. *Endocrinol Metab (Seoul)* (2016) 31:245–53. doi: 10.3803/EnM.2016.31.2.245
111. Abcouwer SF, Gardner TW. Diabetic Retinopathy: Loss of Neuroretinal Adaptation to the Diabetic Metabolic Environment. *Ann N Y Acad Sci* (2014) 1311:174–90. doi: 10.1111/nyas.12412
112. Fiori A, Terlizzi V, Kremer H, Gebauer J, Hammes HP, Harmsen MC, et al. Mesenchymal Stromal/Stem Cells as Potential Therapy in Diabetic Retinopathy. *Immunobiology* (2018) 223:729–43. doi: 10.1016/j.imbio.2018.01.001
113. Harvey HB, Wu CC, Gilman MD, Vartanians V, Halpern EF, Pandharipande PV, et al. Correlation of the Strength of Recommendations for Additional Imaging to Adherence Rate and Diagnostic Yield. *J Am Coll Radiol* (2015) 12:1016–22. doi: 10.1016/j.jacr.2015.03.038
114. Khaksar M, Sayyari M, Rezaie J, Pouyafar A, Montazersaheb S, Rahbarghazi R. High Glucose Condition Limited the Angiogenic/Cardiogenic Capacity of Murine Cardiac Progenitor Cells in *In Vitro* and *In Vivo* Milieu. *Cell Biochem Funct* (2018) 36:346–56. doi: 10.1002/cbf.3354
115. Liao XB, Zhang ZY, Yuan K, Liu Y, Feng X, Cui RR, et al. MiR-133a Modulates Osteogenic Differentiation of Vascular Smooth Muscle Cells. *Endocrinology* (2013) 154:3344–52. doi: 10.1210/en.2012-2236
116. Peng YQ, Xiong D, Lin X, Cui RR, Xu F, Zhong JY, et al. Oestrogen Inhibits Arterial Calcification by Promoting Autophagy. *Sci Rep* (2017) 7:3549. doi: 10.1038/s41598-017-03801-x
117. Lin X, Xu F, Cui RR, Xiong D, Zhong JY, Zhu T, et al. Arterial Calcification Is Regulated *Via* an miR-204/DNMT3a Regulatory Circuit Both *In Vitro* and in Female Mice. *Endocrinology* (2018) 159:2905–16. doi: 10.1210/en.2018-00320
118. Xu F, Zhong JY, Lin X, Shan SK, Guo B, Zheng MH, et al. Melatonin Alleviates Vascular Calcification and Ageing Through Exosomal miR-204/miR-211 Cluster in a Paracrine Manner. *J Pineal Res* (2020) 68:e12631. doi: 10.1111/jpi.12631
119. Bodiga VL, Eda SR, Bodiga S. Advanced Glycation End Products: Role in Pathology of Diabetic Cardiomyopathy. *Heart Fail Rev* (2014) 19:49–63. doi: 10.1007/s10741-013-9374-y
120. Devi TS, Lee I, Hüttemann M, Kumar A, Nantwi KD, Singh LP. TXNIP Links Innate Host Defense Mechanisms to Oxidative Stress and Inflammation in Retinal Muller Glia Under Chronic Hyperglycemia: Implications for Diabetic Retinopathy. *Exp Diabetes Res* (2012) 2012:438238. doi: 10.1155/2012/438238
121. Newton WC, Kim JW, Luo JZQ, Luo L. Stem Cell-Derived Exosomes: A Novel Vector for Tissue Repair and Diabetic Therapy. *J Mol Endocrinol* (2017) 59:R155–r165. doi: 10.1530/JME-17-0080
122. Wrighten SA, Piroli GG, Grillo CA, Reagan LP. A Look Inside the Diabetic Brain: Contributors to Diabetes-Induced Brain Aging. *Biochim Biophys Acta* (2009) 1792:444–53. doi: 10.1016/j.bbadis.2008.10.013

123. Cui C, Ye X, Chopp M, Venkat P, Zacharek A, Yan T, et al. miR-145 Regulates Diabetes-Bone Marrow Stromal Cell-Induced Neurorestorative Effects in Diabetes Stroke Rats. *Stem Cells Transl Med* (2016) 5:1656–67. doi: 10.5966/sctm.2015-0349
124. Brownlee M. Biochemistry and Molecular Cell Biology of Diabetic Complications. *Nature* (2001) 414:813–20. doi: 10.1038/414813a
125. Said G. Diabetic Neuropathy–A Review. *Nat Clin Pract Neurol* (2007) 3:331–40. doi: 10.1038/ncpneuro0504
126. Thorve VS, Kshirsagar AD, Vyawahare NS, Joshi VS, Ingale KG, Mohite RJ. Diabetes-Induced Erectile Dysfunction: Epidemiology, Pathophysiology and Management. *J Diabetes Complications* (2011) 25:129–36. doi: 10.1016/j.jdiacomp.2010.03.003
127. Fandel TM, Albersen M, Lin G, Qiu X, Ning H, Banie L, et al. Recruitment of Intracavernously Injected Adipose-Derived Stem Cells to the Major Pelvic Ganglion Improves Erectile Function in a Rat Model of Cavernous Nerve Injury. *Eur Urol* (2012) 61:201–10. doi: 10.1016/j.eururo.2011.07.061
128. Matz EL, Terlecki R, Zhang Y, Jackson J, Atala A. Stem Cell Therapy for Erectile Dysfunction. *Sex Med Rev* (2019) 7:321–8. doi: 10.1016/j.sxmr.2017.12.008
129. Boulton AJ, Vileikyte L, Ragnarson-Tennvall G, Apelqvist J. The Global Burden of Diabetic Foot Disease. *Lancet* (2005) 366:1719–24. doi: 10.1016/S0140-6736(05)67698-2
130. Geiger A, Walker A, Nissen E. Human Fibrocyte-Derived Exosomes Accelerate Wound Healing in Genetically Diabetic Mice. *Biochem Biophys Res Commun* (2015) 467:303–9. doi: 10.1016/j.bbrc.2015.09.166
131. Zhou Q, Gallagher R, Ufret-Vincenty R, Li X, Olson EN, Wang S. Regulation of Angiogenesis and Choroidal Neovascularization by Members of microRNA-23~27~24 Clusters. *Proc Natl Acad Sci USA* (2011) 108:8287–92. doi: 10.1073/pnas.1105254108
132. Madhyastha R, Madhyastha H, Pengjam Y, Nakajima Y, Omura S, Maruyama M. NFkappaB Activation Is Essential for miR-21 Induction by Tgfβ1 in High Glucose Conditions. *Biochem Biophys Res Commun* (2014) 451:615–21. doi: 10.1016/j.bbrc.2014.08.035
133. Zhang N, Geng T, Wang Z, Zhang R, Cao T, Camporez JP, et al. Elevated Hepatic Expression of H19 Long Noncoding RNA Contributes to Diabetic Hyperglycemia. *JCI Insight* (2018) 3:e120304. doi: 10.1172/jci.insight.120304
134. Chen JJ, Zhou SH. Mesenchymal Stem Cells Overexpressing MiR-126 Enhance Ischemic Angiogenesis *via* the AKT/ERK-Related Pathway. *Cardiol J* (2011) 18:675–81. doi: 10.5603/CJ.2011.0032
135. Hu J, Zeng L, Huang J, Wang G, Lu H. miR-126 Promotes Angiogenesis and Attenuates Inflammation After Contusion Spinal Cord Injury in Rats. *Brain Res* (2015) 1608:191–202. doi: 10.1016/j.brainres.2015.02.036
136. Amin KN, Umapathy D, Anandharaj A, Ravichandran J, Sasikumar CS, Chandra SKR, et al. miR-23c Regulates Wound Healing by Targeting Stromal Cell-Derived Factor-1α (SDF-1α/CXCL12) Among Patients With Diabetic Foot Ulcer. *Microvasc Res* (2020) 127:103924. doi: 10.1016/j.mvr.2019.103924
137. An T, Chen Y. Mesenchymal Stromal Cell-Derived Extracellular Vesicles in the Treatment of Diabetic Foot Ulcers: Application and Challenges. *Stem Cell Rev Rep* (2020) 17:369–78. doi: 10.1007/s12015-020-10014-9
138. Wang C, Wang M, Xu T, Zhang X, Lin C, Gao W, et al. Engineering Bioactive Self-Healing Antibacterial Exosomes Hydrogel for Promoting Chronic Diabetic Wound Healing and Complete Skin Regeneration. *Theranostics* (2019) 9:65–76. doi: 10.7150/thno.29766
139. Guo SC, Tao SC, Yin WJ, Qi X, Yuan T, Zhang CQ. Exosomes Derived From Platelet-Rich Plasma Promote the Re-Epithelization of Chronic Cutaneous Wounds *via* Activation of YAP in a Diabetic Rat Model. *Theranostics* (2017) 7:81–96. doi: 10.7150/thno.16803
140. Kranendonk ME, Visseren FL, Van Balkom BW, Nolte-'T Hoen EN, Van Herwaarden JA, De Jager W, et al. Human Adipocyte Extracellular Vesicles in Reciprocal Signaling Between Adipocytes and Macrophages. *Obes (Silver Spring)* (2014) 22:1296–308. doi: 10.1002/oby.20679
141. Zhang Y, Mei H, Chang X, Chen F, Zhu Y, Han X. Adipocyte-Derived Microvesicles From Obese Mice Induce M1 Macrophage Phenotype Through Secreted miR-155. *J Mol Cell Biol* (2016) 8:505–17. doi: 10.1093/jmcb/mjw040
142. Kang T, Jones TM, Naddell C, Bacanamwo M, Calvert JW, Thompson WE, et al. Adipose-Derived Stem Cells Induce Angiogenesis *via* Microvesicle Transport of miRNA-31. *Stem Cells Transl Med* (2016) 5:440–50. doi: 10.5966/sctm.2015-0177
143. Liang X, Zhang L, Wang S, Han Q, Zhao RC. Exosomes Secreted by Mesenchymal Stem Cells Promote Endothelial Cell Angiogenesis by Transferring miR-125a. *J Cell Sci* (2016) 129:2182–9. doi: 10.1242/jcs.170373
144. Hu L, Wang J, Zhou X, Xiong Z, Zhao J, Yu R, et al. Exosomes Derived From Human Adipose Mensenchymal Stem Cells Accelerates Cutaneous Wound Healing *via* Optimizing the Characteristics of Fibroblasts. *Sci Rep* (2016) 6:32993. doi: 10.1038/srep32993
145. Blazquez R, Sanchez-Margallo FM, de la Rosa O, Dalemans W, Alvarez V, Tarazona R, et al. Immunomodulatory Potential of Human Adipose Mesenchymal Stem Cells Derived Exosomes on *In Vitro* Stimulated T Cells. *Front Immunol* (2014) 5:556. doi: 10.3389/fimmu.2014.00556
146. Wang L, Hu L, Zhou X, Xiong Z, Zhang C, Shehada HMA, et al. Exosomes Secreted by Human Adipose Mesenchymal Stem Cells Promote Scarless Cutaneous Repair by Regulating Extracellular Matrix Remodelling. *Sci Rep* (2017) 7:13321. doi: 10.1038/s41598-017-12919-x
147. Bagno L, Hatzistergos KE, Balkan W, Hare JM. Mesenchymal Stem Cell-Based Therapy for Cardiovascular Disease: Progress and Challenges. *Mol Ther* (2018) 7:1610–23. doi: 10.1016/j.ymthe.2018.05.009
148. Basu J, Ludlow JW. Exosomes for Repair, Regeneration and Rejuvenation. *Expert Opin Biol Ther* (2016) 16:489–506. doi: 10.1517/14712598.2016.1131976
149. Nassar W, El-Ansary M, Sabry D, Mostafa MA, Fayad T, Kotb E, et al. Umbilical Cord Mesenchymal Stem Cells Derived Extracellular Vesicles Can Safely Ameliorate the Progression of Chronic Kidney Diseases. *Biomater Res* (2016) 20:21. doi: 10.1186/s40824-016-0068-0
150. Wang X, Gu H, Huang W, Peng J, Li Y, Yang L, et al. Hsp20-Mediated Activation of Exosome Biogenesis in Cardiomyocytes Improves Cardiac Function and Angiogenesis in Diabetic Mice. *Diabetes* (2016) 65:3111–28. doi: 10.2337/db15-1563
151. Tomasoni S, Longaretti L, Rota C, Morigi M, Conti S, Gotti E, et al. Transfer of Growth Factor Receptor mRNA *via* Exosomes Unravels the Regenerative Effect of Mesenchymal Stem Cells. *Stem Cells Dev* (2013) 22:772–80. doi: 10.1089/scd.2012.0266
152. Xie J, Ameres SL, Friedline R, Hung JH, Zhang Y, Xie Q, et al. Long-Term, Efficient Inhibition of microRNA Function in Mice Using rAAV Vectors. *Nat Methods* (2012) 9:403–9. doi: 10.1038/nmeth.1903
153. Beuzelin D, Kaeffer B. Exosomes and miRNA-Loaded Biomimetic Nanovehicles, a Focus on Their Potentials Preventing Type-2 Diabetes Linked to Metabolic Syndrome. *Front Immunol* (2018) 9:2711. doi: 10.3389/fimmu.2018.02711
154. Prockop DJ, Brenner M, Fibbe WE, Horwitz E, Le Blanc K, Phinney DG, et al. Defining the Risks of Mesenchymal Stromal Cell Therapy. *Cytotherapy* (2010) 12:576–8. doi: 10.3109/14653249.2010.507330
155. Klopp AH, Gupta A, Spaeth E, Andreeff M, Marini F3rd. Concise Review: Dissecting a Discrepancy in the Literature: Do Mesenchymal Stem Cells Support or Suppress Tumor Growth? *Stem Cells* (2011) 29:11–9. doi: 10.1002/stem.559
156. Pham PV. Concise Review: Extracellular Vesicles From Mesenchymal Stem Cells as Cellular Therapy. *Biomed Res Ther* (2017) 4. doi: 10.15419/bmrat.v4i08.287
157. Ankrum JA, Ong JF, Karp JM. Mesenchymal Stem Cells: Immune Evasive, Not Immune Privileged. *Nat Biotechnol* (2014) 32:252–60. doi: 10.1038/nbt.2816
158. Wu Y, Huang S, Enhe J, Ma K, Yang S, Sun T, et al. Bone Marrow-Derived Mesenchymal Stem Cell Attenuates Skin Fibrosis Development in Mice. *Int Wound J* (2014) 11:701–10. doi: 10.1111/iwj.12034
159. Lee Y, El Andaloussi S, Wood MJ. Exosomes and Microvesicles: Extracellular Vesicles for Genetic Information Transfer and Gene Therapy. *Hum Mol Genet* (2012) 21:R125–134. doi: 10.1093/hmg/dds317
160. Alvarez-Erviti L, Seow Y, Yin H, Betts C, Lakhal S, Wood MJ. Delivery of siRNA to the Mouse Brain by Systemic Injection of Targeted Exosomes. *Nat Biotechnol* (2011) 29:341–5. doi: 10.1038/nbt.1807

161. Koritzinsky EH, Street JM, Star RA, Yuen PS. Quantification of Exosomes. *J Cell Physiol* (2017) 232:1587–90. doi: 10.1002/jcp.25387
162. Lőrincz M, Timár CI, Marosvári KA, Veres DS, Otrokocsi L, Kittel, et al. Effect of Storage on Physical and Functional Properties of Extracellular Vesicles Derived From Neutrophilic Granulocytes. *J Extracell Vesicles* (2014) 3:25465. doi: 10.3402/jev.v3.25465
163. Lener T, Gimona M, Aigner L, Börger V, Buzas E, Camussi G, et al. Applying Extracellular Vesicles Based Therapeutics in Clinical Trials - an ISEV Position Paper. *J Extracell Vesicles* (2015) 4:30087. doi: 10.3402/jev.v4.30087
164. Watson DC, Bayik D, Srivatsan A, Bergamaschi C, Valentin A, Niu G, et al. Efficient Production and Enhanced Tumor Delivery of Engineered Extracellular Vesicles. *Biomaterials* (2016) 105:195–205. doi: 10.1016/j.biomaterials.2016.07.003
165. Pachler K, Lener T, Streif D, Dunai ZA, Desgeorges A, Feichtner M, et al. A Good Manufacturing Practice-Grade Standard Protocol for Exclusively Human Mesenchymal Stromal Cell-Derived Extracellular Vesicles. *Cytotherapy* (2017) 19:458–72. doi: 10.1016/j.jcyt.2017.01.001

Conflict of Interest: The authors declare that the research was conducted in the absence of any commercial or financial relationships that could be construed as a potential conflict of interest.

Publisher's Note: All claims expressed in this article are solely those of the authors and do not necessarily represent those of their affiliated organizations, or those of the publisher, the editors and the reviewers. Any product that may be evaluated in this article, or claim that may be made by its manufacturer, is not guaranteed or endorsed by the publisher.

frontiers in Endocrinology

ORIGINAL RESEARCH
published: 24 December 2021
doi: 10.3389/fendo.2021.791363

Let-7e-5p Regulates IGF2BP2, and Induces Muscle Atrophy

Takuro Okamura[1], *Hiroshi Okada*[1,2], *Yoshitaka Hashimoto*[1], *Saori Majima*[1], *Takafumi Senmaru*[1], *Naoko Nakanishi*[1], *Mai Asano*[1], *Masahiro Yamazaki*[1], *Masahide Hamaguchi*[1] *and Michiaki Fukui*[1]*

[1] *Department of Endocrinology and Metabolism, Graduate School of Medical Science, Kyoto Prefectural University of Medicine, Kyoto, Japan,* [2] *Department of Diabetes and Endocrinology, Matsushita Memorial Hospital, Moriguchi, Japan*

Background and Aims: To understand the role of microRNAs in muscle atrophy caused by androgen-depletion, we performed microarray analysis of microRNA expression in the skeletal muscles of Sham, orchiectomized (ORX), and androgen-treated ORX mice.

Methods: To clarify role and mechanisms of let-7e-5p in the muscle, the effect of let-7e-5p overexpression or knockdown on the expression of myosin heavy chain, glucose uptake, and mitochondrial function was investigated in C2C12 myotube cells. Moreover, we examined serum let-7e-5p levels among male subjects with type 2 diabetes.

Results: We found that the expression of the miRNA, lethal *(let)-7e-5p* was significantly lower in ORX mice than that in Sham mice (p = 0.027); however, *let-7e-5p* expression in androgen-treated ORX mice was higher (p = 0.047). Suppression of let-7e-5p significantly upregulated the expression of myosin heavy chain, glucose uptake, and mitochondrial function. Real-time PCR revealed a possible regulation involving let-7e-5p and *Igf2bp2* mRNA and protein in C2C12 cells. The serum let-7e-5p levels were significantly lower, which might be in compensation, in subjects with decreased muscle mass compared to subjects without decreased muscle mass. Let-7e-5p downregulates the expression of *Igf2bp2* in myotube cells and inhibits the growth of the myosin heavy chain.

Conclusions: Based on our study, serum level of let-7e-5p may be used as a potential diagnostic marker for muscle atrophy.

Keywords: micro RNA, let-7e-5p, muscle atrophy, Igf2bp2, sarcopenia

OPEN ACCESS

Edited by:
Pieter de Lange, University of Campania Luigi Vanvitelli, Italy

Reviewed by:
Atsushi P. Kimura, Hokkaido University, Japan
Xianyong Lan, Northwest A&F University, China

***Correspondence:**
Michiaki Fukui
michiaki@koto.kpu-m.ac.jp

Specialty section:
This article was submitted to Cellular Endocrinology, a section of the journal Frontiers in Endocrinology

Received: *08 October 2021*
Accepted: *06 December 2021*
Published: *24 December 2021*

Citation:
Okamura T, Okada H, Hashimoto Y, Majima S, Senmaru T, Nakanishi N, Asano M, Yamazaki M, Hamaguchi M and Fukui M (2021) Let-7e-5p Regulates IGF2BP2, and Induces Muscle Atrophy. Front. Endocrinol. 12:791363. doi: 10.3389/fendo.2021.791363

INTRODUCTION

Sarcopenia, an aging-related condition characterized by the loss of muscle mass, strength, and function, is an important global health concern (1). Sarcopenia-associated muscular atrophy not only impairs motor function, but also increases the likelihood of falls and fractures, affects daily activities (2, 3), and increases the risk of mortality (4). The pathogenesis of skeletal muscle atrophy includes reduced regenerative capacity of muscle satellite cells, reduced protein synthesis, and accelerated degradation of myotube cells (5). Although the exact mechanism is unknown, reduced androgen production has been implicated in the pathogenesis of skeletal muscle atrophy. Roy et al. reported an association between serum androgen concentration and skeletal muscle mass and

strength (6). In addition, Basualto-Alarcón et al. showed that androgen signals induce muscle hypertrophy through the mTOR and androgen receptor pathways (7). However, androgen replacement therapy has been reported to have several adverse effects (8). Therefore, there is an urgent need to develop new therapeutic options to prevent androgen deficiency-induced skeletal muscle atrophy.

Micro RNAs (miRNAs) are short single-stranded non-coding RNAs approximately 19–23 nucleotides in length that regulate gene expression in the post-transcriptional control phase of target messenger RNAs (mRNAs). MiRNA-mediated transcriptional repression is known to play an important role in biological processes such as cell proliferation and differentiation (9), apoptosis (10), metabolism (11), and development (12). MiRNAs bind to their target mRNAs with incomplete homology, thereby destabilizing the target mRNA, and inhibiting protein synthesis (13).

Recent studies have shown that a single miRNA can regulate the expression of multiple genes associated with a single pathology. Abnormal expression of miRNAs in the skeletal and cardiac muscles is associated with muscle damage (14). We previously reported that activation of the Akt-mTOR pathway, caused by miR-23b-3p overexpression-mediated PTEN repression, counteracts skeletal muscle atrophy and has beneficial effects on the skeletal muscles, including increased expression of myosin heavy chain, myoD, and myogenin, and increased glucose uptake and ATP activity (15). In contrast, in this study, using microarray analyses of miRNA in skeletal muscles, we found that the miRNA, lethal (let)-7e-5p, was overexpressed in androgen-treated orchidectomized (ORX) mice, compared to ORX mice. Let-7 family has been reported to be related with muscle atrophy. Muscle biopsy studies found that the expression of let-7b and let-7e was increased in the skeletal muscle in older men with less lean mass compared to young men (16). In another study, in healthy men with 21-days bed rest let-7 in muscle was increased (17). On the other hand, the expression of let-7 was decreased in skeletal muscle at 10-days of bed rest in healthy man (18), and the expression of the let-7 family within atrophied skeletal muscle has been reported in various ways and no clear conclusions have been reached. In this study, we investigated the association between skeletal muscle atrophy and let-7e-5p using murine C2C12 myotube cells. In addition, we examined the relationship between let-7e-5p levels in human serum and muscle atrophy.

MATERIALS AND METHODS

Animals and Experimental Design

All experimental procedures were approved by the Committee for Animal Research, Kyoto Prefectural University of Medicine (M2020-40). Six-week-old C57BL/6 J male mice were purchased from Shimizu Laboratory Supplies (Kyoto, Japan) and housed in specific pathogen-free controlled environment. The mice were fed a standard diet (SD; 344.9 kcal/100 g, fat kcal 4.6%; CLEA Japan, Tokyo) for 4 weeks starting at 8 weeks of age.

Mice were either orchiectomized (ORX group) or sham-operated (Sham group) at 7 weeks of age. Under isoflurane inhalation anesthesia, the skin of the testicle area is cut by 1 cm, the testicle is removed, and compression hemostasis is applied until obvious bleeding stops. In the sham group, the skin at the testicle area is cut by 1 cm, and the testicle is not removed, and only the skin is sutured. For the androgen-treatment group (ORX+A), 8-week-old ORX mice were treated with testosterone, administered once every 2 days for 4 weeks *via* subcutaneous injection of androgen enanthate (3.6 μg/g body weight; ISEI, Yamagata, Japan) diluted in sesame oil (19).

When the mice reached 12 weeks of age, mice were sacrificed by the administration of a combination of anesthetics including 0.3 mg/kg medetomidine, 4.0 mg/kg midazolam, and 5.0 mg/kg butorphanol (20). The soleus muscle was obtained, frozen immediately, and stored at -80°C until use. QIAzol Lysis reagent (Qiagen, Hilden, Germany) was used for miRNA extraction.

MiRNA Microarray Analysis

The soleus muscles were obtained from the mice in the ORX, ORX+A, and Sham groups, and subjected to GeneChip miRNA 4.0 Array (cat. #902412, Applied Biosystems, Foster City, CA, USA). The relative abundance of the miRNAs within the groups was evaluated using the weighted average distance (WAD) method using R (21) and paired t-tests. The WAD method ranked the genes based on high expression, high weightage, or fold-change. WAD was found to be an effective method of transcriptome analysis. The data were preprocessed with Robust Multichip Average normalization, and the global miRNA expression was visualized as a volcano plot.

Mouse Skeletal Muscle Cell Culture

C2C12 cells (a mouse myoblast cell line; KAC Co. Ltd., Kyoto, Japan), were plated in 24-well plates and grown in Dulbecco's modified Eagle's medium (DMEM) supplemented with 20% fetal bovine serum (day 2). The medium was changed every other day. When the cells reached 80% confluence, they were differentiated in DMEM supplemented with 2% horse serum (differentiation medium) (day 0). At 24 h after the medium change, the cells were transfected with 30 nM let-7e-5p mimic/inhibitor or a scrambled sequence (mirVana ®), which were purchased from Thermo Fisher Scientific, using X-treme Gene siRNA transfection kit (Roche, Mannheim, Germany) according to the manufacturer's recommendations (day 1). At 96 h (day 5) post-transfection, the myotube cells were evaluated through various experiments.

Gene Expression in C2C12 Cells

Gene expression in the C2C12 cells was analyzed on day 5. Medium was removed and the cells were washed with cold phosphate buffered saline (PBS) twice. Cells were detached from the dish using cell scrapers, homogenized in ice-cold QIAzol Lysis reagent, and total RNA was isolated following the manufacturer's instructions. Total RNA (0.5 μg) was reverse transcribed into cDNA using a High-Capacity cDNA Reverse Transcription Kit (Applied Biosystems) with oligodT and random hexamer primers according to the manufacturer's recommendations. The reverse transcription reaction was

performed for 120 min at 37°C and the reaction was inactivated for 5 min at 85°C. We chose the *let-7e-5p* target mRNA, *Igf2bp2*, for further studies. We used real-time reverse transcription-polymerase chain reaction (RT-PCR) to quantify the mRNA expression of *Igf2bp2*, *Trim63*, *Fbxo32*, and *Hdac4*, which are involved in muscle atrophy (22). RT-PCR was performed using TaqMan Fast Advanced Master Mix (Applied Biosystems) according to the manufacturer's instructions. The PCR conditions were as follows: 1 cycle of 2 min at 50°C and 20 s at 95°C, followed by 40 cycles of 1 s at 95°C, and 20 s at 60°C.

The relative expression of each target gene was normalized to the threshold cycle (CT) value of *Gapdh* quantified using the comparative threshold cycle 2−ΔΔCT method as described previously (23). Signals from the Sham mice were assigned a relative value of 1.0. Six mice were examined in each group, and RT-PCR was performed in triplicate for each sample. Total miRNA was extracted from the soleus muscle using the miRNeasy mini kit (Qiagen, Hilden, Germany).

For the miRNA RT-PCR experiments, cDNA was synthesized from 200 ng of total miRNA using a Taqman miRNA Reverse Transcription kit (Applied Biosystems). U6 was used as an endogenous control. RT-PCR was performed using TaqMan Fast Advanced Master Mix (Applied Biosystems) according to the manufacturer's instructions. The PCR conditions used were as follows: 1 cycle of 2 min at 50°C and 20 s at 95°C, followed by 40 cycles of 1 s at 95°C, and 20 s at 60°C. We extracted and quantified let-7e-5p and U6 small nucleolar RNA using the 2 −ΔΔCT method. Signals from the Sham mice were assigned a relative value of 1.0.

Luciferase Reporter Assay

The putative let-7e-5p targets were predicted using TargetScan Human 6.2 (http://www.targetscan.org/). The putative recognition sites of let-7e-5p in the IGF2BP2 3'-untranslated region (3'-UTR) and its sequences are shown in **Supplementary Figure 2**. The reporter plasmids containing the wild-type (WT) 3′UTR (pmirGLO3-IGF2BP2-WT-3′UTR) and mutant (MUT) 3′UTR (pmirGLO3-IGF2BP2-MUT-3′UTR) were synthesised (Genecopoeia). C2C12 myotube cells in 96-well plates were transfected with 30 nM scrambled sequence (NC), a combination of let-7e-5p mimicking substrate (Applied Biosystems) and IGF2BP2 reporter vector or pEZX-MT01 control vector, which were purchased from Merk, using an X-treme GENE siRNA transfection kit according to the manufacturer's instructions. All transfection experiments were performed in triplicate. Luciferase activity was assayed at 48 h after transfection, using a dual-luciferase reporter assay system (Genecopoeia).

Protein Extracts and Western Blot Incubated With Antibodies

Whole C2C12 myotube cell extracts were prepared in a radio immunoprecipitation assay buffer (RIPA, ATTO, Tokyo; 50 mmol/L Tris (pH 8.0), 150 mmol/L NaCl, 0.5% deoxycholate, 0.1% SDS and 1.0% NP-40) containing a protease inhibitor cocktail (BioVision, Milpitas, CA, USA). Protein assays were performed using a BCA protein assay kit (Pierce/Thermo Scientific, Rockford, IL, USA) according with the manufacturer's instructions. Total protein (20μg) was electrophoresed in 12% SDS-PAGE gels, and western blotting was carried out using standard protocols and proteins detected by ImageQuant LAS 500 (GE Healthcare, Piscataway, NJ, USA).

C2C12 myotube cells were subjected to protein extractions. First, 40–60 μg of protein extraction were incubated with the following primary antibodies; Igf2bp2 (1:1000), MY32 or gapdh (1:1500) diluted with EzBlock Chemi (ATTO, Osaka, Japan) overnight at 4°C, followed by incubation with goat anti-mouse IgG secondary antibodies conjugated to horseradish peroxidase diluted with EzBlock Chemi for 30 minutes at room temperature. All the antibodies listed in this section were obtained from Santa Cruz Biotechnology (Santa Cruz, Dallas, TX, USA).

Immunocytochemistry

C2C12 cells were cultured in 8-well chamber slides and immunocytochemistry was performed on day 5. The cells were fixed in 4% paraformaldehyde and incubated with MY32, a primary monoclonal antibody against myosin heavy chain (Sigma-Aldrich, St. Louis, MO, USA), or F12B, anti-myogenin, (Sigma-Aldrich), diluted in PBS/1% BSA/0.3% TritonTM X-100 (Sigma-Aldrich) overnight at 4°C, and then with Texas-red-conjugated anti-mouse secondary antibody (Jackson ImmunoResearch) diluted in PBS/1% BSA/0.3% TritonTM X-100 overnight at 4°C for 1 h. The nuclei were stained with DAPI (Sigma-Aldrich). Images were captured with a BZ-X710 fluorescence microscope, and the fluorescence intensity of the cells and the nuclei count per image with a 20-fold magnification were analyzed using ImageJ (NIH). In addition, the fusion index was defined and determined according to a previous study (24).

Apoptosis Detection by Flow Cytometry Analysis

C2C12 cells were cultured in 24-well chamber slides and flow cytometry analyses were performed on day 5 with Annexin V-FITC Apoptosis Detection Kit (Nacalai tesque, Kyoto, Japan) according to the manufacturer's recommendations. FACS Canto II and FlowJo version 10 software were used for obtained data and analyzation.

ATP Activity

C2C12 cells were cultured in 24-well plates, and cellular ATP was extracted on day 5 using an Intracellular ATP assay kit (Toyo-B-Net, Tokyo, Japan) according to the manufacturer's instructions. The medium was removed, cells were washed twice with cold PBS, and then treated with ATP extraction buffer (400 μL/well) at room temperature for 5 min. The lysate was then dispensed into 96-well plates (on ice) in triplicate and luminescent reagent (100 μL/well) was added. ATP activity was quantitated as a measure of the luminescence using an Orion L microplate luminometer (Berthold Detection Systems, Pforzheim, Germany).

2-Deoxyglucose Uptake by C2C12 Cells

The uptake of [^{3}H]2-deoxyglucose (PerkinElmer, Boston, MA) by C2C12 cells cultured in 24-well plates was measured. Cells were washed twice with serum-free DMEM, incubated in serum-

free DMEM for 2 h at 37°C, and washed twice with PBS. Then, Krebs-Ringer-phosphate buffer (10 mM phosphate [pH 7.5], 113 mM NaCl, 5 mM KCl, 1.3 mM $CaCl_2$, 1.2 mM $MgSO_4$, and 1.2 mM KH_2PO_4 containing 0.3% BSA) was added in the presence or absence of 10 mU/mL bovine insulin for 30 min at 37°C. The uptake of 10 μM [^{3}H]2-deoxyglucose was then measured over a 5-min period. Reactions were terminated by rapidly washing the cells twice with ice-cold Krebs ringer bicarbonate buffer.

Cells were then extracted using 0.2% SDS, and aliquots of the cell extract were counted by liquid scintillation and used to determine the protein concentration. Nonspecific uptake was measured in the presence of 10 μM of cytochalasin-B, and the values were subtracted from those corresponding to specific binding.

Measurement of Cellular Oxygen Consumption Rate (OCR) in C2C12 Cells

OCR of C2C12 cells was determined using a Seahorse Extracellular Flux Analyzer XFp (Agilent Technologies, Santa Clara, CA). C2C12 cells (0.5 × 104 cells/well) were plated and cultured in normal medium in a Seahorse plate, and the experiment was conducted 5 days after changing the cells to differentiation medium. On the day of the measurement, the medium was replaced with XF assay medium supplemented with 10 mM glucose, 2 mM glutamine, and 1 mM pyruvate, and the cell culture plate was placed in a CO2-free incubator for 1 h. OCR was determined using a Seahorse Analyzer in combination with a Cell Mito Stress Test assay kit according to the manufacturer's instructions. For the Cell Mito Stress Test, 2 μM oligomycin, 2 μM carbonyl cyanide 4-(trifluoromethoxy) phenylhydrazone (FCCP), and 1 μM rotenone /antimycin A were subsequently added to the assay medium to monitor different aspects of mitochondrial respiration. Two plates with the same conditions were prepared, one for the experiment and the other for cell counting after stripping the cells with trypsin EDTA, and OCR was normalized to the total number of cells.

Study Population

The present study population was derived from the KAMOGAWA-DM cohort study, which is an ongoing prospective cohort study that began in 2014 (25). Approval for the study was obtained from the research ethics committees of the Kyoto Prefectural University of Medicine and Kameoka Municipal Hospital (E-466), and written informed consent was obtained from all the patients. For the present study, we collected information pertaining to male patients aged ≥ 65 years with type 2 diabetes, all of whom were Japanese, physically active, and KAMOGAWA-DM participants recruited from the outpatient clinic of the Kyoto Prefectural University of Medicine or Kameoka Municipal Hospital between August 2015 and September 2017. Patients with diabetic nephropathy stage 3 or higher (26) and those with inflammatory disease, malignancy, or endocrine disease were excluded from the study. Patients with class NYHA II–IV cardiac insufficiency (27) or severe chronic obstructive pulmonary disease were also excluded (27) as these conditions may influence the patient's physical activity.

Next, we examined the decrease in muscle mass by determining each patient's skeletal muscle index (SMI) based on the algorithms proposed by the Asian Working Group for Sarcopenia (28). The body composition of each patient was evaluated using a multifrequency impedance body composition analyzer (InBody 720, InBody Japan, Tokyo) (29), which is well correlated with the dual-energy X-ray absorptiometry (30). We obtained each patient's body weight (BW, kg), body fat mass (kg), skeletal muscle mass (kg), and appendicular muscle mass (kg) and then calculated the skeletal muscle mass index (SMI) (kg/m2) by dividing the appendicular muscle mass (kg) by the square of the patient's height (m) (30). The body mass index was defined as weight in kilograms divided by height in meters squared. The cut-off value for SMI was set to < 7.0 kg/m2. In this study, we selected a total of 32 male patients to form two groups of 16 patients with or without decreased muscle mass, matched for age. Approval for the study was obtained from the research ethics committees of the Kyoto Prefectural University of Medicine and Kameoka Municipal Hospital, and written informed consent was obtained from all the patients.

Serum miRNA Extraction

RNA was extracted from serum samples using miRNeasy Serum/Plasma Kit (Qiagen) according to the manufacturer's instructions. Briefly, 250 μL of serum was thawed on ice and centrifuged at 12,000 g at 4°C for 10 min to remove cellular debris. Thereafter, 200 μL of the supernatant was lysed in 1000 μL of QIAzol Lysis Reagent. After incubation for 5 min, 25 fmol of synthetic cel-miR-39 (Syn-cel-miR-39-3p miScript miRNA Mimic, Qiagen) was added to each sample as an external spiked-in control.

Total RNA, including small RNA, was extracted and eluted in 30 μL of RNase-free water using a QIAcube device (Qiagen). Serum levels of let-7e-5p and cel-miR-39 were examined by real-time PCR. A fixed volume of 2 μL of total RNA was reverse transcribed using Taqman miRNA Reverse Transcription kit (cat. #4366597, Applied Biosystems) in a total volume of 15 μL under the following cycling conditions: 16°C for 30 min, 42°C for 30 min, 85°C for 5 min, and then maintained at 4°C.

Real-time PCR was performed (in duplicate) using MiRNA Assay Kit and TaqMan Universal Master Mix II (no UNG; cat. #4440040, Applied Biosystems) on the StepOne Plus system (Applied Biosystems) under the following cycling conditions: 95°C for 10 min, followed by 40 cycles of 95°C for 15 s and 60°C for 1 min. The cycle threshold (Ct) values were calculated using StepOne Software v2.3 (Applied Biosystems). The miRNAs expression levels were normalized to those of cel-miR-39 determined using the $2^{-\Delta\Delta Ct}$ method.

Statistical Analysis

Data were analyzed using JMP ver. 13.0 software (SAS, Cary, NC). Student's t-test was used to compare the different groups. P = 0.05 was considered significant. Moreover, when necessary, Kruskal-Wallis tests followed by Bonferroni correction of the Mann-Whitney U test were used for multiple comparisons. In addition, the area under the curve (AUC) of serum let-7e-5p

levels, for the presence of sarcopenia, was calculated by the receiver operating characteristic curve.

RESULTS

MiRNA Array Analyses of Murine Soleus Muscle

We examined the changes in miRNA expression in the soleus muscle of ORX mice by performing microarray analysis comparing the Sham and ORX mice administered with androgen (ORX+A). The differentially expressed genes in the Sham and ORX mice, and ORX and ORX+A mice were determined using the WAD algorithm, and the full ranking is shown in **Supplementary Tables 1** and **2**. Top 20 miRNAs were ranked from top to bottom, as shown in **Figures 1A, B**. Additionally, volcano plots and heatmap of microarrays data displaying the pattern of gene expression values for ORX mice versus sham or ORX+A mice were shown in **Supplementary Figures 1A, B** and **3**. In microarray analyses, the fold change of let-7e 5p expression in ORX mice was 0.73 ± 0.16 compared to that in sham mice, and 0.60 ± 0.12 ($p = 0.047$). In real-time PCR, the expression of let-7e-5p was significantly reduced in the ORX mice, compared to that in Sham mice ($p = 0.027$), whereas replacement of testosterone restored the expression of let-7e-5p ($p = 0.135$) (**Supplementary Table 3**). In addition, the expression of let-7e-5p evaluated by RT-PCR in soleus muscle of ORX mice was significantly decreased, compared to that of sham or ORX+A mice ($p = 0.001$), whereas that of ORX+A mice was restored to the same levels as that of sham mice ($p = 0.167$) (**Supplementary Figure 1C**).

Igf2bp2 Is a Potential Target of Let-7e-5p

Putative let-7e-5p targets were predicted using TargetScan Human 6.2 (http://www.targetscan.org/). The putative let-7e-5p recognition sites in the 3'-untranslated region (3'-UTR) of insulin-like growth factor-2 mRNA-binding proteins 2 (Igf2bp2) and their sequences are shown in **Supplementary Figure 2**. We confirmed that the expression of let-7e-5p in C2C12 cells was significantly increased following transfection of the mimicking substrate, and decreased following transfection of an inhibitor ($p = 0.001$) (**Figure 2A**). Expression of *Igf2bp2* in C2C12 cells was significantly decreased following transfection with the let-7e-5p mimicking substrate ($p = 0.001$) (**Supplementary Figure 1D**). Conversely, the expression of Igf2bp2 in C2C12 cells was significantly increased by the let-7e-5p inhibitor ($p = 0.001$) (**Supplementary Figure 1D**). Moreover, in Western blot analyses, the Igf2bp2 protein levels were investigated. The Igf2bp2 protein levels of C2C12 cells transfected with the let-7e-5p inhibitor was higher than those with the let-7e-5p mimicking substrate (**Figure 2C**). In addition, the luciferase reporter assays using a 3'UTR of Igf2bp2 construct with let-7e-5p or a miR-Control construct expressing C2C12 myotube cells revealed a consistent reduction of luciferase activity in the let-7e-5p transfectants, suggesting that let-7e-5p represses Igf2bp2 directly (**Figure 2D**). The expression of genes related to muscle atrophy such as Trim63, Fbxo32, and Hdac4, was significantly increased in C2C12 cells transfected with the let-7e-5p

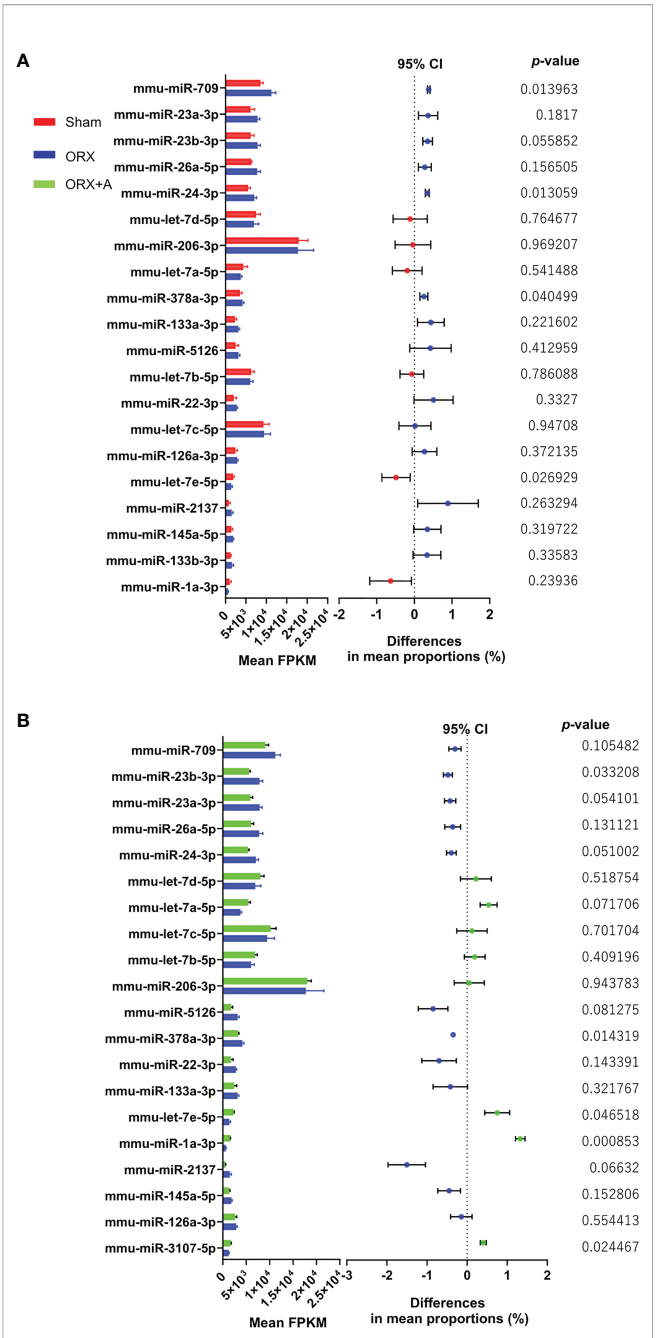

FIGURE 1 | Top 20 miRNAs in the soleus muscle ranked using the weighted average difference method. Influence of miRNAs in Sham, ORX, and ORX+A mice was assessed using the weighted average differences method, and the assessed influence of the genera are ranked from top to bottom. Top 20 miRNAs are shown. Differences between these miRNAs were evaluated using paired t-tests (n = 3). Left, histogram showing the mean fragments per kilobase of exon per million reads mapped (FPKM) of miRNAs (mean + standard deviation); right, 95% confidence interval (CI) of the differences in mean proportion and P- value by paired t-test are shown. **(A)** Sham vs. ORX mice. **(B)** ORX vs. ORX+A mice. Sham: red, ORX: blue, ORX+A: green.

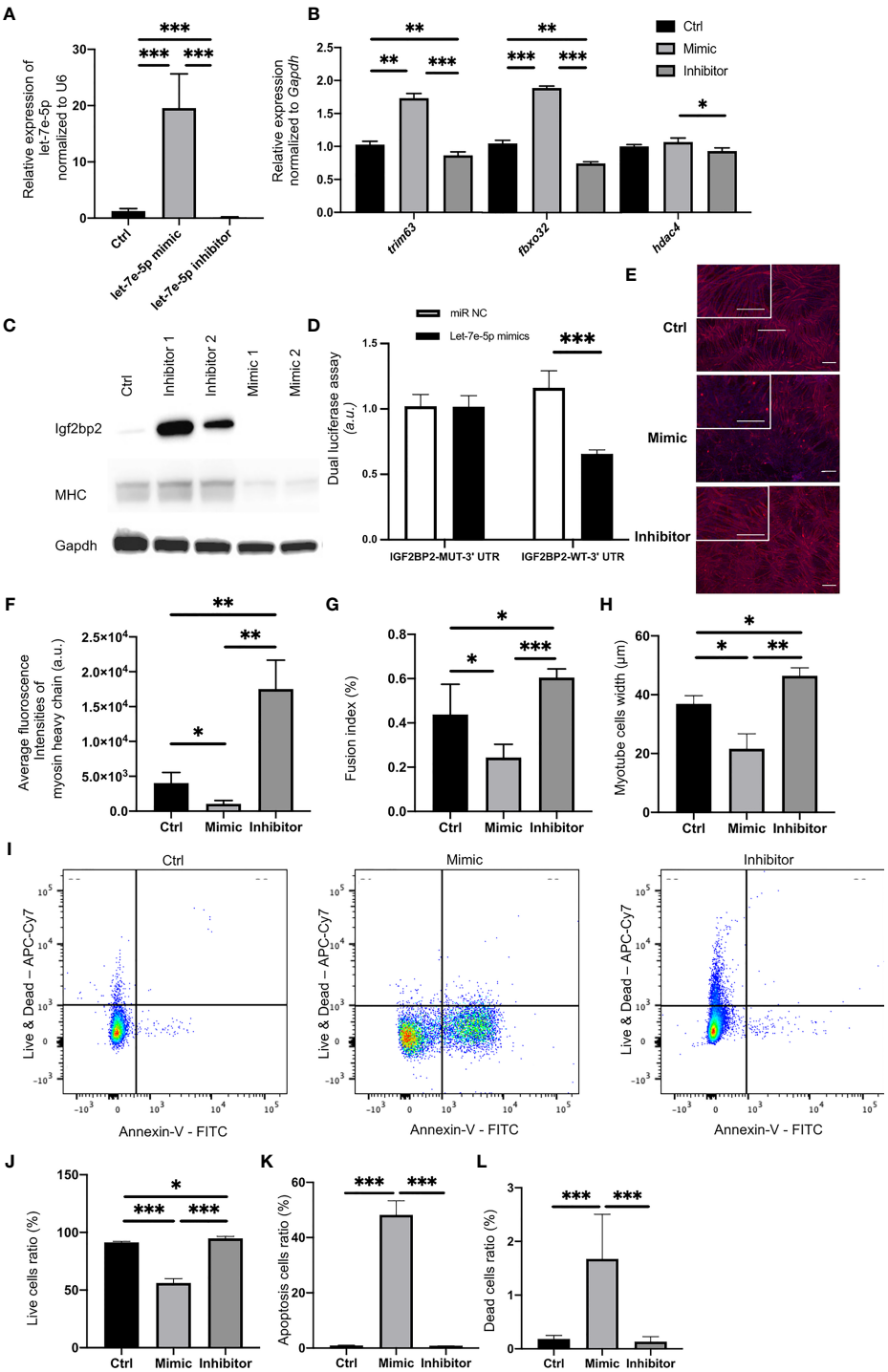

FIGURE 2 | Let-7e-5p inhibits myotube formation in C2C12 cells *via* repression of Igf2bp2. **(A)** Let-7e-5p expression in C2C12 cells was assessed after transfection with a let-7e-5p mimic/inhibitor (30 nM) (n = 6). **(B)** Relative expression of mRNAs of indicated genes in C2C12 cells normalized to *Gapdh* expression (n = 6). **(C)** Western blotting to detect the levels of Igf2bp2 and MHC and Gapdh in C2C12 myotube cells transfected with a let-7e-5p mimic/inhibitor (n=6). **(D)** Target validation study by luciferase assay (n=6). **(E)** Immunocytochemistry in C2C12 cells (n = 6). *Red:* Myosin heavy chain. *Blue:* DAPI. Scale bar, 50 μm. **(F)** Fluorescence intensity of myosin heavy chain (arbitrary units, a.u.) was compared (n = 6). **(G)** Fusion indices of C2C12 cells are shown (n = 6). **(H)** Width of myosin heavy chain are shown (n=6). **(I)** Representative flow cytometry plots of C2C12 cells Annexin V- PI- live cells, Annexin V+ PI- apoptosis cells, and Annexin V+ PI+ dead cells. **(J)** The ratio of live cells is shown (n=6). **(K)** The ratio of apoptosis cells is shown (n=6). **(L)** The ratio of dead cells is shown (n=6). Data represent the means ± standard deviation (SD). *p = 0.05, **p = 0.01, ***p = 0.001 by one-way ANOVA. Kruskal-Wallis tests followed by Bonferroni correction of the Mann-Whitney U test were used for multiple comparisons. Ctrl: negative control, MHC: myosin heavy chain.

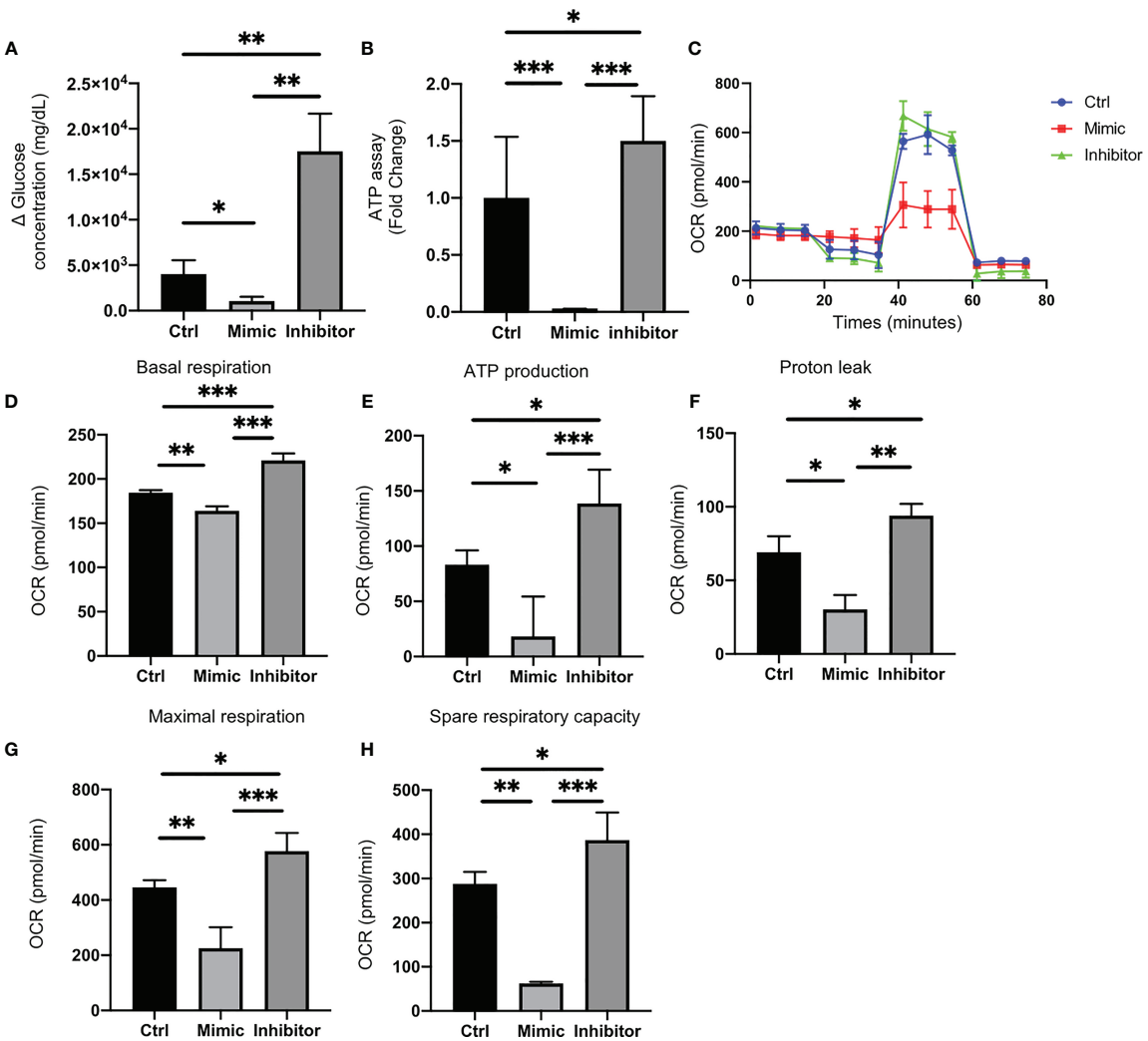

FIGURE 3 | Let-7e-5p decreases glucose uptake and downregulates mitochondrial function in C2C12 cells. **(A)** Glucose uptake by C2C12 cells was monitored after transfection with let-7e-5p mimic/inhibitor. Glucose uptake was downregulated by let-7e-5p mimicking substrate and upregulated by let-7e-5p inhibitor, compared to negative control (n = 6). **(B)** ATP assay following transfection with let-7e-5p mimic/inhibitor. ATP production was downregulated by let-7e-5p mimicking substrate and upregulated by let-7e-5p inhibitor, compared to negative control (n = 6). **(C)** Raw data of oxygen consumption rate (OCR), **(D)** basal respiration, **(E)** ATP-linked respiration (oligomycin-sensitive OCR), **(F)** proton leak, **(G)** maximal mitochondrial respiration (FCCP-stimulated OCR), and **(H)** spare respiratory capacity. OCRs were normalized to the total number of cells. Data represent the means ± SD; *p = 0.05, **p = 0.01, ***p = 0.001 by one-way ANOVA.

mimicking substrate compared to that in cells transfected with the inhibitor (**Figure 2B**).

Suppression of Let-7e-5p Upregulated the Expression of Myosin Heavy Chain in C2C12 Cells and Decreased the Apoptosis

In Western blot analyses, the MHC protein levels of C2C12 cells transfected with the let-7e-5p inhibitor was higher than those with the let-7e-5p mimicking substrate (**Figure 2C**). Next, we immunostained the cells with monoclonal antibodies against myosin heavy chain. Immunostaining revealed induction of growth in myotube cells transfected with the let-7e-5p inhibitor, while cells transfected with the let-7e-5p mimicking substrate atrophied (**Figure 2E**). In addition, the fluorescence intensity of myosin heavy chain in the C2C12 cells transfected with the let-7e-5p inhibitor was significantly higher than that in the cells transfected with the negative control ($p = 0.006$), whereas the level in cells transfected with the let-7e-5p mimicking substrate was significantly lower than that in the negative control ($p = 0.032$) (**Figure 2F**). The fusion index of the let-7e-5p mimicking substrate was significantly less than that of the negative control ($p = 0.041$) or the inhibitor ($p = 0.001$) (**Figure 2G**). Additionally, myotube width of the C2C12 cells transfected with the let-7e-5p inhibitor was significantly higher than that with the negative control ($p = 0.001$) (**Figure 2H**). Moreover, the viability was investigated with Annexin V by flowcytometry. Then, the ratio of apoptosis and dead cells was increased by transfection with the let-7e-5p mimicking substrate,

compared to negative control, whereas transfection with the let-7e-5p inhibitor significantly decreased the apoptosis and dead cells (p = 0.001) (**Figures 2I–L**). In addition, the fluorescence intensity of myogenin in the C2C12 cells transfected with the let-7e-5p inhibitor was significantly higher than that in the cells transfected with the negative control (p = 0.001), whereas the level in cells transfected with the let-7e-5p mimicking substrate was significantly lower than that in the negative control (p = 0.034) (**Supplementary Figures 4A, B**).

Let-7e-5p Downregulated Glucose Uptake in C2C12 Cells

Glucose uptake in C2C12 cells transfected with let-7e-5p inhibitor was significantly increased (p = 0.002), whereas that in cells transfected with let-7e-5p mimicking substrate was significantly decreased (p = 0.026) compared to the negative control (**Figure 3A**).

Let-7e-5p Downregulated ATP Activity in C2C12 Cells

ATP activity in C2C12 cells transfected with let-7e-5p mimicking substrate was significantly downregulated, compared to that of the negative control (p = 0.001), whereas the ATP activity in cells transfected with let-7e-5p inhibitor was upregulated (p = 0.039) (**Figure 3B**). Next, we investigated the mitochondrial OCR of C2C12 cells using an extracellular flux analyzer. C2C12 cells transfected with let-7e-5p mimicking substrate showed decreased basal respiration. In addition, C2C12 cells transfected with let-7e-5p mimicking substrate had significantly decreased ATP production, proton leak, maximal respiration, and spare respiratory capacity, compared to negative control and cells transfected with let-7e-5p inhibitor. On the contrary, their mitochondrial function was upregulated by the inhibition of let-7e-5p (**Figures 3C–H**).

Expression of Let-7e-5p in Serum of Patients With Muscle Atrophy Was Significantly Lower Than That in Patients Without Muscle Atrophy

Since let-7e-5p was suggested to have an effect on skeletal muscle in animal and cell experiments, we investigated serum let-7e-5p levels to test whether it is a biomarker for sarcopenia in our human studies. The characteristics of the 32 male patients with diabetes (with and without muscle atrophy) are summarized in **Table 1**. We investigated the differences in the expression of let-7e-5p in the serum between the two groups. Serum let-7e-5p expression in patients with muscle atrophy was significantly lower than that in patients without muscle atrophy (p = 0.028) (**Figure 4A**). Serum let-7e-5p level of 1.302 was identified as the cut-off for the presence of sarcopenia in the patients with diabetes (**Figure 4B**). Serum let-7e-5p level was found to be negatively associated with the presence of muscle atrophy in both univariate logistic regression analysis (OR of 1-unit increment: 0.70, 95% confidence interval (CI): 0.50–0.99, p = 0.011) and multivariate logistic regression analysis after adjusting for covariates (OR of 1-unit increment: 0.68, 95% CI: 048–0.99, p = 0.009) (**Table 2**).

DISCUSSION

Androgen deficiency is known to be associated not only with muscle atrophy (31), but also with insulin resistance, type 2 diabetes, metabolic syndrome, and visceral fat accumulation (32, 33). In the present study, the expression of the miRNA, let-7e-5p, was found to be decreased in the soleus muscle of ORX mice compared to that in Sham mice, whereas replacement of testosterone restored the expression of let-7e-5p. Furthermore, let-7e-5p was found to promote muscle atrophy by inhibiting the function of Igf2bp2, thereby reducing glucose uptake by myotube cells, and thus impairing mitochondrial function. In addition, serum let-7e-5p levels were significantly lower in patients with muscle atrophy than in those without. In this study, we also identified that the cut-off value of serum let-7e-5p level in patients with diabetes, for the presence of muscle atrophy, was 1.302.

The lethal-7 (let-7) gene was first discovered as an important developmental regulator in Caenorhabditis elegans. Let-7e-5p inhibits proliferation and metastasis of glioma stem cells (34) and colorectal cancer (35), and its functions are being intensively investigated in the field of oncology. Several target genes of let-7e-5p have been identified. In this study, we focused on Igf2bp2 and found that let-7e-5p regulates Igf2bp2. Igf2bps 1, 2, and 3 belong to a highly conserved family of RNA-binding proteins that influence the fate of transcripts (36–38). In contrast to Igf2bp1 and Igf2bp3, which are expressed during development, Igf2bp2 is widely expressed in many adult tissues, including the gut, muscles, and brain. In these organs, small quantitative differences in Igf2bp2 expression subtly affects processes such as food uptake, metabolism, feeding behavior, or more complex behavioral features that affects physical activity and, ultimately, the lifetime risk of developing obesity and diabetes (39). In their study of the relationship between IGFBP2 and skeletal muscle, Caron et al. (40) demonstrated that overexpression of high mobility group A2, an upstream target of Igf2bp2, enhanced myogenesis and myosin heavy chain expression in embryonic stem cells. Furthermore, since the muscle atrophy-related genes investigated in this study, such as A, B, and C, do not share a

TABLE 1 | Characteristics of the study patients with and without muscle atrophy.

	With Muscle atrophy n=16	Without Muscle atrophy n=16	*p*-value
Age, yrs	69.8 (6.9)	69.4 (6.3)	0.817
SMI, kg/m^2	5.7 (0.8)	7.8 (1.0)	< 0.001
Let-7e-5p	2.0 (1.8)	7.1 (10.1)	0.028

Data are mean (SD). SMI: skeletal muscle mass index.

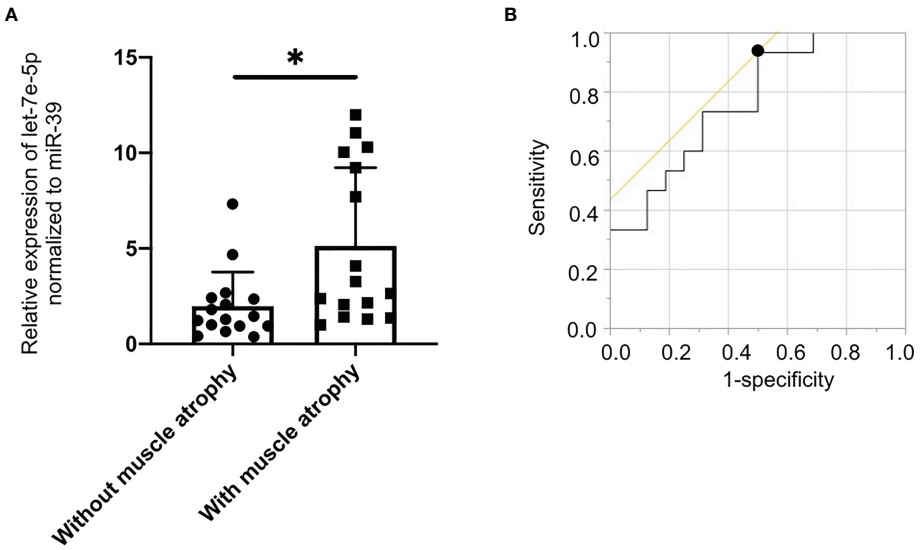

FIGURE 4 | Decreased levels of serum circulating let-7e-5p in patients with muscle atrophy compared to patients without muscle atrophy. **(A)** Relative expression of serum circulating let-7e-5p normalized to miR-39 in the patients with and without muscle atrophy is shown. Serum let-7e-5p expression in patients without muscle atrophy (7.1 ± 10.1) was significantly higher than that in patients with muscle atrophy (2.0 ± 1.8) (p = 0.028). Data represent the means ± SD. **(B)** Optimal cut-off point for serum circulating let-7e-5p level, for the presence of sarcopenia, is 1.302 (AUC 0.767, 95% CI, 0.600–0.934, sensitivity = 0.933, specificity = 0.500, p = 0.001). *p = 0.05 by Pearson's chi-square test.

common binding site with let-7e-5p, we hypothesized that the gene expression of IGF2BP2 indirectly alters the expression of these muscle atrophy-related genes. Moreover, Igf2bp2 promotes translation of IGF2 through internal ribosomal entry and downstream PI3K/Akt signaling (41), which inhibits FOXO1 and MURF1, and suppresses muscle atrophy (42). A previous study has shown that Igf2bp2 functions as a key regulator of satellite cell activation and skeletal muscle development (43). Adjusting the expression of let-7e-5p altered the expression of myogenin, one of the differentiation markers of myotubular cells (44), suggesting that let-7e-5p may also be involved in muscle differentiation through the regulation of IGF2BP2 expression. In addition, the other previous study reported that postnatal Igf2bp2 inactivation in mouse skeletal muscles reduces muscle mass accompanied by a reduction in overall protein synthesis due to reduced autocrine production of IGF2 and impaired activation of Akt1, Gsk3α, and eIF2Bϵ (45). In this study, suppression of let-7e-5p in C2C12 cells significantly increased the expression of Igf2bp2, which resulted in muscle hypertrophy. Furthermore, Igf2bp2 promotes the transport of mRNAs into the vicinity of mitochondria, and subsequent translation and mediation of cellular functions (46). In contrast, the suppression of Igf2bp2 reduces the OCR (47). In fact, in our study, mitochondrial function was enhanced by the suppression of let-7e-5p in C2C12 cells.

Serum let-7e-5p levels were significantly lower in diabetic patients with sarcopenia compared to that in patients without sarcopenia. This suggests that serum let-7e-5p level can be used as a diagnostic marker for sarcopenia. We hypothesize that serum let-7e-5p levels in patients were lower to reduce atrophy of skeletal muscles caused by deficiency in androgen. However, it is difficult to derive a causal relationship from this cross-sectional analysis. Therefore, we intend to perform longitudinal analyses to understand this relationship further in future studies.

Our study has the following limitation. The effects of let-7e-5p on skeletal muscles was only demonstrated through cellular experiments in this study. In the future, we intend to examine the influence of impaired glucose tolerance on skeletal muscles in animal experiments using conditional knockout mice. In addition, the possibility of mRNA-miRNA interaction needed to be evaluated not only by dual-luciferase assay but also by ribonucleoprotein immunoprecipitation.

TABLE 2 | Logistic regression analyses for muscle atrophy.

	Univariate		Multivariate	
	OR (95%CI)	***p*-value**	**OR (95%CI)**	***p*-value**
Age, yrs	1.01 (0.91-1.11)	0.881	1.04 (0.92-1.17)	0.507
Let-7e-5p	0.70 (0.50-0.99)	0.011	0.68 (0.48-0.99)	0.009

Multivariate analysis was adjusted for age.
CI, confidential interval; OR, odds ratio.

In conclusion, this study revealed that the overexpression of Igf2bp2 in C2C12 cells using a let-7e-5p inhibitor improves sarcopenia mainly *via* suppression of genes associated with muscle atrophy and enhanced mitochondrial function. Therefore, inhibition of let-7e-5p in skeletal muscles represents a potential therapeutic target for sarcopenia. Additionally, serum let-7e-5p level may be used as a marker for sarcopenia.

DATA AVAILABILITY STATEMENT

The data that support the findings of this study are available from the corresponding author upon reasonable request.

ETHICS STATEMENT

The studies involving human participants were reviewed and approved by the research ethics committees of the Kyoto Prefectural University of Medicine and Kameoka Municipal Hospital. The patients/participants provided their written informed consent to participate in this study. The animal study was reviewed and approved by the Committee for Animal Research, Kyoto Prefectural University of Medicine.

AUTHOR CONTRIBUTIONS

TO originated and designed the study, researched the data, and wrote the manuscript. HO and YH originated and designed the study, researched the data, and reviewed the manuscript. HO, YH, and MH researched the data and contributed to the discussion. MF originated and designed the study, researched the data, and reviewed and edited the manuscript. MF is the guarantor of this work and, as such, had full access to all of the data in the study and takes responsibility for the integrity of the data and the accuracy of the data analysis. All authors were involved in the writing of the manuscript and approved the final version of this article.

FUNDING

This work was supported by KAKENHI, Grant-in-Aid for Young Scientists (19K17966).

ACKNOWLEDGMENTS

We thank all of the staff members of the Kyoto Prefectural University of Medicine. We would like to thank Editage (www.editage.com) for English language editing.

SUPPLEMENTARY MATERIAL

The Supplementary Material for this article can be found online at: https://www.frontiersin.org/articles/10.3389/fendo.2021.791363/full#supplementary-material

REFERENCES

1. Chen LK, Woo J, Assantachai P, Auyeung TW, Chou MY, Iijima K, et al. Asian Working Group for Sarcopenia: 2019 Consensus Update on Sarcopenia Diagnosis and Treatment. *J Am Med Dir Assoc* (2020) 21:300–7.e2. doi: 10.1016/j.jamda.2019.12.012
2. Delmonico MJ, Harris TB, Lee J-S, Visser M, Nevitt M, Kritchevsky SB, et al. Health, Aging and Body Composition Study. Alternative Definitions of Sarcopenia, Lower Extremity Performance, and Functional Impairment With Aging in Older Men and Women. *J Am Geriatr Soc* (2007) 55:769–74. doi: 10.1111/j.1532-5415.2007.01140.x
3. Goodpaster BH, Park SW, Harris TB, Kritchevsky SB, Nevitt M, Schwartz A v, et al. The Loss of Skeletal Muscle Strength, Mass, and Quality in Older Adults: The Health, Aging and Body Composition Study. *J Gerontol Ser A Biol Sci Med Sci* (2006) 61:1059–64. doi: 10.1093/gerona/61.10.1059
4. Cruz-Jentoft AJ, Baeyens JP, Bauer JM, Boirie Y, Cederholm T, Landi F, et al. Sarcopenia: European Consensus on Definition and Diagnosis: Report of the European Working Group on Sarcopenia in Older People. *Age Ageing* (2010) 39:412–23. doi: 10.1093/ageing/afq034
5. le Grand F, Rudnicki MA. Skeletal Muscle Satellite Cells and Adult Myogenesis. *Curr Opin Cell Biol* (2007) 19:628–33. doi: 10.1016/j.ceb.2007.09.012
6. Roy TA, Blackman MR, Harman SM, Tobin JD, Schrager M, Metter EJ. Interrelationships of Serum Testosterone and Free Testosterone Index With FFM and Strength in Aging Men. *Am J Physiol Endocrinol Metab* (2002) 283:E284–94. doi: 10.1152/ajpendo.00334.2001
7. Basualto-Alarcón C, Jorquera G, Altamirano F, Jaimovich E, Estrada M. Testosterone Signals Through mTOR and Androgen Receptor to Induce Muscle Hypertrophy. *Med Sci Sports Exercise* (2013) 45:1712–20. doi: 10.1249/MSS.0b013e31828cf5f3
8. Grech A, Breck J, Heidelbaugh J. Adverse Effects of Testosterone Replacement Therapy: An Update on the Evidence and Controversy. *Ther Adv Drug Saf* (2014) 5:190–200. doi: 10.1177/2042098614548680
9. Hwang HW, Mendell JT. MicroRNAs in Cell Proliferation, Cell Death, and Tumorigenesis. *Br J Cancer* (2006) 94:776–80. doi: 10.1038/sj.bjc.6603023
10. Pileczki V, Cojocneanu-Petric R, Maralani M, Neagoe IB, Sandulescu R. MicroRNAs as Regulators of Apoptosis Mechanisms in Cancer. *Clujul Med* (2016) 89:50–5. doi: 10.15386/cjmed-512
11. Rottiers V, Näär AM. MicroRNAs in Metabolism and Metabolic Disorders. *Nat Rev Mol Cell Biol* (2012) 13:239–51. doi: 10.1038/nrm3313
12. Alvarez-Garcia I, Miska EA. MicroRNA Functions in Animal Development and Human Disease. *Development* (2005) 132:4653–62. doi: 10.1242/dev.02073
13. Esteller M. Non-Coding RNAs in Human Disease. *Nat Rev Genet* (2011) 12:861–74. doi: 10.1038/nrg3074
14. Eisenberg I, Alexander MS, Kunkel LM. miRNAS in Normal and Diseased Skeletal Muscle. *J Cell Mol Med* (2009) 13:2–11. doi: 10.1111/j.1582-4934.2008.00524.x
15. Okamura T, Hashimoto Y, Osaka T, Senmaru T, Fukuda T, Hamaguchi M, et al. MiR-23b-3p Acts as a Counter-Response Against Skeletal Muscle Atrophy. *J Endocrinol* (2020) 244:535–47. doi: 10.1530/JOE-19-0425
16. Drummond MJ, McCarthy JJ, Sinha M, Spratt HM, Volpi E, Esser KA, et al. Aging and microRNA Expression in Human Skeletal Muscle: A Microarray and Bioinformatics Analysis. *Physiol Genomics* (2011) 43:595–603. doi: 10.1152/physiolgenomics.00148.2010
17. Rullman E, Mekjavic IB, Fischer H, Eiken O. PlanHab (Planetary Habitat Simulation): The Combined and Separate Effects of 21 Days Bed Rest and Hypoxic Confinement on Human Skeletal Muscle miRNA Expression. *Physiol Rep* (2016) 4:e12753. doi: 10.14814/phy2.12753

18. Režen T, Kovanda A, Eiken O, Mekjavic IB, Rogelj B. Expression Changes in Human Skeletal Muscle miRNAs Following 10 Days of Bed Rest in Young Healthy Males. *Acta Physiol* (2014) 210:655–66. doi: 10.1111/apha.12228
19. Senmaru T, Fukui M, Okada H, Mineoka Y, Yamazaki M, Tsujikawa M, et al. Testosterone Deficiency Induces Markedly Decreased Serum Triglycerides, Increased Small Dense LDL, and Hepatic Steatosis Mediated by Dysregulation of Lipid Assembly and Secretion in Mice Fed a High-Fat Diet. *Metabolism* (2013) 62:851–60. doi: 10.1016/j.metabol.2012.12.007
20. Kawai S, Takagi Y, Kaneko S, Kurosawa T. Effect of Three Types of Mixed Anesthetic Agents Alternate to Ketamine in Mice. *Exp Anim* (2011) 60:481–7. doi: 10.1538/expanim.60.481
21. Kadota K, Nakai Y, Shimizu K. A Weighted Average Difference Method for Detecting Differentially Expressed Genes From Microarray Data. *Algorithms Mol Biol* (2008) 3:8. doi: 10.1186/1748-7188-3-8
22. Castets P, Rion N, Théodore M, Falcetta D, Lin S, Reischl M, et al. Mtorc1 and PKB/Akt Control the Muscle Response to Denervation by Regulating Autophagy and HDAC4. *Nat Commun* (2019) 10:3187. doi: 10.1038/s41467-019-11227-4
23. Livak KJ, Schmittgen TD. Analysis of Relative Gene Expression Data Using Real-Time Quantitative PCR and the 2(-Delta Delta C(T)) Method. *Methods (San Diego Calif)* (2001) 25:402–8. doi: 10.1006/meth.2001.1262
24. Yamaguchi T, Suzuki T, Arai H, Tanabe S, Atomi Y. Continuous Mild Heat Stress Induces Differentiation of Mammalian Myoblasts, Shifting Fiber Type From Fast to Slow. *Am J Physiol Cell Physiol* (2010) 298:C140–8. doi: 10.1152/ajpcell.00050.2009
25. Sakai R, Hashimoto Y, Ushigome E, Miki A, Okamura T, Matsugasumi M, et al. Late-Night-Dinner Is Associated With Poor Glycemic Control in People With Type 2 Diabetes: The KAMOGAWA-DM Cohort Study. *Endocr J* (2018) 65:395–402. doi: 10.1507/endocrj.EJ17-0414
26. Haneda M, Utsunomiya K, Koya D, Babazono T, Moriya T, Makino H, et al. A New Classification of Diabetic Nephropathy 2014: A Report From Joint Committee on Diabetic Nephropathy. *J Diabetes Invest* (2015) 6:242–6. doi: 10.1111/jdi.12319
27. Fulster S, Tacke M, Sandek A, Ebner N, Tschope C, Doehner W, et al. Muscle Wasting in Patients With Chronic Heart Failure: Results From the Studies Investigating Co-Morbidities Aggravating Heart Failure (SICA-Hf). *Eur Heart J* (2013) 34:512–9. doi: 10.1093/eurheartj/ehs381
28. Chen L-K, Liu L-K, Woo J, Assantachai P, Auyeung T-W, Bahyah KS, et al. Sarcopenia in Asia: Consensus Report of the Asian Working Group for Sarcopenia. *J Am Med Dir Assoc* (2014) 15:95–101. doi: 10.1016/j.jamda.2013.11.025
29. Okamura T, Miki A, Hashimoto Y, Kaji A, Sakai R, Osaka T, et al. Shortage of Energy Intake Rather Than Protein Intake Is Associated With Sarcopenia in Elderly Patients With Type 2 Diabetes: A Cross-Sectional Study of the KAMOGAWA-DM Cohort. *J Diabetes* (2019) 11:477–83. doi: 10.1111/1753-0407.12874
30. Kim M, Shinkai S, Murayama H, Mori S. Comparison of Segmental Multifrequency Bioelectrical Impedance Analysis With Dual-Energy X-Ray Absorptiometry for the Assessment of Body Composition in a Community-Dwelling Older Population. *Geriatr Gerontol Int* (2015) 15:1013–22. doi: 10.1111/ggi.12384
31. Axell A-M, MacLean HE, Plant DR, Harcourt LJ, Davis JA, Jimenez M, et al. Continuous Testosterone Administration Prevents Skeletal Muscle Atrophy and Enhances Resistance to Fatigue in Orchidectomized Male Mice. *Am J Physiol Endocrinol Metab* (2006) 291:E506–16. doi: 10.1152/ajpendo.00058.2006
32. Traish AM, Saad F, Guay A. The Dark Side of Testosterone Deficiency: II. Type 2 Diabetes and Insulin Resistance. *J Androl* (2008) 30:23–32. doi: 10.2164/jandrol.108.005751
33. Fukui M, Kitagawa Y, Ose H, Hasegawa G, Yoshikawa T, Nakamura N. Role of Endogenous Androgen Against Insulin Resistance and Athero-Sclerosis in Men With Type 2 Diabetes. *Curr Diabetes Rev* (2007) 3:25–31. doi: 10.2174/157339907779802094
34. Gong W, Zheng J, Liu X, Ma J, Liu Y, Xue Y. Knockdown of NEAT1 Restrained the Malignant Progression of Glioma Stem Cells by Activating microRNA Let-7e. *Oncotarget* (2016) 7:62208–23. doi: 10.18632/oncotarget.11403
35. Shan Y, Liu Y, Zhao L, Liu B, Li Y, Jia L. MicroRNA-33a and Let-7e Inhibit Human Colorectal Cancer Progression by Targeting ST8SIA1. *Int J Biochem Cell Biol* (2017) 90:48–58. doi: 10.1016/j.biocel.2017.07.016
36. Oleynikov Y, Singer RH. Real-Time Visualization of ZBP1 Association With β-Actin mRNA During Transcription and Localization. *Curr Biol* (2003) 13:199–207. doi: 10.1016/S0960-9822(03)00044-7
37. Hüttelmaier S, Zenklusen D, Lederer M, Dictenberg J, Lorenz M, Meng XH, et al. Spatial Regulation of β-Actin Translation by Src-Dependent Phosphorylation of ZBP1. *Nature* (2005) 438:512–5. doi: 10.1038/nature04115
38. Pan F, Hüttelmaier S, Singer RH, Gu W. ZBP2 Facilitates Binding of ZBP1 to β-Actin mRNA During Transcription. *Mol Cell Biol* (2007) 27:8340–51. doi: 10.1128/mcb.00972-07
39. Christiansen J, Kolte AM, Hansen TVO, Nielsen FC. IGF2 mRNA-Binding Protein 2: Biological Function and Putative Role in Type 2 Diabetes. *J Mol Endocrinol* (2009) 43:187–95. doi: 10.1677/JME-09-0016
40. Caron L, Bost F, Prot M, Hofman P, Binétruy B. A New Role for the Oncogenic High-Mobility Group A2 Transcription Factor in Myogenesis of Embryonic Stem Cells. *Oncogene* (2005) 24:6281–91. doi: 10.1038/sj.onc.1208781
41. Mu Q, Wang L, Yu F, Gao H, Lei T, Li P, et al. Imp2 Regulates GBM Progression by Activating IGF2/PI3K/Akt Pathway. *Cancer Biol Ther* (2015) 16:623–33. doi: 10.1080/15384047.2015.1019185
42. Stitt TN, Drujan D, Clarke BA, Panaro F, Timofeyva Y, Kline WO, et al. The IGF-1/PI3K/Akt Pathway Prevents Expression of Muscle Atrophy-Induced Ubiquitin Ligases by Inhibiting FOXO Transcription Factors. *Mol Cell* (2004) 14:395–403. doi: 10.1016/S1097-2765(04)00211-4
43. Li Z, Gilbert JA, Zhang Y, Zhang M, Qiu Q, Ramanujan K, et al. An HMGA2-IGF2BP2 Axis Regulates Myoblast Proliferation and Myogenesis. *Dev Cell* (2012) 23:1176–88. doi: 10.1016/j.devcel.2012.10.019
44. Brunetti A, Goldfine ID. Differential Effects of Fibroblast Growth Factor on Insulin Receptor and Muscle Specific Protein Gene Expression in Bc3h-1 Myocytes. *Mol Endocrinol* (1990) 4:880–5. doi: 10.1210/MEND-4-6-880
45. Regué L, Ji F, Flicker D, Kramer D, Pierce W, Davidoff T, et al. IMP2 Increases Mouse Skeletal Muscle Mass and Voluntary Activity by Enhancing Autocrine Insulin-Like Growth Factor 2 Production and Optimizing Muscle Metabolism. *Mol Cell Biol* (2019) 39. doi: 10.1128/mcb.00528-18
46. Janiszewska M, Suvà ML, Riggi N, Houtkooper RH, Auwerx J, Clément-Schatlo V, et al. Imp2 Controls Oxidative Phosphorylation and Is Crucial for Preservin Glioblastoma Cancer Stem Cells. *Genes Dev* (2012) 26:1926–44. doi: 10.1101/gad.188292.112
47. Fujii Y, Kishi Y, Gotoh Y. IMP2 Regulates Differentiation Potentials of Mouse Neocortical Neural Precursor Cells. *Genes Cells* (2013) 18:79–89. doi: 10.1111/gtc.12024

Conflict of Interest: YH has received grants from Asahi Kasei Pharma, personal fees from Daiichi Sankyo Co., Ltd., personal fees from Mitsubishi Tanabe Pharma Corp., personal fees from Sanofi K.K., personal fees from Novo Nordisk Pharma Ltd., outside the submitted work. TS has received personal fees from Ono Pharma Co., Ltd., Mitsubishi Tanabe Pharma Co, Astellas Pharma Inc., Kyowa Hakko Kirin Co., Ltd., Sanofi K.K., MSD K.K., Kowa Pharma Co., Ltd., Taisho Toyama Pharma Co., Ltd., Takeda Pharma Co., Ltd., Kissei Pharma Co., Ltd., Novo Nordisk Pharma Ltd., Eli Lilly Japan K.K. outside the submitted work. EU has received grants from the Japanese Study Group for Physiology and Management of Blood Pressure, the Astellas Foundation for Research on Metabolic Disorders (Grant number: 4024). Donated Fund Laboratory of Diabetes therapeutics is an endowment department, supported with an unrestricted grant from Ono Pharmaceutical Co., Ltd., and received personal fees from AstraZeneca plc, Astellas Pharma Inc., Daiichi Sankyo Co., Ltd., Kyowa Hakko Kirin Company Ltd., Kowa Pharmaceutical Co., Ltd., MSD K.K., Mitsubishi Tanabe Pharma Corp., Novo Nordisk Pharma Ltd., Taisho Toyama Pharmaceutical Co., Ltd., Takeda Pharmaceutical Co., Ltd., Nippon Boehringer Ingelheim Co., Ltd., and Sumitomo Dainippon Pharma Co., Ltd., outside the submitted work. MH has received grants from Asahi Kasei Pharma, Nippon Boehringer Ingelheim Co., Ltd., Mitsubishi Tanabe Pharma Corporation, Daiichi Sankyo Co., Ltd., Sanofi K.K., Takeda Pharmaceutical Company Limited, Astellas Pharma Inc., Kyowa Kirin Co., Ltd., Sumitomo Dainippon Pharma Co., Ltd., Novo Nordisk Pharma Ltd., and Eli Lilly Japan K.K., outside the submitted work. MA received personal fees from Novo Nordisk Pharma Ltd., Abbott Japan Co., Ltd., AstraZeneca plc, Kowa Pharmaceutical Co., Ltd., Ono Pharmaceutical Co., Ltd., Takeda Pharmaceutical Co., Ltd., outside the submitted work. MY reports personal fees from MSD K.K., Sumitomo Dainippon Pharma Co., Ltd., Kowa

Company, Limited, AstraZeneca PLC, Takeda Pharmaceutical Company Limited, Kyowa Hakko Kirin Co., Ltd., Daiichi Sankyo Co., Ltd., Kowa Pharmaceutical Co., Ltd., Ono Pharma Co., Ltd., outside the submitted work. MF has received grants from Nippon Boehringer Ingelheim Co., Ltd., Kissei Pharma Co., Ltd., Mitsubishi Tanabe Pharma Co, Daiichi Sankyo Co., Ltd., Sanofi K.K., Takeda Pharma Co., Ltd., Astellas Pharma Inc., MSD K.K., Kyowa Hakko Kirin Co., Ltd., Sumitomo Dainippon Pharma Co., Ltd., Kowa Pharmaceutical Co., Ltd., Novo Nordisk Pharma Ltd., Ono Pharma Co., Ltd., Sanwa Kagaku Kenkyusho Co., Ltd. Eli Lilly Japan K.K., Taisho Pharma Co., Ltd., Terumo Co., Teijin Pharma Ltd., Nippon Chemiphar Co., Ltd., and Johnson & Johnson K.K. Medical Co., Abbott Japan Co., Ltd., and received personal fees from Nippon Boehringer Ingelheim Co., Ltd., Kissei Pharma Co., Ltd., Mitsubishi Tanabe Pharma Corp., Daiichi Sankyo Co., Ltd., Sanofi K.K., Takeda Pharma Co., Ltd., Astellas Pharma Inc., MSD K.K., Kyowa Kirin Co., Ltd., Sumitomo Dainippon Pharma Co., Ltd., Kowa Pharma Co., Ltd., Novo Nordisk Pharma Ltd., Ono Pharma Co., Ltd., Sanwa Kagaku Kenkyusho Co., Ltd., Eli Lilly Japan K.K., Taisho Pharma Co., Ltd., Bayer Yakuhin, Ltd., AstraZeneca K.K., Mochida Pharma Co., Ltd., Abbott Japan Co., Ltd., Medtronic Japan Co., Ltd., Arkley Inc., Teijin Pharma Ltd. and Nipro Cor., outside the submitted work.

The remaining authors declare that the research was conducted in the absence of any commercial or financial relationships that could be construed as a potential conflict of interest.

Publisher's Note: All claims expressed in this article are solely those of the authors and do not necessarily represent those of their affiliated organizations, or those of the publisher, the editors and the reviewers. Any product that may be evaluated in this article, or claim that may be made by its manufacturer, is not guaranteed or endorsed by the publisher.

frontiers in Endocrinology

ORIGINAL RESEARCH
published: 24 December 2021
doi: 10.3389/fendo.2021.809916

Maternal Glucose and LDL-Cholesterol Levels Are Related to Placental Leptin Gene Methylation, and, Together With Nutritional Factors, Largely Explain a Higher Methylation Level Among Ethnic South Asians

Line Sletner[1,2], Aina E. F. Moen[2,3,4], Chittaranjan S. Yajnik[5], Nadezhda Lekanova[3], Christine Sommer[6], Kåre I. Birkeland[7], Anne K. Jenum[8] and Yvonne Böttcher[2,3]*

[1] Department of Pediatric and Adolescents Medicine, Akershus University Hospital, Lørenskog, Norway, [2] Institute of Clinical Medicine, University of Oslo, Lørenskog, Norway, [3] Department of Clinical Molecular Biology, Akershus University Hospital, Lørenskog, Norway, [4] Division of Infection Control and Environmental Health, The Norwegian Institute of Public Health, Oslo, Norway, [5] Diabetes Unit, King Edward Memorial (KEM) Hospital and Research Centre, Pune, India, [6] Department of Endocrinology, Morbid Obesity and Preventive Medicine, Oslo University Hospital, Oslo, Norway, [7] Institute of Clinical Medicine, University of Oslo, Oslo, Norway, [8] General Practice Research Unit, Department of General Practice, Institute of Health and Society, Faculty of Medicine, University of Oslo, Oslo, Norway

OPEN ACCESS

Edited by:
GianLuca Colussi, University of Udine, Italy

Reviewed by:
Judit Bassols, Institute of Biomedical Research of Girona, Spain
Marion Ouidir, National Institutes of Health (NIH), United States

***Correspondence:**
Line Sletner
line.sletner@medisin.uio.no

Specialty section:
This article was submitted to Translational Endocrinology, a section of the journal Frontiers in Endocrinology

Received: *05 November 2021*
Accepted: *06 December 2021*
Published: *24 December 2021*

Citation:
Sletner L, Moen AEF, Yajnik CS, Lekanova N, Sommer C, Birkeland KI, Jenum AK and Böttcher Y (2021) Maternal Glucose and LDL-Cholesterol Levels Are Related to Placental Leptin Gene Methylation, and, Together With Nutritional Factors, Largely Explain a Higher Methylation Level Among Ethnic South Asians. Front. Endocrinol. 12:809916. doi: 10.3389/fendo.2021.809916

Background: Leptin, mainly secreted by fat cells, plays a core role in the regulation of appetite and body weight, and has been proposed as a mediator of metabolic programming. During pregnancy leptin is also secreted by the placenta, as well as being a key regulatory cytokine for the development, homeostatic regulation and nutrient transport within the placenta. South Asians have a high burden of type 2 diabetes, partly attributed to a "thin-fat-phenotype".

Objective: Our aim was to investigate how maternal ethnicity, adiposity and glucose- and lipid/cholesterol levels in pregnancy are related to placental leptin gene (*LEP*) DNA methylation.

Methods: We performed DNA methylation analyses of 13 placental *LEP* CpG sites in 40 ethnic Europeans and 40 ethnic South Asians participating in the STORK-Groruddalen cohort.

Results: South Asian ethnicity and gestational diabetes (GDM) were associated with higher placental *LEP* methylation. The largest ethnic difference was found for CpG11 [5.8% (95% CI: 2.4, 9.2), p<0.001], and the strongest associations with GDM was seen for CpG5 [5.2% (1.4, 9.0), p=0.008]. Higher maternal LDL-cholesterol was associated with lower placental *LEP* methylation, in particular for CpG11 [-3.6% (-5.5, -1.4) per one mmol/L increase in LDL, p<0.001]. After adjustments, including for nutritional factors involved in the one-carbon-metabolism cycle (vitamin D, B12 and folate levels), ethnic

differences in placental *LEP* methylation were strongly attenuated, while associations with glucose and LDL-cholesterol persisted.

Conclusions: Maternal glucose and lipid metabolism is related to placental *LEP* methylation, whilst metabolic and nutritional factors largely explain a higher methylation level among ethnic South Asians.

Keywords: Leptin, placenta, methylation, cholesterol, ethnicity, gestational diabetes

BACKGROUND

During normal pregnancy, physiological changes in maternal body composition and glucose and lipid metabolism occur to ensure appropriate supply of nutrients to the growing fetus (1). After an initial small decrease in insulin resistance, fasting glucose and lipid levels in early pregnancy, there is a progressive increase in insulin resistance, triglycerides, high-density lipoprotein (HDL) cholesterol and low-density lipoprotein (LDL) cholesterol as pregnancy progress (2). Glucose is the major nutrient required for fetal growth and is primarily sourced from the maternal circulation and transported across placenta by facilitated diffusion (1). Triglycerides are hydrolysed by lipases on the maternal side of the placental syncytiotrophoblast, and free fatty acids are released and taken up by the placenta. Cholesterol is important for placental and fetal growth and maturation and necessary for steroid hormone synthesis, including estrogen. Cholesterol is probably mainly delivered to the placenta by LDL-cholesterol, taken up by endocytosis (3).

Leptin is a peptide hormone central for energy homeostasis. It is secreted mainly by the adipose tissue, regulating energy balance by inhibiting hunger (4). During pregnancy leptin is also secreted from the placenta, and the maternal circulating leptin levels increase substantially with increasing gestation (5, 6). Within the placenta leptin has physiological effects on placenta development including angiogenesis, growth and immunomodulation, and there is support for it's role in the regulation of placental nutrient transport (e.g. glucose and amino-acids), by up-regulating specific placental nutrient transporter isoforms (5, 7). Expression of the leptin gene (*LEP)* is regulated in parts by epigenetic mechanisms. Several CpG islands are found in the *LEP* promoter region and methylation in these regions will affect the *LEP* expression (7–11).

Across the life span, ethnic South Asians have a high burden of type 2 diabetes and are diagnosed at a younger age and at a lower BMI than ethnic Europeans (12, 13). The increased risk is thought to be partly explained by South Asians being smaller and thinner at birth, but with relatively more adiposity, a phenotype that persists throughout life (14). This "thin-fat-phenotype" has been partly related to "the double burden of malnutrition", defined as the simultaneous manifestation of both undernutrition (primarily micronutrient deficiencies) and overnutrition (increased adiposity, hyperlipidemia and hyperglycemia), also during pregnancy (15). It is likely that the placenta plays an important role for these relationships.

Studies of maternal obesity and diabetes have reported inconsistent findings of methylation or gene expression in placental tissue (16, 17). Most studies exploring epigenetic mechanisms in placenta have been performed in Caucasian populations, and some suggest that maternal obesity and hyperglycemia are associated with hyper-methylation and hypo-expression of the *LEP* gene in placenta (8, 10, 17). Few studies have examined relations with maternal lipid concentrations or micronutrient levels. Leptin has been proposed as a mediator of metabolic programming. Given the differences in body composition, as well as different exposures to socioeconomic and nutritional factors across the life course, studying relations between maternal adiposity, glucose and lipid metabolism and placental *LEP* methylation in ethnic South Asian and European mothers living in Europe could thus shed light on mechanisms involved in developmental programming of metabolic diseases.

We therefore investigated the relationships of maternal ethnicity (European vs. South Asian), adiposity, hyperglycemia and lipid levels with placental DNA methylation in *LEP*, also taking nutritional factors into account, in a well characterized Norwegian cohort of pregnant women.

MATERIALS AND METHODS

Population and Design

Data are from a population-based cohort study of 823 presumably healthy pregnant women attending the Child Health Clinics in three city districts in Groruddalen, Oslo, Norway, for primary antenatal care from May 2008 to May 2010. The study design has been presented in detail elsewhere (18). The women were included at <20 weeks' gestation (Mean=15, standard deviation (s.d.)=3) and reexamined at 28 ± 2 weeks' gestation. All women were given oral and written information about the Stork Groruddalen project when attending the Child Health Clinics for antenatal care and invited to participate. The women who chose to participate gave informed written consent at inclusion, on behalf of themselves and their offspring.

The women were eligible if they were: (1) living in one of the three city districts, (2) would give birth at the study hospitals, (3) in gestational week < 20, (4) not suffering from diseases necessitating intensive hospital follow-up during pregnancy, (5) not already included in the study with a previous pregnancy lasting > 22 weeks, (6) could communicate (orally) in Norwegian or one of the other eight languages, and (7) were

able to provide informed written consent. Overall participation rate was 74% and the study cohort was representative for women attending the Child Health Clinics with respect to ethnicity and age, and fairly representative with respect to parity. Questionnaire data (through interview) and fasting blood samples were collected at both visits by specially trained study midwifes, supported by a professional interpreter and translated material when needed. At birth the weight of the baby was measured on calibrated electronic scales and umbilical cord serum was collected and frozen directly on -80°C.

Maternal Factors

The participants' ethnic origin was defined by her country of birth. If the participant's mother was born outside Europe or North America, country of origin was defined by the participant's mother's country of birth (18). All women with non-European ancestry were either born or had mothers born outside Europe.

Maternal height was measured at enrollment to the nearest 0.1 cm with a fixed stadiometer (18). Body weight and estimated body fat were measured with a bioelectrical impedance analysis (BIA) scale (Tanita-BC 418 MA, Tanita Corporation, Tokyo, Japan) at both visits with light clothing and without shoes. Pre-pregnant body mass index (BMI, weight (kg)/height $(m)^2$) was calculated using pre-pregnant weight (self-reported at inclusion), to the nearest kg, and measured height.

Parity was categorized as "primiparous" or "parous" (at least one previous pregnancy lasting more than 22 weeks). Maternal age was recorded in years at enrolment. Maternal present socioeconomic position was a score derived from a principal components analysis (PCA) of 11 different demographic variables (19). The variables contributing most to the score, were individual level data about education, occupational class and employment status, and household variables as own or renting tenure and rooms per person in the household. This score was normally distributed (mean=0, median=0.1, SD=1 range:-2.91 to 2.59). Maternal childhood socioeconomic position was derived from a separate PCA of three sociodemographic variables (family occupational class (highest of mother and father), rooms per person in household and family ownership of car, all referring to maternal age of 10 years), and was also normally distributed.

Biochemical Analyses

A standard 75 g oral glucose tolerance test (OGTT) was performed at Visit 2 at 28 ± 2 weeks' gestation. Women were diagnosed with gestational diabetes (GDM) according to the criteria recommended by the World Health Organization (WHO) between 1999-2013 (fasting plasma glucose >7 mmol/L or 2-hour glucose >7.8nmol/L) and given life style advise or specialist follow-up according to guidelines. However, for the present study we have defined GDM by the WHO 2013 criteria (fasting glucose ≥5.1 mmol/l or 2-h glucose ≥8.5 mmol/l) (20).

Fasting triglycerides, HDL- and total cholesterol (all measured in mmol/L) were analysed in serum, consecutively at each study visit, with a colorimetric method (Vitros 5.1 FS, Ortho clinical diagnostic at the routine laboratory at Akershus University Hospital). Serum 25-OH vitamin D was analysed by competitive RIA (Dia-Sorin) at the Hormone Laboratory, Oslo University Hospital. LDL-cholesterol was calculated using Friedewald`s formula (21) as follows: LDL-cholesterol = total cholesterol – HDL-cholesterol – (0.45 x triglycerides) mmol/L, which correlate well with directly measured LDL both early and late in pregnancy (r=0.97) (22). No women used lipid-lowering agents at any visit. Maternal and umbilical cord S-leptin (pg/ml) was analyzed in 2012 from biobanked (-80°C) material with the Luminex xMAP technology (Millipore Corporation, Billerica, MA, USA) at the Hormone Laboratory, Oslo University Hospital. Serum vitamin B12 and folate were measured from biobanked material in 2016, using electrochemiluminescence (ECLIA) assays, Roche, at Medical Biochemistry, Oslo University Hospital.

Placental Macroscopic Examinations and Processing

Placentas were refrigerated immediately after birth. The next working day placentas were macroscopically examined by a placental pathologist according to a standardized protocol, including weight before and after removal of membranes and cord, length (largest diameter), width (smallest diameter), thickness (central) and description of pathological changes. Further, section samples from the umbilical cord, membranes and two cross sections from macroscopic normal looking placental tissue in the central part of the disc, cross sections from pathological looking tissue and additional sections from the maternal plate, were taken. Tissue sections were fixed in buffered formalin and routinely processed and paraffin embedded (FFPE). For this study, FFPE tissue from the cross-sections of central normal looking placenta were used.

Placental Tissue Sample Preparation

DNA and RNA were purified using the Allprep DNA/RNA FFPE Kit (Qiagen, Hilden, Germany) according to manufacturer's instructions. In the present study only DNA was further analyzed. DNA quantity was obtained using Qubit™ dsDNA HS Assay Kit (Invitrogen,Thermo Fisher Scientific, Waltham, MA, USA). Samples were stored at -20°C until further processed. Bisulfite conversion was performed using the EpiTect Fast DNA Bisulfite Kit (Qiagen) according to manufacturer's instructions. In total, 500 ng of DNA was bisulfite converted for subsequent pyrosequencing analyses, with exception of samples where purified DNA concentrations were less than 20 ng/µl, where 300 ng of DNA was used.

Pyrosequencing

DNA methylation analyses of *LEP* and 13 CpG sites were performed as described by Bekkering et al. (23) The CpG annotation is also according to Bekkering et al. and the CpG site locations relative to *LEP* transcription start site (TSS) and nucleotide position are given in **Table 1**. Briefly, the PCR and sequencing primers were ordered using PyroMark Custom Assay (Qiagen). PCR amplification of the bisulfite converted DNA was performed using the PyroMark PCR Kit (Qiagen) and 1µl

TABLE 1 | The CpG site location relative to *LEP* transcription start site (TSS) and nucleotide position.

CpG	Location relative to TSS	GRCh38.p7 CpG nucleotide position
CpG1	-127	chr7:128.241.151
CpG2	-123	chr7:128.241.155
CpG3	-118	chr7:128.241.160
CpG4	-115	chr7:128.241.163
CpG5	-100	chr7:128.241.178
CpG6	-95	chr7:128.241.183
CpG7	-85	chr7:128.241.193
CpG8	-74	chr7:128.241.204
CpG9	-71	chr7:128.241.207
CpG10	-62	chr7:128.241.216
CpG11	-51	chr7:128.241.227
CpG12	-38	chr7:128.241.240
CpG13	-33	chr7:128.241.245

bisulfite template, and cycling conditions as described in the PyroMark PCR Kit protocol.

Pyrosequencing was performed using the PyroMarkQ48 Autoprep (Qiagen) according to manufacturer's instructions. All reactions were conducted in duplicates and for each sequencing run three controls, non-template (RNase-free water), unmethylated DNA and methylated DNA, were included. The two latter from the EpiTect PCR Control DNA Set (Qiagen). All duplicates were restricted to a minimum difference in % methylation of < 5%. If the criteria were not met the samples were re-run. The mean percentage DNA methylation was used per sample. The sequencing data for all 13 CpG sites in *LEP* were quality control checked by the PyroMarkQ48 Autoprep software and the percentage of DNA methylation were calculated. For samples where CpG site(s) did not pass quality control, analyses were repeated until satisfactory results were obtained. Two samples were excluded as they repeatedly failed quality control.

Statistical Methods

Descriptives are given as mean (SD), median (IQR) and n (%) as appropriate. We examined the correlation between the methylation of the different CpGs using scatterplots and the Pearson's correlation coefficient. Univariate linear regression analyses were first used to explore associations of maternal factors, placental characteristics and circulating leptin with *LEP* methylation (CpG 1-13). Based on these results we further performed multivariate general linear model analyses to explore the independent effects of the maternal factors of most interest according to our aim (ethnicity, GDM, LDL-cholesterol and fat mass) on*LEP* methylation, adjusting for clinically important covariates; age, parity, socioeconomic status and height. In a final model we also adjusted for maternal vitamin B12, folate and 25-OH vitamin D levels. We assessed potential interactions with ethnicity by examining scatterplots and by performing our analyses stratified by ethnic group; first univariate and then in the fully adjusted models. We also entered interaction terms between ethnicity*GDM or ethnicity*LDL-cholesterol, one by one into the fully adjusted models. In sensitivity analyses we replaced "total fat mass at enrollment" as the measure of maternal adiposity with either pre-pregnant BMI, total fat mass at 28 weeks' gestation or maternal sum of skinfolds, with similar results.

A priori, we planned to draw conclusions based on effect estimates and their CIs, rather than statistical tests using an arbitrary P-value cut-off. Nevertheless, in tables p-values <0.05 are written in bold and in figures the point estimates are marked with * reflecting the precision of the estimate (* when p<0.05 but >0.01, ** when p ≤ 0.01 but >0.001 and *** when p<0.001). All P-values given are uncorrected for multiple testing, i.e. we did not take into account the number of CpG sites tested (*N*=13).

RESULTS

Sample Characteristics

Eligible for the present study were ethnic Western European and South Asian mothers participating in the STORK-Groruddalen cohort, with singleton pregnancies, gestational age ≥35 weeks and a valid weight at birth, a macroscopic placenta examination performed, and data regarding GDM from an oral glucose tolerance test (OGTT), offered to all study participants (**Figure S1**, Flow chart). From these we randomly chose 80 placentas, 40 European (36 with Norwegian and 4 with other Western European background) and 40 South Asian (26 with Pakistani and 14 with Sri Lankan or Indian background), with similar numbers of boys and girls in both groups.

Characteristics of the study participants are presented in **Table 2**. South Asian mothers were slightly younger, had a lower early life and present socioeconomic position and were shorter. They also had lower levels of vitamin B12, folate and 25-OH vitamin D in early pregnancy. Mean body fat did not differ significantly, while 2-hour glucose levels from the OGTT at 28 weeks' gestation was slightly higher and LDL-cholesterol was lower in the South Asians. Differences between the two ethnic groups reflected the differences previously reported in the total cohort (n=823) (6, 19, 20). [+(Waage,et. al. submitted)] South Asian mothers also had smaller placentas, represented by a lower weight and smaller length and width, but a similar thickness, and birthweight of the offspring was lower (**Table 2**).

Associations Between Maternal Factors and Placental *LEP* Methylation

The mean *LEP* methylation level in the placental tissue differed considerably between the 13 *LEP* CpGs, ranging between 8% (CpG3) and 63% (CpG11) (**Table S1**). The methylation of the different CpGs were highly correlated with each other (Pearson's correlation coefficient >0.8), except for CpG11, which was less correlated with CpG 1, 2, 3, 4, 7, 9 and 10, and for CpG5, which was less correlated with CpG 2 and 3 (correlation coefficients between 0.5-0.7) (data not shown). For all CpGs, the mean placental methylation level was numerically higher in South Asians than in Europeans, and the differences were significant for 10 out of 13 CpGs (**Figure 1** and **Tables S2A**–**E**). The largest difference was observed for CpG11 (mean difference: 5.8% (95% CI: 2.4, 9.2), p<0.001), followed by CpG5 (5.0% (1.3, 8.8), p=0.01).

TABLE 2 | Maternal and placental characteristics.

	n	Total sample	n	Western European	n	South Asian	p
Maternal characteristics							
Gestational week at enrollment	80	15.0 (3.3)	40	14.0 (2.2)	40	**16.0 (3.8)**	**0.007**
Gestational week at OGTT[a]	80	28.2 (1.1)	40	28.2 (1.3)	40	28.2 (0.9)	0.8
Age (years), mean (sd)	80	29.5 (4.6)	40	30.7 (4.5)	40	**28.3 (4.3)**	**0.02**
Parity (number of previous births)	80		40		40		0.2
Nullipara		30 (37%)		16 (40%)		14 (35%)	
Para 1		36 (45%)		20 (50%)		16 (40%)	
Para 2+		14 (18%)		4 (10%)		10 (25%)	
Born in Norway	80	40 (50%)	40	36 (90%)	40	**4 (10%)**	**<0.001**
Childhood socioeconomic score[b]	79	0.02 (1.0)	40	0.72 (0.77)	39	**-0.60 (0.67)**	**<0.001**
Present socioeconomic score[c]	80	0.2 (0.8)	40	0.5 (0.7)	40	**-0.2 (0.8)**	**0.001**
Any smoking at OGTT	80	0	40	0	40	0	–
Height (cm)	80	164.7 (5.8)	40	168.0 (5.4)	40	**161.3 (4.0)**	**<0.001**
Prepregnant BMI (kg/m2)	78	24.1 (3.9)	39	24.7 (3.7)	39	23.5 (4.0)	0.2
Total fat mass (kg) at enrollment[d]	80	23.2 (8.4)	40	24.2 (8.5)	40	22.1 (8.2)	0.3
Sum of skinfolds (mm) at enrollment[e]	73	72.2 (19.6)	36	69.3 (20.5)	37	75.0 (18.5)	0.2
Nutritional factors (at enrollment)							
Vitamin B12 (pmol/L)	79	247 (86)	39	268 (93)	40	**227 (76)**	**0.03**
Folate (nmol/L)	79	23.7 (10.9)	39	28.6 (9.6)	40	**18.9 (10.0)**	**<0.001**
25OH-Vitamin D (nmol/L)	79	50.8 (27.7)	39	70.0 (22.7)	40	**32.1 (17.4)**	**<0.001**
Glucose measures (at OGTT)							
Gestational diabetes[f]	80	34 (43%)	40	15 (38%)	40	19 (48%)	0.4
Fasting glucose (mmol/L)	80	4.9 (0.6)	40	4.9 (0.6)	40	5.0 (0.5)	0.4
2-hour plasma glucose (mmol/L)	79	6.1 (1.4)	40	5.7 (1.2)	39	6.4 (1.5)	**0.02**
Lipids (at OGTT)							
Fasting HDL (mmol/L)	79	1.9 (0.4)	39	2.0 (0.5)	40	1.8 (0.4)	0.2
Fasting LDL (mmol/L)	78	3.5 (0.9)	39	3.9 (0.8)	39	**3.2 (0.9)**	**0.001**
Fasting Triglycerides (mmol/L)	79	2.0 (0.8)	39	2.0 (0.8)	40	2.0 (0.7)	0.8
Placental characteristics							
Weight (g) excl. cord and membr.	80	495 (115)	40	520 (116)	40	**469 (110)**	**0.04**
Thickness (cm)	77	2.5 (0.5)	38	2.6 (0.5)	39	2.6 (0.5)	0.9
The larger diameter (cm)	79	18.5 (2.1)	39	19.1 (2.3)	40	**18.0 (1.8)**	**0.02**
The smaller diameter (cm)	79	16.6 (2.0)	39	17.0 (1.8)	40	**16.1 (2.0)**	**0.03**
Morphological changes	80	14 (18%)	40	5 (13%)[g]	40	9 (23%)[h]	–
Birth characteristics							
Gestational age (days)	80	282 (10)	40	283 (10)	40	279 (10)	0.1
Birthweight (g)	80	3413 (550)	40	3583 (541)	40	**3242 (511)**	**0.005**
Serum leptin							
S-leptin (pg/ml) at enrollment	80	1411 (912, 1998)	40	1116 (802, 1752)	40	1727 (1213, 2137)	0.07
S-leptin (pg/ml) at OGTT	78	1925 (1158, 3055)	40	1708 (970, 2457)	38	2225 (1380, 3089)	0.2
Umbilical cord S-leptin (pg/ml)	72	1980 (1056, 3463)	37	1982 (879, 3078)	35	1945 (1148, 4023)	0.7

Numbers are mean (sd), n (%) or median (IQR) as appropriate. Differences between the two ethnic groups were assesses using Pearson Chi-Square tests or t-tests, as appropriate. P-values for such possible differences are given in the right column. Significant differences are marked in bold.

[a]*OGTT = Oral glucose tolerance test performed at 28 ± 2 weeks' gestation (glucose measured fasting and 2 hours after drinking 75g glucose; to diagnose gestational diabetes) GDM classified by WHO 2013 criteria = Fasting glucose ≥ 5.1 mmol/L or 2-hour glucose ≥ 8.5 mmol/L.*

[b]*Score extracted form a Principal Components Analyses of 3 demographic variables reflecting maternal socioeconomic status at age 10 years. Mean=0, median=0.1, SD=1 range:-2.91 to 2.59).*

[c]*Score extracted form a Principal Components Analyses of 11 demographic variables reflecting maternal socioeconomic status at enrolment.*

[d]*Measured with a bioelectrical impedance analysis (BIA) scale (Tanita-BC 418 MA).*

[e]*Sum of suprailiac, triceps and subscapular skinfolds, measured by Holtain T/W Caliper 0-48mm (Holtain Ltd., Crymych; UK).*

[f]*As defined by the WHO 2013 criteria (fasting glucose ≥5.1 mmol/l or 2-h glucose ≥8.5 mmol/l).*

[g]*Two placentas with signs of chorioamnionitis, three placentas with small infarctions (<5% of volume).*

[h]*One placenta with signs of chorioamnionitis, six placentas with small infarctions (five < 5% of volume, one 25% of volume), one placenta with signs of vilitis.*

Measures of placental size (weight, length, width or thickness) were not consistently associated with *LEP* methylation (**Tables S2A–E**). We also found no associations with any of the measures of maternal adiposity (total fat mass at enrollment, pre-pregnant BMI, total fat mass at 28 weeks' gestation or maternal sum of skinfolds), or with circulating s-leptin in maternal nor umbilical cord venous blood (**Tables S2A–E**), in any of the two ethnic groups (data not shown).

In univariate analyses GDM was associated with higher placental *LEP* methylation, with higher levels for 8 out of 13 CpGs (**Tables S2A–E**). The strongest association was seen for CpG5 (5.2% (1.4, 9.0), p=0.008, **Table S2B**), followed by CpG12 (4.6 (1.6, 7.5), p=0.003, **Table S2D**). However, while univariate nominal associations with GDM were observed for 11 out of 13 CpGs in South Asians, only smaller, non-significant trends were seen in Europeans (**Table 3**). Exploration of scatteplots and

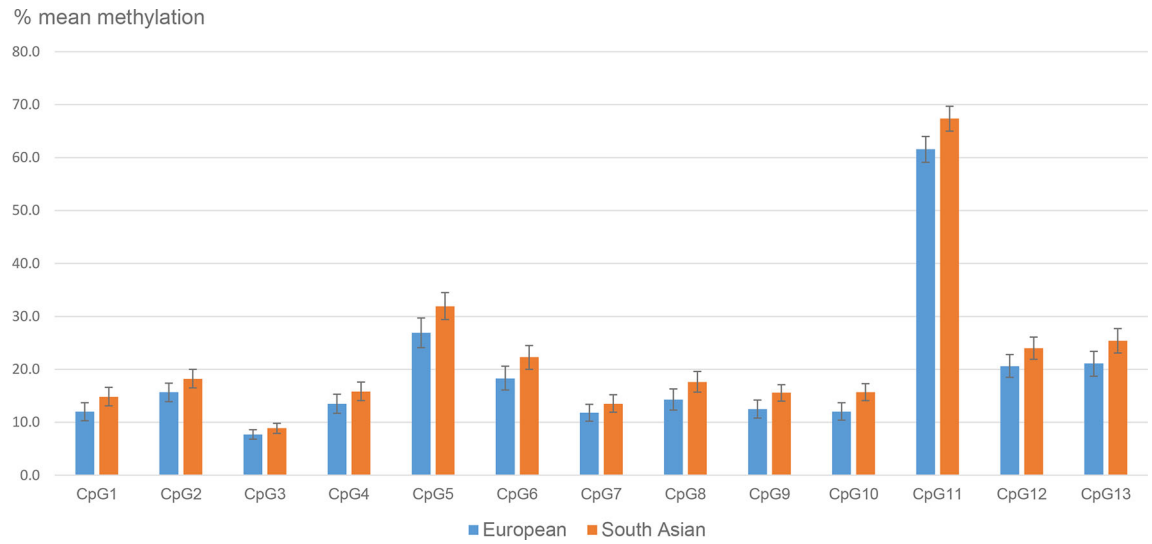

FIGURE 1 | Mean placental *LEP* methylation (95% CI) in ethnic European and South Asian women.

univariate analyses did not indicate similar differential effects of LDL-cholesterol in the two ethnic groups.

Regarding maternal lipids, higher fasting LDL-cholesterol levels at 28 weeks' gestation was associated with lower placental *LEP* methylation in 12 out of 13 CpGs (**Tables S2A–E**). The strongest association was seen for CpG11, where one mmol/L increase in LDL-cholesterol was associated with 3.6% (-5.5, -1.4) lower methylation (p<0.001, **Table S2D**), followed by CpG5 (-3.2% (-5.3, -1.2, p=0.003), **Table S2B**). HDL-cholesterol was not consistently associated with *LEP* methylation, although nominally negatively associated with CpG11 methylation (p=0.03). For fasting triglycerides, we observed no significant associations with DNA methylation for any of the 13 CpG sites in *LEP*.

Using multivariate linear models we further examined the independent effects of ethnicity and metabolic factors on placental *LEP* methylation. As the strongest associations with ethnicity were found for CpG11, 5 and 13, results from multivariate are shown for these three CpGs in **Tables 4A–C**. However, similar results are shown for all CpGs in **Table S3**. As described above, South Asian ethnic origin and GDM were positively and LDL-cholesterol negatively associated with the *LEP* methylation level in univariate analyses. After mutual adjustments, and adjustments for maternal age, height, early life socioeconomic position and parity, GDM and LDL-cholesterol remained significantly associated with the methylation level, while the effect estimate for ethnicity was attenuated and no longer significant (**Table 4**, Model 1). When further adjusting for maternal vitamin D, B12 and folate status, the association with ethnicity disappeared (**Table 4**, Model 2), the association with GDM was somewhat attenuated and only

TABLE 3 | Mean % placental *LEP* methylation (95% CI) of CpG 1-13 in ethnic European and South Asian women with and without GDM.

	Europe			South Asia		
	non-GDM n = 25	GDM n = 15	p	non-GDM n = 21	GDM n = 19	p
CpG1	11.5 (9.4, 13.6)	12.8 (10.1, 15.5)	0.5	12.6 (10.4, 14.9)	17.3 (14.9, 19.7)	**0.007**
CpG2	15.5 (13.3, 17.7)	15.9 (13.2, 18.6)	0.8	16.5 (14.2, 18.8)	20.3 (17.8, 22.7)	**0.04**
CpG3	7.2 (6.1, 8.4)	8.4 (6.9, 9.9)	0.2	8.1 (6.9, 9.4)	9.8 (8.4, 11.3)	0.08
CpG4	12.8 (10.5, 15.0)	14.5 (10.5, 15.0)	0.4	14.3 (11.9, 16.6)	17.8 (15.2, 20.4)	**0.04**
CpG5	26.0 (22.7, 29.3)	28.7 (24.1, 33.2)	0.4	29.1 (25.8, 32.4)	35.4 (31.7, 39.1)	**0.01**
CpG6	18.4 (15.5, 21.3)	18.3 (14.9, 21.7)	0.9	20.0 (17.1, 22.9)	25.3 (22.0, 28.6)	**0.02**
CpG7	11.2 (9.1, 13.3)	12.7 (10.2, 15.2)	0.4	12.4 (10.3, 14.6)	14.9 (12.4, 17.3)	0.1
CpG8	14.1 (11.7, 16.6)	14.7 (11.5, 17.8)	0.8	15.7 (13.1, 18.3)	19.9 (17.1, 22.7)	**0.03**
CpG9	12.1 (10.1, 14.1)	13.2 (10.5, 15.8)	0.5	13.7 (11.6, 15.8)	17.7 (15.5, 20.0)	**0.02**
CpG10	11.8 (9.8, 13.8)	12.4 (9.9, 14.9)	0.7	13.7 (11.6, 15.8)	17.8 (15.6, 20.1)	**0.01**
CpG11	60.7 (57.7, 63.8)	62.9 (59.1, 66.7)	0.4	65.3 (62.1, 68.5)	69.7 (57.7, 63.8)	**0.03**
CpG12	19.5 (16.9, 22.0)	22.5 (19.2, 25.7)	0.2	21.5 (18.9, 24.1)	27.3 (24.3, 30.3)	**0.004**
CpG13	20.8 (17.8, 23.9)	21.6 (18.0, 25.2)	0.7	22.9 (20.0, 25.9)	28.4 (25.1, 31.7)	**0.02**

p-values represents the significance level for the difference between GDM and non-GDM from univariate general linear models (similar to t-tests). Significant differences are written in bold.

borderline significant while the association with LDL-cholesterol remained significant. In fully adjusted models higher maternal folate was associated with higher *LEP* metylation.

Last, we checked for interactions with ethnicity, by entering interaction terms ethnicity* GDM or ethnicity*LDL-cholesterol one by one into the fully adjusted models. No significant interactions were observed (p>0.3 for all, and >0.7 for CpG5 and CpG11). We also performed multivariate analyses stratified by ethnic group. Although not significant in all, effect estimates for GDM, LDL-cholesterol, adiposity and nutritional factors were similar across the two ethnic groups (data not shown). In supplementary analyses, exchanging GDM with maternal fasting or 2-hour glucose as explanatory factors, we found similar results as when using GDM (**Tables S4A–C**).

DISCUSSION

As far as we are aware, this is the first study exploring ethnic differences in placental *LEP* methylation, and relationships with both maternal glycaemia, lipid levels and adiposity. We found that South Asian ethnic origin and maternal GDM were associated with higher placental *LEP* methylation, while higher LDL-cholesterol was associated with lower *LEP* methylation. The strongest associations with these three maternal factors were found for CpG11 and CpG5, which are known binding sites for important transcription factors. Ethnic differences were, however, strongly attenuated and no longer significant when adjusting for metabolic factors and vitamin status. In contrast, measures of placental size, maternal adiposity or circulating leptin levels were not associated with placental *LEP* methylation.

Leptin is involved in the regulation of multiple aspects of maternal metabolic homeostasis (7). Furthermore, leptin has been shown to also be important for placentation and maternal–fetal exchange processes (5). We did not find any associations between maternal or fetal circulating levels of leptin and placental *LEP* methylation. Hence, placental *LEP* methylation seems to be related to other factors than maternal and offspring leptin levels.

To the best of our knowledge, no other studies have so far investigated variations in placental *LEP* methylation across different ethnic groups. Limited information also exists from other tissues. A study from US comparing whole blood *LEP*

TABLE 4 | Associations between maternal factors and placental *LEP* CpG5, CpG11 and CpG13 methylation.

Table 4a | Associations with CpG5 methylation.

	Univariate		Model 1		Model 2	
	β (95% CI)	p	β (95% CI)	p	β (95% CI)	p
South Asian ethnicity	5.0 (1.3, 8.8)	**0.01**	2.9 (-3.6, 9.4)	0.4	1.4 (-5.9, 8.7)	0.7
Gestational diabetes	5.2 (1.4, 9.0)	**0.008**	4.8 (0.6, 8.9)	**0.03**	4.0 (-0.1, 8.1)	0.05
Fat mass (kg)	0.0 (-0.2, 0.3)	0.9	-0.1 (-0.4, 0.2)	0.6	-0.0 (-0.3, 0.3)	0.9
LDL cholesterol	-3.2 (-5.3, -1.2)	**0.003**	-2.1 (-4.3, 0.2)	**0.07**	-2.8 (-5.0, -0.6)	**0.02**
Vitamin B12	-0.01 (-0.04, 0.02)	0.5			-0.02 (-0.05, 0.25)	0.2
Folate	-0.00 (-0.19, 0.18)	1			0.26 (0.05, 0.48)	**0.02**
Vitamin D	-0.08 (-0.15, -0.01)	**0.02**			-0.07 (-0.17, 0.04)	0.2

Table 4b | Associations with CpG11 methylation.

	Univariate β (95% CI)	p	Model 1 β (95% CI)	p	Model 2 β (95% CI)	p
South Asian ethnicity	5.8 (2.4, 9.2)	**0.001**	3.8 (-1.5, 9.1)	0.2	0.7 (-5.1, 6.5)	0.8
Gestational diabetes	3.8 (0.2, 7.3)	**0.04**	3.9 (0.2, 7.5)	**0.04**	2.7 (-0.9, 6.3)	0.1
Fat mass (kg)	-0.1 (-0.3, 0.2)	0.6	-0.1 (-0.4, 0.1)	0.4	-0.1 (-0.3, 0.2)	0.6
LDL cholesterol	-3.6 (-5.5, -1.8)	**<0.001**	-2.5 (-4.4, -0.5)	**0.02**	-3.1 (-5.1, -1.2)	**0.002**
Vitamin B12	-0.01 (-0.04, 0.01)	0.2			-0.02 (-0.04, 0.01)	0.1
Folate	-0.07 (-0.24, 0.10)	0.4			0.15 (-0.02, 0.32)	0.09
Vitamin D	-0.10 (-0.17, -0.04)	**0.001**			-0.07 (-0.16, 0.02)	0.1

Table 4c | Associations with CpG13 metylation.

	Univariate β (95% CI)	p	Model 1 β (95% CI)	p	Model 2 β (95% CI)	p
South Asian ethnicity	4.2 (0.9, 7.5)	**0.01**	4.3 (-0.9, 9.6)	0.1	3.6 (-2.2, 9.5)	0.2
Gestational diabetes	3.4 (0.05, 6.8)	**0.04**	4.4 (0.8, 8.0)	**0.02**	3.4 (-0.3, 7.1)	0.07
Fat mass (kg)	-0.1 (-0.3, 0.1)	0.3	-0.2 (-0.4, 0.02)	0.07	-0.1 (-0.4, 0.1)	0.4
LDL cholesterol	-2.4 (-4.3, -0.6)	**0.01**	-1.5 (-3.4, 0.5)	**0.1**	-2.2 (-4.2, -0.3)	**0.03**
Vitamin B12	-0.01 (-0.04, 0.01)	0.2			-0.02 (-0.04, 0.01)	0.2
Folate	0.03 (-0.13, 0.19)	0.7			0.22 (0.04, 0.40)	**0.02**
Vitamin D	-0.05 (-0.11, 0.01)	0.1			-0.02 (-0.11, 0.07)	0.7

Betas are effect estimates from univariate and multivariate general linear models, adjusting for covariates. Significant effects (p < 0.05) are written in bold.
Model 1: Variables included in the model: ethnicity, age, height, early life socioeconomic position, parity, gestational diabetes, total fat mass and LDL-cholesterol.
Model 2: Variables included in the model: ethnicity, age, height, early life socioeconomic position, parity, gestational diabetes, total fat mass, LDL-cholesterol, vit B12, folate and 25-OH Vit D.

methylation in adults and children with Northern European vs Vietnamese (East Asian) origin showed a lower methylation level in ethnic Vietnamese participants (24). Interestingly, in line with our data they also found the largest difference in the CpG-site that corresponds to our CpG11. However, the relationship to ethnicity was in the opposite direction compared to our findings in placentas from South Asian mothers. We can only speculate as to whether this merely reflects that methylation is tissue-specific, or whether it could be related to differences between these two Asian sub-groups.

Consistently, higher DNA methylation levels in South Asians were observed across all CpG sites investigated in the present study, suggesting a general hypermethylation of *LEP* in placentas of South Asians compared with individuals of European descent. The mechanistic background remains elusive, but could partly be due to genetic factors, as genetic variation may partly influence DNA methylation, e.g. by SNP markers introducing or deleting CpG sites (25, 26). However, people belonging to different ethnic groups may also differ on several other environmental factors not captured by genetic ancestry. For example, changes in the methylation of *LEP* have been observed in blood cells in adults exposed to famine when *in-utero* (27). In our study, 90% of the women with South Asian ancestry were born in Pakistan, India or Sri Lanka, classified as low or middle income countries, and had a lower socioeconomic position in childhood, compared with women of European origin. Although we did not find significant associations with maternal height or early life socioeconomic position, this could potentially have induced adaptive effects on regulatory mechanisms within the placenta.

In our cohort of pregnant women with expected normal pregnancies, all women were offered screening for GDM, and the majority hence had a relatively mild GDM (20). Nevertheless, we found that GDM was associated with higher *LEP* methylation. This is in line with some previous studies (17, 28). One study by Lesseur et al., obtaining GDM status from medical charts, found that placentas from mothers with GDM had 2.5% higher *LEP* methylation levels than in mothers not diagnosed with GDM (28). This effect estimate was slightly smaller than in our study. In another study by Bouchard et al. they found that in women with impaired glucose tolerance, placental leptin gene DNA methylation levels were associated with maternal 2-h glucose levels. However, this association depended on the placental site the tissue was sampled from (10). The different methodology makes direct comparison with our findings difficult and illustrates the complexity involved in these relationships.

In contrast to our findings, Lesseur et al. reported an association between maternal obesity and placental *LEP* methylation, and that this was largely mediated through an effect on GDM (28). Further, a study from France observed placental hypermethylation and hypoexpression of *LEP* in relation with maternal obesity (8), while a study from Spain did not find any obesity-related changes in placental *LEP* expression (29). We found no differences in placental *LEP* methylation across various levels of maternal adiposity. These findings were similar in the two ethnic groups and across different measures of adiposity, suggesting that adiposity is not the primary explanation for the observed associations with ethnicity and glucose- and lipid metabolism.

We have not been able to find any previous studies exploring associations between maternal lipid/lipoprotein levels and placental *LEP* methylation. A study by Houde et al. did show that in severely obese non-pregnant adults, LDL-cholesterol levels were positively associated with *LEP* methylation levels both in whole blood and in adipose tissue, suggesting that LDL-cholesterol might be involved in the epigenetic regulation of leptin (30). However, the positive associations were, in contrast to the negative association observed in placental tissue in our study. LDL-cholesterol is possibly the most important source of cholesterol for the fetus (3). A recent Norwegian *in vivo* study showed that fetal cholesterol uptake was related to the uteroplacental uptake of cholesterol from LDL-cholesterol, suggesting that the placenta influences maternal-fetal cholesterol transfer (31). Some previous studies have indicated that leptin plays a role in the regulation of placental glucose and amino-acid transport, by up-regulating specific placental nutrient transporter isoforms (5). From our finding we could thus speculate that placental leptin may also be involved in the regulation of LDL-cholesterol transport in the placenta.

Interestingly, in the study by Houde et al., as in our study, the strongest associations with LDL cholesterol were found for the two CpG sites that corresponds to our CpG11 and CpG5. In our study the strongest relations with ethnicity and GDM were also seen for CpG11 and CpG5. Methylation of these two CpGs, and in particular CpG11, were less correlated with the metylation of other CpGs. These two CpGs are located at binding sites for known transcription factors (32). CpG5 is located at the binding site for the specificity protein 1 (SP1), known to be involved in the *LEP* gene expression regulation in adipocytes (32, 33), especially in the induction of leptin by insulin-stimulated glucose metabolism as reported by Moreno-Aliaga et al. (34) Further, CpG11 is located at a binding site for CCAAT/enhancer binding protein-α (CEBPA). The gene coding for CEBPA is considered a core regulatory gene in the control of adipogenesis (11). Binding of CEBPA at this site highly activates the transcription of *LEP*, and methylation of this site has been shown to repress transcription of the *LEP* gene (32, 35). Our results support that also in placental tissue it is likely that these sites are subject to regulatory mechanisms and changes in gene expression affected by maternal glucose metabolism, and thus could have important functions during pregnancy beyond its accepted action on maturation of adipocytes for energy storage (7). However, our findings further suggest that the regulation of *LEP* expression in placental tissue differs from blood and adipose tissue.

In univariate stratified analyses we found that effect estimates for the association between GDM and placental *LEP* methylation were nominally larger, and only significant for South Asians. We could speculate that this finding reflect that GDM in South Asians to a larger extent represent pre-gestational dysglycemia and hence more "severe" GDM. We had limited statistical power

to do formal interaction analyses and to test direct vs. indirect effects of the different exposures. However, interaction analyses and stratified analyses in fully adjusted models did not suggest that the effects of GDM, LDL-cholesterol and nutritional factors differed between the two ethnic groups. This indicate that the suggested stronger effect of GDM in South Asians from univariate analyses are mainly related to differences in other covariates.

In our study, South Asian mothers had lower levels of vitamin D, B12 and folate than ethnic European mothers in early pregnancy. Folate and vitamin B12 are key factors in generating methionine that represents a major source of S-adenosylmethionine (SAM), the major methyl-donating substrate for DNA methylation, and hence strongly influences DNA methylation levels (36). Also, vitamin D has effects on genome wide DNA methylation levels and was recently reported to influence long-chain polyunsaturated fatty acids and oxidative stress in the placenta *via* one-carbon metabolism (37). The relations between nutritional factors and the methylation of regulatory cytokines in placenta is likely very complicated, where not only the level of each nutritional factor itself, but also the combination of different factors may be important (38, 39). Differences in vitamin levels could also be proxy measures of other complex life-style factors. Nevertheless, our findings suggest that nutritional factors may be involved in the regulation of key placental cytokines also in generally well-nourished multi-ethnic European populations.

The present study has several strengths. First, we have studied relationships with *LEP* methylation in two distinct ethnic groups, known to have different metabolic phenotypes, participating in the same cohort study, ruling out methodological issues to explain observed ethnic differences. Second, this cohort of pregnant women were followed from early pregnancy, and we have an extensive maternal dataset, including information about early life socioeconomic conditions, lipids/lipoproteins, glucose data from universal screening of GDM, different measures of adiposity and micronutrient status, specifically vitamins known to be involved in the one-carbon metabolism cycle, and more. Nevertheless, there are also important limitations to the study. We had a relatively small sample size, which limited our power; e.g. for interaction analyses and to test direct vs. indirect effects. Although transversal tissue sections from the central placenta will mainly consist of tissue from the fetal compartment (chorionic plate, villi), it could possibly also contain smaller amounts of tissue of maternal origin (intervillous space and basal plate). Moreover, even within fetal tissue different cell types may be present. As methylation is cell-type specific, this could have implications for our results. However, in our study such differences between placental samples should occur completely at random, and would thus not explain the observed associations with ethnicity or lipid and glucose levels. As we observed similar patterns of associations with ethnicity, GDM and LDL-cholesterol across all CpGs, and we consider this study as exploratory and hypothesis generating, we did not correct the p-values for multiple testing, i.e. we did not take into account the number of CpG sites tested (N=13). If we had applied Bonferroni correction for association analyses, the study-specific significance threshold for the analyses would have been lowered to P=0.0038 (0.05/13). Some of the observed associations would hence still be significant.

CONCLUSIONS

The relationships between maternal factors, placental function and fetal development are probably mediated through a complex system likely affected by genomic differences and adaptive processes. Leptin is considered a key regulatory cytokine within the placenta. Our findings suggest that maternal glucose and cholesterol metabolism in pregnancy can alter placental *LEP* metylation, in particular at some CpG sites which are known as binding sites for important transcription factors. Further, our results indicate that differences in maternal metabolism and nutritional status between ethnic Europeans and South Asians could explain most of the ethnic variation in placental *LEP* methylation. Understanding the impact of maternal metabolic and nutritional factors on placental epigenetic marks is particularly important given the current rise in prevalence of obesity, GDM and type 2 diabetes, not least in the South Asian population, and the possible consequences on later-life disease susceptibility.

DATA AVAILABILITY STATEMENT

The datasets presented in this article are not readily available because of restrictions e.g. their containing information that could compromise the privacy of the study participants. Requests to access the datasets should be directed to the corresponding author.

ETHICS STATEMENT

The studies involving human participants were reviewed and approved by the Regional Committee for Medical and Health Research Ethics for South Eastern Norway. The patients/participants provided their written informed consent to participate in this study.

AUTHOR CONTRIBUTIONS

LS, AJ, and KB contributed in the data acquisition. LS and YB planned the study. AM and NL performed the epigenetic laboratory analyses. LS performed the statistical analyses and wrote the manuscript. LS, AM, YB, CY, and CS contributed on the interpretation of the data. All authors critically revised the paper and approved the final manuscript.

FUNDING

This work is funded by The South-Eastern Norway Regional Health Authority through a research project grant to LS (Grant number 2017-063). The funder had no role in data collection, analyses or interpretation of data or in writing the paper.

ACKNOWLEDGMENTS

The authors thank study staff at the Child Health Clinics in Stovner, Grorud and Bjerke districts in Oslo for help with collecting the maternal data. We also thank B. Casati, G. Turowski, B. Roald and other staff at the dept. of pathology at Akershus University Hospital and Oslo University Hospital for performing the placental macroscopic examinations and tissue preparation.

SUPPLEMENTARY MATERIAL

The Supplementary Material for this article can be found online at: https://www.frontiersin.org/articles/10.3389/fendo.2021.809916/full#supplementary-material

REFERENCES

1. Lager S, Powell TL. Regulation of Nutrient Transport Across the Placenta. *J Pregnancy* (2012) 2012:179827. doi: 10.1155/2012/179827
2. Butte NF. Carbohydrate and Lipid Metabolism in Pregnancy: Normal Compared With Gestational Diabetes Mellitus. *Am J Clin Nutr* (2000) 71 (5):1256s–61s. doi: 10.1093/ajcn/71.5.1256s
3. Malassine A, Alsat E, Besse C, Rebourcet R, Cedard L. Acetylated Low Density Lipoprotein Endocytosis by Human Syncytiotrophoblast in Culture. *Placenta* (1990) 11(2):191–204. doi: 10.1016/S0143-4004(05)80180-8
4. Friedman JM. Leptin and the Endocrine Control of Energy Balance. *Nat Metab* (2019) 1(8):754–64. doi: 10.1038/s42255-019-0095-y
5. Tessier DR, Ferraro ZM, Gruslin A. Role of Leptin in Pregnancy: Consequences of Maternal Obesity. *Placenta* (2013) 34(3):205–11. doi: 10.1016/j.placenta.2012.11.035
6. Sommer C, Jenum AK, Waage CW, Morkrid K, Sletner L, Birkeland KI. Ethnic Differences in BMI, Subcutaneous Fat, and Serum Leptin Levels During and After Pregnancy and Risk of Gestational Diabetes. *Eur J Endocrinol* (2015) 172(6):649–56. doi: 10.1530/EJE-15-0060
7. Schanton M, Maymo JL, Perez-Perez A, Sanchez-Margalet V, Varone CL. Involvement of Leptin in the Molecular Physiology of the Placenta. *Reproduction* (2018) 155(1):R1–R12. doi: 10.1530/REP-17-0512
8. Nogues P, Dos Santos E, Jammes H, Berveiller P, Arnould L, Vialard F, et al. Maternal Obesity Influences Expression and DNA Methylation of the Adiponectin and Leptin Systems in Human Third-Trimester Placenta. *Clin Epigenet* (2019) 11(1):20. doi: 10.1186/s13148-019-0612-6
9. D'Ippolito S, Tersigni C, Scambia G, Di Simone N. Adipokines, An Adipose Tissue and Placental Product With Biological Functions During Pregnancy. *Biofactors* (2012) 38(1):14–23. doi: 10.1002/biof.201
10. Bouchard L, Thibault S, Guay SP, Santure M, Monpetit A, St-Pierre J, et al. Leptin Gene Epigenetic Adaptation to Impaired Glucose Metabolism During Pregnancy. *Diabetes Care* (2010) 33(11):2436–41. doi: 10.2337/dc10-1024
11. Wroblewski A, Strycharz J, Swiderska E, Drewniak K, Drzewoski J, Szemraj J, et al. Molecular Insight Into the Interaction Between Epigenetics and Leptin in Metabolic Disorders. *Nutrients* (2019) 11(8):1872. doi: 10.3390/nu11081872
12. Tran AT, Diep LM, Cooper JG, Claudi T, Straand J, Birkeland K, et al. Quality of Care for Patients With Type 2 Diabetes in General Practice According to Patients' Ethnic Background: A Cross-Sectional Study From Oslo, Norway. *BMC Health Serv Res* (2010) 10:145. doi: 10.1186/1472-6963-10-145
13. Sattar N, Gill JM. Type 2 Diabetes in Migrant South Asians: Mechanisms, Mitigation, and Management. *Lancet Diabetes Endocrinol* (2015) 3(12):1004–16. doi: 10.1016/S2213-8587(15)00326-5
14. Bhopal RS. A Four-Stage Model Explaining the Higher Risk of Type 2 Diabetes Mellitus in South Asians Compared With European Populations. *Diabetes Med* (2013) 30(1):35–42. doi: 10.1111/dme.12016
15. Wells JC, Sawaya AL, Wibaek R, Mwangome M, Poullas MS, Yajnik CS, et al. The Double Burden of Malnutrition: Aetiological Pathways and Consequences for Health. *Lancet* (2020) 395(10217):75–88. doi: 10.1016/S0140-6736(19)32472-9
16. Moen GH, Sommer C, Prasad RB, Sletner L, Groop L, Qvigstad E, et al. Mechanisms in Endocrinology: Epigenetic Modifications and Gestational Diabetes: A Systematic Review of Published Literature. *Eur J Endocrinol* (2017) 176(5):R247–R67. doi: 10.1530/EJE-16-1017
17. Lesseur C, Chen J. Adverse Maternal Metabolic Intrauterine Environment and Placental Epigenetics: Implications for Fetal Metabolic Programming. *Curr Environ Health Rep* (2018) 5(4):531–43. doi: 10.1007/s40572-018-0217-9
18. Jenum AK, Sletner L, Voldner N, Vangen S, Morkrid K, Andersen LF, et al. The STORK Groruddalen Research Programme: A Population-Based Cohort Study of Gestational Diabetes, Physical Activity, and Obesity in Pregnancy in a Multiethnic Population. Rationale, Methods, Study Population, and Participation Rates. *Scand J Public Health* (2010) 38(5 Suppl):60–70. doi: 10.1177/1403494810378921
19. Sletner L, Jenum AK, Morkrid K, Vangen S, Holme IM, Birkeland KI, et al. Maternal Life Course Socio-Economic Position and Offspring Body Composition at Birth in a Multi-Ethnic Population. *Paediatr Perinat Epidemiol* (2014) 28(5):445–54. doi: 10.1111/ppe.12137
20. Jenum AK, Morkrid K, Sletner L, Vangen S, Torper JL, Nakstad B, et al. Impact of Ethnicity on Gestational Diabetes Identified With the WHO and the Modified International Association of Diabetes and Pregnancy Study Groups Criteria: A Population-Based Cohort Study. *Eur J Endocrinol* (2012) 166 (2):317–24. doi: 10.1530/EJE-11-0866
21. Friedewald WT, Levy RI, Fredrickson DS. Estimation of the Concentration of Low-Density Lipoprotein Cholesterol in Plasma, Without Use of the Preparative Ultracentrifuge. *Clin Chem* (1972) 18(6):499–502. doi: 10.1093/clinchem/18.6.499
22. Christensen JJ, Retterstøl K, Godang K, Roland MC, Qvigstad E, Bollerslev J, et al. LDL Cholesterol in Early Pregnancy and Offspring Cardiovascular Disease Risk Factors. *J Clin Lipidol* (2016) 10(6):1369–78.e7. doi: 10.1016/j.jacl.2016.08.016
23. Bekkering I, Leeuwerke M, Tanis JC, Schoots MH, Verkaik-Schakel RN, Plosch T, et al. Differential Placental DNA Methylation of VEGFA and LEP in Small-For-Gestational Age Fetuses With an Abnormal Cerebroplacental Ratio. *PloS One* (2019) 14(8):e0221972. doi: 10.1371/journal.pone.0221972
24. Mosher MJ, Melton PE, Stapleton P, Schanfield MS, Crawford MH. Patterns of DNA Methylation Across the Leptin Core Promoter in Four Diverse Asian and North American Populations. *Hum Biol* (2016) 88(2):121–35. doi: 10.13110/humanbiology.88.2.0121
25. Galanter JM, Gignoux CR, Oh SS, Torgerson D, Pino-Yanes M, Thakur N, et al. Differential Methylation Between Ethnic Sub-Groups Reflects the Effect of Genetic Ancestry and Environmental Exposures. *Elife* (2017) 6:e20532. doi: 10.7554/eLife.20532
26. Yuan V, Price EM, Del Gobbo G, Mostafavi S, Cox B, Binder AM, et al. Accurate Ethnicity Prediction From Placental DNA Methylation Data. *Epigenet Chromatin* (2019) 12(1):51. doi: 10.1186/s13072-019-0296-3
27. Tobi EW, Lumey LH, Talens RP, Kremer D, Putter H, Stein AD, et al. DNA Methylation Differences After Exposure to Prenatal Famine Are Common and Timing- and Sex-Specific. *Hum Mol Genet* (2009) 18(21):4046–53. doi: 10.1093/hmg/ddp353
28. Lesseur C, Armstrong DA, Paquette AG, Li Z, Padbury JF, Marsit CJ. Maternal Obesity and Gestational Diabetes Are Associated With Placental Leptin DNA Methylation. *Am J Obstet Gynecol* (2014) 211(6):654.e1–9. doi: 10.1016/j.ajog.2014.06.037

29. Martino J, Sebert S, Segura MT, Garcia-Valdes L, Florido J, Padilla MC, et al. Maternal Body Weight and Gestational Diabetes Differentially Influence Placental and Pregnancy Outcomes. *J Clin Endocrinol Metab* (2016) 101 (1):59–68. doi: 10.1210/jc.2015-2590
30. Houde AA, Legare C, Biron S, Lescelleur O, Biertho L, Marceau S, et al. Leptin and Adiponectin DNA Methylation Levels in Adipose Tissues and Blood Cells Are Associated With BMI, Waist Girth and LDL-Cholesterol Levels in Severely Obese Men and Women. *BMC Med Genet* (2015) 16:29. doi: 10.1186/s12881-015-0174-1
31. Horne H, Holme AM, Roland MCP, Holm MB, Haugen G, Henriksen T, et al. Maternal-Fetal Cholesterol Transfer in Human Term Pregnancies. *Placenta* (2019) 87:23–9. doi: 10.1016/j.placenta.2019.09.001
32. Melzner I, Scott V, Dorsch K, Fischer P, Wabitsch M, Bruderlein S, et al. Leptin Gene Expression in Human Preadipocytes Is Switched on by Maturation-Induced Demethylation of Distinct Cpgs in its Proximal Promoter. *J Biol Chem* (2002) 277(47):45420–7. doi: 10.1074/jbc.M208511200
33. Mason MM, He Y, Chen H, Quon MJ, Reitman M. Regulation of Leptin Promoter Function by Sp1, C/EBP, and a Novel Factor. *Endocrinology* (1998) 139(3):1013–22. doi: 10.1210/endo.139.3.5792
34. Moreno-Aliaga MJ, Swarbrick MM, Lorente-Cebrian S, Stanhope KL, Havel PJ, Martinez JA. Sp1-Mediated Transcription Is Involved in the Induction of Leptin by Insulin-Stimulated Glucose Metabolism. *J Mol Endocrinol* (2007) 38 (5):537–46. doi: 10.1677/JME-06-0034
35. Krempler F, Breban D, Oberkofler H, Esterbauer H, Hell E, Paulweber B, et al. Leptin, Peroxisome Proliferator-Activated Receptor-Gamma, and CCAAT/Enhancer Binding Protein-Alpha Mrna Expression in Adipose Tissue of Humans and Their Relation to Cardiovascular Risk Factors. *Arterioscler Thromb Vasc Biol* (2000) 20(2):443–9. doi: 10.1161/01.ATV.20.2.443
36. Rush EC, Katre P, Yajnik CS. Vitamin B12: One Carbon Metabolism, Fetal Growth and Programming for Chronic Disease. *Eur J Clin Nutr* (2014) 68 (1):2–7. doi: 10.1038/ejcn.2013.232
37. Nandi AA, Wadhwani NS, Randhir KN, Madiwale SD, Deshpande JS, Wagh GN, et al. Maternal Vitamin D Deficiency Influences Long-Chain Polyunsaturated Fatty Acids and Pregnancy Outcome in Association With Alterations in One-Carbon Metabolism. *Nutr Res* (2021) 86:37–49. doi: 10.1016/j.nutres.2020.11.009
38. Saravanan P, Sukumar N, Adaikalakoteswari A, Goljan I, Venkataraman H, Gopinath A, et al. Association of Maternal Vitamin B12 and Folate Levels in Early Pregnancy With Gestational Diabetes: A Prospective UK Cohort Study (Pride Study). *Diabetologia* (2021) 64(10):2170–82. doi: 10.1007/s00125-021-05510-7
39. Behere RV, Deshmukh AS, Otiv S, Gupte MD, Yajnik CS. Maternal Vitamin B12 Status During Pregnancy and Its Association With Outcomes of Pregnancy and Health of the Offspring: A Systematic Review and Implications for Policy in India. *Front Endocrinol* (2021) 12:619176. doi: 10.3389/fendo.2021.619176

Conflict of Interest: The authors declare that the research was conducted in the absence of any commercial or financial relationships that could be construed as a potential conflict of interest.

Publisher's Note: All claims expressed in this article are solely those of the authors and do not necessarily represent those of their affiliated organizations, or those of the publisher, the editors and the reviewers. Any product that may be evaluated in this article, or claim that may be made by its manufacturer, is not guaranteed or endorsed by the publisher.

frontiers in Endocrinology

ORIGINAL RESEARCH
published: 03 January 2022
doi: 10.3389/fendo.2021.750261

Adipocyte-Specific Inhibition of *Mir221/222* Ameliorates Diet-Induced Obesity Through Targeting *Ddit4*

*Satoshi Yamaguchi, Dongxiao Zhang, Akihiro Katayama, Naoko Kurooka, Ryosuke Sugawara, Haya Hamed Hassan Albuayjan, Atsuko Nakatsuka, Jun Eguchi and Jun Wada**

Department of Nephrology, Rheumatology, Endocrinology and Metabolism, Okayama University Graduate School of Medicine, Dentistry and Pharmaceutical Sciences, Okayama, Japan

MicroRNAs expressed in adipocytes are involved in transcriptional regulation of target mRNAs in obesity, but miRNAs critically involved in this process is not well characterized. Here, we identified upregulation of miR-221-3p and miR-222-3p in the white adipose tissues in C57BL/6 mice fed with high fat-high sucrose (HFHS) chow by RNA sequencing. *Mir221* and *Mir222* are paralogous genes and share the common seed sequence and *Mir221/222AdipoKO* mice fed with HFHS chow demonstrated resistance to the development of obesity compared with *Mir221/222*$^{flox/y}$. *Ddit4* is a direct target of *Mir221* and *Mir222*, and the upregulation of *Ddit4* in *Mir221/222AdipoKO* was associated with the suppression of TSC2 (tuberous sclerosis complex 2)/mammalian target of rapamycin complex 1 (mTORC1)/S6K (ribosomal protein S6 kinase) pathway. The overexpression of miR-222-3p linked to enhanced adipogenesis, and it may be a potential candidate for miRNA-based therapy.

Keywords: non-coding RNAs, microRNA, adipose tissues, Adipogenesis, mTORC1

OPEN ACCESS

Edited by:
Marc Thibonnier, AptamiR Therapeutics. Inc., United States

Reviewed by:
Soonkyu Chung, University of Massachusetts Amherst, United States
Naima Moustaid-Moussa, Texas Tech University, United States

***Correspondence:**
Jun Wada
junwada@okayama-u.ac.jp

Specialty section:
This article was submitted to Obesity, a section of the journal Frontiers in Endocrinology

Received: *30 July 2021*
Accepted: *07 December 2021*
Published: *03 January 2022*

Citation:
Yamaguchi S, Zhang D, Katayama A, Kurooka N, Sugawara R, Albuayjan HHH, Nakatsuka A, Eguchi J and Wada J (2022) Adipocyte-Specific Inhibition of Mir221/222 Ameliorates Diet-Induced Obesity Through Targeting Ddit4. Front. Endocrinol. 12:750261. doi: 10.3389/fendo.2021.750261

INTRODUCTION

In obesity, the excess and ectopic accumulation of adipose tissue leads to the clusters of metabolic disorders such as low-grade inflammation, type 2 diabetes (T2D), dyslipidemia, hypertension, nonalcoholic fatty liver disorder (NAFLD), cardiovascular diseases (CVDs), chronic kidney disease (CKD) and cancer. As an endocrine organ, the adipose tissue communicates with other tissues by secreting peptide hormones, inflammatory cytokines, signaling lipids and miRNAs packed in exosomes (1). The alteration of expression profile of miRNA both in cytoplasm and extracellular vesicles leads to changes in the transcriptional and translational activities of the genes, which control inflammation, whole body insulin sensitivity, lipid metabolism, adipogenesis of white, beige, and brown adipose tissues (2). For instance, miR-34a secreted by mature adipocytes in exosomes were transported into macrophages, suppresses M2 polarization, and stimulates inflammatory responses by repressing Krüppel-like factor 4 (3). Lentivirus-mediated suppression of miR-34a increased the beige and brown fat formation in diet-induced obese mice by increasing fibroblast growth factor 21 and sirtuin 1 (4). The genetic ablation of miR-128-1 in mouse metabolic disease models resulted in increased energy expenditure, amelioration of diet-induced obesity and enhanced insulin sensitivity (5). In lipid metabolism, miR-425 overexpression in mice resulted in the promotion of diet-induced

obesity and overexpression of miR-425 in 3T3-L1 cells accelerated adipogenesis and lipogenesis, while knock down of miR-425 remarkably enhanced lipolysis and lipid oxidation (6).

We also attempted to identify specific miRNAs critically involved in the process of obesity, we surveyed expression profile of miRNAs in liver, muscle, white adipose tissues (WATs), and sera of C57BL/6JJcl mice fed with standard (STD) and high fat-high sucrose (HFHS) chow by RNA sequencing (GSE61959) (7). miR-221-3p and miR-222-3p are highly up-regulated in epididymal adipose tissues in mice fed with high fat high sucrose (HFHS). miR-221 and miR-222 both locate in the close proximity on the X chromosome and share the identical seed sequence (8). In meta-analysis, circulating miR-221-3p was reduced in T2D, while miR-222-3p was elevated in obesity and T2D (9). Although miR-221-3p and miR-222-3p are differentially expressed in sera and adipose tissues, the functional *in vivo* experiments to elucidate the roles of *Mir221* and *Mir222* in obesity has not been reported. Here, we investigated the adipocyte specific *Mir221* and *Mir222* knockout (*Mir221/222AdipoKO*) mice fed with HFHS chow, and they were protected from the development of obesity by targeting DDIT4 (DNA damage inducible transcript 4)/TSC2 (tuberous sclerosis complex 2)/S6K (ribosomal protein S6 kinase) pathway.

MATERIALS AND METHODS

Animal Models

We obtained Mir 221 KO cond (*Mir221*^{tm2}; EMMA ID, EM:05507) from EMMA (the European Mouse Mutant Archive) and Helmholz Zentrum München (Neuherberg, Germany). The targeting vector cassette composed of *Neo* flanked by FRT and distal loxP sites was inserted outside the genomic region encoding *Mir221* and *Mir222* precursors. *Neo* was removed by Flp in the conditional KO allele of Mir 221 KO cond. The conditional KO allele was confirmed by primer pair; 1544_29 (5'- GCT CTG TTT TCC TAA GTG ATG G-3') and 1544_30 (5'-CTG ACA GGA AGT AAA TCA TCT TAG C-3'). The expected fragments were 265 bp in wild and 384 bp in conditional KO allele. We also used B6.FVB-Tg (Adipoq-cre) 1Evdr/J to produce *Mir221/222AdipoKO* mice by crossing to Mir 221 KO cond. Adipoq-cre transgene was screened by primers, Forward (5'-AGC GAT GGA TTT CCG TCT CT-3') and Reverse (5'-CAC CAG CTT GCA TGA TCT CC-3'). The primers, oIMR7338 (5'-CTA GGC CAC AGA ATT GAA AGA TCT-3') and oIMR7339 (5'-GTA GGT GGA AAT TCT AGC ATC ATC C-3'), were used for internal positive control. The expected sizes for transgene and internal positive control were 200 bp and 324 bp, respectively. By crossing male Tg (Adipoq-cre) and female *Mir221*^{tm2}*/y* C57BL/6JJcl mice, we generated male *Mir221/222*$^{flox/y}$ and male *Mir221/222AdipoKO* littermates.

Five-week-old mice were randomly assigned to standard diet (STD) group (MF, Oriental Yeast, Japan) or high fat high sucrose diet (HFHS) group (D12331, Research Diets, New Brunswick, NJ). The detailed formulation of STD (10) (https://www.oyc.co.jp/bio/LAD-equipment/LAD/ingredient.html and https://www.oyc.co.jp/bio/LAD-equipment/LAD/rodents.html) and HFHS (https://www.eptrading.co.jp/service/researchdiets/pdf/D12328-D12331.pdf) diets are shown in **Supplementary Table 1**. At 22 weeks of age, we obtained various organs and they were subjected to following experiments.

3T3-L1 Cell Cultures

3T3-L1 pre-adipocytes were cultured in Dulbecco's modified eagle's medium (DMEM, 2124951, Gibco). On day 0, the cells were treated with the differentiation media; DMEM supplemented with 10% FBS, 10 μg/ml insulin (I1882, Sigma), 1 μM DEX (D2915, Sigma) and 0.5 mM IBMX (I5879, Sigma). Then, the media were changed to DMEM supplemented with 10 μg/ml insulin and 10% FBS on day 2 and cultured for 10 or 20 days. Undifferentiated 3T3-L1 cells were subjected to Lentiviral miRNA expression, Lentiviral miRNA inhibition studies, and luciferase reporter assays.

Human Serum Samples

Human serum samples were collected from 69 patients with type 2 diabetes in Okayama University Hospital and 45 subjects with normal fasting glucose (NGT).

Insulin Tolerance Test and Glucose Tolerance Test (ITT and GTT)

The 13-week-old mice were fasted for 16 hours in GTT and for 3 hours in ITT. They were then intraperitoneally injected with glucose solution (1 mg/g body weight) and human insulin (1 unit/kg in HFHS groups and 0.75 unit/kg in STD groups) for GTT and ITT, respectively.

Basal Metabolic Rate, Locomotor Activity, and Food Intake

At 18 weeks of age, O_2/CO_2 metabolism measuring system (MK-5000, Muromachi Kikai, Tokyo, Japan) were used to quantify oxygen consumption rate and carbon dioxide production for the estimation of $\dot{V}O2$ and respiratory quotient (RQ). The locomotor activity was recorded for 24 hours by the frequency of interrupting an infrared sensor (ACTIMO-100, Shinfactory, Fukuoka, Japan). Daily food intake was measured and calculated; daily food intake [g/day/body weight (BW)] = [initial food weight (g) – leftover food weight (g)]/measurement period (days)/BW (g). The 6-10 mice in each experimental group were examined.

Reverse Transcription-Quantitative Polymerase Chain Reaction (RT-qPCR)

RNAs were extracted from frozen tissues and cultured 3T3-L1 cells with RNeasy Mini kit (74106, Qiagen). The QIAamp Circulating Nucleic Acid Kit (Qiagen) were used for the isolation of total RNAs from serum. For gene expression analyses, cDNAs were prepared with High-Capacity RNA-to-cDNA Kit (Thermo Fisher Scientific). TaqMan gene expression primers, *Ddit4* (Mm00512504_g1), *Rplp0* (Mm00725448_s1), *Rn18s* (Mm03928990_g1), *Adipoq* (Mm00456425_m1), *Lep* (Mm00434759_m1), *Lpl* (Mm01345523_m1), *Srebf1* (Mm00550338_m1), *Cebpa* (Mm00514283_s1), *Fabp4* (Mm00445878_m1), *Pparg* (Mm01184322_m1), *Lipe* (Mm00495359_m1), *Pnpla2*

(Mm00503040_m1), *Ucp1* (Mm01244861_m1), *Cox8b* (Mm00432648_m1), *Prdm16* (Mm00712556_m1), *Cidea* (Mm00432554_m1), *Ppargc1a* (Mm01208835_m1), *G6pc* (Mm00839363_m1), *Gck* (Mm00439129_m1), *Fasn* (Mm00662319_m1), *Ppara* (Mm00440939_m1), *Il6* (Mm00446190_m1), *Ifng* (Mm01168134_m1), *Tnf* (Mm00443258_m1), *Il1b* (Mm01336189_m1) were used (Thermo Fisher Scientific). For miRNA expression studies, cDNAs were prepared from total RNAs by TaqMan MicroRNA Reverse Transcription Kit (Life Technologies). MicroRNA primers, *mmu-miR-222-3p* (CTAAJ3), *hsa-miR-221-3p* (000524), *hsa-miR-222-3p* (002276), snoRNA202 (001232), snoRNA234 (001234), and cel-miR-39 (000200) were used (Thermo Fisher Scientific). Rplp0, Rn18s, snoRNA202, snoRNA234, and cel-miR-39 were served as the invariant controls. The RT-qPCR was performed using TaqMan Universal PCR Master mix II (no UNG) at a StepOne Plus Real-Time PCR system. The quantification was performed by the $2^{-\Delta\Delta CT}$ analysis method.

Cloning of Mir221 Host Gene (*Mir221hg*)

Long non-coding RNA, *Mir221hg*, was cloned using SMARTer RACE 5'/3' Kit (634858, Clontech). 5'- and 3'-RACE-Ready cDNAs from epididymal adipose tissues poly A^+ RNA were prepared by SMARTScribe Reverse Transcriptase. 5'- and 3'-RACE-Ready cDNAs were amplified by PCR using 5' GSP (5'-GAT TAC GCC AAG CTT CCA GCA GAC AAT GTA GC TGT TGC-3') and 3' GSP (5'-GAT TAC GCC AAG CTT TCC AGG TCT GGG GCA TGA ACC TG-3'), respectively. Furthermore, nested PCR was performed using 5' NGSP (5'-GAT TAC GCC AAG CTT GTA TGC CAG GTT CAT GCC CCA GAC-3') and 3' NGSP (5'-GAT TAC GCC AAG CTT GCA ACA GCT ACA TTG TCT GCT GG-3'). PCR products were analyzed by agarose/EtBr gel and purified by NucleoSpin Gel and PCR Clean-Up Kit. The purified RACE products were subcloned into pRACE vector by In-Fusion Cloning (Clontech). Independent 4 clones of both 5'- and 3'-RACE were sequenced.

Western Blot Analysis

The epididymal fat tissues from 22-week-old mice and cultured 3T3-L1 cells were homogenized in RIPA lysis buffer (radioimmunoprecipitation buffer) plus protease inhibitors. The samples were boiled in SDS-PAGE loading buffer, separated on 12% Mini-PROTEAN TGX Precast Protein Gels (Bio-Rad), and transferred to a PVDF Blotting Membrane (cytiva). After blocking with 5% nonfat milk for 1 hour at room temperature (RT), the blots were incubated with REDD-1/DDIT4 Antibody, rabbit polyclonal (ab106356, RRID: AB_10864294), C/EBPα Antibody, rabbit polyclonal (2295, RRID: AB_10692506), PPARγ (D69) Antibody, rabbit polyclonal (2430, RRID: AB_823599), mTOR (7C10) Rabbit mAb (2983, RRID: AB_2105622), Phospho-mTOR (Ser2448) (D9C2) XP Rabbit mAb (5536, RRID: AB_10691552), Akt Antibody, rabbit polyclonal (9272, RRID: AB_329827), Phospho-Akt (Thr308) Antibody, rabbit polyclonal (9275, RRID: AB_329828), p70 S6 Kinase (49D7) Rabbit mAb (2708, RRID: AB_390722), Phospho-p70 S6 Kinase (Thr389) Antibody, rabbit polyclonal (9205, RRID: AB_330944), Tuberin/TSC2 Antibody, rabbit polyclonal (3612, RRID: AB_2207804), Phospho-Tuberin/TSC2 (Thr1462) Antibody, rabbit polyclonal (3611, RRID: AB_329855, Cell Signaling Technology) overnight at 4°C. GAPDH (D16H11) XP Rabbit mAb (HRP Conjugate) (8884, RRID: AB_11129865) was used as a loading control (Cell Signaling Technology). After washing three times with Tris-buffered saline (TBS), the blots were incubated with ECL Donkey Anti-Rabbit IgG, HRP-Conjugated Antibodies (NA934V, GE healthcare Life science, 1:10000) at RT for 1 hour. The blots were developed with Pierce ECL Western Blotting Substrate (TE261327, Thermo Fisher Scientific). The chemiluminescence was analyzed using ImageQuant LAS-4000 mini (FUJIFILM).

Morphometric Analysis for Adipocyte Size

Epididymal adipose tissues were fixed by 10% formalin, embedded with paraffin. The 5-μm paraffin sections were prepared and stained with PAS. The images were captured using an Olympus BX51 microscope. The size of the adipocytes was analyzed by Keyence Hybrid cell count software. Epididymal adipose tissues were taken from 3-5 individual animals from each experimental group.

Isolation of Stromal Vascular Fraction (SVF) From White Adipose Tissues

SVF was isolated from epididymal adipose tissue of 24-week-old mice. Briefly, fresh mouse epididymal fat pads were minced and digested with collagenase type 1 (CLSS1, Worthington) in HBSS containing 10% FBS for 45 minutes at 37°C. The mixture was filtered through a nylon mesh (100 μm), then centrifuged at 400 g for 1 minute. The adipocyte fraction was obtained from the supernatant, they were again centrifuged at 800 g for 10 minutes, and the SVF was obtained from the pellet.

Identification of *Mir221/222* Target mRNAs

The mRNA microarray was performed by GeneChip Mouse Gene 2.0 array using total RNA of epididymal fat obtained from 16-week-old mice (1 animal from each group) and analyzed by Filgen (Nagoya, Japan). The raw data are available in Gene Expression Omnibus (GEO; https://www.ncbi.nlm.nih.gov/geo/) (GSE163921). TargetScan (http://www.targetscan.org/vert_72/), miRDB (http://www.mirdb.org/), and DIANA-microT v5.0 (https://bio.tools/DIANA-microT) and were used to identify potential target genes for *Mir221/222*.

Lentiviral miRNA Expression and Lentiviral miRNA Inhibitor

Lentiviral transduction using pLV-miRNA and pLV-miR-Locker system to 3T3-L1 cells were performed according to the manufacturer's manual (Biosettia). After transformation to *E. coli* JM109 cells, pLV-[mmu-mir-221] plasmid (mir-p177m, Biosettia), pLV-[mmu-mir-222] plasmid (mir-p178m, Biosettia), pLV-[mmu-mir-221-3p] locker plasmid (mir-mp0337, Biosettia), pLV-[mmu-mir-222-3p] locker plasmid (mir-mp0339, Biosettia), pLV-[mir-control] plasmid (mir-p000, Biosettia), pLV-miR-locker control plasmid (mir-locker-ctrl, Biosettia), pMDLg/pRRE (12251, Addgene), pRSV/Rev (12253, Addgene), and pMD2.G (12259, Addgene) were isolated with EndoFree Plasmid Maxi Kit (12362, Qiagen).

293T cells (10×10^7/5 mL) were transfected with each pLV plasmid, pMDLg/pRRE, pRSV/Rev, pMD2.G, Lipofectamine LTX, and 1.5 mL Opti-MEM. The supernatants were collected after 48 hours after transfection. 3T3-L1 cells were transduced with lentivirus stock in complete media containing 10 μg/mL polybrene for 12 hours, replaced with fresh complete medium

Luciferase Reporter Assay

To quantitatively evaluate miRNA activity on cloned miRNA target sequence from 3'-untranslated region (3'-UTR) of *Ddit4*, pmirGLO dual luciferase miRNA Target expression vector (E1330, Promega) was used. Firstly, the pmirGLO plasmid was linearized by double digestion with *Xho*I and *Sal*I. The cDNA of *Ddit4* wild type (WT) 3′-UTR was amplified by PCR and ligated with CIP treated pmirGLO Vector. The primers are Forward-*Xho*I-3'UTR-*Ddit4*: 5'-GGG GGG CTC GAG CAG CTG CTC ATT GAA GAG TG-3′, and Reverse-*Sal*I-3'UTR-*Ddit4*: 5'-GGG GGG GTCGAC CAA ACC AAC AGA GGA GAC AG-3′. pmirGLO-*Ddit4* MT 3'-UTR was prepared by site directed mutagenesis by PCR using primers; Forward-MT-Seed-*Ddit4*: 5'-CTG GAT GTG TAT CTG CAT GTA C-3' and Reverse-MT-Seed-*Ddit4*: 5'-GTA CAT GCA GAT ACA CAT CCA G-3'. The seed sequence "CGATGTA" was mutated to "CGTCTA". After transformation to *E. coli* JM109 cells, pmirGLO-*Ddit4* WT 3'-UTR, pmirGLO-*Ddit4* MT 3'-UTR, and pmirGLO no-insert control plasmids were isolated with EndoFree Plasmid Maxi Kit (12362, Qiagen). 3T3-L1 cells were seeded at a density of 120,000 cells/mL, then co-transfected with Syn-mmu-miR-221-3p (MIMAT0000669, Qiagen), Syn-mmu-miR-222-3p (MIMAT0000670, Qiagen), negative control siRNA (1027280, Qiagen), inhibitor negative control (1027271, Qiagen), pmirGLO-*Ddit4* WT 3'-UTR, pmirGLO-*Ddit4* MT 3'-UTR, and pmirGLO no-insert control plasmids. Twenty-four hours after transfection, the cells were analyzed to measure luciferase activities using the Dual-Glo Luciferase Assay System and a GloMax 20/20 luminometer (Promega).

Statistical Analysis

All values were represented as the mean ± standard deviation (SD). Statistical analyses were conducted using IBM SPSS Statistics 23 and GraphPad Prism (version 8.0). Independent *t*-test, Mann-Whitney's U test, and one-way ANOVA with Tukey test was used to determine the differences. For correlation, non-parametric Spearman r coefficient was used. $p<0.05$ was considered statistically significant.

RESULTS

Mir221/222AdipoKO Mice Are Resistant to Diet-Induced Obesity

To identify miRNAs critically involved in the disease process of obesity and type 2 diabetes (T2D), we performed miRNA profiling of serum, liver and epididymal fat tissues in C57BL/6JJcl mice fed with standard (STD) and high fat-high sucrose (HFHS) chow. The Illumina RNA sequencing data (Gene Expression Omnibus number GSE61959) demonstrated that the read numbers of *Mir221* and *Mir222* were 5.7 and 8.2-fold up-regulated in epididymal adipose tissues in HFHS group compared with STD group (**Supplementary Table 2**). *Mir221* and *Mir222* are paralog genes located in proximity on X chromosome and they share identical seed sequence. To further investigate the role of *Mir221/222* in obesity and diabetes, we crossed male Tg (Adipoq-cre) mice and female *Mir221*$^{tm2/y}$ C57BL/6JJcl mice and generated male *Mir221/222*$^{flox/y}$ and male *Mir221/222AdipoKO* littermates.

Body weight of *Mir221/222AdipoKO* mice fed with HFHS chow was significantly reduced compared with *Mir221/222*$^{flox/y}$ mice (**Figure 1A**). The weight of epididymal, mesenteric, subdermal, and brown fat was also reduced in *Mir221/222AdipoKO* mice (**Figure 1B**). The *Mir221/222*$^{flox/y}$ and *Mir221/222AdipoKO* mice fed with STD chow demonstrated no significant differences in their body and tissue weight (**Figures 1A, B**). The average size of adipocytes in epididymal adipose tissues derived from *Mir221/222AdipoKO* mice fed with HFHS chow was smaller compared with *Mir221/222*$^{flox/y}$ mice (**Figure 1C**). To investigate glucose homeostasis, we performed insulin tolerance test (ITT) and glucose tolerance test (GTT). The blood glucose levels of *Mir221/222AdipoKO* mice fed with HFHS chow were reduced in GTT and ITT compared with *Mir221/222*$^{flox/y}$, but they did not reach significant differences (**Figure 1D**). The serum insulin concentrations of *Mir221/222AdipoKO* mice were significantly lower than *Mir221/222*$^{flox/y}$, suggesting the improvement of insulin sensitivity in *Mir221/222AdipoKO* mice (**Figure 1D**). To investigate whether reduced adiposity in *Mir221/222AdipoKO* mice was due to changes in energy expenditure or energy intake, we measured basal metabolic rates, locomotor activity and food intake. Basal metabolic rate such as respiratory quotient and oxygen consumption were not altered between *Mir221/222*$^{flox/y}$ and *Mir221/222AdipoKO* mice fed with HFHS chow (**Supplementary Figures 1A, B**). The locomotor activity was recorded for 24 hours, most of the activities were observed during the dark phase. Increased activity was observed in *Mir221/222AdipoKO* mice under HFHS chow compared with *Mir221/222*$^{flox/y}$ during light (0.944 ± 0.309 *vs* 1.60 ± 0.764 counts/min, p=0.036) and dark (6.67 ± 4.38 *vs* 7.94 ± 4.38 counts/min, p=0.497) periods (**Supplementary Figure 1C**). Food consumptions were not altered in *Mir221/222AdipoKO* and *Mir221/222*$^{flox/y}$ fed with HFHS (**Supplementary Figure 1D**). Under HFHS chow, serum leptin concentrations were significantly reduced in *Mir221/222AdipoKO* compared with *Mir221/222*$^{flox/y}$ (24.5 ± 2.35 *vs* 21.5 ± 1.85 ng/ml, p=0.043), while serum adiponectin concentrations were not altered (**Supplementary Figures 1E, F**). In quantitative RT-PCR in epididymal adipose tissues, mRNA expression of *Lep* was significantly reduced in *Mir221/222AdipoKO*. The genes related to adipogenesis, such as *Pparg*, *Cebpa*, *Ppargc1* and *Prdm16*, were not altered in *Mir221/222AdipoKO* (**Supplementary Figure 2**).

Expression *Mir221* and *Mir222* Are Highly Induced by HFHS Chow Feeding in Mature Adipocytes From Epidydimal Adipose Tissue

We investigated the expression of *Mir221* and *Mir222* in various organs. Both miR-221-3p and miR-222-3p were abundantly

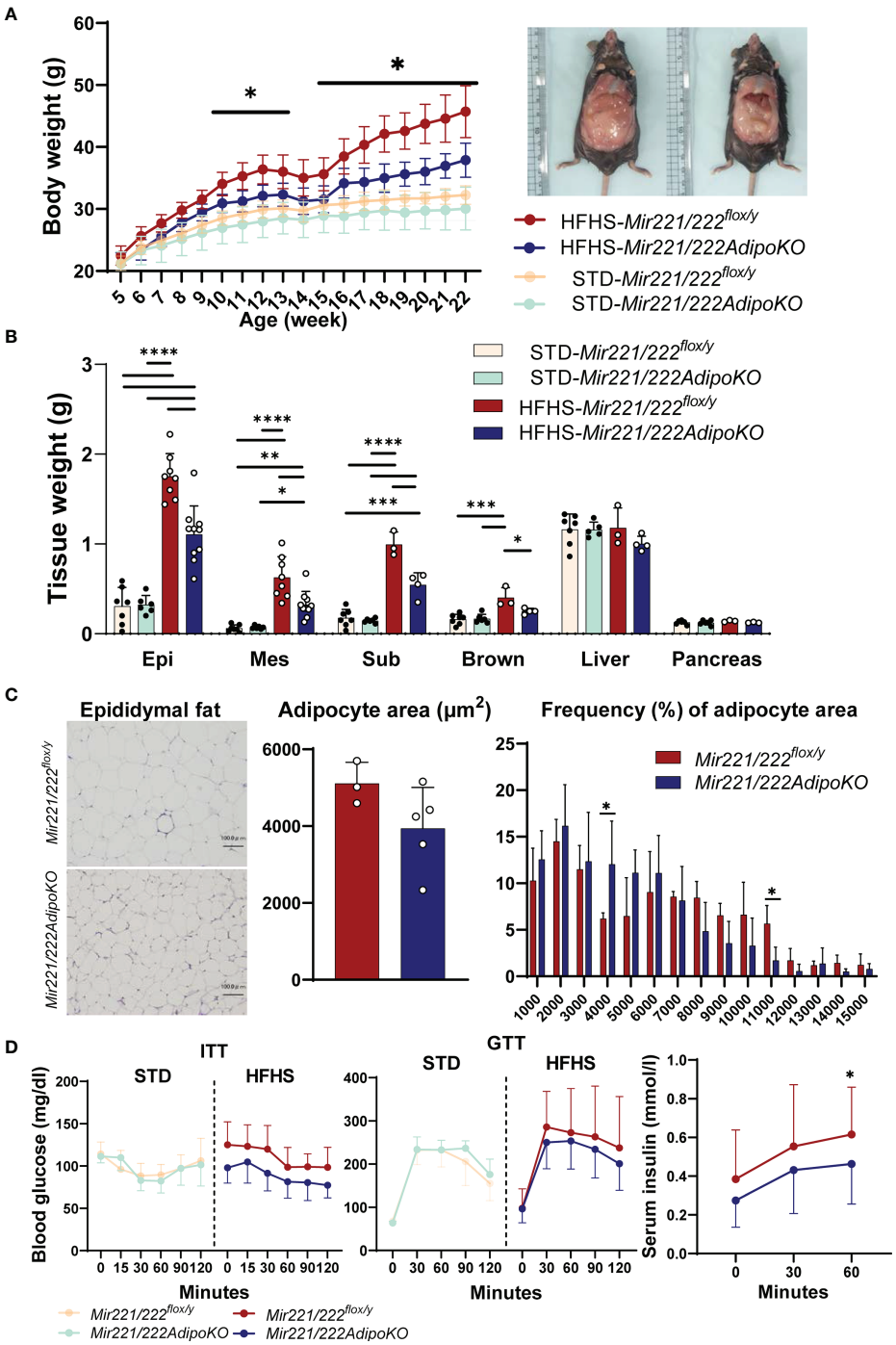

FIGURE 1 | The metabolic phenotypes of *Mir221/222*$^{flox/y}$ and *Mir221/222AdipoKO* male mice fed with high fat high sucrose (HFHS) or standard (STD) chow. **(A)** Body weight of *Mir221/222*$^{flox/y}$ and *Mir221/222AdipoKO* mice fed with HFHS (n=7) or STD chow (n=6), respectively. **(B)** Tissue weight of *Mir221/222*$^{flox/y}$ and *Mir221/222AdipoKO* mice fed with HFHS or STD chow at 24 weeks of age. (Epi, epididymal; Mes, mesenteric; Sub, inguinal; Brown, Brown adipose tissues) **(C)** Adipocyte area in epididymal adipose tissues of *Mir221/222*$^{flox/y}$ (n=3) and *Mir221/222AdipoKO* (n=5) mice fed with HFHS or STD. Quantitative analyses were carried out on PAS-stained paraffin sections. **(D)** Insulin tolerance test (ITT) in Mir221/222flox/y (n=7) and Mir221/222AdipoKO (n=6). Glucose tolerance test (GTT) in Mir221/222flox/y fed with HFHS (n=13) or STD chow (n=7) and Mir221/222AdipoKO fed with HFHS (n=16) or STD chow (n=6). Data shown as mean ± SD and analyzed by one-way ANOVA with Tukey test in **(A, B)**, and Mann-Whitney's U test in **(C, D)** (*p<0.05; **p<0.01; ***p<0.001; ****p<0.0001).

expressed in brain, kidney, and lung in *Mir221/222*$^{flox/y}$ and they were down-regulated or not altered by the HFHS feeding compared with STD chow. In contrast, both miR-221-3p and miR-222-3p were significantly upregulated in the epididymal fat tissues, and such upregulation was canceled in the epididymal fat tissues of *Mir221/222AdipoKO* fed with HFHS chow (**Figures 2A, B**). Next, we investigated the localization of *Mir221* and *Mir222* in the cell fractions of epididymal adipose tissues. Both miR-221-3p and miR-222-3p were significantly induced by HFHS chow in mature adipocytes of *Mir221/222*$^{flox/y}$, while the upregulation was significantly reversed in the mature adipocyte of *Mir221/222AdipoKO* fed with HFHS chow. In contrast, miR-221-3p and miR-222-3p were not significantly upregulated in the stromal vascular fraction (SVF) from *Mir221/222*$^{flox/y}$ fed with HFHS chow (**Figure 2C**). We also assessed the expression of miR-221-3p and miR-222-3p during 3T3-L1 adipocyte differentiation. Both miR-221-3p and miR-222-3p continuously down-regulated after the induction of adipocyte differentiation (**Supplementary Figure 3A**). Finally, we assessed the serum concentrations of mmu-miR-221-3p and mmu-miR-222-3p by quantitative PCR and they were not altered in *Mir221/222*$^{flox/y}$ and *Mir221/222AdipoKO* fed with STD and

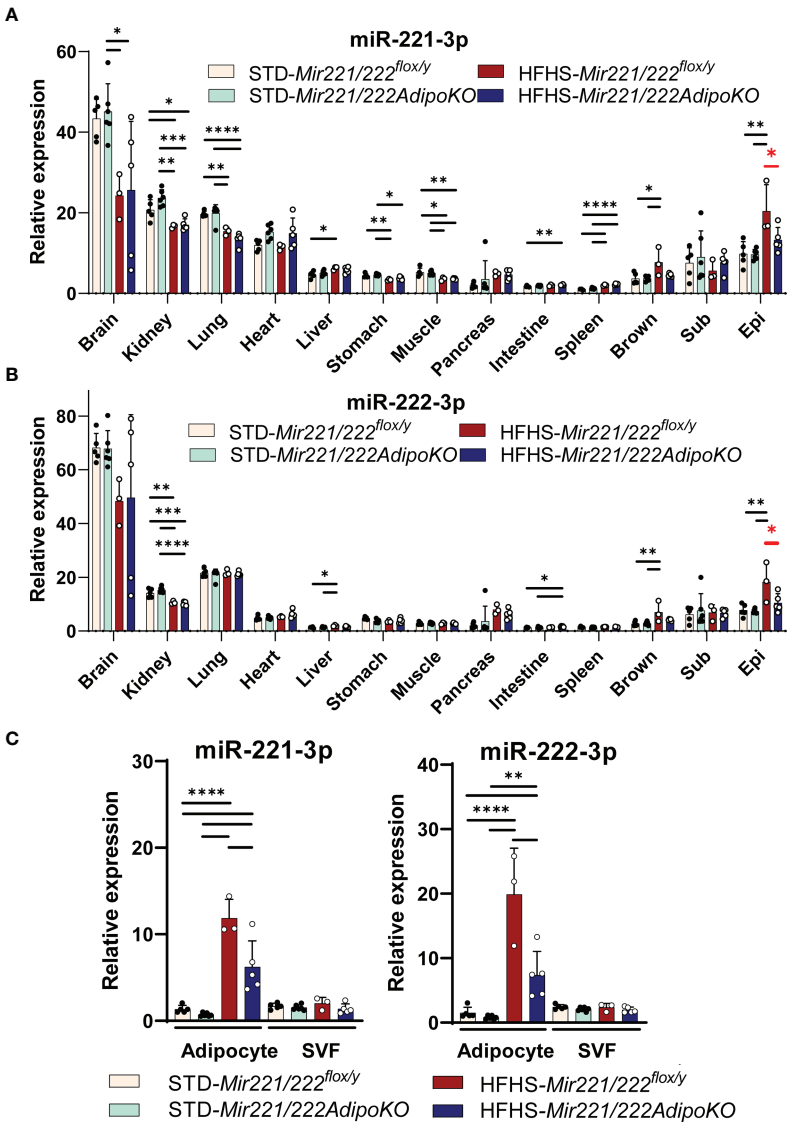

FIGURE 2 | Expression of Mir221 and Mir222 in *Mir221/222*$^{flox/y}$ and *Mir221/222AdipoKO* male mice fed with high fat high sucrose (HFHS) or standard (STD) chow. **(A, B)** In various tissues, the expression of miR-221-3p and miR-222-3p is normalized by snoRNA202 and snoRNA234. The HFHS-induced up-regulation of miR-221-3p and miR-222-3p in epididymal adipose tissues was reversed in *Mir221/222AdipoKO* (red asterisks). (Epi, epididymal; Mes, mesenteric; Sub, inguinal; Brown, Brown adipose tissues) **(C)** Serum concentration of miR-221-3p and miR-222-3p. HFHS *Mir221/222*$^{flox/y}$ (n=3), HFHS *Mir221/222AdipoKO* (n=5), STD *Mir221/222*$^{flox/y}$ (n=5) and STD *Mir221/222AdipoKO* mice (n=6). Data shown as mean ± SD and analyzed by one-way ANOVA with Tukey test (*p<0.05; **p<0.01; ***p<0.001; ****p<0.0001).

HFHS chow, suggesting serum mature forms of *Mir221* and *Mir222* were derived from various organs but not exclusively from adipose tissues (**Supplementary Figure 4A**). In human samples from the subjects with normal glucose tolerance (NGT, n=45) and impaired glucose tolerance (IGT, n=69), hsa-miR-221-3p and hsa-miR-222-3p demonstrated negative (R^2 = 0.1311, p<0.0001) and positive correlations (R2 = 0.03841, p=0.0441) with HbA1c levels, respectively (**Supplementary Figures 4B, C**).

Identification of *Mir221hg* and Its Expression

The miRNA genes are classified as intergenic and intragenic miRNAs, and the intragenic miRNAs and related host genes share the common transcriptional regulation. The long non-coding RNA (lncRNA), namely mir-221 host gene (MIR221HG), has been reported in bovine, which inhibits the adipocyte differentiation in cultured cells (11). Thus, we performed 5' and 3' rapid amplification of cDNA ends (5'/3'RACE) using poly A^+ RNA purified from epididymal fat tissues of C57BL/6JJcl mice and cloned 1537 bp single exon lncRNA (*Mir221hg*, MW581002) which overlap *Mir221* (**Supplementary Figure 5A**). Next, we designed primers for quantitative PCR of *Mir221hg* and evaluated gene expression in various tissue. *Mir221hg* was abundantly expressed in brain in *Mir221/222*$^{flox/y}$ and they were upregulated in brain, heart, liver, intestine, spleen by the HFHS feeding compared with STD chow. The expression of *Mir221hg* was rather low in various adipose tissues and its lncRNA expression was not changed in *Mir221/222AdipoKO* fed with STD and HFHS chow (**Supplementary Figures 5B, C**). Although *Mir221hg* lncRNA may be functional as a reservoir for miR-221-3p, the role of *Mir221hg* lncRNA in adipose tissues was limited in our experiments.

miR-221-3p and miR-222-3p Target *Ddit4*

To investigate the mechanism for the resistance to diet-induced obesity in *Mir221/222AdipoKO*, we attempted to identify the potential target genes for miR-221-3p and miR-222-3p. We performed mRNA profiling by GeneChip Mouse Gene 2.0 array using total RNA purified from epididymal fat tissues of *Mir221/222*$^{flox/y}$ fed with STD or HFHS, *Mir221/222AdipoKO* fed with STD or HFHS chow (**Supplementary Tables 3–5**). Then, we made the list of 355 target genes commonly predicted by TargetScan, miRDB, and DIANA-microT, and their seed sequences were conserved in both human and mouse genome (**Supplementary Table 6**). By searching upregulated genes in *Mir221/222AdipoKO* compared with *Mir221/222*$^{flox/y}$ in both STD and HFHS fed groups, we identified that DNA-damage-inducible transcript 4 (*Ddit4*) demonstrated 1.9-fold and 2.58-fold upregulation in *Mir221/222AdipoKO* fed with HFHS and STD chow, respectively (**Supplementary Table 7**). To evaluate miRNA activity of miR-221-3p and miR-222-3p by the binding to 3'-untranslated region (3'-UTR) of *Ddit4*, we performed luciferase reporter assay in 3T3-L1 cells. We cloned 3'-UTR regions of *Ddit4* gene and prepared the wild-type reporter vector, pmirGLO-*Ddit4* WT 3'-UTR, and the mutant vector, pmirGLO-*Ddit4* MT 3'-UTR, in which mutagenesis was induced on the seed sequence binding site (**Figure 3A**). The luciferase reporter vectors were co-transfected with Syn-mmu-miR-221-3p or Syn-mmu-miR-222-3p or negative control siRNA in 3T3-L1 cells. As a result, reporter activity of pmirGLO-*Ddit4* WT 3'-UTR were significantly inhibited in the presence of both Syn-mmu-miR-221-3p and Syn-mmu-miR-222-3p. In contrast, Syn-mmu-miR-221-3p or Syn-mmu-miR-222-3p had almost no effect on the reporter activity of pmirGLO-*Ddit4* MT 3'-UTR (**Figure 3A**). Next, we checked the expression of *Ddit4* in the epididymal adipose tissues of *Mir221/222*$^{flox/y}$ and *Mir221/222AdipoKO* fed with HFHS by quantitative PCR and Western blot. Although the mRNA expression of *Ddit4* was increased in *Mir221/222AdipoKO* without statistical significance, DDIT4 protein expression was significantly upregulated in the *Mir221/222AdipoKO* compared with *Mir221/222*$^{flox/y}$ (**Figure 3B**), suggesting the possible involvement of translational repression by miR-221-3p and miR-222-3p.

Mir221/Mir222 Promotes Adipogenesis by *DDIT4*-Mediated Inhibition of mTORC1

DDIT4 is known to activate tuberous sclerosis complex 1 (TSC1)/TSC2 complex by the inhibition of AKT (protein kinase B) and the release of 14-3-3 from TSC2 (12). It further negatively regulates mammalian target of rapamycin complex 1 (mTORC1) (13). Increased activity of the mTORC1 signaling has been associated with obesity (14), and the knockout mice for the mTORC1 downstream ribosomal protein S6 kinase (S6K) are protected against diet-induced-obesity (15). Thus, we further checked the inactivated form of p-TSC2 (Thr-1462) and activated form of p-S6K (16) in the epididymal adipose tissues of *Mir221/222*$^{flox/y}$ and *Mir221/222AdipoKO*. After overnight fasting, the mice were injected intraperitoneally with insulin and the epididymal fat tissues were harvested at 7 min after insulin injection. In *Mir221/222AdipoKO* mice, both p-AKT and p-TSC2 (Thr-1462) were significantly reduced, and accordingly p-S6K was also significantly reduced (**Figures 4A, B**). p-mTOR was reduced in *Mir221/222AdipoKO* mice, however, it did not reach the statistically significant differences (**Figures 4A, B**).

Since mTOR has been shown to positively regulate adipogenesis and lipogenesis while inhibiting lipolysis, fatty acid oxidation and ketogenesis (17), we performed adipogenesis and glycerol assays in 3T3-L1 adipocytes. We constructed lentiviral vector expressing miRNA inhibitors (pLV-locker 221, pLV-locker 222, pLV-locker control) and miRNA mimics (pLV 221, pLV 222, pLV control). The efficiency for inhibitors and mimics was confirmed in 3T3-L1 cells at 3-7 days after the transduction (**Supplementary Figures 3B, C**). Lentiviral vectors were transduced to 3T3-L1 cells at 2 days before the induction of differentiation and cultured for 7 days. The pLV-locker 221, pLV-locker 222, and pLV-locker 221/222 did not alter the accumulation of lipid droplets demonstrated by oil red O staining measured by absorbance at 490 nm (**Figure 5A**). Similarly, pLV 221, pLV 222, and pLV221/222 only show slight increase in the accumulation of lipid droplets in 3T3-L1 cells without statistical significance (**Figure 5B**). Western blot analysis demonstrated that the

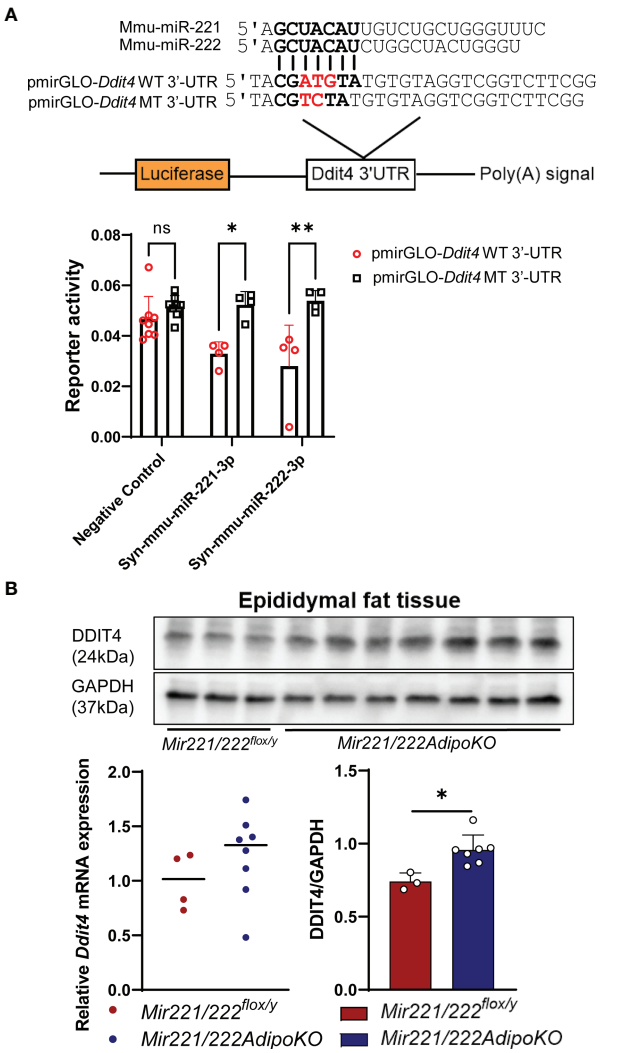

FIGURE 3 | Dual-luciferase reporter assay for *Ddit4* 3'UTR and expression of *Ddit4* in mice. **(A)** Dual-luciferase reporter assay using pmirGLO-*Ddit4* WT 3'-UTR, pmirGLO-*Ddit4* MT 3'-UTR, and pmirGLO no-insert control plasmids. 3T3-L1 cells were co-transfected with Syn-mmu-miR-221-3p (n=4), Syn-mmu-miR-222-3p (n=4), negative control siRNA (n=8). (ns, not significant). **(B)** Quantitative RT-PCR for *Ddit4* in epididymal adipose tissues of *Mir221/222*$^{flox/y}$ (n=4) and *Mir221/222AdipoKO* (n=8) mice fed with high fat high sucrose (HFHS). Western blot analyses for DDIT4 and GAPDH (glyceraldehyde-3-phosphate dehydrogenase) in epididymal adipose tissues of *Mir221/222*$^{flox/y}$ (n=3) and *Mir221/222AdipoKO* (n=7) mice fed with high fat high sucrose (HFHS). Data shown as mean ± SD and analyzed by Mann-Whitney's U test (*p<0.05; **p<0.01).

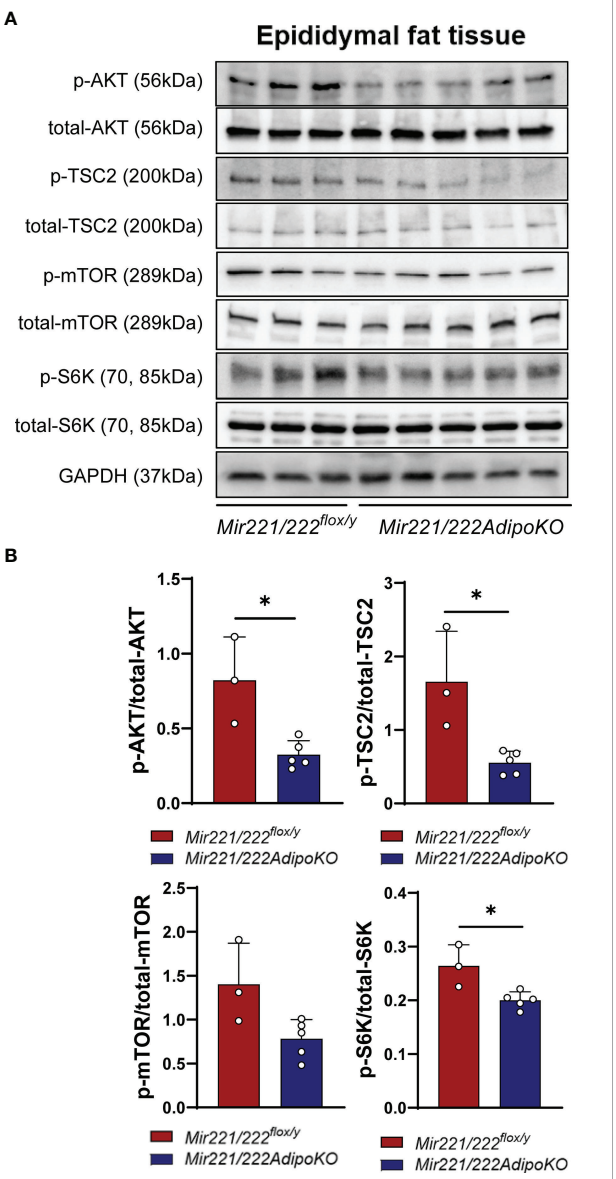

FIGURE 4 | Western blot analyses. **(A)** Western blot analyses for AKT (protein kinase B), TSC2 (tuberous sclerosis complex 2), mTOR (mammalian target of rapamycin) and S6K (ribosomal protein S6 kinase) in *Mir221/222*$^{flox/y}$ (n=3) and in epididymal adipose tissues of *Mir221/222AdipoKO* (n=5) male mice fed with high fat high sucrose (HFHS). Activated form of p-AKT and Inactivated form of p-TSC2 (Thr-1462) and activated form of p-S6K are shown. **(B)** Densitometric analyses of Western blots. Data shown as mean ± SD and analyzed by Mann-Whitney's U test (*p<0.05).

expression of C/EBPα and PPARγ were not changed by pLV-locker 221 and pLV-locker 222 (**Figure 5C**), while they were significantly up-regulated by treatment with pLV 222 (**Figure 5D**). To investigate lipolysis, lentiviral vectors were transduced to the fully differentiated 3T3-L1 adipocyte and we performed glycerol assay 7 days after lentiviral transduction. pLV-locker 221/222 and pLV 221/222 did not alter the glycerol release (**Figure 5E**).

DISCUSSION

The adipocyte-specific inhibition of *Mir221/Mir222* expression protected the mice fed with HFHS chow from the obesity. We demonstrated that the direct target of miR-221-3p and miR-222-3p was *Ddit4* and the inhibition of *Mir221/Mir222* expression resulted in upregulation of DDIT4, inactivation of AKT, activation of TSC2 and subsequent inactivation of S6K, the

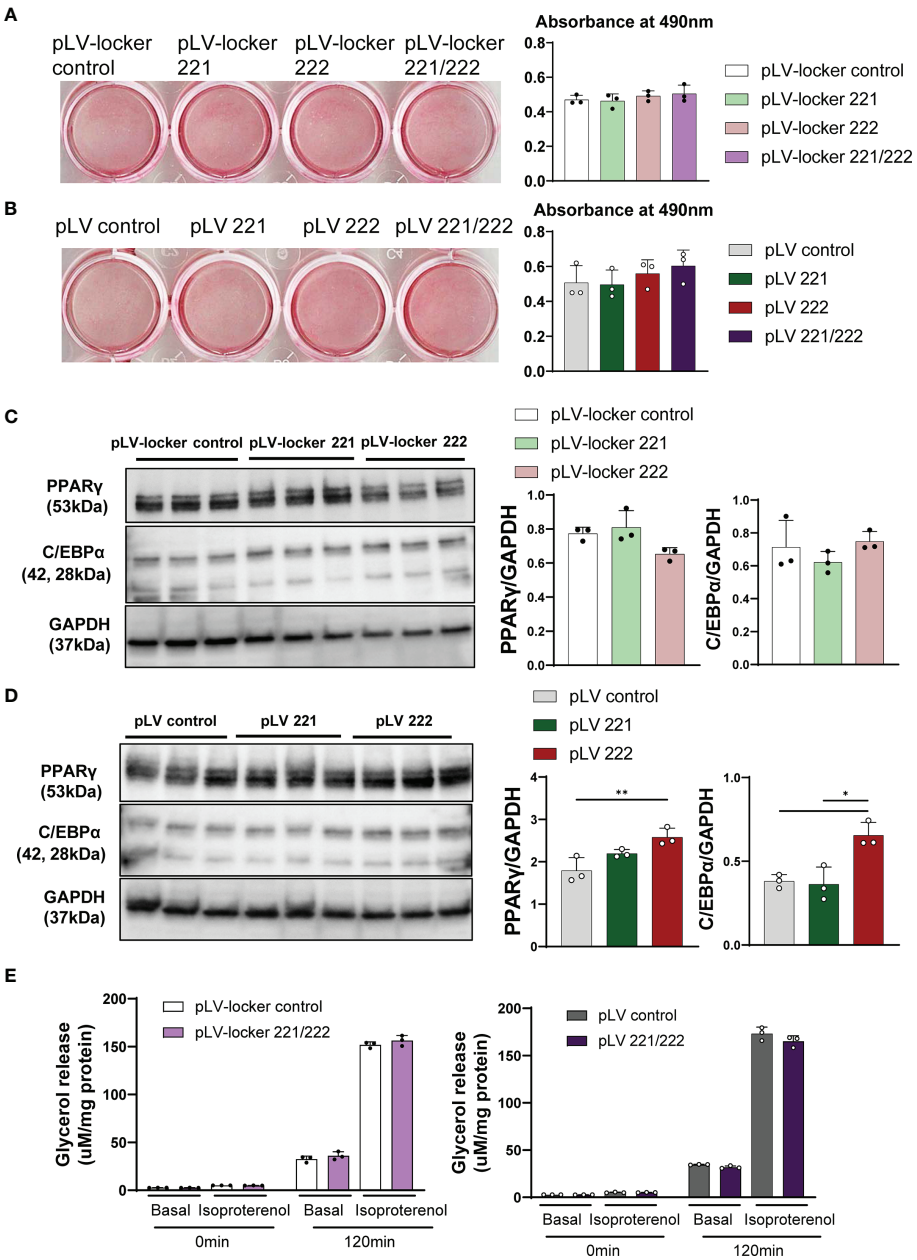

FIGURE 5 | Adipogenesis, lipogenesis and lipolysis in 3T3-L1 cells. Lentiviral vectors were transduced to 3T3-L1 cells at 2 days before the induction of differentiation and cultured for 7 days. **(A)** Oil-red O staining of differentiated 3T3-L1 cells treated with pLV-locker control, pLV-locker 221, pLV-locker 222, and pLV-locker 221/222. **(B)** Oil-red O staining of differentiated 3T3-L1 cells treated with pVL control, pLV 221, pLV 222, and pLV221/222. **(C)** Western blot analysis of PPARγ in differentiated 3T3-L1 cells treated with pLV-locker control, pLV-locker 221, pLV-locker 222, and pLV-locker 221/222. **(D)** Western blot analysis of PPARγ in differentiated 3T3-L1 cells treated with pVL control, pLV 221, pLV 222, and pLV221/222. **(E)** Lipolysis assay in 3T3-L1 cells stimulated with isoproterenol. Differentiated 3T3-L1 cells were treated with pLV-locker 221/222 and pLV 221/222. Data shown as mean ± SD and analyzed by one-way ANOVA with Tukey test (*p<0.05; **p<0.01).

latter is a major target of mTORC1. The lentivirus-mediated transfer of *Mir222* gene promoted the adipogenesis demonstrated by up-regulation of C/EBPα and PPARγ in differentiated 3T3-L1 cells. We concluded that the inhibition of miR-221-3p and miR-222-3p and DDIT4-mediated inhibition of mTORC1 signaling is one of the major mechanisms for the protection from diet-induced obesity. The role of *Mir221* in adipogenesis has been focused by series of investigation and Ahonen et al. reported miR-221-3p overexpression in Simpson-Golabi-Behmel syndrome (SGBS) preadipocytes inhibited *de novo* lipogenesis and adipogenesis (18). In our investigation, overexpression by pLV 221 did not alter the lipogenesis and

adipogenesis in 3T3-L1 cells; however, pLV 222 enhanced the adipogenesis. In bovine adipocyte differentiation, long non-coding RNA (lncRNA), *MIR221HG*, significantly increased adipocyte differentiation associated with dramatic increment of PPARγ (11). We also cloned mouse *Mir221hg* with 1,537 bp and identified that 1,054 bp of 5'-flanking region was deleted in *Mir221/222AdipoKO* mice. The expression of *Mir221hg* is barely detected in brown and WATs in wild type mice and we speculated that the influence of deletion of *Mir221hg* is minimal in *Mir221/222AdipoKO* mice. Although the functional studies to elucidate the role of *Mir222* in adipogenesis and lipogenesis were not reported in cultured adipocytes in previously published studies, we demonstrated that *Mir222* expression was upregulated in WATs of obese mice and in serum of obese patients. The importance of *Mir222* in the pathogenesis of obesity is supported by the analysis of adipose tissue-specific Dicer knockout mice, in which gonadal adipose tissue was the main source of serum exosomal miR-222 (19). The exosome-packed *Mir222* influenced remote organs, and overexpression of *Mir222* inhibits the expression of IRS-1 by directly binding to untranslated regions in the muscle (20) and liver (21). In current investigation, we firstly demonstrated that overexpression of *Mir222* promoted the adipogenesis in 3T3-L1 cells.

Under the presence of amino acids, mTORC1 is activated by GTP-bound Rheb. In the upstream of the Rheb, AKT inhibits TSC2 and TBC1D7 (TBC1 Domain Family Member 7) complex, which further inhibits the activation of mTORC1 by acting as a GTPase-activating protein. mTORC1 promotes the lipid synthesis and storage and adipogenesis, while it inhibits the lipolysis, β-oxidation and ketogenesis. SREBP (sterol regulatory element-binding protein) processing and activation is promoted by mTORC1 by the activation of S6K and lipin 1 leading to transcriptional activation of SREPB1, SREBP2, and many other lipogenic genes. mTORC1 also committed mesenchymal stem cells to adipocyte lineage by the activation of S6K, promotes the initial step of adipocyte differentiation by inhibiting 4E-BP1/2 (eIF4E-binding protein 1/2), and completes the final differentiation by the activation of PPARγ (22). Many researchers screened the agents or intrinsic factors to inhibit mTORC1 signaling and lipogenesis for the treatment of obesity. Lee et al. reported that ezetimibe reduced lipid accumulation by inhibiting mTORC1 signaling, leading to the downregulation of lipogenesis-related genes (23). Shi et al. reported that the inhibition of miR-196b-5p blocked adipogenesis and lipogenesis by directly targeting TSC1 and TGFBR1 (transforming growth factor-β receptor 1) (24). We demonstrated that the inhibition of miR-221-3p and miR-222-3p and subsequent DDIT4-mediated inhibition of mTORC1 signaling is a therapeutic target for the treatment of obesity.

The activation of mTORC1 links to various pathological processes in adipose tissues such as inflammation, beige adipogenesis and angiogenesis. mTORC1 loss and gain of function studies in macrophages resulted in amelioration and exacerbation of inflammatory response, as well as macrophage polarization to both M1 and M2 profiles (25). miR-221 mediates M1 macrophage polarization (26, 27), while suppression of miR-222 alleviate the inflammatory response (28, 29). However, we did not observe the apparent changes in gene expression of cytokines such as *Il1b*, *Il6*, *Ifng*, and *Tnf* in adipose tissues in *Mir221/222AdipoKO* mice (**Supplementary Figure 2**). The phenotyping of T cells and macrophages in WATs should be performed in the future investigation. In beige adipogenesis, the adipose-specific deletion of Raptor, a key component of mTORC1, promoted beige adipogenesis by inhibiting prostaglandins (PGs) synthesized by cyclooxygenase-2 (COX-2) (30). Supporting this notion, ketoprofen alleviated diet-induced obesity and promotes the fat browning by the COX-2 and mTORC1-p38 signaling pathway (31). In our investigation, the genes related to beige adipogenesis such as *Ppargc1* and *Prdm16* tended to be upregulated in WATs without statistical differences. However, in WATs in *Mir221/222AdipoKO* mice, apparent beige adipogenesis was not observed by histological examinations. In tumor microenvironment and angiogenesis, mTORC1 under a hypoxic condition promotes the translation of hypoxia-inducible factor (HIF) 1-2, which lead to the expression of angiogenic growth factors such as vascular endothelial growth factor (VEGF), TGF-α, and platelet-derived growth factor β (PDGF-β) (32). *Mir221* and *Mir222* demonstrated the angiogenic activities in vascular cells (33) and cancers (34), however, we did not observe the angiogenesis activities in WATs in *Mir221/222AdipoKO* mice.

LIMITATION OF STUDY

We hypothesized that circulating miR-221-3p and miR-222-3p play important roles in both mouse obese models and the patients with obesity and T2D. However, the circulating levels of miR-221-3p and miR-222-3p were not altered in *Mir221/222$^{flox/y}$* and *Mir221/222AdipoKO* mice fed with STD and HFHS. In addition, the human serum levels of miR-221-3p and miR-222-3p showed correlations with HbA1c, however, they did not show significant correlations with body weight and BMI. Although we show the roles of miR-221-3p and miR-222-3p in the adipocytes, we did not clearly demonstrate the role of circulating miR-221-3p and miR-222-3p in the pathogenesis of obesity. Another limitation is that it is still unknown why *Mir221/222AdipoKO* mice did not show significant improvement of insulin sensitivity although the body weight was significantly reduced compared with *Mir221/222$^{flox/y}$* fed with HFHS. Finally, the micronutrient composition is not matched between the STD and HFHS diets and it may possibly impact the observed outcomes. Ideally, a matched diet should be used for mineral and vitamin mix.

DATA AVAILABILITY STATEMENT

The datasets presented in this study can be found in online repositories. The names of the repository/repositories and accession number(s) can be found in the article/**Supplementary Material**.

ETHICS STATEMENT

The studies involving human participants were reviewed and approved by Okayama University Graduate School of Medicine, Dentistry and Pharmaceutical Sciences and Okayama University Hospital, Ethics Committee. The patients/participants provided their written informed consent to participate in this study. The animal study was reviewed and approved by the Animal Care and Use Committee of the Department of Animal Resources, Advanced Science Research Center, Okayama University.

AUTHOR CONTRIBUTIONS

SY, DZ, AK, and JW designed the project and experiments and wrote the manuscript. SY, DZ, AK, NK, RS, and HA performed animal experiments and analyzed and interpreted data. AN and JE performed culture and molecular biology experiments. SY, AK, NK, RS, AN, JE, and JW designed and performed clinical study. All authors contributed to the article and approved the submitted version.

FUNDING

This work was supported by Grant-in-Aid for Young Scientists (19K17984), Grant-in-Aid for Scientific Research (B) (19H03675), Japan Agency for Medical Research and development (AMED, grant no: 17ek0210095h0001, 20ek0109445h0001).

ACKNOWLEDGMENTS

We acknowledge support from Central Research Laboratory, Okayama University Medical School; usage of Kubota High Speed Refrigerated Centrifuge Model 7780II, ABI PRISM3130, and producing paraffin blocks and sections.

SUPPLEMENTARY MATERIAL

The Supplementary Material for this article can be found online at: https://www.frontiersin.org/articles/10.3389/fendo.2021.750261/full#supplementary-material

REFERENCES

1. Kahn CR, Wang G, Lee KY. Altered Adipose Tissue and Adipocyte Function in the Pathogenesis of Metabolic Syndrome. *J Clin Invest* (2019) 129:3990–4000. doi: 10.1172/JCI129187
2. Huang Z, Xu A. Adipose Extracellular Vesicles in Intercellular and Inter-Organ Crosstalk in Metabolic Health and Diseases. *Front Immunol* (2021) 12:608680. doi: 10.3389/fimmu.2021.608680
3. Pan Y, Hui X, Hoo RLC, Ye D, Chan CYC, Feng T, et al. Adipocyte-Secreted Exosomal microRNA-34a Inhibits M2 Macrophage Polarization to Promote Obesity-Induced Adipose Inflammation. *J Clin Invest* (2019) 129:834–49. doi: 10.1172/JCI123069
4. Fu T, Seok S, Choi S, Huang Z, Suino-Powell K, Xu HE, et al. MicroRNA 34a Inhibits Beige and Brown Fat Formation in Obesity in Part by Suppressing Adipocyte Fibroblast Growth Factor 21 Signaling and SIRT1 Function. *Mol Cell Biol* (2014) 34:4130–42. doi: 10.1128/MCB.00596-14
5. Wang L, Sinnott-Armstrong N, Wagschal A, Wark AR, Camporez JP, Perry RJ, et al. A MicroRNA Linking Human Positive Selection and Metabolic Disorders. *Cell* (2020) 183:684–701.e14. doi: 10.1016/j.cell.2020.09.017
6. Qi R, Wang J, Wang Q, Qiu X, Yang F, Liu Z, et al. MicroRNA-425 Controls Lipogenesis and Lipolysis in Adipocytes. *Biochim Biophys Acta Mol Cell Biol Lipids* (2019) 1864:744–55. doi: 10.1016/j.bbalip.2019.02.007
7. Higuchi C, Nakatsuka A, Eguchi J, Teshigawara S, Kanzaki M, Katayama A, et al. Identification of Circulating miR-101, miR-375 and miR-802 as Biomarkers for Type 2 Diabetes. *Metabolism* (2015) 64:489–97. doi: 10.1016/j.metabol.2014.12.003
8. Deiuliis JA. MicroRNAs as Regulators of Metabolic Disease: Pathophysiologic Significance and Emerging Role as Biomarkers and Therapeutics. *Int J Obes (Lond)* (2016) 40:88–101. doi: 10.1038/ijo.2015.170
9. Villard A, Marchand L, Thivolet C, Rome S. Diagnostic Value of Cell-Free Circulating MicroRNAs for Obesity and Type 2 Diabetes: A Meta-Analysis. *J Mol Biomark Diagn* (2015) 6(6):251. doi: 10.4172/2155-9929.1000251
10. Nakagawa Y, Ishimura K, Oya S, Kamino M, Fujii Y, Nanba F, et al. Comparison of the Sympathetic Stimulatory Abilities of B-Type Procyanidins Based on Induction of Uncoupling Protein-1 in Brown Adipose Tissue (BAT) and Increased Plasma Catecholamine (CA) in Mice. *PloS One* (2018) 13:e0201203. doi: 10.1371/journal.pone.0201203
11. Li M, Gao Q, Tian Z, Lu X, Sun Y, Chen Z, et al. MIR221HG Is a Novel Long Noncoding RNA That Inhibits Bovine Adipocyte Differentiation. *Genes (Basel)* (2019) 11(1):29. doi: 10.3390/genes11010029
12. Britto FA, Dumas K, Giorgetti-Peraldi S, Ollendorff V, Favier FB. Is REDD1 a Metabolic Double Agent? Lessons From Physiology and Pathology. *Am J Physiol Cell Physiol* (2020) 319:C807–24. doi: 10.1152/ajpcell.00340.2020
13. Tirado-Hurtado I, Fajardo W, Pinto JA. DNA Damage Inducible Transcript 4 Gene: The Switch of the Metabolism as Potential Target in Cancer. *Front Oncol* (2018) 8:106. doi: 10.3389/fonc.2018.00106
14. Khamzina L, Veilleux A, Bergeron S, Marette A. Increased Activation of the Mammalian Target of Rapamycin Pathway in Liver and Skeletal Muscle of Obese Rats: Possible Involvement in Obesity-Linked Insulin Resistance. *Endocrinol* (2005) 146:1473–81. doi: 10.1210/en.2004-0921
15. Yu R, Li Z, Liu S, Huwatibieke B, Li Y, Yin Y, et al. Activation of Mtorc1 Signaling in Gastric X/A-Like Cells Induces Spontaneous Pancreatic Fibrosis and Derangement of Glucose Metabolism by Reducing Ghrelin Production. *EBioMed* (2018) 36:304–15. doi: 10.1016/j.ebiom.2018.09.027
16. Manning BD, Tee AR, Logsdon MN, Blenis J, Cantley LC. Identification of the Tuberous Sclerosis Complex-2 Tumor Suppressor Gene Product Tuberin as a Target of the Phosphoinositide 3-Kinase/Akt Pathway. *Mol Cell* (2002) 10:151–62. doi: 10.1016/s1097-2765(02)00568-3
17. Pena-Leon V, Perez-Lois R, Seoane LM. mTOR Pathway is Involved in Energy Homeostasis Regulation as a Part of the Gut-Brain Axis. *Int J Mol Sci* (2020) 21(16):5715. doi: 10.3390/ijms21165715
18. Ahonen MA, Asghar MY, Parviainen SJ, Liebisch G, Horing M, Leidenius M, et al. Human Adipocyte Differentiation and Composition of Disease-Relevant Lipids Are Regulated by miR-221-3p. *Biochim Biophys Acta Mol Cell Biol Lipids* (2021) 1866:158841. doi: 10.1016/j.bbalip.2020.158841
19. Li D, Song H, Shuo L, Wang L, Xie P, Li W, et al. Gonadal White Adipose Tissue-Derived Exosomal MiR-222 Promotes Obesity-Associated Insulin Resistance. *Aging (Albany NY)* (2020) 12:22719–43. doi: 10.18632/aging.103891
20. de Mendonca M, de Sousa E, da Paixao AO, Araujo Dos Santos B, Roveratti Spagnol A, Murata GM, et al. MicroRNA miR-222 Mediates Pioglitazone Beneficial Effects on Skeletal Muscle of Diet-Induced Obese Mice. *Mol Cell Endocrinol* (2020) 501:110661. doi: 10.1016/j.mce.2019.110661
21. Ono K, Igata M, Kondo T, Kitano S, Takaki Y, Hanatani S, et al. Identification of microRNA That Represses IRS-1 Expression in Liver. *PloS One* (2018) 13:e0191553. doi: 10.1371/journal.pone.0191553
22. Epstein Y, Seidman DS, Moran D, Arnon R, Arad M, Varssano D. Heat-Exercise Performance of Pyridostigmine-Treated Subjects Wearing Chemical Protective Clothing. *Aviat Space Environ Med* (1990) 61:310–3.

23. Lee YS, Park JS, Lee DH, Han J, Bae SH. Ezetimibe Ameliorates Lipid Accumulation During Adipogenesis by Regulating the AMPK-Mtorc1 Pathway. *FASEB J* (2020) 34:898–911. doi: 10.1096/fj.201901569R
24. Shi Y, Li F, Wang S, Wang C, Xie Y, Zhou J, et al. miR-196b-5p Controls Adipocyte Differentiation and Lipogenesis Through Regulating Mtorc1 and TGF-Beta Signaling. *FASEB J* (2020) 34:9207–22. doi: 10.1096/fj.201901562RR
25. Festuccia WT. Regulation of Adipocyte and Macrophage Functions by Mtorc1 and 2 in Metabolic Diseases. *Mol Nutr Food Res* (2021) 65:e1900768. doi: 10.1002/mnfr.201900768
26. Cai M, Shi Y, Zheng T, Hu S, Du K, Ren A, et al. Mammary Epithelial Cell Derived Exosomal MiR-221 Mediates M1 Macrophage Polarization *via* SOCS1/STATs to Promote Inflammatory Response. *Int Immunopharmacol* (2020) 83:106493. doi: 10.1016/j.intimp.2020.106493
27. Quero L, Tiaden AN, Hanser E, Roux J, Laski A, Hall J, et al. miR-221-3p Drives the Shift of M2-Macrophages to a Pro-Inflammatory Function by Suppressing JAK3/STAT3 Activation. *Front Immunol* (2019) 10:3087. doi: 10.3389/fimmu.2019.03087
28. Zhang H, Luan S, Xiao X, Lin L, Zhao X, Liu X. Silenced microRNA-222 Suppresses Inflammatory Response in Gestational Diabetes Mellitus Mice by Promoting CXCR4. *Life Sci* (2021) 266:118850. doi: 10.1016/j.lfs.2020.118850
29. Zhang Y, Yang J, Zhou X, Wang N, Li Z, Zhou Y, et al. Knockdown of miR-222 Inhibits Inflammation and the Apoptosis of LPS-Stimulated Human Intervertebral Disc Nucleus Pulposus Cells. *Int J Mol Med* (2019) 44:1357–65. doi: 10.3892/ijmm.2019.4314
30. Zhang X, Luo Y, Wang C, Ding X, Yang X, Wu D, et al. Adipose Mtorc1 Suppresses Prostaglandin Signaling and Beige Adipogenesis *via* CRTC2-COX-2 Pathway. *Cell Rep* (2018) 24:3180–93. doi: 10.1016/j.celrep.2018.08.055
31. Kang NH, Mukherjee S, Jang MH, Pham HG, Choi M, Yun JW. Ketoprofen Alleviates Diet-Induced Obesity and Promotes White Fat Browning in Mice *via* the Activation of COX-2 Through Mtorc1-P38 Signaling Pathway. *Pflugers Arch* (2020) 472:583–96. doi: 10.1007/s00424-020-02380-7
32. Conciatori F, Bazzichetto C, Falcone I, Pilotto S, Bria E, Cognetti F, et al. Role of mTOR Signaling in Tumor Microenvironment: An Overview. *Int J Mol Sci* (2018) 19(8):2453. doi: 10.3390/ijms19082453
33. Poliseno L, Tuccoli A, Mariani L, Evangelista M, Citti L, Woods K, et al. MicroRNAs Modulate the Angiogenic Properties of HUVECs. *Blood* (2006) 108:3068–71. doi: 10.1182/blood-2006-01-012369
34. Xu CH, Liu Y, Xiao LM, Chen LK, Zheng SY, Zeng EM, et al. Silencing microRNA-221/222 Cluster Suppresses Glioblastoma Angiogenesis by Suppressor of Cytokine Signaling-3-Dependent JAK/STAT Pathway. *J Cell Physiol* (2019) 234:22272–84. doi: 10.1002/jcp.28794

Conflict of Interest: JW receives speaker honoraria from Astra Zeneca, Daiichi Sankyo, Novartis, Novo Nordisk Pharma, Tanabe Mitsubishi and receives grant support from Astellas, Baxter, Bayer, Chugai, Dainippon Sumitomo, Kyowa Kirin, Novo Nordisk Pharma, Ono, Otsuka, Tanabe Mitsubishi, and Teijin.

The remaining authors declare that the research was conducted in the absence of any commercial or financial relationships that could be construed as a potential conflict of interest.

Publisher's Note: All claims expressed in this article are solely those of the authors and do not necessarily represent those of their affiliated organizations, or those of the publisher, the editors and the reviewers. Any product that may be evaluated in this article, or claim that may be made by its manufacturer, is not guaranteed or endorsed by the publisher.

frontiers in Endocrinology

ORIGINAL RESEARCH
published: 10 January 2022
doi: 10.3389/fendo.2021.690555

Profile Screening of Differentially Expressed lncRNAs of Circulating Leukocytes in Type 2 Diabetes Patients and Differences From Type 1 Diabetes

*Jianyi Lv[1], Yihan Liu[1], Jia Cui[2], Hongjuan Fang[3], Ying Wu[1], Xiao Zhu[1], Meng Guo[1], Changlong Li[1], Jingtao Dou[2], Zhenwen Chen[1] and Xiaoyan Du[1]**

[1] School of Basic Medical Sciences, Capital Medical University, Beijing, China, [2] Department of Endocrinology, Chinese PLA General Hospital, Beijing, China, [3] Department of Endocrinology, Beijing TianTan Hospital, Capital Medical University, Beijing, China

OPEN ACCESS

Edited by:
Marcia Hiriart, Universidad Nacional Autonoma de Mexico, Mexico

Reviewed by:
Haitao Luo, University of Jinan, China
Yu-Hang Zhang, Brigham and Women's Hospital, United States

***Correspondence:**
Xiaoyan Du
duduyan@ccmu.edu.cn

Specialty section:
This article was submitted to Diabetes: Molecular Mechanisms, a section of the journal Frontiers in Endocrinology

Received: 03 April 2021
Accepted: 13 December 2021
Published: 10 January 2022

Citation:
Lv J, Liu Y, Cui J, Fang H, Wu Y, Zhu X, Guo M, Li C, Dou J, Chen Z and Du X (2022) Profile Screening of Differentially Expressed lncRNAs of Circulating Leukocytes in Type 2 Diabetes Patients and Differences From Type 1 Diabetes. Front. Endocrinol. 12:690555. doi: 10.3389/fendo.2021.690555

Long noncoding RNAs (lncRNAs) have been reported to have multiple functions and can be used as markers of various diseases, including diabetes. This study was conducted to determine the lncRNA profile in leukocytes from patients with type 2 diabetes (T2D). Differential expression of lncRNAs in T2D and type 1 diabetes (T1D) was also examined. RNA sequencing was performed in a critically grouped sample of leukocytes from T2D patients and healthy persons. A total of 845 significantly differentially expressed lncRNAs were identified, with 260 downregulated and 585 upregulated lncRNAs in T2D. The analysis of functions of DE-lncRNA and constructed co-expression networks (CNC) showed that 21 lncRNAs and 117 mRNAs harbored more than 10 related genes in CNC. Fourteen of 21 lncRNAs were confirmed to be significantly differentially expressed was detected by qPCR between the T2D and control validation cohorts. We also identified a panel of 4 lncRNAs showing significant differences in expression between T1D and T2D. Collectively, hundreds of novel DE-lncRNAs we identified in leukocytes from T2D patients will aid in epigenetic mechanism studies. Fourteen confirmed DE-lncRNAs can be regarded as diagnostic markers or regulators of T2D, including 4 lncRNAs that chould distinguish T1D and T2D in clinical practice to avoid misdiagnosis.

Keywords: circulating leukocyte, distinguishing diagnosis, lncRNA, RNA sequencing, type 2 diabetes, type 1 diabetes

INTRODUCTION

Diabetes mellitus (DM) is one of the most widespread chronic diseases, creating a burden for both patients and their families. DM is always divided into four main types, among which patients with type 2 diabetes (T2D) account for over 90% and type 1 diabetes (T1D) with approximately 10% of all cases (1). Genetic and environmental factors are important causes of T2D. Although the characteristics of type 1 and 2 diabetes differ, quickly or easily distinguishing these types is difficult

in clinical practice. Additionally, as the age of T2D patients decreases, it becomes difficult to distinguish type 1 and 2 diabetes in patients 20–30 years old (1). Thus, T1D patients may be misdiagnosed as having T2D, resulting in incorrect treatment. Diagnosing different types of diabetes mellitus still remains a challenge. Therefore, new markers or therapy targets are urgently needed for T2D. Also, simple, convenient, and efficient molecular technological methods that aid in the diagnoses of different types of diabetes are needed as well.

Long noncoding RNAs (lncRNAs) are a class of RNAs with transcripts longer than 200 nucleotides and limited protein coding potential (2). Studies have demonstrated that lncRNAs are involved in a wide range of biological processes (3). A growing mass of literature has revealed that lncRNAs are useful markers of disease status and in diagnosis (4). Few previous studies have investigated lncRNAs in diabetes (5). Most reports of lncRNAs in diabetes have mainly focused on the lncRNA profile in pancreatic beta cells and regulation of glucose homeostasis (6), diabetes with vascular complications (7), nephropathy (8), obesity (9), and retinopathy (10). Researchers have established a connection between lincRNA transcriptome of human monocyte-derived macrophages and cardiometabolic disorders (11). However, studies aimed at identifying lncRNAs involved in T2D in circulating leukocytes are rare. Systemic low-grade inflammation is a hallmark of T2D and contributes to the pathogenesis of several associated complications (12). Activation of monocytes and macrophages plays an important role in inflammatory processes needed for the protection against invading pathogens or toxins (13). We predicted that lncRNA in peripheral blood cells may play a regulatory role in the pathogenesis of T2D. Wang et al. performed microarray analysis to screen out differential expressed mRNAs and lncRNAs between T2D patients and healthy control (14). Marpadga et al. revealed downregulation of anti-inflammatory cytokines and antiproliferative genes, along with several lncRNAs, may promote chronic inflammation in T2D with RNA sequencing (15). Whether lncRNAs are involved blood cells or if they can be used to distinguish type 1 and 2 diabetes has not been explored. Therefore, we identified differentially expressed lncRNAs in leukocytes, the most nucleated cells in circulation, and explored novel lncRNAs as diagnostic markers and potential regulators for T2D. We also evaluated lncRNAs that can discriminate type 2 and type 1 diabetes by analyzing the present data and our previous data (GEO accession number GSE130279).

MATERIALS AND METHODS

Subjects

Human blood samples collected from the Department of Endocrinology, Chinese PLA General Hospital, were grouped into healthy control (CTR, n = 5), and T2D (n = 11, 6 with family history and 5 without family history) as discovery cohort by clinical examination. The expanded validation cohort were grouped by healthy control (CTR, n = 36), T2D (n = 56), and T1D (n = 11). The information of these T2D participants in discovery cohort and validation cohort are showed in **Table S1**. All consenting adult subjects (18–65 years old) with no past medical history were consecutively enrolled between March 2017 and January 2018. Blood samples were subsequently collected in the morning after an overnight fast of 10 to 12 h. The study was approved by the Ethics Committee of the Chinese PLA General Hospital (Permitted No. S2016-147-03) and all patients gave informed consent before participation in the study.

Detailed Information of Type 2 Diabetes Diagnosed Criteria and Excluded Requirements

The individuals in this study either suffered from T2D, T1D or were healthy controls, as part of discovery or validation cohorts. The subjects in the T2D or T1D group were involved based on criteria including: 1) diagnosed with T2D or T1D according the World Health Organization (WHO) screening criteria; 2) aged 18–65 years without a gender limit; 3) with normal triglyceride serum level; 4) no complications occurred; and 5) with the approval of the participants themselves or their guardian. Patients with family history were defined as such by the existence of a parent and grandparent also diagnosed as having T2D. The subjects in the healthy control group were included based on the following criteria: 1) healthy with a negative diagnosis of T2D and T1D according the World Health Organization (WHO) screening diabetes criteria and confirmed with normal blood biochemical indexes, free from all endocrine disease and infectious disease by consulting; 2) aged 18–65 years without a gender limit; 3) with the approval of the participants themselves or their guardian. Exclusion criteria were: 1) severe disease or tumors in the heart, brain, liver, kidney currently or previously; 2) severe gastrointestinal disease; 3) presenting with other conditions such as severe infection or active tuberculosis and applying multiple antibiotics; 4) pregnant or lactating women; 5) with a history of or alcohol and/or drug abuse currently; 6) with a history of mental illness or with family history; and 7) stressful life incidents having occurred within one year. The information of healthy control was gained by consulting.

Total RNA Extraction and Purification From Leukocytes

Total RNA was extracted from leukocytes isolated from peripheral blood. Briefly, approximately 2.5 ml of blood from each subject was static settlement for less than 4 h, followed by centrifugation for 10 min at 3,000×*g*. The cell pellets were then incubated with 1 ml red blood cell lysate (Solarbio Technology Co., Ltd.) and the resultant lysate was centrifuged for 3 min at 3,000×*g*. After that, the supernatant was removed and the above steps were repeated three times. Total RNA was extracted using TRIzol, as per the manufacturer's instructions (Invitrogen). Ribosomal RNA was removed using the Ribo Zero Magnetic Gold kit (MRZG126, Illumina). Quality and integrity of the isolated RNA was verified by NanoDrop (Thermo scientific) and Bioanalyzer (Agilent). OD260/280 ratio ranged between 1.9 and 2.1 and RIN >7.0.

RNA-Sequencing and Analysis

RNA sequencing was performed by Annoroad Gene Tech. Co., Ltd. Sequence libraries were prepared using the NEB Next Ultra Directional RNA LibraryPrep Kit for Illumina (NEB, Ispawich, USA) selection in order to include all the lncRNA transcripts that were not polyadenylated. Libraries were sequenced on the Illumina HiSeq X Ten with 150 bp paired-end reads. The paired-end reads from the samples were mapped to the hg19 reference genome by HISAT (v2.0.5). *Ab initio* transcript reconstruction was performed using String Tie, version 1.3.2d, with the reference genome download from the ENSEMBL. Novel transcripts were filtered for having at least 2 exons. Read counts were then calculated per gene from the alignment bam files using HTSeq (v0.6.0) and FPKM (Fragments Per Kilobase Millon Mapped Reads) were then calculated to represent the expression level of genes in each sample. The protein-coding potential of transcripts was evaluated using the CNCI, CPC, PFAM, and CPAT analysis. Novel lncRNAs were identified as non-coding RNA in all four analyses. Conservative analysis of the identified novel lncRNAs was performed by PhastCons. RefSeq gene counts were normalized by trimmed mean of M value (TMM) method. DEGs were identified using Bioconductor package edgeR using criteria of fold change ≥2, FDR <0.05, and average coverage ≥1 in at least 1 sample. Empirical Bayes moderated statistics and corresponding *p* values were computed for comparisons and *p*-values were adjusted for multiple comparisons using the Benjamini–Hochberg procedure. Genes with an adjusted *p*-value of <0.05 were considered differentially expressed and defined as optimized data. The DE-lncRNA and mRNA between T1D and T2D were analyzed by the present data and our previous data.

Construction of the Coding Non-Coding Gene Co-Expression Network and Correlation Analysis

To explore the association between lncRNAs and target mRNAs, a coding non-coding co-expression (CNC) network was constructed based on correlation analysis between DE-lncRNAs and mRNAs. Target mRNAs were selected with High Spearman correlation Coefficient ($p \geq 0.9$) or with distance less than 50 kb. The network was constructed with Cytoscape (http://www.cytoscape.org) and STRING (https://string-db.org).

To obtain DE-lncRNA associated protein-coding genes, correlation analysis was performed by R studio (v1.2.1335). The expression level of fourteen DE-lncRNAs and all mRNAs were calculated the correlation co-efficient. Pearson's correlations ranging from 0.3 to 0.5, 0.5 to 0.7 or >0.7 are classified as weak, moderate, and strong, respectively. P-value is less than 0.05.

GO Term and KEGG Pathway Analysis

Differentially expression genes (DEGs) between T2D and healthy control were set to the Gene Ontology (GO) database to analyze the potential functions of lncRNAs and their associated mRNAs. The terms were supplied as annotation to genes and gene products. In this study, we mainly focused on the biological process (BP), cellular component (CC), and molecular function (MF) domains and a *P*-value of <0.05 was considered statistically significant. KEGG pathway analysis of DEGs was performed using the KOBAS online analysis database (available online: http://kobas.cbi.pku.edu.cn/). We analyzed the significantly differentially expressed co-expression mRNAs of lncRNAs as determined from CNC network.

qPCR for Validation of Differential lncRNA in Expanded Cohort

A total of 21 lncRNAs were chosen to be validated further by qPCR in independently expanded samples of CTL (n = 36), T2D (n = 56), respectively. These 21 candidate lncRNAs were chosen based on the following criteria: 1) the biotype of both the lncRNA or antisense-lncRNA was included; 2) lncRNAs with no significant different expression between T2D and control were randomly selected; 3) both novel and known lncRNAs were included; 4) both up and downregulated DE-lncRNAs were included; and 5) the lncRNAs in the CNC network were chosen. After primer design and optimization of PCR conditions, 21 lncRNAs were tested and the information is presented in **Table S2**. The 9 DE-lncRNA between T1D and T2D were tested by 56 T2D and 11 T1D samples as well. cDNA was reverse transcribed by 5× All-In-One MasterMix (with AccuRT Genomic DNA Removal Kit) (Applied Biological Materials Inc., Canada) according to the manufacturer's instructions. The qPCR was performed using EvaGreen 2× qPCR MasteMix—No dye (SYBR Green) (Applied Biological Materials Inc., Canada) and samples were amplified using the CFX Connect qPCR System (Biorad, Hercules, CA, USA). All experiments were conducted in triplicate and these triplicates were repeated three times. The $2^{-\Delta\Delta CT}$ method was used to quantify the relative expression of each lncRNA, and β-actin was used as an internal control.

Statistical Analysis

Statistical analysis was performed using SPSS 19.0 software (SPSS Inc., USA). All values were expressed as the mean ± SEM. Differences were considered statistically significant at $p < 0.05$. Differential expression levels of lncRNA in the expanded samples were evaluated with the Mann–Whitney U test. Differences were considered statistically significant at $p < 0.05$.

RESULTS

Transcriptomic Profiles in Patients With Type 2 Diabetes

To determine the transcriptomic profiles of T2D patients, we evaluated 11 patients diagnosed T2D and 5 healthy volunteers as controls. The data process flow chart shown in **Figure 1A**. The information about the T2D participants is shown in **Table 1**, which demonstrates that most clinical characteristics in the discovery cohort and expanded cohort were not significantly different. Thus, the lncRNAs selected in the discovery cohort could be reliably validated in the expanded cohort.

We first described the transcriptomic profiles of T2D to identify critical genes and lncRNAs in the T2D patients. In total, 14,503 lncRNAs and 17,487 mRNAs (8,331 upregulated and 9,156 downregulated) were detected in leukocytes from T2D patients. Of these, 8,706 lncRNAs have been registered in databases (defined

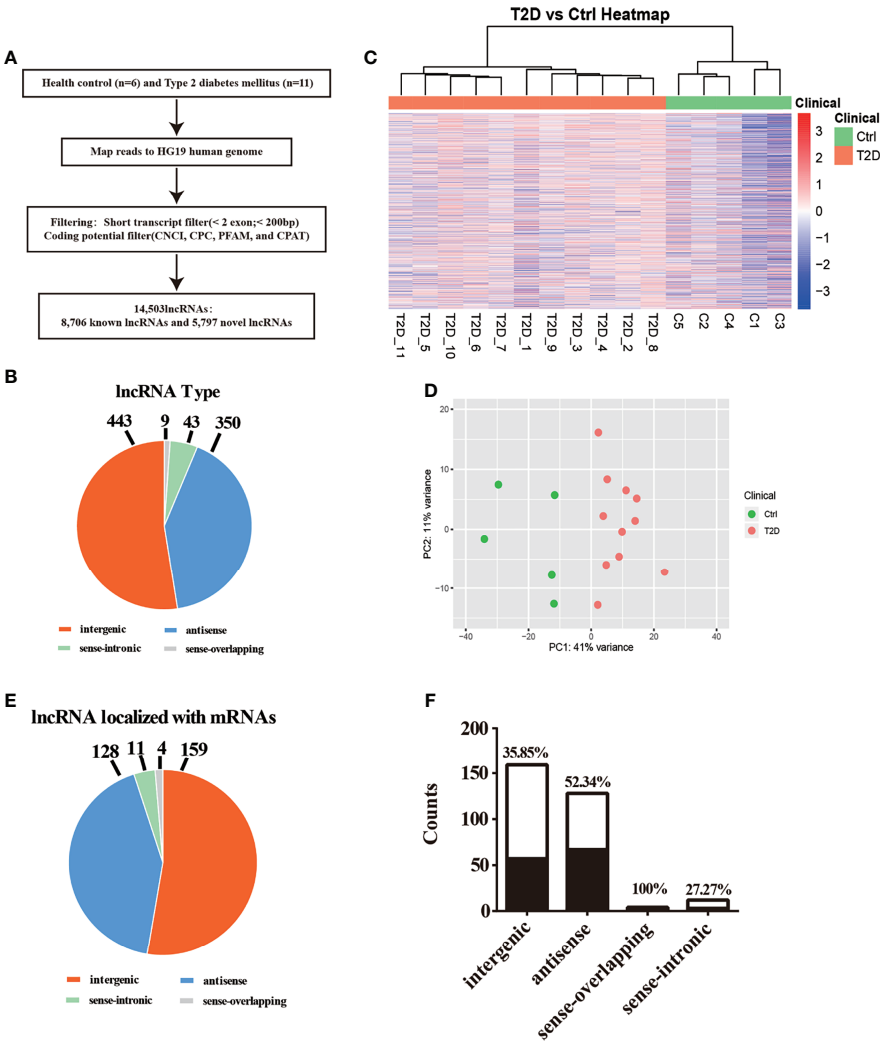

FIGURE 1 | Transcriptomic landscape of T2D-lncRNAs. **(A)** A schematic illustration of the procedure used to identify and define lncRNAs in the leukocytes of patients with type 2 diabetes and to discover lncRNAs different between type 1 diabetes and type 2 diabetes. **(B)** Pie chart representations show the proportion of type 2 diabetes associated lncRNAs that are transcribed as antisense, intergenic, sense-overlapping, and sense-intronic lncRNAs, analyzed post-optimization. **(C)** Differential lncRNA expression profiles were hierarchical cluster analyzed and shown as a heatmap. **(D)** Principal component analysis shows similar results also presented as a heatmap. **(E)** The different classes of T2D-lncRNAs with significant differential expression derived from coding genes classified into intergenic, antisense, sense-overlapping, and sense-intronic lncRNAs according biotype. **(F)** The ratio of different classes T2D-lncRNA with significant co-expression mRNAs.

TABLE 1 | Clinical characteristics of included patients of type 2 diabetes in discovery cohorts (n=11) and in validation cohorts (n=56).

Items	Type 2 diabetes in discovery cohorts (n=11)	Type 2 diabetes in validation cohorts (n=56)	t-test/chi-square test (p value)
Age (years)	40.91±11.77	47.55±12.12	0.1098
Sex (male%)	90.91%	39.13%	0.1078
BMI (kg/m2)	25.63±4.26	27.68±5.50	0.1822
Fasting glucose (mmo/L)	7.55±1.98	8.08±3.08	0.4762
OGTT insulin (0h,μU/mL)	17.98±29.23	20.20±46.10	0.8628
OGTT insulin (2h,μU/mL)	57.24±75.06	61.52±78.30	0.8869
HbA1c	8.46±1.97	8.82±1.95	0.5904
Total cholesterol (mg/dL)	5.05±3.01	4.46±1.21	0.5375
Fasting triglycerides (mg/dL)	2.53±3.09	2.66±2.56	0.9021
HDL (mg/dL)	1.04±0.22	1.01±0.39	0.7092
LDL (mg/dL)	2.66±0.66	2.65±0.92	0.9663

as known), namely, 4,821 upregulated and 3,885 downregulated lncRNAs. Additionally, 5,797 lncRNAs were identified for the first time (defined as novel) with 3,663 upregulated and 2,134 downregulated. After optimization using an adjusted *p*-value (threshold of $p < 0.05$), we identified 845 significantly differentially expressed (DE) lncRNAs (T2D-lncRNAs) (**Table S3**), among which 260 were downregulated and 585 were upregulated (**Figure S1A**). The top 20 lncRNAs are shown in **Table 2**. Further, 1,305 mRNAs (T2D-mRNAs) were found in T2D by similar optimization, with 559 downregulated and 746 upregulated (**Figure S1A**). Of the DE-lncRNAs, 350 (41.4%) were antisense, 443 (52.4%) were intergenic (lincRNA), and 52 belonged to sense-overlapping (5.09%), and sense-intronic (1.06%) lncRNAs (**Figure 1B** and **Table S3**). Both T2D-lncRNA and T2D-mRNA were clearly distinguished in T2D patients and healthy controls by hierarchical clustering (**Figure 1C** and **Figure S1A**) and principal content analysis (**Figure 1D** and **Figure S1B**). Taken together, the difference between healthy controls and T2D patients was significantly reflected by both the expression of protein coding genes and hundreds of lncRNAs in the leukocytes.

We further analyzed the different classes of T2D-lncRNAs derived from coding genes. In the T2D-lncRNAs dataset, 302 lncRNAs were localized with their mRNAs, but only 131 of lncRNAs showed significantly altered expression levels of their localized mRNA. The biotype of the 302 lncRNA including intergenic (159 lncRNAs), antisense (128 lncRNAs), sense-overlapping (4 lncRNAs), and sense-intronic (11 lncRNAs) are shown in **Figure 1E**. Sense-overlapping lncRNAs showed the highest ratio (100%, 4/4) of significant co-expression in each biotype group (**Figure 1F**).

Features of Novel lncRNAs Identified in Patients With Type 2 Diabetes

The characteristics of 9,114 transcripts (some lncRNAs have more than one transcript) identified in T2D patients were first disentangled as novel lncRNAs. Most novel lncRNA transcripts harbored 2 exons (7,106/9,114, 77.97%) (**Figure 2A**). The lengths of most novel lncRNAs (6,570/9,114, 72.09%) were less than 2,000 bp (**Figure 2B**). The results of conservation analysis of the novel lncRNAs in humans indicated that more than half (5,587/9,114, 61.3%) had low conservation scores (CS less than 0.1) (**Figure 2C**) and 6.77% of lncRNA transcripts (617/9,114) had CS less than 0.01 between human and other species. Analysis of the distribution of transcripts on chromosomes demonstrated that novel lncRNAs were mainly distributed on chr1, chr2, chr3, chr5, chr6, and chr7 and that most lncRNAs with low CS in humans were from the same chromosome (**Figure S2**).

CNC Network of lncRNAs and mRNAs in Type 2 Diabetes

We structured co-expression networks to determine if lncRNAs are associated with one to dozens of lncRNAs and mRNAs. There were 1,076 genes involved in our co-expression networks consisting of 618 lncRNAs and 458 mRNAs (**Figure S3A**). In total, 21 lncRNAs and 117 mRNAs harbored more than 10 related genes in the CNC network. The top 10 lncRNAs and mRNAs with the number of genes to which they were related are shown in **Table 3**. The lncRNAs used for further validation and their CNC network are shown in **Figures 3A–F**. LncRNA MSTRG.172533 was the top-ranking lncRNA harboring 57 genes in its network, among which RACK1 (16), SLC9A8 (17), and others have been reported as related to diabetes. The mRNA RAC1 harbored 37 genes and ranked first in CNC analysis, which has been explored in diabetes (18), diabetic retinopathy (19), and so on. We also performed correlation analysis to obtain DE-lncRNA associated protein-coding genes. As shown in **Figure 3G**, Pearson's correlations ranging from 0.3 to 0.5, 0.5 to 0.7 or >0.7 are classified as weak, moderate, and strong, respectively. P-value is less than 0.05.

Taken together, these results confirm that lncRNA and mRNA in leukocytes are important in type 2 diabetes and

TABLE 2 | The top 20 lncRNA with significantly differential expression in white blood cell from type 2 diabetes (T2D) and health control (C).

Gene	C normalize	T2D normalize	Log2 Fold Change	FDR	Up/Down	Biotype
ENSG00000267257	19.44	0.55	-5.13	8.5E-07	down	antisense
ENSG00000276107	39.88	3.37	-3.56	1.79E-06	down	sense_intronic
MSTRG.103146	598.79	214.23	-1.48	1.74E-05	down	antisense
MSTRG.19495	0.65	12.42	4.26	5.77E-05	up	linc
ENSG00000273338	104.62	15.05	-2.8	6.36E-05	down	antisense
MSTRG.180057	0.83	13.65	4.04	7.37E-05	up	linc
MSTRG.22781	3.1	26.47	3.1	8.32E-05	up	antisense
MSTRG.161229	27.29	128.52	2.24	8.34E-05	up	antisense
MSTRG.180437	201.79	585.68	1.54	9.34E-05	up	linc
MSTRG.180334	0.6	11.82	4.31	9.76E-05	up	linc
MSTRG.182419	88.48	13.76	-2.69	9.78E-05	down	linc
MSTRG.106807	2940.94	1210	-1.28	0.000101	down	antisense
MSTRG.195300	54.62	0.59	-6.53	0.000105	down	linc
MSTRG.62902	0.64	11.46	4.17	0.000105	up	antisense
MSTRG.125714	8.73	47.42	2.44	0.000106	up	antisense
MSTRG.10587	4.64	28.06	2.59	0.000123	up	antisense
MSTRG.80841	1.05	12.84	3.61	0.000139	up	linc
MSTRG.181523	1.29	18	3.8	0.000185	up	antisense
ENSG00000260244	281.53	76.87	-1.87	0.000222	down	sense_overlapping
MSTRG.183281	335.1	117.4	-1.51	0.000315	down	antisense

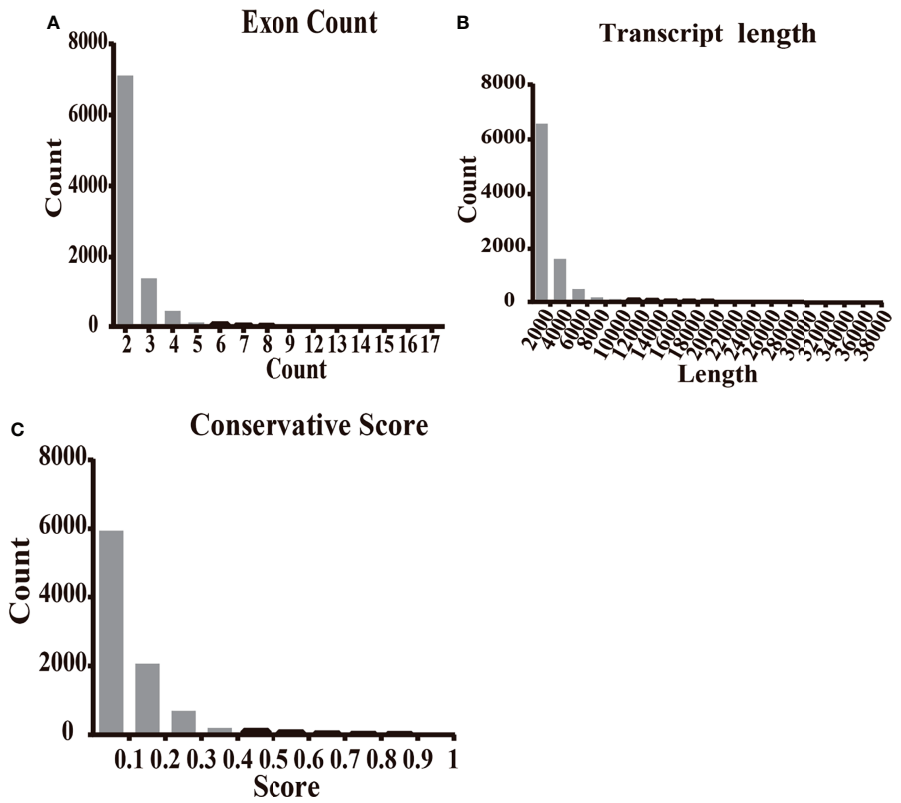

FIGURE 2 | The features of novel lncRNAs in T2D patients compared with healthy controls. **(A)** The transcripts of novel lncRNAs were mainly distributed in 2, 3, and 4 exons. **(B)** The largest amount of novel lncRNA transcripts distributed as the length less than 2,500 nt. **(C)** The transcripts of novel lncRNAs distributed at the conservation score range. The ratio of transcript with conservation scores less than 0.1 was 61.3%.

these association between lncRNAs and their related genes should be further investigated.

GO and KEGG Pathway Analyses

We further applied the Gene Ontology (GO) enrichment analysis to classify the DE-lncRNAs associated-mRNAs of T2D into three main categories, namely, biological process, molecular function, and cellular component (**Figures 4A, B**). In the biological process group, the DEGs were mainly enriched in metabolic process, response to stimulus, cell communication, nitrogen compound metabolic process and immune system process are among the top 15 items (**Figure 4A**). Under the molecular function category, ion binding, catalytic activity, nucleic acid binding, and organic cyclic compound binding showed the highest percentages (**Figure 4A**). Next, we compared 6 T2D patients with family histories and 5 samples without family histories to 5 healthy controls, respectively. Their overlapped genes were undertaken GO analysis. It was very similar to the previous one (**Figure S3**). These data indicate that genetic factors (e.g., family history) may not have important impacts on lncRNA functions in T2D. We further performed KEGG pathway analysis. As shown in **Figure 4B**, the DEgene-enriched pathway included the metabolic pathways, Rap1 signaling pathway, Toll-like receptor signaling pathway, MAPK pathway and PI3K-Akt signaling pathway. Among them, 9 DEGs were enriched in MAPK pathway, which participate in the development of pathological traits resulting from excessive caloric intake and obesity that cause metabolic syndrome and type 2 diabetes (**Figure 4C**).

TABLE 3 | The top 10 lncRNAs and mRNAs with numbers of related genes in co-expression network.

Gene	Biotype	Target gene counts
MSTRG.172533	lncRNA	57
MSTRG.118864	lncRNA	52
ENSG00000276649	lncRNA	39
ENSG00000246263	lncRNA	39
RAC1	mRNA	37
ENSG00000279463	lncRNA	35
POLR2K	mRNA	32
APP	mRNA	32
MAPK3	mRNA	32
RHOA	mRNA	30

Measurement of Chosen lncRNAs in Validation Groups

To further confirm the DE-lncRNAs, we independently measured 21 lncRNAs in the validation groups of T2D patients (n = 56) and healthy controls (n = 36) by qPCR. The expression

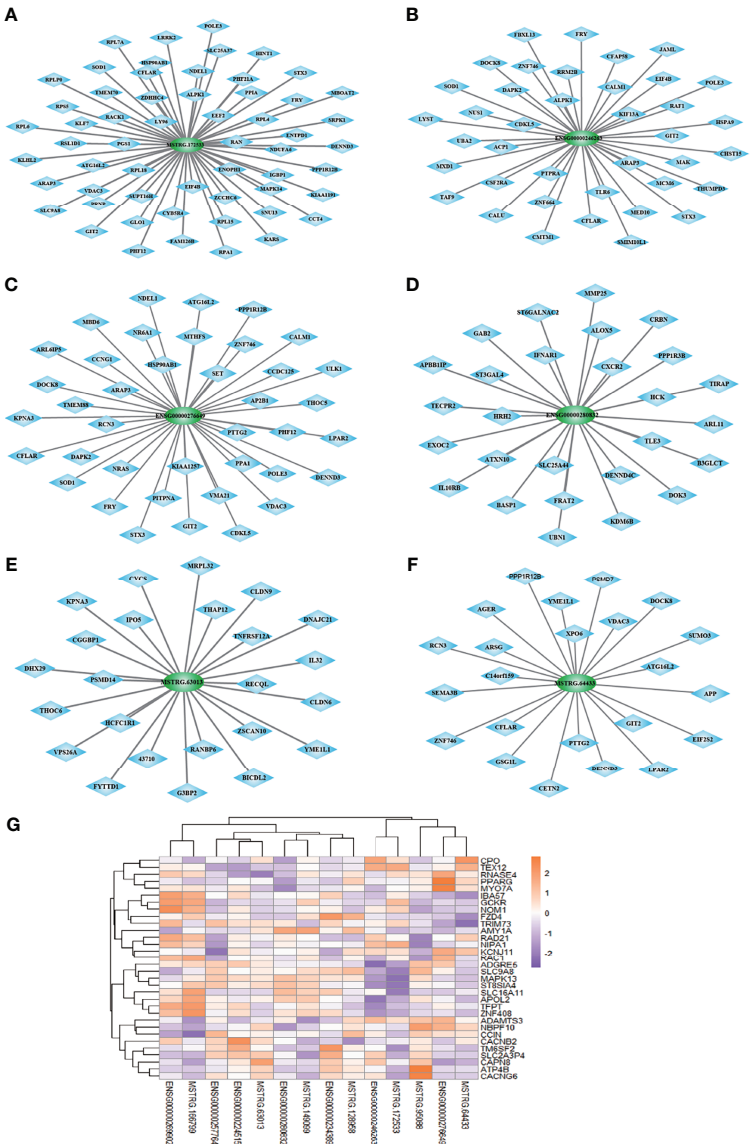

FIGURE 3 | **(A–F)** The co-expression network of 6 lncRNAs validated in expanded cohort which selected from top 10 lncRNA with most related mRNA. **(G)** Correlation analysis was performed to obtain DE-lncRNA associated protein-coding genes. Pearson's correlations ranging from 0.3 to 0.5, 0.5 to 0.7 or >0.7 are classified as weak, moderate and strong, respectively. P-value is less than 0.05.

levels of these lncRNAs in the validation cohort are shown in **Figure 5**. Fourteen of 21 (66.67%) lncRNAs displayed obviously different expression levels between T2D and healthy control groups; 4 lncRNAs were downregulated and the others were upregulated in T2D. Ten novel lncRNAs and 4 known lncRNAs were confirmed as positive in the expanded cohort. Among them, 8 lncRNAs belonged to the lincRNA, whereas 5 lncRNAs belonged to the antisense (**Table 4**). We then compared the validation results and sequencing data, which showed that most lncRNAs (85.71%, 18/21) in the expanded group displayed similar trends as the sequencing data (**Figure 6**). Particularly, 9 lncRNAs exhibited the same significantly positive results as observed in the sequencing data. Furthermore, we compared the validation positive ratio by categorizing these lncRNAs with their features (**Table 4**). The results demonstrated that 4 of 8 lncRNAs (50%) without significant differences in the sequenced data were significantly different in the validation test. The validation-positive ratios of the known- and novel-lncRNAs were 57.14 and 71.43%, respectively, in the validation cohorts (**Table 4**). Six known and 7 novel lncRNAs with significant differences in the sequencing data demonstrated positive ratios of 50 and 85.71%, respectively (**Table 4**). Only 1 of 2 lncRNAs with no expression in either the control or T2D group in the sequencing data displayed significant differences in the

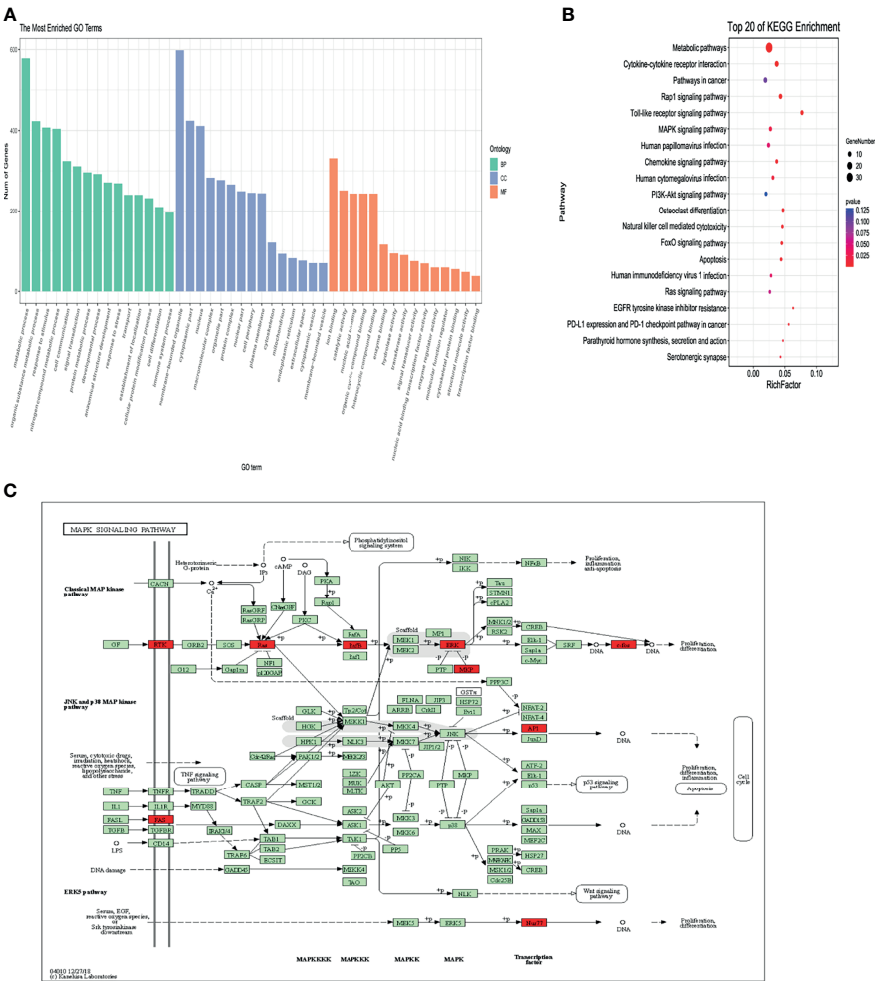

FIGURE 4 | Bioinformation analysis by enrichment analysis of pathways and GO terms for T2D-lncRNA and T2D-mRNA using optimized data. **(A)** Gene ontology analysis of lncRNA-associated mRNAs of T2D in biological processes, molecular functions, and cellular components. **(B)** KEGG pathway analysis of lncRNA-associated mRNAs of T2D. **(C)** Differentially expressed DEGs enriched in MAPK signaling pathway.

expanded cohort (**Table 4**). When validation-positive lncRNAs were analyzed by biotype, the results showed that the positive ratios in lincRNA and antisense lncRNA were 61.54% (8/13) vs. 71.43% (5/7). The positive ratios in the lncRNAs with and without predicted mRNAs were 88.89% (8/9) and 50% (6/12), respectively (**Table 4**).

We also sought to identify potential orthologs of 21 lncRNAs by comparing their sequences with previously identified murine lncRNAs. Based on pairwise genomic alignments, we found that 11 lncRNA sequences (52.38%) harbored orthologs in mouse genomic sequences without annotation, whereas the other 10 lncRNAs were had no orthologs in mice (**Table 5**). Of the 14 validation-positive lncRNA, 5 (35.71%) exhibited orthologous sequences in the mouse genome (**Table 5**). Thus, the validated lncRNAs exhibited evolutionary conservation in humans and should be further investigated to determine their relationship with the human T2D epigenetic mechanism or as biomarkers.

DE-lncRNA Between Type 1 and 2 Diabetes

To further screen for lncRNAs differentially expressed in T1D and T2D with potential as diagnostic markers for distinguishing T1D and T2D, the transcriptome sequencing cohort comprised of 11 patients diagnosed with T2D and 6 patients diagnosed with T1D (Accession number: GSE130279) was analyzed. Only 10 lncRNAs showed significant difference between the two groups, with 7 upregulated and 3 downregulated lncRNAs (**Table S5**); 15 mRNAs with 6 upregulated and 9 downregulated mRNAs (**Table S6**). We independently measured 9 lncRNAs (4 showed significant differences in sequencing data, **Table S7**) by qPCR in validating T1D (n = 11), and T2D (n = 56). We found 4 lncRNAs (MSTRG.128697, MSTRG.74858, MSTRG.63013, and ENSG00000269902) showed significantly differential expression between T1D and T2D. Their expression levels in the discovery cohort and validation cohort are shown in **Figure 7**. Thus, this panel of 4 lncRNAs may be valuable as diagnostically distinguishable markers in T1D and T2D.

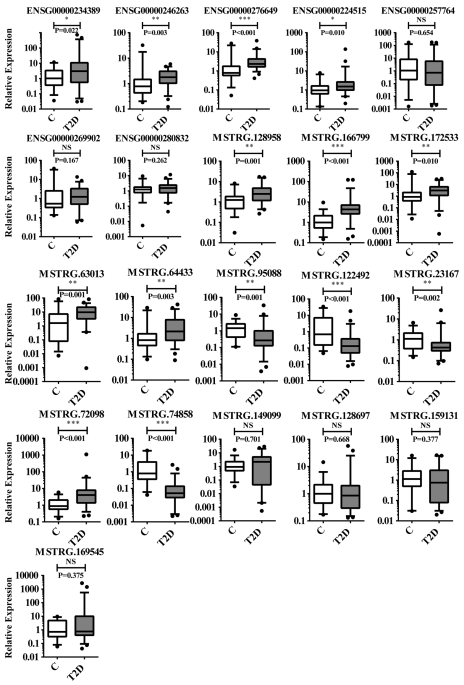

FIGURE 5 | Results of 21 lncRNAs further confirmed in the validation cohorts by qPCR. There are 14 lncRNAs that showed significant difference in expression levels between T2D patients (n = 56) and healthy controls (n = 36). NS, no significant difference; "*" indicated significant difference with $p < 0.05$, "**" indicated $p < 0.01$ and "***" indicated $p < 0.001$.

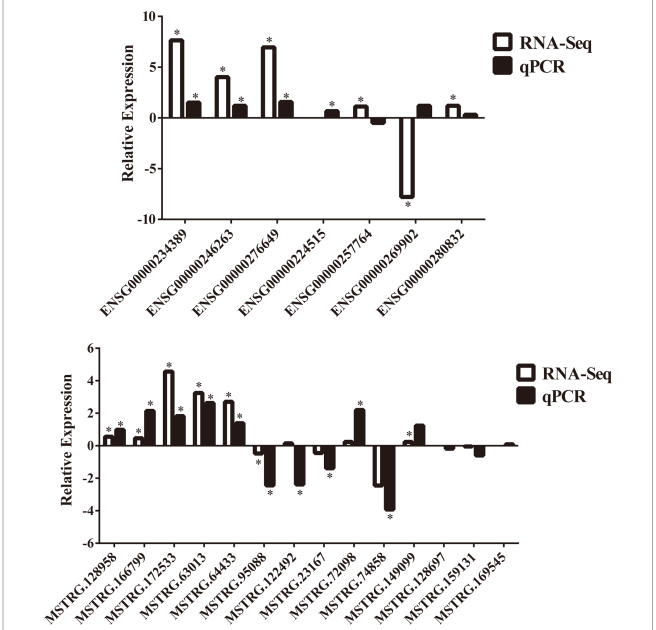

FIGURE 6 | Comparisons of trends between RNA sequencing data and further confirmation of 21 lncRNAs in the validation cohorts by qPCR. "*" indicated significant difference in RNA sequencing data or validation cohorts by qPCR.

DISCUSSION

LncRNAs participate in the epigenetic regulation of various diseases by altering the expression of lncRNA target genes and displaying clear clinical significance (20). An increasing number of studies have demonstrated that causal variants of diabetes-related lncRNA are significantly enriched in the islet regions and transcription factor-binding sites (21). However, studies aimed at identifying lncRNAs involved in T2D in circulating leukocytes are very limited. A very recent report showed that circulating lncRNAs were aberrantly expressed in T2D by microarray analysis, indicating their potential roles in chronic inflammation and insulin resistance (14). We predicted that in addition to islet beta cells, lncRNAs may play a regulatory role in peripheral blood cells such as leukocytes and alter cellular phenotypes and disease risk. In the present study, we determined the full profile of circulating lncRNA and mRNA in T2D patients to describe their characteristics and differential expression compared to healthy controls. In total, 14,503 lncRNAs were identified in T2D leukocytes and 5,797 lncRNAs were defined as novel lncRNAs. Adjusted data showed that 845 lncRNAs were significantly different between T2D patients and healthy controls. We report more data than in previous studies in which the peripheral blood of patients with diabetes was screened for associated lncRNAs by microarrays (14), but fewer than those reported by transcriptomic sequencing or microarrays in beta cells (6). Here, we constructed DE-lncRNA and DE-mRNA networks to explore the biological functions of lncRNAs during the development of diabetes mellitus. There were 1,076 genes involved in our CNC results, among which 21 lncRNAs and 117 mRNAs harbored more than 10 related genes. Further analysis indicated that the top lncRNA (MSTRG.172533) harbored 57 genes in its network. Genes in this network such as RACK1 (16), SLC9A8 (17), PPIA (22), and others have been explored in diabetes. These results strongly support that circulating leukocytes from T2D harbor enriched lncRNAs and may represent important targets for further diabetes research. Newly obtained data of lncRNAs and mRNAs in our study may extend the knowledge of molecular alterations in the T2D transcriptome.

Murine disease models are often chosen as the first alternative to avoid highly heterogeneous human genetic backgrounds and low RNA integrity from cadaveric islets in exploring the role of lncRNAs (21). However, considering that the evolutional conservation of lncRNA is much lower than that of mRNA between mice and humans, it is important to evaluate whether mouse models are useful in this case. In fact, notable species differences in lncRNA expression have been reported in comparisons of the transcriptional landscape of mouse and human beta cells (23). It was reported that most adipose-enriched lincRNAs (~85%) were not conserved in mice, and as few as 15% of human lincRNA loci contain syntenic non-coding transcripts expressed in mouse (24). It has putatively been confirmed that there are mouse orthologues for 70% of human lncRNAs but only 47% have been confirmed by RNA-seq (6). Approximately 85% of human macrophage lincRNAs are not

TABLE 4 | The results of analysis by the categorical features of 21 lncRNAs which were chosen in validation cohorts. "*" marked the validation positive lncRNA.

Categorical features	LncRNA	Ratio of lncRNA with significant difference
No significant difference in sequencing cohorts	MSTRG.169545, MSTRG.23167*, MSTRG.72098*, MSTRG.74858*, ENSG00000224515*, MSTRG.128697, MSTRG.122492*, MSTRG.159131	4/8 (50.0%)
No expression in either group of sequencing cohorts	ENSG00000224515*, MSTRG.128697	1/2 (50.0%)
Known lncRNA with significant difference in sequencing cohorts	ENSG00000234389*, ENSG00000246263*, ENSG00000257764, ENSG00000269902, ENSG00000276649*, ENSG00000280832	3/6 (50.0%)
Novel lncRNA with significant difference in sequencing cohorts	MSTRG.128958*, MSTRG.149099, MSTRG.166799*, MSTRG.172533*, MSTRG.63013*, MSTRG.64433*, MSTRG.95088*	6/7 (85.71%)
Known lncRNA	ENSG00000234389*, ENSG00000246263*, ENSG00000257764, ENSG00000269902, ENSG00000276649*, ENSG00000280832, ENSG00000224515*	4/7 (57.14%)
Novel lncRNA	MSTRG.128958*, MSTRG.149099, MSTRG.166799*, MSTRG.172533*, MSTRG.63013*, MSTRG.64433*, MSTRG.95088*, MSTRG.169545, MSTRG.23167*, MSTRG.72098*, MSTRG.74858*, MSTRG.128697, MSTRG.122492*, MSTRG.159131	10/14 (71.43%)
LincRNA	ENSG00000269902, MSTRG.149099, MSTRG.169545, MSTRG.172533*, MSTRG.23167*, MSTRG.63013*, MSTRG.64433*, MSTRG.72098*, MSTRG.74858*, MSTRG.95088*, MSTRG.128697, MSTRG.122492*, MSTRG.159131	8/13 (61.54%)
Antisense lncRNA	ENSG00000246263*, ENSG00000257764, ENSG00000276649*, ENSG00000280832, ENSG00000224515*, MSTRG.128958*, MSTRG.166799*	5/7(71.43%)
LncRNA with predicted mRNA	ENSG00000234389*, ENSG00000246263*, ENSG00000276649*, ENSG00000280832, MSTRG.149099, MSTRG.166799*, MSTRG.172533*, MSTRG.63013*, MSTRG.64433*	7/9 (77.78%)
LncRNA without predicted mRNA	ENSG00000257764, ENSG00000269902, ENSG00000224515*, MSTRG.128958*, MSTRG.95088*, MSTRG.169545, MSTRG.23167*, MSTRG.72098*, MSTRG.74858*, MSTRG.128697, MSTRG.122492*, MSTRG.159131	7/12 (58.33%)

expressed in mice, and only 24% show significant sequence conservation between humans and mice (11). These studies indicate that although mouse diabetic models and their lncRNAs are convenient for research, there are some clear barriers and limitations to the conclusions that can be drawn from these data because of the lack of sequence conservation. In the current study, we analyzed the evolutionary conservation of novel lncRNAs and 14 positively validation lncRNAs. Among the novel lncRNAs, 61.3% had a conservation score of less than 0.1, indicating that they exhibited high evolutionary conservation in humans. Of the set of validated 14 lncRNAs, only 35.71% (5 lncRNAs) had orthologs in mice with no further annotation. Thus, these validated 14 lncRNAs can be used directly in clinical research without considering the conservation problem. Therefore, the large amounts of lncRNAs and mRNAs obtained from convenient circulating leukocytes of T2D

TABLE 5 | The information of 14 lncRNAs positively validated in the expanding cohort in present study and their potential orthologous sequences comparing with mouse data.

LncRNAs	Novel/known	The log2 value in the RNA-seq data	Significant difference in validation cohort	Orthologous sequence with mouse
ENSG00000224515	known	–	yes	Not found
ENSG00000234389	known	1.79	yes	Not found
ENSG00000246263	known	1.03	yes	Not found
ENSG00000257764	known	3.55	no	Not found
ENSG00000269902	known	-1.6	no	Not found
ENSG00000276649	known	1.77	yes	Not found
ENSG00000280832	known	1.63	no	Not found
MSTRG.122492	novel	0.6	yes	chr3:58,478,307-58,478,532
MSTRG.128697	novel	–	no	Not found
MSTRG.128958	novel	5.21	yes	chr5:66,016,825-66,017,169
MSTRG.149099	novel	5.32	no	Not found
MSTRG.159131	novel	-0.65	no	Not found
MSTRG.166799	novel	3.88	yes	chr6:39,016,934-39,045,231
MSTRG.169545	novel	1.44	no	chr14:70,790,722-70,791,594
MSTRG.172533	novel	1.99	yes	Not found
MSTRG.23167	novel	-1.12	yes	chr19:35,211,979-35,262,091
MSTRG.63013	novel	2.66	yes	chr17:23,644,824-23,660,240
MSTRG.64433	novel	2.11	yes	chr7:126,093,191-126,095,342
MSTRG.72098	novel	2.06	yes	chr11:95,397,976-95,398,838
MSTRG.74858	novel	-1.51	yes	chr11:121,806,938-121,808,036
MSTRG.95088	novel	-2.66	yes	chr2:45,237,395-45,239,069

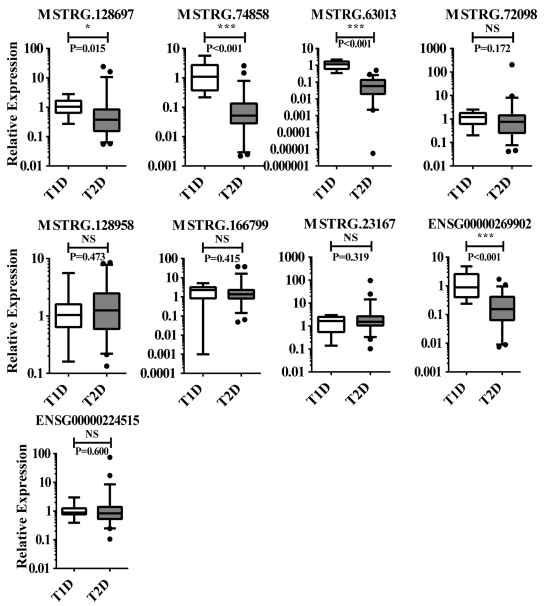

FIGURE 7 | The 9 lncRNAs tested in T1D (n = 11), and T2D (n = 56) using qPCR, of which 4 lncRNAs with significant difference and 6 with non-significant difference. NS, no significant difference; "*" indicated significant difference with $p < 0.05$ and "***" indicated $p < 0.001$.

patients in the present study contribute valuable information based on an urgent need for human data.

To confirm and understand lncRNAs in T2D more detail, we validated 21 lncRNAs, 14 lncRNAs (14/21, 66.67%) displayed expression levels that were significantly different between T2D patients and healthy controls. Compared to the identification of lncRNAs in osteoarthritis chondrocytes (11/16, 68.75%) (25), in human coronary artery smooth muscle and endothelial cells (21/31, 67.74%) (26), and in blood samples from patients with diabetic neuropathy (2/6, 33.33%) (27), the detection rate we describe here is comparable. We found that the positive validation ratio of lncRNAs with predicted mRNAs (77.78%) in CNC was higher than those without predicted mRNAs (58.33%). The novel lncRNAs showed a higher positive validation ratio than known lncRNAs. These results indicate that candidate lncRNAs for validation can be chosen from a wider range, particularly from lncRNAs in the CNC.

LncRNAs can be classified into two large groups: lincRNAs with no direct relationship with protein-coding genes or those partially overlapping the protein coding sequences as sense- or antisense transcripts (28). When choosing candidate lncRNAs, the analysis of antisense-lncRNAs in peripheral blood mononuclear cells and the spinal cord have been prioritized (29). LincRNAs were first characterized to play important roles in macrophage activation in cardiometabolic diseases in human genetic studies (11). We found that lincRNAs exhibited lower validation positive ratios (61.54%) than antisense lncRNAs (71.43%). Nevertheless, both were comparable. Thus, our work is a reminder that it would be a better choice to investigate T2D in terms of both lincRNA and antisense-lncRNAs, as T2D has been considerably understudied compared to lncRNAs in general. In the 14 positively validated lncRNAs, 7 lncRNAs had predicted mRNA targets related to 144 genes (**Table S8**); of these, many genes have been confirmed as related to diabetes. For instance, in the network of lncRNA MSTRG.63013, 24 related genes, including G3BP2 (30), and others may affect diabetes development. The rest 7 lncRNAs lacked predicted mRNA targets, which may be because of our currently limited understanding of the human genome (or those of other animals). As a pioneering study, our results can be used to investigate the regulatory function of these lncRNAs in T2D in the future.

LncRNAs have been reported as disease biomarkers in diagnosis, prognosis, or therapeutic targeting because of their sensitivity and convenience (31). As the most common diabetes subtypes, type 1 and 2 diabetes are difficult to diagnose in many cases. Current methods include evaluation of clinical symptoms, C-peptide, and antibodies or other auto-immunobiomarkers related T1D. However, these indicators are not sufficiently specific and sensitive to meet the diagnosis requirement. Therefore, exploring new molecular biomarkers for accurately diagnosing type 1 and 2 diabetes is urgent. In fact, it was reported that lncRNAs are modulated during the development of T1D (32). Thus, we identified lncRNAs showing differential expression between type 1 and 2 diabetes which may be useful as distinguishing markers. We screened 4 lncRNAs that were significantly different expressed in circulating leukocytes from patients with type 1 and 2 diabetes. This panel may be used to develop a convenient and efficient molecular method for distinguishing type 1 and 2 diabetes in clinical practice.

There were several limitations to this study. First, the expanded cohort number was limited, particularly the number of T1D patients. This is because we grouped the samples very critically and collected samples without any treatment over a short term. Second, leukocytes may not completely represent the circulating conditions. Therefore, we plan to screen lncRNAs in circulating exosomes, which are extracellular vesicles that may play more important roles in regulating diabetes; these results will be compared to the lncRNAs identified in leukocytes in the current study. Finally, we did not investigate the relationship of lncRNAs and their regulatory or predicted mRNAs, although some lncRNAs and mRNAs were in the CNC. These regulatory relationships should be further analyzed.

In conclusion, the present RNA sequencing work identified thousands of lncRNAs and mapped their expression profiles in T2D. The many novel non-coding RNAs identified may function as key modulators of T2D. Importantly, the leukocyte specificity found for the 14 lncRNAs identified (together with other data presented) may be useful for future functional studies, and a set of 4 DE-lncRNAs may aid in accurately diagnosing type 1 and 2 diabetes.

DATA AVAILABILITY STATEMENT

The datasets presented in this study can be found in online repositories. The names of the repository/repositories and accession number(s) can be found below: NCBI Gene Expression Omnibus (https://www.ncbi.nlm.nih.gov/geo): GEO accession, GSE134594.

ETHICS STATEMENT

The studies involving human participants were reviewed and approved by the Ethics Committee of the Chinese PLA General Hospital (Permitted No. S2016-147-03). The patients/participants provided their written informed consent to participate in this study.

AUTHOR CONTRIBUTIONS

All authors listed have made a substantial, direct, and intellectual contribution to the work and approved it for publication.

FUNDING

This study was supported by the National Natural Science Foundation of China (Nos. 31970512, 32070531 and 31872308).

SUPPLEMENTARY MATERIAL

The Supplementary Material for this article can be found online at: https://www.frontiersin.org/articles/10.3389/fendo.2021.690555/full#supplementary-material

Supplementary Figure 1 | (A) Differentially expressed lncRNAs (T2D-lncRNAs) and type 2 diabetes mRNA were identified from a Volcano plot showing data from type 2 diabetes patient relative to healthy controls. The vertical black lines correspond to 2-fold up and downregulations, respectively; and the horizontal black line represents a *p*-value of 0.05. The red and green points in the plots represent the differentially expressed genes with statistical significance for upregulation and downregulation of lncRNA and mRNA, respectively. **(B)** Differential mRNA expression profiles were hierarchical cluster analyzed and shown as a heatmap. **(C)** Principal component analysis showed similar results as presented in heatmap.

Supplementary Figure 2 | The conservation of novel lncRNAs on chromosomes.

Supplementary Figure 3 | (A) Co-expression networks of lncRNA-mRNA involved 1076 genes, consisted by 618 lncRNAs and 458 mRNAs. Venn plot for the differentially expressed lncRNAs **(B)** and mRNAs **(C)** between T2DM with- and without- family history samples. **(D)** Go analysis for the overlapped genes of T2DM with- and without family history samples.

REFERENCES

1. Cho NH, Shaw JE, Karuranga S, Huang Y, da Rocha Fernandes JD, Ohlrogge AW, et al. IDF Diabetes Atlas: Global Estimates of Diabetes Prevalence for 2017 and Projections for 2045. *Diabetes Res Clin Pract* (2018) 138:271–81. doi: 10.1016/j.diabres.2018.02.023
2. Feng SD, Yang JH, Yao CH, Yang SS, Zhu ZM, Wu D, et al. Potential Regulatory Mechanisms of Lncrna in Diabetes and its Complications. *Biochem Cell Biol* (2017) 95:361–7. doi: 10.1139/bcb-2016-0110
3. Peng WX, Koirala P, Mo YY. Lncrna-Mediated Regulation of Cell Signaling in Cancer. *Oncogene* (2017) 36:5661–7. doi: 10.1038/onc.2017.184
4. Wu T, Du Y. LncRNAs: From Basic Research to Medical Application. *Int J Biol Sci* (2017) 13:295–307. doi: 10.7150/ijbs.16968
5. Gong W, Zhu G, Li J, Yang X. Lncrna MALAT1 Promotes the Apoptosis and Oxidative Stress of Human Lens Epithelial Cells *via* P38mapk Pathway in Diabetic Cataract. *Diabetes Res Clin Pract* (2018) 144:314–21. doi: 10.1016/j.diabres.2018.06.020
6. Moran I, Akerman I, van de Bunt M, Xie R, Benazra M, Nammo T, et al. Human Beta Cell Transcriptome Analysis Uncovers LncRNAs That are Tissue-Specific, Dynamically Regulated, and Abnormally Expressed in Type 2 Diabetes. *Cell Metab* (2012) 16:435–48. doi: 10.1016/j.cmet.2012.08.010
7. Michalik KM, You X, Manavski Y, Doddaballapur A, Zornig M, Braun T, et al. Long Noncoding RNA MALAT1 Regulates Endothelial Cell Function and Vessel Growth. *Circ Res* (2014) 114:1389–97. doi: 10.1161/CIRCRESAHA.114.303265
8. Alvarez ML, Khosroheidari M, Eddy E, Kiefer J. Role of Microrna 1207-5P and its Host Gene, the Long Non-Coding RNA Pvt1, as Mediators of Extracellular Matrix Accumulation in the Kidney: Implications for Diabetic Nephropathy. *PloS One* (2013) 8:e77468. doi: 10.1371/journal.pone.0077468
9. Liu S, Sheng L, Miao H, Saunders TL, MacDougald OA, Koenig RJ, et al. SRA Gene Knockout Protects Against Diet-Induced Obesity and Improves Glucose Tolerance. *J Biol Chem* (2014) 289:13000–9. doi: 10.1074/jbc.M114.564658
10. Yau JW, Rogers SL, Kawasaki R, Lamoureux EL, Kowalski JW, Bek T, et al. Global Prevalence and Major Risk Factors of Diabetic Retinopathy. *Diabetes Care* (2012) 35:556–64. doi: 10.2337/dc11-1909
11. Zhang H, Xue C, Wang Y, Shi J, Zhang X, Li W, et al. Deep RNA Sequencing Uncovers a Repertoire of Human Macrophage Long Intergenic Noncoding RNAs Modulated by Macrophage Activation and Associated With Cardiometabolic Diseases. *J Am Heart Assoc* (2017) 6(11):e007431. doi: 10.1161/JAHA.117.007431
12. Bhupathiraju SN, Hu FB. Epidemiology of Obesity and Diabetes and Their Cardiovascular Complications. *Circ Res* (2016) 118:1723–35. doi: 10.1161/CIRCRESAHA.115.306825
13. Donath MY. Targeting Inflammation in the Treatment of Type 2 Diabetes: Time to Start. *Nat Rev Drug Discovery* (2014) 13:465–76. doi: 10.1038/nrd4275
14. Wang X, Chang X, Zhang P, Fan L, Zhou T, Sun K. Aberrant Expression of Long Non-Coding RNAs in Newly Diagnosed Type 2 Diabetes Indicates Potential Roles in Chronic Inflammation and Insulin Resistance. *Cell Physiol Biochem: Int J Exp Cell Physiol Biochem Pharmacol* (2017) 43:2367–78. doi: 10.1159/000484388
15. Reddy MA, Amaram V, Das S, Tanwar VS, Ganguly R, Wang M, et al. Lncrna DRAIR is Downregulated in Diabetic Monocytes and Modulates the Inflammatory Phenotype *via* Epigenetic Mechanisms. *JCI Insight* (2021) 6(11):e143289. doi: 10.1172/jci.insight.143289
16. Qiu Y, Mao T, Zhang Y, Shao M, You J, Ding Q, et al. A Crucial Role for RACK1 in the Regulation of Glucose-Stimulated IRE1alpha Activation in Pancreatic Beta Cells. *Sci Signal* (2010) 3:ra7. doi: 10.1126/scisignal.2000514
17. Lokman FE, Seman NA, Ismail AA, Yaacob NA, Mustafa N, Khir AS, et al. Gene Expression Profiling in Ethnic Malays With Type 2 Diabetes Mellitus, With and Without Diabetic Nephropathy. *J Nephrol* (2011) 24:778–89. doi: 10.5301/JN.2011.6382
18. Damacharla D, Thamilselvan V, Zhang X, Mestareehi A, Yi Z, Kowluru A. Quantitative Proteomics Reveals Novel Interaction Partners of Rac1 in Pancreatic Beta-Cells: Evidence for Increased Interaction With Rac1 Under Hyperglycemic Conditions. *Mol Cell Endocrinol* (2019) 494:110489. doi: 10.1016/j.mce.2019.110489
19. Sahajpal N, Kowluru A, Kowluru RA. The Regulatory Role of Rac1, a Small Molecular Weight Gtpase, in the Development of Diabetic Retinopathy. *J Clin Med* (2019) 8:pii: E965. doi: 10.3390/jcm8070965
20. Cao M, Zhao J, Hu G. Genome-Wide Methods for Investigating Long Noncoding RNAs. *BioMed Pharmacother* (2019) 111:395–401. doi: 10.1016/j.biopha.2018.12.078
21. Singer RA, Sussel L. Islet Long Noncoding RNAs: A Playbook for Discovery and Characterization. *Diabetes* (2018) 67:1461–70. doi: 10.2337/dbi18-0001
22. Zhang L, Li Z, Zhang B, He H, Bai Y. PPIA is a Novel Adipogenic Factor Implicated in Obesity. *Obes (Silver Spring)* (2015) 23:2093–100. doi: 10.1002/oby.21208
23. Benner C, Meulen TVD, Cacéres E, Tigyi K, Donaldson CJ, Huising MO. The Transcriptional Landscape of Mouse Beta Cells Compared to Human Beta Cells Reveals Notable Species Differences in Long Non-Coding RNA and Protein-Coding Gene Expression. *BMC Genomics* (2014) 15:620. doi: 10.1186/1471-2164-15-620

24. Zhang X, Xue C, Lin J, Ferguson JF, Weiner A, Liu W, et al. Interrogation of Nonconserved Human Adipose LincRNAs Identifies a Regulatory Role of Linc-ADAL in Adipocyte Metabolism. *Sci Transl Med* (2018) 10:eaar5987. doi: 10.1126/scitranslmed.aar5987
25. Pearson MJ, Philp AM, Heward JA, Roux BT, Walsh DA, Davis ET, et al. Long Intergenic Noncoding RNAs Mediate the Human Chondrocyte Inflammatory Response and Are Differentially Expressed in Osteoarthritis Cartilage. *Arthritis Rheumatol* (2016) 68:845–56. doi: 10.1002/art.39520
26. Bell RD, Long X, Lin M, Bergmann JH, Nanda V, Cowan SL, et al. Identification and Initial Functional Characterization of a Human Vascular Cell-Enriched Long Noncoding RNA. *Arterioscler Thromb Vasc Biol* (2014) 34:1249–59. doi: 10.1161/ATVBAHA.114.303240
27. Luo L, Ji LD, Cai JJ, Feng M, Zhou M, Hu SP, et al. Microarray Analysis of Long Noncoding RNAs in Female Diabetic Peripheral Neuropathy Patients. *Cell Physiol Biochem* (2018) 46:1209–17. doi: 10.1159/000489071
28. Motterle A, Sanchez-Parra C, Regazzi R. Role of Long Non-Coding RNAs in the Determination of β-Cell Identity. *Diabetes Obes Metab* (2016) 18:41–50. doi: 10.1111/dom.12714
29. Gagliardi S, Zucca S, Pandini C, Diamanti L, Bordoni M, Sproviero D, et al. Long Non-Coding and Coding RNAs Characterization in Peripheral Blood Mononuclear Cells and Spinal Cord From Amyotrophic Lateral Sclerosis Patients. *Sci Rep* (2018) 8:2378. doi: 10.1038/s41598-018-20679-5
30. Zhao B, Li H, Liu J, Han P, Zhang C, Bai H, et al. MicroRNA-23b Targets Ras Gtpase-Activating Protein SH3 Domain-Binding Protein 2 to Alleviate Fibrosis and Albuminuria in Diabetic Nephropathy. *J Am Soc Nephrol* (2016) 27:2597–608. doi: 10.1681/ASN.2015030300
31. Kumarswamy R, Bauters C, Volkmann I, Maury F, Fetisch J, Holzmann A, et al. Circulating Long Noncoding RNA, LIPCAR, Predicts Survival in Patients With Heart Failure. *Circ Res* (2014) 114:1569–75. doi: 10.1161/CIRCRESAHA.114.303915
32. Anna M, Sonia G, Dorothée C, Paolo M, Romano R. Involvement of Long Non-Coding RNAs in Beta Cell Failure at the Onset of Type 1 Diabetes in NOD Mice. *Diabetologia* (2015) 58:1827–35. doi: 10.1007/s00125-015-3641-5

Conflict of Interest: The authors declare that the research was conducted in the absence of any commercial or financial relationships that could be construed as a potential conflict of interest.

Publisher's Note: All claims expressed in this article are solely those of the authors and do not necessarily represent those of their affiliated organizations, or those of the publisher, the editors and the reviewers. Any product that may be evaluated in this article, or claim that may be made by its manufacturer, is not guaranteed or endorsed by the publisher.

frontiers in Endocrinology

ORIGINAL RESEARCH
published: 24 January 2022
doi: 10.3389/fendo.2021.800123

Identification of Key LncRNAs and Pathways in Prediabetes and Type 2 Diabetes Mellitus for Hypertriglyceridemia Patients Based on Weighted Gene Co-Expression Network Analysis

Shoumeng Yan[1†], Mengzi Sun[1†], Lichao Gao[2], Nan Yao[1], Tianyu Feng[1], Yixue Yang[1], Xiaotong Li[1], Wenyu Hu[1], Weiwei Cui[3] and Bo Li[1*]*

[1] Department of Epidemiology and Biostatistics, School of Public Health, Jilin University, Changchun, China, [2] Department of Endocrinology, The First Hospital of Jilin University, Changchun, China, [3] Department of Nutrition and Food Hygiene, School of Public Health, Jilin University, Changchun, China

OPEN ACCESS

Edited by:
Katsumi Iizuka,
Fujita Health University, Japan

Reviewed by:
Baocheng Chang,
Tianjin Medical University, China
Agnese Filippello,
University of Catania, Italy

***Correspondence:**
Weiwei Cui
cuiweiwei@jlu.edu.cn
Bo Li
li_bo@jlu.edu.cn

[†]These authors have contributed equally to this work

Specialty section:
This article was submitted to Diabetes: Molecular Mechanisms, a section of the journal Frontiers in Endocrinology

Received: 22 October 2021
Accepted: 13 December 2021
Published: 24 January 2022

Citation:
Yan S, Sun M, Gao L, Yao N, Feng T, Yang Y, Li X, Hu W, Cui W and Li B (2022) Identification of Key LncRNAs and Pathways in Prediabetes and Type 2 Diabetes Mellitus for Hypertriglyceridemia Patients Based on Weighted Gene Co-Expression Network Analysis. Front. Endocrinol. 12:800123. doi: 10.3389/fendo.2021.800123

Aims: Prevalence of prediabetes and type 2 diabetes mellitus(T2DM) are increasing worldwide. Key lncRNAs were detected to provide a reference for searching potential biomarkers of prediabetes and T2DM in hypertriglyceridemia patients.

Methods: The study included 18 hypertriglyceridemia patients: 6 newly diagnosed type 2 diabetes patients, 6 samples with prediabetes and 6 samples with normal blood glucose. Weighted gene co-expression network analysis (WGCNA) was conducted to construct co-expression network and obtain modules related to blood glucose, thus detecting key lncRNAs.

Results: The green, yellow and yellow module was significantly related to blood glucose in T2DM versus normal controls, T2DM versus prediabetes, prediabetes versus normal controls, respectively. ENST00000503273, ENST00000462720, ENST00000480633 and ENST00000485392 were detected as key lncRNAs for the above three groups, respectively.

Conclusions: For hypertriglyceridemia patients with different blood glucose levels, ENST00000503273, ENST00000462720 and ENST00000480633 could be potential biomarkers of T2DM.

Keywords: diabetes, lncRNAs, qRT-PCR, WGCNA, hypertriglyceridemia

INTRODUCTION

Hyperglycemia promotes a variety of reactions, including oxidative stress and the formation of advanced glycosylated end products, which have been associated with structural and functional changes in blood vessels that eventually cause dysfunction of several organs, especially the heart, nerves, eyes, and kidneys (1). Prevalence of prediabetes is increasing worldwide and more than 470 million people will have

prediabetes by 2030 (2). Previous studies indicated that prediabetes was associated with an increased risk of coronary heart disease, stroke, and all-cause mortality (3). Meanwhile, it is estimated that the number of patients with diabetes were expected to increase to 693 million by 2045. Type 2 diabetes mellitus accounts for about 90%-95% of patients with diabetes (4). Compared with people who do not have diabetes, T2DM patients have a 15% increased risk of all-cause mortality (5). Specially, hypertriglyceridemia can reduce peripheral insulin sensitivity. Meanwhile, insulin resistance leads to the occurrence of hypertriglyceridemia. Therefore, a vicious circle is established (6). Furthermore, T2DM patients with hypertriglyceridemia usually have a higher prevalence of diabetic complications (7). Therefore, whether from a public health perspective or a clinical perspective, prediabetes and T2DM patients with high triglycerides should be paid more attention.

Current research is still searching for novel reliable non-invasive biomarkers to replace the invasive sampling methods for the diagnostic protocols (8, 9). Meanwhile, healthy individuals release exosomes with a cargo of different RNA, DNA, and protein contents into the circulation. Therefore, the above molecules can be measured non-invasively as biomarkers of healthy and diseased states (10). Long noncoding RNAs (lncRNAs) represent a class of transcripts longer than 200 nucleotides with limited protein-coding potential (11). Increasing evidence indicated that lncRNAs could interfere with gene expressions and signaling pathways at various stages, play important roles in the regulation of tissue homeostasis and pathophysiological conditions (12). Existing research have indicated that lncRNA were involved in the entire prediabetes biological process (13). Therefore, as a biomarker, lncRNA plays an important role in the prediction and diagnosis of diseases. Li et al. reported that lncRNA ENST00000550337.1 could be a potential diagnostic biomarker for prediabetes (14). In addition, studies have shown that lncRNAs were related to T2DM *via* producing a complex regulatory network through interactions with transcription factors (15). The abnormal expression of lncRNA NONRATT021972 participates in the occurrence and progression of T2DM, in which it was a potential clinical biomarker (16). The emerging evidence indicated that the role of MALAT1 in diabetes complications is both pro-inflammatory and apoptosis in different cell types (17). However, conventional method only focuses on the role of the single gene, the external sample traits cannot be combined (18). Fortunately, weighted gene co-expression network analysis (WGCNA) could solve the problem.

WGCNA was a method of scale-free network analysis proposed by Peter Langfelder and Steve Horvath in 2008. WGCNA can be used for detecting modules of highly correlated genes, and summarizing such modules *via* the module eigengene or an intramodular hub gene, and relating modules to one another and to external sample traits (18). Meanwhile, WGCNA also alleviates the multiple testing problems inherent in microarray data analysis (19). In addition, WGCNA focused on the whole genome information to overview of the signature of gene networks in phenotypes which can avoid bias and subject judgement (20). Based on the above characteristics of WGCNA, we used it to construct a co-expression network and obtain modules related to blood glucose, thus detecting key genes, and providing a reference for searching potential biomarkers of prediabetes and T2DM in hypertriglyceridemia patients. We present the following article in accordance with the STROBE reporting checklist.

MATERIALS AND METHODS

Participants

The study included 18 hypertriglyceridemia patients: six newly diagnosed type 2 diabetes patients, six samples with prediabetes and six samples with normal blood glucose. All participants were Han Chinese aged 40-65 years and were recruited at the First Hospital of Jilin University from July to September 2020. Patients were diagnosed based on the guidelines for the prevention and control of type 2 diabetes in China (2017 Edition): Patients with type 2 diabetes were defined as fasting plasma glucose (FPG)≥7.0 mmol/L or oral glucose tolerance test (OGTT) two-hour blood glucose ≥11.1 mmol/L. The range of FPG from 6.1-7.0 or the range of OGTT from 7.8-11.1 were regarded as patients with prediabetes. Besides, FPG<6.1 mmol/L and OGTT<7.8 mmol/L could be regarded as the normal controls. Meanwhile, the level of triglycerides (TG) in all participants was >1.7 mmol/L based on the guidelines for prevention and treatment of dyslipidemia in China(2016 Edition). Additionally, all participants had not controlled their blood glucose through drugs or other treatments previously. Meanwhile, all patients with the history of coronary artery disease (CAD), hypertension, atrial fibrillation, myocardial infarction, tumor, acute infectious disease, immune disease, and hematological disease were excluded from the study. All participants have written informed consent and the study was approved by Ethics Committee of the Public Health of the Jilin University, and the privacy of the participants are strictly confidential.

Blood Sample Collection and RNA Sequencing

For each sample, 9 ml trizol (TAKARA BIO INC., CA, Japan) was added into the whole blood immediately after the blood samples (3 ml) were collected. The ratio of trizol to whole blood is 3:1. And total RNA was isolated and purified using total RNA extraction kit. NanoPhotometer® spectrophotometer (IMPLEN, CA, USA) was used to detect the RNA purity. Meanwhile, RNA integrity was evaluated using the RNA Nano 6000 Assay Kit of the Agilent Bioanalyzer 2100 system (Agilent Technologies, CA, USA). The chain-specific library was constructed by removing the ribosomal RNA. After the library was qualified, Illumina PE150 sequencing was performed according to pooling of the effective concentration of the library and the data output requirements. Followed by the sequencing, we removed reads with adapter and N (N means that the nucleobase information cannot be determined) ≥ 0.002, and low-quality reads from raw data. Meanwhile, Q20, Q30, and GC content were calculated. Finally, we obtained the clean reads. All analyses in the study were based on the clean data.

Weighted Gene Co-Expression Network Analysis

We used R version 4.0.4 and the package 'WGCNA' for data analysis. The WGCNA R software package is a comprehensive

collection of R functions for performing various aspects of weighted correlation network analysis (18). We selected the 5000 genes using the Median Absolute Deviation (MAD) algorithm to ensure heterogeneity and accuracy of bioinformatics for co-expression network analysis (21). Then, to make the constructed network more consistent with the characteristics of scale-free network and amplify the correlation between genes, an appropriate soft threshold β is selected (20, 22). Subsequently, we converted the adjacency matrix into a topological overlap matrix (TOM) to evaluate gene connectivity in the network. Finally, an average linkage hierarchical clustering was performed based on TOM-based dissimilarity, with a gene dendrogram>30 and cutting height < 0.25 to construct module dendrograms for further analysis (21, 23).

Screening for Key Modules and Differentially Expressed LncRNAs

The principal component analysis was performed for module eigengenes (ME). Meanwhile, we can assess the relation between MEs and blood glucose and determine the T2DM-related module by combining the clinical data of participants. Meanwhile, the limma R package, based on empirical Bayes methods and linear models, was used to get differentially expressed lncRNAs. The threshold was P<0.05 (22).

Identification of Key lncRNAs and Functional Enrichment Analysis

We take the intersection of all genes in T2DM-related module and differentially expressed lncRNAs to obtain key lncRNAs. Subsequently, these key lncRNAs were mapped to the DAVID (Database for Annotation, Visualization, and Integrated Discovery) dataset (https://david.ncifcrf.gov/) to convert gene symbol to gene ID. Then, we used KOBAS 3.0 (http://kobas.cbi.pku.edu.cn/) to conduct the Functional Enrichment Analysis.

Quantitative Real-Time Polymerase Chain Reaction

The blood samples in qRT-PCR experiment were from a cross-sectional survey in Jilin Province. There were 125 T2DM patients and prediabetes who met the inclusion criteria, respectively. Meanwhile, based on the matching of gender and age, we selected the corresponding control blood samples. The total RNA was extracted using the MolPure® Blood RNA Kit (19241ES50, YEASEN) based on the manufacturer's instructions. Subsequently, we used lnRcute lncRNA First-Strand cDNA Kit (KR202, TIANGEN) to conduct reverse transcription. The cDNA was then analyzed by qRT-PCR using lnRcute lncRNA qPCR Kit (FP402, TIANGEN) on QuantStudio 3 system (Applied Biosystems). The PCR amplification was performed with one cycle at 95°C for 3 min, followed by 40 cycles at 95°C for 5 sec, at 55°C for 10 sec, and at 72°C for 15 sec. The following PCR primers were used: ENST00000503273 primers, forward: 5′- CCTGCCCGCTATGTGACCAATG -3′, reverse: 5′- ACTCCAGCCTGTATCTTCCTCCATC -3′; ENST00000462720 primers, forward: 5′- CTGTGCTTCTG CTTGACTGAGGATC -3′, reverse: 5′-AGGGTGACTGTGA GAGGGTGATG -3′; ENST00000480633 primers, forward: 5′- GAGCCTCGTTCACGGTTCTATGC -3′, reverse: 5′- CAGCCA GCTTGCAGTGACCTTC -3′; ENST00000485392 primers, forward: 5′- TGACGATGAGGTGGCGGTAA -3′, reverse: 5′- GCTCTCGCTGAAACCAGTCC -3′. Expression data were normalized to the expression of β-actin with the $2^{-\Delta\Delta Ct}$ method.

Statistical Analysis

All statistical analyses were performed by IBM SPSS 24.0 and R version 4.0.4. The package 'WGCNA' was used to construct a weighted gene co-expression network. Mean and standard deviation were used to describe the normal continues variables, and the analysis of variance (ANOVA) was performed for the comparison. Meanwhile, median and quartiles were calculated to describe the skewed continues variables, and the Kruskal-Wallis test was used for the comparison. Moreover, Chi-square tests were used to compare categorical variables. A 2-sided P value less than 0.05 was considered significant.

RESULTS

Basic Situation of the Transcriptome Data and the Determination of Soft Threshold

Basic information of six newly diagnosed type 2 diabetes patients, six samples with prediabetes and six normal controls was shown in **Table 1**. And the transcriptome data were used to perform the study. To ensure the quality of analysis, the cleaned data were used after eliminating low-quality data. The detailed situation was shown in **Table 2**. In order to assess the effect of lncRNA in people with different blood glucose levels, we performed pairwise analysis on the three group: type 2 diabetes versus normal controls, type 2 diabetes versus prediabetes, and prediabetes versus normal controls. Meanwhile, the appropriate soft threshold β were ·determined based on the selected criteria of power value, which was 16, 18 and 16, respectively (**Figures S1–S3**).

Type 2 Diabetes *Versus* Normal Controls

Eight models (black, blue, brown, green, grey, red, turquoise, yellow) were obtained through constructing co-expression networks (**Figure 1A**). The number of genes in different modules was shown in **Table 3**. Specially, the genes classified in grey model indicated that they were not assigned to any module. The correlation between genes was displayed in **Figures 2A, B** indicated the correlation between different modules. Meanwhile, by combining clinical data (gender, age, blood glucose and BMI) of T2DM patients and normal controls, we could get the relevant modules and corresponding genes. Based on the aims of the study, modules that are highly related to blood glucose have received attention. As shown in **Figure 3A**, the green module (r=0.7, P=0.01) was significantly related to blood glucose. Additionally, the results of differentially expressed lncRNAs between T2DM patients and normal controls were shown in **Figures 4A, B**, which revealing that 528 lncRNAs were up-regulated and 622 lncRNAs were down-regulated. Subsequently, we take the intersection of all genes in green module and differentially expressed lncRNAs to obtain key lncRNAs (**Table S1**). Then, the pathway analysis to the target genes corresponding to these lncRNAs was performed. **Figure 5A** indicated that Glycolysis/Gluconeogenesis, Metabolic pathways, Type II diabetes mellitus and other signaling pathway were

TABLE 1 | Basic Situation of Participants in the Study.

	T2DM (n=6)	Prediabetes (n=6)	Control (n=6)	χ^2/F	*P*
Gender (male/female)	4/2	4/2	2/4	1.761	0.589
Age (year)	54 ± 6.03	53.17 ± 3.13	52 ± 6.26	0.213	0.811
Weight (kg)	65 (61.25, 75)	65 (62.25, 66.25)	60 (58.75, 77.5)	0.693	0.707
Height (cm)	170.33 ± 5.16	168.67 ± 6.98	164.83 ± 6.80	1.178	0.335
BMI (kg/m^2)	22.62 ± 2.49	22.84 ± 2.39	24.1 ± 2.7	0.594	0.565
TC (mmol/L)	4.86 ± 0.92	5.19 ± 0.63	5.94 ± 1.2	2.072	0.160
LDL (mmol/L)	2.65 ± 0.52	2.92 ± 0.47	3.52 ± 0.56	4.496	0.030
HDL (mmol/L)	1.09 (0.85, 1.23)	1.04 (0.86, 1.35)	1.31 (1.1, 2.11)	4.060	0.131
TG (mmo/L)	2.59 (2.24, 6.51)	2.5 (1.98, 7.59)	2.29 (1.98, 3.24)	0.947	0.623
Lipoprotein (a) (mg/L)	30.5 (13.5, 213.5)	121 (24.25, 267.5)	66 (36.5, 340.75)	1.263	0.532
Creatinine (μmol/L)	63.2 ± 7.26	106.5 ± 7.78	68 ± 13.29	13.103	0.002
Uric acid (μmol/L)	352.5 ± 40	389 ± 65.05	399 ± 116.84	0.314	0.739
ALT (U/L)	18.75 ± 0.96	22.25 ± 5.74	19 ± 4.08	0.906	0.438
AST (U/L)	22 (19, 24.25)	19.5 (12.25, 35)	23 (16.25, 24.5)	0.554	0.758
FPG (mmol/L)	8.8 (7.95, 13.15)	6.55 (6.28, 6.65)	5.25 (4.88, 5.5)	15.205	<0.001
A1C (mmol/mol)	85.8 ± 17.43	46.67 ± 1.53	38.5 ± 2.12	13.081	0.004
A1C (%)	9.96 ± 1.58	6.47 ± 0.15	5.7 ± 0.14	12.832	0.005

enriched. We found hexokinase-3(HK3) was involved in all above pathways. The corresponding lncRNA of HK3 was ENST00000503273. All enriched signaling pathways of HK3 were displayed in **Tables S2** and **S5**.

Type 2 Diabetes *Versus* Prediabetes

By constructing co-expression networks, eleven models (black, blue, brown, green, grey, magenta, pink, purple, red, turquoise, yellow) were obtained (**Figure 1B**). The number of genes in different modules was shown in **Table 3**. The correlation between genes was shown in **Figures 2C, D** indicated the correlation between different modules. Meanwhile, we could get the blood glucose related modules and corresponding genes *via* combining clinical data of T2DM and prediabetes patients. As shown in **Figure 3B**, the yellow module (r=0.69, P=0.01) was significantly related to blood glucose. Additionally, the results of differentially expressed lncRNAs between T2DM and prediabetes patients were displayed in **Figures 4C, D**, which containing 807 up-regulated lncRNAs and 809 down-regulated lncRNAs. Similarly, we take the intersection of all genes in yellow module and differentially expressed lncRNAs to obtain key lncRNAs (**Table S1**), and the pathway analysis was performed. **Figure 5B** indicated that Type II diabetes mellitus, Insulin resistance, Fc gamma R-mediated phagocytosis, Inflammatory mediator regulation of TRP channels and other signaling pathway were enriched. Protein kinase C-epsilon (PRKCE) was involved in all above pathways and corresponding lncRNA was ENST00000462720 and ENST00000480633. All enriched signaling pathways of PRKCE were shown in **Tables S3** and **S5**.

Prediabetes *Versus* Normal Controls

Eight models were obtained by using WGCNA (**Figure 1C**). The number of genes in each module was shown in **Table 3**. The correlation between genes was shown in **Figures 2E, F** shown the correlation between different modules. Similarly, as shown in **Figure 3C**, the yellow module (r=-0.61, P=0.03) was significantly

TABLE 2 | Summary of data from RNA sequencing.

	Raw_reads	Clean_reads	Raw_bases (G)	Clean_bases (G)	Error rate (%)	Q20 (%)	Q30 (%)	GC_content (%)
HTG_D_1	95930240	93380952	14.39	14.01	0.02	98.25	95.03	58.36
HTG_D_2	95047612	93684148	14.26	14.05	0.02	98.08	94.78	60.28
HTG_D_3	87308266	85200132	13.10	12.78	0.02	98.14	94.77	56.51
HTG_D_4	93872544	92111104	14.08	13.82	0.03	97.60	93.34	59.32
HTG_D_5	98171594	95680364	14.73	14.35	0.02	98.03	94.36	59.55
HTG_D_6	92939324	90560052	13.94	13.58	0.03	97.77	93.84	56.14
HTG_P_1	94041630	92351516	14.11	13.85	0.03	97.78	94.36	62.02
HTG_P_2	92027882	90468058	13.80	13.57	0.02	98.29	95.24	59.29
HTG_P_3	93457176	91128506	14.02	13.67	0.02	98.41	95.54	60.52
HTG_P_4	84170598	81790586	12.63	12.27	0.02	97.91	94.53	59.49
HTG_P_5	97877050	95285304	14.68	14.29	0.03	97.47	93.82	63.35
HTG_P_6	93912472	92728294	14.09	13.91	0.02	98.00	94.60	59.82
HTG_N_1	85958252	84363446	12.89	12.65	0.02	98.32	95.41	60.36
HTG_N_2	85005964	83070364	12.75	12.46	0.02	97.83	94.44	61.92
HTG_N_3	91876150	89511812	13.78	13.43	0.02	97.92	94.57	59.15
HTG_N_4	91519536	89611444	13.73	13.44	0.02	98.14	94.97	57.04
HTG_N_5	91153458	89365918	13.67	13.40	0.02	98.20	95.04	58.43
HTG_N_6	84993186	83520980	12.75	12.53	0.02	98.21	95.01	57.19

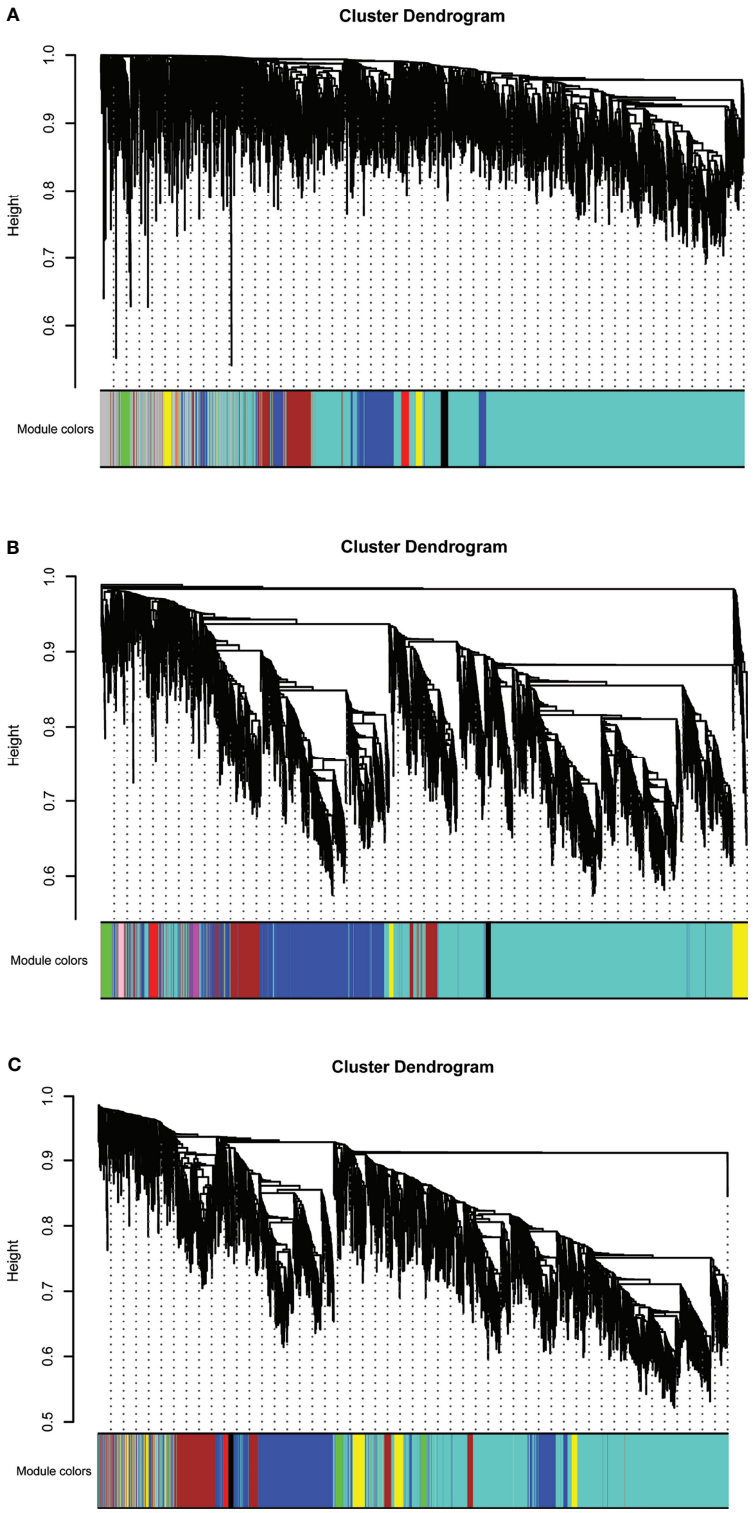

FIGURE 1 | Hierarchical clustering dendrograms of identified co-expressed genes in modules in **(A)** T2DM versus normal controls, **(B)** T2DM versus prediabetes and **(C)** prediabetes versus normal controls (different colors represent different modules).

TABLE 3 | Number of lncRNAs contained in different modules.

Type 2 diabetes mellitus versus normal controls						
Module	black		blue		brown	green
Number	67		549		364	97
Module	grey		red		turquoise	yellow
Number	491		76		3230	126
Type 2 diabetes mellitus versus prediabetes						
Module	black	blue	brown	green	grey	magenta
Number	44	1237	464	86	25	40
Module	pink	purple	red	turquoise	yellow	
Number	44	34	76	2811	139	
Prediabetes versus normal controls						
Module	black		blue		brown	green
Number	46		1207		587	124
Module	grey		red		turquoise	yellow
Number	62		56		2592	326

related to blood glucose. And the results of differentially expressed lncRNAs between prediabetes and Normal Controls were shown in **Figures 4E, F**. Subsequently, we used the same method to obtain key lncRNAs and conducted the pathway analysis (**Table S1**). **Figure 5C** indicated that PI3K-Akt signaling pathway, Cortisol synthesis and secretion, TNF signaling pathway and other signaling pathway were enriched. Activating transcription factor 6-β (ATF6B) was enriched in all above pathways and the corresponding lncRNA was ENST00000485392. All enriched signaling pathways of ATF6B were displayed in **Tables S4** and **S5**.

Validation *via* qRT-PCR, GEO Data Set and ROC Curve

As shown in **Figure 6A**, there were significant differences for ENST00000503273 between the T2DM patients and normal controls *via* the validation of qRT-PCR (*z=-2.472, P=0.013*). Meanwhile, significant differences for ENST00000462720(*z=-2.389, P=0.017*) and ENST00000480633(*z=-5.477, P<0.001*) were observed between the T2DM and prediabetes patients based on **Figures 6B, C**, respectively. However, no significant difference was found for ENST00000485392 between the prediabetes and normal controls based on qRT-PCR. Meanwhile, the corresponding genes of above lncRNAs were verified *via* GSE 130991 data set. 74 T2DM, 23 prediabetes patients and 112 controls were selected from the data set. However, the corresponding gene of ENST00000485392 was not detected in this array. The p-value and log2 fold change of all genes were shown in **Table S6**. Moreover, the ROC curve was used to evaluate the diagnostic power of above lncRNAs. Detailed situation was shown in **Table 4** and **Figure 7**.

DISCUSSION

The prevalence of diabetes in adults aged 18–99 years was estimated to be 8.4% in 2017 and predicted to rise to 9.9% in 2045. Meanwhile, there were 374 million people, equaling 7.7% of the world population, who have impaired glucose tolerance. Based on this, the healthcare expenditure due to hyperglycemia has brought a large social, financial and health system burden to the world (4). We used WGCNA to find the key lncRNA was ENST00000503273 and the corresponding mRNA was HK3 between T2DM patients and normal controls. Similarly, the key lncRNAs were ENST00000462720 and ENST00000480633, and the corresponding mRNA was PRKCE between T2DM and prediabetes patients. Moreover, the key lncRNA was ENST00000485392 and the corresponding mRNA was ATF6B between prediabetes and normal controls.

Hexokinase was involved in phosphorylation of glucose to produce glucose-6-phosphate, the initial step in glycolysis and most glucose metabolism pathways (24). When hungry, the body mobilizes stored fat to decompose and oxidize to produce large amounts of acetyl-CoA, which can be condensed with oxaloacetic acid to form citric acid to reduce glycolysis. Meanwhile, under fed conditions, glycolytic substrates appear to contribute at most 50% of the acetyl-CoA requirements for oxidation to fat (25). Previous studies have indicated that PRKCE could regulate Protein kinase C-delta (PRKCD), and PRKCD is related to the accumulation of triglycerides and the production of lipogenic enzymes in liver for mouse (26). Meanwhile, existing researches have shown that along with increased triglyceride and FFA levels, ATF6 protein was elevated after infusion (27). Therefore, these genes seem to be related to triglycerides or lipids.

Glycolysis pathway is one of the most critical pathways of glucose metabolism, and it is also a pathway that links the metabolism of glucose, fat and amino acids. For diabetes, the activities of hexokinase and glycogen synthase in the liver and skeletal muscle are reduced, resulting in hepatic glycogen increased and glycogen synthesis decreased, thus promoting blood glucose. Meanwhile, for patients with T2DM, insulin is relatively insufficient due to decreased insulin sensitivity in the liver, leading to the synthesis of glycolysis-related enzyme reduced and glycolysis weakened. Subsequently, the ability to

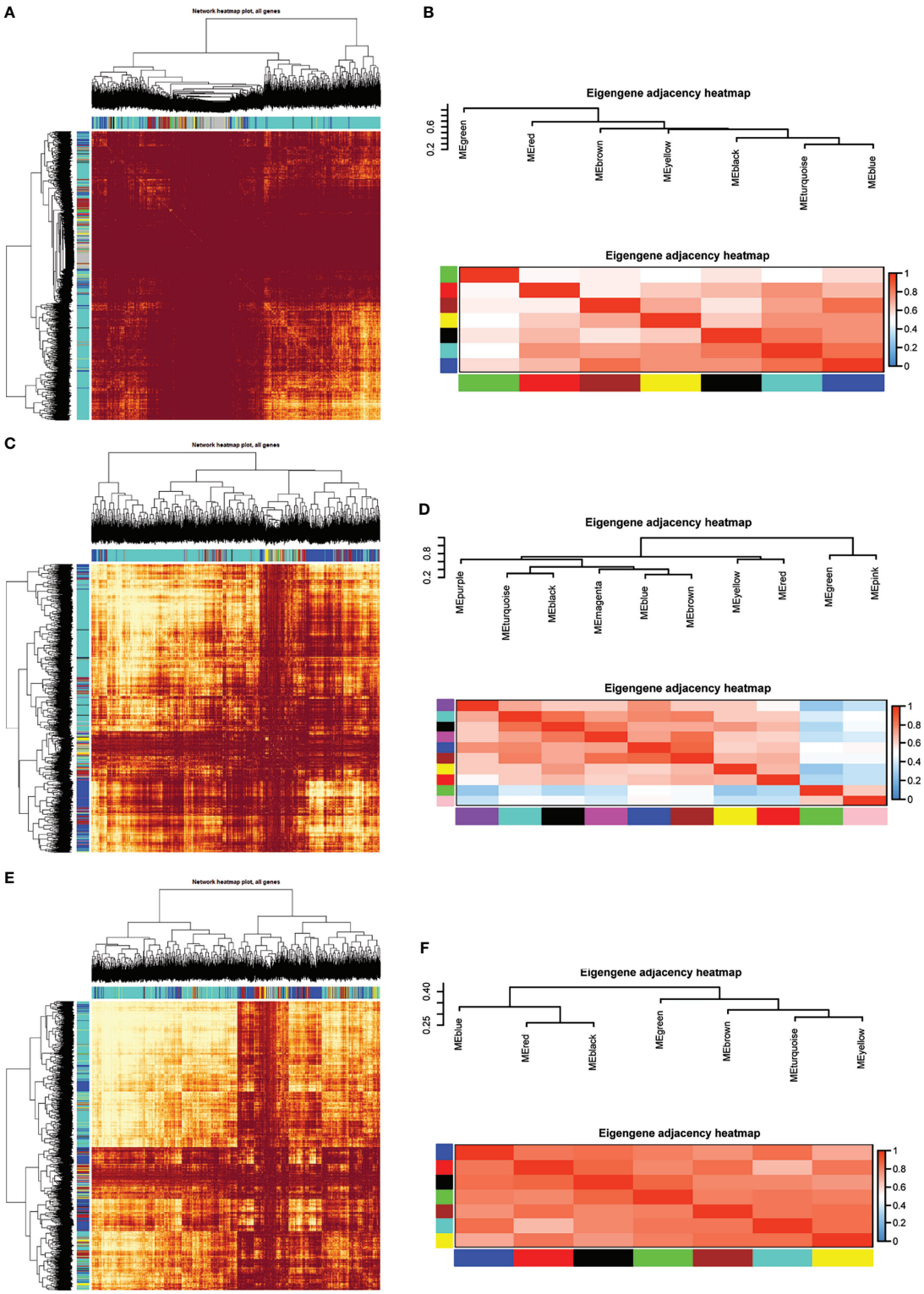

FIGURE 2 | Module preservation analysis. Visualization of the WGCNA network using a heatmap plot in **(A)** T2DM versus normal controls, **(C)** T2DM versus prediabetes and **(E)** prediabetes versus normal controls (The heatmap depicts the topological overlap matrix (TOM) among all genes included in the analysis). **(B, D, F)** represented the heatmap plot of the adjacencies of modules in T2DM versus normal controls, T2DM versus prediabetes and prediabetes versus normal controls, respectively.

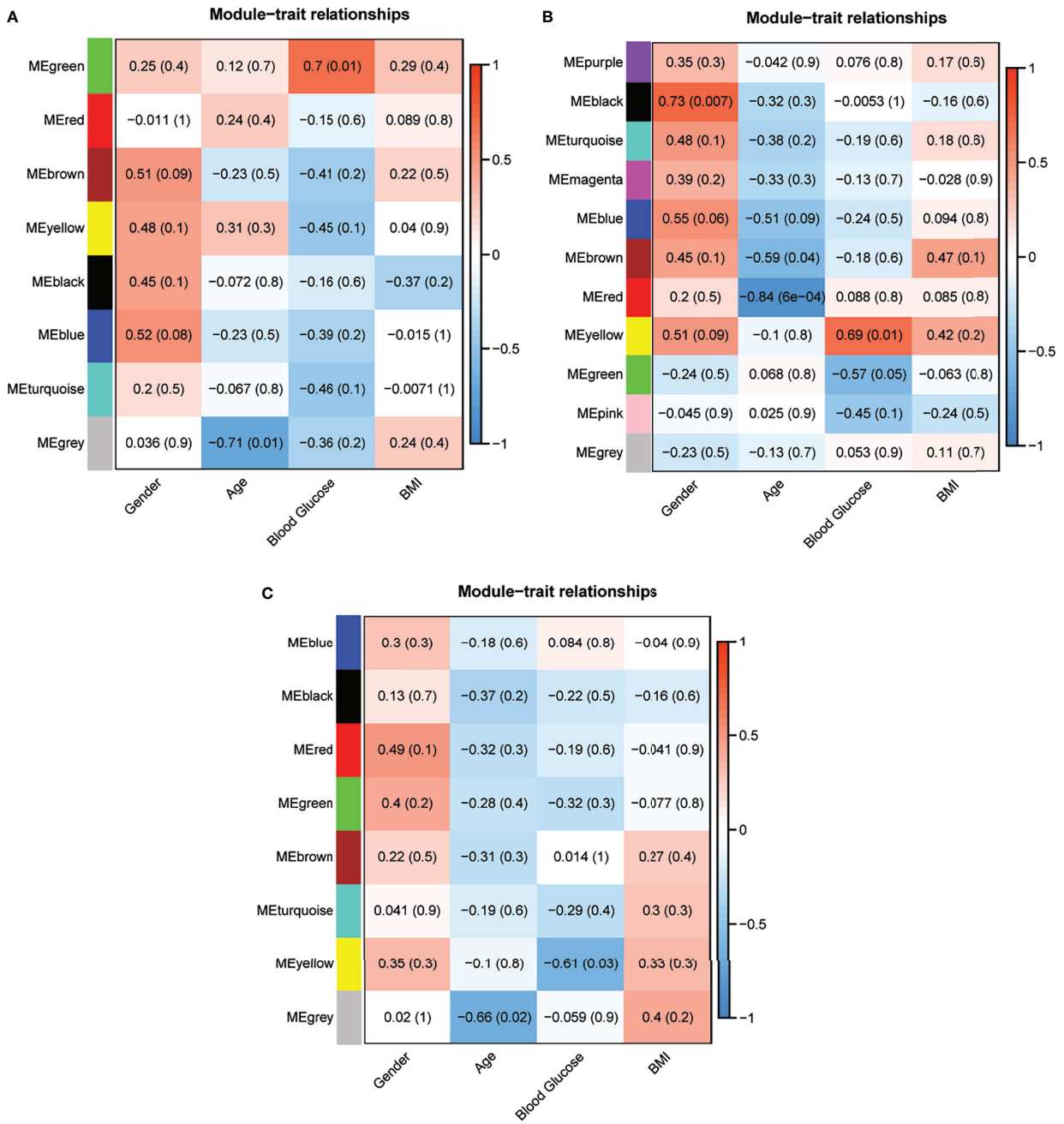

FIGURE 3 | Correlation analysis of the modules and clinical traits in **(A)** T2DM versus normal controls, **(B)** T2DM versus prediabetes and **(C)** prediabetes versus normal controls (Each cell contained the corresponding correlation and P value).

metabolize glucose is lessened. Finally, it has a certain impact on the blood glucose balance (28, 29). Notably, there are a number of genes are related to insulin sensitivity. For example, an increase in HK3 could contribute to the improvement of insulin sensitivity (30). Meanwhile, previous studies have indicated that some synthase appears to stimulate HK3 expression to improve insulin sensitivity (31). Therefore, through the glycolysis pathway, the mechanism of HK3 affecting the development of T2DM could be improving insulin sensitivity.

Early study found that overexpression of PRKCE could be associated with the development of insulin resistance by decreasing the insulin receptors in animals (32). The current literature indicated that increased PRKCE activation was related to marked increases TG in liver, which further led to insulin resistance (33). Meanwhile, PRKCE could also impairs insulin

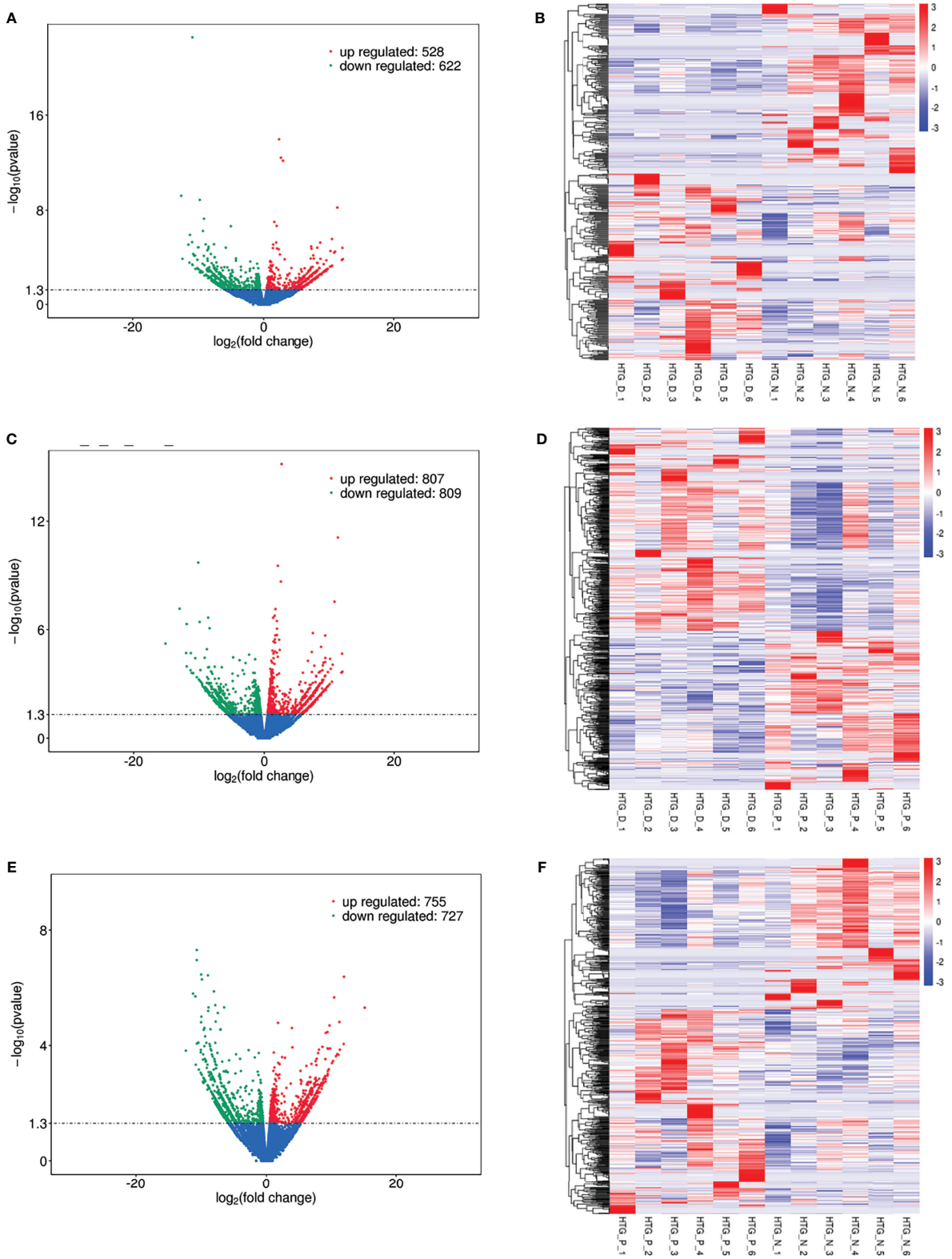

FIGURE 4 | Differentially expressed lncRNAs in **(A)** T2DM versus normal controls, **(C)** T2DM versus prediabetes and **(E)** prediabetes versus normal controls with volcano plot, and **(B, D, F)** represented the heatmap plot for above groups, respectively.

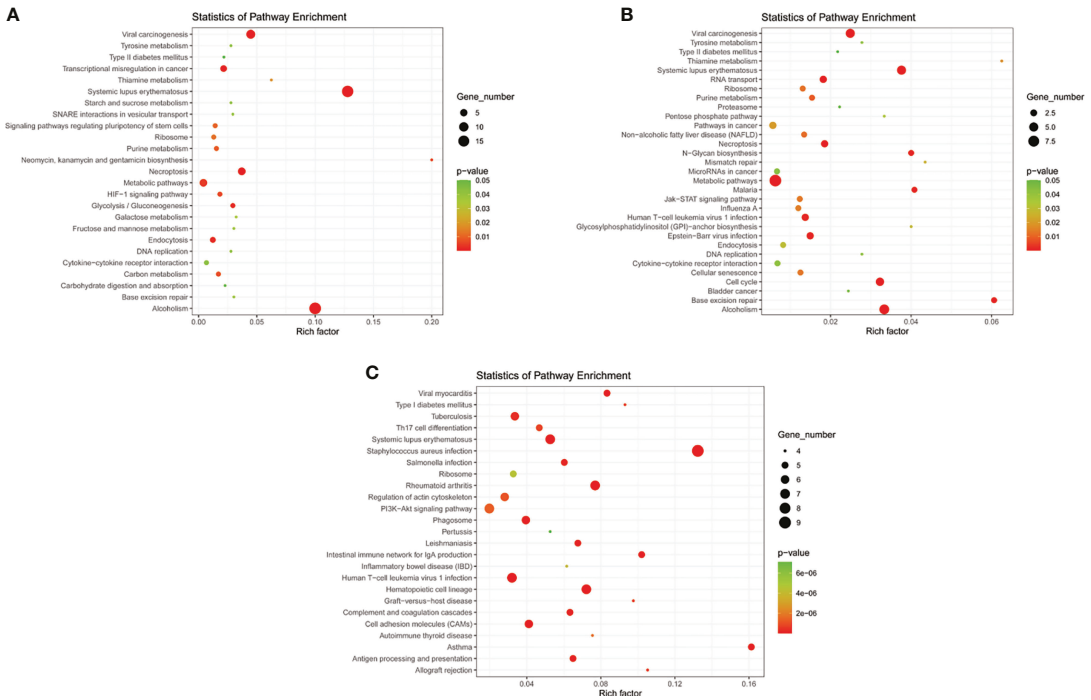

FIGURE 5 | KEGG pathway analyses of important lncRNAs (intersection of all genes in selected module and differentially expressed lncRNAs) in **(A)** T2DM versus normal controls, **(B)** T2DM versus prediabetes and **(C)** prediabetes versus normal controls.

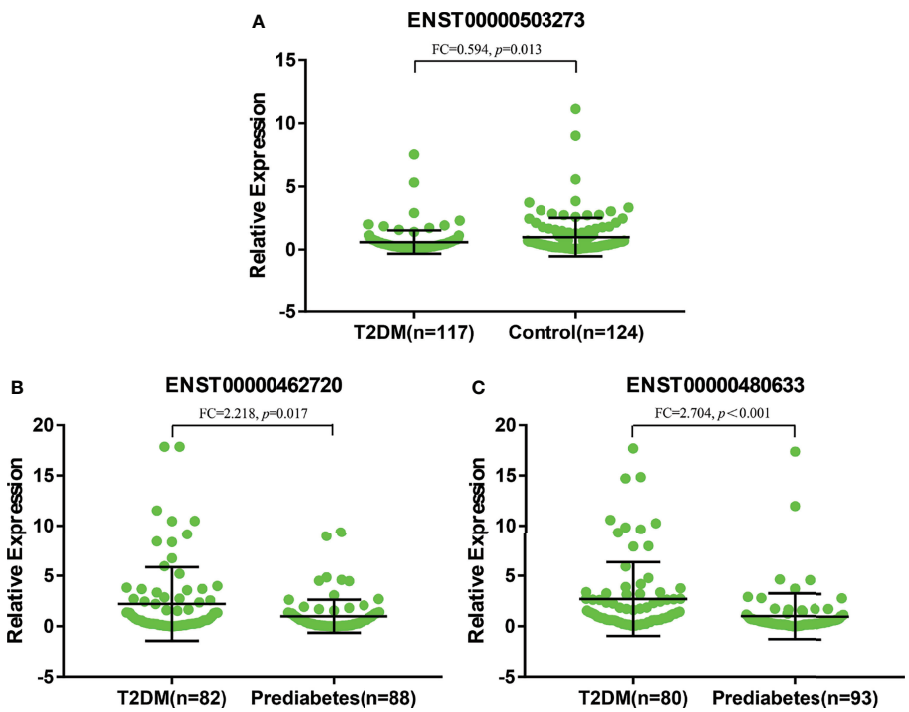

FIGURE 6 | **(A)** represented relative expression of lncRNAs for ENST00000503273 between T2DM and normal controls. **(B, C)** represented relative expression of lncRNAs for ENST00000462720 and ENST00000480633 between T2DM and prediabetes, respectively.

TABLE 4 | The Diagnostic Values of LncRNAs (ROC curve).

	Sensitivity (%)	Specificity (%)	AUC	*P*	*95%CI*
ENST00000503273	89.7	29.8	0.592	0.013	0.520-0.664
ENST00000462720	29.3	89.8	0.606	0.017	0.521-0.691
ENST00000480633	66.3	76.3	0.742	<0.001	0.667-0.816

signaling and its ability to activate glycogen synthesis and inhibit neoglucogenesis, resulting in insulin resistance (34). It is well known that insulin resistance is a core defect in T2DM (35). Besides, PRKCE is a critical gene in steatosis for NAFLD patients, and NAFLD is a risk factor for T2DM (36, 37). Moreover, the association of PRKCE with insulin granules is essential for insulin secretion (38). Therefore, it seems that PRKCE can cause the further development of T2DM through a variety of ways. Meanwhile, the activation of protein kinase C (PKC) is considered to be one of the ways that hyperglycemia leads to the development of diabetic vascular complications and other diabetic complications (39, 40).

PI3K-Akt signaling pathway is related to endoplasmic reticulum (ER) stress (41). ER stress is a key phenomenon in the obesity- and T2DM-associated adverse metabolic outcomes, including insulin resistance in key metabolic organs (42). Studies have indicated that ATF6 is a key transcription factor regulating ER stress (43). Mammals express two homologous ATF6(ATF6α and ATF6β), and ATF6β contributes to adipogenic processes (44). Correspondingly, PI3K-AKT signaling pathway promotes lipid biosynthesis and inhibits lipolysis (45). Therefore, ATF6β could promote the production of adipocytokines, and then the adipocytokines lead to insulin resistance *via* blocking PI3K-AKT-mediated inhibition of lipolysis attenuating the capacity of glucose utilization (45). Meanwhile, ATF6 could increase expression of TNF-α and other inflammatory cytokines in response to ER stress (46). The inflammatory cytokines enhance lipolysis by reducing perilipin and fat-specific protein 27 levels, and then the hepatic insulin-AKT signaling was impaired (47–49). Therefore, ATF6β could involve in insulin resistance through PI3K-Akt signaling pathway, which also included the role of TNF-α. and in turn, insulin resistance aggravates the PI3K-AKT pathway, forming a vicious circle (45). Specially, literatures have indicated that the genetic variation in ATF6 is related to prediabetes in the Chinese Han population (50). However, no significant difference was found for its corresponding lncRNA based on qRT-PCR in our study, more sample was needed in the future.

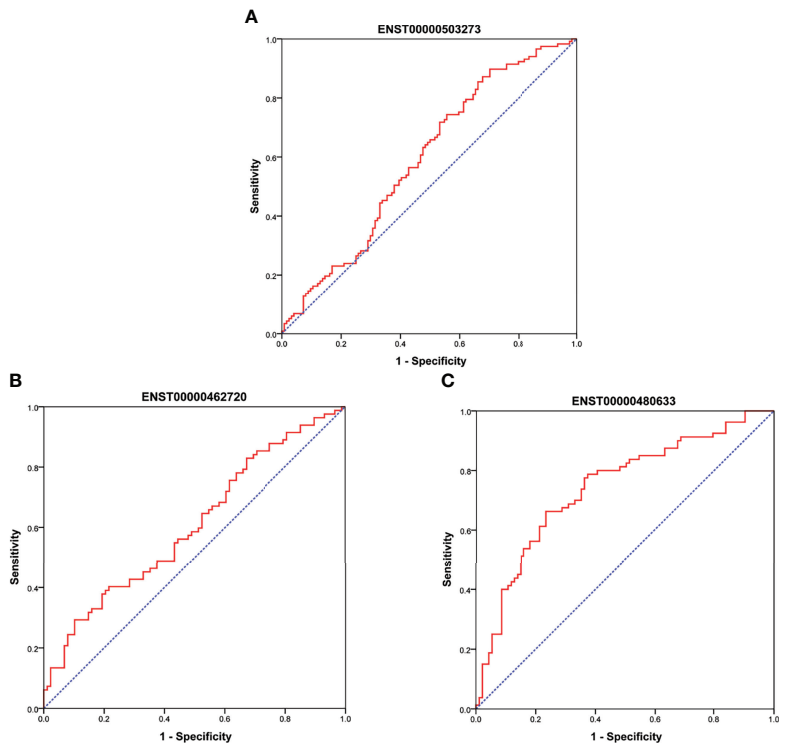

FIGURE 7 | **(A)** showed ROC curve for ENST00000503273 between T2DM and normal controls. **(B, C)** showed ROC curve for ENST00000462720 and ENST00000480633 between T2DM and prediabetes, respectively.

This research has some limitations. In order to get reliable results, a larger sample size will be needed. Moreover, although we have used qRT-PCR to verify the key lncRNA, more molecular biology experiments and functional studies are required to help validate our findings in the future.

CONCLUSION

For hypertriglyceridemia patients with different blood glucose levels, ENST00000503273, ENST00000462720 and ENST00000480633 could be potential biomarkers of T2DM.

DATA AVAILABILITY STATEMENT

The original contributions presented in the study are publicly available. This data can be found here: NCBI, GEO, GSE193436.

ETHICS STATEMENT

The studies involving human participants were reviewed and approved by the Ethics Committee of the Public Health of the Jilin University. The patients/participants provided their written informed consent to participate in this study.

AUTHOR CONTRIBUTIONS

BL, WC, and SY made the study design. SY, MS, LG, and NY conducted the study. SY, MS, TF, and YY analyzed the data and wrote the manuscript. SY, MS, XL, and WH participated amending the manuscript. All authors contributed to the article and approved the submitted version.

FUNDING

This work was supported by the National Natural Science Foundation of China (81973129) and the Graduate Innovative Research Program of Jilin University (101832020CX265).

SUPPLEMENTARY MATERIAL

The Supplementary Material for this article can be found online at: https://www.frontiersin.org/articles/10.3389/fendo.2021.800123/full#supplementary-material

REFERENCES

1. Yan S, Li M, Ma X, Jiang S, Sun M, Wang C, et al. Association of Multiple Mineral and Vitamin B Group Intake With Blood Glucose Using Quantile Regression Analysis: NHANES 2007-2014. *Food Nutr Res* (2019) 63. doi: 10.29219/fnr.v63.3560
2. Tabák AG, Herder C, Rathmann W, Brunner EJ, Kivimäki M. Prediabetes: A High-Risk State for Diabetes Development. *Lancet (London England)* (2012) 379(9833):2279–90. doi: 10.1016/S0140-6736(12)60283-9
3. Zand A, Ibrahim K, Patham B. Prediabetes: Why Should We Care? *Methodist DeBakey Cardiovasc J* (2018) 14(4):289–97. doi: 10.14797/mdcj-14-4-289
4. Cho NH, Shaw JE, Karuranga S, Huang Y, da Rocha Fernandes JD, Ohlrogge AW, et al. IDF Diabetes Atlas: Global Estimates of Diabetes Prevalence for 2017 and Projections for 2045. *Diabetes Res Clin Pract* (2018) 138:271–81. doi: 10.1016/j.diabres.2018.02.023
5. Chatterjee S, Khunti K, Davies MJ. Type 2 Diabetes. *Lancet (London England)* (2017) 389(10085):2239–51. doi: 10.1016/S0140-6736(17)30058-2
6. Jung UJ, Choi MS. Obesity and its Metabolic Complications: The Role of Adipokines and the Relationship Between Obesity, Inflammation, Insulin Resistance, Dyslipidemia and Nonalcoholic Fatty Liver Disease. *Int J Mol Sci* (2014) 15(4):6184–223. doi: 10.3390/ijms15046184
7. Miñambres I, Sánchez-Hernández J, Cuixart G, Sánchez-Pinto A, Sarroca J, Pérez A. Characterization of the Hypertriglyceridemic Waist Phenotype in Patients With Type2 Diabetes Mellitus in Spain: An Epidemiological Study. *Rev Clin Espanola* (2020) 221:576–81. doi: 10.1016/j.rce.2020.06.013
8. Pös O, Biró O, Szemes T, Nagy B. Circulating Cell Free Nucleic Acids: Characteristics and Applications Running Title: Cell-Free Nucleic Acids. *Eur J Hum Genet* (2018) 26:937–45. doi: 10.1038/s41431-018-0132-4
9. Mauro SD, Scamporrino A, Fruciano M, Filippello A, Piro S. Circulating Coding and Long Non-Coding RNAs as Potential Biomarkers of Idiopathic Pulmonary Fibrosis. *Int J Mol Sci* (2020) 21(22):8812. doi: 10.3390/ijms21228812
10. Happel C, Ganguly A, Tagle DA. Extracellular RNAs as Potential Biomarkers for Cancer. *J Cancer Metastasis Treat* (2020) 6. doi: 10.20517/2394-4722.2020.71
11. Yan B, Yao J, Liu JY, Li XM, Wang XQ, Li YJ, et al. lncRNA-MIAT Regulates Microvascular Dysfunction by Functioning as a Competing Endogenous RNA. *Circ Res* (2015) 116(7):1143–56. doi: 10.1161/CIRCRESAHA.116.305510
12. Uchida S, Dimmeler S. Long Noncoding RNAs in Cardiovascular Diseases. *Circ Res* (2015) 116(4):737–50. doi: 10.1161/CIRCRESAHA.116.302521
13. Zhang P, Zhu X, Du Y, Dong Z, Qiao C, Li T, et al. Screening and Functional Studies of Long Noncoding RNA in Subjects With Prediabetes. *Endocrine* (2020) 68(2):296–305. doi: 10.1007/s12020-020-02226-3
14. Li X, Zhao Z, Gao C, Rao L, Hao P, Jian D, et al. The Diagnostic Value of Whole Blood lncRNA ENST00000550337.1 for Pre-Diabetes and Type 2 Diabetes Mellitus. *Exp Clin Endocrinol Diabetes* (2017) 125(6):377–83. doi: 10.1055/s-0043-100018
15. Treede RD, Jensen TS, Campbell JN, Cruccu G, Dostrovsky JO, Griffin JW, et al. Neuropathic Pain: Redefinition and a Grading System for Clinical and Research Purposes. *Neurology* (2008) 70(18):1630–5. doi: 10.1212/01.wnl.0000282763.29778.59
16. Yu W, Zhao GQ, Cao RJ, Zhu ZH, Kai L. LncRNA NONRATT021972 Was Associated With Neuropathic Pain Scoring in Patients With Type 2 Diabetes. *Behav Neurol* (2017) 2017:2941297. doi: 10.1155/2017/2941297
17. Abdulle LE, Hao JL, Pant OP, Liu XF, Zhou DD, Gao Y, et al. MALAT1 as a Diagnostic and Therapeutic Target in Diabetes-Related Complications: A Promising Long-Noncoding RNA. *Int J Med Sci* (2019) 16(4):548–55. doi: 10.7150/ijms.30097
18. Langfelder P, Horvath S. WGCNA: An R Package for Weighted Correlation Network Analysis. *BMC Bioinf* (2008) 9:559. doi: 10.1186/1471-2105-9-559
19. Zhao W, Langfelder P, Fuller T, Dong J, Li A, Hovarth S. Weighted Gene Coexpression Network Analysis: State of the Art. *J Biopharmaceut Stat* (2010) 20(2):281–300. doi: 10.1080/10543400903572753
20. Zhou J, Guo H, Liu L, Hao S, Guo Z, Zhang F, et al. Construction of Co-Expression Modules Related to Survival by WGCNA and Identification of Potential Prognostic Biomarkers in Glioblastoma. *J Cell Mol Med* (2021) 25(3):1633–44. doi: 10.1111/jcmm.16264
21. Bai KH, He SY, Shu LL, Wang WD, Lin SY, Zhang QY, et al. Identification of Cancer Stem Cell Characteristics in Liver Hepatocellular Carcinoma by

WGCNA Analysis of Transcriptome Stemness Index. *Cancer Med* (2020) 9 (12):4290–8. doi: 10.1002/cam4.3047
22. Xiong Y, Yuan L, Chen L, Zhu Y, Zhang S, Liu X, et al. Identifying a Novel Biomarker TOP2A of Clear Cell Renal Cell Carcinoma (ccRCC) Associated With Smoking by Co-Expression Network Analysis. *J Cancer* (2018) 9 (21):3912–22. doi: 10.7150/jca.25900
23. Feng T, Li K, Zheng P, Wang Y, Yao Y. Weighted Gene Coexpression Network Analysis Identified MicroRNA Coexpression Modules and Related Pathways in Type 2 Diabetes Mellitus. *Oxid Med Cell Longevity* (2019) 2019:9567641. doi: 10.1155/2019/9567641
24. Printz RL, Koch S, Potter LR, O'Doherty RM, Tiesinga JJ, Moritz S, et al. Hexokinase II mRNA and Gene Structure, Regulation by Insulin, and Evolution. *J Biol Chem* (1993) 268(7):5209–19. doi: 10.1016/S0021-9258(18)53521-3
25. Jones JG. Hepatic Glucose and Lipid Metabolism. *Diabetologia* (2016) 59 (6):1098–103. doi: 10.1007/s00125-016-3940-5
26. Frangioudakis G, Burchfield JG, Narasimhan S, Cooney GJ, Leitges M, Biden TJ, et al. Diverse Roles for Protein Kinase C Delta and Protein Kinase C Epsilon in the Generation of High-Fat-Diet-Induced Glucose Intolerance in Mice: Regulation of Lipogenesis by Protein Kinase C Delta. *Diabetologia* (2009) 52(12):2616–20. doi: 10.1007/s00125-009-1543-0
27. Tampakakis E, Tabit CE, Holbrook M, Linder EA, Berk BD, Frame AA, et al. Intravenous Lipid Infusion Induces Endoplasmic Reticulum Stress in Endothelial Cells and Blood Mononuclear Cells of Healthy Adults. *J Am Heart Assoc* (2016) 5(1). doi: 10.1161/JAHA.115.002574
28. Hue L, Rider MH. Role of Fructose 2,6-Bisphosphate in the Control of Glycolysis in Mammalian Tissues. *Biochem J* (1987) 245(2):313–24. doi: 10.1042/bj2450313
29. Moore MC, Coate KC, Winnick JJ, An Z, Cherrington AD. Regulation of Hepatic Glucose Uptake and Storage In Vivo. *Adv Nutr (Bethesda Md)* (2012) 3(3):286–94. doi: 10.3945/an.112.002089
30. Miranda DN, Coletta DK, Mandarino LJ, Shaibi GQ. Increases in Insulin Sensitivity Among Obese Youth Are Associated With Gene Expression Changes in Whole Blood. *Obes (Silver Spring Md)* (2014) 22(5):1337–44. doi: 10.1002/oby.20711
31. Ragolia L, Hall CE, Palaia T. Lipocalin-Type Prostaglandin D(2) Synthase Stimulates Glucose Transport *via* Enhanced GLUT4 Translocation. *Prostaglandins Other Lipid Mediators* (2008) 87(1-4):34–41. doi: 10.1016/j.prostaglandins.2008.06.001
32. Ikeda Y, Olsen GS, Ziv E, Hansen LL, Busch AK, Hansen BF, et al. Cellular Mechanism of Nutritionally Induced Insulin Resistance in Psammomys Obesus: Overexpression of Protein Kinase Cepsilon in Skeletal Muscle Precedes the Onset of Hyperinsulinemia and Hyperglycemia. *Diabetes* (2001) 50(3):584–92. doi: 10.2337/diabetes.50.3.584
33. Camporez JP, Wang Y, Faarkrog K, Chukijrungroat N, Petersen KF, Shulman GI. Mechanism by Which Arylamine N-Acetyltransferase 1 Ablation Causes Insulin Resistance in Mice. *Proc Natl Acad Sci USA* (2017) 114(52):E11285–92. doi: 10.1073/pnas.1716990115
34. Ntandja Wandji LC, Gnemmi V, Mathurin P, Louvet A. Combined Alcoholic and non-Alcoholic Steatohepatitis. *JHEP Rep: Innovation Hepatol* (2020) 2 (3):100101. doi: 10.1016/j.jhepr.2020.100101
35. Laakso M. Insulin Resistance and its Impact on the Approach to Therapy of Type 2 Diabetes. *Int J Clin Pract Supplement* (2001) (121):8–12.
36. Rezaei Tavirani M, Rezaei Tavirani M, Zamanian Azodi M. ANXA2, PRKCE, and OXT are Critical Differentially Genes in Nonalcoholic Fatty Liver Disease. *Gastroenterol Hepatol Bed To Bench* (2019) Spring12(2):131–7.
37. Petersen MC, Madiraju AK, Gassaway BM, Marcel M, Nasiri AR, Butrico G, et al. Insulin Receptor Thr1160 Phosphorylation Mediates Lipid-Induced Hepatic Insulin Resistance. *J Clin Invest* (2016) 126(11):4361–71. doi: 10.1172/JCI86013
38. Mendez CF, Leibiger IB, Leibiger B, Høy M, Gromada J, Berggren PO, et al. Rapid Association of Protein Kinase C-Epsilon With Insulin Granules Is Essential for Insulin Exocytosis. *J Biol Chem* (2003) 278(45):44753–7. doi: 10.1074/jbc.M308664200
39. Kizub IV, Klymenko KI, Soloviev AI. Protein Kinase C in Enhanced Vascular Tone in Diabetes Mellitus. *Int J Cardiol* (2014) 174(2):230–42. doi: 10.1016/j.ijcard.2014.04.117
40. Ways DK, Sheetz MJ. The Role of Protein Kinase C in the Development of the Complications of Diabetes. *Vitamins Hormones* (2000) 60:149–93. doi: 10.1016/S0083-6729(00)60019-5
41. Song Q, Han CC, Xiong XP, He F, Gan W, Wei SH, et al. PI3K-Akt-mTOR Signal Inhibition Affects Expression of Genes Related to Endoplasmic Reticulum Stress. *Genet Mol Res: GMR* (2016) 15(3). doi: 10.4238/gmr.15037868
42. Villalobos-Labra R, Subiabre M, Toledo F, Pardo F, Sobrevia L. Endoplasmic Reticulum Stress and Development of Insulin Resistance in Adipose, Skeletal, Liver, and Foetoplacental Tissue in Diabesity. *Mol Aspects Med* (2018) 66:49–61. doi: 10.1016/j.mam.2018.11.001
43. Hillary RF, Una FG. A Lifetime of Stress: ATF6 in Development and Homeostasis. *J Biomed Sci* (2018) 25(1):48. doi: 10.1186/s12929-018-0453-1
44. Bou M, Montfort J, Le Cam A, Rallière C, Lebret V, Gabillard JC, et al. Gene Expression Profile During Proliferation and Differentiation of Rainbow Trout Adipocyte Precursor Cells. *BMC Genomics* (2017) 18(1):347. doi: 10.1186/s12864-017-3728-0
45. Huang X, Liu G, Guo J, Su Z. The PI3K/AKT Pathway in Obesity and Type 2 Diabetes. *Int J Biol Sci* (2018) 14(11):1483–96. doi: 10.7150/ijbs.27173
46. Stengel ST, Fazio A, Lipinski S, Jahn MT, Aden K, Ito G, et al. Activating Transcription Factor 6 Mediates Inflammatory Signals in Intestinal Epithelial Cells Upon Endoplasmic Reticulum Stress. *Gastroenterology* (2020) 159 (4):1357–74. doi: 10.1053/j.gastro.2020.06.088
47. Ranjit S, Boutet E, Gandhi P, Prot M, Tamori Y, Chawla A, et al. Regulation of Fat Specific Protein 27 by Isoproterenol and TNF-α to Control Lipolysis in Murine Adipocytes. *J Lipid Res* (2011) 52(2):221–36. doi: 10.1194/jlr.M008771
48. Hotamisligil GS. Endoplasmic Reticulum Stress and the Inflammatory Basis of Metabolic Disease. *Cell* (2010) 140(6):900–17. doi: 10.1016/j.cell.2010.02.034
49. Yang L, Calay ES, Fan J, Arduini A, Kunz RC, Gygi SP, et al. METABOLISM. S-Nitrosylation Links Obesity-Associated Inflammation to Endoplasmic Reticulum Dysfunction. *Science (New York NY)* (2015) 349(6247):500–6. doi: 10.1126/science.aaa0079
50. Gu N, Ma X, Zhang J, Dong A, Jin M, Feng N, et al. Obesity has an Interactive Effect With Genetic Variation in the Activating Transcription Factor 6 Gene on the Risk of Pre-Diabetes in Individuals of Chinese Han Descent. *PLoS One* (2014) 9(10):e109805. doi: 10.1371/journal.pone.0109805

Conflict of Interest: The authors declare that the research was conducted in the absence of any commercial or financial relationships that could be construed as a potential conflict of interest.

frontiers in Endocrinology

ORIGINAL RESEARCH
published: 23 February 2022
doi: 10.3389/fendo.2022.834075

Papillary Thyroid Carcinoma: Molecular Distinction by MicroRNA Profiling

Francesca Galuppini[1], Simona Censi[2], Isabella Merante Boschin[2], Matteo Fassan[1,3], Marta Sbaraglia[1], Nicola Valeri[4], Jens Claus Hahne[4], Loris Bertazza[2], Giada Munari[1], Marco Galasso[5], Luciano Cascione[6], Susi Barollo[2], Massimo Rugge[1], Federica Vianello[7], Angelo Paolo Dei Tos[1], Caterina Mian[2] and Gianmaria Pennelli[1]*

[1] Pathology Unit, Department of Medicine (DIMED), University of Padua, Padua, Italy, [2] Endocrinology Unit, Department of Medicine (DIMED), University of Padua, Padua, Italy, [3] Veneto Institute of Oncology, Istituto Di Ricovero E Cura a Carattere Scientifico (IRCCS), Padua, Italy, [4] Division of Molecular Pathology, The Institute of Cancer Research, London, United Kingdom, [5] Laboratorio per le Tecnologie delle Terapie Avanzate (LTTA), Department of Morphology, Surgery and Experimental Medicine, University of Ferrara, Ferrara, Italy, [6] Bioinformatics Core Unit, Institute of Oncology Research, Bellinzona, Switzerland, [7] Department of Radiotherapy, Veneto Institute of Oncology, Istituto Di Ricovero E Cura a Carattere Scientifico (IRCCS), Padua, Italy

OPEN ACCESS

Edited by:
Vasyl Vasko, Uniformed Services University of the Health Sciences, United States

Reviewed by:
Fulvio Basolo, University of Pisa, Italy
Dorina Ylli, MedStar Health Research Institute (MHRI), United States

***Correspondence:**
Francesca Galuppini
francesca.galuppini@gmail.com

Specialty section:
This article was submitted to Thyroid Endocrinology, a section of the journal Frontiers in Endocrinology

Received: *13 December 2021*
Accepted: *26 January 2022*
Published: *23 February 2022*

Citation:
Galuppini F, Censi S, Merante Boschin I, Fassan M, Sbaraglia M, Valeri N, Hahne JC, Bertazza L, Munari G, Galasso M, Cascione L, Barollo S, Rugge M, Vianello F, Dei Tos AP, Mian C and Pennelli G (2022) Papillary Thyroid Carcinoma: Molecular Distinction by MicroRNA Profiling. Front. Endocrinol. 13:834075. doi: 10.3389/fendo.2022.834075

Papillary thyroid carcinoma (PTC) is a miscellaneous disease with a variety of histological variants, each with its own mutational profile, and clinical and prognostic characteristics. Identification of microRNA (miRNA) expression profiles represents an important benchmark for understanding the molecular mechanisms underlying the biological behavior of these unique PTC subtypes in order that they be better characterized. We considered a series of 35 PTC samples with a histological diagnosis of either hobnail (17 cases) or classical variant (nine cases) and with a specific *BRAF* p.K601E mutation (nine cases). We determined the overall miRNA expression profile with NanoString technology, and both quantitative reverse transcription–PCR and *in situ* hybridization were used to confirm selected miRNAs. The miRNA signature was found to consistently differentiate specific histotypes and mutational profiles. In contrast to the *BRAF* p.K601E mutation and classic PTCs, three miRNAs (miR-21-5p, miR-146b-5p, and miR-205-5p) were substantially overexpressed in the hobnail variant. The current study found that different miRNA signature profiles were linked to unique histological variants and *BRAF* mutations in PTC. Further studies focusing on the downstream pathogenetic functions of mRNAs in thyroid neoplasms are warranted.

Keywords: microRNA, papillary thyroid cancer, histological variant, miR-205, miR-146, miR-21, hobnail, *BRAF*

INTRODUCTION

Papillary thyroid carcinoma (PTC) is the most common thyroid malignancy, accounting for 80%–90% of all tumors affecting this gland, and predominantly affects women (1, 2). Despite the prognosis of PTC being excellent (10-year survival is up to 90%) (3), a rise in mortality has been mainly linked to local tumor persistence or recurrence (10-year survival is from 49% to 68%) or distant metastases (10-year survival between 25% and 42%) (3). Therefore, it is fundamental to

identify those patients who have an increased risk of recurrence and, therefore, who need more extensive surgery or a targeted postsurgical follow-up. Several factors have already been identified to be prognostic in the assessment of tumor aggressiveness such as age, gender, tumor size, pTNM, stage, and extrathyroid extension. Recently, of these prognostic factors, interest has focused on two particular variables: histological variants and molecular features.

In addition to the classic morphology of PTC, more than 10 different histologic variants have been described. Some of these can be distinguished solely based on a peculiar microscopic appearance, whereas others appear to have distinct clinical and prognostic characteristics. The latter group includes the follicular variant, characterized by a favorable prognosis (to the point where some capsulated variants have been renamed noninvasive follicular thyroid neoplasm with papillary-like nuclear features or "NIFTP" (4)). Other variants have been characterized by more aggressive behavior: tall cells, columnar, and hobnail. In particular, hobnail PTC (HoV-PTC) has been recently identified as a rare but aggressive histological variant (about 0.2% of all PTCs). It typically is found at an advanced stage at the time of diagnosis and tends to develop in lymph nodes as distant metastases. The hobnail variant shows a significant mortality rate, and its disease-specific survival rate is approximately 46%–66% (5–7). *BRAF* p.V600E is the most common mutation in these tumors, which is present in 50%–65% of HoV-PTC cases, followed by *TP53* (56%). Recent studies have also reported *RET/PTC1* rearrangements and *TERT* promoter mutations in HoV-PTC (8, 9). Because of its low incidence and recent identification, further studies are needed to clearly define this variant from molecular, histological, and clinical points of view.

To date, with regard to molecular features of thyroid tumors, *BRAF* and *TERT* promoters have been the genes most investigated as possible outcome indicators. *BRAF* p.V600E mutations are considered reliable preoperative prognostic factors with regard to optimizing the choice of surgical treatment. In fact, this mutation is very frequent in PTC, varying from 14% to 64% of cases (10). *BRAF* p.V600E is more frequent in classic and tall-cell variants (11), while the p.K601E mutation is peculiar to the follicular variant (*BRAF* p.K601E FV-PTC), and seems to be a favorable prognostic factor (12). Although numerous studies have correlated the p.V600E mutation with well-known prognostic factors, such as extrathyroid extension and advanced stages at diagnosis, a significant correlation with an outcome has not yet been demonstrated (13). Therefore, the identification of a new marker associated with *BRAF*-mutated tumors and a poor prognosis is required and may be used as a new therapeutic target and follow-up marker in PTC.

In response to this necessity, a new class of molecules has been studied during the last decade: microRNAs (miRNAs). MiRNAs are small noncoding single-stranded RNA filaments that act as negative regulators of gene expression at the posttranscriptional level. MiRNAs bind the untranslated region (UTR) of target mRNAs and block their translation or degradation, regulating the downstream cascade (14, 15). The role of miRNAs has therefore proved to be crucial when researching regulatory mechanisms of the main genes involved in neoplastic development, becoming both therapeutic targets and diagnostic and prognostic markers. In recent literature, several miRNAs, including miR-222, miR-221, and miR-21, have been found to be overexpressed in PTC tissues compared to normal thyroid tissue (16). These results suggest that distinct miRNA profiles are correlated with PTC tumorigenesis, progression, and prognosis (17).

In light of these data, we wanted to undertake a pilot study to test whether there was an association between rare histological variants of PTC with more aggressive clinicopathological features or conversely with more benign course between core genetic mutations of PTC and between miRNA signatures. For these reasons, we decided to trace the miRNA expression profiles of representative samples of p.K601E-PTC, hobnail, and classic variants of PTC, which had been previously investigated for *BRAF* p.V600E, with the aim of identifying new markers associated with the characteristic biological behavior of this type of carcinoma.

MATERIALS AND METHODS

Study Population

All patients underwent a total thyroidectomy or lobectomy between 2008 and 2016 at the University Hospital of Padua, with a histological diagnosis of PTC. Patient material was collected from the archives of the Surgical Pathology Unit at Padua University Hospital (Padua, Italy). Hematoxylin and eosin-stained slides from formalin-fixed paraffin-embedded tissues were reviewed by two pathologists (GP and FG).

All cases of HoV-PTC and p.K601E-PTC were selected. Nine CV-PTC cases were included as a control cohort. In all patients, a fine-needle aspiration biopsy was performed on a suspicious node at each ultrasound examination and part of the biopsied material was used for the molecular evaluation of the mutational status of *BRAF*.

All patients involved in the study gave their written informed consent, and the study was approved by the Center's Ethics Committee of the University Hospital of Padua. All experiments were performed in accordance with relevant guidelines and regulations.

BRAF Mutational Profiling

The genetic material necessary for the molecular analysis of the *BRAF* gene was extracted from the primary tumor of all study patients. Since each sample was initially fixed in formalin and embedded in paraffin for storage, a deparaffining process was carried out for DNA extraction using a "DNeasy Blood & Tissue Handbook" according to the manufacturer's instructions. After this procedure, qualitative control of the extracted DNA and the determination of its concentration were performed.

DNA Amplification by PCR and Sequencing

Once the DNA was extracted, the specific sequences encoding the gene under study were amplified by PCR. Each amplification

reaction was verified by electrophoresis through a 2% (P/V) agarose gel in Tris-acetate-EDTA (50×). Using Millipore Microcon columns (centrifugal filter device), the amplification products were separated from primers, proteins, salts, and resins. Direct sequencing of the aforementioned exons was performed using a Big-dye Terminator protocol according to the manufacturer's instructions. Subsequently, each product was purified using Autoseq G-50 Dye Terminator Removal Kit (GE Healthcare, Little Chalfont, UK) columns and then processed by an automatic sequencer ABI PRISM (Applied Biosystems, Bedford, MA, USA).

NanoString nCounter® and Bioinformatics Analysis

Total RNA extraction was performed using an Ambion Recover All Isolation Kit (Life Technologies, Carlsbad, CA, USA), according to the manufacturer's instructions. The purity and quality of the extracted RNA were determined by Bio-Analyser (Agilent Technologies, Santa Clara, CA, USA).

MiRNA expression was analyzed using an nCounter® Human v2 miR Expression Assay Kit (NanoString, Seattle, WA, USA) as previously described (18).

This assay detects 800 endogenous miRNAs, five housekeeping transcripts plus six positive and six negative controls. About 150 ng of each total RNA sample was used as input into the nCounter Human miRNA sample preparation. Hybridization was conducted for 16 h at 65°C. Subsequently, the strip tubes were placed into the nCounter Prep Station for automated sample purification and subsequent reporter capture. Each sample was scanned for 555 fields of view on an nCounter® Digital Analyzer (NanoString). Data were extracted using an nCounter® RCC Collector (NanoString). Six samples (three HoV-PTC and three p.K601E-PTC) failed quality control and were excluded from further analysis. Raw data, which were proportional to copy number, were log-transformed and normalized by the quantile method after application of a manufacturer-supplied correction factor for several miRNAs (19). Data were filtered to exclude relatively invariant features (interquartile range = 0.5) and features below the detection threshold defined for each sample by a cutoff corresponding to Δ2 standard deviations of negative control probes plus their mean in at least half of the samples. After the preprocessing steps described above, we plotted relative differences in transcriptional profile between the samples using a multidimensional scaling plot. Using R/Bioconductor and the filtered dataset, limma data analysis were employed with a contrast matrix for the comparisons of interest (19, 20). *P*-values were used to rank miRNAs of interest, and a correction for multiple comparisons was performed using the Benjamini–Hochberg method (21). Raw data that were above background, as well as the corresponding quantile-normalized data, were imported into MultiExperiment Viewer (http://mev.tm4.org/) for visual inspection. Only miRNAs with a *P*-value <0.01 were included in heatmaps. The color red indicates the strong expression of a miRNA, whereas a green point mirrors a reduced level of a determined miRNA.

Quantitative Real-Time Polymerase Chain Reaction Analysis

Expression of three of the most important dysregulated miRNAs detected using NanoString nCounter® Analysis (hsa-miR-21-5p, hsa-miR-146b-5p, hsa-miR-205-5p) was investigated by quantitative reverse transcription (qRT)–PCR.

For qRT–PCR analysis, an NCodeTM miRNA qRT–PCR kit was used (Invitrogen, Carlsbad, CA, USA) according to the manufacturer's instructions with the following primers:

- hsa-miR-21-5p (primer: 5′-cgg tag ctt atc aga ctg atg ttg a-3′)
- hsa-miR-146b-5p (primer: 5′-ggg tga gaa ctg aat tcc a-3′)
- hsa-miR-205-5p (primer: 5′-ggt cct tca ttc cac cg-3′)

Results were normalized relative to the values of *RNU6B* nuclear RNA expression (5′-gtt ggc tct ggt gca gg gcc tcc gag gta ttc gca-3′). Reactions were performed in a LightCycler 480 Real Time PCR cycler System (Roche, Milan, Italy). All qRT–PCR reactions were conducted in duplicate, and the results were calculated according to the comparative CT method. This method uses the equation 2^{-dCt}, where Ct is the threshold cycle (i.e., the number of cycles at which the fluorescence generated in one reaction exceeds a given threshold), and dCt is the difference between the mean Ct of the gene sample and the mean Ct of the *RNU6B* probe.

MiR-21 and MiR-205 *In Situ* Hybridization Analysis

In situ hybridization (ISH) was conducted on tissues of all samples under examination. The ISH was performed using a signal amplification system (GenPointTMCatalyzed Signal Amplification System; DakoCytomation, Carpinteria, CA, USA) following the protocol provided by the manufacturer and modifications made by Yamamichi et al. (22).

The sections on slides were incubated at 60°C for 30 min, deparaffinized, and subsequently treated with proteinase K (DakoCytomation) for 30 min at room temperature. After gentle rinsing in distilled water and immersion in a 95% ethanol solution for 10 s, sections were air-dried. They were then prehybridized at 49°C–56°C for 1 h with RNA ISH buffer (Ambion, Carlsbad, CA, USA). They were subsequently incubated overnight at 49°C–56°C in RNA ISH buffer containing miRCURYTM LNA probes and labeled with biotin for the detection of hsa-miR-21 (Exiqon, Woburn, MA, USA). As a control, a probe (*U6*, Exiqon) was used at a final concentration of 200 nM. The slides were then washed in TBST and then GenPointTM stringent wash solution (at 54°C for 30 min). The slides were exposed to a fixative containing H_2O_2 (DakoCytomation) for 20 min and then a further solution fixative (DakoCytomation) for 30 min. The slides were then exposed to primary streptavidin-horseradish peroxidase antibody, a biotinylated tiamide, a streptavidin-labeled secondary antibody, and a solution chromogen nitroblue tetrazolium, according to the manufacturer's instructions. The sections were then mildly counterstained with hematoxylin and washed with TBST and water before assembly.

Statistical Analysis

The *t*-test was used to assess the differences in miRNA expression levels, obtained by qRT–PCR, between Hobnail variant–PTCs,

BRAF K601E mutation FV-PTCs, and classic variant–PTCs or in different subgroups classified by *BRAF* V600E status. Statistical analyses were performed using MedCalc Statistical Software version 16.4.3 (MedCalc Software bvba, Ostend, Belgium; https://www.medcalc.org; 2016). A $P < 0.05$ was considered statistically significant.

RESULTS

Clinicopathological Features

Of the original 32 patients recruited with a histological and molecular diagnosis of HoV-PTC and p.K601E-PTC, 26 patients were included in our study (six patients were excluded from the analysis, and details are shown in **Figure 1**). Nine classic variant (CV)-PTC cases were included as a control cohort. All cases of p.K601E-PTC resulted in a follicular variant (*BRAF* p.K601E FV-PTC). Clinicopathological features are summarized in **Table 1**.

BRAF p.V600E Mutation Analysis

A *BRAF* p.V600E mutation was found in 8/17 (47%) of HoV-PTC cases and in 4/9 (44%) of CV-PTC cases. A p.V600E mutation was not found in any patient with p.K601E, as previously detected in cytological specimens. All *BRAF* p.K601E mutations were identified in histological samples.

Identification of MiRNAs Associated With Histological and Mutational Features

In order to define miRNAs that distinguished between patients with characteristic histological variants and mutational profiles, we performed miRNA expression analysis in a cohort of 17 HoV-PTC cases, nine *BRAF* p.K601E FV-PTC cases, and in a randomly selected cohort of nine CV-PTC cases.

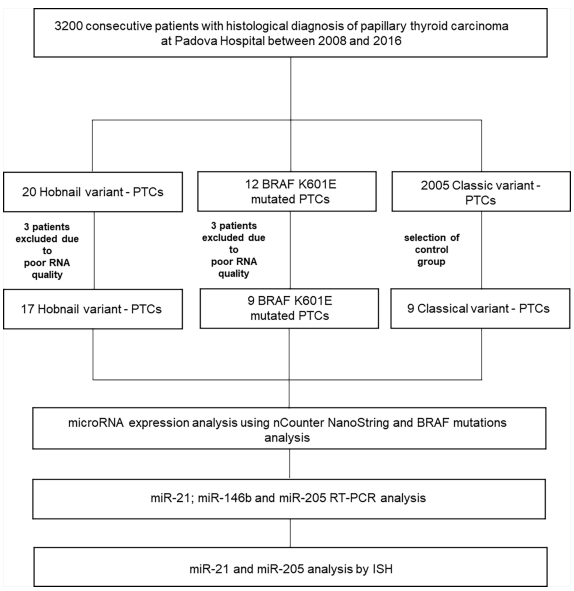

FIGURE 1 | Overview of the study. ISH, *in situ* hybridization; PTC, papillary thyroid carcinoma; RT–PCR, reverse transcription–PCR.

Forty-six miRNAs were deregulated ($P < 0.05$) in a comparison between HoV-PTC and *BRAF* p.K601E FV-PTC cases (regardless of other *BRAF* mutations; **Figure 2A**). **Table 2** shows 14 deregulated miRNAs with a *P*-value <0.01; seven of these were upregulated in HoV-PTC, while the remaining seven were downregulated.

Dividing the cohort of HoV-PTC cases based on the results of *BRAF* p.V600E analysis, we noted that a set of 127 miRNAs was deregulated between the two subgroups ($P < 0.01$). If we compare only the HoV-PTC p.V600E mutated subgroup with *BRAF* p.K601E FV-PTC cases, a large set of 324 miRNAs were significantly deregulated.

When HoV-PTC and CV-PTC samples were compared, 40 miRNAs were found to be downregulated in HoV-PTC patients, while 14 were overexpressed ($P < 0.05$). **Table 3** shows deregulated miRNAs with a *P*-value <0.01.

When the analysis focused on *BRAF* status, 14 miRNAs were deregulated in p.V600E HoV-PTC compared to p.V600E CV-PTC cases (seven were downregulated and seven upregulated; $P < 0.01$). Instead, comparing p.V600E CV-PTC to HoV-PTC wild type (wt), 43 miRNAs showed statistically significant differences in expression levels.

When the analysis compared *BRAF* p.K601E FV-PTC and CV-PTC samples, a set of 153 miRNAs were found to be deregulated ($P < 0.05$); in particular, only 14 were overexpressed in *BRAF* p.K601E FV-PTC patients, while the others were downregulated. **Table 4** shows the deregulated miRNAs with a *P*-value <0.01.

Dividing the cohort of CV-PTC cases on the basis of a *BRAF* p.V600E analysis, we noted that a set of 65 miRNAs was deregulated between the two subgroups. In particular, only three miRNAs were upregulated in a *BRAF* p.K601E FV-PTC compared to p.V600E CV-PTC cohort, while all the others were downregulated ($P < 0.05$).

Validation of MiRNAs Found to Be Deregulated in the Investigated Cohorts

For the validation of miRNAs associated with the histological and molecular features of PTC, we focused on miRNAs upregulated in a comparison of hobnail variant of PTC vs. p.K601E mutation and the classic variant of PTC based on the following observations: (1) since the hobnail variant is associated with a worse prognosis than those of patients with the classic variant and *BRAF* p.K601E mutation, miRNAs overexpressed in these samples might be important in determining the biological behavior of disease; (2) overexpressed rather than silenced miRNAs might be easier to detect in tissues and biological fluids. The expression of the three miRNAs (miR-21-5p, miR-146b-5p, and miR-205) deregulated in HoV-PTC vs. *BRAF* p.K601E FV-PTC and CV-PTC detected in the cohorts by nCounter® was confirmed in the same cohorts (n = 35) using qRT–PCR. All three miRNAs were shown to be significantly upregulated in HoV-PTC patients (**Table 5**). Moreover, when the three miRNAs were analyzed in the subgroups divided for the *BRAF* p.V600E mutation, two of them (miR-146b and miR-21)

TABLE 1 | Clinicopathological features of patients included in this study.

Patient	Age at diagnosis (years)	Gender	Tumor size (cm)	Histological variant	t	n	m	Stage	*BRAF* status
1	52	F	1.7	Hobnail	1b	0	0	I	wt
2	24	M	4.3	Hobnail	4a	1b	0	I	wt
3	46	M	1.2	Hobnail	1b	0	0	I	wt
4	38	M	2.2	Hobnail	2	1a	0	I	wt
5	48	F	2.4	Hobnail	3b(m)	1b	0	I	wt
6	48	M	3.8	Hobnail	3	X	0	I	wt
7	63	M	n.v.	Hobnail	4a(m)	1a	0	IVA	wt
8	73	F	2.1	Hobnail	2	0	0	I	wt
9	56	F	4.5	Hobnail	3b(m)	1a	0	II	wt
10	36	F	1.6	Hobnail	1b	1a	0	I	V600E
11	65	F	3.7	Hobnail	3a(m)	1a	0	II	V600E
12	38	F	1.1	Hobnail	3a(m)	0	0	I	V600E
13	29	F	4.1	Hobnail	3a	1a	0	I	V600E
14	38	M	2.3	Hobnail	3a(m)	1a	0	I	V600E
15	55	M	2.9	Hobnail	3a(m)	1a	0	II	V600E
16	32	F	3.0	Hobnail	2(m)	0	0	I	V600E
17	69	F	1.8	Hobnail	1b(m)	1a	0	II	V600E
18	53	F	1.0	Follicular	1b(m)	0	0	I	K601E
19	78	M	8.0	Follicular	3a	X	0	II	K601E
20	34	M	1.2	Follicular	1b	0	0	I	K601E
21	29	F	3.7	Follicular	2	X	0	I	K601E
22	78	F	0.7	Follicular	1a(m)	0	0	I	K601E
23	45	F	0.6	Follicular	1a(m)	0	0	I	K601E
24	43	F	3.0	Follicular	2	X	0	I	K601E
25	42	F	4.5	Follicular	3	X	0	I	K601E
26	34	F	2.1	Follicular	2	0	0	I	K601E
27	52	F	1.3	Classical	1b(m)	1a	0	I	V600E
28	38	F	1.2	Classical	3b(m)	1a	0	I	V600E
29	23	F	2.8	Classical	3b(m)	0	0	I	V600E
30	35	F	1.5	Classical	1b	1a	0	I	V600E
31	61	F	1.1	Classical	1b	0	0	I	wt
32	25	F	1.7	Classical	1b(m)	0	0	I	wt
33	27	F	1.5	Classical	1b	0	0	I	wt
34	43	F	2.2	Classical	2(m)	0	0	I	wt
35	54	F	3.0	Classical	2	1a	0	I	wt

M, male; F, female; wt, wild-type.

were found to be overexpressed in all *BRAF* wt samples, while miR-205 was overexpressed in CV-PTC wt vs. CV-PTC p.V600E but downregulated in HoV-PTC wt vs. HoV-PTC p.V600E (**Figure 2B**).

MiR-21 and MiR-205 *In Situ* Hybridization Results

To further confirm nCounter® and qRT–PCR findings, miR-21 and miR-205 expressions were investigated in all samples (n = 35) by ISH analysis. The expression of miR-21 and miR-205 was identifiable as a granular blue cytoplasmic stain that was scored according to a three-tiered scale (score 0, no cytoplasmic staining; score 1, faint cytoplasmic staining; score 2, strong cytoplasmic staining). In HoV-PTC, miR-21 was significantly overexpressed: all (9/9) wt HoV-PTC cases were given a score of 2; 63% (5/8) of p.V600E HoV-PTC cases were scored 2, and 37% (3/8) were scored 1 (by comparison with adjacent normal thyroid tissue). Instead, all *BRAF* p.K601E FV-PTC cases were given a score of 0; all (5/5) wt CV-PTC cases and 75% (3/4) of p.V600E CV-PTC cases were given a score of 1, while 25% (1/4) of p.V600E CV-PTC cases were given a score of 2 (by comparison with adjacent normal thyroid tissue; **Figure 3**). Also, miR-205 was significantly overexpressed in HoV-PTC cases (14/17 scored 2); instead, all *BRAF* p.K601E FV-PTC cases were negative (score 0) for the stain. CV-PTC cases were principally given a score of 1 (7/9; **Figure 3**).

DISCUSSION

PTC is a heterogeneous neoplasia comprising several histological variants that are associated with specific mutational profiles with distinct clinical and prognostic features. Therefore, novel markers are being studied in order to better characterize these particular subtypes of PTC and to achieve targeted follow-up and treatments.

For this purpose, we used an innovative method that can simultaneously analyze a wide range of miRNAs, generating a "miRnoma" of the cancer. Researchers have demonstrated the value of the automated platform, NanoString Technologies nCounter®, in several publications, with results derived from a variety of tissues and in different biological settings, including cancer development, neurobiology, and immunology. Through NanoString, it is possible to analyze up to 800 miRNAs for each

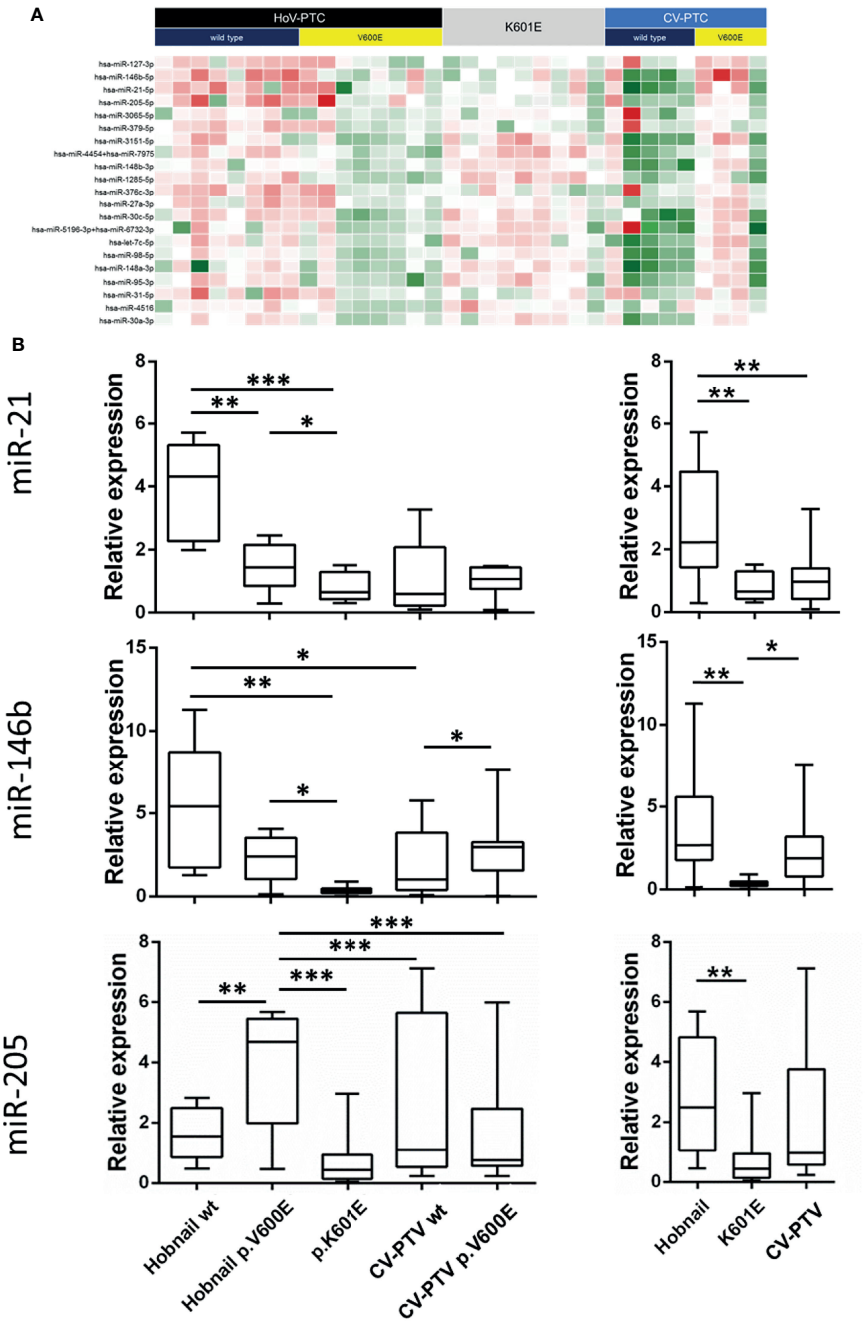

FIGURE 2 | **(A, B)** Heatmap showing miRNA expression in all PTC subgroups. The miRs with a *P*-value <0.01 are shown **(A)**. Plot showing miR-21-5p, miR-146b-5p, and miR-205-5p expression in subgroups divided for a *BRAF* p.V600E mutation (left panel) and in hobnail papillary thyroid carcinoma (HoV-PTC) vs. *BRAF* p.K601E FV-PTC and classic variant (CV)-PTC (right panel). All qRT–PCR reactions were conducted in duplicate, and the results were calculated according to the comparative CT method. **(B)** wt, wild-type. **P* < 0.01, ***P* < 0.001, ****P* < 0.0001.

single sample—thanks to a hybridization system using fluorescent barcodes. The main advantages of using this platform concern the high sensitivity and reproducibility of the results even with samples that are usually difficult to analyze, such as formalin-fixed paraffin-embedded tissues (23).

In our series, we decided to compare forms of PTC with completely different clinical behavior, obviously considering them from a histological but also a molecular point of view, taking into consideration the particular variant with the p.K601E BRAF mutation. The latter is identified almost exclusively in the

TABLE 2 | List of miRNAs deregulated in the comparison of HoV-PTCs vs. p.K601E-PTCs ($P < 0.01$).

MicroRNA_ID	HoV-PTCs (Relative expression)	*BRAF* p.K601E FV-PTC (Relative expression)	*P*-value
hsa-miR-127-3p	38.97	20.19	0.00008
hsa-miR-146b-5p	1,087.18	208.17	0.00017
hsa-miR-21-5p	3,828.23	920.68	0.00080
hsa-miR-205-5p	83.43	21.71	0.00154
hsa-miR-3065-5p	35.89	69.93	0.00176
hsa-miR-379-5p	24.53	20	0.00387
hsa-miR-3151-5p	159.86	583	0.00481
hsa-miR-4454+hsa-miR-7975	27,491.2	61,250.01	0.00670
hsa-miR-148b-3p	133.24	281.28	0.00718
hsa-miR-1285-5p	47.04	142.18	0.00728
hsa-miR-376c-3p	25.61	20	0.00919
hsa-miR-27a-3p	24.65	20	0.00934
hsa-miR-30c-5p	190.54	408.81	0.01074
hsa-miR-5196-3p+hsa-miR-6732-3p	96.18	210.32	0.01387

HoV-PTC, hobnail papillary thyroid carcinoma; BRAF p.K601E FV-PTC, BRAF K601E mutated papillary thyroid carcinoma.

TABLE 3 | List of miRNAs deregulated in the comparison of HoV-PTCs vs. CV-PTCs.

MicroRNA_ID	HoV-PTCs (Relative expression)	CV-PTCs (Relative expression)	*P*-value
hsa-miR-330-3p	2.06	6.74	7.1E-06
hsa-miR-3180-5p	1.67	3.59	0.00188
hsa-miR-519b-5p+hsa-miR-519c-5p+hsa-miR-523-5p+hsa-miR-518e-5p+hsa-miR-522-5p +hsa-miR-519a-5p	1.94	3.96	0.00524
hsa-miR-4286	4,923.05	1,195.28	0.00776
hsa-miR-539-5p	20.73	9.54	0.01012
hsa-miR-486-3p	2.04	4.21	0.01065
hsa-miR-556-5p	2.01	3.66	0.01075
hsa-miR-323b-3p	3.14	6.99	0.01329
hsa-miR-875-3p	1.57	3.32	0.01392
hsa-miR-503-5p	66.96	25.52	0.01489

HoV-PTC, hobnail papillary thyroid carcinoma; CV-PTCs, classic papillary thyroid carcinoma.

follicular histological variant of PTC, as we reported in our series, and usually also distinguishes capsulated forms of the follicular variant, therefore with even less aggressive characteristics (24). We preferred to go beyond the concept of the histological variant of PTC by including in the categorization also molecular information to further stratify the neoplastic behavior.

Our analysis revealed significant differences in terms of a miRNA expression profile between the different cohorts analyzed. In particular, 46 miRNAs were deregulated in a comparison of HoV-PTCs and *BRAF* p.K601E FV-PTCs. A set of 153 miRNAs were found to be deregulated between *BRAF* p.K601E FV-PTC and CV-PTC samples. And in a comparison between HoV-PTC and CV-PTC samples, 54 miRNAs were deregulated ($P < 0.05$). After a subdivision of the two cohorts (HoV-PTC and CV-PTC) according to molecular results for *BRAF* p.V600E, a statistically significant difference was found in the expression profile of the same cohorts (for example, p.V600E HoV-PTC vs. wt HoV-PTC) and between different cohorts (for example, p.V600E HoV-PTC vs. p.V600E CV-PTC). Among the more deregulated miRNAs, three miRNAs primarily emerged: miR-21-5p, miR 146b-5p, and miR-205-5p. Validation analysis (RT–PCR and ISH) confirmed these results.

The miRNA, miR-21-5p, is a crucial oncomir that has been found to be linked to proliferation, apoptosis, invasion, and migration of malignant cell lines (25). Thus, miR-21-5p plays a fundamental role in malignant behavior and transformation. In thyroid carcinogenesis and specifically in PTC, the deregulation of miR-21-5p has been demonstrated (26). The role of miR-21-5p lies in its specific targeting of the three prime UTR (3′-UTR) of *PDCD4*, which negatively regulates protein expression and is a well-known tumor suppressor. The importance of this molecular pathway (which might not necessarily be the sole one) in regulation by miR-21-5p is supported by the finding that miR-21-5p upregulation consistently parallels programmed cell death 4 protein downregulation (27).

The second miRNA, miR-146-5p, has a regulatory role in several tumors by acting on invasiveness and metastasis. For example, it has been shown that breast cancer metastasis-suppressor 1 (BRMS1) affects mir-146 (28). Nuclear factor-κB (NF-κB), which is regulated by BRMS1 and mir-146, is involved in the development of cancer by influencing the proliferative and antiapoptotic signals of thyroid carcinomas (29). NF-κB is implicated in anaplastic thyroid carcinoma through the overexpression of mir-146a. It has been shown that the upregulation of mir-146b reduces the growth of primary brain tumors as gliomas. Several studies have shown that transforming growth factor (TGF)-β1 regulates specific miRNAs, such as mir-146b-5p, in normal cells and cancer. Because TGF-β1 also

TABLE 4 | List of miRNAs deregulated in the comparison of *BRAF* p.K601E FV-PTC vs. CV-PTCs ($P < 0.01$).

MicroRNA_ID	*BRAF* p.K601E FV-PTC (Relative expression)	CV-PTCs (Relative expression)	*P*-value
hsa-miR-675-5p	1.2	4.07	0.000003
hsa-miR-1250-5p	1.53	5.06	0.000004
hsa-miR-589-5p	1.81	4.11	0.00011
hsa-miR-433-5p	2.03	6.6	0.00016
hsa-miR-381-3p	2.42	6.15	0.00044
hsa-miR-92b-3p	3.01	10.72	0.00047
hsa-miR-4755-5p	1.63	5.28	0.00071
hsa-miR-34c-3p	2.88	8.97	0.00135
hsa-miR-208a-3p	1.19	3.4	0.00136
hsa-miR-376a-2-5p	2.09	5.37	0.00162
hsa-miR-1296-5p	1.32	3.52	0.00169
hsa-miR-640	2.59	7.21	0.00200
hsa-miR-129-2-3p	3.11	6.98	0.00203
hsa-miR-1193	2.09	6.06	0.00230
hsa-miR-196a-5p	3.12	13.93	0.00230
hsa-miR-526a+hsa-miR-518c-5p+hsa-miR-518d-5p	2.8	10.04	0.00319
hsa-miR-2053	1.95	7.53	0.00323
hsa-miR-330-3p	2.38	6.74	0.00426
hsa-miR-1298-5p	2.63	8.15	0.00547
hsa-miR-608	2.4	6.61	0.00573
hsa-miR-889-3p	2.13	4.86	0.00650
hsa-miR-1226-3p	2.13	6.16	0.00654
hsa-miR-561-5p	14.97	5.85	0.00665
hsa-miR-4454+hsa-miR-7975	51,688.68	16,905.97	0.00673
hsa-miR-488-3p	1.91	4.74	0.00697
hsa-miR-1245b-5p	1.25	4.73	0.00768
hsa-miR-1273c	1.73	3.43	0.00776
hsa-miR-875-3p	1.38	3.32	0.00836
hsa-miR-328-5p	1.57	4.29	0.00855
hsa-miR-941	2.63	6.29	0.00905
hsa-miR-542-3p	2.14	9.32	0.00954
hsa-miR-215-5p	1.6	3.72	0.00993
hsa-miR-197-5p	5.98	15.91	0.01000

BRAF p.K601E FV-PTC, BRAF K601E mutated papillary thyroid carcinoma; CV-PTC, classic papillary thyroid carcinoma.

TABLE 5 | MiRNA expression determined by qRT–PCR in investigated cohort.

Variable	Compared cohorts	*P*-value
miR-21-5p	HoV-PTC vs. *BRAF* p.K601E FV-PTC	0.0059
	HoV-PTC vs. CV-PTC	0.0081
	BRAF p.K601E FV-PTC vs. CV-PTC	n.s.
	p.V600E HoV-PTC vs. *BRAF* p.K601E FV-PTC	0.06
	wt HoV-PTC vs. *BRAF* p.K601E FV-PTC	0.0001
	wt HoV-PTC vs. p.V600E HoV-PTC	0.0038
miR-146b-5p	HoV-PTC vs. *BRAF* p.K601E FV-PTC	0.0056
	HoV-PTC vs. CV-PTC	n.s.
	BRAF p.K601E FV-PTC vs. CV-PTC	0.0132
miR-205-5p	HoV-PTC vs. *BRAF* p.K601E FV-PTC	0.0098
	HoV-PTC vs. CV-PTC	n.s.
	BRAF p.K601E FV-PTC vs. CV-PTC	n.s.

HoV-PTC, hobnail papillary thyroid carcinoma; BRAF p.K601E FV-PTC, BRAF K601E mutated papillary thyroid carcinoma; CV-PTC, classic papillary thyroid carcinoma; n.s., not significant.

regulates epithelial–mesenchymal transition in PTC, this growth factor has important roles in the expression of specific miRNAs for the progression of thyroid cancer (30–32). Inactivating miR-146b has been considered as a promising strategy also in thyroid cancer therapy. For example, Santa-Inez et al. (33) targeted miR-146b in an experimental model conducted on anaplastic thyroid cancer cell line using Clustered Regularly Interspaced Short Palindromic Repeats / Cas9n (CRISPR/Cas9n) editing system. Also in follicular thyroid cancer (FTC), miR-146b was found to be associated with the process of cancerization and increased aggressiveness of the neoplasm. In particular, Knyazeva et al. (34) analyzed a series of 84 follicular lesions with different histological diagnosis and found a correlation with miR-146b dysregulation and follicular cell malignant transformation and follicular thyroid cancer

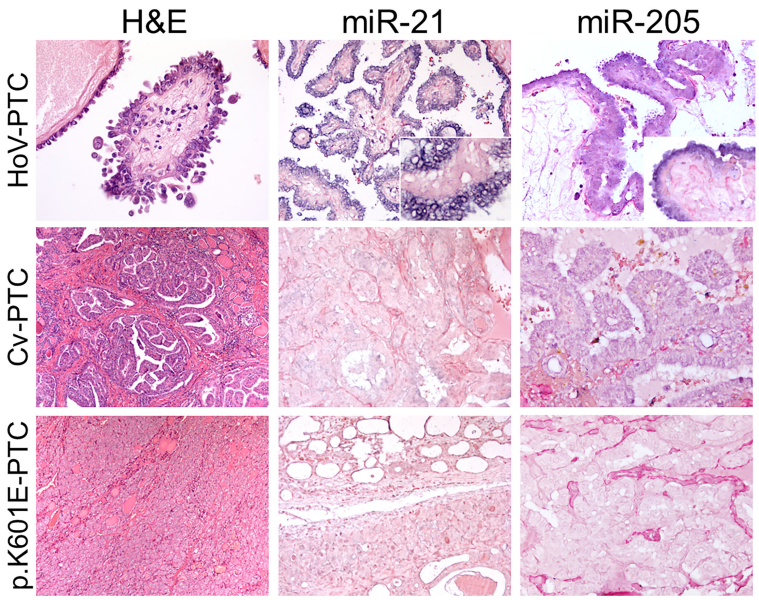

FIGURE 3 | MiR-21 and miR-205 *in situ* hybridization in HoV-PTC, CV-PTC, and *BRAF* p.K601E FV-PTC. The first column represents hobnail papillary thyroid carcinoma (HoV-PTC), classic variant (CV)-PTC, and *BRAF* p.K601E FV-PTC tissues stained with hematoxylin and eosin. The expression of miRs was detectable as a grainy blue cytoplasmic stain. Significant overexpression of miR-21 and miR-205 (score 2) was observed in HoV. In CV-PTC samples, faint miR-21 and miR-205 (score 1) staining was observed. Positive cytoplasmic staining for miR-21 and miR-205 in *BRAF* p.K601E FV-PTC tissue compared with adjacent normal thyroid tissue was not observed (×200 and ×100 original magnification).

progression. miR-146b has also been proposed as a circulating marker of PTC, both diagnostically and prognostically, but future studies will be necessary for this application (35).

In particular, the overexpression of miR-205-5p in the hobnail variant vs. p.K601E-PTC is noteworthy. Importantly, miR-205 is a driver miRNA whose deregulation may induce cancer development and progression (36, 37). Moreover, miR-205 has a double function: i) it can play a role as an oncogene in several cancers (for example, lung, bladder, cervical, and head/neck malignancies); and ii) it can be downregulated in breast cancer, prostatic cancer, and glioma (38, 39). The only previous study that investigated miR-205 expression in thyroid neoplasia suggested that miR-205 overexpression might have a potential tumor suppressive role, which could be exerted through miR-205 binding to 3-UTR of vascular endothelial growth factor A (VEGFA) protein in thyroid cancer. That the overexpression of this miRNA has been found in cases of aggressive variant PTC, such as hobnail-PTC, underlies the hypothesis that the regulatory mechanism of this miRNA is more complex and, therefore, requires further investigation to be clearly understood.

In conclusion, PTC is a heterogeneous neoplasm from both morphological and molecular points of view. The present study highlights this by demonstrating how the different histological variants and specific *BRAF* mutations, which are associated with a different prognosis, are characterized by different miRNA expression profiles. The miRNAs, miR-21-5p, miR-146b-5p, and miR-205-5p, were the most significantly overexpressed miRNAs in the analyzed cohorts. In light of these data, although results are preliminary, these markers appear to play a role in PTC carcinogenesis and, in particular, seem to correlate with its different biological behavior. This is a seminal study that will be deepened considering the most relevant emerged miRNAs in large series for each of the groups. One of the limitations of this study is the low number of analyzed samples mainly due to the rarity of the categories considered such as the p.K601E *BRAF* mutation and the hobnail variant. Further studies are necessary in order to validate these results in a wider population-based cohort and to understand the exact mechanism of action of these miRNAs.

DATA AVAILABILITY STATEMENT

The original contributions presented in the study are included in the article/supplementary material. Further inquiries can be directed to the corresponding author.

ETHICS STATEMENT

The studies involving human participants were reviewed and approved by the University Hospital of Padua Ethics Committee. Written informed consent for participation was not required for this study in accordance with the national legislation and the institutional requirements.

AUTHOR CONTRIBUTIONS

FG designed the study, performed the research, analyzed the data, and wrote the article. SC, IMB, MF, NV, MR, FV, ADT, CM, and GP designed the study and performed the research. MS, JCH, LB, GM, MG, LC, and SB contributed to the acquisition of clinical samples and data and to the statistical analysis. All authors contributed to the article and approved the submitted version.

FUNDING

This research did not receive any specific grant from any funding agency in the public, commercial, or not-for-profit sectors. MF is supported by a grant from the Italian Health Ministry/Veneto region research program NET-2016–02363853 and Fondazione AIRC under 5 per mille, grant ID 22759.

REFERENCES

1. Collini P, Sampietro G, Rosai J, Pilotti S. Minimally Invasive (Encapsulated) Follicular Carcinoma of the Thyroid Gland Is the Low-Risk Counterpart of Widely Invasive Follicular Carcinoma But Not of Insular Carcinoma. *Virchows Archiv* (2003) 442:71–6. doi: 10.1007/s00428-002-0701-2
2. Beaugie JM, Brown CL, Doniach I, Richardson JE. Primary Malignant Tumours of the Thyroid: The Relationship Between Histological Classification and Clinical Behaviour. *Br J Surg* (1976) 63:173–81. doi: 10.1002/bjs.1800630303
3. Nucera C, Goldfarb M, Hodin R, Parangi S. Role of B-Raf(V600e) in Differentiated Thyroid Cancer and Preclinical Validation of Compounds Against B-Raf(V600e). *Biochim Biophys Acta* (2009) 1795:152–61. doi: 10.1016/j.bbcan.2009.01.003
4. Nikiforov YE, Seethala RR, Tallini G, Baloch ZW, Basolo F, Thompson LD, et al. Nomenclature Revision for Encapsulated Follicular Variant of Papillary Thyroid Carcinoma: A Paradigm Shift to Reduce Overtreatment of Indolent Tumors. *JAMA Oncol* (2016) 2:1023–9. doi: 10.1001/jamaoncol.2016.0386
5. Asioli S, Erickson LA, Sebo TJ, Zhang J, Jin L, Thompson GB, et al. Papillary Thyroid Carcinoma With Prominent Hobnail Features: A New Aggressive Variant of Moderately Differentiated Papillary Carcinoma. A Clinicopathologic, Immunohistochemical, and Molecular Study of Eight Cases. *Am J Surg Pathol* (2010) 34:44–52. doi: 10.1097/PAS.0b013e3181c46677
6. Ieni A, Barresi V, Cardia R, Licata L, Di Bari F, Benvenga S, et al. The Micropapillary/Hobnail Variant of Papillary Thyroid Carcinoma: A Review of Series Described in the Literature Compared to a Series From One Southern Italy Pathology Institution. *Rev Endocr Metab Disord* (2016) 17:521–7. doi: 10.1007/s11154-016-9398-4
7. Watutantrige-Fernando S, Vianello F, Barollo S, Bertazza L, Galuppini F, Cavedon E, et al. The Hobnail Variant of Papillary Thyroid Carcinoma: Clinical/Molecular Characteristics of a Large Monocentric Series and Comparison With Conventional Histotypes. *Thyroid* (2018) 28:96–103. doi: 10.1089/thy.2017.0248
8. Morandi L, Righi A, Maletta F, Rucci P, Pagni F, Gallo M, et al. Somatic Mutation Profiling of Hobnail Variant of Papillary Thyroid Carcinoma. *Endocr Relat Cancer* (2017) 24:107–17. doi: 10.1530/ERC-16-0546
9. Lubitz CC, Economopoulos KP, Pawlak AC, Lynch K, Dias-Santagata D, Faquin WC, et al. Hobnail Variant of Papillary Thyroid Carcinoma: An Institutional Case Series and Molecular Profile. *Thyroid* (2014) 24:958–65. doi: 10.1089/thy.2013.0573
10. Nikiforova MN, Kimura ET, Gandhi M, Biddinger PW, Knauf JA, Basolo F, et al. Braf Mutations in Thyroid Tumors are Restricted to Papillary Carcinomas and Anaplastic or Poorly Differentiated Carcinomas Arising From Papillary Carcinomas. *J Clin Endocr Metab* (2003) 88:5399–404. doi: 10.1210/jc.2003-030838
11. Frattini M, Ferrario C, Bressan P, Balestra D, De Cecco L, Mondellini P, et al. Alternative Mutations of Braf, Ret and Ntrk1 Are Associated With Similar But Distinct Gene Expression Patterns in Papillary Thyroid Cancer. *Oncogene* (2004) 23:7436–40. doi: 10.1038/sj.onc.1207980
12. Trovisco V, Soares P, Preto A, de Castro IV, Lima J, Castro P, et al. Type And Prevalence Of Braf Mutations Are Closely Associated With Papillary Thyroid Carcinoma Histotype And Patients' Age But Not With Tumour Aggressiveness. *Virchows Arch* (2005) 446:589–95. doi: 10.1007/s00428-005-1236-0
13. Galuppini F, Pennelli G, Vianello F, Censi S, Zambonin L, Watutantrige-Fernando S, et al. BRAF Analysis Before Surgery for Papillary Thyroid Carcinoma: Correlation With Clinicopathological Features and Prognosis in a Single-Institution Prospective Experience. *Clin Chem Lab Med* (2016) 54:1531–9. doi: 10.1515/cclm-2015-0218
14. Nikiforova MN, Tseng GC, Steward D, Diorio D, Nikiforov YE, et al. Microrna Expression Profiling of Thyroid Tumors: Biological Significance and Diagnostic Utility. *J Clin Endocr Metab* (2008) 93:1600–8. doi: 10.1210/jc.2007-2696
15. Galuppini F, Censi S, Moro M, Carraro S, Sbaraglia M, Iacobone M, et al. MicroRNAs in Medullary Thyroid Carcinoma: A State of the Art Review of the Regulatory Mechanisms and Future Perspectives. *Cells* (2021) 10:955. doi: 10.3390/cells10040955
16. Chou CK, Chen RF, Chou FF, Chang HW, Chen YJ, Lee YF, et al. miR-146b is Highly Expressed in Adult Papillary Thyroid Carcinomas With High Risk Features Including Extrathyroidal Invasion and the BRAFV600E Mutation. *Thyroid* (2010) 20:489–94. doi: 10.1089/thy.2009.0027
17. Yip L, Kelly L, Shuai Y, Armstrong MJ, Nikiforov YE, Carty SE, et al. MicroRNA Signature Distinguishes the Degree of Aggressiveness of Papillary Thyroid Carcinoma. *Ann Surg Oncol* (2011) 18:2035–41. doi: 10.1245/s10434-011-1733-0
18. Valeri N, Braconi C, Gasparini P, Murgia C, Lampis A, Paulus-Hock V, et al. MicroRNA-135b Promotes Cancer Progression by Acting as a Downstream Effector of Oncogenic Pathways in Colon Cancer. *Cancer Cell* (2014) 25:469–83. doi: 10.1016/j.ccr.2014.03.006
19. Cascione L, Gasparini P, Lovat F, Carasi S, Pulvirenti A, Ferro A, et al. Integrated microRNA and mRNA Signatures Associated With Survival in Triple Negative Breast Cancer. *PloS One* (2013) 8:e55910. doi: 10.1371/journal.pone.0055910
20. Trevisani F, Ghidini M, Larcher A, Lampis A, Lote H, Manunta P, et al. MicroRNA 193b-3p as a Predictive Biomarker of Chronic Kidney Disease in Patients Undergoing Radical Nephrectomy for Renal Cell Carcinoma. *Br J Cancer* (2016) 115:1343–50. doi: 10.1038/bjc.2016.329
21. Benjamini Y, Hochberg Y. Controlling the False Discovery Rate: A Practical and Powerful Approach to Multiple Testing. *J R Stat Soc Series B Methodol* (1995) 57:289–300. doi: 10.1111/j.2517-6161.1995.tb02031.x
22. Yamamichi N, Shimomura R, Inada K, Sakurai K, Haraguchi T, Ozaki Y, et al. Locked Nucleic Acid *in Situ* Hybridization Analysis of miR-21 Expression During Colorectal Cancer Development. *Clin Cancer Res* (2009) 15:4009–16. doi: 10.1158/1078-0432.CCR-08-3257
23. Veldman-Jones MH, Brant R, Rooney C, Geh C, Emery H, Harbron CG, et al. Evaluating Robustness and Sensitivity of the NanoString Technologies Ncounter Platform to Enable Multiplexed Gene Expression Analysis of Clinical Samples. *Cancer Res* (2015) 75:2587–93. doi: 10.1158/0008-5472.CAN-15-0262
24. Afkhami M, Karunamurthy A, Chiosea S, Nikiforova MN, Seethala R, Nikiforov YE, et al. Histopathologic and Clinical Characterization of Thyroid Tumors Carrying the BRAF(K601E) Mutation. *Thyroid* (2016) 26:242–7. doi: 10.1089/thy.2015.0227
25. Volinia S, Calin GA, Liu CG, Ambs S, Cimmino A, Petrocca F, et al. A microRNA Expression Signature of Human Solid Tumors Defines Cancer Gene Targets. *Proc Natl Acad Sci USA* (2006) 14:2257–61. doi: 10.1073/pnas.0510565103
26. Zang C, Sun J, Liu W, Chu C, Jiang L, Ge R. miRNA-21 Promotes Cell Proliferation and Invasion *via* VHL/PI3K/AKT in Papillary Thyroid Carcinoma. *Hum Cell* (2019) 32:428–36. doi: 10.1007/s13577-019-00254-4
27. Pennelli G, Fassan M, Mian C, Pizzi M, Balistreri M, Barollo S, et al. PDCD4 Expression in Thyroid Neoplasia. *Virchows Arch* (2013) 462:95–100. doi: 10.1007/s00428-012-1352-6

28. Bhaumik D, Scott GK, Schokrpur S, Patil CK, Campisi J, Benz CC. Expression of microRNA-146 Suppresses NF-kB Activity With Reduction of Metastatic Potential in Breast Cancer Cells. *Oncogene* (2008) 27:5643–7. doi: 10.1038/onc.2008.171
29. Taganov KD, Boldin MP, Chang KJ, Baltimore D. NF-kB-Dependent Induction of microRNA miR-146, an Inhibitor Targeted to Signaling Proteins of Innate Immune Responses. *Proc Natl Acad Sci USA* (2006) 103:12481–6. doi: 10.1073/pnas.0605298103
30. Chou CK, Liu RT, Kang HY. MicroRNA-146b: A Novel Biomarker and Therapeutic Target for Human Papillary Thyroid Cancer. *Int J Mol Sci* (2017) 18, pii:E636. doi: 10.3390/ijms18030636
31. Pan Y, Yun W, Shi B, Cui R, Liu C, Ding Z, et al. Downregulation of miR-146b-5p *via* Iodine Involvement Repressed Papillary Thyroid Carcinoma Cell Proliferation. *J Mol Endocrinol* (2020) 65:1–10. doi: 10.1530/JME-19-0198
32. Celakovsky P, Kovarikova H, Chrobok V, Mejzlik J, Laco J, Vosmikova H, et al. MicroRNA Deregulation in Papillary Thyroid Cancer and its Relationship With BRAF V600E Mutation. *In Vivo* (2021) 35:319–23. doi: 10.21873/invivo.12262
33. Santa-Inez DC, Fuziwara CS, Saito KC, Kimura ET. Targeting the Highly Expressed microRNA miR-146b With CRISPR/Cas9n Gene Editing System in Thyroid Cancer. *Int J Mol Sci* (2021) 22:7992. doi: 10.3390/ijms22157992
34. Knyazeva M, Korobkina E, Karizky A, Sorokin M, Buzdin A, Vorobyev S, et al. Reciprocal Dysregulation of MiR-146b and MiR-451 Contributes in Malignant Phenotype of Follicular Thyroid Tumor. *Int J Mol Sci* (2020) 21:5950. doi: 10.3390/ijms21175950
35. Liu Y, Geng G, Liu X, Cao M, Zhang X. A Meta-Analysis of Circulating microRNAs in the Diagnosis of Papillary Thyroid Carcinoma. *PloS One* (2021) 16:e0251676. doi: 10.1371/journal.pone.0251676
36. Gregory PA, Bert AG, Paterson EL, Barry SC, Tsykin A, Farshid G, et al. The miR-200 Family and miR-205 Regulate Epithelial to Mesenchymal Transition by Targeting ZEB1 and SIP1. *Nat Cell Biol* (2008) 10:593–601. doi: 10.1038/ncb1722
37. Chauhan N, Dhasmana A, Jaggi M, Chauhan SC, Yallapu MM. miR-205: A Potential Biomedicine for Cancer Therapy. *Cells* (2020) 25:1957. doi: 10.3390/cells9091957
38. Vosgha H, Salajegheh A, Smith RA, Lam AK, et al. The Important Roles of miR-205 in Normal Ph,Ysiology, Cancers and as a Potential Therapeutic Target. *Curr Cancer Drug Targets* (2014) 14:621–37. doi: 10.2174/1568009614071409261056 34
39. Salajegheh A, Vosgha H, Md Rahman A, Amin M, Smith RA, Lam AK. Modulatory Role of miR-205 in Angiogenesis and Progression of Thyroid Cancer. *J Mol Endocrinol* (2015) 55:183–96. doi: 10.1530/JME-15-0182

Conflict of Interest: The authors declare that the research was conducted in the absence of any commercial or financial relationships that could be construed as a potential conflict of interest.

Publisher's Note: All claims expressed in this article are solely those of the authors and do not necessarily represent those of their affiliated organizations, or those of the publisher, the editors and the reviewers. Any product that may be evaluated in this article, or claim that may be made by its manufacturer, is not guaranteed or endorsed by the publisher.

frontiers in Endocrinology

ORIGINAL RESEARCH
published: 16 March 2022
doi: 10.3389/fendo.2022.841463

Association of Organochlorine Pesticides With Genetic Markers of Endoplasmic Reticulum Stress in Type 2 Diabetes Mellitus: A Case–Control Study Among the North-Indian Population

Neha Tawar[1], Basu Dev Banerjee[1]*, Sri Venkata Madhu[2], Vivek Agrawal[3] and Sanjay Gupta[3]*

[1] Department of Biochemistry, University College of Medical Sciences (UCMS) and Guru Teg Bahadur (GTB) Hospital (University of Delhi), Delhi, India, [2] Department of Endocrinology and Metabolism, UCMS and Guru Teg Bahadur (GTB) Hospital (University of Delhi), Delhi, India, [3] Department of Surgery, UCMS and Guru Teg Bahadur (GTB) Hospital (University of Delhi), Delhi, India

OPEN ACCESS

Edited by:
Alok Raghav, Ganesh Shankar Vidyarthi Memorial Medical College, India

Reviewed by:
Shahid Banday, University of Massachusetts Medical School, United States
Jamal Ahmad, Aligarh Muslim University, India
Kirti Amresh Gautam, G D Goenka University, India

***Correspondence:**
Neha Tawar
tawar.neha145@gmail.com
Basu Dev Banerjee
banerjeebd@hotmail.com

Specialty section:
This article was submitted to Clinical Diabetes, a section of the journal Frontiers in Endocrinology

Received: *22 December 2021*
Accepted: *03 February 2022*
Published: *16 March 2022*

Citation:
Tawar N, Banerjee BD, Madhu SV, Agrawal V and Gupta S (2022) Association of Organochlorine Pesticides With Genetic Markers of Endoplasmic Reticulum Stress in Type 2 Diabetes Mellitus: A Case–Control Study Among the North-Indian Population. Front. Endocrinol. 13:841463. doi: 10.3389/fendo.2022.841463

Background: Organochlorine pesticides (OCPs) have been long linked to type 2 diabetes mellitus (T2DM); however, this relation at the molecular level has not been explored yet. Endoplasmic reticulum (ER) stress and pro-inflammatory pathways are considered vital ones in the pathogenesis of T2DM. We aimed to investigate the existence of any association between OCPs, ER stress, and pro-inflammatory pathways in subjects with known T2DM.

Methods: Seventy subjects each with T2DM and normal glucose tolerance were recruited from the surgery department. Their visceral adipose tissue was collected intraoperatively. OCP concentration, ER stress, and pro-inflammatory markers were analyzed and compared between two study groups.

Results: We found 18 OCPs and their metabolites in visceral adipose tissue samples of study participants. The levels of δ-HCH, heptachlor, endrin, and p,p′DDT were significantly higher in the T2DM group and were also positively correlated with fasting and postprandial plasma glucose levels ($p < 0.01$). We observed a positive association of δ-HCH ($p < 0.01$), heptachlor ($p < 0.05$), and endrin ($p < 0.05$) with central adiposity and ER stress markers. However, we failed to establish the correlation of OCPs with any of the pro-inflammatory markers.

Conclusion: The existence and simultaneous complex correlation of OCPs with ER stress may explain their role in the pathogenesis of T2DM, revealing the persistence of the gene–environment interaction in the etiology of T2DM.

Keywords: OCP, T2DM, normal glucose tolerance, inflammation, ER stress, visceral adipose tissue

INTRODUCTION

Exposure to environmental toxicants such as organochlorine pesticides (OCPs) has been strongly associated with type 2 diabetes mellitus (T2DM) (1–6). Their property of persistence and bioaccumulation in the environment has generated a surge of global interest (7). Due to their lipophilic nature, they remain stored in the adipose tissue without disintegration for a long time (8); in consequence, even a minimal continuous exposure over time can still lead to potential health hazards (9). OCPs are the most investigated insecticides linked with obesity in humans (10). India is among one of the top producers and consumers of OCPs (11, 12), and their exposure might be a possible risk factor for higher vulnerability for developing T2DM (3).

Adipose tissue, which is considered an energy storage site, has also been associated with several adverse metabolic consequences, providing visceral adipose tissue more physiological relevance, as it is a leading determinant of insulin resistance and excessive inflammatory state (13). With the development of obesity, the adipose tissue undergoes some molecular and cellular adaptations with a significant generation of pro-inflammatory molecules such as tumor necrosis factor α (TNFα) and interleukin 6 (IL-6) (14). Chronic inflammation may be a consequence of endoplasmic reticulum (ER) stress and/or trigger the same (15), which ensures a self-perpetuating cycle. Chronic ER stress, which is considered to be a vital one in diabetes pathogenesis (16, 17), leads to a self-protective mechanism to maintain cellular viability and function by reducing misfolded and unfolded protein load by unfolded protein response (UPR) (18). Upregulated ER stress has been observed in the adipose tissue of various obese and lean insulin-resistant animals and humans (19–21).

In spite of major advancements in the acknowledgement of the pathophysiology of T2DM, the mechanisms are still incompletely understood and its susceptibility might be explained by the complex gene–environment interaction (22). Although the previous literature supports the evidence for the complex interplay of ER stress and inflammation in chronic metabolic disorders, there is a dearth of studies showing the interconnectivity of these environmental contaminants with such cellular stress mechanisms. Hence, the present study was conducted in order to evaluate the possible synergy of OCP compounds with pro-survival and pro-apoptotic ER stress and inflammatory pathways at the molecular level in human subjects with T2DM.

METHODOLOGY

This was a case–control study carried out in the Department of Surgery and Biochemistry, University College of Medical Sciences (UCMS), and Guru Teg Bahadur (GTB) Hospital, Delhi. Ethical clearance (certificate no. IHEC-UCMS 08112015) was obtained from the Institutional Ethics Committee for Human Research, UCMS, and GTB Hospital, Delhi, before initiating the study. The patient information sheet was explained to each subject, and their written consent was obtained. The study was conducted between the periods of January 2016 to January 2020.

Study Subjects

The study included 70 subjects each with known T2DM and normal glucose tolerance (NGT) subjects attending the OPD of the surgery department for their elective abdominal surgeries for clinical conditions such as cholecystectomy, appendectomy, and hernia. Subjects with life-threatening cardiovascular disease, known pancreatic disease, and Cushing syndrome as well as females with pregnancy and known polycystic ovarian syndrome were excluded from the study.

The T2DM subjects were categorized based on clinical guidelines set by the American Diabetes Association (ADA) (23), while a standardized 75-g oral glucose tolerance test was performed for identifying subjects with NGT (23). Both the groups were matched based on their gender, age, and BMI.

Anthropometric Measurements

A detailed questionnaire was used to record the demographical and clinical characteristics of the recruited subjects. Demographical characteristics including age, gender, body mass index (weight (kg)/height (m^2)), pulse rate, blood pressure, diet pattern, socioeconomic status (24), and any other medical history were documented for each subject.

Sample Collection and Storage

The visceral adipose tissue sample weighing about 5 g was collected intraoperatively in a sterile container and cryopreserved in liquid nitrogen followed by their storage at -80°C for estimation of OCP levels and gene expression levels. Also, blood samples were collected for the estimation of fasting and postprandial plasma glucose.

Organochlorine Pesticide Analysis

Pesticide extraction for each sample was done in triplicates by using the method given by Bush et al. (25). Briefly, 1 g of finely chopped visceral adipose tissue was shaken in a flask with 1:2 parts of acetone (Merck, Kenilworth, NJ, USA) and n-hexane (Merck, USA) at 100–120 rpm at room temperature for 4 to 5 h on a mechanical shaker. The solvent was collected and the extraction procedure was repeated twice using the same process, and the fractions were added to the previous solvent fractions. The cleanup of the collected solvent fraction was done by adsorption column chromatography using heat-activated Florisil (SRL, Mumbai, India) and anhydrous sodium sulfate (SRL, India). The collected n-hexane was evaporated by a vacuum rotary evaporator and reconstituted in n-hexane to 1-ml quantity. Quantification of organochlorine residue levels was done using a gas chromatograph (PerkinElmer Clarus 500) equipped with a Ni63 electron capture detector. The sample (1 μl) was automated injected at 170°C with a hold of 1 min. The temperature was raised at the rate of 5°C/min to 225°C and the time for the hold was 5 min, and then to 275°C at the rate of 6°C/min with a 15-min hold. Nitrogen gas with a flow rate of 35 ml/min was used as a carrier. The limit of detection for each pesticide was 4 pg/ml. The adipose tissue samples were analyzed for the following organochlorine residues: α-hexachlorocyclohexane (α-HCH), β-HCH, γ-HCH, δ-HCH, heptachlor, aldrin, heptachlor epoxide B (HTEB), heptachlor epoxide A (HTEA), endosulfan I, endosulfan II, dieldrin, endrin, methoxychlor, o,p′-dichlorodiphenyldichloroethylene (o,p′-DDE),

p,p′-DDE, p,p′-dichlorodiphenyldichloroethane (p,p′-DDD), o,p′-dichlorodiphenyltrichloroethane (o,p′-DDT), and p,p′-DDT. A quantitative analysis of pesticide residues in each sample was done by comparing the peak area with those obtained from a chromatogram of a mixed OCP standard (AccuStandard, New Haven, CT, USA) of known concentrations. The concentration of OCPs in samples has been presented in ng/gm (ppb) wet weight.

Gene Expression Analysis at the Transcriptional Level

The mRNA expression of protein kinase R-like ER kinase (PERK), activating transcription factor (ATF-4), C/EBP homologous protein (CHOP), inositol-requiring enzyme-1α (IRE-1α), X box-binding protein (spliced) (XBP-1s), glucose-regulated protein-78 (GRP-78), TNFα, and IL-6 were analyzed by quantitative real-time PCR (qPCR) in triplicates along with negative control.

Total RNA extraction from visceral adipose tissue was done by using the TRIzol reagent (Invitrogen, Thermo Fisher Scientific, Waltham, MA, USA) standard method as per the manufacturer's protocol. The quality and concentration of total RNA were measured spectrophotometrically on a NanoDrop spectrophotometer (ND2000, Thermo Fisher Scientific, USA). Total RNA (1 μg) was used for complementary DNA synthesis using an iScript cDNA synthesis kit (Bio-Rad, Hercules, CA, USA) as per the manufacturer's protocol. The NCBI tool, Primer BLAST, was used to design the primers of genes of interest. The Sso EvaGreen Supermix (Bio-Rad, USA) (dNTPs, Sso7d fusion polymerase, $MgCl_2$, EvaGreen dye, stabilizers) was used for the reaction mixture of qPCR. The concentration of 10 pmol of primer was used for each qPCR reaction (primer sequences presented in **Table 1**). The PCR amplification was performed on a CFX Connect Real-Time PCR Detection System (Bio-Rad, USA). The amplification cycle included initial denaturation at 95°C for 1 min followed by 40 cycles of denaturation at 95°C for 30 s and annealing at 60°C for 45 s and lastly extension at 72°C for 30 s. β-Actin was used as the gene normalizer. The gene expression was determined by the 2-ΔΔCt method (26).

Gene Expression Analysis at the Translational Level

The total proteins from 100 mg visceral adipose tissue samples were isolated by radioimmunoprecipitation buffer (G-Biosciences, St. Louis, MO, USA) followed by their quantification using a bicinchoninic acid protein assay kit (G-Biosciences, USA). In brief, 30 μg denatured protein was resolved on 10% Tris–glycine gel and transferred to a polyvinylidene fluoride membrane (Bio-Rad, USA). The non-specific binding sites on the membrane were blocked with 5% skimmed milk. The membrane was incubated with corresponding primary antibodies (Abbkine, USA) at 1:700 dilutions overnight at 4°C, and after washing the membrane was treated with an HRP-conjugated secondary antibody (Abbkine, USA) for 2 h. The detection of signals was recorded by the use of an ECL Reagent Kit (Thermo Fisher Scientific, USA) in the gel imaging system (Thermo Fisher Scientific ECL Imager). The protein band density was measured and compared using the ImageJ software.

TABLE 1 | Primer sequences of specific genes.

Genes	Primer sequence
PERK	Forward 5′ TGTCGCCAATGGGATAGTGACGA 3′
	Reverse 5′ AATCCGGCTCTCGTTTCCATGTCT 3′
ATF-4	Forward 5′ GGGAGTTGGCTTCTGATTCTCA 3′
	Reverse 5′ ATCAAGTCCCCCACCAACAC 3′
CHOP	Forward 5′ AAACAGGCATCAGACCAGCTT 3′
	Reverse 5′ CTGCCATCTCTGCAGTTGGA 3′
IRE-1α	Forward 5′ ACACCATCACCATGTACGACACCA 3′
	Reverse 5′ ATTCACTGTCCACAGTCACCACCA 3′
XBP-1s	Forward 5′ TGCTGAGTCCGCAGCAGGTG 3′
	Reverse 5′ GCTGGCAGGCTCTGGGGAAG 3′
GRP-78	Forward 5′ CATCACGCCGTCCTATGTCG 3′
	Reverse 5′ CGTCAAAGACCGTGTTCTCG 3′
IL-6	Forward 5′ AAAGATGTAGCCGCCCCAC 3′
	Reverse 5′ AGGCAAGTCTCCTCATTGAATCC 3′
TNF α	Forward 5′ CCCAGGCAGTCAGATCAT 3′
	Reverse 5′ TCAGCTCCACGCCATT 3′
β-Actin	Forward 5′ GTCTTCCCCTCCATCGT 3′
	Reverse 5′ CGTCGCCCACATAGGAAT 3′

Statistical Analysis

The data for continuous variables were expressed as mean ± standard deviation. Different variables between cases and controls were compared by the independent t-test. The Mann–Whitney U test was used to compare the pesticide level between cases and controls. The adjusted odds ratio (OR) with 95% confidence interval was calculated for defining the risk of T2DM by OCPs. The Spearman correlation matrix was used to analyze data for biochemical variables with pesticides, and gene–environment interaction. p values <0.05 were considered statistically significant. Collected data were analyzed using IBM SPSS software (version 21).

RESULTS

Demographic Characteristics of Study Groups

The demographic characteristics of the study subjects are presented in **Table 2**. The study subjects in both T2DM and NGT groups shared similar anthropometric characteristics with a comparable proportion of males and females ($p = 0.856$). The two groups did not share a significant age difference ($p = 0.409$). There were no significant differences in BMI ($p = 0.291$) between the study groups; however, their waist circumference differs significantly ($p \leq 0.001$). There was no significant difference observed in blood pressure between the groups ($p = 0.102$). The case group shared a higher history of familial diabetes ($p = 0.003$) as compared to controls. The socioeconomic status also differed significantly between the two groups (0.018); the subjects with T2DM belonged to a higher socioeconomic group compared to subjects of the control group.

Organochlorine Pesticide Analysis

The analysis of visceral adipose tissue samples disclosed the presence of various OCPs and their metabolites. By comparing the OCP levels, we found that every pesticide concentration was

TABLE 2 | Demographic characteristics of the T2DM and NGT groups.

Parameters	NGT (N = 70)	T2DM (N = 70)	p-value
Gender (male/female)	23/47	21/49	0.856
Age (years)	43.65 ± 9.22	44.9 ± 8.61	0.409
BMI (kg/m^2)	24.3 ± 3.3	24.9 ± 3.3	0.291
Waist circumference (cm)	88 ± 7.2	95.3 ± 10	**0.000*****
BP diastolic/systolic (mmHg)	80.4 ± 6.2/123.5 ± 8.1	81.5 ± 6.1/126.1 ± 10.9	0.102
Positive family history of T2DM	16	34	**0.003****
Socioeconomic status (I/II/III/IV/V)	0/0/4/16/50	0/8/7/14/41	**0.018***

*Values presented as mean ± SD; *p ≤ 0.05; **p ≤ 0.01; ***p ≤ 0.001.*

higher in the T2DM group as compared to the NGT group (**Table 3**); however, δ-HCH ($p \leq 0.001$), heptachlor ($p \leq 0.001$), endrin ($p \leq 0.001$), and p,p′-DDT ($p = 0.002$) levels were significantly higher in T2DM patients (**Figure 1**). Multivariable binary logistic regression, adjusted for confounding factors such as age, gender, BMI, and family history of T2DM, revealed that of these four pesticides, δ-HCH ($p = 0.003$) and endrin ($p \leq 0.001$) were positively associated with the risk of T2DM (**Table 4**).

The Correlation of Glycemic and Anthropometric Markers With OCP Levels

The correlation analysis also revealed the significant positive correlation of fasting and postprandial plasma glucose with δ-HCH, heptachlor, endrin, and p,p′-DDT (**Figure 2**). The waist circumference was also found to be positively correlated with δ-HCH ($r = 0.242$, $p = 0.004$), heptachlor ($r = 0.207$, $p = 0.014$), and endrin ($r = 0.211$, $p = 0.012$).

ER Stress and Pro-Inflammatory Marker Gene Expression

The parallel transcriptional and translational gene expression analysis revealed that all the ER stress markers except PERK were upregulated in visceral adipose tissue of T2DM patients as compared to NGT. A higher expression of both the pro-inflammatory markers was also observed in the T2DM group. The mRNA expressions of ATF-4, CHOP, IRE-1α, XBP-1s, and GRP-78 were 2.6-, 2.4-, 5.5-, 3.8-, 2.3-fold upregulated respectively in the T2DM group compared with the NGT group, whereas PERK was found to be 3.5-fold downregulated. Similarly, the mRNA expression of IL-6 and TNFα was found to be 4.6- and 1.9-fold significantly higher in T2DM subjects compared to NGT subjects, respectively. The protein expression of the respective genes was found to be in synchronization with their transcriptional expression (**Figure 3**).

The Gene–Gene Interaction

Interestingly, the mRNA expression of all the ER stress markers significantly and positively correlated among themselves and with both the pro-inflammatory markers (**Table 5**).

The Correlation of Glycemic and Anthropometric Markers With ER Stress and Pro-Inflammatory Gene Expression

By correlating the studied genes with fasting and postprandial plasma glucose, all genes except PERK and TNFα were found to be significantly positively correlated with plasma glucose indices.

TABLE 3 | Comparison of visceral adipose tissue OCP levels between the T2DM and NGT groups.

Organochlorine pesticides (ng/gm)	Controls (mean ± SD) N = 70	Cases (mean ± SD) N = 70	p-value
α-HCH	0.41 ± 1.07	0.90 ± 2.45	0.131
β-HCH	0.89 ± 2.54	1.25 ± 5.56	0.624
γ-HCH	0.86 ± 1.88	1.17 ± 2.88	0.451
δ-HCH	0.79 ± 0.50	2.70 ± 2.73	**0.000*****
Heptachlor	1.22 ± 1.17	4.20 ± 3.74	**0.000*****
Aldrin	0.57 ± 1.77	0.65 ± 2.34	0.830
HTEB	0.12 ± 0.45	0.36 ± 0.93	0.053
HTEA	1.81 ± 2.99	1.81 ± 4.70	0.244
o,p′-DDE	1.07 ± 2.71	1.82 ± 6.48	0.378
Endosulfan I	1.15 ± 4.23	1.77 ± 4.25	0.391
Dieldrin	0.09 ± 0.64	0.38 ± 1.09	0.062
p,p′-DDE	0.53 ± 2.19	1.11 ± 4.80	0.368
Endrin	0.60 ± 0.56	6.01 ± 5.08	**0.000*****
Endosulfan II	0.37 ± 1.89	0.61 ± 2.20	0.062
p,p′-DDD	1.74 ± 3.21	2.53 ± 3.80	0.193
o,p′-DDT	0.35 ± 0.99	0.72 ± 1.48	0.121
Methoxychlor	0.23 ± 1.22	0.62 ± 1.46	0.105
p,p′-DDT	1.13 ± 0.94	2.09 ± 1.77	**0.000*****

SD, standard deviation.
*****p ≤ 0.001.*

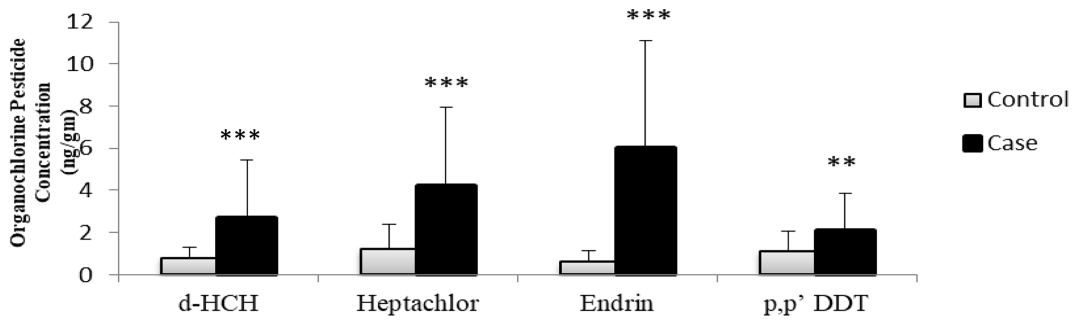

FIGURE 1 | Comparison of OCP levels (ng/gm) in the T2DM (N = 70) and NGT (N = 70) groups. **p ≤ 0.01; ***p ≤ 0.001.

TABLE 4 | The risk of development of T2DM with visceral adipose tissue accumulation of OCPs.

Organochlorine pesticides	Adjusted odds ratio	95% CI	p-value
δ-HCH	3.835	1.581–9.302	**0.003****
Endrin	4.127	1.905–8.838	**0.000*****
Heptachlor	1.309	0.928–1.846	0.125
p,p′-DDT	1.149	0.610–2.165	0.666

Adjusted for age, gender, BMI, and family history of T2DM.
CI, confidence interval.
***p ≤ 0.01; ***p ≤ 0.001.*

Interestingly, the weight of the study subjects was found to be positively correlated with mRNA expressions of CHOP and GRP-78. Waist circumference showed a significant positive correlation with ATF-4, CHOP and GRP-78, and BP (systolic and diastolic) with IRE-1α, and XBP-1s (**Table 6**).

The Gene–Environment Interaction

A significant positive correlation between transcriptional ER stress expression and OCPs was observed in this study. δ-HCH was positively correlated with the expression of ATF-4 (p = 0.010), IRE-1α (p = 0.030), and XBP-1s (p = 0.038) genes. Heptachlor was found to be positively correlated with IRE-1α (p = 0.044) and XBP-1s (p = 0.006) genes, whereas endrin was positively correlated with ATF-4 (p = 0.025), CHOP (p = 0.017), IRE-1α (p = 0.039), XBP-1s (p = 0.003), and GRP-78 (p = 0.020) genes (**Table 7**). However, a significant correlation of genes with p,p′-DDT was not observed in our study.

DISCUSSION

Our study demonstrated the presence of several OCPs and their metabolites in the visceral adipose tissue, of which δ-HCH, heptachlor, endrin, and p,p′-DDT were found to be significantly higher in the T2DM group as compared to the NGT group. These pesticides were positively associated with central adiposity, linking their obesogenic role in the etiology of T2DM. Nevertheless, the odds ratios of δ-HCH and endrin were significantly associated with the occurrence of T2DM. Our study is the first to show the interplay of ER stress with OCP compounds in T2DM and establish the possible cross talk between genetics and the environment. We found endrin to be correlated with all ER stress genetic markers except the PERK gene; however, we failed to establish the synergistic relation between pro-inflammatory markers and OCPs.

Upregulation of ER stress and pro-inflammatory markers in the visceral adipose tissue and their significant positive correlation with fasting and postprandial plasma glucose have been found in our study, which indicates that both of these pathways might be considered as an attractive target for T2DM.

Discussing the part of OCPs in diabetes, numerous epidemiological studies have associated OCP exposure with increased risks of obesity and/or T2DM (27–30). Due to their lipophilic nature, many pesticides tend to get accumulated in adipose tissue depots and therefore may interrupt the function of adipose tissue and promote obesity and T2DM (30, 31). The role of OCPs as endocrine-disrupting chemicals is also well known (32). In this study, we detected various OCP compounds in the visceral adipose tissue, but only four pesticides, δ-HCH, heptachlor, endrin, and p,p′-DDT, had a mean concentration significantly higher in T2DM subjects as compared to the NGT group. Of these four OCPs, δ-HCH and endrin were found to have a significantly higher relative risk associated with T2DM. These results have never been reported previously in an epidemiological study. However, as per the previous literature, β-HCH was strongly associated with T2DM (2), but δ-HCH has not been linked to T2DM yet, to the best of our knowledge. Heptachlor has been reported to increase the gluconeogenic enzymatic activity in the liver, which in turn upregulates the glucose synthesis from glycogen (33). Kamel et al. uncovered the cumulative effect of heptachlor in the pathogenesis of diabetes (34, 35). Higher serum endrin levels were observed in children with type 1 diabetes (36). Endrin was also found to stimulate

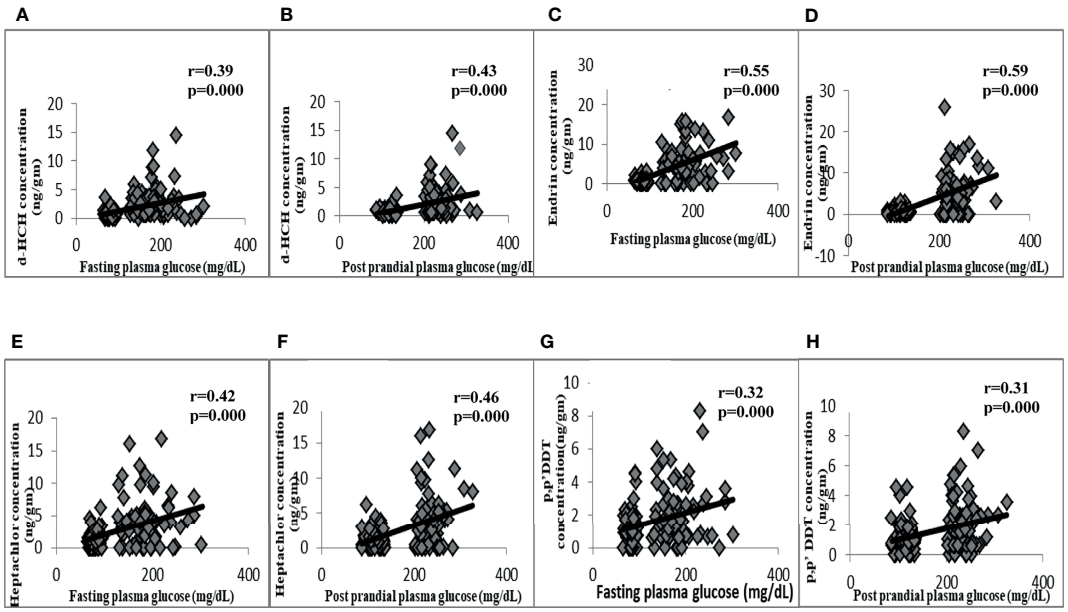

FIGURE 2 | Correlation of OCPs with plasma glucose indices. Positive correlation of fasting plasma glucose with d-HCH **(A)**, endrin **(C)**, heptachlor **(E)**, and p, p'DDT **(G)**. Positive correlation of postprandial plasma glucose with d-HCH **(B)**, endrin **(D)**, heptachlor **(F)**, and p,p'DDT **(H)**.

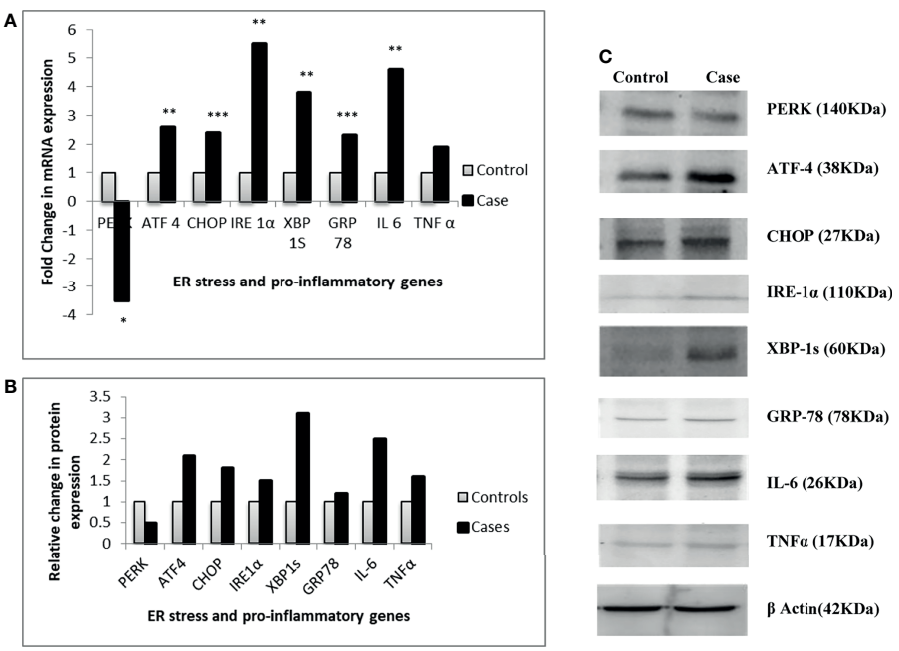

FIGURE 3 | Relative gene expression of ER stress and pro-inflammatory genes between thetwo groups. **(A)** Relative change in transcriptional expression of the genes. **(B)** Relative change in translational expression of the genes. **(C)** Western blot images of the genes. *p ≤ 0.05; **p ≤ 0.01; ***p ≤ 0.001.

lipid accumulation in adipocytes in an *in vitro* study (37). DDT and its metabolites being ubiquitous in the environment have long been linked to endocrine disruption; however, the actual mechanism remains unclear (38). A significant association of visceral adipose tissue levels of DDT with T2DM has also been reported (39). *In vitro* and *in vivo* studies have shown the inhibition of insulin-dependent glucose uptake when treated with an OCP mixture (40).

TABLE 5 | Correlation matrix showing the gene–gene interaction among ER stress and pro-inflammatory markers in visceral adipose tissue.

Gene	PERK	ATF-4	CHOP	IRE-1α	XBP-1s	GRP-78	IL-6	TNFα
	r	r	r	r	r	r	r	r
PERK	1	0.000	**0.274***	0.091	**0.249***	**0.272***	**0.409*****	**0.480*****
ATF-4	0.000	1	**0.404****	0.188	**0.279***	**0.458*****	0.176	**0.245***
CHOP	**0.274***	**0.404****	1	**0.379****	**0.471*****	**0.571*****	**0.600*****	**0.417*****
IRE-1α	0.091	0.188	**0.379****	1	**0.637*****	0.212	**0.443*****	**0.250***
XBP-1s	**0.249***	**0.279***	**0.471*****	**0.637*****	1	**0.279***	**0.420*****	**0.398****
GRP-78	**0.272***	**0.458*****	**0.571*****	0.212	**0.279***	1	**0.283***	**0.390****
IL-6	**0.409*****	0.176	**0.600*****	**0.443*****	**0.420*****	**0.283***	1	**0.580*****
TNF α	**0.480*****	**0.245***	**0.417*****	**0.250***	**0.398****	**0.390****	**0.580*****	1

r, correlation coefficient.
**p ≤ 0.05; **p ≤ 0.01; ***p ≤ 0.001.*

TABLE 6 | Correlation matrix showing the association of mRNA expression of ER stress and pro-inflammatory genes with anthropometric and clinical variables.

Variables	Δ Ct PERK	Δ Ct ATF-4	Δ Ct CHOP	Δ Ct IRE-1α	Δ Ct XBP-1s	Δ Ct GRP-78	Δ Ct IL-6	Δ Ct TNFα
	r	r	r	r	r	r	r	r
Height	0.11	0.14	0.4	0.24	0.15	0.4	0.32	0.2
Weight	0.08	0.32	0.5*	0.31	0.15	**0.53***	0.27	0.32
BMI	0.02	0.31	0.31	0.19	0.05	0.38	0.07	0.28
Waist circumference	0.02	**0.49***	**0.64****	0.38	0.26	**0.66*****	0.37	0.43
BP systolic	0.06	**0.59****	0.42	**0.64****	**0.66****	0.36	0.42	0.3
BP diastolic	0.02	0.44	0.23	**0.61***	**0.58****	0.14	0.28	0.21
Fasting plasma glucose	-0.29	**0.40*****	**0.41*****	**0.43*****	**0.46*****	**0.32****	**0.35*****	0.15
Postprandial plasma glucose	-0.23	**0.44*****	**0.42*****	**0.40*****	**0.50*****	**0.37*****	**0.29***	0.17

r, correlation coefficient.
**p ≤ 0.05; **p ≤ 0.01; ***p ≤ 0.001.*

TABLE 7 | Correlation matrix showing gene–environment interaction between ER stress markers and OCPs.

Genes/OCPs	δ-HCH	Heptachlor	Endrin
	r	r	r
ATF-4	0.284**	0.039	0.247*
CHOP	0.175	0.219	0.286*
IRE-1α	0.261*	0.243*	0.250*
XBP-1s	0.250*	0.328**	0.353**
GRP-78	0.167	0.145	0.280*

r, correlation coefficient.
**p ≤ 0.05; **p ≤ 0.01.*

By the correlation matrix findings, we brought to light the positive correlation of δ-HCH, heptachlor, endrin, and p,p'-DDT with fasting and postprandial plasma glucose. The levels of serum p,p′-DDE were reported to be positively correlated with fasting and postprandial plasma glucose and glycated hemoglobin as well (41). Al-Othman also reported the strong correlation of HCH with homeostatic model assessment for insulin resistance (HOMA-IR) (42); likewise, β-HCH serum levels were found to be elevated in patients with high serum glucose levels (5). Discussing the molecular axis in T2DM, accruing evidence revealed the increased unfolded protein response (UPR)-initiating molecules, PERK and IRE1α, in the adipose tissue of obese humans (19, 20, 43), and human islet cells from T2DM subjects as well (44). Nakatani et al. also showed that ER stress plays a crucial role in the insulin resistance found in diabetes and thus could be a potential therapeutic target for diabetes (45). Our results were consistent with the literature as the markers of the IRE-1α-XBP1-GRP-78 pathway, an early trigger of UPR, were overexpressed in the visceral adipose tissue of T2DM subjects. IRE-1α, a proximal ER stress sensor and central mediator of UPR, upregulates the expression of genes for GRP-78, an ER chaperon *via* splicing of a transcription activator, XBP-1, that ultimately facilitate cellular recovery. GRP-78 also acts as a central regulator for ER stress owing to its role in the induction of stress *via* three transmembrane ER stress sensors through a binding-release mechanism (46).

Considering the PERK-ATF-4-GRP-78 pathway, PERK was found to be downregulated in T2DM subjects in our study, which might be explained by the fact that, during acute or chronic gluco-lipotoxic stresses in secretory cells, pancreatic β cells, and adipocytes, in particular, excessive demand of protein synthesis arises (47). The increased frequency of transcription and translation was observed for the pathway's downstream markers, ATF-4, mainly responsible for the induction of a pro-apoptotic molecule, CHOP, indicating their activation in the visceral adipose tissue of T2DM subjects. CHOP usually remains expressed at lower levels in unstressed cells; however, under irredeemable ER stress, its expression raises significantly (48) but at the same time its pro-apoptotic effect may be dependent on the corresponding expression of other components of the UPR (49).

ER stress has been positively associated with chronic inflammation in humans as shown in many studies. A study by Lenin et al. in PBMC of T2DM patients as a surrogate cell model demonstrated the elevated ER stress markers and association of these stress molecules with pro-inflammatory markers, TNFα and IL-6 (50). Our results were consistent with previous results as gene expression levels of these two pro-

inflammatory markers in the visceral adipose tissue of T2DM subjects were significantly positively correlated with all ER stress markers.

Focusing on the gene expression correlation with blood glucose indices, our study results were consistent with the previously existing data as significant positive correlations between fasting and postprandial plasma glucose and ER stress markers (ATF-4, CHOP, IRE-1α, XBP-1, and GRP-78) and IL-6 were observed. Lenin et al. reported the positive correlations of ATF-4, CHOP, IRE-1α, XBP-1, and GRP-78 with glycated hemoglobin; also later, three markers were closely linked to fasting plasma sugar (50). The serum IL-6 levels have been associated with T2DM by many authors (51, 52), and elevation of this cytokine caused a direct influence on insulin signal intensity (53). However, any considerable association of PERK and TNFα was not found with plasma glucose levels. Being a well-recognized molecular link between obesity, declining insulin action, and eventually the development of T2DM, ER stress enacts in a complex way (54). Early experiments using cell culture and mouse models have demonstrated that excessive adiposity results in chronic ER stress, particularly in the liver and adipose tissue (21). The present study demonstrated the strong correlation of CHOP and GRP-78 with the body weight and waist circumference of the study subjects. Besides, ATF-4 was also significantly correlated with waist circumference. Recent studies have provided evidence that moderate weight loss promotes the amelioration of ER stress in the adipose tissue (20, 55).

Addressing the gene–environment interaction, only a few studies have reported the correlation between several types of insecticides and ER stress. An *in-vitro* study reported the GRP-78 upregulation by endosulfan treatment (56). The existence of a correlation between transcriptional ER stress markers and OCPs in our study suggests some interplay between the two. The results indicate that upregulation of these genes may occur in the presence of a higher concentration of OCP levels in the adipose tissue or its reverse may also be true. Our results demonstrated a positive correlation of δ-HCH with ATF-4, IRE-1α, and XBP-1s, heptachlor with IRE-1α, and XBP-1s, whereas endrin correlated with all ER stress markers except PERK. We did not observe any significant association of OCPs with any of the pro-inflammatory markers. Taken together, these data demonstrate that there might be considerable cross talk between the environmental signaling and cellular pathways. Obesogenic effects of OCPs may contribute to the development of cellular stress which in the long run may be responsible for the pathogenesis of T2DM.

Although there are inadequate data on the underlying mechanisms of OCP toxicity in relation to disease etiology, multiple factors for pollutant exposure and physiological responses also cause some limitations to the study. Concurrently, because of the cross-sectional nature of our work, the study could not reveal any causal relationship between ER stress and T2DM, and for this, we need prospective follow-up studies. In addition, further studies using a larger sample size are needed to identify the association between ER stress and other toxic compounds and confirm their role in the etiology of T2DM.

CONCLUSION

The existence of the correlation between OCPs and ER stress markers suggests some interplay between genetics and the environmental factors. The upregulation of genes involved in ER stress may occur in the presence of higher concentration of OCPs levels in the visceral adipose tissue. The study shows the potential role of OCPs in the development of T2DM *via* disrupting the ER stress pathway.

DATA AVAILABILITY STATEMENT

The raw data supporting the conclusions of this article will be made available by the authors, without undue reservation.

ETHICS STATEMENT

The study involving human participants were reviewed and approved by the Institutional Ethics Committee-Human Research, University College of Medical Sciences. The patients/participants provided their written informed consent to participate in this study.

AUTHOR CONTRIBUTIONS

NT: conceptualization, methodology, data curation, writing—original draft preparation. BD: conceptualization, supervision, visualization. SM: supervision, visualization. VA: supervision, visualization, sample collection. SG: supervision, visualization, sample collection. All authors contributed to the article and approved the submitted version.

FUNDING

This study was supported by a Junior Research Fellowship provided by the University Grant Commission (no. 132003443).

REFERENCES

1. Tyagi S, Siddarth M, Mishra BK, Banerjee BD, Urfi AJ, Madhu SV. High Levels of Organochlorine Pesticides in Drinking Water as a Risk Factor for Type 2 Diabetes: A Study in North India. *Environ Pollut* (2021) 271:116287. doi: 10.1016/j.envpol.2020.116287
2. Daniels SI, Chambers JC, Sanchez SS, Merrill MA, Hubbard AE, Macherone A, et al. Elevated Levels of Organochlorine Pesticides in South Asian

Immigrants Are Associated With an Increased Risk of Diabetes. *J Endocr Soc* (2018) 2(8):832–41. doi: 10.1210/js.2017-00480
3. Taylor KW, Novak RF, Anderson HA, Birnbaum LS, Blystone C, Devito M, et al. Evaluation of the Association Between Persistent Organic Pollutants (POPs) and Diabetes in Epidemiological Studies: A National Toxicology Program Workshop Review. *Environ Health Perspect* (2013) 121(7):774–83. doi: 10.1289/ehp.1205502
4. Lee DH, Lind PM, Jacobs DR, Salihovic S, Van Bavel B, Lind L. Polychlorinated Biphenyls and Organochlorine Pesticides in Plasma Predict Development of Type 2 Diabetes in the Elderly: The Prospective Investigation of the Vasculature in Uppsala Seniors (PIVUS) Study. *Diabetes Care* (2011) 34(8):1778–84. doi: 10.2337/dc10-2116
5. Cox S, Niskar AS, Venkat Narayan KM, Marcus M. Prevalence of Self-Reported Diabetes and Exposure to Organochlorine Pesticides Among Mexican Americans: Hispanic Health and Nutrition Examination Survey, 1982-1984. *Environ Health Perspect* (2007) 115(12):1747–52. doi: 10.1289/ehp.10258
6. Tyagi S, Mishra BK, Sharma T, Tawar N, Urfi A, Banerjee B, et al. Level of Organochlorine Pesticide in Prediabetic and Newly Diagnosed Diabetes Mellitus Patients With Varying Degree of Glucose Intolerance and Insulin Resistance Among North Indian Population. *Diabetes Metab J* (2021) 45 (4):558–68. doi: 10.4093/DMJ.2020.0093
7. Taiwo AM. A Review of Environmental and Health Effects of Organochlorine Pesticide Residues in Africa. *Chemosphere* (2019) 220:1126–40. doi: 10.1016/j.chemosphere.2019.01.001
8. Jayaraj R, Megha P, Sreedev P. Review Article. Organochlorine Pesticides, Their Toxic Effects on Living Organisms and Their Fate in the Environment. *Interdiscip Toxicol* (2016) 9(3-4):90–100. doi: 10.1515/intox-2016-0012
9. Kim KH, Kabir E, Jahan SA. Exposure to Pesticides and the Associated Human Health Effects. *Sci Total Environ* (2017) 575:525–35. doi: 10.1016/j.scitotenv.2016.09.009
10. Xiao X, Clark JM, Park Y. Potential Contribution of Insecticide Exposure and Development of Obesity and Type 2 Diabetes. *Food Chem Toxicol* (2017) 105:456–74. doi: 10.1016/j.fct.2017.05.003
11. Ali U, Syed JH, Malik RN, Katsoyiannis A, Li J, Zhang G, et al. Organochlorine Pesticides (OCPs) in South Asian Region: A Review. *Sci Total Environ* (2014) 476-477:705–17. doi: 10.1016/j.scitotenv.2013.12.107
12. Chakraborty P, Zhang G, Li J, Xu Y, Liu X, Tanabe S, et al. Selected Organochlorine Pesticides in the Atmosphere of Major Indian Cities: Levels, Regional *Versus* Local Variations, and Sources. *Environ Sci Technol* (2010) 44(21):8038–43. doi: 10.1021/es102029t
13. Kumar KVSH, Sharma R, Manrai M, Sood AK. Visceral Adipose Tissue as a Risk Factor for Diabetes Mellitus in Patients With Chronic Pancreatitis: A Cross-Sectional, Observational Study. *Diabetes Ther* (2017) 8(5):1057–64. doi: 10.1007/s13300-017-0304-1
14. Goyal R, Faizy AF, Siddiqui SS, Singhai M. Evaluation of TNF-α and IL-6 Levels in Obese and Non-Obese Diabetics: Pre- and Postinsulin Effects. *N Am J Med Sci* (2012) 4(4):180–4. doi: 10.4103/1947-2714.94944
15. Hasnain SZ, Lourie R, Das I, Chen AC, Mcguckin MA. The Interplay Between Endoplasmic Reticulum Stress and Inflammation. *Immunol Cell Biol* (2012) :260–70. doi: 10.1038/icb.2011.112
16. Back SH, Kaufman RJ. Endoplasmic Reticulum Stress and Type 2 Diabetes. *Annu Rev Biochem* (2012) 81:767–93. doi: 10.1146/annurev-biochem-072909-095555
17. Eizirik DL, Cardozo AK, Cnop M. The Role for Endoplasmic Reticulum Stress in Diabetes Mellitus. *Endocr Rev* (2008) 29(1):42–61. doi: 10.1210/er.2007-0015
18. Hetz C. The Unfolded Protein Response: Controlling Cell Fate Decisions Under ER Stress and Beyond. *Nat Rev Mol Cell Biol* (2012) 13(2):89–102. doi: 10.1038/nrm3270
19. Boden G, Duan X, Homko C, Molina EJ, Song WW, Perez O, et al. Increase in Endoplasmic Reticulum Stress-Related Proteins and Genes in Adipose Tissue of Obese, Insulin-Resistant Individuals. *Diabetes* (2008) 57(9):2438–44. doi: 10.2337/db08-0604
20. Gregor MF, Yang L, Fabbrini E, Mohammed BS, Eagon JC, Hotamisligil GS, et al. Endoplasmic Reticulum Stress is Reduced in Tissues of Obese Subjects After Weight Loss. *Diabetes* (2009) 58(3):693–700. doi: 10.2337/db08-1220
21. Özcan U, Cao Q, Yilmaz E, Lee A-H, Iwakoshi NN, Ozdelen E, et al. Endoplasmic Reticulum Stress Links Obesity, Insulin Action, and Type 2 Diabetes. *Sci (80-)* (2004) 306(5695):457–61. doi: 10.1126/science.1103160
22. Jin W, Patti ME. Genetic Determinants and Molecular Pathways in the Pathogenesis of Type 2 Diabetes. *Clin Sci* (2009) 116(2):99–111. doi: 10.1042/CS20080090
23. Association AD. Classification and Diagnosis of Diabetes: Standards of Medical Care in Diabetes-2020. *Diabetes Care* (2020) 43(Supplement 1): S14–31. doi: 10.2337/dc20-S002
24. Wani R. Socioeconomic Status Scales-Modified Kuppuswamy and Udai Pareekh's Scale Updated for 2019. *J Fam Med Prim Care* (2019) 8(6):1846. doi: 10.4103/jfmpc.jfmpc_288_19
25. Bush B, Snow J, Koblintz R. Polychlorobiphenyl (PCB) Congeners, P,P′-DDE, and Hexachlorobenzene in Maternal and Fetal Cord Blood From Mothers in Upstate New York. *Arch Environ Contam Toxicol* (1984) 13(5):517–27. doi: 10.1007/BF01056331
26. Livak KJ, Schmittgen TD. Analysis of Relative Gene Expression Data Using Real-Time Quantitative PCR and the 2-ΔΔCT Method. *Methods* (2001) 25 (4):402–8. doi: 10.1006/meth.2001.1262
27. Meek EC, Jones DD, Crow JA, Wills RW, Cooke WH, Chambers JE. Association of Serum Levels of P,P'- Dichlorodiphenyldichloroethylene (DDE) With Type 2 Diabetes in African American and Caucasian Adult Men From Agricultural (Delta) and non-Agricultural (Non-Delta) Regions of Mississippi. *J Toxicol Environ Heal - Part A Curr Issues* (2019) 82(6):387–400. doi: 10.1080/15287394.2019.1610678
28. Tang M, Chen K, Yang F, Liu W. Exposure to Organochlorine Pollutants and Type 2 Diabetes: A Systematic Review and Meta-Analysis. *PloS One* (2014) 9 (10). doi: 10.1371/journal.pone.0085556
29. Karami-Mohajeri S, Abdollahi M. Toxic Influence of Organophosphate, Carbamate, and Organochlorine Pesticides on Cellular Metabolism of Lipids, Proteins, and Carbohydrates: A Systematic Review. *Hum Exp Toxicol* (2011) 30(9):1119–40. doi: 10.1177/0960327110388959
30. Tawar N, Banerjee B, Mishra BK, Sharma T, Tyagi S, Madhu SV, et al. Adipose Tissue Levels of DDT as Risk Factor for Obesity and Type 2 Diabetes Mellitus. *Indian J Endocrinol Metab* (2021) 25(2):160–5. doi: 10.4103/IJEM.IJEM_198_21
31. Gutgesell RM, Tsakiridis EE, Jamshed S, Steinberg GR, Holloway AC. Impact of Pesticide Exposure on Adipose Tissue Development and Function. *Biochem J* (2020) 477(14):2639–53. doi: 10.1042/BCJ20200324
32. Kumar M, Sarma DK, Shubham S, Kumawat M, Verma V, Prakash A, et al. Environmental Endocrine-Disrupting Chemical Exposure: Role in Non-Communicable Diseases. *Front Public Heal* (2020) 8:553850/BIBTEX. doi: 10.3389/FPUBH.2020.553850/BIBTEX
33. Komori M, Nishio K, Kitada M, Shiramatsu K, Muroya K, Soma M, et al. Fetus-Specific Expression of a Form of Cytochrome P-450 in Human Livers. *Biochemistry* (1990) 29(18):4430–3. doi: 10.1021/bi00470a024
34. Montgomery MP, Kamel F, Saldana TM, Alavanja MCR, Sandler DP. Incident Diabetes and Pesticide Exposure Among Licensed Pesticide Applicators: Agricultural Health Study, 1993-2003. *Am J Epidemiol* (2008) 167 (10):1235–46. doi: 10.1093/aje/kwn028
35. Park SK, Son HK, Lee SK, Kang JH, Chang YS, Jacobs DR, et al. Relationship Between Serum Concentrations of Organochlorine Pesticides and Metabolic Syndrome Among Non-Diabetic Adults. *J Prev Med Public Heal* (2010) 43 (1):1–18. doi: 10.3961/jpmph.2010.43.1.1
36. El-morsi DA, Rahman RHA, Abou-arab AAK. Pesticides Residues in Egyptian Diabetic Children : A Preliminary Study Journal of Clinical Toxicology. *J Clinic Toxicol* (2012) 2(6). doi: 10.4172/2161-0495.1000138
37. Sargis RM, Johnson DN, Choudhury RA, Brady MJ. Environmental Endocrine Disruptors Promote Adipogenesis in the 3T3-L1 Cell Line Through Glucocorticoid Receptor Activation. *Obesity* (2010) 18(7):1283–8. doi: 10.1038/oby.2009.419
38. Zhuang S, Zhang J, Wen Y, Zhang C, Liu W. Distinct Mechanisms of Endocrine Disruption of DDT-Related Pesticides Toward Estrogen Receptor α and Estrogen-Related Receptor γ. *Environ Toxicol Chem* (2012) 31(11):2597–605. doi: 10.1002/etc.1986
39. Kim K, Lee Y, Geol S, Lee I-K, Lee H-J, Kim J-H, et al. Chemosphere Associations of Organochlorine Pesticides and Polychlorinated Biphenyls in Visceral *vs.* Subcutaneous Adipose Tissue With Type 2 Diabetes and Insulin Resistance. *Chemosphere* (2014) 94:151–7. doi: 10.1016/j.chemosphere.2013.09.066

40. Ruzzin J, Petersen R, Meugnier E, Madsen L, Lock E-J, Lillefosse H, et al. Persistent Organic Pollutant Exposure Leads to Insulin Resistance Syndrome. *Environ Health Perspect* (2010) 118(4):465–71. doi: 10.1289/ehp.0901321
41. Gupta S, Mishra BK, Banerjee BD, Jhamb R, Aslam M, Madhu SV. Effect of Postprandial Triglycerides on DDT/ppDDE Levels in Subjects With Varying Degree of Glucose Intolerance. *Eur J Pharm Sci* (2021) 157. doi: 10.1016/J.EJPS.2020.105635
42. Al-Othman AA, Abd-Alrahman SH, Al-Daghri NM. DDT and its Metabolites are Linked to Increased Risk of Type 2 Diabetes Among Saudi Adults: A Cross-Sectional Study. *Environ Sci Pollut Res* (2014) 22(1):379–86. doi: 10.1007/s11356-014-3371-0
43. Alhusaini S, McGee K, Schisano B, Harte A, McTernan P, Kumar S, et al. Lipopolysaccharide, High Glucose and Saturated Fatty Acids Induce Endoplasmic Reticulum Stress in Cultured Primary Human Adipocytes: Salicylate Alleviates This Stress. *Biochem Biophys Res Commun* (2010) 397 (3):472–8. doi: 10.1016/j.bbrc.2010.05.138
44. Huang CJ, Lin CY, Haataja L, Gurlo T, Butler AE, Rizza RA, et al. High Expression Rates of Human Islet Amyloid Polypeptide Induce Endoplasmic Reticulum Stress-Mediated β-Cell Apoptosis, a Characteristic of Humans With Type 2 But Not Type 1 Diabetes. *Diabetes* (2007) 56(8):2016–27. doi: 10.2337/db07-0197
45. Nakatani Y, Kaneto H, Kawamori D, Yoshiuchi K, Hatazaki M, Matsuoka T-A, et al. Involvement of Endoplasmic Reticulum Stress in Insulin Resistance and Diabetes. *J Biol Chem* (2005) 280: (1):847–51. doi: 10.1074/jbc.M411860200
46. Lee AS. The ER Chaperone and Signaling Regulator GRP78/BiP as a Monitor of Endoplasmic Reticulum Stress. *Methods* (2005) 35(4):373–81. doi: 10.1016/j.ymeth.2004.10.010
47. Komura T, Sakai Y, Honda M, Takamura T, Matsushima K, Kaneko S. CD14+ Monocytes Are Vulnerable and Functionally Impaired Under Endoplasmic Reticulum Stress in Patients With Type 2 Diabetes. *Diabetes* (2010) 59 (3):634–43. doi: 10.2337/db09-0659
48. Oyadomari S, Mori M. Roles of CHOP/GADD153 in Endoplasmic Reticulum Stress. *Cell Death Differ* (2004) 11(4):381–9. doi: 10.1038/sj.cdd.4401373
49. Williams BL, Lipkin WI. Endoplasmic Reticulum Stress and Neurodegeneration in Rats Neonatally Infected With Borna Disease Virus. *J Virol* (2006) 80(17):8613–26. doi: 10.1128/jvi.00836-06
50. Lenin R, Sankaramoorthy A, Mohan V, Balasubramanyam M. Altered Immunometabolism at the Interface of Increased Endoplasmic Reticulum (ER) Stress in Patients With Type 2 Diabetes. *J Leukoc Biol* (2015) 98(4):615–22. doi: 10.1189/jlb.3a1214-609r
51. Phosat C, Panprathip P, Chumpathat N, Prangthip P, Chantratita N, Soonthornworasiri N, et al. Elevated C-Reactive Protein, Interleukin 6, Tumor Necrosis Factor Alpha and Glycemic Load Associated With Type 2 Diabetes Mellitus in Rural Thais: A Cross-Sectional Study. *BMC Endocr Disord* (2017) 17(1):44. doi: 10.1186/s12902-017-0189-z
52. Belfki H, Ben Ali S, Bougatef S, Ahmed DB, Haddad N, Jmal A, et al. Association Between C-Reactive Protein and Type 2 Diabetes in a Tunisian Population. *Inflammation* (2012) 35(2):684–9. doi: 10.1007/s10753-011-9361-1
53. Lainampetch J, Panprathip P, Phosat C, Chumpathat N, Prangthip P, Soonthornworasiri N, et al. Association of Tumor Necrosis Factor Alpha, Interleukin 6, and C-Reactive Protein With the Risk of Developing Type 2 Diabetes: A Retrospective Cohort Study of Rural Thais. *J Diabetes Res* (2019) 2019. doi: 10.1155/2019/9051929
54. Wang M, Li Z, Li C, Liu Y, Jiang H, Jia L, et al. Endoplasmic Reticulum Stress in Adipose Tissue at the Intersection of Childhood Obesity-Associated Type 2 Diabetes/Insulin Resistance and Atherosclerosis. *Int J Clin Exp Med* (2019) 12 (4):3095–106.
55. López-Domènech S, Abad-Jiménez Z, Iannantuoni F, de Marañón AM, Rovira-Llopis S, Morillas C, et al. Moderate Weight Loss Attenuates Chronic Endoplasmic Reticulum Stress and Mitochondrial Dysfunction in Human Obesity. *Mol Metab* (2019) 19:24–33. doi: 10.1016/j.molmet.2018.10.005
56. Skandrani D, Gaubin Y, Vincent C, Beau B, Murat JC, Soleihavoup J-P, et al. Relationship Between Toxicity of Selected Insecticides and Expression of Stress Proteins (HSP, GRP) in Cultured Human Cells: Effects of Commercial Formulations *Versus* Pure Active Molecules. *Biochim Biophys Acta - Gen Subj* (2006) 1760(1):95–103. doi: 10.1016/j.bbagen.2005.09.015

Conflict of Interest: The authors declare that the research was conducted in the absence of any commercial or financial relationships that could be construed as a potential conflict of interest.

Publisher's Note: All claims expressed in this article are solely those of the authors and do not necessarily represent those of their affiliated organizations, or those of the publisher, the editors and the reviewers. Any product that may be evaluated in this article, or claim that may be made by its manufacturer, is not guaranteed or endorsed by the publisher.

frontiers | Frontiers in Endocrinology

ORIGINAL RESEARCH
published: 13 May 2022
doi: 10.3389/fendo.2022.864299

Menopausal Transition: Prospective Study of Estrogen Status, Circulating MicroRNAs, and Biomarkers of Bone Metabolism

*Jiri Baloun[1,2], Aneta Pekacova[1,2], Laszlo Wenchich[1], Hana Hruskova[3,4], Ladislav Senolt[1,2], Xiao Svec[1], Karel Pavelka[1,2] and Jan J. Stepan[1,2]**

[1] Institute of Rheumatology, Prague, Czechia, [2] Department of Rheumatology, First Faculty of Medicine, Charles University in Prague, Prague, Czechia, [3] Department of Obstetrics and Gynecology, First Faculty of Medicine, Charles University in Prague, Prague, Czechia, [4] General University Hospital in Prague, Prague, Czechia

Objective: Osteoporosis is associated with an impaired balance between bone resorption and formation, which in turn leads to bone loss and fractures. Many recent studies have underlined the regulatory role of microRNAs (miRNAs) in bone remodeling processes and their potential as biomarkers of osteoporosis. The purpose of this study was to prospectively examine the association of circulating miRNAs and bone biomarkers with estrogen status in women before and after oophorectomy, as well as in oophorectomized women on estrogen therapy.

Methods: In this prospective study, we included 11 women before oophorectomy and hysterectomy and at 201 ± 24 days after the surgery. Another 11 women were evaluated 508 ± 127 days after oophorectomy and hysterectomy and after an additional 203 ± 71 days of estradiol treatment. Serum miRNAs were profiled by sequencing. Estrogen status and biomarkers of bone metabolism were quantified. Bone mineral density was assessed in the lumbar spine.

Results: Our analysis revealed 17 miRNAs associated with estrogen levels. Of those miRNAs that were upregulated with estrogen deficiency and downregulated after estrogen therapy, miR-422a correlated with serum beta-carboxy-terminal type I collagen crosslinks (β-CTX) and procollagen 1 N-terminal propeptide (P1NP); and miR-1278 correlated with serum β-CTX, P1NP, osteocalcin, sclerostin, and Dickkopf-1(Dkk1). In contrast, we found an inverse association of miR-24-1-5p with estrogen status and a negative correlation with serum β-CTX, P1NP, osteoprotegerin, and sclerostin levels.

Conclusion: The reported miRNAs associated with estrogen status and bone metabolism could be potential biomarkers of bone pathophysiology and would facilitate studies on the prevention of postmenopausal osteoporosis. Our findings require validation in an extended cohort.

Keywords: estrogen, circulating miRNA, bone remodeling, oophorectomy, osteoporosis prevention and control

OPEN ACCESS

Edited by:
Daniela Merlotti, University of Siena, Italy

Reviewed by:
Athanasios D. Anastasilakis, 424 General Military Hospital, Greece
Bente L. Langdahl, Aarhus University, Denmark

***Correspondence:**
Jan J. Stepan
stepan@revma.cz

Specialty section:
This article was submitted to Bone Research, a section of the journal Frontiers in Endocrinology

Received: *28 January 2022*
Accepted: *28 March 2022*
Published: *13 May 2022*

Citation:
Baloun J, Pekacova A, Wenchich L, Hruskova H, Senolt L, Svec X, Pavelka K and Stepan JJ (2022) Menopausal Transition: Prospective Study of Estrogen Status, Circulating MicroRNAs, and Biomarkers of Bone Metabolism. Front. Endocrinol. 13:864299. doi: 10.3389/fendo.2022.864299

INTRODUCTION

Osteoporosis is a skeletal disease characterized by low bone mass and microarchitectural deterioration, which are related to unbalanced bone resorption and bone formation (1), leading to bone fragility and susceptibility to fracture (2). The consequences of osteoporosis substantially increase the consumption of medical and economic resources worldwide (3). Until now, many expression profiling studies have revealed that bone remodeling processes are well-tuned at the transcriptional level and controlled by noncoding RNAs, especially long non-coding RNAs and microRNAs (miRNAs) (4–6).

MiRNAs are short RNAs of typically 18-22 nucleotides that operate as post-transcriptional regulators of protein-coding genes and the non-coding genome (7). They regulate many developmental and functional pathways, and their aberrant expression has been associated with various disorders (8), including osteoporosis (7, 9). In particular, several miRNAs with distinguishable expression profiles have been identified in bone samples from patients with osteoporosis and those with low impact fractures in most studies (10–15). Generally, during the bone remodeling process, miRNAs regulate differentiation of osteoblast and osteoclast and bone formation by targeting the regulators of osteogenesis or osteoclastogenesis, namely, transcription factors and signaling pathways (7, 16, 17). MiRNAs can escape from tissues into the bloodstream and become circulating miRNAs, providing additional information related to bone metabolism (7). The existing literature has mainly assessed the profiles of circulating miRNAs in patients with established osteoporosis and low-impact fractures. Recent research has drawn attention to the association of circulating miRNAs with bone remodeling in menstrual cessation (18). In the early postmenopausal period, the bone mineral density is not decreased but the bone resorption rate excessively exceeds new bone formation, posing a possible osteoporosis risk (19). The purpose of this study was to prospectively examine the association of circulating miRNAs and bone biomarkers with estrogen status in women before and after oophorectomy, as well as in oophorectomized women on estrogen therapy.

PATIENTS AND METHODS

Patients

Between July 2018 and May 2019, 22 women who had been consecutively referred for bone status assessment through the Department of Obstetrics and Gynecology, General University Hospital in Prague, and had hysterectomy and bilateral oophorectomy before menopause were included in the present study. Surgery was indicated for benign gynecological diseases, including leiomyoma (14), metrorrhagia (3), breast cancer gene mutation (3), dysplasia of the cervix (1), and benign ovarian cyst (1). Of these subjects, 11 women were evaluated 18 ± 10 days before oophorectomy and hysterectomy and 201 ± 24 days after the surgery. None of these women received hormone therapy after surgery. The other 11 women who had previously undergone oophorectomy and hysterectomy were evaluated at baseline 508 ± 127 days after the surgery. Hormone treatment was initiated by their gynecologist. A check-up was performed after 203 ± 71 days of oral hormonal treatment, corresponding to 1 mg of estradiol per day.

Complete medical histories and dietary questionnaires were obtained from all subjects. No subject had bone- or calcium-related metabolic disease or received medications that are known to affect bone or calcium metabolism. No woman had a history of alcohol abuse, diabetes mellitus, active neoplastic disease, liver disease, known endocrine and rheumatologic disease, immunosuppressive treatment, treatment with corticosteroids, aromatase inhibitors, anti-osteoporotic drugs, anticonvulsants, or a history of fragility fractures or had previously received hormone replacement therapy. Subjects were advised to maintain their usual physical activity and dietary pattern throughout the study.

The study was approved by the Institutional Review Board at the Institute of Rheumatology, Prague, Czech Republic. All participants signed written informed consent forms to participate and agreed to DXA and blood tests. All study procedures were carried out in compliance with the laws and regulations governing the use of human subjects (Declaration of Helsinki) (20).

Blood Collection

Venous blood samples were obtained after an overnight fast from each subject at baseline and follow-up visits for laboratory analyses. To separate the serum, whole blood was collected into commercially available collection tubes. After one hour of clotting, the blood was centrifuged at 2000xg for 20 minutes. Serum (supernatant) was transferred into a new tube and frozen at -70°C until further processing.

MiRNA Isolation

MiRNAs were extracted from 200 μL of blood serum using NucleoSpin miRNA Plasma (Macherey-Nagel) according to the manufacturer's protocol. Isolated miRNAs were not quantified since concentrations were below the detection limits of the NanoDrop 2000. Follow-up procedures were conducted with undiluted samples.

Massively Parallel Sequencing

Library Preparation

Libraries for massively parallel sequencing (MPS) were prepared from 10.5 μL of isolated miRNAs using Kit v3 (Bioo Scientific) according to the manufacturer's protocol. Fragments after the amplification step were analyzed using a Fragment Analyzer (Advanced Analytical), and fragments of the miRNA library (145 bp) were quantified. Samples were pooled in equal concentrations of miRNA library fragments, which were isolated using the Pippin Prep system with 3% agarose (Sage Science) before sequencing. The isolated fragments were quantified using a Qubit 2.0 fluorometer (Thermo Fisher Scientific) and were used for sequencing on a NextSeq 500 (Illumina) according to the manufacturer's protocol.

Bioinformatics Analyses

Adaptor sequences in MPS data were identified and removed with Cutadapt (v2.5) software (21). Only high-quality reads with a length between 16 and 28 bp after adapter trimming were retained as potential miRNA reads. The quality of both raw and processed reads was evaluated using FastQC software (22).

Count-based miRNA expression data were generated by the Chimira tool (23) from FASTQ files. All sequences were adapter trimmed and mapped against miRBase v22 (24), allowing up to two mismatches per sequence. All samples were evaluated for differential expression using DESeq2 (25). Further analyses were performed using R/Bioconductor packages. Raw data and annotated sequences of the small RNA libraries were uploaded to the GEO database.

DESeq2 computed the normalized miRNA-read count, dispersion, and base mean (the average of the normalized count values, divided by the size factors, taken over all samples). The dispersion can be understood as a squared coefficient of variation and the mean dispersion value of 26.04 represents the coefficient of variation of 4.49. miRNAs with a base mean < 10 were indistinguishable from the sampling noise and were filtered out of the dataset.

Bone Densitometry

The areal bone mineral density (aBMD) of the lumbar spine (LS-BMD) was evaluated using dual-energy X-ray absorptiometry (DXA) (GE Healthcare Lunar software version 14.1) and expressed in grams/cm^2 and T-score. The T-score was calculated using the National Health and Nutrition Examination Survey (NHANES) of young women as a reference. Quality control assurance measurements were performed following the manufacturer's recommendations. The short-term *in vivo* precision error for the lumbar spine (L1–L4) was 0.7%; the long-term *in vivo* precision error was 0.31%. Trained examiners with extensive experience conducted the measurements.

Biochemical Analysis

The concentrations of total serum calcium, phosphate, glucose, total alkaline phosphatase, γ-glutamyltransferase (GGT), thyroid-stimulating hormone (TSH), 1-84 amino acid fragment of parathyroid hormone (intact PTH), 25(OH)D, beta-carboxy-terminal type I collagen crosslinks (β-CTX), procollagen 1 N-terminal propeptide (P1NP), osteocalcin, estradiol, and FSH were determined using the Beckman Coulter AU 680 (Beckman Coulter, USA), Roche cobas e601 (Roche, Switzerland), and Liaison XL (Diasorin, Italy) analytical systems. The plasma estradiol measuring range was 18.4-11,000 pmol/l with intra- and interassay CV < 12%. The plasma FSH measuring range was 0.1-200 IU/l with intra- and interassay CV < 6%. The serum β-CTX measuring range was 0.01-6 μg/l with intra- and interassay CV < 6%. The serum PINP measuring range was 5-1200 μg/l with intra- and interassay CV < 6%. The estimated glomerular filtration rate (eGFR) was calculated (26). Serum sclerostin was assessed using the Bioactive Sclerostin ELISA (Biomedica, Austria), and the measuring range was 10-320 pmol/l with intra- and interassay CV < 5%. Serum Dickkopf-1 (DKK1) was analyzed using the DKK-1 ELISA (Biomedica, Austria), and the measuring range was 10-160 pmol/l with intra- and interassay CV < 3%. Serum osteoprotegerin was measured using the Human Osteoprotegerin ELISA (Biovendor, Czech Republic), and the measuring range was 1.5-60 pmol/l with intra- and interassay CV < 7%.

Biostatistical Analyses

Characteristics of the population were computed using SigmaPlot version 14.0, Systat Software, San Jose, CA, USA. The Kolmogorov–Smirnov test was applied to assess the normality of the data. Data with a normal distribution are presented as the mean ± SD, while nonparametric data are presented as the median and quartiles. The paired t-test was used to compare biochemical variables, depending on the normality of the variables. Univariate analysis with Pearson correlation was used. Statistical significance was defined as a p-value < 0.05.

DESeq2 algorithm provided a matrix of normalized read counts, which were analyzed with RStudio software and relevant packages (27, 28). Since miRNAs had normalized read count equal to zero in several samples, we employed glmmTMB R package (28), in which we can specify fixed and random effects models for the conditional and zero-inflated components of the model with negative binomial assumption. Using this R extension, we fitted a GLMM-NB, using the normalized read count of miRNAs as the outcome variable, with fixed effects of the level of estrogen (or the biomarker of bone metabolism) and follicle-stimulating hormone (FSH) as a confounding variable. We also fitted a random-effects structure, which includes a random intercept for patient ID. To test differential miRNA expression between patients with optimal and low estrogen levels (estrogen status) or the association with the biomarkers of bone remodelling (adjusted with FSH level and a random intercept for patient ID), the following model was used:

$$\log(\mu_{ij}) = (\beta_0 + \gamma_{0j}) + \beta_1(estrogen\ \ status\ \ or\ \ biomarker) + \beta_2(FSH) + \epsilon_{ij}$$

$$normalized\ \ read\ \ counts \sim NB(u_{ij}, \theta)$$

where i - the miRNA; j – patients ID; β – regression coefficient; γ – random parameter; and ϵ – error. The effect of estrogen level was represented as the incidence rate ratio (IRR), which means that the number of expected observations on the miRNAs' count changes by the value of IRR if the estrogen level changes from optimal to low. The association of the bone modelling biomarkers is represented as the slope, which is the change of normalized read counts if the value of the biomarkers changes by one unit. The adjusted p-value was calculated using Benjamini-Hochberg (BH) method (29) and indicated in **Supplementary Tables**.

RESULTS

Demographic and Clinical Characteristics

At baseline, no differences were observed in age, body mass index (BMI), serum 1-84 amino acid fragment of parathyroid hormone (intact PTH), creatinine, glucose, thyroid stimulating hormone (TSH), or creatinine clearance between women before and after oophorectomy (Groups A and C, **Table 1**). At follow-up 201 days after oophorectomy (Group B), lumbar spine bone mineral density (LS BMD) and serum estradiol decreased significantly, while serum follicle-stimulating hormone (FSH), type 1 collagen crosslinked C-telopeptide (β-CTX), intact amino-terminal propeptide of type I procollagen (P1NP), alkaline phosphatase, osteocalcin, sclerostin, calcium, and phosphate significantly increased compared to values before oophorectomy (Group A). Similar differences were observed between the variables before oophorectomy (Group A) and 508 days after oophorectomy (Group C), except for sclerostin. In women on oral hormonal therapy for 203 days (from 508 days, Group C, to 711 days after oophorectomy, Group D), LS-BMD and serum estradiol increased significantly, while serum FSH, β-CTX, P1NP, alkaline phosphatase, osteocalcin, sclerostin, osteoprotegerin, calcium, phosphate, and PTH decreased. Dkk1and OPG serum levels did not correlate with bone remodeling markers (β-CTX and P1NP), while levels of β-CTX and P1NP were highly correlated (**Table 2**; **Figure 1**).

Of the 48 sequenced samples, 22 samples were paired up as having sufficient and low levels of estrogen. The four remaining samples were additional measurements to four paired samples and were thus discarded.

MiRNome Profiling in Patient Serum – Sequencing Study

Sequencing revealed a median coverage of over 10 million unprocessed reads per sample, but after trimming and aligning to miRBase v22, we found that the median was 4.9 million reads per sample with a balanced distribution (SD = 0.043).

After alignment, we found 1305 unique miRNA sequences. Since low-read count miRNAs with high dispersion might be indistinguishable from sampling noise and increase the false-positive rate, we filtered out all miRNAs with a base mean of > 10 and found 439 miRNAs.

Since patients were paired up, we employed generalized linear mixed-effects modeling with the negative binomial assumption (GLMM-NB) and patients as the random effect. The first analysis focused on changes in miRNA concentrations in serum with sufficient and low levels of estrogen, and we found 17 miRNAs with $p < 0.05$ and a difference in fold change of > 50%. To affirm their connection to osteoporosis, we examined their relationship to lumbar spine BMD, biomarkers and hormones associated with bone metabolism, and biomarkers of low-grade inflammation. Significant associations are given in **Table 2** and **Tables S1**, **S2** in detail.

The concentrations of 14 miRNAs showed an inverse association with changes in estrogen status (**Table 2**). Serum concentrations of miR-422a were positively associated with serum β-CTX and P1NP levels (**Figure 2**). The amount of miR-1278 was positively associated with serum β-CTX, P1NP, sclerostin, osteocalcin, and Dkk1 levels. Increased miR-422a levels were associated with increased serum β-CTX and P1NP levels (**Table 2**).

In contrast, the levels of miR-132-5p, miR-24-1-5p, and miR-619-5p showed a positive association with estrogen status (**Figure 2**). Of these, miR-24-1-5p was negatively associated

TABLE 1 | Characteristics of 11 untreated women prior to oophorectomy (A) and 201 days after oophorectomy (B) and 11 untreated women 508 days after oophorectomy (C) and then after 203 days of estradiol treatment (D).

Characteristics	A Prior to oophorectomy	B After oophorectomy	p	C Untreated after oophorectomy	D Treated after oophorectomy	p
Age (years)	47.9 (2.5)	48.5 (2.4)	<0.001	48.6 (5.1)	49.3 (5.2)	<0.001
BMI (kg/m^2)	29.7 (26.3 - 34.5)	29.2 (25.5 - 35.3)	0.766	24.3 (20.8 - 31.1)	23.6 (21.0 - 31.2)	0.388
Spine BMD (g/cm^2)	1.327 (0.140)	1.266 (0.139)	<0.001	1.012 (0.181)	1.048 (0.183)	<0.001
βCTX (µg/l)	0.24 (0.18 - 0.36)	0.57 (0.55 - 0.92)	<0.001	0.86 (0.54 - 0.99)	0.33 (0.26 - 0.41)	<0.001
PINP (µg/l)	39.8 (33.4 - 51.0)	73.2 (59.7 - 109.8)	<0.001	104.5 (74.3 - 111.9)	50.7 (42.7 - 60.9)	<0.001
Osteokalcin (µg/l) Osteoprotegerin (pmol/l)	17.0 (13.3 - 19.2)	22.4 (20.1 - 27.7)	<0.001	32.4 (25.3 - 38.2)	22.2 (19.6 - 27.6)	0.002
Osteoprotegerin (pmol/l) Sclerostin (pmol/l)	5.19 (3.61)	6.34 (1.62)	0.067	5.57 (1.40)	4.79 (1.36)	0.002
Sclerostin (pmol/l) DKK1	111.9 (66.0 - 157.2)	133.1 (112.7-177.5)	0.001	120.3 (111.6 - 134.9)	95.1 (78.5 - 106.9)	0.001
DKK1 (pmol/l)	46.2 (17.8)	56.0 (19.2)	0.012	54.6 (13.5)	46.0 (14.4)	0.014
Phosphate (mmol/l) Calcium	1.06 (0.12)	1.22 (0.14)	0.004	1.31 (0.09)	1.07 (0.11)	<0.001
Calcium (mmol/l)	2.42 (0.10)	2.52 (0.16)	0.042	2.47 (0.05)	2.36 (0.09)	0.001
Intact PTH (pmol/l) 25(OH)D	3.12 (1.20)	2.92 (1.54)	0.470	2.38 (0.85)	2.89 (0.86)	0.037
25(OH)D (nmol/l)	46.8 (22.8)	63.2 (17.3)	0.045	71.3 (20.1)	78.5 (14.6)	0.346
Estradiol (pmol/l)	338.5 (188.3)	36.3 (18.2)	<0.001	22.3 (5.8)	161.4 (66.3)	<0.001
FSH (IU/l)	6.6 (4.2)	86.1 (31.6)	<0.001	111.0 (51.8)	65.5 (38.5)	<0.001
Glucose (mmol/l)	5.2 (0.5)	5.3 (0.5)	0.739	5.3 (0.4)	5.2 (0.5)	0.098
ALP (µkat/l)	1.22 (0.99 - 1.57)	1.69 (1.54 - 2.8)	<0.001	1.45 (1.20 - 1.78)	1.05 (1.01 - 1.34)	<0.001
TSH (mIU/l)	2.32 (2.00 - 3.73)	3.13 (1.41 - 4.36)	0.803	2.36 (1.78 - 4.93)	2.18 (1.83 - 3.27)	0.767
eGFR (ml/sec/1.73 m^2)	1.60 (0.12)	1.66 (0.22)	0.139	1.57 (0.17)	1.60 (0.20)	0.535

Data are the mean (SD) or median (IQR).

TABLE 2 | Association of changes in 17 miRNAs with disparate concentrations between sufficient and low estrogen levels in serum with biomarkers in 11 untreated women before oophorectomy and 201 days after, and in 11 women initially untreated for 508 days and then treated with estradiol for 203 days.

miRNA	Estradiol	βCTX	PINP	Sclerostin	Dkk1	Osteoprotegrin
miR-195-5p	2.12	0.22	0.00	0.00	0.00	-0.06
	0.048	0.759	0.370	0.502	0.832	0.381
miR-196a-5p	162.96	2.54	0.01	0.02	0.07	0.25
	0.008	0.390	0.549	0.482	**0.001**	0.605
miR-200a-3p	4.92	1.78	0.01	0.00	0.03	-0.01
	0.028	0.350	0.665	0.852	0.114	0.929
miR-424-3p	3.41	1.68	0.01	0.00	-0.01	0.00
	0.050	0.138	0.133	0.596	0.746	0.972
miR-505-5p	1262.52	7.67	0.02	-0.06	-0.01	0.11
	0.033	0.095	0.402	0.167	0.889	0.756
miR-550a-3-5p	225659839.00	-6.19	-0.03	0.02	-0.19	-2.75
	0.002	0.674	0.725	0.782	0.352	0.226
miR-3120-3p	12.03	1.88	0.02	0.00	0.02	0.24
	0.032	0.427	0.191	0.874	0.679	0.441
miR-100-5p	3.19	1.30	0.01	0.00	0.02	-0.04
	0.018	0.183	0.094	0.724	0.112	0.733
miR-122-5p	5.23	1.57	0.02	0.00	0.04	-0.12
	0.045	0.383	0.136	0.998	0.162	0.616
miR-1278	413.22	11.70	0.04	0.06	0.18	-0.45
	<0.001	**0.002**	**<0.001**	**0.035**	**0.002**	0.176
miR-1304-5p	25.08	5.05	0.04	-0.01	-0.02	-0.34
	0.004	0.089	0.168	0.688	0.831	0.147
miR-422a	2.21	1.29	0.01	0.00	-0.01	0.05
	0.013	**0.015**	**0.001**	0.669	0.501	0.475
miR-566	42.85	3.20	0.01	0.02	0.00	-0.07
	0.018	0.246	0.483	0.573	0.940	0.873
let-7d-3p	1.89	1.03	0.01	0.00	0.01	-0.07
	0.038	0.053	0.259	0.904	0.307	0.271
miR-132-5p	0.16	-1.91	-0.01	0.00	0.00	-0.15
	0.034	0.079	0.322	0.713	0.951	0.177
miR-24-1-5p	0.00	-6.71	-0.05	-0.04	-0.02	-1.11
	<0.001	**0.006**	**0.020**	**0.029**	0.766	**<0.001**
miR-619-5p	0.07	-2.60	-0.01	-0.01	-0.09	-0.10
	0.011	0.088	0.141	0.621	**0.007**	0.511

Data are presented as the incident rate ratios and p values for estradiol (bold). Data for biomarkers are presented as the slope (β) and p-values.

with β-CTX, PINP, osteoprotegerin, and sclerostin levels. The remaining miRNAs were not associated with any biomarker of bone metabolism or inflammation. Furthermore, the associations between miRNA concentrations and lumbar spine BMD were not significant.

MiRNome Profiling in Patient Serum – osteomiR®

An association between osteoporosis and circulating miRNA profiles can be assessed using commercially available kits, such as osteomiR® (TAmiRNA, Austria). This complete kit includes materials for miRNA isolation, reverse transcription, and qRT–PCR with LNA probes. In addition to quality control (QC) probes, this kit screened ten miRNAs connected to osteoporosis. However, in most of our samples, these miRNAs were below the detection limit of qRT–PCR (C_T > 30), and the QC probes indicated low concentrations after isolation. We verified these results by additional miRNA isolation from serum and quantification by TaqMan Advanced miRNA assays (Thermo).

All ten miRNAs included in the osteomiR® kit were detected in our miRNA-Seq analysis, and their relation to estrogen levels and biomarkers was assessed using GLMM-NB with patients as a random effect and FSH as a confounding variable. Nonetheless, no miRNA was significantly different between samples with sufficient and low estrogen levels (**Table S3**), but we found an association of miR-375 with β-CTX and P1NP (**Table S4**).

DISCUSSION

In this study, we screened the profile of circulating miRNAs in women before and after oophorectomy, as well as in oophorectomized women on estrogen therapy. We identified 17 miRNAs, which were different in sera with either sufficient or low estrogen levels. Of the 14 miRNAs upregulated after oophorectomy and downregulated with estrogen therapy, miR-1278, miR-24-1-5p, and miR-422awere associated with biomarkers of bone metabolism, suggesting their role in the pathogenesis of osteoporosis (11, 30–33).

The expression of miR-422a was previously detected in monocytes and was considered a potential biomarker for postmenopausal osteoporosis (34). We observed a decrease in miR-422a levels after estradiol treatment, and a positive correlation of miR-422a levels with β-CTX and PINP but not with sclerostin levels. These findings support the role of miR-

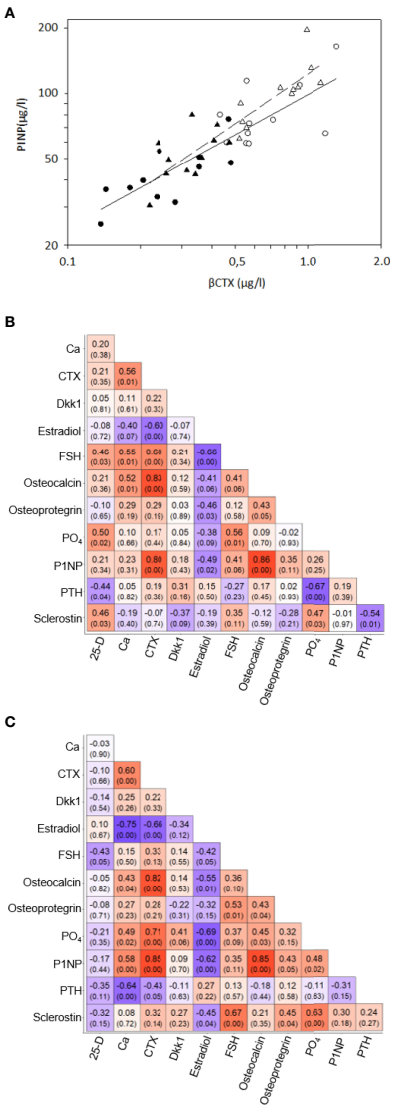

FIGURE 1 | Correlations of bone remodeling biomarkers – **(A)** Correlations between serum βCTX and P1NP in 11 women before oophorectomy, Group A (•) and untreated after surgery, Group B (o) (solid line), and in 11 oophorectomized women untreated, Group C (Δ) and treated with estradiol, Group D (▲). **(B)** Correlation matrix of selected the bone remodelling biomarkers in the Group A and B. The matrix included Pearson's correlation coefficients and p-value in the bracket below. The color indicates the strength and direction of the coefficient. **(C)** Correlation matrix of selected the bone remodelling biomarkers in the Group C and D. The matrix included Pearson's correlation coefficients and p-value in the bracket below. The color indicates the strength and direction of the coefficient.

422a expression in bone remodeling associated with estrogen status (35–39).

The linkage of miR-1278 to bone metabolism was not explored previously, but we found associations of miR-1278 with serum levels of bone remodeling biomarkers (β-CTX, P1NP, and osteocalcin). In addition, miR-1278 was positively associated with sclerostin and Dkk1, which are inhibitors of the WNT signaling pathway. These associations are in concordance with previous studies on the association between inhibitors of the WNT signaling pathway and estrogen status (40–44). The Wnt/β-catenin pathway activation enhances bone mass not only by stimulating osteoblastogenesis but, at least to some extent, also by inhibiting osteoclastogenesis as well (44).

In contrast, estrogen deficiency in our patients was associated with decreased serum levels of miR-24-1-5p and increased serum levels of β-CTX, P1NP, and sclerostin compared to those of women with sufficient estrogen status. Similarly, postmenopausal women treated with teriparatide had a significant and inverse correlation of miR-24-3p at 3 months with P1NP at 3 and 12 months and with β-CTX at 12 months (45). However, Seeliger et al. observed an upregulated miR-24-3p concentration in sera and bone tissue of osteoporotic patients (11), while another study did not find any differences in the relative expression of miR-24-3p between healthy, osteoporotic, and sarcopenic postmenopausal women (14). The discrepancy observed among these studies might arise from the quantification of different isoforms of this miRNA.

In this study, levels of β-CTX and P1NP were highly correlated, reflecting the coupling of bone resorption and bone formation (46). The early phase after oophorectomy is characterized by the prevalence of bone resorption over bone formation; following initiation of estrogen treatment, a decrease in markers of bone resorption is later followed by a decrease in markers of bone formation (47). Compared with women before oophorectomy and women treated with estrogen, untreated oophorectomized women showed higher serum β-CTX, PINP, and osteocalcin, but also higher sclerostin, Dkk1, and OPG, and levels. Our sclerostin data correspond with a negative correlation of sclerostin levels with the free estradiol index in postmenopausal women (48), with significantly higher serum sclerostin levels in postmenopausal women than premenopausal women (49), and with a decrease in serum (42, 50) and bone mRNA sclerostin levels (43) after the administration of estrogen. DKK1 expression in bone was enhanced after ovariectomy in mice, and DKK1 antisense oligonucleotide treatment reduced the promoting effect of estrogen deficiency on DKK1 (51). Postmenopausal women with significantly increased serum DKK1 had more significant osteoporosis (51). Osteoprotegerin levels are higher in postmenopausal osteoporotic women, compared with controls (52), and the inverse relationship between serum OPG and serum oestradiol levels was demonstrated in females (53). Serum OPG levels measured after 3 months and 1 year of HT decreased significantly compared to baseline (54).

In this study, while miR-1278, miR-24-1-5p, and miR-422a correlated with markers of bone remodeling (β-CTX and P1NP), only miR-1278 and miR-24-1-5p correlated with serum sclerostin levels. Both in our untreated and treated women, serum levels of inhibitors of bone formation (sclerostin and Dkk1), and bone resorption (OPG), were not correlated with markers of bone remodeling. Interestingly, circulating sclerostin levels do not decrease in postmenopausal women on antiresorptive therapy with bisphosphonates (55). Taken together, in agreement with previous data (49, 54), our results indicate that changes in serum sclerostin, Dkk1 and OPG levels may represent a compensatory response of the osteocyte

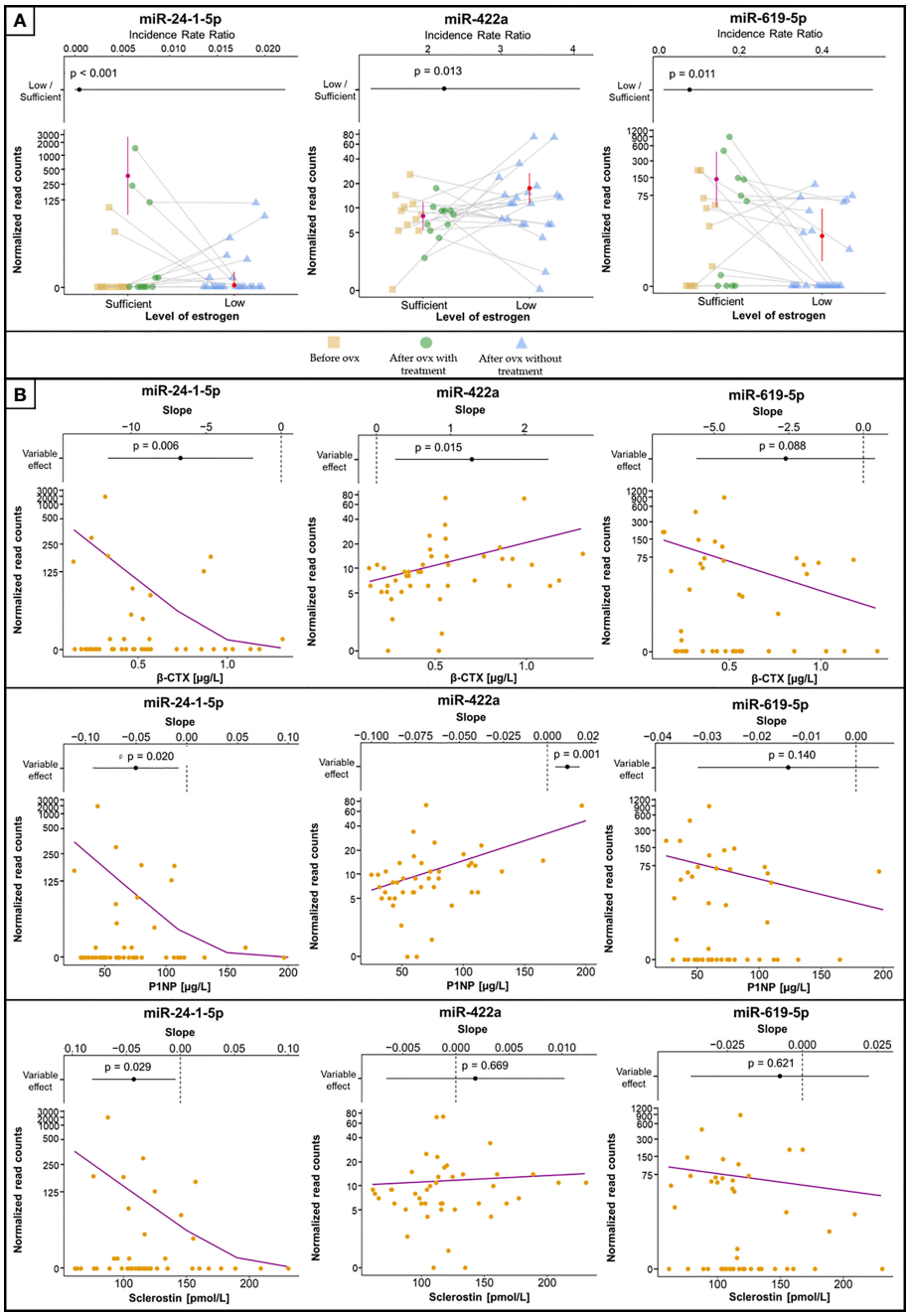

FIGURE 2 | Selected miRNAs associated with estrogen status and biomarkers of bone metabolism or inflammation. **(A)** MiRNA concentrations between groups, with error bars representing 95% confidence intervals and estimated means (filled circles). Samples from the same patient are connected with grey lines. The plots at the top are visualizations of the 95% confidence intervals with IRR (filled circles), where values > 1 indicate increased concentrations in samples with low estrogen levels and vice versa. The vertical dashed line indicates IRR equal to 1 (= no difference). p values denoting the statistical significance between the groups are specified above the slope and were computed using GLMM-NB. **(B)** The association of selected miRNAs with levels of biomarkers. The violet line is the regression line computed using GLMM-NB. The plots at the top are visualizations of 95% confidence intervals with the slope (β) (filled circles), where a positive value indicates a positive association of the miRNA with the biomarker and vice versa. The vertical dashed line indicates a slope equal to 0 (= no difference). p values denoting the statistical significance of the association are specified above the slope and were computed using GLMM-NB.

functional activity reflecting acute estrogen deficiency and/or estrogen replete state, rather than changes in remodeling of bone.

Above all, the amount of miR-200a-3p was elevated in our patients with low estrogen levels and downregulated in women with high estrogen. Physiologically, miR-200s are overexpressed in several clinical conditions related to estrogen status, such as in the mammary glands during mammary gland development, pregnancy, and lactation (56), as well as in estrogen-dependent cancers (57). In humans, miR-200a-3p was associated with osteoporosis (4), albeit not significantly expressed in patients with osteoporotic bone fractures (11, 13), whereas our GLMM-NB analysis did not reveal any pertinence of miR-200a-3p to lumbar spine BMD or biomarkers. This particular miRNA is notable due to its substantial increase in our patients with low estrogen levels and its apparent relevance to osteoporosis.

Our study did not aim to establish an association of miRNAs with the probability of osteoporosis and low impact fractures. To assess osteoporosis in our cohort, we used the commercially available kit osteomiR® (TamiRNA) (58). However, the screening failed due to an insufficient amount of miRNAs after isolation, and we speculate that our serum samples contained insufficient levels of miRNA for qRT–PCR. Fortunately, our well-designed MPS could detect miRNAs at low concentrations, so we were able to quantify all miRNAs included in osteomiR®. This underlines the importance of sample processing and highlights the advantage of MPS.

Although our study is informative, there are several limitations. First, several lifestyle factors that can influence estrogen levels, such as nutritional status and exercise, were not addressed. Second, the miRNAs of interest had zero counts in several samples; however, we employed a statistical approach, which should resolve this problem. Third, the cohort of 22 pairs of samples might be insufficient for a proper statistical analysis, but recruitment of such a uniform cohort is complicated and time-consuming. Fourth, the duration of our study was relatively short, as it was an exploratory study. Given the short duration of the study and the low number of cases, changes in BMD should be interpreted with caution. Fifth, the ovariectomized women in this study were treated with 1 mg of estradiol. Bone remodeling is dose-dependently regulated by estrogen (59, 60). Estradiol at follicular to periovulatory levels is needed to suppress a mildly activated immune system responsible for increased postmenopausal bone resorption (59). However, women in this study were referred for bone status assessment, and the estrogen therapy was prescribed by their gynecologists. Sixth, the MPS results were not validated by qRT–PCR due to the low miRNA concentration in sera. Seventh, as smoking was reported by only one woman treated with estrogen after oophorectomy, the effects of smoking on the liver metabolism of sex hormones were not taken into consideration in the analyses. Further significant limitations include seasonal variability, vitamin D status, and the effects of PTH on osteocytic sclerostin production (61, 62). In our patients treated with estrogen, no significant correlation was observed between serum sclerostin, serum vitamin D and PTH. Six out of 11 women before oophorectomy were vitamin D insufficient. They were supplemented with 800 IU vitamin D. Previously, such a supplementation did not significantly change sclerostin levels in women (63). In patients with vitamin D severe deficiency (25-hydroxyvitamin D level ≤ 20 ng/mL) receiving a monthly intramuscular injection of 300,000 IU of cholecalciferol, serum sclerostin levels decreased (64). In our untreated patients, after oophorectomy, an increase in serum 25- hydroxyvitamin D was correlated with the increase in sclerostin levels. Finally, this study is descriptive, and our results warrant further validation by additional research.

To our knowledge, this is the first prospective study to compare the associations between changes in estrogen status and relative serum levels of circulating miRNAs with BMD and biomarkers of both bone metabolism in women before and after ovariectomy as well as in ovariectomized women after estrogen treatment. The design of this study eliminates the confounding effects of age on the association between the levels of circulating miRNAs, estradiol, follicle-stimulating hormone, and bone variables (65, 66). The present findings corroborate a few previous studies on the expression of miRNAs during treatment with anti-osteoporotic agents (45), as well as studies comparing profiles in postmenopausal osteoporotic and healthy premenopausal women (66, 67). Although this study reported substantial changes in several miRNAs (let-7d-3p, miR-1278, miR-24-1-5p, miR-422a, and miR-619-5p) that regulate osteoblast and osteoclast differentiation in association with estrogen status, these results require further research and validation in an extended cohort.

In summary, of the 14 miRNAs that showed upregulation with estrogen deficiency and downregulation after estrogen therapy, miR-422a correlated with serum β-CTX and P1NP and miR-1278 correlated with serum β-CTX, P1NP, osteocalcin, sclerostin, and Dkk1. Of the 3 miRNAs showing downregulation with estrogen deficiency and upregulation after estrogen therapy, miR-24-1-5p showed a negative correlation with serum β-CTX, P1NP, osteoprotegerin, and sclerostin levels. These miRNAs represent promising biomarkers in bone pathophysiology in studies on the prevention of postmenopausal osteoporosis and the mechanism of antiresorptive therapies. Future prospective studies are required to validate the potential clinical application of our findings.

DATA AVAILABILITY STATEMENT

The original contributions presented in the study are publicly available. This data can be found in GEO database (accession number GSE194086).

ETHICS STATEMENT

The studies involving human participants were reviewed and approved by The Institutional Review Board of the Institute of Rheumatology, Prague, Czechia. The patients/participants provided their written informed consent to participate in this study.

AUTHOR CONTRIBUTIONS

All authors were involved in drafting the article or in revising it critically for important intellectual content. All authors take responsibility for the integrity of the data and the accuracy of the data analysis JB was responsible for serum miRNA profiling, biostatistical analyses, data interpretation and manuscript preparation. AP was responsible for miRNA isolation and preparation of MPS libraries. LW was responsible for biochemical analyses and data interpretation. HH performed the clinical diagnoses. KP and LŠ performed the critical revision of the manuscript. XS was responsible for data interpretation. JS designed the study, was responsible for blood collection, patient follow-up, bone densitometry, immunoassays and manuscript preparation. All authors had access to the data, and have read and accepted the final version of the manuscript for submission.

FUNDING

This research was funded by the Ministry of Health of the Czech Republic under grant NV18-05-00394 and by RVO 00023728 (Institute of Rheumatology), Charles University project SVV 260 523.

ACKNOWLEDGMENTS

We thank Alena Adamová Ludmila Hauptvoglová, and Tereza Malá, for their excellent technical assistance in this project. We acknowledge the Core Facility Genomics supported by the NCMG research infrastructure (LM2015091 funded by MEYS CR) for their support with obtaining scientific data presented in this paper.

SUPPLEMENTARY MATERIAL

The Supplementary Material for this article can be found online at: https://www.frontiersin.org/articles/10.3389/fendo.2022.864299/full#supplementary-material

REFERENCES

1. Khosla S, Oursler MJ, Monroe DG. Estrogen and the Skeleton. *Trends Endocrinol Metab* (2012) 23(11):576–81. doi: 10.1016/j.tem.2012.03.008
2. Klibanski A, Adams-Campbell L, Bassford T, Blair SN, Boden SD. Osteoporosis Prevention, Diagnosis, and Therapy. *JAMA* (2001) 285 (6):785–95. doi: 10.1001/jama.285.6.785
3. Hernlund E, Svedbom A, Ivergard M, Compston J. Osteoporosis in the European Union: Medical Management, Epidemiology and Economic Burden. *Arch Osteo* (2013) 8:136. doi: 10.1007/s11657-013-0136-1
4. Huai Y, Zhang W, Chen Z, Zhao F, Wang W, Dang K, et al. A Comprehensive Analysis of MicroRNAs in Human Osteoporosis. *Front Endocrinol* (2020) 11:516213. doi: 10.3389/fendo.2020.516213
5. An JH, Ohn JH, Song JA, Yang JY, Park H, Choi HJ, et al. Changes of MicroRNA Profile and MicroRNA-MRNA Regulatory Network in Bones of Ovariectomized Mice. *J Bone Mine Res* (2014) 29(3):644–56. doi: 10.1002/jbmr.2060
6. Yavropoulou MP, Yovos JG. The "Dark Matter" of DNA and the Regulation of Bone Metabolism: The Role of Non-Coding RNAs. *J Musculos Neuro Interact* (2018) 18(1):18–31.
7. Jones TL, Esa MS, Li KHC, Krishnan SRG, Elgallab GM, Pearce MS, et al. Osteoporosis, Fracture, Osteoarthritis & Sarcopenia: A Systematic Review of Circulating MicroRNA Association. *Bone* (2021) 152:116068. doi: 10.1016/j.bone.2021.116068
8. Condrat CE, Thompson DC, Barbu MG, Bugnar OL, Boboc A, Cretoiu D, et al. MiRNAs as Biomarkers in Disease: Latest Findings Regarding Their Role in Diagnosis and Prognosis. *Cells* (2020) 9(2):276. doi: 10.3390/cells9020276
9. Grillari J, Makitie RE, Kocijan R, Haschka J, Vazquez DC, Semmelrock E, et al. Circulating MiRNAs in Bone Health and Disease. *Bone* (2020) 145:115787. doi: 10.1016/j.bone.2020.115787
10. Zhao W, Shen G, Ren H, Liang, Yu X, Zhang Z, et al. Therapeutic Potential of MicroRNAs in Osteoporosis Function by Regulating the Biology of Cells Related to Bone Homeostasis. *J Cell Physiol* (2018) 233(12):9191–208. doi: 10.1002/jcp.26939
11. Seeliger C, Karpinski K, Haug AT, Vester H, Schmitt A, Bauer JS, et al. Five Freely Circulating MiRNAs and Bone Tissue MiRNAs Are Associated with Osteoporotic Fractures. *J Bone Mine Res* (2014) 29(8):1718–28. doi: 10.1002/jbmr.2175
12. Kocijan R, Muschitz C, Geiger E, Skalicky S, Baierl A, Dormann R, et al. Circulating Microrna Signatures in Patients with Idiopathic and Postmenopausal Osteoporosis and Fragility Fractures. *J Clin Endocrinol Metab* (2016) 101(11):4125–34. doi: 10.1210/jc.2016-2365
13. Panach L, Mifsut D, Tarin JJ, Cano A, Garcia-Perez MA. Serum Circulating MicroRNAs as Biomarkers of Osteoporotic Fracture. *Calcif Tissue Int* (2015) 97(5):495–505. doi: 10.1007/s00223-015-0036-z
14. Chen Z, Bemben MG, Bemben DA. Bone and Muscle Specific Circulating MicroRNAs in Postmenopausal Women Based on Osteoporosis and Sarcopenia Status. *Bone* (2019) 120:271–8. doi: 10.1016/j.bone.2018.11.001
15. Yavropoulou MP, Anastasilakis AD, Makras P, Tsalikakis DG, Grammatiki M, Yovos JG. Expression of MicroRNAs That Regulate Bone Turnover in the Serum of Postmenopausal Women with Low Bone Mass and Vertebral Fractures. *Eur J Endocrinol* (2017) 176(2):169–76. doi: 10.1530/EJE-16-0583
16. Sun M, Zhou X, Chen L, Huang S, Leung V, Wu N, et al. The Regulatory Roles of MicroRNAs in Bone Remodeling and Perspectives as Biomarkers in Osteoporosis. *BioMed Res Int* (2016) 2016:1652417. doi: 10.1155/2016/1652417
17. Taipaleenmaki H, Bjerre Hokland L, Chen L, Kauppinen S, Kassem M. Mechanisms in Endocrinology: Micro-RNAs: Targets for Enhancing Osteoblast Differentiation and Bone Formation. *Eur J Endocrinol* (2012) 166(3):359–71. doi: 10.1530/EJE-11-0646
18. Anastasilakis AD, Papachatzopoulos S, Makras P, Gkiomisi A, Nikolakopoulos P, Polyzos SA, et al. The Effect of Pharmacological Cessation and Restoration of Menstrual Cycle on Bone Metabolism in Premenopausal Women with Endometriosis. *Bone* (2022) 158:116354. doi: 10.1016/j.bone.2022.116354
19. Stepan JJ, Hruskova H, Kverka M. Update on Menopausal Hormone Therapy for Fracture Prevention. *Curr Osteo Rep* (2019) 17(6):465–73. doi: 10.1007/s11914-019-00549-3
20. World Medical A. World Medical Association Declaration of Helsinki: Ethical Principles for Medical Research Involving Human Subjects. *JAMA* (2013) 310 (20):2191–4. doi: 10.1001/jama.2013.281053
21. Martin M. Cutadapt Removes Adapter Sequences from High-Throughput Sequencing Reads. *EMBnetjournal* (2011) 17:10. doi: 10.14806/ej.17.1.200
22. Andrews S. Babraham Bioinformatics - Fastqc a Quality Control Tool for High Throughput Sequence Data. *Soil* (1973) 5:47–81.
23. Vitsios DM, Enright AJ. Chimira: Analysis of Small RNA Sequencing Data and MicroRNA Modifications. *Bioinformatics* (2015) 31(20):3365–7. doi: 10.1093/bioinformatics/btv380
24. Kozomara A, Griffiths-Jones S. Mirbase: Annotating High Confidence MicroRNAs Using Deep Sequencing Data. *Nucleic Acids Res* (2014) 42 (Database issue):D68–73. doi: 10.1093/nar/gkt1181
25. Team RC. *R: A Language and Environment for Statistical Computing*. Vienna, Austria: R Foundation for Statistical Computing (2021).

26. Levey AS, Stevens LA, Schmid CH, Zhang YL, Castro AF, Feldman HI 3rd, et al. A New Equation to Estimate Glomerular Filtration Rate. *Ann Intern Med* (2009) 150(9):604–12. doi: 10.7326/0003-4819-150-9-200905050-00006
27. Love MI, Huber W, Anders S. Moderated Estimation of Fold Change and Dispersion for RNA-Seq Data with Deseq2. *Genome Biol* (2014) 15(12):550. doi: 10.1186/s13059-014-0550-8
28. Brooks ME, Kristensen K, van Benthem KJ, Magnusson A, Berg CW, Nielsen A, et al. Glmmtmb Balances Speed and Flexibility among Packages for Zero-Inflated Generalized Linear Mixed Modeling. *R J* (2017) 9(2):378–400. doi: 10.32614/RJ-2017-066
29. Benjamini Y, Hochberg Y. Discovery Rate: A Practical and Powerful Approach to Multiple Testing. *J R Stat Soc* (1995) 57(1):289–300.
30. Zeng Y, Qu X, Li H, Huang S, Wang S, Xu Q, et al. MicroRNAa-100 Regulates Osteogenic Differentiation of Human Adipose-Derived Mesenchymal Stem Cells by Targeting Bmpr2. *FEBS Lett* (2012) 586(16):2375–81. doi: 10.1016/j.febslet.2012.05.049
31. Cheng VK, Au PC, Tan KC, Cheung CL. MicroRNA and Human Bone Health. *JBMR Plus* (2019) 3(1):2–13. doi: 10.1002/jbm4.10115
32. Weilner S, Skalicky S, Salzer B, Keider V, Wagner M, Hildner F, et al. Differentially Circulating MiRNAs after Recent Osteoporotic Fractures Can Influence Osteogenic Differentiation. *Bone* (2015) 79:43–51. doi: 10.1016/j.bone.2015.05.027
33. Edmonston D, Wolf M. Fgf23 at the Crossroads of Phosphate, Iron Economy and Erythropoiesis. *Nat Rev Nephrol* (2020) 16(1):7–19. doi: 10.1038/s41581-019-0189-5
34. Cao Z, Moore BT, Wang Y, Peng XH, Lappe JM, Recker RR, et al. Mir-422a as a Potential Cellular MicroRNA Biomarker for Postmenopausal Osteoporosis. *PloS One* (2014) 9(5):e97098. doi: 10.1371/journal.pone.0097098
35. Pacifici R, Brown C, Puscheck E, Friedrich E, Slatopolsky E, Maggio D, et al. Effect of Surgical Menopause and Estrogen Replacement on Cytokine Release from Human Blood Mononuclear Cells. *Proc Natl Acad Sci USA* (1991) 88 (12):5134–8. doi: 10.1073/pnas.88.12.5134
36. D'Amelio P, Grimaldi A, Di Bella S, Brianza SZ, Cristofaro MA, Tamone C, et al. Estrogen Deficiency Increases Osteoclastogenesis up-Regulating T Cells Activity: A Key Mechanism in Osteoporosis. *Bone* (2008) 43(1):92–100. doi: 10.1016/j.bone.2008.02.017
37. Adeel S, Singh K, Vydareny KH, Kumari M, Shah E, Weitzmann MN, et al. Bone Loss in Surgically Ovariectomized Premenopausal Women Is Associated with T Lymphocyte Activation and Thymic Hypertrophy. *J Investig Med* (2013) 61(8):1178–83. doi: 10.2310/JIM.0000000000000016
38. Cauley JA, Danielson ME, Boudreau RM, Forrest KY, Zmuda JM, Pahor M, et al. Inflammatory Markers and Incident Fracture Risk in Older Men and Women: The Health Aging and Body Composition Study. *J Bone Mine Res* (2007) 22(7):1088–95. doi: 10.1359/jbmr.070409
39. Shevde NK, Bendixen AC, Dienger KM, Pike JW. Estrogens Suppress Rank Ligand-Induced Osteoclast Differentiation *Via* a Stromal Cell Independent Mechanism Involving C-Jun Repression. *Proc Natl Acad Sci USA* (2000) 97 (14):7829–34. doi: 10.1073/pnas.130200197
40. Lehmann J, Thiele S, Baschant U, Rachner TD, Niehrs C, Hofbauer LC, et al. Mice Lacking Dkk1 in T Cells Exhibit High Bone Mass and Are Protected from Estrogen-Deficiency-Induced Bone Loss. *iScience* (2021) 24(3):102224. doi: 10.1016/j.isci.2021.102224
41. Tian J, Xu XJ, Shen L, Yang YP, Zhu R, Shuai B, et al. Association of Serum Dkk-1 Levels with Beta-Catenin in Patients with Postmenopausal Osteoporosis. *J Huazhong Univ Sci Tech Med Sci* (2015) 35(2):212–8. doi: 10.1007/s11596-015-1413-6
42. Modder UI, Clowes JA, Hoey K, Peterson JM, McCready L, Oursler MJ, et al. Regulation of Circulating Sclerostin Levels by Sex Steroids in Women and in Men. *J Bone Mine Res* (2011) 26(1):27–34. doi: 10.1002/jbmr.128
43. Fujita K, Roforth MM, Demaray S, McGregor U, Kirmani S, McCready LK, et al. Effects of Estrogen on Bone MRNA Levels of Sclerostin and Other Genes Relevant to Bone Metabolism in Postmenopausal Women. *J Clin Endocrinol Metab* (2014) 99(1):E81–8. doi: 10.1210/jc.2013-3249
44. Glass DA, Bialek P2nd, Ahn JD, Starbuck M, Patel MS, Clevers H, et al. Canonical Wnt Signaling in Differentiated Osteoblasts Controls Osteoclast Differentiation. *Dev Cell* (2005) 8(5):751–64. doi: 10.1016/j.devcel.2005.02.017
45. Anastasilakis AD, Makras P, Pikilidou M, Tournis S, Makris K, Bisbinas I, et al. Changes of Circulating MicroRNAs in Response to Treatment with Teriparatide or Denosumab in Postmenopausal Osteoporosis. *J Clin Endocrinol Metab* (2018) 103(3):1206–13. doi: 10.1210/jc.2017-02406
46. Eriksen EF. Normal and Pathological Remodeling of Human Trabecular Bone: Three Dimensional Reconstruction of the Remodeling Sequence in Normals and in Metabolic Bone Disease. *Endocr Rev* (1986) 7(4):379–408. doi: 10.1210/edrv-7-4-379
47. Hannon R, Blumsohn A, Naylor K, Eastell R. Response of Biochemical Markers of Bone Turnover to Hormone Replacement Therapy: Impact of Biological Variability. *J Bone Mine Res* (1998) 13(7):1124–33. doi: 10.1359/jbmr.1998.13.7.1124
48. Mirza FS, Padhi ID, Raisz LG, Lorenzo JA. Serum Sclerostin Levels Negatively Correlate with Parathyroid Hormone Levels and Free Estrogen Index in Postmenopausal Women. *J Clin Endocrinol Metab* (2010) 95(4):1991–7. doi: 10.1210/jc.2009-2283
49. Ardawi MS, Al-Kadi HA, Rouzi AA, Qari MH. Determinants of Serum Sclerostin in Healthy Pre- and Postmenopausal Women. *J Bone Mine Res* (2011) 26(12):2812–22. doi: 10.1002/jbmr.479
50. O'Brien CA, Plotkin LI, Galli C, Goellner JJ, Gortazar AR, Allen MR, et al. Control of Bone Mass and Remodeling by Pth Receptor Signaling in Osteocytes. *PloS One* (2008) 3(8):e2942. doi: 10.1371/journal.pone.0002942
51. Ahmed SF, Fouda N, Abbas AA. Serum Dickkopf-1 Level in Postmenopausal Females: Correlation with Bone Mineral Density and Serum Biochemical Markers. *J Osteo* (2013) 2013:460210. doi: 10.1155/2013/460210
52. Yano K, Tsuda E, Washida N, Kobayashi F, Goto M, Harada A, et al. Immunological Characterization of Circulating Osteoprotegerin/Osteoclastogenesis Inhibitory Factor: Increased Serum Concentrations in Postmenopausal Women with Osteoporosis. *J Bone Mine Res* (1999) 14 (4):518–27. doi: 10.1359/jbmr.1999.14.4.518
53. Kudlacek S, Schneider B, Woloszczuk W, Pietschmann P, Willvonseder R. Serum Levels of Osteoprotegerin Increase with Age in a Healthy Adult Population. *Bone* (2003) 32(6):681–6. doi: 10.1016/S8756-3282(03)00090-5
54. Han KO, Choi JT, Choi HA, Moon IG, Yim CH, Park WK, et al. The Changes in Circulating Osteoprotegerin after Hormone Therapy in Postmenopausal Women and Their Relationship with Oestrogen Responsiveness on Bone. *Clin Endocrinol (Oxf)* (2005) 62(3):349–53. doi: 10.1111/j.1365-2265.2005.02221.x
55. Chung YE, Lee SH, Lee SY, Kim SY, Kim HH, Mirza FS, et al. Long-Term Treatment with Raloxifene, but Not Bisphosphonates, Reduces Circulating Sclerostin Levels in Postmenopausal Women. *Osteo Int* (2012) 23(4):1235–43. doi: 10.1007/s00198-011-1675-1
56. Roth MJ, Moorehead RA. The Mir-200 Family in Normal Mammary Gland Development. *BMC Dev Biol* (2021) 21(1):12. doi: 10.1186/s12861-021-00243-7
57. Fontana A, Barbano R, Dama E, Pasculli B, Rendina M, Morritti MG, et al. Combined Analysis of Mir-200 Family and Its Significance for Breast Cancer. *Sci Rep* (2021) 11(1):2980. doi: 10.1038/s41598-021-82286-1
58. Kerschan-Schindl K, Hackl M, Boschitsch E, Foger-Samwald U, Nagele O, Skalicky S, et al. Diagnostic Performance of a Panel of MiRNAs (Osteomir) for Osteoporosis in a Cohort of Postmenopausal Women. *Calcif Tissue Int* (2021) 108(6):725–37. doi: 10.1007/s00223-020-00802-3
59. Straub RH. The Complex Role of Estrogens in Inflammation. *Endocr Rev* (2007) 28(5):521–74. doi: 10.1210/er.2007-0001
60. Faubion L, White TA, Peterson BJ, Geske JR, LeBrasseur NK, Schafer MJ, et al. Effect of Menopausal Hormone Therapy on Proteins Associated with Senescence and Inflammation. *Physiol Rep* (2020) 8(16):e14535. doi: 10.14814/phy2.14535
61. Lisse TS, Chun RF, Rieger S, Adams JS, Hewison M. Vitamin D Activation of Functionally Distinct Regulatory MiRNAs in Primary Human Osteoblasts. *J Bone Mine Res* (2013) 28(6):1478–88. doi: 10.1002/jbmr.1882
62. Bellido T, Ali AA, Gubrij I, Plotkin LI, Fu Q, O'Brien CA, et al. Chronic Elevation of Parathyroid Hormone in Mice Reduces Expression of Sclerostin by Osteocytes: A Novel Mechanism for Hormonal Control of Osteoblastogenesis. *Endocrinology* (2005) 146(11):4577–83. doi: 10.1210/en.2005-0239

63. Dawson-Hughes B, Harris SS, Ceglia L, Palermo NJ. Effect of Supplemental Vitamin D and Calcium on Serum Sclerostin Levels. *Eur J Endocrinol* (2014) 170(4):645–50. doi: 10.1530/EJE-13-0862
64. Acibucu F, Dokmetas HS, Acibucu DO, Kilicli F, Aydemir M, Cakmak E. Effect of Vitamin D Treatment on Serum Sclerostin Level. *Exp Clin Endocrinol Diabetes* (2017) 125(9):634–7. doi: 10.1055/s-0035-1559790
65. Randolph JF Jr, Sowers M, Bondarenko IV, Harlow SD, Luborsky JL, Little RJ. Change in Estradiol and Follicle-Stimulating Hormone across the Early Menopausal Transition: Effects of Ethnicity and Age. *J Clin Endocrinol Metab* (2004) 89(4):1555–61. doi: 10.1210/jc.2003-031183
66. Feurer E, Kan C, Croset M, Sornay-Rendu E, Chapurlat R. Lack of Association between Select Circulating MiRNAs and Bone Mass, Turnover, and Fractures: Data from the Ofely Cohort. *J Bone Mine Res* (2019) 34(6):1074–85. doi: 10.1002/jbmr.3685
67. You L, Pan L, Chen L, Gu W, Chen J. Mir-27a Is Essential for the Shift from Osteogenic Differentiation to Adipogenic Differentiation of Mesenchymal Stem Cells in Postmenopausal Osteoporosis. *Cell Physiol Biochem* (2016) 39(1):253–65. doi: 10.1159/000445621

Conflict of Interest: The authors declare that the research was conducted in the absence of any commercial or financial relationships that could be construed as a potential conflict of interest.

frontiers | Frontiers in Endocrinology

ORIGINAL RESEARCH
published: 22 June 2022
doi: 10.3389/fendo.2022.896640

Specific miRNAs Change After 3 Months of GH treatment and Contribute to Explain the Growth Response After 12 Months

*Cecilia Catellani[1,2], Gloria Ravegnini[3], Chiara Sartori[1], Beatrice Righi[1], Pietro Lazzeroni[1], Laura Bonvicini[4], Silvia Poluzzi[5], Francesca Cirillo[1], Barbara Predieri[5], Lorenzo Iughetti[5], Paolo Giorgi Rossi[4], Sabrina Angelini[3] and Maria Elisabeth Street[1,6]**

[1] Department of Mother and Child, Azienda Unità Sanitaria Locale – IRCCS di Reggio Emilia, Reggio Emilia, Italy, [2] PhD Program in Clinical and Experimental Medicine, University of Modena and Reggio Emilia, Modena, Italy, [3] Department of Pharmacy and Biotechnology, University of Bologna, Bologna, Italy, [4] Epidemiology Unit, Azienda Unità Sanitaria Locale – IRCCS di Reggio Emilia, Reggio Emilia, Italy, [5] Department of Medical and Surgical Sciences of the Mother, Children and Adults, University of Modena and Reggio Emilia, Modena, Italy, [6] Department of Medicine and Surgery, University of Parma, Parma, Italy

OPEN ACCESS

Edited by:
Mariacarolina Salerno, University of Naples Federico II, Italy

Reviewed by:
Donatella Capalbo, Federico II University Hospital, Italy
Anna Grandone, University of Campania Luigi Vanvitelli, Italy

***Correspondence:**
Maria Elisabeth Street
mariaelisabeth.street@unipr.it

Specialty section:
This article was submitted to Pediatric Endocrinology, a section of the journal Frontiers in Endocrinology

Received: *15 March 2022*
Accepted: *21 April 2022*
Published: *22 June 2022*

Citation:
Catellani C, Ravegnini G, Sartori C, Righi B, Lazzeroni P, Bonvicini L, Poluzzi S, Cirillo F, Predieri B, Iughetti L, Giorgi Rossi P, Angelini S and Street ME (2022) Specific miRNAs Change After 3 Months of GH treatment and Contribute to Explain the Growth Response After 12 Months. Front. Endocrinol. 13:896640. doi: 10.3389/fendo.2022.896640

Context: There is growing evidence of the role of epigenetic regulation of growth, and miRNAs potentially play a role.

Objective: The aim of this study is to identify changes in circulating miRNAs following GH treatment in subjects with isolated idiopathic GH deficiency (IIGHD) after the first 3 months of treatment, and verify whether these early changes can predict growth response.

Design and Methods: The expression profiles of 384 miRNAs were analyzed in serum in 10 prepubertal patients with IIGHD (5 M, 5 F) at two time points before starting GH treatment (t–3, t0), and at 3 months on treatment (t+3). MiRNAs with a fold change (FC) > +1.5 or <-1.5 at t+3 were considered as differentially expressed. *In silico* analysis of target genes and pathways led to a validation step on 8 miRNAs in 25 patients. Clinical and biochemical parameters were collected at baseline, and at 6 and 12 months. Simple linear regression analysis and multiple stepwise linear regression models were used to explain the growth response.

Results: Sixteen miRNAs were upregulated and 2 were downregulated at t+3 months. MiR-199a-5p (p = 0.020), miR-335-5p (p = 0.001), and miR-494-3p (p = 0.026) were confirmed to be upregulated at t+3. Changes were independent of GH peak values at testing, and levels stabilized after 12 months. The predicted growth response at 12 months was considerably improved compared with models using the common clinical and biochemical parameters.

Conclusions: MiR-199a-5p, miR-335-5p, and miR-494-3p changed after 3 months of GH treatment and likely reflected both the degree of GH deficiency and the sensitivity to treatment. Furthermore, they were of considerable importance to predict growth response.

Keywords: miR-199a-5p, miR-335-5p, miR-494-3p, growth, GH deficiency, GH treatment

1 INTRODUCTION

During the last decade, knowledge on epigenetics has increased, and in this context, microRNAs (miRNAs) have attracted the interest of researchers given their role as key regulators of multiple biological processes. MiRNAs are endogenous small non-coding RNAs that act as transcriptional (1, 2) and post-transcriptional regulators (3). Multiple changes in miRNA abundance can occur, where simultaneously up- and downregulated miRNAs can target the same gene with a range of predicted effects and, *vice versa*, a single miRNA can regulate several target genes (4). To date, the miRNA network is considered of fundamental importance for the regulation of gene expression (5). MiRNAs are key regulators of metabolic pathways (6–9), and are currently studied as biomarkers of disease and response to drug administration (10, 11). Evidence on longitudinal growth regulation by miRNAs has been reported in different *in vitro* and animal models (12, 13) and miRNAs have been described to contribute to the regulation of the hypothalamic–pituitary–IGF axis and to growth plate function (12). Currently, only one study has shown that miRNAs change under conditions of dysregulated growth hormone (GH) levels in humans (14). One *in vitro* study highlighted that the GH receptor can be regulated by specific miRNAs, suggesting that this regulatory system could be of importance for the GH axis (15). Finally, one recent study described that circulating miRNAs in adult patients and mice with congenital GH deficiency were regulated in relationship with aging (16). However, so far, no studies have investigated the changes in miRNA circulating levels in response to GH treatment in childhood.

The growth response in patients on GH treatment is variable depending both on the patient's basal conditions and on personal innate sensitivity to therapy (17). Often, the measured growth rate does not coincide with the expected one and the degree of correlation between clinical–auxological parameters and dose and GH peak vary enormously, both inter- and intra-individually during treatment. In this context, some patients run the risk of receiving an excessively low or high GH dose (18–20). Currently, in the attempt to improve the growth response, some medical devices on web platforms have become available in clinical practice (21). However, these interactive tools use universal algorithms based on growth prediction models built by collecting clinical data stored in international databases, and they can be used only after the first year of treatment.

This study aimed to identify changes in circulating miRNAs following GH treatment in children with isolated idiopathic GH deficiency (IIGHD) after the first 3 months of treatment, to explore their associations with clinical and biochemical parameters during the first 12 months of therapy, and to test the ability of early changes in these selected miRNAs to predict the clinical outcome in terms of growth on GH treatment.

2 PATIENTS AND METHODS

2.1 Patients

Ten prepubertal children at diagnosis of idiopathic isolated GH deficiency were enrolled for a preliminary profiling step [chronological age (CA): 8.80 ± 2.60 years; 5 male patients (M) and 5 female patients (F)]. Twenty-five prepubertal patients were included in the following validation step (CA: 9.08 ± 3.05 years); the main characteristics of the study cohort at diagnosis are reported in **Table 1**. All subjects were diagnosed with isolated idiopathic growth hormone deficiency (IIGHD) according to the official indications (22) and remained prepubertal throughout this 12-month study. At diagnosis, 24 subjects underwent an arginine stimulation test, and 1 underwent a clonidine stimulation test as the first test. Nineteen underwent a glucagon stimulation test and six underwent a clonidine stimulation test as the second test. All the subjects underwent a magnetic resonance imaging (MRI) scan of the hypothalamus and pituitary gland. Patients were enrolled at the pediatric endocrine centers in Reggio Emilia and Modena. Patients with ascertained or probable genetic syndromes (e.g., skeletal dysplasia, Silver-Russell syndrome) and/or obesity were excluded to further reduce the chances of confounding factors. The patients were treated with GH, according to the indications of the Italian Regulatory Agency (AIFA Note 39) and underwent routine practice for treatment. Both biosimilar and recombinant human GH were used.

For the purpose of analyses, patients were also subdivided according to GH peak concentrations (highest peak > or < 5 ng/ml) at testing, and based on response to GH treatment [change in height (Ht) SDS after 12 months on treatment > or < +0.3 SDS, defined as responders and non-responders, respectively) (23).

The study was approved by the local Ethical Committee (Study title: "Role of miRNAs as predictors of response to growth hormone (GH) in patients with GH deficiency" Prot no. 2016/0002409) at the Institutions. Written informed consent was obtained from all participants and their parents as appropriate.

The general workflow of the study is described in **Figure 1**.

2.2 Sample Processing and Total RNA Isolation

Whole blood was drawn in BD Vacutainer Serum Separator Tubes, and it was processed within 2 h from collection and after overnight fasting, between 7:30 and 8:30 a.m. Whole blood was then centrifuged at 2,000 *g* for 10 min at 4°C. Serum was aliquoted in 1.5-ml sterile RNase-free tubes and further centrifuged at 2,500 *g* for 10 min at 4°C to remove any contaminant cells and debris. Serum was then collected in sterile RNase-free tubes and stored at −80°C until use. Blood samples were collected at two time points before the beginning of treatment (3 months before, t−3, and just before the treatment, t0), and at 3 and 12 months after the beginning of the treatment (t+3 and t+12) in the context of routine controls. Total RNA was isolated from 400 µl of serum using the miRVana PARIS kit (Invitrogen Cat No. AM1556) according to the manufacturer's protocol and the eluate was stored at −80°C. RNA was reverse-transcribed using the TaqMan™ Advanced miRNA cDNA Synthesis Kit (Applied Biosystems Cat No. A28007) following the manufacturer's instructions.

2.3 Discovery Step: miRNA Expression Profiling

The expression profiles of 384 miRNAs were analyzed in 10 patients, of which 5 were male patients and 5 were female

TABLE 1 | Auxological and biochemical features of patients at baseline, and at 6 and 12 months of GH treatment.

	Baseline	6 months of treatment	12 months of treatment
Sex, M/F	17/8		
CA, years	9.08 ± 3.05		
Target height, cm	166.1 ± 8.12		
Target height SDS	−0.96 ± 0.81		
Highest GH peak N<5 ng/ml/N>5 ng/ml	7/18		
GH peak at first test, ng/ml	4.23 ± 2.06		
GH peak at second test, ng/ml	5.14 ± 2.01		
Bone age, years	7.35 ± 2.77		8.41 ± 2.88
Height, cm	119.22 ± 16.79	124.22 ± 16.88	127.96 ± 16.78
Height SDS	−1.92 ± 0.37	−1.61 ± 0.39*	−1.48 ± 0.39#
Weight, kg	23.17 ± 7.39	25.38 ± 8.51	27.39 ± 9.10
Weight SDS	−1.79 ± 0.74	−1.62 ± 0.79*	−1.45 ± 0.79#
BMI, kg/m^2	15.85 ± 1.48	15.92 ± 1.78	16.21 ± 1.93
BMI SDS	−0.49 ± 0.79	−0.61 ± 0.88	−0.55 ± 0.91
Growth velocity, cm/year §	4.49 ± 1.59	8.03 ± 1.69	7.19 ± 1.51
Growth velocity SDS §	−1.60 ± 1.04	2.78 ± 1.99*	1.82 ± 2.40#
IGF-I, ng/ml	150.96 ± 62.86	281.22 ± 127.69	284.33 ± 113.92
IGF-I SDS	−0.03 ± 0.59	0.88 ± 0.76*	0.79 ± 0.63#
Fasting blood glucose, mg/dl	81.44 ± 4.75	85.44 ± 8.61	86.07 ± 7.14
Insulin, μU/ml		7.73 ± 4.41	8.83 ± 5.30
HbA1c, mmol/mol		33.18 ± 3.00	32.83 ± 2.96
Alkaline phosphatase, U/L	267.43 ± 136.97	603.59 ± 216.75	448.33 ± 227.44
Drug, N recombinant/N biosimilar	11/14		
GH dose, mg/kg/day	0.028 ± 0.004	0.023 ± 0.004	0.023 ± 0.004
Hypothalamus–pituitary MRI	*N* = 1 Rathke's cleft cyst *N* = 2 small pituitary gland *N* = 22 normal		

*BMI, body mass index; CA, chronological age; F, females; FBG, fasting blood glucose; GH, growth hormone; HbA1c, glycated hemoglobin; IGF-I, insulin-like growth factor 1; M, males; N, number; SD, standard deviation; SDS, standard deviation score; U, units. §calculated on the previous 6 months. *p < 0.0001 baseline vs. 6 months on treatment. #p < 0.0001, baseline vs. 12 months on treatment. Data are reported as mean ± SD.*

patients (10 samples collected at t−3, 10 samples at t0, and 10 samples at t+3) to avoid gender-specific miRNAs, using TaqMan Advanced miRNA Human A Cards (Applied Biosystems Cat No. A34714) that contain 384 miRNA assays. Briefly, 2 μl of RNA eluate was reverse-transcribed to cDNA, using the TaqMan Advanced miRNA cDNA synthesis kit (Applied Biosystems Cat No. A28007) following the manufacturer's instructions in the Thermal Cycler T100 (Bio-Rad). The cDNA was loaded into the TaqMan Advanced miRNA array Card A and run in a 7900HT Fast PCR system (Applied Biosystems). Array data were normalized using the standard internal reference hsa-miR-16-5p (Assay ID: 477860_mir) as endogenous control (24); to be sure about its validity, we selected hsa-miR-16-5p after assessment of its stability in our study cohort and further review of the literature (24). The data were analyzed using the $2^{-\Delta\Delta Ct}$ method and miRNAs with Ct > 35 were considered as not expressed and excluded from further analysis. Moreover, those miRNAs changing significantly (p-value at paired Student's t-test ≤0.05) in the two time points before starting treatment (t−3 and t0) were excluded in order to not consider those miRNAs changing for other causes independent of treatment. Considering the exploratory purpose of the study and based on the number of subjects analyzed, we did not perform FDR correction. The miRNAs having a fold change (FC) ($\log_2 2^{-\Delta\Delta Ct}$) >+1.5 or FC ($\log_2 2^{-\Delta\Delta Ct}$) < −1.5 between baseline and 3 months on treatment were considered as differentially expressed.

An *in silico* analysis was performed to identify the validated target genes and pathways for each differentially expressed miRNA in order to select those expected to be involved with growth. In particular, the network that represents miRNA target interactions and highlights the most impacted pathways was obtained from the miRNet v 2.0 online tool (25). This tool collects data from three well-annotated databases, miRTarBase v8.0, TarBase v8.0, and miRecords. The significance was set at a p-value of 0.05.

2.4 Validation of the Profiling Results by Real-Time qRT-PCR

MiRNAs for the validation step were chosen based on FC (>+1.5 or <−1.5) between baseline and 3 months on treatment, and based on miRNA target gene analysis. Eight miRNAs were selected and evaluated by TaqMan Advanced miRNA assays (Applied Biosystems): hsa-miR-22-3p (Assay ID: 477985_mir), hsa-miR-30c-5p (Assay ID: 478008_mir), hsa-miR-106a-5p (Assay ID: 478225_mir), hsa-miR-140-5p (Assay ID: 477909_mir), hsa-miR-199a-5p (Assay ID: 478231_mir), hsa-miR-335-5p (Assay ID: 478324_mir), hsa-miR-340-5p (Assay ID: 478042_mir), and hsa-miR-494-3p (Assay ID: 478135_mir). cDNA was prepared as described above (*Section 2.3*), and miRNA expression was evaluated according to the manufacturer's protocol and run in triplicate in a 7900HT Fast PCR system (Applied Biosystems). Data were normalized using hsa-miR-16-5p (Assay ID: 477860_mir) as endogenous control (24). The validation analysis was performed at two time points t0 and t+3. In addition, miRNA levels were analyzed at 12 months on treatment (t+12).

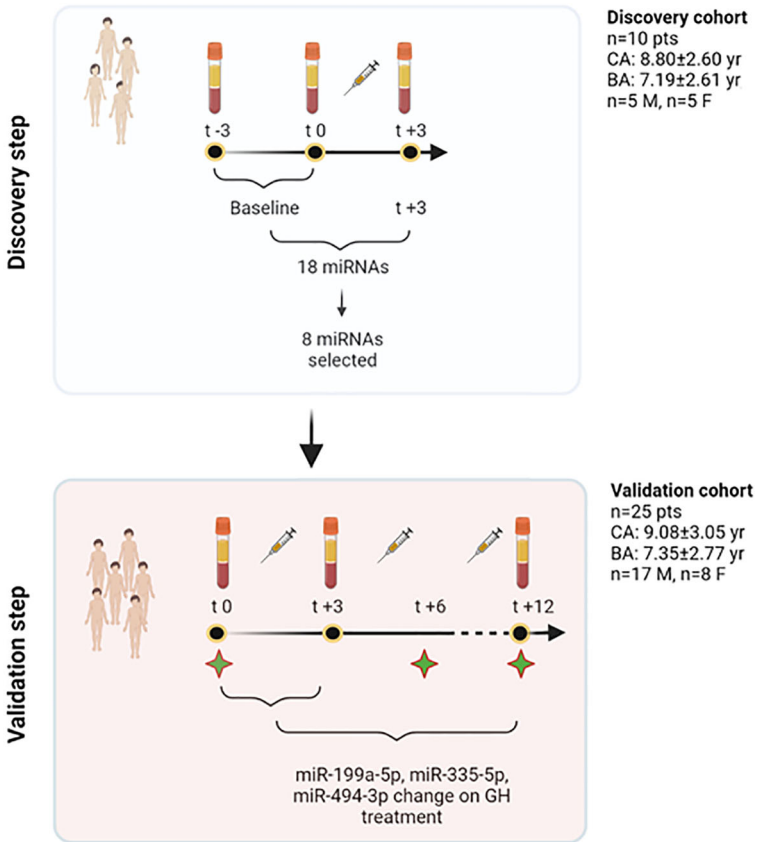

FIGURE 1 | Study workflow. In the discovery step, a profiling approach was used, and all those miRNAs showing spontaneous variations independent of treatment (–3 and 0 months) were excluded from further analyses. Eighteen miRNAs were found to show changes at +3 months. Based on their function, 8 miRNAs were selected out of this initial pool of 18. The validation phase used TaqMan Real-Time qRT-PCR approach and studied the response of these 8 miRNAs at 3 months on GH treatment in 25 patients. Three specific miRNAs were found to change significantly on treatment, and were included, together with other clinical and biochemical variables, to contribute to explain growth after 1 year of treatment. To further understand miRNA changes on treatment, these were further measured in serum at 12 months. Green stars in the figure represent time points in which clinical and biochemical data have been recorded (t0, t+6, t+12). BA, bone age; CA, chronological age; F, females; GH, growth hormone; M, males; n, number; pts, patients; yr, years. Created with BioRender.com.

2.5 Auxological Parameters and Bone Age

A full auxological assessment was done at baseline, 6 months, and 12 months on treatment and medical history was taken. Body mass index (BMI), calculated as weight/height^2 (kg/m^2), and weight were converted to standard deviation scores (SDS) using the references of Cole et al. (26). Height (Ht) and target height (THt) were recorded and expressed as SDS, using the Tanner reference data (27). Height velocity SDS was calculated using Tanner's references (27). Bone age was assessed according to the Greulich and Pyle Atlas reference (28). Puberty in all subjects was staged according to the criteria of Marshall and Tanner (29, 30).

2.6 Biochemical Parameters

Alkaline phosphatase and blood glucose were measured using Atellica CH Alkaline Phosphatase Concentrated (ref. 11097600) and Atellica CH Glucose Hexokinase 3 (ref. 11097592) assays on the Atellica CH Analyzer, respectively. HbA1c was assayed by HPLC on the D-100 System (Bio-Rad). Insulin, GH, and IGF-I levels were measured using chemiluminescence methods: LIAISON Insulin (Ref. 310360), LIAISON hGH (ref. 310340), and LIAISON IGF-I (ref. 313231) immunoassays, respectively, on the LIAISON Analyzer Diasorin. IGF-I concentrations were converted to SDS based on the reference values provided by the manufacturer.

2.7 Statistical Analysis

Paired Student's *t*-test ($p \leq 0.05$) was used to identify miRNAs that were differentially expressed after 3 months of GH treatment with respect to the baseline (t0, t+3). Moreover, paired Student's *t*-test was used to evaluate differences between baseline patient's characteristics and after 6 and 12 months of treatment. These comparisons were made only on the standardized parameters.

The associations of miRNA values at baseline, at 3 months and their change during this time frame (delta 0–3 months) with baseline clinical features, and with 6- and 12-month recorded

clinical and biochemical data were analyzed. In addition, the associations of 12-month miRNA levels with clinical and biochemical parameters at 12 months were investigated by means of simple linear regression analysis. The distribution of height SDS and growth rate SDS at baseline and at 6 and 12 months were also analyzed (**Figure 2**) in order to select the meaningful time horizon for measuring the two outcomes.

Multiple linear regression models were performed in order to investigate the major determinants of height variations between 0 and 6 months and between 0 and 12 months, and the variance of growth rate variation between 0 and 6 months. A set of models that considered only auxological parameters at baseline were estimated: the first one included only auxological parameters; the other models were estimated by adding, one by one, as independent variables, GH peaks at testing, GH dose at the beginning of treatment, IGF-I SDS at baseline, the difference between CA and bone age at baseline, and baseline levels and change in miRNA levels during the first 3 months of treatment. Finally, the models were estimated with a backward stepwise selection estimation method with significance level for removal from the model set to 0.2 considering the following as independent variables: sex, CA at the beginning of treatment, genetic target SDS, treatment dose (mg/kg/day), height SDS at baseline, weight SDS at baseline, peak at first GH stimulation test (ng/ml), peak at second GH simulation test (ng/ml), IGF-I SDS (t0), difference between CA and bone age at baseline, miR-199a-5p (t0), delta (0–3) miR-199a-5p, miR-355-5p (t0), delta (0–3) miR-335-5p, miR-494-3p (t0), and delta (0–3) miR-494-3p.

To define the degree of accuracy or predictive effectiveness of the model, leave-one-out cross-validation analysis was performed for each model. Specifically, we reported the variations in adjusted R^2, meaning the percentage of variance in the outcome explained by the variable included in the model adjusted for the number of degrees of freedom spent by the model parameters, and R^2 CV as a measure of the variance, explained by the models corrected with the cross-validation method. In this way, we built 25 models excluding patients one by one, and we predicted the growth parameter of the excluded patient with the parameters estimated by the model. The best models obtained are reported in the text. For the associations explored in these models, we did not perform a formal statistical test of hypothesis, and p-values should be interpreted as continuous variables without any threshold. Furthermore, p-values should be interpreted cautiously because there is an issue of multiple testing, but no easy solutions for false discovery rate adjustments were identified since it is not possible to determine the total set of independent comparisons. Comparison of miRNA expression levels in responders vs. non responders was also performed, as well as a comparison according to GH peak concentrations as specified above. Statistical analyses were performed using STATA v16.0 (STATA Corp., College Station, TX, USA).

3 RESULTS

3.1 Growth and Biochemical Outcomes During the First Year of Treatment

All clinical and biochemical characteristics of the subjects are summarized in **Table 1**. Height SDS both at 6 months and at 1 months on treatment was significantly increased with respect to baseline (-1.92 ± 0.37 vs. −1.61 ± 0.39, $p < 0.0001$, and −1.92 ± 0.37 vs. −1.48 ± 0.39, $p < 0.0001$, respectively) (**Figure 2**). Although BMI SDS decreased on treatment, no significant change was observed. Growth velocity (GV) SDS after 6 months (−1.60 ± 1.04 vs. 2.78 ± 1.99, $p < 0.0001$) and 12 months on treatment was significantly increased with respect to pre-treatment growth velocity, but decreased during the second 6 months on GH (2.78 ± 1.99 vs. 1.82 ± 2.40) (**Figure 2**). IGF-I SDS increased after 6 months on treatment with respect to baseline (0.88 ± 0.76 vs. −0.03 ± 0.59, $p <$ 0.0001), remaining almost stable in the following 6 months on treatment. Alkaline phosphatase increased on treatment but changes were not statistically significant, whereas fasting blood glucose and HbA1c remained stable.

3.2 Discovery miRNA Profiling Step

The profiling step was preliminarily performed in order to select a pool of miRNAs of interest for the following analyses. Among

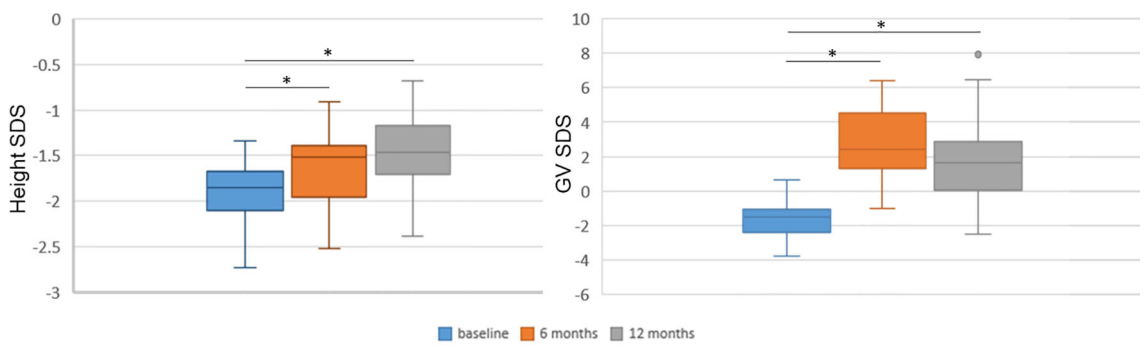

FIGURE 2 | Height and growth velocity over time. Height and growth velocity are represented with respect to the previous 6 months. Height and growth velocity (GV) were standardized according to Tanner's standards. SDS, standard deviation score. *$p < 0.0001$ versus baseline at paired Student's t-test.

the miRNAs analyzed, 186 were detectable and measured in the serum of patients. Those miRNAs changing significantly ($p < 0.05$ at paired Student's *t*-test) between the two time points before starting treatment (t−3; t0) were excluded, as changes were considered to be independent of treatment. Sixteen miRNAs (hsa-let-7a-5p, hsa-let-7e-5p, hsa-miR-30c-5p, hsa-miR-34a-5p, hsa-miR-132-3p, hsa-miR-140-5p, hsa-miR-199a-5p, hsa-miR-330-3p, hsa-miR-335-5p, hsa-miR-340-5p, hsa-miR-369-3p, hsa-miR-375, hsa-miR-450a-5p, hsa-miR-494-3p, hsa-miR-582-5p, and hsa-miR-421) had an FC >+1.5 and were considered as upregulated after 3 months of treatment with respect to baseline; two miRNAs (hsa-miR-22-3p and hsa-miR-106a-5p) had an FC < −1.5 and were considered to be downregulated after 3 months of GH treatment with respect to baseline.

3.3 Pathway Enrichment Analysis

Pathway enrichment analysis of these 18 miRNAs evidenced that they were significantly involved in the regulation of 100 different pathways ($p < 0.05$). Among these 18 miRNAs (**Table 2**), those predicted to be involved in the regulation of longitudinal growth and bone development were selected for the validation step, namely, miR-22-3p, miR-30c-5p, miR-106a-5p, miR-140-5p, miR-199a-5p, miR-335-5p, miR-340-5p, and miR-494-3p (**Figure 3**). These miRNAs were predicted to regulate genes involved in Wnt-β-catenin signaling, Notch signaling, PI3K/AKT, and TGF-β signaling that are relevant for growth (**Figure 3**).

3.4 miRNA Validation Step

MiR-22-3p, miR-30c-5p, miR-106a-5p, miR-140-5p, miR-199a-5p, miR-335-5p, miR-340-5p, and miR-494-3p were selected to be validated in single assay, at baseline, and at 3 months on treatment, in the larger group of patients (**Table 2**). This study highlighted that miR-199a-5p ($p = 0.020$), miR-335-5p ($p = 0.001$), and miR-494-3p ($p = 0.026$) were upregulated after 3 months with respect to baseline (**Figure 4**). The measurements at 12 months of treatment showed that the circulating levels of these specific miRNAs were more stable and that the inter-individual variance was smaller than that observed at the other two time points (**Figures 5A, C, E**, **S1**).

Based on the GH peaks (highest peak > or < 5 ng/ml), no differences in miRNA levels were observed at baseline or at 3 and 12 months, nor was there any difference in the change at 3 months versus baseline. MiRNA levels were more variable in the non-responder patients with respect to responders (< or > +0.3 SDS) (**Figures 5B, D, F**). No differences in miRNA levels were observed based on the type of GH used for treatment (biosimilar vs. rhGH).

TABLE 2 | Differentially expressed miRNAs after 3 months of GH treatment with respect to the baseline in 10 prepubertal patients with IIGHD.

miRNA	Fold Change ($log_2 2^{-\Delta\Delta Ct}$)	Up/down
hsa-miR-375	3.1	Up
hsa-let-7e-5p	2.5	Up
hsa-miR-340-5p	2.4	Up
hsa-miR-494-3p	2.1	Up
hsa-miR-34a-5p	2.1	Up
hsa-miR-30c-5p	1.9	Up
hsa-let-7a-5p	1.8	Up
hsa-miR-140-5p	1.8	Up
hsa-miR-421	1.8	Up
hsa-miR-132-3p	1.7	Up
hsa-miR-330-3p	1.7	Up
hsa-miR-369-3p	1.7	Up
hsa-miR-582-5p	1.7	Up
hsa-miR-450a-5p	1.6	Up
hsa-miR-335-5p	1.6	Up
hsa-miR-199a-5p	1.6	Up
hsa-miR-106a-5p	−1.8	Down
hsa-miR-22-3p	−3.1	Down

Fold change (FC) was calculated as $log_2 2^{-\Delta\Delta Ct}$. MiRNAs with an FC > 1.5 were considered as upregulated and miRNAs with an FC < −1.5 were considered as downregulated.

3.5 Simple Linear Regression Analysis and Multiple Stepwise Linear Regression Models to Explain Growth Response

All possible associations between baseline characteristics and miRNA values at baseline, at 3 months of treatment, and miRNA variations during the first 3 months (ΔΔCt 0–3 months) were analyzed in order to evaluate whether a variable could be critical for the building of a model (**Tables 3A–C**) . Several models starting from auxological parameters at baseline, GH peaks at testing, and GH dose at the beginning of treatment, IGF-I SDS at baseline, bone age and difference between CA and bone age, baseline levels, and change in miRNA levels during the first 3 months of treatment were used to explain the change in height SDS over the first 6 and 12 months of treatment, and growth velocity during the first 6 months of treatment (**Tables 4A–C**). Change in growth velocity from 0 to 12 months after treatment was not included, since the change in growth velocity was not constant during the period as shown in **Figure 2**.

With regard to the change in HtSDS (0–6 months), each single miRNA gave a contribution to the model comparable to that given by IGF-I SDS and the peak GH value, without a substantial improvement in the model that used auxological parameters only. The difference between chronological age and bone age substantially increased the ability of the model to predict the outcome. The final model, obtained with a stepwise procedure, included miR-335-5p and miR-494-3p together with the other variables (**Table 4A**).

Considering the outcome delta HtSDS (0–12 months), miR-199a-5p was the miRNA that most improved the model containing the auxological parameters only, and its contribution was more important than that of IGF-I SDS and peak GH values. The difference between chronological age and bone age was the single best predictor, whereas the stepwise procedure identified a model including miR-335-5p, miR-494-3p, sex, CA, target height SDS, GH dose, and the difference between chronological age and bone age as the best highly predictive model (**Table 4B**).

With regard to growth velocity SDS (0–6 months), only one miRNA (miR-199a-5p) contributed to the model when the miRNAs were included one by one. The variance was explained better by this miRNA than by IGF-I SDS at baseline, GH peak values, and the difference between chronological age and bone age. The stepwise procedure identified a highly predictive model including miR-335-5p, miR-199a-5p, sex, CA,

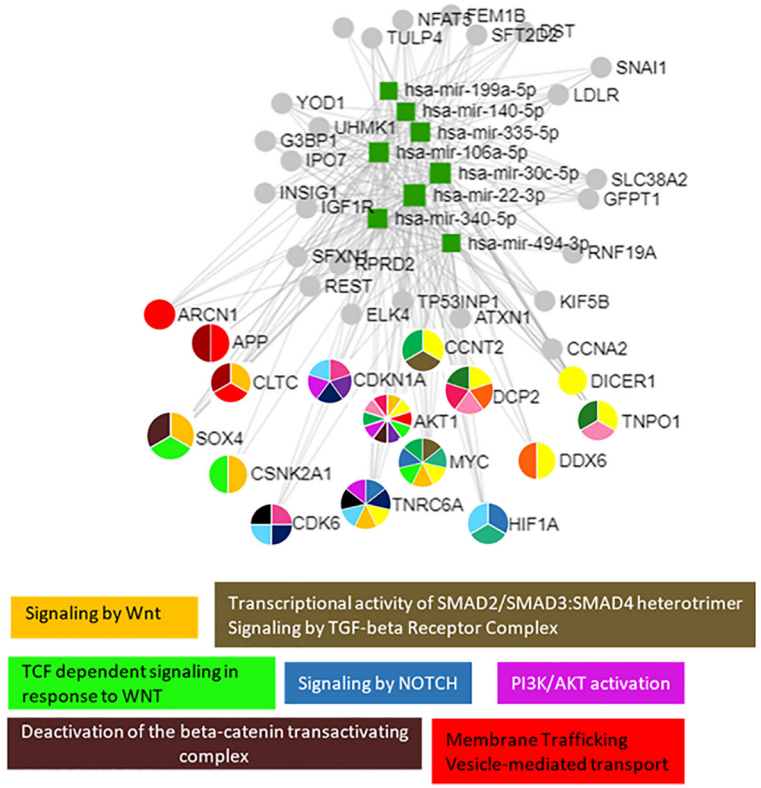

FIGURE 3 | The 8 selected miRNAs regulated genes and pathways that are important for growth. Analyses were carried out using miRNet v 2.0 and only significantly predicted pathways ($p < 0.05$) were selected to generate the figure.

weight SDS, target height SDS, GH dose, peak GH values at testing, and the difference between chronological age and bone age (**Table 4C**).

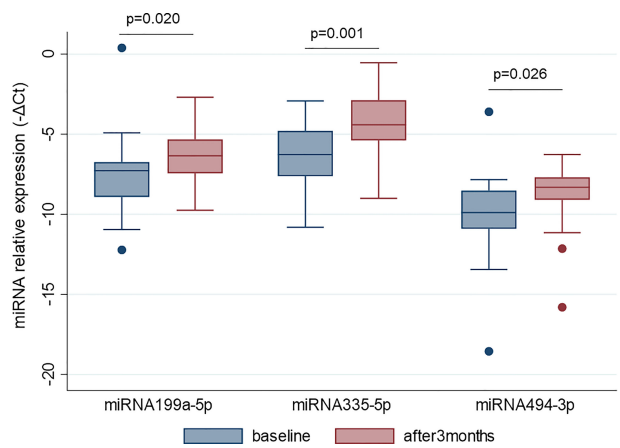

FIGURE 4 | MiR-199a-5p, miR-335-5p and miR-494-3p are upregulated after 3 months of GH treatment with respect to the baseline. MiRNA levels are expressed as –ΔCt where ΔCt is calculated as: Ct miRNA – Ct miR-16-5p. p-value ≤ 0.05 at paired Student's t-test.

4 DISCUSSION

Using an miRNA profiling approach, 18 miRNAs were found to change after the first 3 months of GH treatment in IIGHD prepubertal patients. The subsequent validation phase in a larger group of patients showed that miR-335-5p, miR-199a-5p, and miR-494-3p were significantly upregulated at 3 months, and both the baseline circulating levels and their change (0–3 months) contributed to explain growth at 12 months of treatment improving the growth prediction substantially based on baseline clinical features, and GH peaks during the stimulation tests at diagnosis.

To the best of our knowledge, this is the first study that analyzes the change in circulating miRNA levels in response to GH treatment. This study considered only prepubertal subjects with IIGHD in order to reduce confounding factors. In fact, as the miRNA network is a key modulator of gene expression, it changes throughout life (13, 31, 32), and is also dependent on body weight (33).

A previous paper by Kelly et al. (15) considered miRNA expression levels as potential markers of GH administration in humans to evaluate whether they could detect doping in sports. In particular, this study involved a total of 20 subjects subdivided into three groups (6 individuals receiving replacement doses of GH, 11 acromegalic patients, and 3 individuals with no abnormalities in GH secretion); miRNA microarray analyses were performed on a

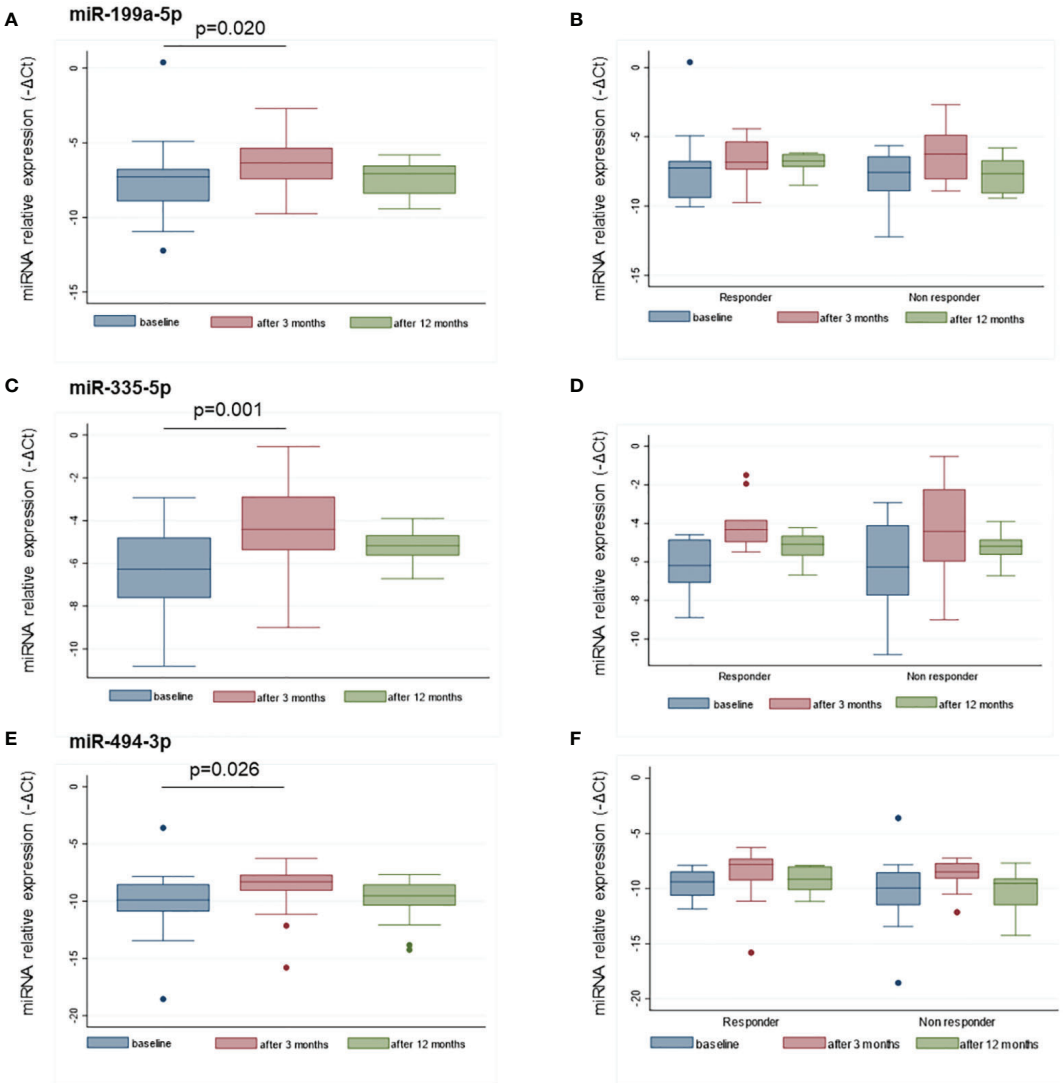

FIGURE 5 | Distributions of miR-199a-5p **(A)**, miR-335-5p **(C)**, and miR-494-3p **(E)** at baseline, and after 3 and 12 months of treatment. The distribution of the same miRNAs in responders and non-responders to GH treatment are reported at the same time points in panels **(B, D, F)**. MiRNA levels are expressed as –ΔCt where ΔCt is calculated as: Ct miRNA – Ct miR-16-5p. *p*-value ≤ 0.05 at paired Student's *t*-test.

subgroup of 4 acromegalic patients, 3 rhGH users, and 2 individuals with no known pituitary disorders evidencing that miR-2861, miR-663, miR-3152, and miR-3185 were reduced when rhGH was administered (15). A previous *in vitro* study reported that the GH receptor was regulated by specific miRNAs that inhibited GH receptor expression (16), suggesting that this regulatory system was of importance for the GH axis. We recently reviewed the regulation by miRNAs not only at the GH receptor level but also on the GH signaling pathway, on IGFs, and IGF1 receptor signaling in different *in vitro* and animal models highlighting their importance for growth (13). Interestingly, the miRNAs we found to be differentially expressed in the current study have not been investigated previously in the context of GH secretion, signaling, and the IGF system. These findings suggest that further relationships between miRNAs, the GH/IGF-1 axis, and the IGF system will be disclosed in the near future. With regard to the function of the specific miRNAs, miR-199a-5p and miR-335-5p, they play a role in bone formation and osteoblast differentiation *in vitro*. In particular, miR-199a-5p is involved in osteoblast differentiation, and its upregulation increases alkaline phosphatase (ALP) activity, calcification, and the expression of osteoblast differentiation markers such as Runx2, Osterix, and Osteocalcin in human bone marrow stem cells (34). The overexpression of miR-335-5p has been reported to promote bone formation and regeneration in a transgenic mouse model (35). A previous study from this same group highlighted that miR-335-5p reduced the expression of DKK1, an inhibitor of the Wnt signaling pathway, which is pivotal for bone development (36). Moreover, miR-335-5p overexpression

TABLE 3 | Associations between baseline characteristics, miR-199a-5p **(A),** miR-335-5p **(B),** and miR-494-3p **(C)** levels at baseline, their change between baseline and 3 months (delta), and after 3 months of treatment.

A: miRNA-199a-5p												
Baseline characteristics	**miRNA-199a-5p**											
	Baseline				**delta 0–3 months**				**3 months**			
	coef	***p*-value**	**95% CI**		**coef**	***p*-value**	**95% CI**		**coef**	***p*-value**	**95% CI**	
Sex, M/F	0.49	0.646	−1.68	2.65	−0.72	0.503	−2.89	1.46	−0.23	0.767	−1.80	1.34
Bone age, years	0.06	0.765	−0.35	0.46	−0.18	0.368	−0.58	0.23	−0.12	0.388	−0.40	0.16
CA, years	0.03	0.876	−0.31	0.36	−0.15	0.361	−0.49	0.18	−0.13	0.288	−0.37	0.11
Height SDS	3.34	0.009	0.91	5.78	−3.20	0.015	−5.71	−0.70	0.14	0.891	−1.91	2.19
Weight SDS	0.81	0.222	−0.53	2.16	−0.28	0.687	−1.67	1.12	0.54	0.266	−0.44	1.52
BMI SDS	0.38	0.545	−0.91	1.67	0.37	0.567	−0.94	1.67	0.75	0.093	−0.14	1.64
IGF-I SDS	1.42	0.088	−0.23	3.06	−0.70	0.415	−2.45	1.05	0.72	0.242	−0.52	1.95
Alkaline phosphatase, U/L	0.01	0.136	−0.00	0.02	−0.00	0.936	−0.02	0.02	0.01	0.108	−0.00	0.02
GH peak at first stimulation test, ng/ml	−0.14	0.573	−0.64	0.36	0.12	0.616	−0.38	0.63	−0.01	0.938	−0.38	0.35
GH peak at second stimulation test, ng/ml	−0.11	0.666	−0.62	0.40	0.12	0.640	−0.40	0.64	0.01	0.955	−0.36	0.38
Biosimilar vs. human recombinant GH	−0.24	0.807	−2.28	1.80	−0.00	0.999	−2.07	2.07	−0.24	0.737	−1.72	1.23
GH dose, mg/kg/day	34.16	0.796	−236.45	−304.78	24.37	0.856	−249.54	298.28	58.53	0.54	−136.05	253.12
B: miRNA-335-5p												
Baseline characteristics	**miRNA-335-5p**											
	Baseline				**Delta 0–3 months**				**3 months**			
	coef	***p*-value**	**95% CI**		**coef**	***p*-value**	**95% CI**		**coef**	***p*-value**	**95% CI**	
Sex, M/F	0.97	0.309	−0.96	2.91	−0.48	0.699	−2.99	2.04	0.50	0.592	−1.39	2.39
Bone age, years	0.22	0.200	−0.13	0.57	−0.12	0.551	−0.54	0.29	0.10	0.520	−0.22	0.42
CA, years	0.13	0.371	−0.17	0.44	−0.04	0.827	−0.44	0.35	0.09	0.525	−0.20	0.39
Height SDS	−0.07	0.954	−2.65	2.50	0.21	0.896	−3.07	3.49	0.14	0.909	−2.34	2.61
Weight SDS	0.31	0.611	−0.94	1.57	0.55	0.486	−1.05	2.14	−0.86	0.138	−2.02	0.30
BMI SDS	0.34	0.554	−0.83	1.52	0.46	0.529	−1.04	1.96	0.80	0.139	−0.28	1.89
IGF-I SDS	−1.26	0.097	−2.76	0.25	1.12	0.254	−0.86	3.1	−0.14	0.854	−1.67	1.40
Alkaline phosphatase, U/L	0.00	0.856	−0.02	0.02	0.01	0.253	−0.01	0.03	0.01	0.264	−0.01	0.03
GH peak at first stimulation test, ng/ml	−0.04	0.863	−0.50	0.42	−0.03	0.903	−0.62	0.55	−0.07	0.733	−0.51	0.37
GH peak at second stimulation test, ng/ml	0.24	0.413	−0.35	0.83	0.24	0.413	−0.35	0.83	0.23	0.296	−0.21	0.67
Biosimilar vs. human recombinant GH	0.98	0.276	−0.83	2.79	−0.96	0.403	−3.3	1.37	0.02	0.985	−1.77	1.80
GH dose, mg/kg/day	87.36	0.466	−156.39	331.11	−215.9	0.151	−516.31	84.51	−128.54	0.260	−358.94	101.86
C: miRNA-494-3p												
Baseline characteristics	**miRNA-494-3p**											
	Baseline				**Delta 0–3 months**				**3 months**			
	coef	***p*-value**	**95% CI**		**coef**	***p*-value**	**95% CI**		**coef**	***p*-value**	**95% CI**	
Sex, M/F	0.08	0.942	−2.27	2.44	−1.65	0.142	−3.90	0.60	−1.57	0.066	−3.25	0.11
Bone age, years	−0.31	0.141	−0.72	0.11	0.31	0.138	−0.11	0.72	−0.00	0.993	−0.34	0.34
CA, years	−0.24	0.168	−0.59	0.11	0.18	0.318	−0.18	0.54	−0.06	0.638	−0.35	0.22
Height SDS	0.36	0.808	−2.70	3.43	−2.20	0.134	−5.12	0.73	−1.83	0.102	−4.05	0.39
Weight SDS	0.83	0.249	−0.63	2.30	−0.78	0.282	−2.25	0.69	0.05	0.927	−1.10	1.21
BMI SDS	1.17	0.078	−0.14	2.49	−0.75	0.272	−2.12	0.63	0.42	0.420	−0.64	1.49
IGF-I SDS	2.14	0.014	0.47	3.80	−1.66	0.065	−3.42	0.11	0.48	0.499	−0.97	1.93
Alkaline phosphatase, U/L	0.01	0.273	−0.01	0.04	−0.01	0.491	−0.03	0.02	0.01	0.058	−0.00	0.01
GH peak at first stimulation test, ng/ml	0.18	0.503	−0.36	0.72	0.03	0.903	−0.51	0.58	0.21	0.299	−0.20	0.62
GH peak at second stimulation test, ng/ml	−0.01	0.977	−0.57	0.55	−0.01	0.971	−0.57	0.55	−0.02	0.932	−0.45	0.41
Biosimilar vs. human recombinant GH	−1.15	0.281	−3.31	1.01	0.24	0.822	−1.97	2.46	−0.91	0.268	−2.56	0.75
GH dose, mg/kg/day	−95.24	0.505	−385.97	195.49	50.98	0.722	−242.33	344.3	−44.25	0.688	−269.2	180.69

Data are presented as linear regression coefficients, p*-value, and 95% CI.*

BMI, body mass index; CA, chronological age; CI, confidence interval; coef, coefficient; F, females; GH, growth hormone; IGF-I, insulin-like growth factor 1; M, males; SDS, standard deviation score. U, units.

TABLE 4 | Multiple regression models to predict the change in height SDS during the first 6 months **(A)** and 12 months **(B)** of treatment, and growth velocity during the first 6 months of treatment **(C)**.

A

		Delta height 0–6	
		Adj R^2	R^2 CV
Model 1	Sex, CA (years), GH dose (mg/kg/day), height (SDS), weight (SDS), target height (SDS)	0.53	0.11
Model 2	Sex, CA (years) GH dose (mg/kg/day), height (SDS), weight (SDS), target height (SDS), GH peaks (ng/ml)	0.49	0.04
Model 3	Sex, CA (years), GH dose (mg/kg/day), height (SDS), weight (SDS), target height (SDS), IGF-I (SDS)	0.51	0.08
Model 4	Sex, CA (years), GH dose (mg/kg/day), height (SDS), weight (SDS), target height (SDS), difference between CA and bone age	0.62	0.21
Model 5	Sex, CA (years), GH dose (mg/kg/day), height (SDS), weight (SDS), target height (SDS) and:		
	miR-199a-5p (baseline and delta 0–3)	0.59	0.15
	miR-355-5p (baseline and delta 0–3)	0.49	0.07
	miR-494 -3p (baseline and delta 0–3)	0.48	0.06
Model 6—STEPWISE	Selected variables: sex, CA (years), target height (SDS), GH dose (mg/kg/day), height (SDS), weight (SDS), difference between CA and bone age (years), GH peak at second test (ng/ml), miR-335-5p baseline, delta 0–3 months miR-335-5p, delta 0–3 months miR-494-3p.	0.72	0.02

B

		Delta height 0–12	
		Adj R^2	R^2 CV
Model 1	Sex, CA (years), GH dose (mg/kg/day), height (SDS), weight (SDS), target height (SDS)	0.36	0.15
Model 2	Sex, CA (years), GH dose (mg/kg/day), height (SDS), weight (SDS), target height (SDS), GH peaks (ng/ml)	0.31	0.02
Model 3	Sex, CA (years), GH dose (mg/kg/day), height (SDS), weight (SDS), target height (SDS), IGF-I (SDS)	0.36	0.10
Model 4	Sex, CA (years), GH dose (mg/kg/day), height (SDS), weight (SDS), target height (SDS), difference between chronological age and bone age	0.67	0.44
Model 5	Sex, CA (years), GH dose (mg/kg/day), height (SDS), weight (SDS), target height (SDS), and:		
	miR-199a-5p (baseline and delta 0–3)	0.41	0.20
	miR-355-5p (baseline and delta 0–3)	0.34	0.01
	miR-494 -3p (baseline and delta 0–3)	0.29	0.12
Model 6—STEPWISE	Selected variables: sex, CA (years), target height (SDS), GH dose (mg/kg/day), difference between CA and bone age, delta 0–3 months miR-335-5p, delta 0–3 months miR-494-3p.	0.79	0.43

C

		Delta growth rate 0–6	
		Adj R^2	R^2 CV
Model 1	Sex, CA (years), GH dose (mg/kg/day), height (SDS), weight (SDS), target height (SDS)	–0.12	0.07
Model 2	Sex, CA (years) GH dose (mg/kg/day), height (SDS), weight (SDS), target height (SDS), GH peaks (ng/ml)	–0.23	0.14
Model 3	Sex, CA (years), GH dose (mg/kg/day), height (SDS), weight (SDS), target height (SDS), IGF-I (SDS)	–0.17	0.08
Model 4	Sex, CA (years), GH dose (mg/kg/day), height (SDS), weight (SDS), target height (SDS), difference between CA and bone age	0.00	0.00
Model 5	Sex, CA (years), GH dose (mg/kg/day), height (SDS), weight (SDS), target height (SDS) and:		
	miR-199a-5p (baseline and delta 0–3)	0.39	0.23
	miR-355-5p (baseline and delta 0–3)	0.02	0.00
	miR-494 -3p (baseline and delta 0–3)	–0.05	0.01
Model 6—STEPWISE	Selected variables: sex, CA (years), GH dose (mg/kg/day), target height (SDS), weight (SDS), difference between CA and bone age, GH peak at first test (ng/ml), GH peak at second test (ng/ml), miR-199a- 5p baseline, delta 0–3 months miR-335-5p, delta 0–3 months miR-199a-5p.	0.75	0.63

Adj, adjusted; CA, chronological age; CV, cross-validated; GH, growth hormone; IGF-I, insulin-like growth factor 1; SDS, standard deviation score.

has been shown to promote chondrogenic differentiation of mesenchymal stem cells (37). MiR-494-3p has not been studied yet in the context of bone or growth plate development; however, it has been reported to promote PI3K/AKT pathway hyperactivation in hepatocellular carcinoma by targeting PTEN (38). The PI3K/AKT pathway is known to control hypertrophic chondrocyte differentiation and to be involved in endochondral bone growth (39), and promotes osteoblast differentiation (40).

Our findings also suggest that early changes in these three specific miRNAs could reflect both sensitivity to GH treatment as well as the degree of GH deficiency at diagnosis. In support of this, we observed little difference in the levels among single subjects after 12 months of treatment, whereas a clear change occurred during the first 3 months that could depend both on the initial degree of GH deficiency and on the sensitivity to the GH being administered for treatment: in fact, different doses are often needed in different subjects. Interestingly, in the growth prediction models, the GH dose was selected among the variables that gave substantial contribution to the explanation of variance in growth. The changes in the miRNA levels were found to be independent of

GH peak levels in response to stimulation tests, possibly confirming that GH peaks do not reflect the degree of GH deficiency, consistent with the well-known fact that the response to tests is variable (41). Furthermore, the degree of response to treatment did not seem to affect their change during the first 3 months of treatment.

Finally, in our series, these miRNAs proved to considerably increase the capacity to predict growth response compared with the use of clinical parameters only and compared to current models (21). Some previous good prediction models have been published but have never been used routinely in clinical practice because they are too complicated. Among these, one model considered markers of bone metabolism in 24-h urine collections at different time points besides auxological parameters (42). Stepwise prediction models that had height SDS 0–6 months, height SDS 0–12 months, and growth velocity 0–6 months as outcomes selected both the baseline levels and the change (0–3 months) in the levels of the three miRNAs we validated. Whereas predicted height SDS at 6 months was not significantly improved by the new model with respect to the use of auxological parameters alone; height prediction at 12 months and growth rate at 6 months were highly explained. These latter models also included the GH dose, anticipating the possibility that these models should be further studied for potential use for personalized and optimized treatment. We are aware that the small number of patients could have influenced the findings, and the data need to be confirmed in a much larger dataset; however, we should keep in mind that this type of patient cohort was quite difficult to collect. Further studies are needed to verify whether these miRNAs change or not at puberty, and whether they could be used in growth prediction models in other conditions having GH treatment as an indication. A further use could be hypothesized for the diagnosis of GH deficiency. It is of interest that the value of the information contained in the three miRNA levels and their early variation in predicting growth was greater than that contained in IGF-I serum levels (43, 44), suggesting that miRNAs could effectively be of value for further research.

In conclusion, this exploratory study has shown that miRNAs change on GH treatment, and has led to the identification of three miRNAs that show significant changes in the early period of treatment and contribute to predict the growth response after 12 months. These results are promising and suggest that including miRNAs in the set of variables used to predict treatment response could substantially improve timeliness of correct treatment and contribute to personalized therapy. However, we are aware that these results should be validated in a larger independent cohort of patients and further studies will be required to corroborate miRNA efficacy in the prediction of treatment response. A control group of healthy subjects would also be useful to compare results. In addition, the results suggest that we need to explore these miRNAs as possible identifiers of GH deficiency and finally their potential implication as a cause of idiopathic short stature.

DATA AVAILABILITY STATEMENT

The original contributions presented in the study are publicly available. These data can be found here: https://www.ncbi.nlm.nih.gov/geo/query/acc.cgi?acc=GSE193450, GSE193450.

ETHICS STATEMENT

This study involving human participants was reviewed and approved by the Ethics Committees of Reggio Emilia and Modena. Written informed consent to participate in this study was provided by the participants' legal guardian/next of kin.

AUTHOR CONTRIBUTIONS

MS conceived, designed, and supervised this study. MES, CS, BR, PL, SP, and BP enrolled the patients. CC, GR, and FC performed the experiments. LB and PGR performed statistical analyses of the data. MES, CC, GR, SA, PGR, LB, and LI contributed to the interpretation of the results. MES, CC, GR, BR, SA, PGR, and LI contributed to writing the manuscript. All the authors read, revised, and approved the final manuscript.

FUNDING

This study received funding from the Grant for Growth Innovation (GGI) 2018—Merck. Financial support was also provided by Ipsen S.p.A. and in addition by Fondazione del Monte di Bologna e Ravenna and Ferring S.p.A. The funders were not involved in the study design; collection, analysis, and interpretation of data; the writing of this article; or the decision to submit it for publication.

SUPPLEMENTARY MATERIAL

The Supplementary Material for this article can be found online at: https://www.frontiersin.org/articles/10.3389/fendo.2022.896640/full#supplementary-material

REFERENCES

1. O'Brien J, Hayder H, Zayed Y, Peng C. Overview of MicroRNA Biogenesis, Mechanisms of Actions, and Circulation. *Front Endocrinol (Lausanne)* (2018) 9:402. doi: 10.3389/fendo.2018.00402
2. Catalanotto C, Cogoni C, Zardo G. MicroRNA in Control of Gene Expression: An Overview of Nuclear Functions. *Int J Mol Sci* (2016) 17:1712. doi: 10.3390/ijms17101712
3. Filipowicz W, Bhattacharyya SN, Sonenberg N. Mechanisms of Post-Transcriptional Regulation by microRNAs: Are the Answers in Sight? *Nat Rev Genet* (2008) 9:102–14. doi: 10.1038/nrg2290
4. Bartel DP. MicroRNAs: Target Recognition and Regulatory Functions. *Cell* (2009) 136:215–33. doi: 10.1016/j.cell.2009.01.002
5. Kang K, Peng X, Luo J, Gou D. Identification of Circulating miRNA Biomarkers Based on Global Quantitative Real-Time PCR Profiling. *J Anim Sci Biotechnol* (2012) 3:4. doi: 10.1186/2049-1891-3-4
6. Jung HJ, Suh Y. Regulation of IGF -1 Signaling by microRNAs. *Front Genet* (2015) 5:472. doi: 10.3389/fgene.2014.00472
7. Faghihi MA, Modarresi F, Khalil AM, Wood DE, Sahagan BG, Morgan TE, et al. Expression of a Noncoding RNA Is Elevated in Alzheimer's Disease and Drives Rapid Feed-Forward Regulation of Beta-Secretase. *Nat Med* (2008) 14:723–30. doi: 10.1038/nm1784

8. Eisenberg I, Eran A, Nishino I, Moggio M, Lamperti C, Amato AA, et al. Distinctive Patterns of microRNA Expression in Primary Muscular Disorders. *Proc Natl Acad Sci USA* (2007) 104:17016–21. doi: 10.1073/pnas.0708115104
9. Bramnert M, Segerlantz M, Laurila E, Daugaard JR, Manhem P, Groop L. Growth Hormone Replacement Therapy Induces Insulin Resistance by Activating the Glucose-Fatty Acid Cycle. *J Clin Endocrinol Metab* (2003) 88:1455–63. doi: 10.1210/jc.2002-020542
10. El-Awady RA, Herzi F, Al-Tunaiji H, Saleh EM, Abdel-Wahab AH, Al Homossi A, et al. Epigenetics and miRNA as Predictive Markers and Targets for Lung Cancer Chemotherapy. *Cancer Biol Ther* (2015) 16:1056–70. doi: 10.1080/15384047.2015.1046023
11. Yan S, Cao Y, Mao AW. MicroRNAs in Colorectal Cancer: Potential Biomarkers and Therapeutic Targets. *Front Biosci* (2015) 20:1092–103. doi: 10.2741/4361
12. Cirillo F, Catellani C, Lazzeroni P, Sartori C, Street ME. The Role of MicroRNAs in Influencing Body Growth and Development. *Horm Res Paediatr* (2020) 93:7–15. doi: 10.1159/000504669
13. Cirillo F, Lazzeroni P, Catellani C, Sartori C, Amarri S, Street ME. MicroRNAs Link Chronic Inflammation in Childhood to Growth Impairment and Insulin-Resistance. *Cytokine Growth Factor Rev* (2018) 39:1–18. doi: 10.1016/j.cytogfr.2017.12.004
14. Kelly BN, Haverstick DM, Lee JK, Thorner MO, Vance ML, Xin W, et al. Circulating microRNA as a Biomarker of Human Growth Hormone Administration to Patients. *Drug Test Anal* (2014) 6:234–8. doi: 10.1002/dta.1469
15. Elzein S, Goodyer CG. Regulation of Human Growth Hormone Receptor Expression by microRNAs. *Mol Endocrinol* (2014) 28:1448–59. doi: 10.1210/me.2014-1183
16. Saccon TD, Schneider A, Marinho CG, Nunes ADC, Noureddine S, Dhahbi J, et al. Circulating microRNA Profile in Humans and Mice With Congenital GH Deficiency. *Aging Cell* (2021) 20:e13420. doi: 10.1111/acel.13420
17. Reed ML, Merriam GR, Kargi AY. Adult Growth Hormone Deficiency – Benefits, Side Effects, and Risks of Growth Hormone Replacement. *Front Endocrinol (Lausanne)* (2013) 4:64. doi: 10.3389/fendo.2013.00064
18. Cappa M, Iughetti L, Loche S, Maghnie M, Vottero A. GeNeSIS National Board on Behalf of the GeNeSIS Italian Investigators. Efficacy and Safety of Growth Hormone Treatment in Children With Short Stature: The Italian Cohort of the GENeSIS Clinical Study. *J Endoocrinol Invest* (2016) 39:667–77. doi: 10.1007/s40618-015-0418-0
19. Sävendahl L, Pournara E, Pedersen BT, Blankenstein O. Is Safety of Childhood Growth Hormone Therapy Related to Dose? Data From a Large Observational Study. *Eur J Endocrinol* (2016) 174:681–91. doi: 10.1530/EJE-15-1017
20. Shimatsu A, Tai S, Imori M, Ihara K, Taketsuna M, Funai J, et al. Efficacy and Safety of Growth Hormone Replacement Therapy in Japanese Adults With Growth Hormone Deficiency: A Postmarketing Observational Study. *Endocr J* (2013) 60:1131–44. doi: 10.1507/endocrj.EJ13-0083
21. Loftus J, Lindberg A, Aydin F, Gomez R, Maghnie M, Rooman R, et al. Individualised Growth Response Optimisation (iGRO) Tool: An Accessible and Easy-to-Use Growth Prediction System to Enable Treatment Optimisation for Children Treated With Growth Hormone. *J Pediatr Endocrinol Metab* (2017) 30:1019–26. doi: 10.1515/jpem-2017-0120
22. Growth Hormone Research Society. Consensus Guidelines for the Diagnosis and Treatment of Growth Hormone (GH) Deficiency in Childhood and Adolescence: Summary Statement of the GH Research Society. *J Clin Endocrinol Metab* (2000) 85:3990–3. GH Research Society. doi: 10.1210/jc.85.11.3990
23. Wit JM, Deeb A, Bin-Abbas B, Al Mutair A, Koledova E, Savage MO. Achieving Optimal Short- and Long-Term Responses to Paediatric Growth Hormone Therapy. *J Clin Res Pediatr Endocrinol* (2019) 11:329–40. doi: 10.4274/jcrpe.galenos.2019.2019.0088
24. Schwarzenbach H, da Silva AM, Calin G, Pantel K. Data Normalization Strategies for MicroRNA Quantification. *Clin Chem* (2015) 61:1333–42. doi: 10.1373/clinchem.2015.239459
25. Chang L, Zhou G, Soufan O, Xia J. Mirnet 2.0: Network-Based Visual Analytics for miRNA Functional Analysis and Systems Biology. *Nucleic Acids Res* (2020) 48:W244–51. doi:10.1093/nar/gkaa467.
26. Cole TJ, Freeman JV, Preece MA. Body Mass Index Reference Curves for the UK, 1990. *Arch Dis Child* (1995) 73:25–9. doi: 10.1136/adc.73.1.25
27. Tanner JM, Whitehouse RH, Takaishi M. Standards From Birth to Maturity for Height, Weight, Height Velocity, and Weight Velocity: British Children 1965, Part II. *Arch Dis Child* (1966) 41:613–36. doi: 10.1136/adc.41.220.613
28. Greulich WW, Pyle SI. *Radiographic Atlas Of Skeletal Development Of The Hand And Wrist. 2nd Edition*. Stanford, California: Stanford University Press (1959). ISBN: 0804703981.
29. Marshall WA, Tanner JM. Variations in the Pattern of Pubertal Changes In Boys. *Arch Dis Child* (1970) 45(239):13–23. doi: 10.1136/adc.45.239.13
30. Marshall WA, Tanner J. Variations in Pattern of Pubertal Changes in Girls. *Arch Dis Child* (1969) 44:291–303. doi: 10.1136/adc.44.235.291
31. Huen K, Lizarraga D, Kogut K, Eskenazi B, Holland N. Age-Related Differences in miRNA Expression in Mexican-American Newborns and Children. *Int J Environ Res Public Health* (2019) 16:524. doi: 10.3390/ijerph16040524
32. Lai CY, Wu YT, Yu SL, Yu YH, Lee SY, Liu CM, et al. Modulated Expression of Human Peripheral Blood microRNAs From Infancy to Adulthood and Its Role in Aging. *Aging Cell* (2014) 13:679–89. doi: 10.1111/acel.12225
33. Thompson MD, Cismowski MJ, Serpico M, Pusateri A, Brigstock DR. Elevation of Circulating microRNA Levels in Obese Children Compared to Healthy Controls. *Clin Obes* (2017) 7:216–21. doi: 10.1111/cob.12192
34. Qi XB, Jia B, Wang W, Xu GH, Guo JC, Li X, et al. Role of miR-199a-5p in Osteoblast Differentiation by Targeting TET2. *Gene* (2020) 726:144193. doi: 10.1016/j.gene.2019.144193
35. Zhang L, Tang Y, Zhu X, Tu T, Sui L, Han Q, et al. Overexpression of MiR-335-5p Promotes Bone Formation and Regeneration in Mice. *J Bone Miner Res* (2017) 32:2466–75. doi: 10.1002/jbmr.3230
36. Zhang J, Tu Q, Bonewald LF, He X, Stein G, Lian J, et al. Effects of miR-335-5p in Modulating Osteogenic Differentiation by Specifically Downregulating Wnt Antagonist DKK1. *J Bone Miner Res* (2011) 26:1953–63. doi: 10.1002/jbmr.377
37. Lin X, Wu L, Zhang Z, Yang R, Guan Y, Hou X, et al. MiR-335-5p Promotes Chondrogenesis in Mouse Mesenchymal Stem Cells and is Regulated Through Two Positive Feedback Loops. *J Bone Miner Res* (2014) 29:1575–85. doi: 10.1002/jbmr.2163
38. Lin H, Huang ZP, Liu J, Qiu Y, Tao YP, Wang MC, et al. MiR-494-3p Promotes PI3K/AKT Pathway Hyperactivation and Human Hepatocellular Carcinoma Progression by Targeting PTEN. *Sci Rep* (2018) 8:10461. doi: 10.1038/s41598-018-28519-2
39. Ulici V, Hoenselaar KD, Gillespie JR, Beier F. The PI3K Pathway Regulates Endochondral Bone Growth Through Control of Hypertrophic Chondrocyte Differentiation. *BMC Dev Biol* (2008) 8:40. doi: 10.1186/1471-213X-8-40
40. Mukherjee A, Rotwein P. Akt Promotes BMP2-Mediated Osteoblast Differentiation and Bone Development. *J Cell Sci* (2009) 122:716–26. doi: 10.1242/jcs.042770
41. Hilczer M, Smyczynska J, Stawerska R, Lewinski A. Stability of IGF-I Concentration Despite Divergent Results of Repeated GH Stimulating Tests Indicates Poor Reproducibility of Test Results. *Endocr Regul* (2006) 40:37–45 PMID: 17100545.
42. Schönau E, Westermann F, Rauch F, Stabrey A, Wassmer G, Keller E, et al. A New and Accurate Prediction Model for Growth Response to Growth Hormone Treatment in Children With Growth Hormone Deficiency. *Eur J Endocrinol* (2001) 144:13–20. doi: 10.1530/eje.0.1440013
43. Smyczyńska J, Stawerska R, Hilczer M, Lewiński A. Secondary IGF-I Deficiency as a Prognostic Factor of Growth Hormone (GH) Therapy Effectiveness in Children With Isolated, Non-Acquired GH Deficiency. *Exp Clin Endocrinol Diabetes* (2015) 123:209–14. doi: 10.1055/s-0034-1395665
44. Federico G, Street ME, Maghnie M, Caruso-Nicoletti M, Loche S, Bertelloni S, et al. Assessment of Serum IGF-I Concentrations in the Diagnosis of Isolated Childhood-Onset GH Deficiency: A Proposal of the Italian Society for Pediatric Endocrinology and Diabetes (SIEDP/ISPED). *J Endocrinol Invest* (2006) 29:732–7. doi: 10.1007/BF03344184

Conflict of Interest: The authors declare that the research was conducted in the absence of any commercial or financial relationships that could be construed as a potential conflict of interest.

frontiers | Frontiers in Endocrinology

REVIEW
published: 08 July 2022
doi: 10.3389/fendo.2022.929924

Circulating MicroRNAs as Potential Diagnostic Biomarkers for Diabetic Retinopathy: A Meta-Analysis

Lingli Ma[1], *Yan Wen*[1], *Zimeng Li*[1], *Nan Wu*[2] *and Qing Wang*[1]*

[1] *Department of Endocrinology and Metabolism, China-Japan Union Hospital of Jilin University, Changchun, China,*
[2] *Department of Dermatology, China-Japan Union Hospital of Jilin University, Changchun, China*

OPEN ACCESS

Edited by:
Pranav Kumar Prabhakar, Lovely Professional University, India

Reviewed by:
Pranay Pankaj, Jaipur National University, India
Yao Jiang, The Affiliated Hospital of Southwest Medical University, China

***Correspondence:**
Qing Wang
wang_qing@jlu.edu.cn

Specialty section:
This article was submitted to Diabetes: Molecular Mechanisms, a section of the journal Frontiers in Endocrinology

Received: *27 April 2022*
Accepted: *13 June 2022*
Published: *08 July 2022*

Citation:
Ma L, Wen Y, Li Z, Wu N and Wang Q (2022) Circulating MicroRNAs as Potential Diagnostic Biomarkers for Diabetic Retinopathy: A Meta-Analysis. Front. Endocrinol. 13:929924. doi: 10.3389/fendo.2022.929924

Objective: Diabetic retinopathy (DR) is a common diabetic microvascular complication and a major cause of acquired vision loss. Finding effective biomarkers for the early identification and diagnosis of DR is crucial. This study aimed to comprehensively evaluate the accuracy of microRNAs (miRNAs) in the diagnosis of DR *via* a meta-analysis of previously published diagnostic studies. This study has been registered on the PROSPERO website, with the number CRD42022323238.

Methods: We searched PubMed, Cochrane Library, Embase, Web of Science, China Wanfang database, and China Knowledge Network database to identify relevant articles published from the time of database creation to April 10, 2022. Stata 14.0 software was used to calculate the pooled sensitivity, specificity, positive likelihood ratio (PLR), negative likelihood ratio (NLR), diagnostic ratio (DOR), and area under the summary receiver operating characteristic (ROC) curve to assess the accuracy of miRNAs in the diagnosis of DR. Heterogeneity between studies was assessed using Cochran-Q test and I^2 statistic for quantitative analysis. The random-effect model was selected due to significant heterogeneity. Subgroup analysis and regression analysis were also performed to determine the potential sources of heterogeneity.

Results: We included 25 articles detailing 52 studies with 1987 patients with DR and 1771 non-DR controls. The findings demonstrated overall sensitivity (0.82, 95% CI: 0.78 ~ 0.85), specificity (0.84, 95% CI: 0.81 ~ 0.86), PLR (5.0, 95% CI: 4.2 ~ 5.9), NLR (0.22, 95% CI: 0.18 ~ 0.26), and the area under the summary ROC curve (0.90, 95% CI: 0.87 ~ 0.92). Furthermore, we performed subgroup analysis and found that panels of multiple miRNAs could enhance the pooled sensitivity (sensitivity, specificity, and AUC values were 0.89, 0.87, and 0.94, respectively).

Conclusion: The meta-analysis showed that miRNAs can be used as potential diagnostic markers for DR, with high accuracy of diagnoses observed with the detection of miRNAs in plasma and serum.

Keywords: miRNA, diabetic retinopathy, diagnosis, biomarkers, meta-analysis

INTRODUCTION

Diabetic retinopathy (DR) is a diabetic microvascular complication (1) and an important cause of visual impairment and blindness in adults worldwide (2). Among individuals with diabetes, the global prevalence of DR is 22.27%. In 2020, the number of adults diagnosed with DR was estimated to be 103.12 million (3), and this number is expected to increase to 160.5 million by 2045 (4). The early stages of DR have no conscious symptoms, and as the extent of the disease progresses vision loss can occur to varying degrees, and if untreated progresses to the proliferative stage, irreversible vision loss can result, therefore, it is critical to prevent progression from the early stages of DR (5, 6). Fundus fluorescein angiography is the gold standard for the diagnosis of DR (7, 8), and fundoscopy, fundus photography, and optical coherence tomography have emerged in the clinical setting (8). However, because fluorescein angiography is invasive, time-consuming, and risky, and in addition, interpretation of fundoscopic examinations and photographic reports requires physicians with expertise and skills in diabetes-related eye diseases (9), these methods are not applicable to the routine screening of DR in clinical practice. In recent years, miRNAs have been shown to play an important role in various diabetic complications (10, 11). The application of circulating miRNAs as biomarkers of DR has garnered significant interest (12, 13). Therefore, the construction of circulating markers for early diagnosis of DR and timely treatment are fundamental goals to improve its diagnosis and treatment.

MicroRNAs (miRNAs) are a group of endogenous non-coding single-stranded small molecule RNAs of 19-24 nucleotides in length (14), which are involved in the post-transcriptional regulation of gene expression and are closely associated with various pathophysiological processes in the human body (15–17). Since abnormal alterations in miRNA expression precedes the expression of the corresponding regulated proteins, the abnormal expression of miRNAs may already be present when patients with diabetes have not yet developed retinal microvascular damage, or when the damage has not yet affected visual function (18). miRNAs are not only widely present in a variety of human tissues and cells, but can also bind to Argonaute proteins (19), which, in turn, prevents the degradation of RNA enzymes, allowing miRNAs to be stably expressed in serum, plasma, and other body fluids (20). This stability, ubiquity, high specificity, high sensitivity, and recent advances in the detection and analysis methods render miRNAs potentially useful novel biomarkers for DR diagnosis (21).

However, there is little consistency in previous studies; hence, no reliable conclusions can be drawn regarding the relationship between miRNAs and DR. In addition, most of the available data are derived from retrospective studies with a small sample size lacking quantitative criteria. Therefore, we performed a diagnostic meta-analysis for the first time to determine the potential diagnostic value of miRNAs in patients with DR.

MATERIALS AND METHODS

We have registered our protocol on PROSPERO (CRD42022323238) and can be found at: https://www.crd.york.ac.uk/prospero/. This meta-analysis follows the PRISMA statement of preferred reporting items for systematic evaluation and meta-analysis (**Supplementary Table 1**).

Search Strategy

We searched PubMed, Cochrane Library, Embase, Web of Science, China Wanfang database, and China Knowledge Network (CNKI) database to identify relevant articles published from the time of database creation to April 10, 2022, without restricting the language of publication. A search strategy for diagnostic DR of circulating microRNAs was developed based on PICOS principles. We obtained all the medical subject headings (MeSH) and entry words on the National Center for Biotechnology Information (NCBI) website, and search terms included "Diabetic Retinopathy" OR "Diabetic Retinopathies" OR "Retinopathies, Diabetic" OR "Retinopathy, Diabetic" AND "MicroRNAs" OR "MicroRNA" OR "miRNAs" OR "Micro RNA" OR "RNA, Micro" OR "Primary MicroRNA" OR "MicroRNA, Primary" OR "Primary miRNA" OR "pri-miRNA" OR "pri miRNA" OR "RNA, Small Temporal" OR "Temporal RNA, Small" OR "stRNA" OR "Small Temporal RNA" OR "pre-miRNA" OR "pre miRNA" AND "sensitiv*" OR "sensitivity and specificity" OR "predictive" OR "value*" OR "accuracy*". We searched PubMed using the following strategy: ((((Diabetic Retinopathy[Title/Abstract]) OR (Diabetic Retinopathies[Title/Abstract])) OR (Retinopathies, Diabetic [Title/Abstract])) AND ((((((MicroRNAs[Title/Abstract]) OR (miRNA[Title/Abstract])) OR (Micro RNA[Title/Abstract])) OR (pri-miRNA[Title/Abstract])) OR (stRNA[Title/Abstract])) OR (miR[Title/Abstract]))) AND (sensitiv*[Title/Abstract] OR sensitivity and specificity[MeSH Terms] OR (predictive[Title/Abstract] AND value*[Title/Abstract]) OR predictive value of tests[MeSH Term] OR accuracy*[Title/Abstract]).

Eligibility Criteria and Quality Assessment

Subjects were recruited with the following inclusion criteria: (1) all patients in the case group were diagnosed following clinically recognized diagnostic criteria; (2) the intervention was characterized by the diagnosis of DR performed using miRNA examination; (3) false positive (FP), true positive (TP), false

negative (FN), and true negative (TN) could be derived directly or calculated from the literature. The exclusion criteria were set as follows: (1) non-human trials; (2) non-case-control studies; (3) reviews, letters, or conference proceedings; (4) insufficient data.

Two investigators used the Quality Assessment of Diagnostic Accuracy Studies-2 (QUADAS-2) (22) tool to independently assess the risk of bias and clinical applicability of included studies. The tool comprised four main components: selection of cases, trials to be evaluated, gold standard, and case flow and progression. Disagreements were resolved by agreement between the two investigators through negotiation or by involving a third reviewer.

Data Extraction

Data and information were extracted independently by two investigators from eligible studies, including first author, year of publication, country, miRNAs, number of samples, internal reference, cut-off values, control source, sample source, assay method, miRNAs expression, AUC with 95% confidence intervals (CIs), sensitivity, specificity, TP, FP, FN, and TN.

Statistical Analysis

We extracted TP, FP, FN, and TN values to calculate pooled sensitivity, specificity, positive likelihood ratio (PLR), negative likelihood ratio (NLR), diagnostic ratio (DOR), and corresponding 95% confidence interval (CI). Summary receiver operating characteristic (SROC) curves were plotted to calculate the area under the curve (AUC) to test the pooled diagnostic value of miRNAs. We used the chi-square test and I^2 test to assess the heterogeneity between studies. Heterogeneity between studies was assessed using Cochran-Q test and I^2 statistic for quantitative analysis, with *P*-value was less than 0.05 for Cochran-Q test and I^2>50%, indicating significant heterogeneity between studies and selection of random-effect model (23, 24). We performed subgroup analysis and regression analysis to determine the source of heterogeneity. Sensitivity analysis was performed to determine the robustness of the meta-analysis results. Deeks' funnel plots were used to examine publication bias. In addition, Fagan′s nomogram was drawn to further assess the diagnostic efficacy of miRNAs. Review Manager 5.3 was used to evaluate the quality of the literature, and Stata 14.0 was used to analyze all data. A *P*-value < 0.05 was considered statistically significant.

RESULTS

Literature Search and Study Characteristics

We searched 423 records in PubMed, Cochrane Library, Embase, Web of Science, China Wanfang database, and CNKI database. Of these, 296 duplicate studies were excluded. Subsequently, based on the titles and abstracts, 246 irrelevant studies, reviews, conference proceedings, and commentaries were excluded, and we evaluated 50 full-text articles and excluded 25 studies based on the exclusion criteria, including 16 studies with insufficient data and six reviews and three studies that were not related to miRNAs. The remaining 25 documents were included in the meta-analysis. The screening flow chart is shown in **Figure 1**.

In total, 25 documents (spanning years 2014 to 2022) included in this meta-analysis involved 52 studies (11, 18, 20, 25–46) (**Table 1**), all of which were case-control studies that included a total of 1987 patients with DR and 1771 non-DR controls, with the source of controls being diabetic patients not diagnosed with DR, healthy population, and patients with cataract. Among these 52 studies, 41 studies reported a single miRNA, and 11 studies discussed a panel of miRNAs. A total of 38 studies detected miRNAs in serum, 10 studies extracted miRNAs in plasma, and four studies extracted miRNAs from the aqueous humor. A total of four studies were conducted in Africa, two studies were conducted in Europe, and the remaining studies were conducted in Asian populations. In addition, 7 of the included studies involved the examination of miRNA-21, and miRNA-20b, miRNA-93, and miRNA-15 were examined in five studies.

Quality Assessment

The quality of the included studies was evaluated using the QUADAS-2, and the results were analyzed by applying Review Manager 5.3. The results are shown in **Figure 2**. Most of the studies included in our meta-analysis were continuous and time scaled. Given that all patients with DR included in the study were diagnosed by clinically recognized diagnostic criteria, all trials involved case-control studies, introducing high or unclear risks in the selection field.

Diagnostic Accuracy of MiRNAs in DR

The sensitivity and specificity of miRNAs in diagnosing DR are shown in **Figure 3**. Forest plots of pooled data showed I^2 = 85.11% for sensitivity and I^2 = 76.96% for specificity, suggesting a large

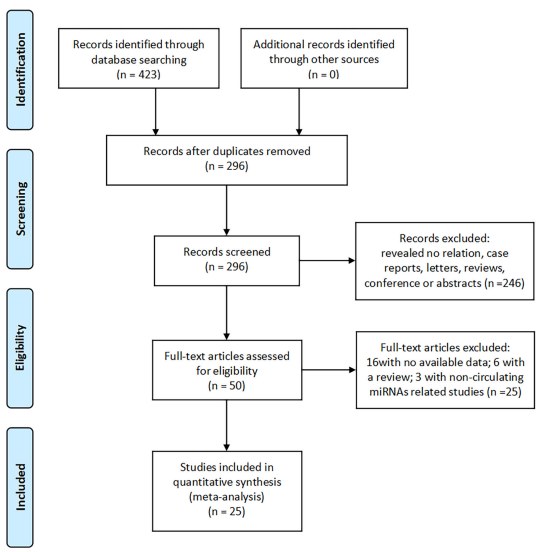

FIGURE 1 | Flow diagram showing selection of studies for meta-analysis.

TABLE 1 | Characteristics of the included studies.

First author/Year	Ethnicity	miRNAs	Expression	Reference	Cut-off	Case/ Control	Controls	Method	Specimen	Sen (%)	Spe (%)	AUC (95% CI)
Qing 2014 (23)	Asian	miR-21、1179 miR-181c	up	U6	NA	30/30	HI	qRT-PCR	Serum	82	95	0.89 (0.86-0.96)
Fu 2017 (24)	Asian	miR-93	up	U6	1.42	98/80	DM	qRT-PCR	plasma	80.5	89.6	0.892 (0.824-0.961)
Fu 2017 (24)	Asian	miR-21	Up	U6	1.56	98/80	DM	qRT-PCR	plasma	70.2	90.8	0.836 (0.770-0.905)
Fu 2017 (24)	Asian	miR-93、miR-21	Up	U6	NA	98/80	DM	qRT-PCR	plasma	86.4	91.3	0.937 (0.868-0.992)
Jiang 2017 (26)	Asian	miR-21	Up	U6	NA	124/180	DM/HI	qRT-PCR	plasma	66.1	90.4	0.825 (0.778-0.872)
Qin 2017 (25)	Asian	miR-126	down	U6 snRNA	8.43	81/59	HI	qRT-PCR	Serum	84.8	93.6	0.976
Zou 2017 (27)	Asian	miR-93	Up	U6	1.31	75/127	HI	qRT-PCR	plasma	73.3	89.2	0.866
Sun 2018 (28)	Asian	miR-21	Up	U6	NA	30/70	HI	qRT-PCR	plasma	81.8	86.7	0.797 (0.709-0.886)
Zheng 2018 (29)	Asian	miR-126	down	U6	≤0.64	110/80	HI	qRT-PCR	plasma	83.6	82.5	0.861
Liang 2018 (30)	Asian	has-miR-425-5p 7a5p、miR-28-3p has-miR-425-5p miR-novel-chr5_15976	up		NA	29/50	HI	qRT-PCR	Serum	92.7	87.5	0.937
Dai 2019 (31)	Asian	miR-451	Up	U6	1.86	60/60	DM	qRT-PCR	Serum	61	82.5	0.722
Dai 2019 (31)	Asian	miR-221	Up	U6	0.823	60/60	DM	qRT-PCR	Serum	71.2	85	0.823
Dai 2019 (31)	Asian	miR-200b	Up	U6	0.761	60/60	DM	qRT-PCR	Serum	81.4	72.3	0.761
Dai 2019 (31)	Asian	miR-451、miR-221 miR-200b	Up	U6	NA	60/60	DM	qRT-PCR	Serum	93.2	77.5	0.938
Ma 2019 (32)	Asian	miR-93	up	U6	NA	76/45	HI	qRT-PCR	Serum	81	89	0.883 (0.813-0.950)
Ma 2019 (32)	Asian	miR-21	up	U6	NA	76/45	HI	qRT-PCR	Serum	71	90	0.845 (0.769-0.914)
Ma 2019 (32)	Asian	miR-93、miR-21	Up	U6	NA	76/45	HI	qRT-PCR	Serum	87	92	0.946 (0.857-0.993)
Yu 2019 (17)	Asian	miR-19b	up	NA	NA	39/30	DM	qRT-PCR	Serum	87	80	0.78 (0.66-0.90)
Yu 2019 (17)	Asian	miR-221	up	NA	NA	39/30	DM	qRT-PCR	Serum	100	73	0.89 (0.81-0.97)
Yu 2019 (17)	Asian	miR-18b	up	NA	NA	39/30	DM	qRT-PCR	Serum	69	97	0.78 (0.67-0.90)
Li 2019 (33)	Asian	miR-4448、miR-338-3p miR-190a-5p miR-485-5p、miR-9-5p	down	NA	−43.869	10/11	T2DM	qRT-PCR	Serum	90	90	0.909
Shaker 2019 (19)	African	miR-20b	down	SNORD 68	4.375	50/30	T2DM	qRT-PCR	Serum	62	60	0.858 (0.753-0.963)
Shaker2019 (19)	African	miR-17-3p	down	SNORD 68	0.2	50/30	T2DM	qRT-PCR	Serum	92	56.7	0.678 (0.535-0.821)
Ji 2019 (34)	Asian	miR-2116-5p	up	cel-miR-39	NA	45/45	T2DM	qRT-PCR	Serum	62.2	77.8	0.756

(Continued)

TABLE 1 | Continued

First author/Year	Ethnicity	miRNAs	Expression	Reference	Cut-off	Case/ Control	Controls	Method	Specimen	Sen (%)	Spe (%)	AUC (95% CI)
Ji 2019 (34)	Asian	miR-3197	up	cel-miR-39	NA	45/45	T2DM	qRT-PCR	Serum	93.3	91.1	0.966
Ji 2019 (34)	Asian	miR-2116-5p miR-3197	up	cel-miR-39	NA	45/45	T2DM	qRT-PCR	Serum	97.8	88.9	0.972
Lin 2020 (35)	Asian	miR-15	down	U6	0.63	105/50	HI	qRT-PCR	Serum	84.9	65.3	0.796 (0.724-0.857)
Lin 2020 (35)	Asian	miR-29a	up	U6	0.11	105/50	HI	qRT-PCR	Serum	53.8	79.6	0.677 (0.597-0.749)
Liu 2020 (36)	Asian	miR-15a	up	U6	219.20 copies/μL	34/40	CP	qRT-PCR	AH	82.4	61.5	0.762 (0.654-0.871)
Liu 2020 (36)	Asian	miR-16	up	U6	148.06 copies/μL	34/40	CP	qRT-PCR	AH	67.6	66.7	0.671 (0.546-0.797)
Liu 2020 (36)	Asian	miR-20b	up	U6	244.31 copies/μL	34/40	CP	qRT-PCR	AH	88.2	69.2	0.862 (0.780-0.943)
Liu 2020 (36)	Asian	miR-15a、miR-16 miR-20b	up	U6	NA	34/40	CP	qRT-PCR	AH	91.2	76.9	0.912 (0.848-0.976)
Liu 2020 (36)	Asian	miR-15a	up	U6	2.77	34/40	CP	qRT-PCR	Serum	76.5	76.9	0.798 (0.695-0.901)
Liu 2020 (36)	Asian	miR-16	up	U6	2.39	34/40	CP	qRT-PCR	Serum	70.6	64.1	0.688 (0.565-0.810)
Liu 2020 (36)	Asian	miR-20b	up	U6	3.42	34/40	CP	qRT-PCR	Serum	79.4	82.1	0.886 (0.806-0.967)
Liu 2020 (36)	Asian	miR-15a miR-16、miR-20b	up	U6	NA	34/40	CP	qRT-PCR	Serum	79.4	92.3	0.931 (0.872-0.990)
Yin 2020 (37)	Asian	miR-210	up	U6	1.905	110/60	HI	qRT-PCR	Serum	95.5	95	0.991
Yin 2020 (37)	Asian	miR-210	up	U6	2.335	110/40	DM	qRT-PCR	Serum	83.6	80	0.892
Wan 2020 (38)	Asian	miR-409-5p	up	U6	NA	115/102	T2DM	qRT-PCR	Serum	83.3	57.4	0.757 (0.693-0.820)
Wan 2020 (38)	Asian	miR-216a	down	U6	NA	115/102	T2DM	qRT-PCR	Serum	47.1	87.8	0.703 (0.633-0.772)
Wan 2020 (38)	Asian	miR-409-5p	up	U6	NA	115/100	HI	qRT-PCR	Serum	90	79.1	0.892 (0.848-0.935)
Wan 2020 (38)	Asian	miR-216a	down	U6	NA	115/100	HI	qRT-PCR	Serum	71	87.8	0.859 (0.810-0.908)
Hu 2021 (39)	Asian	miR-29c	up	U6	1.31	65/64	HI	qRT-PCR	Serum	64.6	78.7	0.716 (0.638-0.785)
Liu 2021 (40)	Asian	miR-211	up	U6	2.23	90/90	DM/HI	qRT-PCR	plasma	72.4	75	0.839 (0.785-0.894)
Sun 2021 (41)	Asian	miR-320	down	NA	NA	179/83	DM	qRT-PCR	Serum	63.1	91.6	0.788 (0.734-0.842)
Santovito 2021 (42)	European	miR-25-3p miR-320b miR-495-3p	up/down	miR-19-5p miR-125a-5p	NA	20/20	T2DM/HI	qRT-PCR	plasma	85	85	0.931 (0.853-1.000)

(Continued)

TABLE 1 | Continued

First author/Year	Ethnicity	miRNAs	Expression	Reference	Cut-off	Case/ Control	Controls	Method	Specimen	Sen (%)	Spe (%)	AUC (95% CI)
Santovito 2021 (42)	European	miR-320b miR-495-3p	up/down	miR-19-5p miR-125a-5p	NA	20/20	T2DM/HI	qRT-PCR	plasma	83	79	0.847 (0.722-0.972)
Wang 2021 (43)	Asian	miR-374a	up	snoRNA U6	1.659	137/70	T2DM	qRT-PCR	Serum	82.9	80.3	0.892
Liu 2022 (44)	Asian	miR-425-5p	up	U6	1.565	100/60	HI	qRT-PCR	Serum	91.7	84	0.907
Liu 2022 (44)	Asian	miR-425-5p	up	U6	1.71	100/35	T2DM	qRT-PCR	Serum	85.7	78	0.833
Salem 2022 (14)	African	miR-181C	up	U6	NA	60/60	HI	qRT-PCR	Serum	90	100	0.983 (0.94-1.0)
Salem 2022 (14)	African	miR-1179	up	U6	NA	60/60	HI	qRT-PCR	Serum	90	80	0.927 (0.82-1.0)

up, upregulated; down, downregulated; NA, not available; HI, health individuals; CP, cataract patients; AH, aqueous humor; Sen, sensitivity; Spe, specificity; AUC, area under the curve; CI, confidence interval.

heterogeneity between studies, and a random effects model was used to estimate the diagnostic performance of miRNAs in DR. The results for diagnostic accuracy of miRNA for DR were as follows: sensitivity, 0.82 (95% CI: 0.78-0.85); specificity, 0.84 (95% CI: 0.81-0.86); NLR, 0.22 (95% CI: 0.18 -0.26); PLR, 5.0 (95% CI: 4.2-5.9), and DOR, 23 (95% CI: 17-31). In addition, we plotted the SROC curve to assess the diagnostic accuracy (**Figure 4**). The AUC was 0.90 (95% CI: 0.87-0.92), which indicated a strong overall accuracy of miRNAs in the diagnosis of DR. Aiding in the process of clinical decision during diagnosis is an important value of biomarkers. Therefore, we plotted a graph (**Figure 5**) based on the combination of PLR and NLR to determine their clinical applicability. PLR >10 and NLR <0.1 represent high diagnostic accuracy. We observed superior diagnostic efficacy of miRNAs in two studies in the articles by Yin et al. and Ji et al. (25, 37). Therefore, miR-3197 and miR-210 may be promising miRNAs and should be further examined in future studies (**Figure 5A**). MiRNAs with high diagnostic accuracy were also confirmed by Fagan's nomogram, with post-test probabilities of 0.56 and 0.5 for PLR and NLR, respectively, when the pre-test probability was set at 20% (**Figure 5B**).

Subgroup Analyses, Meta-Regression, and Sensitivity Analyses

To explore the potential heterogeneity, we performed subgroup analysis (**Table 2**) and regression analysis, grouped according to miRNA profiling, sample size, sample source, miRNA expression, ethnicity, internal reference and cut-off values

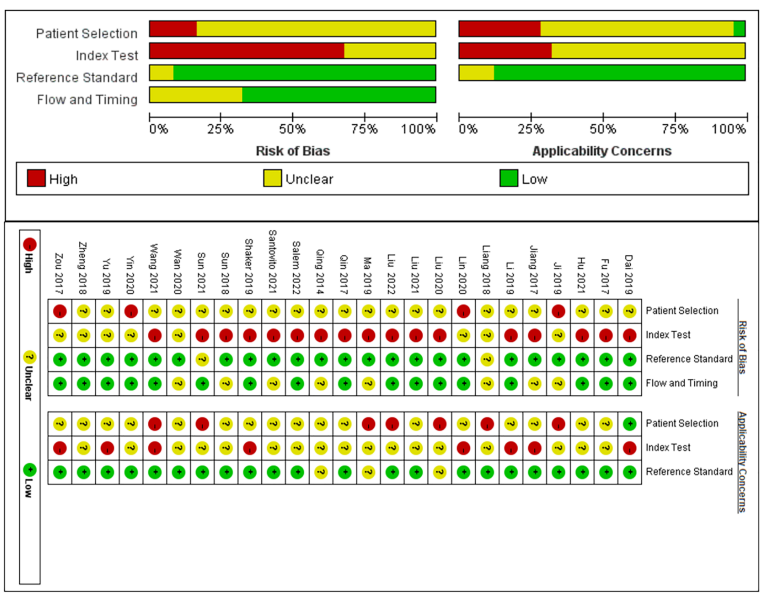

FIGURE 2 | Quality Assessment of Diagnostic Accuracy Studies (QUADAS)-2 assessment for risk of bias and applicability. Red, yellow and green indicate high, unclear and low risk respectively.

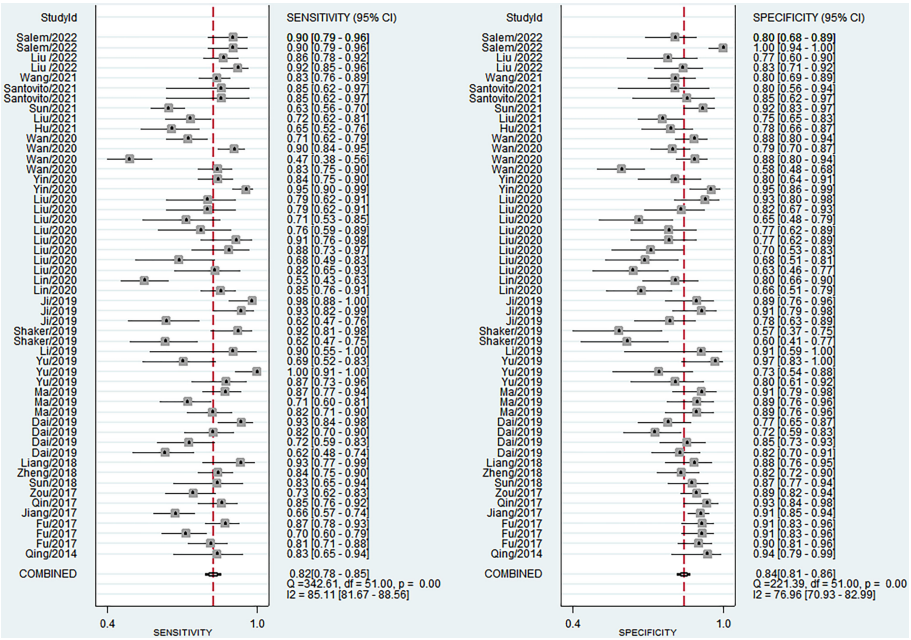

FIGURE 3 | Forest plots of studies examining microRNAs used in the diagnosis of diabetic retinopathy.

setting. Notably, the diagnostic accuracy of miRNA panel was higher compared to single miRNA. The sensitivity, specificity, PLR, NLR, DOR and AUC values for single miRNAs and miRNA panel were 0.80 (95% CI: 0.76-0.83), 0.83 (95% CI: 0.79-0.86), 4.6 (95% CI: 3.8-5.5), 0.24 (95% CI: 0.20-0.30), 19 (95% CI: 14-26) and 0.88 (95% CI: 0.85-0.91) and 0.89 (95% CI: 0.85-0.92), 0.87 (95% CI: 0.83-0.91), 7.1 (95% CI: 5.2-9.6), 0.13 (95% CI: 0.09-0.17), 56 (95% CI: 37-86) and 0.94 (95% CI: 0.92-0.96), respectively. The results of the diagnostic accuracy of DR for sample size <100 and sample ≥100 are listed as follows: the sensitivity was 0.82 (95% CI: 0.79-0.85) vs. 0.80 (95% CI: 0.72-0.86), specificity was 0.84 (95% CI: 0.80-0.87) vs. 0.83 (95% CI: 0.78-0.87), PLR was 5.1 (95% CI: 4.1-6.3) vs. 4.7 (95% CI: 3.6-6.2), NLR was 0.21 (95% CI: 0.17-0.26) vs. 0.24 (95% CI: 0.17-0.34), DOR was 24 (95% CI: 17-35) vs. 20 (95% CI: 12-32), and AUC was 0.90 (95% CI: 0.87-0.92) vs. 0.89 (95% CI: 0.85-0.91). No significant difference was observed in the overall diagnostic accuracy of DR for sample size <100 compared to that observed with sample size ≥100. In plasma samples, the values corresponding to sensitivity, specificity, PLR, NLR, DOR, and AUC were 0.78 (95% CI: 0.73-0.82), 0.87 (95% CI: 0.83-0.90), 6.1 (95% CI: 4.7-7.9), 0.25 (95% CI: 0.20-0.31), 24 (95% CI: 16-36), and 0.90 (95% CI: 0.87-0.92), respectively. In serum samples, the values corresponding to sensitivity, specificity, PLR, NLR, DOR, and AUC were 0.83 (95% CI: 0.78-0.86), 0.84 (95% CI: 0.80-0.87), 5.1 (95% CI: 4.1-6.3), 0.21 (95% CI: 0.16-0.26), 25 (95% CI: 17-36), and 0.90 (95% CI: 0.87-0.92), respectively. In aqueous humor, the values corresponding to sensitivity, specificity, PLR, NLR, DOR, and AUC were 0.83 (95% CI: 0.72-0.91), 0.69 (95% CI: 0.61-0.87), 2.7 (95% CI: 2.0-3.7), 0.24 (95% CI: 0.13-0.43), 11 (95% CI: 5-26), and 0.77 (95% CI: 0.73-0.80), respectively. Interestingly, miRNA expression levels were also correlated with diagnostic value, and our results showed that miRNAs with increased expression exhibited better diagnostic value. In the group demonstrating increased expression of miRNAs, the corresponding values for sensitivity, specificity, PLR, NLR, DOR and AUC were 0.83 (95% CI: 0.79-0.86), 0.84 (95% CI: 0.81-0.87), 5.1 (95% CI: 4.2-6.2), 0.21 (95% CI: 0.17-0.25), 25 (95% CI: 18-35) and 0.90 (95% CI: 0.87-0.92),

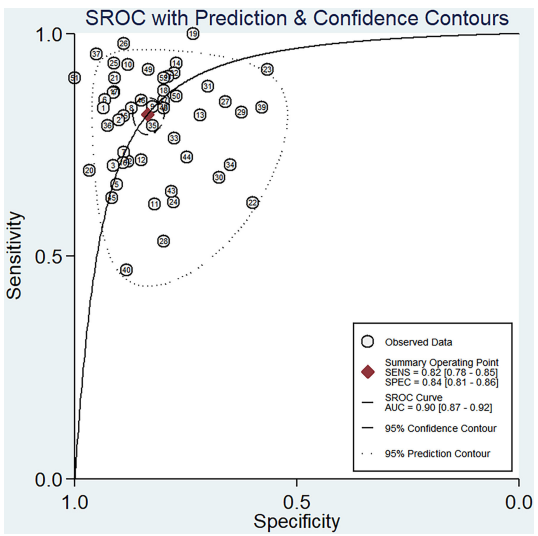

FIGURE 4 | Summary receiver operator characteristic (SROC) curve examining the overall accuracy of miRNAs in the diagnosis of diabetic retinopathy.

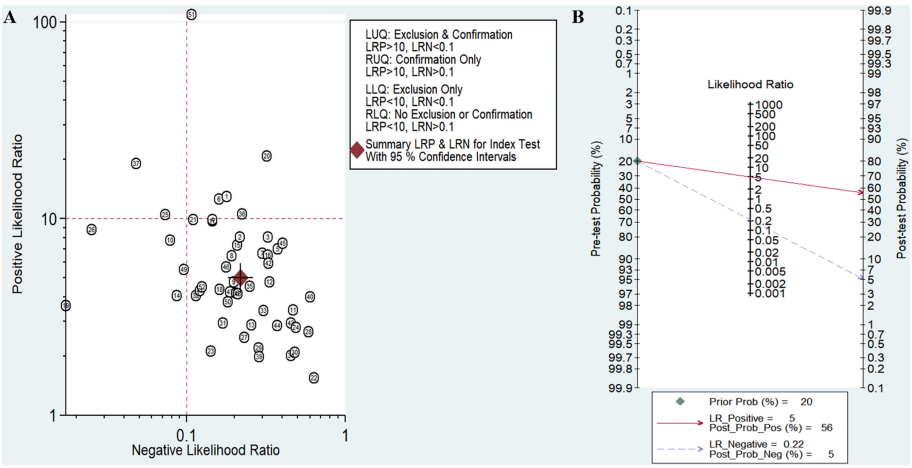

FIGURE 5 | Assessment of clinical applicability of miRNAs for diagnosis of diabetic retinopathy (DR). **(A)** Summary of positive likelihood ratio and negative likelihood ratio for diagnosis of DR; **(B)** Fagan's nomogram of miRNA studies for diagnosis of DR.

respectively. In addition, ethnicity had an impact on the diagnostic value of miRNAs, compared to the Asian population, the non-Asian populations had higher diagnostic accuracy, for sensitivity 0.86 (95% CI: 0.76-0.92), specificity 0.83 (95% CI: 0.61-0.94), PLR 5.0 (95% CI: 1.9 -13.1), NLR 0.17 (95% CI: 0.09-0.32), DOR 29 (95% CI: 7-124), and AUC 0.91 (95% CI: 0.88-0.93). Surprisingly, most studies selected U6 as an internal reference, yet the diagnostic value of the selected other miRNA internal reference groups was more significant than the U6 group, with sensitivity, specificity, PLR, NLR, DOR and AUC for the U6 group, respectively, of 0.80 (95% CI: 0.77-0.83), 0.84 (95% CI: 0.81-0.87), 5.0 (95%CI: 4.1-6.0), 0.24 (95% CI: 0.20-0.28), 21 (95%CI: 16-29) and 0.89 (95%CI: 0.86-0.92), respectively, for the non-U6 group sensitivity, specificity, PLR, NLR, DOR and AUC, respectively, were 0.88 (95% CI: 0.76-0.94), 0.81 (95% CI: 0.71-0.88), 4.5 (95% CI: 2.8-7.3), 0.15 (95% CI: 0.07 -0.33), 29 (95% CI: 9-91) and 0.90 (95% CI: 0.87-0.92), while studies without an explicitly given internal reference had higher diagnostic value, with sensitivity, specificity, PLR, NLR, DOR and AUC were 0.90 (95% CI: 0.70-0.97), 0.86 (95% CI: 0.72-0.94), 6.4 (95% CI: 3.3-12.6), 0.12 (95% CI: 0.04-0.36), 56 (95% CI: 19-164) and 0.93 (95% CI: 0.91-0.95). In addition, studies with optimal cut-off values had pooled results for sensitivity, specificity, PLR, NLR, DOR and AUC of 0.80

TABLE 2 | Summary estimates of diagnostic power and their 95% confidence intervals.

Subgroup	No. studies	Sen (95% CI)	Spe (95% CI)	PLR (95% CI)	NLR (95% CI)	DOR (95% CI)	AUC (95% CI)
MiRNA proliling							
Single miRNA	41	0.80 (0.76-0.83)	0.83 (0.79-0.86)	4.6 (3.8-5.5)	0.24 (0.20-0.30)	19 (14-26)	0.88 (0.85-0.91)
Multiple miRNAs	11	0.89 (0.85-0.92)	0.87 (0.83-0.91)	7.1 (5.2-9.6)	0.13 (0.09-0.17)	56 (37-86)	0.94 (0.92-0.96)
Sample size							
<100	38	0.82 (0.79-0.85)	0.84 (0.80-0.87)	5.1 (4.1-6.3)	0.21 (0.17-0.26)	24 (17-35)	0.90 (0.87-0.92)
≥100	14	0.80 (0.72-0.86)	0.83 (0.78-0.87)	4.7 (3.6-6.2)	0.24 (0.17-0.34)	20 (12-32)	0.89 (0.85-0.91)
Specimen							
Plasma	10	0.78 (0.73-0.82)	0.87 (0.83-0.90)	6.1 (4.7-7.9)	0.25 (0.20-0.31)	24 (16-36)	0.90 (0.87-0.92)
Serum	38	0.83 (0.78-0.86)	0.84 (0.80-0.87)	5.1 (4.1-6.3)	0.21 (0.16-0.26)	25 (17-36)	0.90 (0.87-0.92)
aqueous humor	4	0.83 (0.72-0.91)	0.69 (0.61-0.87)	2.7 (2.0-3.7)	0.24 (0.13-0.43)	11 (5-26)	0.77 (0.73-0.80)
Regulation mode							
Up-regulate	41	0.83 (0.79-0.86)	0.84 (0.81-0.87)	5.1 (4.2-6.2)	0.21 (0.17-0.25)	25 (18-35)	0.90 (0.87-0.92)
Down-regulate	9	0.77 (0.66-0.85)	0.82 (0.73-0.89)	4.3 (2.8-6.6)	0.28 (0.19-0.42)	15 (8-29)	0.87 (0.83-0.89)
Ethnicity							
Asian	46	0.81 (0.78-0.85)	0.84 (0.81-0.86)	5.0 (4.3-5.9)	0.22 (0.18-0.27)	23 (17-30)	0.90 (0.87-0.92)
Non-Asian	6	0.86 (0.76-0.92)	0.83 (0.61-0.94)	5.0 (1.9-13.1)	0.17 (0.09-0.32)	29 (7-124)	0.91 (0.88-0.93)
Internal reference							
U6	40	0.80 (0.77-0.83)	0.84 (0.81-0.87)	5.0 (4.1-6.0)	0.24 (0.20-0.28)	21 (16-29)	0.89 (0.86-0.92)
Non-U6	8	0.88 (0.76-0.94)	0.81 (0.71-0.88)	4.5 (2.8-7.3)	0.15 (0.07-0.33)	29 (9-91)	0.90 (0.87-0.92)
NA	4	0.90 (0.70-0.97)	0.86 (0.72-0.94)	6.4 (3.3-12.6)	0.12 (0.04-0.36)	56 (19-164)	0.93 (0.91-0.95)
Cut-off values							
Given	26	0.80 (0.75-0.83)	0.80 (0.76-0.84)	4.0 (3.2-4.9)	0.26 (0.21-0.32)	15 (11-23)	0.87 (0.83-0.89)
NA	26	0.84 (0.79-0.88)	0.87 (0.83-0.90)	6.4 (5.0-8.1)	0.18 (0.14-0.24)	35 (23-53)	0.92 (0.89-0.94)

Sen, sensitivity; Spe, specificity; PLR, positive likelihood ratio; NLR, negative likelihood ratio; DOR, diagnostic odds ratio; AUC, area under the curve; CI, confidence interval; NA, not available.

(95% CI: 0.75-0.83), 0.80 (95% CI: 0.76-0.84), 4.0 (95% CI: 3.2-4.9), 0.26 (95% CI: 0.21-0.32), 15 (95% CI: 11-23) and 0.87 (95% CI: 0.83-0.89), while studies without cut-off values showed better diagnostic value with sensitivity of 0.84 (95% CI: 0.79–0.88), specificity of 0.87 (95%CI: 0.83–0.90), PLR of 6.4 (95%CI: 5.0–8.1), NLR of 0.18 (95%CI: 0.14–0.24), DOR of 35 (95%CI: 23–53), and AUC of 0.92 (95%CI: 0.89–0.94), respectively.

The results of the sensitivity analysis are shown in **Figure 6**. The goodness of fit (**Figure 6A**) and bivariate normality (**Figure 6B**) showed that the random effects model was suitable. Influence analysis identified that studies of Yu et al, Shaker et al, Yin et al, Wan et al, and Salem et al. were the most dominant studies in weight (**Figure 6C**). Outlier detection implied that heterogeneity may be attributed to the data corresponding to studies of Yu et al, Wan et al, and Salem et al. (**Figure 6D**). After excluding four outlier studies, the I^2 value for heterogeneity decreased to 3.98% for sensitivity and 7.48% for specificity. There was no significant change in the pooled results for diagnostic efficacy (**Table 3**).

We performed meta-regression analysis with ethnicity, miRNA profiling, sample source, sample size, miRNA expression, internal reference and cut-off values as independent variables to explore the sources of heterogeneity. The results are shown in **Figure 7**. For sensitivity and specificity, all seven independent variables were statistically significant, indicating that ethnicity, miRNA profiling, sample source, sample size, miRNA expression, internal reference and cut-off values were sources of heterogeneity.

TABLE 3 | Diagnostic performance of miRNAs in DR.

Analysis	Overall	Outliers excluded
No. of studies	52	48
Sen (95% CI)	0.82 (0.78-0.85)	0.81 (0.78-0.84)
Spe (95% CI)	0.84 (0.81-0.86)	0.83 (0.81-0.86)
PLR (95% CI)	5.0 (4.2-5.9)	4.9 (4.2-5.8)
NLR (95% CI)	0.22 (0.18-0.26)	0.22 (0.19-0.26)
DOR (95% CI)	23 (17-31)	22 (17-30)
AUC (95% CI)	0.90 (0.87-0.92)	0.89 (0.86-0.92)

Sen, sensitivity; Spe, specificity; PLR, positive likelihood ratio; NLR, negative likelihood ratio; DOR, diagnostic odds ratio; AUC, area under the curve; CI, confidence interval.

Publication Bias

Deek's funnel plot was plotted for the 25 included papers (**Figure 8**). The studies were relatively symmetrically distributed on both sides of the regression line with P=0.41, and the differences were not statistically significant, indicating that there was no publication bias in the included data.

DISCUSSION

This meta-analysis of 25 articles including 1987 patients with DR and 1771 non-DR controls showed that miRNAs demonstrate high sensitivity (0.82, 95% CI: 0.78-0.85) and specificity (0.84, 95% CI: 0.81-0.86) in the diagnosis of DR. The pooled PLR of 5.0 indicates a 5.0-fold increase in the probability of an individual being diagnosed with DR. In addition, the NLR was 0.22, implying that the probability of

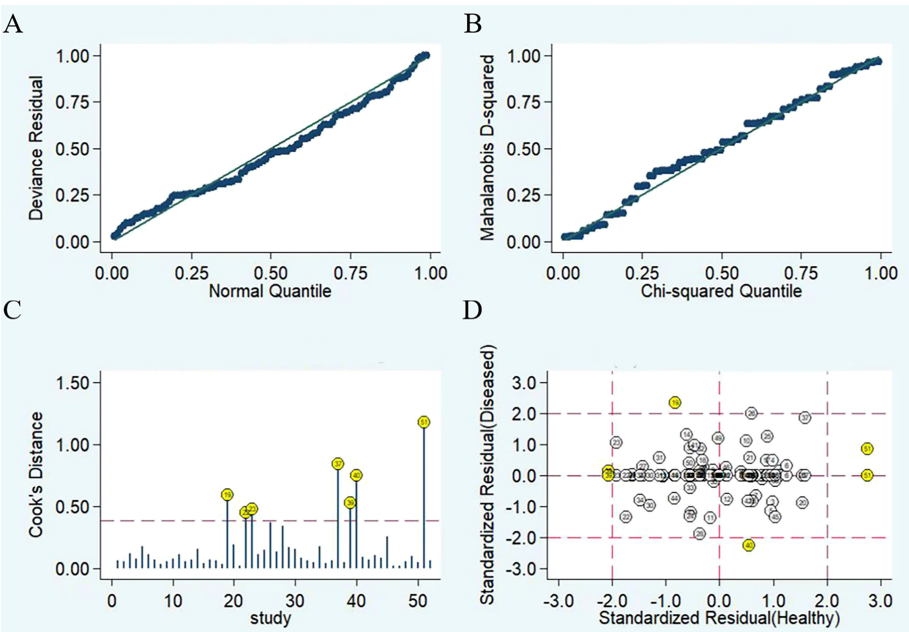

FIGURE 6 | Diagram of sensitivity analysis showing **(A)** goodness-of-fit; **(B)** bivariate normality; **(C)** influence analysis; **(D)** outlier detection.

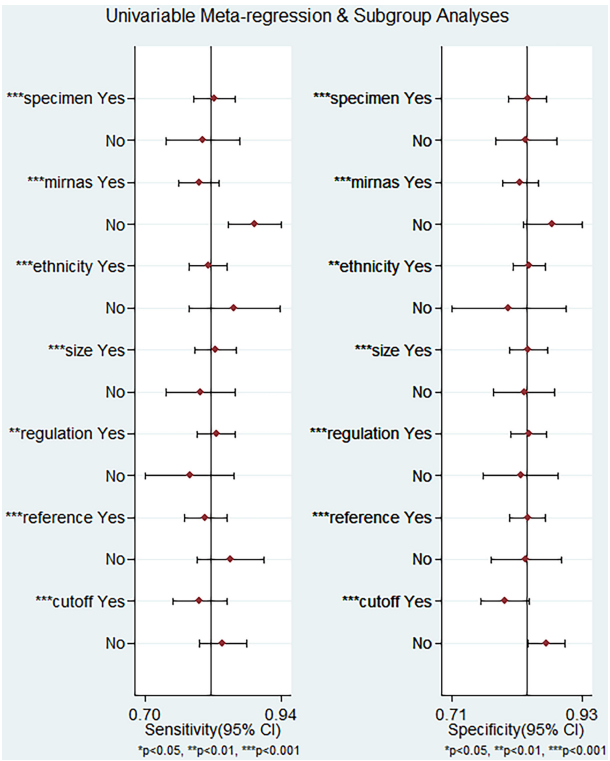

FIGURE 7 | Meta-regression analysis for examining sensitivity and specificity of miRNAs for the diagnosis of diabetic retinopathy.

subjects being diagnosed with DR was only 22%. DOR is an indicator of discriminatory test performance (47), and a DOR value greater than 1 indicates a better diagnostic test, with a DOR of 23, representing the ability of the miRNA to effectively discriminate between DR patients and non-DR control populations. However, due to heterogeneity among the included studies, we explored confounding factors by

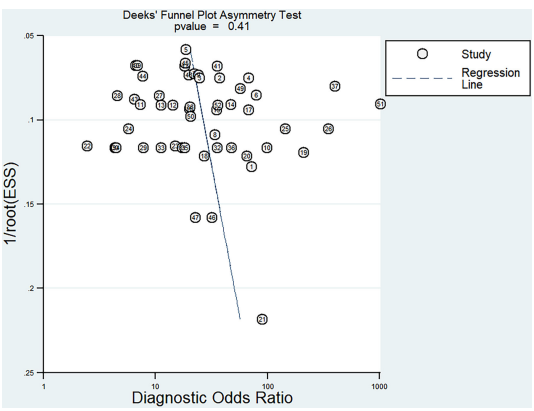

FIGURE 8 | Funnel plot for determining publication bias.

subgroup analysis and meta-regression analysis. Subgroup analysis revealed miRNA profiling, sample size, sample source, miRNA expression, ethnicity, internal reference and cut-off values setting as sources of heterogeneity.The combined detection of pooled miRNAs demonstrated better diagnostic accuracy than single miRNAs, with an AUC value of 0.94 for the miRNA group and 0.88 for single miRNAs. These results are consistent with previous findings by Zhou et al. on differential expression of miRNA in patients with DR (48), which may be explained by multiple gene mutations and epigenetic genetic abnormalities that are involved in the development of DR (49). Therefore, miRNA panel may be more suitable as a diagnostic biomarker for DR, which is the future development trend. One subgroup analysis that requires specific consideration showed that the sensitivity of miRNAs for diagnosis was higher in the non-Asian population (0.86) than in the Asian population (0.81). However, data from only six studies were available for the non-Asian group compared with 46 studies for the Asian group. Hence, we suggest that this difference may be attributed to the smaller number of studies performed with non-Asian populations. In addition, we found that the AUC values of miRNAs in serum, plasma, and aqueous humor were 0.90, 0.90, and 0.77, respectively, indicating that the detection of miRNAs in serum and plasma samples has high accuracy. Since the studies we included all used qRT-PCR to detect miRNAs levels, it was necessary to select appropriate internal reference genes for standardization, and we were surprised to find that although most studies used U6 as an internal reference gene, miRNAs showed higher diagnostic power with the analysis of other materials referred to as non-U6 references. qRT-PCR is the most widely used method for circulating miRNA expression profiling, and the accurate and reliable interpretation of its results depends heavily on the use of suitable reference genes for normalization, but the selection of suitable internal reference genes is still controversial (50), and the future selection of uniform and highly stable internal reference is essential to eliminate or minimize abiotic variation between test samples. Furthermore, in terms of clinical applicability, Fagan′s nomogram demonstrate promising results, with post-test probabilities of 0.56 and 0.5 for PLR and NLR, respectively, when the pre-test probability was set at 20%. This finding indicated that when the samples tested positive for the presence of miRNAs, patients had a 56% probability of developing DR, while the post-test probability of disease was reduced to 5% when the samples were tested negative for miRNAs. Among these studies, the expression of circulating miRNA-21 was reported to be upregulated in five articles. The sensitivity of miR-21 alone for the diagnosis of DR ranged from 0.661 to 0.818, and the specificity ranged from 0.867 to 0.908. Four studies analyzed miRNA-21 alone, and our meta-analysis of the diagnostic efficacy of miRNA-21 showed sensitivity, specificity, PLR, NLR, DOR, and AUC values of 0.70, 0.90, 6.9, 0.33, 21, and 0.89, respectively. Chen et al. demonstrated the protective effect of miR-21 silencing on neovascularization and inflammation in DR through a "knockdown" experiment (51). miR-21 may be an important regulator of reactive oxygen species homeostasis and antioxidant pathways, interfering with superoxide dismutase 2 expression and thereby affecting the

antioxidant response system, which is one of the major causes of cellular damage (52, 53). Therefore, miRNA-21 is considered an early predictor of reactive oxygen species-mediated injury in individuals at high risk for diabetes and has the potential to be an excellent marker for the diagnosis of DR.

These are several strengths of this meta-analysis. This is the first meta-analysis to perform a detailed assessment of the diagnostic value of miRNAs in DR. A more comprehensive list of miRNAs was analyzed in this study. The study also delineated miRNA subtypes that require further examination. Secondly, subgroup analysis and meta-regression analysis were performed to explore the heterogeneity of the studies included based on the high degree of heterogeneity.

Some limitations of this meta-analysis should be highlighted. First, the cutoff values of miRNAs in the included studies differed, which could lead to heterogeneity. Second, we did not assess differences in the accuracy of miRNA detection at different stages of DR for the diagnosis of DR due to a lack of sufficient data. Third, most of the included studies were based on Asian populations, which may contribute to ethnic bias. Fourth, this meta-analysis only included articles published in English and Chinese, which may also contribute to unavoidable bias. Fifth, most studies are retrospective case-control studies, increasing the risk of bias in the quality assessment of patient selection domains, in addition to the fact that there is no consensus on the selection of uniform and stable internal reference genes, which may lead to inconsistent results in the relative quantitative analysis of miRNAs. In addition, the relatively small sample size of each study may have limited the statistical power. Regrettably, due to the lack of a large number of similar miRNAs to pool the results, it is not yet possible to identify specific single miRNA or miRNAs panel as the best diagnostic biomarkers for DR. Therefore, based on the above limitations, these findings need to be interpreted with caution, and the results of our meta-analysis need to be further confirmed by well-designed studies with larger sample sizes in the future.

In conclusion, the current evidence suggests that miRNAs have significant diagnostic value in predicting DR and may be employed as effective non-invasive biomarkers for DR. Furthermore, miRNA panels have higher diagnostic potency than individual miRNAs. However, quality studies with large samples sizes should be conducted to validate our results and confirm the clinical value of miRNAs for patients with DR.

DATA AVAILABILITY STATEMENT

The original contributions presented in the study are included in the article/**Supplementary Material**. Further inquiries can be directed to the corresponding author.

AUTHOR CONTRIBUTIONS

LM and YW wrote the manuscript, responsible for literature retrieval and statistical analysis, ZL participate in editing manuscripts, and QW participate in discussion and review manuscripts. All authors read and approved the final version of the manuscript.

FUNDING

This project was supported by the major project of Chinese Medical Association Fund (No.TW-2018P003).

ACKNOWLEDGMENTS

The authors thank all those who collaborated in the analysis, interpretation of data and writing the article.

SUPPLEMENTARY MATERIAL

The Supplementary Material for this article can be found online at: https://www.frontiersin.org/articles/10.3389/fendo.2022.929924/full#supplementary-material

REFERENCES

1. Nebbioso M, Lambiase A, Armentano M, Tucciarone G, Sacchetti M, Greco A, et al. Diabetic Retinopathy, Oxidative Stress, and Sirtuins: An in Depth Look in Enzymatic Patterns and New Therapeutic Horizons. *Surv Ophthalmol* (2022) 67 (1):168–83. doi: 10.1016/j.survophthal.2021.04.003
2. Stitt AW, Curtis TM, Chen M, Medina RJ, McKay GJ, Jenkins A, et al. The Progress in Understanding and Treatment of Diabetic Retinopathy. *Prog Retinal Eye Res* (2016) 51:156–86. doi: 10.1016/j.preteyeres.2015.08.001
3. Teo ZL, Tham YC, Yu M, Chee ML, Rim TH, Cheung N, et al. Global Prevalence of Diabetic Retinopathy and Projection of Burden Through 2045: Systematic Review and Meta-Analysis. *Ophthalmology* (2021) 128(11):1580–91. doi: 10.1016/j.ophtha.2021.04.027
4. Pu S, Xu Y, Li X, Yu Z, Zhang Y, Tong X, et al. Lncrnas-Modulators of Neurovascular Units in Diabetic Retinopathy. *Eur J Pharmacol* (2022) 925:174937. doi: 10.1016/j.ejphar.2022.174937
5. Lopez-Contreras AK, Martinez-Ruiz MG, Olvera-Montano C, Robles-Rivera RR, Arevalo-Simental DE, Castellanos-Gonzalez JA, et al. Importance of the Use of Oxidative Stress Biomarkers and Inflammatory Profile in Aqueous and Vitreous Humor in Diabetic Retinopathy. *Antioxidants-Basel* (2020) 9(9):891. doi: 10.3390/antiox9090891
6. Antonetti DA, Silva PS, Stitt AW. Current Understanding of the Molecular and Cellular Pathology of Diabetic Retinopathy. *Nat Rev Endocrinol* (2021) 17 (4):195–206. doi: 10.1038/s41574-020-00451-4
7. Mustafi D, Saraf SS, Shang Q, Olmos de Koo LC. New Developments in Angiography for the Diagnosis and Management of Diabetic Retinopathy. *Diabetes Res Clin Pract* (2020) 167:108361. doi: 10.1016/j.diabres.2020.108361
8. Schreur V, Larsen MB, Sobrin L, Bhavsar AR, den Hollander AI, Klevering BJ, et al. Imaging Diabetic Retinal Disease: Clinical Imaging Requirements. *Acta Ophthalmol* (2022). doi: 10.1111/aos.15110
9. Cai S, Liu TYA. The Role of Ultra-Widefield Fundus Imaging and Fluorescein Angiography in Diagnosis and Treatment of Diabetic Retinopathy. *Curr Diabetes Rep* (2021) 21(9):30. doi: 10.1007/s11892-021-01398-0
10. Pirola L, Balcerczyk A, Okabe J, El-Osta A. Epigenetic Phenomena Linked to Diabetic Complications. *Nat Rev Endocrinol* (2010) 6(12):665–75. doi: 10.1038/nrendo.2010.188

11. Salem TI, Eldin NB, Alhusseini NF, Abdullah OA, Ahmed NE. Expression Profile of Micrornas May Be Promising in Diagnosis of Proliferative Diabetic Retinopathy: An Egyptian Study. *Int J Diabetes Developing Countries* (2022). doi: 10.1007/s13410-022-01044-9
12. Zhang J, Cui C, Xu H. Downregulation of Mir-145-5p Elevates Retinal Ganglion Cell Survival to Delay Diabetic Retinopathy Progress by Targeting Fgf5. *Biosci Biotechnol Biochem* (2019) 83(9):1655–62. doi: 10.1080/09168451.2019.1630251
13. Greco M, Chiefari E, Accattato F, Corigliano DM, Arcidiacono B, Mirabelli M, et al. Microrna-1281 as a Novel Circulating Biomarker in Patients With Diabetic Retinopathy. *Front Endocrinol* (2020) 11:528. doi: 10.3389/fendo.2020.00528
14. Ye Z, Li ZH, He SZ. Mirna-1273g-3p Involvement in Development of Diabetic Retinopathy by Modulating the Autophagy-Lysosome Pathway. *Med Sci Monit* (2017) 23:5744–51. doi: 10.12659/msm.905336
15. Mori MA, Ludwig RG, Garcia-Martin R, Brandao BB, Kahn CR. Extracellular Mirnas: From Biomarkers to Mediators of Physiology and Disease. *Cell Metab* (2019) 30(4):656–73. doi: 10.1016/j.cmet.2019.07.011
16. Hill M, Tran N. Mirna Interplay: Mechanisms and Consequences in Cancer. *Dis Model Mech* (2021) 14(4):dmm047662. doi: 10.1242/dmm.047662
17. Stevens MT, Saunders BM. Targets and Regulation of Microrna-652-3p in Homoeostasis and Disease. *J Mol Med (Berl)* (2021) 99(6):755–69. doi: 10.1007/s00109-021-02060-8
18. Yu H, Liu H, Chen X, Wu N. Preliminary Study on Serum Microrna Expression Profile in Patients With Diabetic Retinopathy. *Chin J Ophthalmol Med* (2019) 9(04):246–51. doi: 10.3877/cma.j.issn.2095-2007.2019.04.009
19. Chen X, Rechavi O. Plant and Animal Small Rna Communications Between Cells and Organisms. *Nat Rev Mol Cell Biol* (2022) 23(3):185–203. doi: 10.1038/s41580-021-00425-y
20. Shaker OG, Abdelaleem OO, Mahmoud RH, Abdelghaffar NK, Ahmed TI, Said OM, et al. Diagnostic and Prognostic Role of Serum Mir-20b, Mir-17-3p, Hotair, and Malat1 in Diabetic Retinopathy. *IUBMB Life* (2019) 71(3):310–20. doi: 10.1002/iub.1970
21. Xu YX, Pu SD, Li X, Yu ZW, Zhang YT, Tong XW, et al. Exosomal Ncrnas: Novel Therapeutic Target and Biomarker for Diabetic Complications. *Pharmacol Res* (2022) 178:106135. doi: 10.1016/j.phrs.2022.106135
22. Whiting PF, Rutjes AW, Westwood ME, Mallett S, Deeks JJ, Reitsma JB, et al. Quadas-2: A Revised Tool for the Quality Assessment of Diagnostic Accuracy Studies. *Ann Intern Med* (2011) 155(8):529–36. doi: 10.7326/0003-4819-155-8-201110180-00009
23. Higgins JP, Thompson SG, Deeks JJ, Altman DG. Measuring Inconsistency in Meta-Analyses. *BMJ* (2003) 327(7414):557–60. doi: 10.1136/bmj.327.7414.557
24. Jackson D, White IR, Thompson SG. Extending Dersimonian and Laird's Methodology to Perform Multivariate Random Effects Meta-Analyses. *Stat Med* (2010) 29(12):1282–97. doi: 10.1002/sim.3602
25. Qing S, Yuan S, Yun C, Hui H, Mao P, Wen F, et al. Serum Mirna Biomarkers Serve as a Fingerprint for Proliferative Diabetic Retinopathy. *Cell Physiol Biochem Int J Exp Cell Physiol Biochem Pharmacol* (2014) 34(5):1733–40. doi: 10.1159/000366374
26. Fu C. Expression of Mir-93 and Mir-21 in Patients With Diabetic Retinopathy and Its Clinical Values. *Rec Adv Ophthalmol* (2017) 37(12):1161–4. doi: 10.13389/j.cnki.rao.2017.0293
27. Qin LL, An MX, Liu YL, Xu HC, Lu ZQ. Microrna-126: A Promising Novel Biomarker in Peripheral Blood for Diabetic Retinopathy. *Int J Ophthalmol* (2017) 10(4):530–4. doi: 10.18240/ijo.2017.04.05
28. Jiang Q, Lyu XM, Yuan Y, Wang L. Plasma Mir-21 Expression: An Indicator for the Severity of Type 2 Diabetes With Diabetic Retinopathy. *Biosci Rep* (2017) 37(2):BSR20160589. doi: 10.1042/BSR20160589
29. Zou HL, Wang Y, Gang Q, Zhang Y, Sun Y. Plasma Level of Mir-93 Is Associated With Higher Risk to Develop Type 2 Diabetic Retinopathy. *Graefe's Arch Clin Exp Ophthalmol Albrecht Von Graefes Archiv Fur Klin Und Experimentelle Ophthalmol* (2017) 255(6):1159–66. doi: 10.1007/s00417-017-3638-5
30. Sun J, Cai R, Gao Z, Zhou T, Yin W, Hu H, et al. Correlation of Plasma Microrna-21 Expression With Type 2 Diabetes Mellitus With Retinopathy. *Guizhou Med J* (2018) 42(12):1471–3. doi: CNKI:SUN:GZYI.0.2018-12-033
31. Zheng H, Yu J, Tian N, Wu J. Expression and Significances of Mir-126 and Vegf in Proliferative Diabetic Retinopathy. *J Chin Physician* (2018) 20(10):1477–81. doi: 10.3760/cma.j.issn.1008-1372.2018.10.010
32. Liang Z, Gao KP, Wang YX, Liu ZC, Tian L, Yang XZ, et al. Rna Sequencing Identified Specific Circulating Mirna Biomarkers for Early Detection of Diabetes Retinopathy. *Am J Physiol Endocrinol Metab* (2018) 315(3):E374–e85. doi: 10.1152/ajpendo.00021.2018
33. Dai B, Dai Y. Clinical Value of Serum Mirna in Patients With Diabetic Retinopathy. *Rec Adv Ophthalmol* (2019) 39(08):780–4. doi: 10.13389/j.cnki.rao.2019.0178
34. Ma Y, Zhou LX, Liu Y, Wu W. Prediction of Retinopathy in Type 2 Diabetes Mellitus by Combined Detection of Microrna93 and Microrna21. *Int Eye Sci* (2019) 19(9):1550–3. doi: 10.3980/j.issn.1672-5123.2019.9.24
35. Li Z, Dong Y, He C, Pan X, Liu D, Yang J, et al. Rna-Seq Revealed Novel Non-Proliferative Retinopathy Specific Circulating Mirnas in T2dm Patients. *Front Genet* (2019) 10:531. doi: 10.3389/fgene.2019.00531
36. Ji HH, Yi QY, Chen LS, Wong LP, Liu YF, Xu GD, et al. Circulating Mir-3197 and Mir-2116-5p as Novel Biomarkers for Diabetic Retinopathy. *Clin Chim Acta* (2019) 501:147–53. doi: 10.1016/j.cca.2019.10.036
37. Lin Y, Li Q, Lin X. Expression and Clinical Significances of Mir-15 and Mir-29a in Serum of Patients With Diabetic Retinopathy. *J Chin Physician* (2020) 22(03):399–403. doi: 10.3760/cma.j.cn.431274-20181220-02388
38. Liu L, Wu B, Ni L, Zhang L, Hu X, Wang Z, et al. Changes of Mir-15a,Mir-16 and Mir-20b in Patients With Type 2 Diabetes Mellitus and Their Relationship With Diabetic Retinopathy. *Chin J Gen Pract* (2020) 18(06):954–8. doi: 10.16766/j.cnki.issn.1674-4152.001401
39. Yin C, Lin X, Sun Y, Ji X. Dysregulation of Mir-210 Is Involved in the Development of Diabetic Retinopathy and Serves a Regulatory Role in Retinal Vascular Endothelial Cell Proliferation. *Eur J Med Res* (2020) 25(1):20. doi: 10.1186/s40001-020-00416-3
40. Wan Q, Lei J, Ma T. Risk Factors of Depression and Anxiety and Nursing Intervention in Diabetics During Perioperative Period. *Acta Med Mediterr* (2020) 36(5):3221–7. doi: 10.19193/0393-6384_2020_5_496
41. Hu Q, Luan L, Liu Z. The Relationship Between Serum Mir-29c, Bfgf Levels and Diabetic Retinopathy. *Chin J Atheroscl* (2021) 29(12):1053–8. doi: 10.3969/j.issn.1007-3949.2021.12.008
42. Liu Q, Wang S, Ding L, Qin Y, Maidina N. Diagnostic Value of Serum Mir-211 in Diabetic Retinopathy and Its Influencing Factors. *Chin J Clin Lab Sci* (2021) 39(06):445–8. doi: 10.13602/j.cnki.jcls.2021.06.10
43. Sun Z, Yang J. Correlation Between the Expression of Serum Mir▪320 and Diabetic Retinopathy in Type 2 Diabetic Patients. *Chin J Diabetes* (2021) 29(05):344–8. doi: 10. 3969/j. issn.1006 6187. 2021. 05. 005
44. Santovito D, Toto L, De Nardis V, Marcantonio P, D'Aloisio R, Mastropasqua A, et al. Plasma Microrna Signature Associated With Retinopathy in Patients With Type 2 Diabetes. *Sci Rep* (2021) 11(1):4136. doi: 10.1038/s41598-021-83047-w
45. Wang Z, Zhang X, Wang Y, Xiao D. Dysregulation of Mir-374a Is Involved in the Progression of Diabetic Retinopathy and Regulates the Proliferation and Migration of Retinal Microvascular Endothelial Cells. *Clin Exp Optometry* (2021) 105:1–6. doi: 10.1080/08164622.2021.1913043
46. Liu X, Zhou Y, Liu Y, Wang Q, Pan L. Microrna-425-5p Is Involved in the Development of Diabetic Retinopathy and Regulates the Proliferation and Migration of Retinal Microvascular Endothelial Cells. *Ophthalmic Res* (2022) 65(1):60–7. doi: 10.1159/000516906
47. Glas AS, Lijmer JG, Prins MH, Bonsel GJ, Bossuyt PM. The Diagnostic Odds Ratio: A Single Indicator of Test Performance. *J Clin Epidemiol* (2003) 56(11):1129–35. doi: 10.1016/s0895-4356(03)00177-x
48. Zhou H, Peng C, Huang DS, Liu L, Guan P. Microrna Expression Profiling Based on Microarray Approach in Human Diabetic Retinopathy: A Systematic Review and Meta-Analysis. *DNA Cell Biol* (2020) 39(3):441–50. doi: 10.1089/dna.2019.4942
49. Stavast CJ, Erkeland SJ. The Non-Canonical Aspects of Micrornas: Many Roads to Gene Regulation. *Cells* (2019) 8(11):1465. doi: 10.3390/cells8111465
50. Donati S, Ciuffi S, Brandi ML. Human Circulating Mirnas Real-Time Qrt-Pcr-Based Analysis: An Overview of Endogenous Reference Genes Used for Data Normalization. *Int J Mol Sci* (2019) 20(18):4353. doi: 10.3390/ijms20184353
51. Chen Q, Qiu F, Zhou K, Matlock HG, Takahashi Y, Rajala RVS, et al. Pathogenic Role of Microrna-21 in Diabetic Retinopathy Through Downregulation of Pparalpha. *Diabetes* (2017) 66(6):1671–82. doi: 10.2337/db16-1246

52. La Sala L, Cattaneo M, De Nigris V, Pujadas G, Testa R, Bonfigli AR, et al. Oscillating Glucose Induces Microrna-185 and Impairs an Efficient Antioxidant Response in Human Endothelial Cells. *Cardiovasc Diabetol* (2016) 15:71. doi: 10.1186/s12933-016-0390-9
53. La Sala L, Mrakic-Sposta S, Tagliabue E, Prattichizzo F, Micheloni S, Sangalli E, et al. Circulating Mirorna-21 Is an Early Predictor of Ros-Mediated Damage in Subjects With High Risk of Developing Diabetes and in Drug-Naive T2d. *Cardiovasc Diabetol* (2019) 18(1):18. doi: 10.1186/s12933-019-0824-2

Conflict of Interest: The authors declare that the research was conducted in the absence of any commercial or financial relationships that could be construed as a potential conflict of interest.

Publisher's Note: All claims expressed in this article are solely those of the authors and do not necessarily represent those of their affiliated organizations, or those of the publisher, the editors and the reviewers. Any product that may be evaluated in this article, or claim that may be made by its manufacturer, is not guaranteed or endorsed by the publisher.

frontiers | Frontiers in Endocrinology

ORIGINAL RESEARCH
published: 22 July 2022
doi: 10.3389/fendo.2022.937089

Characteristic MicroRNAs Linked to Dysregulated Metabolic Pathways in Qatari Adult Subjects With Obesity and Metabolic Syndrome

Fayaz Ahmad Mir[1†], Raghvendra Mall[2,3*†], Ahmad Iskandarani[1], Ehsan Ullah[2], Tareq A. Samra[1], Farhan Cyprian[4], Aijaz Parray[5], Meis Alkasem[1], Ibrahem Abdalhakam[1], Faisal Farooq[2] and Abdul-Badi Abou-Samra[1]*

[1] Qatar Metabolic Institute, Academic Health System, Hamad Medical Corporation, Doha, Qatar, [2] Qatar Computing Research Institute (QCRI), Hamad Bin Khalifa University, Doha, Qatar, [3] Department of Immunology, St. Jude Children's Research Hospital, Memphis, TN, United States, [4] College of Medicine, Qatar University (QU) Health, Qatar University, Doha, Qatar, [5] Qatar Neuroscience Institute, Academic Health System, Hamad Medical Corporation, Doha, Qatar

OPEN ACCESS

Edited by:
Davide Povero,
Mayo Clinic, United States

Reviewed by:
Stephanie Burr,
Mayo Clinic, United States
Bei Shi,
China Medical University, China

***Correspondence:**
Fayaz Ahmad Mir
fmir1@hamad.qa
Raghvendra Mall
raghvendra.mall@stjude.org

†These authors have contributed equally to this work and share first authorship

Specialty section:
This article was submitted to Obesity, a section of the journal Frontiers in Endocrinology

Received: 05 May 2022
Accepted: 24 June 2022
Published: 22 July 2022

Citation:
Mir FA, Mall R, Iskandarani A, Ullah E, Samra TA, Cyprian F, Parray A, Alkasem M, Abdalhakam I, Farooq F and Abou-Samra A-B (2022) Characteristic MicroRNAs Linked to Dysregulated Metabolic Pathways in Qatari Adult Subjects With Obesity and Metabolic Syndrome. Front. Endocrinol. 13:937089. doi: 10.3389/fendo.2022.937089

Background: Obesity-associated dysglycemia is associated with metabolic disorders. MicroRNAs (miRNAs) are known regulators of metabolic homeostasis. We aimed to assess the relationship of circulating miRNAs with clinical features in obese Qatari individuals.

Methods: We analyzed a dataset of 39 age-matched patients that includes 18 subjects with obesity only (OBO) and 21 subjects with obesity and metabolic syndrome (OBM). We measured 754 well-characterized human microRNAs (miRNAs) and identified differentially expressed miRNAs along with their significant associations with clinical markers in these patients.

Results: A total of 64 miRNAs were differentially expressed between metabolically healthy obese (OBO) versus metabolically unhealthy obese (OBM) patients. Thirteen out of 64 miRNAs significantly correlated with at least one clinical trait of the metabolic syndrome. Six out of the thirteen demonstrated significant association with HbA1c levels; miR-331-3p, miR-452-3p, and miR-485-5p were over-expressed, whereas miR-153-3p, miR-182-5p, and miR-433-3p were under-expressed in the OBM patients with elevated HbA1c levels. We also identified, miR-106b-3p, miR-652-3p, and miR-93-5p that showed a significant association with creatinine; miR-130b-5p, miR-363-3p, and miR-636 were significantly associated with cholesterol, whereas miR-130a-3p was significantly associated with LDL. Additionally, miR-652-3p's differential expression correlated significantly with HDL and creatinine.

Conclusions: MicroRNAs associated with metabolic syndrome in obese subjects may have a pathophysiologic role and can serve as markers for obese individuals predisposed to various metabolic diseases like diabetes.

Keywords: miRNA, metabolic disorder, HbA1c, obesity, mirDIP, network analysis

INTRODUCTION

The worldwide rise in obesity and its strong association with metabolic diseases have elicited interest in the underlying mechanisms. According to the WHO report 2021, worldwide obesity has nearly tripled since 1975 (1). In 2016, more than 1.9 billion adults, 18 years and older, were overweight and over 650 million were obese (1). The global obesity epidemic is causing an alarming incidence of metabolic disorders. Obesity can be considered a growing epidemic that is associated with hyperglycemia (elevated blood glucose levels >7.0 mmol/L or hemoglobin that is glycosylated HbA1c > 6.5%), insulin resistance, and dyslipidemia (characterized by elevated cholesterol, low-density lipoproteins (LDL) and decreased serum high-density lipoproteins (HDL)), collectively referred to as metabolic syndrome (2). However, there are subjects with an elevated body mass index (BMI) who do not progress to metabolic syndrome; they are generally labeled as "Metabolically Healthy Obese" (2–7), they have obesity only (OBO); but the protective mechanisms are unknown. Body fat distribution is suspected to play an important role (8). High liver fat content and predominantly abdominal adiposity were shown to be linked to the metabolically unhealthy obesity phenotype (obesity with metabolic syndrome or OBM), whereas subcutaneous adiposity is associated with the metabolic healthy obesity phenotype (9, 10). Over the past years, some biological mechanisms and phenotypic characteristics have been identified that differentiate individuals with OBO from OBM (11). The concept of OBO may serve as a model to better understand the pathways and mechanisms linking obesity to metabolic diseases. Therefore, considering the potentially devastating impact of obesity, there is urgency in elucidating underlying mechanisms and identifying novel markers for risk stratification and targeted early treatment.

Impaired adipose tissue metabolism and function are central to the pathogenesis of obesity and associated metabolic disorders. MicroRNAs (miRNAs) play a crucial role in regulating gene expression and are likely to have an essential function in the pathogenesis of obesity and metabolic disorders (12). MicroRNAs are small non-coding RNAs participating in the post-transcriptional regulation of genes by negatively regulating them. Evidence is accumulating that circulating miRNAs, released by many types of cells act as a new class of endocrine factors. MiRNAs might serve as endocrine and paracrine messengers that facilitate communication between donor cells and tissues with receptor cells or target tissues, thereby potentially having important roles in metabolic organ crosstalk (13). In response to various pathophysiological conditions, miRNAs can be released by cells into their environment transported by different extracellular fluids, including blood, and could serve as biomarkers of diverse diseases including diabetes and related metabolic disorders. The role of miRNAs as key regulators of metabolic homeostasis has been intensely explored over the last decade. *Brando et al.* have collated the significant circulating miRNAs that are altered in obese subjects, where microRNAs such as miR-92a-3p, miR-122, miR-122-5p, miR-140-5p, miR-142-3p, miR-151a, miR-155, miR-222, and miR-15a have been shown to be upregulated. On the other hand miR-15a, miR-26a, miR-30b, miR-30c, miR-125b, miR-126, miR-139-5p, miR-144-5p, miR-146a, miR-150, miR-223, and miR-376a are reported to be downregulated in obese adults when compared to healthy lean individuals (14). Controversially, the role of miR-15b remains obscure where it has been upregulated in one study (15) while another group reported downregulation of miR-15b in obese subjects compared to lean counterparts (16). Although obesity is linked to differentially expressed miRNAs, they additionally contribute to various metabolic disorders including hypertension, hepatic steatosis, and insulin resistance by influencing the metabolism of cholesterol, LDL (mir-26a and mir-15b), and elevation of circulating glucose (mir-140-5p, miR-142-3p, miR-222, and mir125b) that eventually glycosylates hemoglobin (HbA1c) respectively (12, 14, 17–21).

Here, we aimed to unravel the associations between the metabolic parameters in obese individuals with miRNA profiling. We identified 64 significantly differentially expressed miRNAs of which 36 were down-regulated and 28 were up-regulated. By undertaking an association discovery approach, we identified the expression of eleven out of the 36 down-regulated miRNAs and two of the 28 up-regulated miRNAs in our patient dataset were significantly correlated with at least one clinical trait of relevance to metabolic syndrome. The down regulated miRNAs include miR-106b-3p, miR-103a-3p, miR-130b-5p, miR-153-3p, miR-182-5p, miR-331-3p, miR-363-3p, miR-433-3p, miR-636, miR-652-3p and miR-93-5p whereas miR-452-3p and miR-485-5p were upregulated. Several of the miRNAs in OBM patients were significantly dysregulated and associated with increased levels of HbA1c and cholesterol. These include miR-130b-5p, miR-153-3p, miR-182-5p, miR-331-3p, miR-363-3p, miR-433-3p, miR-452-3p, miR-485-5p and miR-636. **Figure 1** provides an outline of our experimental design.

MATERIALS AND METHODS

Study Design

The participants were recruited at the Qatar Metabolic Institute, Hamad Medical Corporation, Doha, Qatar. The study protocol was approved by the institutional review board (IRB) of Hamad Medical Corporation (HMC, IRB protocol #16245/16) and all participants provided written informed consent. Obesity was determined according to CDC guidelines. Both Class 1 (BMI of 35 to 40) and Class 2 (BMI > NA). Both Class 1 and Class 2 obesity were referred to as morbid obesity. A total of 120, male and female participants aged between 18 to 65 years with morbid obesity (BMI≥35 kg/m^2) were included. Individuals such as pregnant females and those with identified chronic disease or terminal illness were excluded from the study. The subjects were classified into two groups those without metabolic syndrome (OBO) and with metabolic syndrome (OBM) components of the metabolic syndrome; obesity PLUS any 2 of the following: triglycerides ≥ 150 mg/dL (1.7 mmol/L), HDL< 40 mg/dL (1.03 mmol/L) in men or< 50 mg/dL (1.29 mmol/L) in

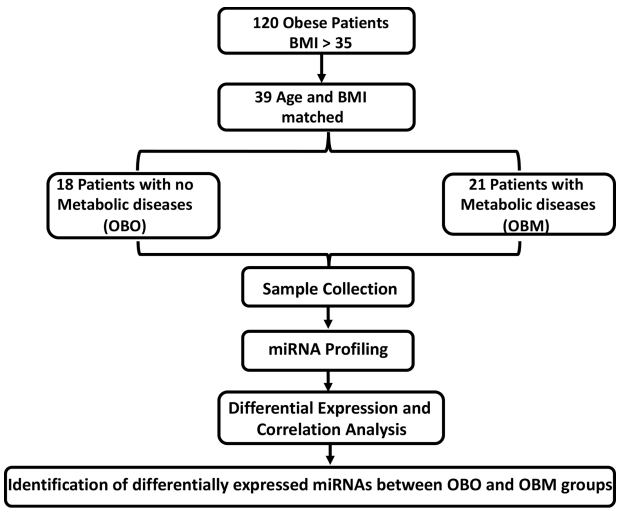

FIGURE 1 | The experimental study design. BMI, Body Mass Index; OBO, Obesity with no metabolic disease; OBM, Obesity with metabolic diseases. To determine the fold-changes of miRNA expression between the OBO vs OBM patients, we used the Relative Quantification (RQ) measure. We considered those miRNAs to be differentially expressed for which $|\log2(RQ)| > 2$ and significance threshold $p < 0.05$. This resulted in the identification of 64 differentially expressed miRNAs. Out of the 64 miRNAs, there were 13 miRNAs whose expression correlated with at least one clinical trait of relevance for metabolic syndrome (including HBA1c, Creatinine, Cholesterol, LDL, and HDL).

women, blood pressure ≥ 130/85 mmHg and fasting blood glucose ≥ 110 mg/dL (5.6 mmol/L) (22). An additional, filter of age and BMI matching yielded 39 subjects that consisted of 18 OBO subjects and 21 OBM subjects. Among the 18 OBO group subjects, none of the subjects had hyperglycemia, 2 individuals were identified with hypertension, 2 with mildly elevated triglycerides, and 6 with a borderline decrease in HDL. Venous blood samples were collected from these 39 subjects for total miRNA isolation.

Participants Characteristics

Height and weight were measured in light clothing without shoes. Fasting blood samples were taken between 7-9 AM after at least 12h of fasting. For serum collection, whole blood was collected *via* BD Vacutainer Serum Separation Tubes (BD Biosciences, Franklin Lakes, NJ, USA). Blood samples were kept at room temperature for 30-60 minutes and then centrifuges at 3000g for 10 minutes. Following centrifugation, serum was separated and immediately stored at -80°C for further use.

Blood biochemistry was performed at the HMC clinical laboratory which has been accredited by the College of American Pathologists (CAP). Measurements included HbA1c with Turbidimetric Inhibition Immunoassay (TINIA Roche Diagnostics, Mannheim, Germany), glucose by enzymatic reference method with hexokinase (Cobas 6000, Roche Diagnostics International, Switzerland), Total cholesterol, triglycerides, and high-density lipoprotein (HDL) cholesterol levels were measured enzymatically using a Synchron LX20 analyzer (Beckman-Coulter, High Wycombe, UK).

RNA Isolation and Quality Control

Whole blood (2.5 ml) was collected into PaXgene Blood RNA Tubes (PreAnalytix). The tubes were inverted 8-10 times then placed at room temperature for at least 2 hours, frozen at -80°C, thawed overnight, then total RNA was isolated with a PAXgene Blood RNA Kit including the DNase Set (Qiagen). The concentrations and purity of the RNA samples were evaluated spectrophotometrically (Nanodrop ND-1000, Thermo, Wilmington, DE USA). The RNA isolation process was validated by analyzing the integrity of several RNAs with the RNA 6000 Nano Chip Kit (Agilent). The presence of the small RNA fraction was confirmed by the Agilent Small RNA Kit (Agilent).

MicroRNA (miRNA) Profiling

The expression levels of 754 miRNAs were profiled using the TaqMan OpenArray Human MicroRNA panels (PN: 4470189; Life Technologies Forster City, CA, USA) on a QuantStudio 12K Flex instrument. For all experimental groups, 3 μL (~10 ng) of total RNA was used for reverse transcription (RT) reactions using MegaPlex RT Primers Human Pool Set v3.0 (PN: 4444745; Pool A v2.1 and Pool B v3.0) according to the manufacturer's optimized protocol for low sample input for profiling human microRNA using the OpenArray platform on BioRad c1000 Touch thermal cycler. No-template controls were included. Pre-amplification of RT products was performed using a 5 μL RT reaction combined with the matching Megaplex PreAmp Primer Pool A v2.1 or B v3.0 and amplified using the thermal cycler (Applied biosystems). The pre-amplified products were diluted at 1:40 in 0.1x TE pH 8. For each experimental set, 10 μL of the diluted products were combined to give a total of 40 μL pooled sample. For both Pool A and Pool B groups, 22.5 μL of the pooled products were combined with an equivalent volume of TaqMan OpenArray Real-Time Master Mix and aliquoted into a 96-well plate. Then, 5 μL from each well were then transferred into a 384 well plate for loading onto OpenArray plates using an AccuFill robotic system. The OpenArray plates were run on a QuantStudio 12K Flex instrument (Life Technologies) and the raw data files were imported and analyzed using the DataAssist software (Life Technologies). Failed reactions were excluded from analysis and undetermined CT values for samples sets determined to have good amplifications were assigned a threshold value of 40, defining low abundance or absence of miRNA expression. Global mean normalization was used to calculate relative fold change for the miRNA expression.

Statistics

Statistical characteristics of clinical measurements were calculated by comparing the OBO and OBM samples using R v4.2.0 (23). The normality of the measurements was tested using Anderson-Darling test using nortest v1.0.4 package (24). The *Student's t-test* was used to calculate the p-value of the normally distributed measurements. For the remaining measurements, Mann-Whitney test from the base package in R was used.

P-values were not corrected for false discovery rate (FDR) owing to the small sample size.

The miRNA expression levels were measured *via* raw CR_T values, which are inversely proportional to miRNA expression i.e., the higher the CR_T value lower the expression of the circulating miRNA (25). However, current miRNA microarray platforms might not have enough miRNAs which are stably expressed as indicated in (26). Thus, to measure fold-changes in miRNA expression, we determined the Relative Quantification (RQ) values using the standard formula (27). An RQ value showcased the fold-change (FC) of a specific miRNA in two populations. An RQ=1 indicated that a specific miRNA was not differentially expressed in the OBO versus OBM samples. Otherwise, if the $|\log2(RQ)| > 2$ and significance threshold ($p< 0.05$), then the miRNA was differentially expressed between the two groups as observed in **Figure 2A**.

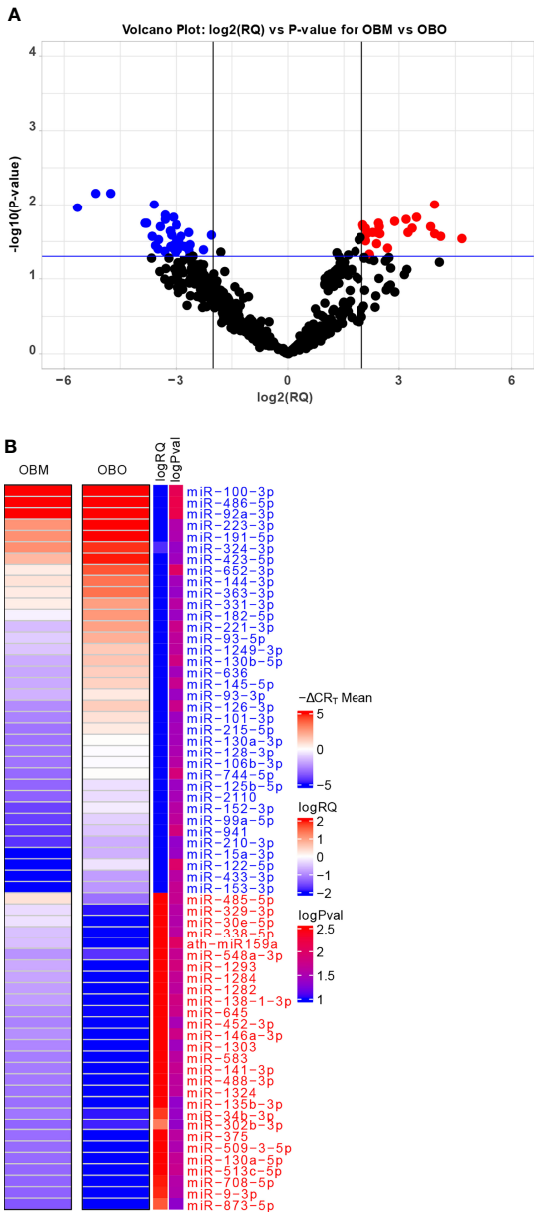

FIGURE 2 | **(A)** Volcano Plot highlighting the differentially expressed microRNAs. The red-colored microRNAs are over-expressed in OBM versus OBO while the blue-colored microRNAs are under-expressed. Here 'RQ' is equivalent to the fold-change of a particular miRNA (Wang, Wang, and Xi 2011) and is ∝ mean $-\Delta CR_T$ values. **(B)** The mean $-\Delta CR_T$ values for the differentially expressed miRNAs for the OBM and OBO groups respectively. The $-\Delta CR_T$ values are ∝ to miRNA expression, where the higher $-\Delta CR_T$ value (or CR_T value) corresponds to higher miRNA expression levels. This is further reflected in the logRQ values which are equivalent to fold-change in the expression of individual miRNA. Here 'logPval' corresponds to -log10 (P-value).

Visualizations

The volcano and scatter plots were constructed using the ggplot2 v3.3.6 package in R. The visualization of the miRNA expression matrix was performed using the ComplexHeatmap v2.12.0 package (28) in R.

Correlation Analysis

We performed a set of correlation analyses, where we correlated the expression (-CR_T value when available) of each differentially expressed miRNAs with the different clinical traits of relevance to metabolic syndrome including HBA1c, Creatinine, Cholesterol, LDL, and HDL. The correlations were estimated using the 'cor.test' function from the stats package using the Pearson correlation method. The correlations between differentially expressed miRNAs and clinical traits were visualized using the corrplot v0.92 package (https://github.com/taiyun/corrplot).

Additionally, we visualize the significantly correlated miRNAs' expression versus individual clinical trait values for the OBO and OBM patients through a scatter plot. We fit a linear regression line along with confidence intervals using the 'geom_smooth' function and annotate the Pearson correlation scores and p-values in the plot using the 'stat_cor' function from the ggplot2 package.

MiRNA-mRNA Interaction Network

We used the microRNA Data Integration Portal, mirDIP v4.1 (http://ophid.utoronto.ca/mirDIP/), which provides nearly 152 million human microRNA–target predictions collected from 30 different resources (21). The mirDIP integrative score was constructed by taking a statistical consensus from the predictions available through myriad resources and was assigned to each unique miRNA-target interaction to provide a unified measure of confidence. The integrated scores range, 0 to 1, was used; higher scores correspond to stronger evidence of potential interaction between miRNA and target gene; the target genes were thus identified.

Pathway Enrichment Analysis

The mRNAs which were identified to be regulated by the differentially expressed miRNAs were then utilized in an overexpression analysis framework. We used the ConsensusPathDB (29) web portal (http://cpdb.molgen.mpg.de/) as utilized in (30–34) to identify significantly enriched pathways choosing the PID (http://pid.nci.nih.gov/) and KEGG (https://www.genome.jp/kegg/pathway.html) database. We also used the ConsensusPathDB web-portal to determine the significantly enriched GO terms. The significantly enriched pathways and GO terms were determined using a hypergeometric test.

The hypergeometric test was performed as described below. Let the total number of genes associated with our differentially expressed miRNAs be n. Out of these n, say k genes are part of a pathway (p). This pathway (p) consists of a total of K genes. The total number of background genes (or all protein-coding genes in humans) be N. Then, the probability of significance of the pathway can be determined by the hypergeometric test as follows:

$$P(p) = \frac{\binom{K}{n}\binom{N-K}{n-k}}{\binom{N}{n}}$$

where $\binom{N}{n}$ represents the combination function (35).

RESULTS

Clinical Characteristics

The clinical characteristics of the study subjects are summarized in **Table 1**. The clinical traits that were significantly different between the two groups include HbA1c (p=0.002), triglycerides (p=0.001), high-density lipoprotein (HDL, p=0.008), glucose (p=0.009), and insulin (p=0.05). Other important clinical traits which were not significantly different between the two sets include clinical variables such as creatinine, low-density lipoprotein (LDL), and cholesterol.

Differential Expression Analysis

We identified a total of 64 miRNAs to be differentially expressed between the OBO and OBM groups (**Figures 2A, B** and **Supplement Table 1**) of which 36 miRNAs were down-regulated and 28 were up-regulated in the OBM patients when compared to the metabolically healthy obese (OBO) patients (**Figure 2A**). Specific miRNAs; miR-873-5p (-ΔCR_T = 1.62), miR-9-3p (-ΔCR_T = 1.91), mir-708-5p (-ΔCR_T = 1.96) were significantly up-regulated in OBM (had higher mean -ΔCR_T) in comparison to OBO patients (**Figure 2B** and **Supplementary Table 1**). On the contrary, miRNAs; miR-100-3p (-ΔCR_T = -9.18), miR-486-5p (-ΔCR_T = -5.16) and miR-92a-3p (-ΔCR_T = -4.76), were among the most significantly downregulated miRNAs in OBM versus OBO patients.

Correlations With Metabolic Syndrome Relevant Clinical Markers

We next performed a set of correlation analyses, where we correlated the expression (-CR_T value when the measurement was available) of each differentially expressed miRNAs with clinical lab traits of relevance to metabolic syndrome including HbA1c, creatinine, cholesterol, LDL, and HDL. 11 out of 36 down-regulated miRNAs and 2 out of 28 up-regulated miRNAs correlated significantly ($p< 0.05$) with at least one of the clinical lab traits (**Figure 3A**). The correlation values across these 13 miRNAs and 5 clinical traits are summarized in **Table 2**. As depicted in **Figure 3A** the miRNAs miR-153-3p, miR-182-5p, and miR-433-3p correlated negatively, while miR-331-3p, miR-452-3p, and miR-485-5p demonstrated a positive correlation with HbA1c. Interestingly, the trend for miRNAs: miR-153-3p, miR-182-5p, and miR-433-3p, the -CR_T values decreased linearly with higher (dysregulated) levels of HbA1c (**Figure 3B**).

TABLE 1 | Clinical and biochemical traits of the study subjects.

Feature	OBO	OBM	P Value
Age (years)	38.06 ± 4.21	40.52 ± 7.26	0.283
Females (N)	11	9	
Males (N)	7	12	
Height (cm)	167.4 ± 11.9	170.8 ± 9.6	0.370
Weight (kg)	113.4 ± 19.6	110.9 ± 27.6	0.782
BMI (kg/m^2)	40.0 ± 4.5	39.6 ± 3.0	0.746
Smoking (%)	6.0	33.0	
HbA1c (%)	5.5 ± 0.27	7.02 ± 1.9	0.002
TG (mmol/L)	1.39 ± 0.48	2.65 ± 1.52	0.001
Cholesterol (mmol/L)	4.9 ± 1.1	4.8 ± 1.1	0.855
LDL (mmol/L)	2.8 ± 1.3	2.6 ± 1.1	0.728
HDL (mmol/L)	1.5 ± 0.7	1.0 ± 0.3	0.008
Glucose (mmol/L)	5.2 ± 0.6	7.4 ± 3.4	0.009
Creatinine (mmol/L)	67.5 ± 14.1	65.3 ± 14.1	0.563
Insulin (miU/mL)	19.0 ± 13.3	27.6 ± 13.2	0.053
CRP (mg/L)	12.8 ± 12.5	7.1 ± 4.5	0.064
ALT (U/L)	20.7 ± 11.6	36.5 ± 35.1	0.063
AST (U/L)	18.8 ± 9.6	23.6 ± 15.0	0.251

OBO (obesity only), and OBM (obesity with metabolic syndrome). Significance was determined by the Student's t-test.

This trend was distinct for the OBM patients, suggesting the loss of expression of these miRNAs in OBM patients was significantly related to increased (↑) HbA1c levels. Similarly, from **Figure 3B** for HbA1c, we could also observe another trend for miRNAs: miR-331-3p, miR-452-3p, and miR-485-5p. The -CR_T values of these miRNAs went significantly up i.e., these miRNAs were significantly over-expressed in OBM patients with increased HbA1c levels.

We further identified that miRNAs: miR-106-3p, miR-652-3p, and miR-93-5p were significantly correlated with creatinine levels of patients in our dataset, and miRNAs: miR-130b-5p, miR-363-3p, and miR-636 were significantly associated with the cholesterol levels of patients as observed in **Figure 3**. However, the ability to distinguish OBM patients from OBO patients through the -CR_T values of these miRNAs was not as stark as of those miRNAs associated with HBA1C (see **Figures 3D, C** respectively). This can also be attributed to the fact that creatinine and cholesterol levels were not significantly different between the two groups as indicated in **Table 1**. We also identified a miRNA, mir-652-3p, that was significantly negatively correlated with LDL (R = -0.34, see **Figure 3E**). Interestingly, the majority of OBM patients had lower LDL values as well as higher expression of mir-652-3p, and the majority of OBO patients had higher LDL values with lower expression of this miRNA. Lastly, we observe a significant negative correlation between mir-130a-3p expression and the clinical trait HDL (R = -0.35, see **Figure 3F**) with no clear distinction between the OBM and OBO groups.

We performed a *Student's* t-test to determine whether the expression values of the 13 miRNAs of interest were significantly different between the males (Gender = 0) and females (Gender = 1) or smokers (Smoking 1 = Yes) versus non-smokers (Smoking 0 = No) in our dataset as illustrated in **Figure 4**. From **Figure 4A**, we observed that miR-106b-3p and miR-652-3p had significantly different expressions in males versus females, where both these miRNAs had lower expression in males when compared to females. Hence the difference in the -CR_T values are positive (Δ-$CR_T > 0$) as indicated in **Figure 4A**. However, for each of these miRNAs, there is no clear segregation of the expression of the miRNA between the OBO versus OBM male patients (Gender = 0) or female patients (Gender = 1) as observed in **Figure 4B**. This suggests that gender does not really have an impact on the differential expression of these miRNAs (miR-106b-3p and miR-652-3p) between the OBO and OBM patient groups.

From **Figure 4C**, we observe that miR-106b-3p has higher expression in patients who don't smoke (0 = No) when compared to patients who smoke (1 = Yes) and the majority of the smokers (4 out of 6) belong to the OBM category. While miR-106b-3p is differentially expressed w.r.t. smoking status, there is no clear segregation of its expression between OBO and OBM groups, for patients who don't smoke. Moreover, owing to the small sample size of patients with a positive smoking status (6 patients only), it is imperative not to draw strong conclusions. However, for a larger population size smoking would be a covariate to regress out when determining differentially expressed miRNAs for the phenotype of interest (i.e. OBO vs OBM patients).

Mechanistic Insights from miRNA-mRNA Networks

We used the mirDIP database to extract information about target mRNAs which can be regulated by the differentially expressed miRNAs with significant associations with clinical traits. We use stringent cutoffs including a minimum of 10 resources and an integrated score of at least 0.75 to retain a potential interaction between miRNA and the target gene. This resulted in a total of 398 interactions between the seven (out of the 13) differentially expressed miRNAs and 378 target genes. Interestingly, we

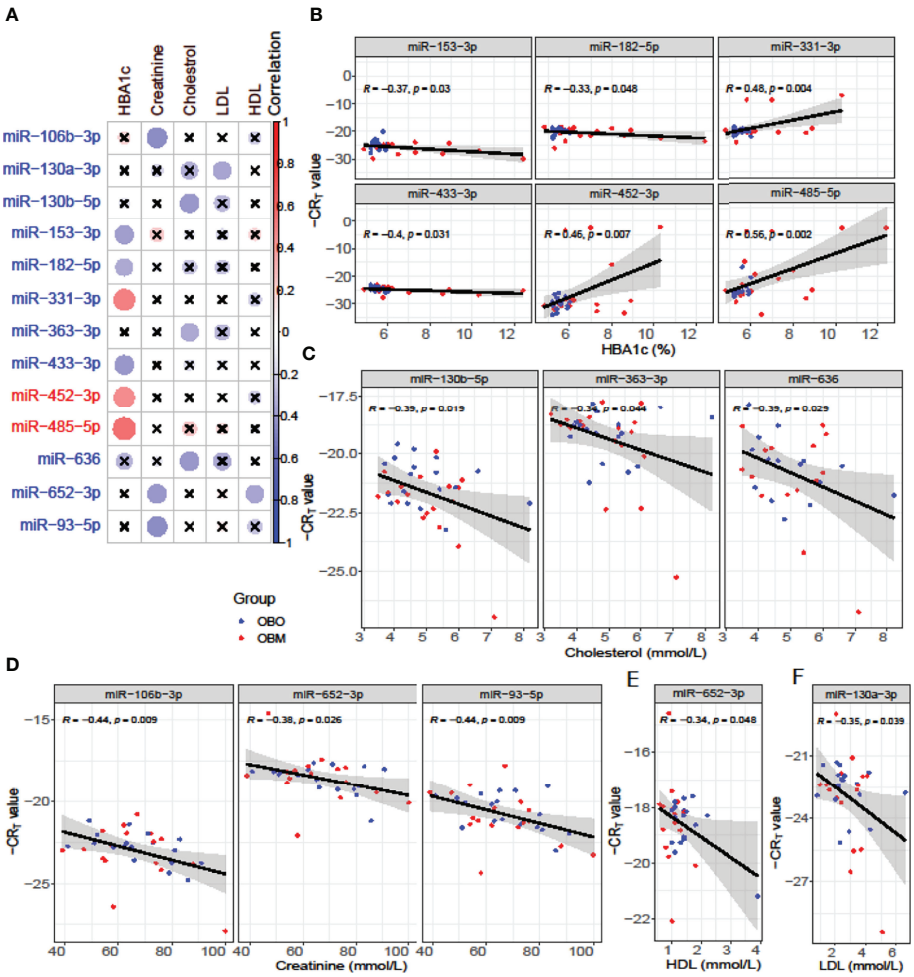

FIGURE 3 | **(A)** Pearson correlation between clinical traits relevant to metabolic syndrome and miRNA expression (-CR_T values). The 'x' represents that the correlation coefficient is not significant. The darker the correlation coefficient ('red' or 'blue') the stronger the correlation (more towards +1 or more towards -1). Significant correlations ($p < 0.05$) of clinical traits with relevance to metabolic syndrome with the differentially expressed miRNAs. **(B)** Correlation with HBA1c; **(C)** Correlation with Cholesterol; **(D)** Correlation with Creatinine; **(E)** Correlation with HDL, and **(F)** Correlation with LDL.

TABLE 2 | Pearson correlation coefficients of the clinical traits associated with metabolic syndrome with the miRNA expression of relevant differentially expressed miRNAs.

Diff MiRNAs	HBA1c	Creatinine	CHOLESTROL	HDL	LDL
miR-106b-3p	0.161	**-0.436**	-0.0776	-0.182	0.001
miR-130a-3p	-0.0913	-0.161	-0.309	0.0669	**-0.351**
miR-130b-5p	-0.111	-0.026	**-0.388**	-0.0154	-0.28
miR-153-3p	**-0.372**	0.219	-0.115	0.168	-0.152
miR-182-5p	**-0.327**	-0.0811	-0.225	0.0626	-0.229
miR-331-3p	**0.484**	-0.0371	0.0247	-0.197	0.0653
miR-363-3p	0.0575	-0.0793	**-0.338**	-0.064	-0.268
miR-433-3p	**-0.395**	0.0775	-0.13	-0.0304	-0.113
miR-452-3p	**0.456**	-0.059	0.0267	-0.183	0.0224
miR-485-5p	**0.555**	0.0405	0.221	-0.0822	0.152
miR-636	-0.282	-0.103	**-0.393**	-0.0614	-0.337
miR-652-3p	0.0627	**-0.383**	-0.00376	**-0.342**	0.0976
miR-93-5p	-0.0617	**-0.437**	-0.033	-0.231	0.0828

The bold values represent strong correlations i.e. |correlation| > 0.3.

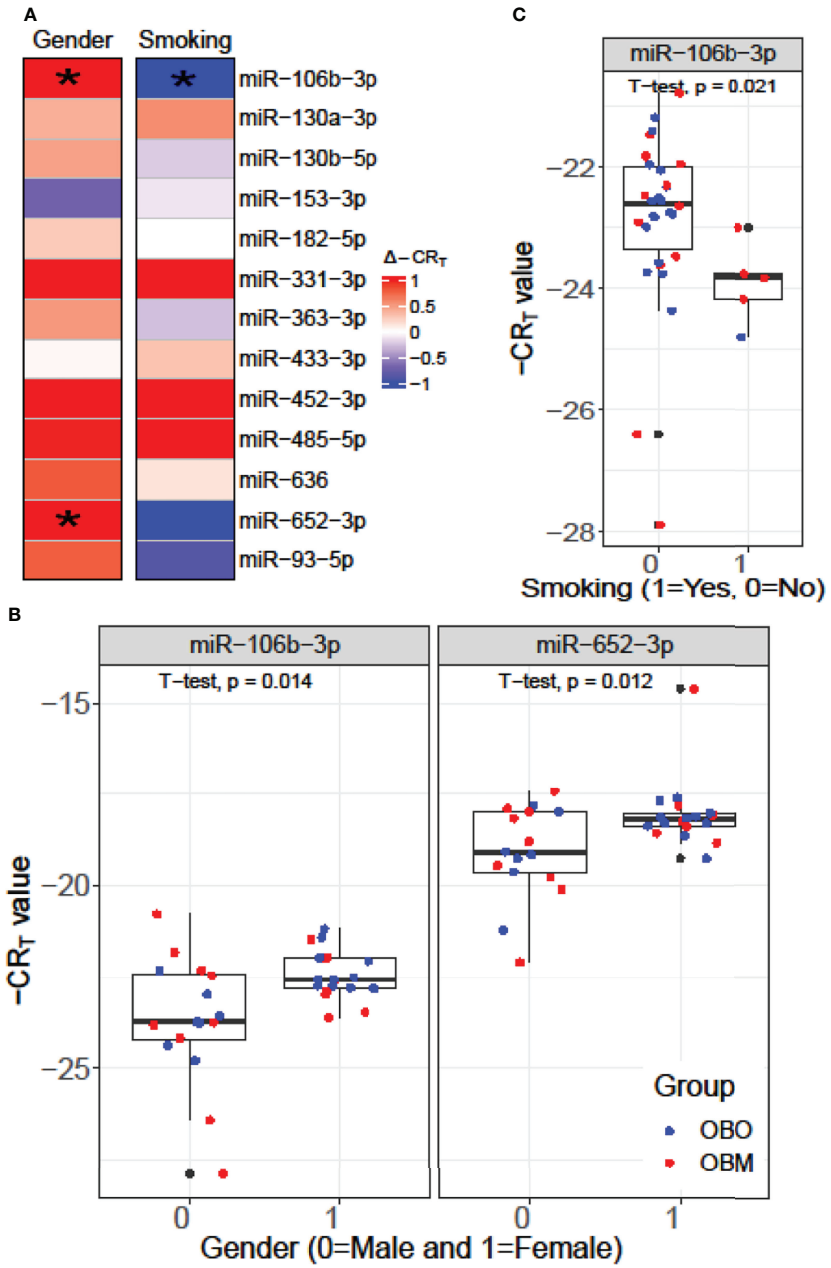

FIGURE 4 | **(A)** Comparison of the expression pattern of the 13 differentially expressed miRNAs for Gender and Smoking status of patients using a *Student's* t-test. Here '*' represents a significant association ($p < 0.05$). **(B)** Boxplot illustrating the significant difference in expression of miR-106b-3p and miR-652-3p between males and females. **(C)** Boxplot highlighting the significant difference in expression of miR-106-3p between patients who smoke versus those who don't.

observed from **Figure 5**, that each of the seven differentially expressed miRNAs forms its own cluster of target genes with small overlaps amidst their interactomes. We then performed downstream pathway enrichment using overexpression analysis through ConsensusPathDB to identify significantly enriched pathways associated with each of these miRNAs. We could determine the enriched pathways and GO terms for four of these seven miRNAs. The top five significantly enriched pathways and top three biological processes, cellular components, and molecular functions for each of these miRNAs were detailed in **Supplementary Tables 2** and **3** respectively.

For example, the miRNA, miR-153-3p, is differentially downregulated with a ΔC_{RTT} of -3.4 ($p=0.02$, **Supplementary Table 1**); the target genes for this miRNA are SPHK2, GNAI3, ROCK1, and PLCB1; which are essential for the Sphingolipid

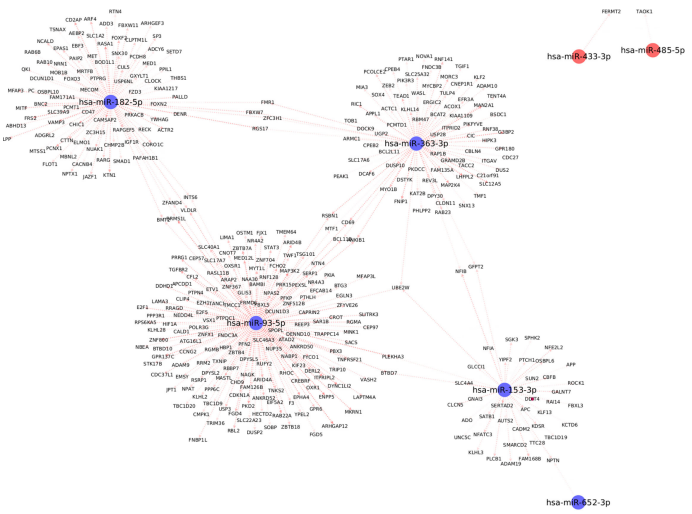

FIGURE 5 | Top differentially expressed miRNAs with strong known interaction (coming from >=10 resources and interaction score>=0.75 from mirDIP) with target genes. Here we highlight only those miRNAs which are significantly correlated with at least one clinical trait relevant to metabolic syndrome.

signaling pathway (**Supplementary Table 2**). The Sphingolipid signaling pathway has been shown to play an important role in the regulation of obesity and type 2 diabetes (36). Similarly, the PDGFR-beta signaling pathway was significantly enriched based on the target genes of both miR-182-5p (USP6NL; CTTN; RASA1; ACTR2; YWHAG) and miR-363-3p (MAP2K4; WASL; ITGAV; RAP1B) respectively. The PDGFR-beta signaling pathway is known to play a role in the regulation of adipose progenitor maintenance and adipocyte-myofibroblast transitions (37). We identified BMP receptor signaling as one of the enriched pathways for miR-93-5p target genes (BAMBI; RGMB; RGMA). It has previously (38) been demonstrated that BMP signaling was relevant for both the white and brown adipogenesis and plays an important role when interconnecting obesity with metabolic and cardiovascular diseases. Finally, we identified the cellular senescence pathway from KEGG as a significantly enriched pathway for miR-93-5p target genes (TGFBR2; E2F5; E2F1; PPP3R1; CDKN1A; RBL2). Interestingly, recently *Smith, Ulf et al.* (39) reviewed that white adipose tissue cells are highly susceptible to becoming senescent both with aging, obesity and type 2 diabetes, independent of the chronological age. The white adipose tissue senescence is associated with the inappropriate expansion of adipocytes, insulin resistance, and dyslipidemia i.e., metabolic syndrome, a finding in line with our phenotype.

Additionally, we identified several different significantly enriched GO terms based on the target genes for each of the top four miRNAs (see **Supplementary Table 3**). These include GO terms associated with biological processes such as positive regulation of metabolic process (GO:0009893), cellular developmental process (GO:0048869), cellular protein modification process (GO:0006464), mitotic cell cycle process (GO:1903047) for miR-153-3p, miR-182-5p, miR-363-3p and miR-93-5p respectively (**Supplementary Table 3**).

DISCUSSION

Individuals with a persistently high BMI are at the risk of developing metabolic syndrome, a medical condition characterized by obesity, insulin resistance, dyslipidemia, and hypertension, with an accompanying risk of type 2 diabetes mellitus and cardiovascular disease (22). There is abundant literature that has investigated the metabolic differences underpinning lean and obese subjects (14). Obese individuals have been the focus of health care in recent years since the reversal of obesity by lifestyle, medical or surgical intervention protects them from metabolic syndrome (40). However, clinical observations identify a proportion of individuals with elevated BMI who led an active and healthy life relatively free of metabolic complications. This population is of particular interest and intensely investigated to elucidate the underpinning mechanisms and gene regulation that confer protection against the development of metabolic syndrome. Moreover, differentiation between OBO and OBM as well as early detection is paramount for clinical management of these individuals.

Several studies have identified the essential role of differentially expressed miRNA in obesity where a cluster of miRNAs; miR-92a-3p, miR-122, miR-122-5p, miR-140-5p, miR-142-3p, miR-151a, miR-155, miR-222, and miR-15a are upregulated and a group of miRNA; miR-15a, miR-26a, miR-30b, miR-30c, miR-125b, miR-126, miR-139-5p, miR-144-5p, miR-146a, miR-150, miR-223 and miR-376a are downregulated in obese adults (14). In this study, we focus particularly on morbidly obese individuals with a BMI>35kg/m^2 who are metabolically protected and susceptible. Our results demonstrate that miR-106b-3p, miR-130a-3p, miR-130b-5p, miR-153-3p, miR-182-5p, miR-331-3p, miR-363-3p, miR-433-3p, miR-636, miR-652-3p, and miR-93-5p were significantly downregulated whereas miR-452-3p, and miR-485-5p were significantly upregulated in morbidly obese patients with metabolic diseases compared to obese patients without any metabolic disease in a

dataset of Qatari population (**Figures 2** and **3**). These miRNAs significantly correlated with at least one clinical trait of relevance to metabolic syndrome like increased levels of HbA1c, creatinine, cholesterol, LDL, and HDL in our dataset (**Figure 3A**). The differentially expressed miRNAs correlate significantly with HbA1c (downregulated miR-153-3p, miR-182-5p and miR-433-3p; upregulated miR-331-3p, miR-452-3p and miR-485-5p), creatinine (downregulated miR-106b-3p, miR-652-3p and miR-93-5p), cholesterol (downregulated miR-130b-5p, miR-363-3p and miR-636), LDL (downregulated miR-130a-3p), and HDL (downregulated miR-652-3p) in our dataset in the context of OBO and OBM. Interestingly, we identify differential expression of miR-92a-3p, miR-122-5p, miR-15a, miR-125b, and miR-146a in our data which have previously been reported to be relevant for obesity (**Figure 2B** and **Supplementary Table 1**) (14).

Our unique dataset with the morbidly obese individuals (OBO and OBM) highlights various differentially expressed miRNAs which have been previously reported in obesity (14) conferring confidence in our study. Although identified in prior studies, these miRNAs (miR-92a-3p, miR-122-5p, miR-15a, miR-125b, and miR-146a) do not associate significantly with clinical lab traits, nor are they upregulated or downregulated in alignment with previous studies. This can be a result of our focus on metabolically healthy and unhealthy obese subjects compared to prior investigations that analyze lean and obese groups. Our findings further demonstrate that miR-153-3p, miR-182-5p, and miR-433-3p are downregulated in the OBM group and negatively correlated with HbA1c. Among these miRNAs, miR-153-3p has been reported to be overexpressed in lupus nephritis patients (28). Through miRNA-mRNA network analysis, we have shown that miR-153-3p regulates sphingolipid signaling. The sphingolipid pathway is known to be extensively involved in obesity and obesity-induced hyperglycemia (36). In agreement with our results, miR-182-5p has been reported to be suppressed in diabetes patients. Interestingly, it was shown that the expression of miR-182-5p is high in newly diagnosed patients compared to healthy control. However, its expression decreased with the increasing duration of T2DM (41). Another miRNA downregulated in the OBM group and positively correlated with HbA1c is miR-433-3p, which has been reported to be overexpressed in serum of hepatocellular carcinoma patients (42), pediatric beta-thalassemia patients, and needs further evaluation in the context of changes to hemoglobin (43). Moreover, miR-331-3p, which was downregulated in metabolically unhealthy obese patients and positively correlated with HbA1c has been reported as a biomarker for HCV-related hepatocellular carcinoma (44), and non-small cell lung cancer (45). Among the upregulated miRNAs in our results, miR-485-5p has been reported earlier to be associated with atherosclerosis (46), and lung and oral cancer (47, 48), whereas, miR-452-3p has been not reported earlier and might be a novel biomarker. Overall, these differentially expressed miRNAs, significantly correlated with HbA1c in obese patients with metabolic diseases and seem to regulate the glycemic pathways. The mechanisms behind the observed correlations of these miRNAs with HbA1c are still unclear and need to be investigated further.

Another set of miRNAs: miR-106b-3p, miR-652-3p, and miR-93-5p, which were downregulated in OBM subjects, negatively correlated with the creatinine levels in these patients. It has been reported earlier that elevated serum creatinine levels are associated with late stages of diabetic nephropathy or renal damage (49). The role of these miRNAs is either a cause or consequence of renal damage or possible existing hypertension in the OBM cohort. The miR-652-3p has been reported to be relevant for insulin resistance (50) and in polycystic ovary syndrome (PCOS) patients, its expression has been shown to be downregulated in the context of creatinine and HDL and is most likely associated with hepatic involvement in cases of insulin resistance (51). miR-106b-3p has been earlier reported to be downregulated in dengue infection (52); its significance in metabolic disorders is unknown. Given the significant association of miR-106b-3p with both gender (higher expression in females in comparison to males) and smoking status (higher expression in non-smokers compared to smokers) of patients in our dataset, this miRNA needs a more detailed mechanistic investigation as its significant correlation with creatinine might be conditioned on the patient's sex and smoking status. Our results indicate that miR-652-3p is not only negatively correlated with creatinine but also with high-density lipopolysaccharides (HDL), indicating its possible role in dyslipidemia in obese patients and warrants more investigation. The results from our study indicate decreased expression of miR-130a-3p, miR-130b-5p, miR-363-3p, miR-636, and miR-652-3p respectively in the OBM subjects. Among these miRNAs, miR-363-3p, miR-130b-5p, and miR-636 correlated with cholesterol, and miR-130a-3p correlated with LDL. It has been reported previously that miR-130a-3p levels were elevated in the pancreatic islets of hyperglycemic subjects (53) as well as progressive cardiac failure (54).

In line with previous studies, we report a significant differential expression of miRNAs that play critical roles in insulin resistance, sensitivity, and release. For example, miR-122-5p, miR-221-3p, miR-126-3p, miR-223-3p, and miR-93-5p, which are downregulated in OBM versus OBO, have been described within the context of insulin sensitivity and resistance (55). In addition, miR-34b-3p, miR-9-3p, miR-375, miR-146a-3p, and miR-30e-5p, which are upregulated in OBM versus OBO have been involved in insulin release in pancreatic β-cells and regulate β-cell fate (56–59). Interestingly, IGF1R, a receptor tyrosine kinase that mediates actions of insulin-like growth factor 1 and one of the factors that are altered in obesity is a key target of differentially expressed miRNAs identified by our framework including miR-182-5p. Another important set of targets for the differentially expressed miRNAs were the MAPK genes (MAP3K2 and MAP2K4) which belong to the family of mitogen-activated protein kinase (MAPK). MAPK genes and their interactors have been reported to protect against adverse effects of high-fat feeding in a murine model, demonstrating a decreased weight gain, improved glucose tolerance, and insulin sensitivity, with markedly diminished adipose tissue inflammation (60).

In conclusion, our data show that subjects with morbid obesity and metabolic syndrome compared to individuals with obesity without metabolic syndrome show differential levels of several miRNAs which can regulate multiple genes and metabolic pathways relevant to glycemic regulation, lipid metabolism, and cellular regeneration. However, the cause or consequence merits further studies. The miRNA group associated with metabolic syndrome in morbidly obese subjects may have a pathophysiologic role that warrants further elucidation. Regardless of their role in disease pathogenesis these groups of miRNAs can serve as additional markers to segregate OBM and OBO that can aid divergent management strategies of treatment. To the best of our knowledge, this is the first study of its kind that addresses the role of miRNAs in morbidly obese healthy versus obese metabolic syndrome adults for a population indigenous to Qatar. We do acknowledge that our dataset is small and further studies are warranted in additional larger cohorts to corroborate the importance of the identified differentially expressed miRNAs.

DATA AVAILABILITY STATEMENT

All the data including processed microRNA and anonymized patient profiles with clinical characteristics as well as the code required to generate the results are available at: https://github.com/raghvendra5688/OBH_vs_OBO_MiRNA_HMC.

ETHICS STATEMENT

The studies involving human participants were reviewed and approved by HMC, IRB protocol #16245/16. The patients/participants provided their written informed consent to participate in this study.

AUTHOR CONTRIBUTIONS

FM, RM, FF, and A-BA-S conceived the study. FM, AI, TS, FC, AP, MA, and IA collected, purified, and harmonized the biological samples. RM and EU built the computational pipeline and performed bioinformatics analysis. FF and A-BA-S supervised the analysis. FM, RM, and EU wrote the manuscript. All authors proofread the manuscript. All authors contributed to the article and approved the submitted version.

ACKNOWLEDGMENTS

We thank Mutasem Shraim, Ayat Fared, Hoda Isam, Elli Concepcion, and Bader Alkhalaf, for technical help. Open access funding provided by the Qatar National Library.

SUPPLEMENTARY MATERIAL

The Supplementary Material for this article can be found online at: https://www.frontiersin.org/articles/10.3389/fendo.2022.937089/full#supplementary-material

Supplementary Table 1 | Differentially expressed miRNAs with their ΔCR_T value, RQ and significance levels (p-value).

Supplementary Table 2 | Top five pathways identified to be significantly enriched w.r.t overexpression analysis of mRNAs estimated to be potentially regulated by the differentially expressed miRNAs of interest through the mirDIP portal. The pathways highlighted in bold have relevant literature specifying their role in obesity and metabolic syndrome.

Supplementary Table 3 | Top three biological processes (bp), molecular functions (mf) and cellular components (cc) identified to be significantly enriched w.r.t overexpression analysis of mRNAs estimated to be potentially regulated by the differentially expressed miRNAs of interest through the mirDIP portal.

REFERENCES

1. WorldHealthOrganisation. *Obesity and Overweight Report*. (2021).
2. Heianza Y, Kato K, Kodama S, Ohara N, Suzuki A, Tanaka S, et al. Risk of the Development of Type 2 Diabetes in Relation to Overall Obesity, Abdominal Obesity and the Clustering of Metabolic Abnormalities in Japanese Individuals: Does Metabolically Healthy Overweight Really Exist? The Niigata Wellness Study. *Diabetes Med* (2015) 32:665–72. doi: 10.1111/dme.12646
3. McLaughlin T, Abbasi F, Lamendola C, Reaven G. Heterogeneity in the Prevalence of Risk Factors for Cardiovascular Disease and Type 2 Diabetes Mellitus in Obese Individuals: Effect of Differences in Insulin Sensitivity. *Arch Intern Med* (2007) 167:642–8. doi: 10.1001/archinte.167.7.642
4. Meigs JB, Wilson PW, Fox CS, Vasan RS, Nathan DM, Sullivan LM, et al. Body Mass Index, Metabolic Syndrome, and Risk of Type 2 Diabetes or Cardiovascular Disease. *J Clin Endocrinol Metab* (2006) 91:2906–12. doi: 10.1210/jc.2006-0594
5. Rey-Lopez JP, de Rezende LF, Pastor-Valero M, Tess BH. The Prevalence of Metabolically Healthy Obesity: A Systematic Review and Critical Evaluation of the Definitions Used. *Obes Rev* (2014) 15:781–90. doi: 10.1111/obr.12198
6. Magkos F. Metabolically Healthy Obesity: What's in a Name? *Am J Clin Nutr* (2019) 110:533–9. doi: 10.1093/ajcn/nqz133
7. van Vliet-Ostaptchouk JV, Nuotio ML, Slagter SN, Doiron D, Fischer K, Foco L, et al. The Prevalence of Metabolic Syndrome and Metabolically Healthy Obesity in Europe: A Collaborative Analysis of Ten Large Cohort Studies. *BMC Endocr Disord* (2014) 14:9. doi: 10.1186/1472-6823-14-9
8. Vague J. The Degree of Masculine Differentiation of Obesities: A Factor Determining Predisposition to Diabetes, Atherosclerosis, Gout, and Uric Calculous Disease. *Am J Clin Nutr* (1956) 4:20–34. doi: 10.1093/ajcn/4.1.20
9. Stefan N, Kantartzis K, Machann J, Schick F, Thamer C, Rittig K, et al. Identification and Characterization of Metabolically Benign Obesity in Humans. *Arch Intern Med* (2008) 168:1609–16. doi: 10.1001/archinte.168.15.1609
10. Stefan N, Schick F, Haring HU. Causes, Characteristics, and Consequences of Metabolically Unhealthy Normal Weight in Humans. *Cell Metab* (2017) 26:292–300. doi: 10.1016/j.cmet.2017.07.008
11. Bluher M. Metabolically Healthy Obesity. *Endocr Rev* (2020) 41:1–16. doi: 10.1210/endrev/bnaa004
12. Rottiers V, Naar AM. MicroRNAs in Metabolism and Metabolic Disorders. *Nat Rev Mol Cell Biol* (2012) 13:239–50. doi: 10.1038/nrm3313
13. Ji C, Guo X. The Clinical Potential of Circulating microRNAs in Obesity. *Nat Rev Endocrinol* (2019) 15:731–43. doi: 10.1038/s41574-019-0260-0
14. Brandao BB, Lino M, Kahn CR. Extracellular miRNAs as Mediators of Obesity-Associated Disease. *J Physiol* (2021) 600(5):1155–69. doi: 10.1113/JP280910

15. Pescador N, Perez-Barba M, Ibarra JM, Corbaton A, Martinez-Larrad MT, Serrano-Rios M. Serum Circulating microRNA Profiling for Identification of Potential Type 2 Diabetes and Obesity Biomarkers. *PloS One* (2013) 8:e77251. doi: 10.1371/journal.pone.0077251
16. Kim NH, Ahn J, Choi YM, Son HJ, Choi WH, Cho HJ, et al. Differential Circulating and Visceral Fat microRNA Expression of Non-Obese and Obese Subjects. *Clin Nutr* (2020) 39:910–6. doi: 10.1016/j.clnu.2019.03.033
17. Ge Q, Brichard S, Yi X, Li Q. microRNAs as a New Mechanism Regulating Adipose Tissue Inflammation in Obesity and as a Novel Therapeutic Strategy in the Metabolic Syndrome. *J Immunol Res* (2014) 2014:987285. doi: 10.1155/2014/987285
18. Karolina DS, Tavintharan S, Armugam A, Sepramaniam S, Pek SL, Wong MT, et al. Circulating miRNA Profiles in Patients With Metabolic Syndrome. *J Clin Endocrinol Metab* (2012) 97:E2271–6. doi: 10.1210/jc.2012-1996
19. Szabo G, Bala S. MicroRNAs in Liver Disease. *Nat Rev Gastroenterol Hepatol* (2013) 10:542–52. doi: 10.1038/nrgastro.2013.87
20. Ortega FJ, Mercader JM, Moreno-Navarrete JM, Rovira O, Guerra E, Esteve E, et al. Profiling of Circulating microRNAs Reveals Common microRNAs Linked to Type 2 Diabetes That Change With Insulin Sensitization. *Diabetes Care* (2014) 37:1375–83. doi: 10.2337/dc13-1847
21. Shah R, Murthy V, Pacold M, Danielson K, Tanriverdi K, Larson MG, et al. Extracellular RNAs Are Associated With Insulin Resistance and Metabolic Phenotypes. *Diabetes Care* (2017) 40:546–53. doi: 10.2337/dc16-1354
22. Fahed G, Aoun L, Bou Zerdan M, Allam S, Bou Zerdan M, Bouferraa Y, et al. Metabolic Syndrome: Updates on Pathophysiology and Management in 2021. *Int J Mol Sci* (2022) 23:1–38. doi: 10.3390/ijms23020786
23. RCoreTeam. R: A Language and Environment for Statistical Computing. In: *R Foundation for Statistical Computing* (2020).
24. D'Agostino RB, Stephens MA. *GOODNESS-OF-FIT TECHNIQUES*. MARCEL DEKKER, INC (1986).
25. Chen Y, Gelfond JA, McManus LM, Shireman PK. Reproducibility of Quantitative RT-PCR Array in miRNA Expression Profiling and Comparison With Microarray Analysis. *BMC Genomics* (2009) 10:407. doi: 10.1186/1471-2164-10-407
26. Davison TS, Johnson CD, Andruss BF. Analyzing Micro-RNA Expression Using Microarrays. *Methods Enzymol* (2006) 411:14–34. doi: 10.1016/S0076-6879(06)11002-2
27. Livak KJ, Schmittgen TD. Analysis of Relative Gene Expression Data Using Real-Time Quantitative PCR and the 2(-Delta Delta C(T)) Method. *Methods* (2001) 25:402–8. doi: 10.1006/meth.2001.1262
28. Navarro-Quiroz E, Pacheco-Lugo L, Navarro-Quiroz R, Lorenzi H, Espana-Puccini P, Diaz-Olmos Y, et al. Profiling Analysis of Circulating microRNA in Peripheral Blood of Patients With Class IV Lupus Nephritis. *PloS One* (2017) 12:e0187973. doi: 10.1371/journal.pone.0187973
29. Herwig R, Hardt C, Lienhard M, Kamburov A. Analyzing and Interpreting Genome Data at the Network Level With ConsensusPathDB. *Nat Protoc* (2016) 11:1889–907. doi: 10.1038/nprot.2016.117
30. Mall R, Saad M, Roelands J, Rinchai D, Kunji K, Almeer H, et al. Network-Based Identification of Key Master Regulators Associated With an Immune-Silent Cancer Phenotype. *Brief Bioinform* (2021) 22:1–14. doi: 10.1093/bib/bbab168
31. Orecchioni M, Fusco L, Mall R, Bordoni V, Fuoco C, Rinchai D, et al. Graphene Oxide Activates B Cells With Upregulation of Granzyme B Expression: Evidence at the Single-Cell Level for Its Immune-Modulatory Properties and Anticancer Activity. *Nanoscale* (2022) 14:333–49. doi: 10.1039/D1NR04355B
32. Roelands J, Mall R, Almeer H, Thomas R, Mohamed MG, Bedri S, et al. Ancestry-Associated Transcriptomic Profiles of Breast Cancer in Patients of African, Arab, and European Ancestry. *NPJ Breast Canc* (2021) 7:10. doi: 10.1038/s41523-021-00215-x
33. Roelands J, Hendrickx W, Zoppoli G, Mall R, Saad M, Halliwill K, et al. Oncogenic States Dictate the Prognostic and Predictive Connotations of Intratumoral Immune Response. *J Immunother Cancer* (2020) 8:1–22. doi: 10.1136/jitc-2020-000617
34. Mall R, Cerulo L, Garofano L, Frattini V, Kunji K, Bensmail H, et al. RGBM: Regularized Gradient Boosting Machines for Identification of the Transcriptional Regulators of Discrete Glioma Subtypes. *Nucleic Acids Res* (2018) 46:e39. doi: 10.1093/nar/gky015
35. Berkopec A. HyperQuick Algorithm for Discrete Hypergeometric Distribution. *J Discrete Algorith* (2007) 5:341–7. doi: 10.1016/j.jda.2006.01.001
36. Guitton J, Bandet CL, Mariko ML, Tan-Chen S, Bourron O, Benomar Y, et al. Sphingosine-1-Phosphate Metabolism in the Regulation of Obesity/Type 2 Diabetes. *Cells* (2020) 9:1–19. doi: 10.3390/cells9071682
37. Dani C, Pfeifer A. The Complexity of PDGFR Signaling: Regulation of Adipose Progenitor Maintenance and Adipocyte-Myofibroblast Transition. *Stem Cell Investig* (2017) 4:28. doi: 10.21037/sci.2017.04.02
38. Blazquez-Medela AM, Jumabay M, Bostrom KI. Beyond the Bone: Bone Morphogenetic Protein Signaling in Adipose Tissue. *Obes Rev* (2019) 20:648–58. doi: 10.1111/obr.12822
39. Smith U, Li Q, Ryden M, Spalding KL. Cellular Senescence and Its Role in White Adipose Tissue. *Int J Obes (Lond)* (2021) 45:934–43. doi: 10.1038/s41366-021-00757-x
40. Taheri S, Zaghloul H, Chagoury O, Elhadad S, Ahmed SH, El Khatib N, et al. Effect of Intensive Lifestyle Intervention on Bodyweight and Glycaemia in Early Type 2 Diabetes (DIADEM-I): An Open-Label, Parallel-Group, Randomised Controlled Trial. *Lancet Diabetes Endocrinol* (2020) 8:477–89. doi: 10.1016/S2213-8587(20)30117-0
41. Weale CJ, Matshazi DM, Davids SFG, Raghubeer S, Erasmus RT, Kengne AP, et al. Expression Profiles of Circulating microRNAs in South African Type 2 Diabetic Individuals on Treatment. *Front Genet* (2021) 12:702410. doi: 10.3389/fgene.2021.702410
42. Tan Y, Ge G, Pan T, Wen D, Chen L, Yu X, et al. A Serum microRNA Panel as Potential Biomarkers for Hepatocellular Carcinoma Related With Hepatitis B Virus. *PloS One* (2014) 9:e107986. doi: 10.1371/journal.pone.0107986
43. Wang H, Chen M, Xu S, Pan Y, Zhang Y, Huang H, et al. Abnormal Regulation of microRNAs and Related Genes in Pediatric Beta-Thalassemia. *J Clin Lab Anal* (2021) 35:e23945. doi: 10.1002/jcla.23945
44. Li J, Jin B, Wang T, Li W, Wang Z, Zhang H, et al. Serum microRNA Expression Profiling Identifies Serum Biomarkers for HCV-Related Hepatocellular Carcinoma. *Cancer Biomark* (2019) 26:501–12. doi: 10.3233/CBM-181970
45. Liu T, Song Z, Gai Y. Circular RNA Circ_0001649 Acts as a Prognostic Biomarker and Inhibits NSCLC Progression *via* Sponging miR-331-3p and miR-338-5p. *Biochem Biophys Res Commun* (2018) 503:1503–9. doi: 10.1016/j.bbrc.2018.07.070
46. Han X, Wang H, Li Y, Liu L, Gao S. A 2 miRNAs-Based Signature for the Diagnosis of Atherosclerosis. *BMC Cardiovasc Disord* (2021) 21:150. doi: 10.1186/s12872-021-01960-4
47. Jiang P, Xu C, Chen L, Chen A, Wu X, Zhou M, et al. Epigallocatechin-3-Gallate Inhibited Cancer Stem Cell-Like Properties by Targeting Hsa-Mir-485-5p/RXRalpha in Lung Cancer. *J Cell Biochem* (2018) 119:8623–35. doi: 10.1002/jcb.27117
48. Lin XJ, He CL, Sun T, Duan XJ, Sun Y, Xiong SJ. hsa-miR-485-5p Reverses Epithelial to Mesenchymal Transition and Promotes Cisplatin-Induced Cell Death by Targeting PAK1 in Oral Tongue Squamous Cell Carcinoma. *Int J Mol Med* (2017) 40:83–9. doi: 10.3892/ijmm.2017.2992
49. DeFronzo RA, Reeves WB, Awad AS. Pathophysiology of Diabetic Kidney Disease: Impact of SGLT2 Inhibitors. *Nat Rev Nephrol* (2021) 17:319–34. doi: 10.1038/s41581-021-00393-8
50. Dahlman I, Belarbi Y, Laurencikiene J, Pettersson AM, Arner P, Kulyte A. Comprehensive Functional Screening of miRNAs Involved in Fat Cell Insulin Sensitivity Among Women. *Am J Physiol Endocrinol Metab* (2017) 312:E482–E94. doi: 10.1152/ajpendo.00251.2016
51. Diaz M, Bassols J, Lopez-Bermejo A, de Zegher F, Ibanez L. Low Circulating Levels of miR-451a in Girls With Polycystic Ovary Syndrome: Different Effects of Randomized Treatments. *J Clin Endocrinol Metab* (2020) 105:e273–e281. doi: 10.1210/clinem/dgz204
52. Teng J, Wang Q, Li X, Chen L, Gu D, Mao W, et al. Analysis of Differentially Expressed Novel MicroRNAs as Potential Biomarkers in Dengue Virus Type 1 Infection. *Clin Lab* (2021) 67:1–10. doi: 10.7754/Clin.Lab.2020.200430
53. Ofori JK, Salunkhe VA, Bagge A, Vishnu N, Nagao M, Mulder H, et al. Elevated miR-130a/Mir130b/miR-152 Expression Reduces Intracellular ATP Levels in the Pancreatic Beta Cell. *Sci Rep* (2017) 7:44986. doi: 10.1038/srep44986

54. Marques FZ, Vizi D, Khammy O, Mariani JA, Kaye DM. The Transcardiac Gradient of Cardio-microRNAs in the Failing Heart. *Eur J Heart Fail* (2016) 18:1000–8. doi: 10.1002/ejhf.517
55. Chen H, Lan HY, Roukos DH, Cho WC. Application of microRNAs in Diabetes Mellitus. *J Endocrinol* (2014) 222:R1–R10. doi: 10.1530/JOE-13-0544
56. Granjon A, Gustin MP, Rieusset J, Lefai E, Meugnier E, Guller I, et al. The microRNA Signature in Response to Insulin Reveals Its Implication in the Transcriptional Action of Insulin in Human Skeletal Muscle and the Role of a Sterol Regulatory Element-Binding Protein-1c/Myocyte Enhancer Factor 2C Pathway. *Diabetes* (2009) 58:2555–64. doi: 10.2337/db09-0165
57. Bai C, Gao Y, Zhang X, Yang W, Guan W. MicroRNA-34c Acts as a Bidirectional Switch in the Maturation of Insulin-Producing Cells Derived From Mesenchymal Stem Cells. *Oncotarget* (2017) 8:106844–57. doi: 10.18632/oncotarget.21883
58. Garcia-Jacobo RE, Uresti-Rivera EE, Portales-Perez DP, Gonzalez-Amaro R, Lara-Ramirez EE, Enciso-Moreno JA, et al. Circulating miR-146a, miR-34a and miR-375 in Type 2 Diabetes Patients, Pre-Diabetic and Normal-Glycaemic Individuals in Relation to Beta-Cell Function, Insulin Resistance and Metabolic Parameters. *Clin Exp Pharmacol Physiol* (2019) 46:1092–100. doi: 10.1111/1440-1681.13147
59. Hu D, Wang Y, Zhang H, Kong D. Identification of miR-9 as a Negative Factor of Insulin Secretion From Beta Cells. *J Physiol Biochem* (2018) 74:291–9. doi: 10.1007/s13105-018-0615-3
60. Moore CE, Pickford J, Cagampang FR, Stead RL, Tian S, Zhao X, et al. MNK1 and MNK2 Mediate Adverse Effects of High-Fat Feeding in Distinct Ways. *Sci Rep* (2016) 6:23476. doi: 10.1038/srep23476

Conflict of Interest: Authors FM, AI, TS, AP, MA, IA, and A-BA-S were employed by HMC.

The remaining authors declare that the research was conducted in the absence of any commercial or financial relationships that could be construed as a potential conflict of interest.

frontiers | Frontiers in Endocrinology

ORIGINAL RESEARCH
published: 26 July 2022
doi: 10.3389/fendo.2022.889858

LncRNA GAS5 Knockdown Mitigates Hepatic Lipid Accumulation *via* Regulating MiR-26a-5p/PDE4B to Activate cAMP/CREB Pathway

Shizan Xu, Yajie Wang, Zhengyang Li, Qian Hua, Miao Jiang and Xiaoming Fan**

Department of Gastroenterology, Jinshan Hospital of Fudan University, Shanghai, China

OPEN ACCESS

Edited by:
Davide Povero,
Mayo Clinic, United States

Reviewed by:
Akiko Eguchi,
Mie University, Japan
Rezvan Noroozi,
Jagiellonian University, Poland

***Correspondence:**
Xiaoming Fan
xiaomingfan57@hotmail.com
Miao Jiang
jiangmiao1978@163.com

Specialty section:
This article was submitted to Obesity, a section of the journal Frontiers in Endocrinology

Received: *04 March 2022*
Accepted: *23 June 2022*
Published: *26 July 2022*

Citation:
Xu S, Wang Y, Li Z, Hua Q, Jiang M and Fan X (2022) LncRNA GAS5 Knockdown Mitigates Hepatic Lipid Accumulation via Regulating MiR-26a-5p/PDE4B to Activate cAMP/CREB Pathway. Front. Endocrinol. 13:889858. doi: 10.3389/fendo.2022.889858

Objective: Non-alcoholic fatty liver disease (NAFLD) can be attributed to the dysregulation of hepatic lipid metabolism; however, its cellular and molecular mechanisms remain unclear. This study aims to explore the effect of long non-coding RNA growth arrest specific 5 (GAS5) on hepatic lipid metabolism in fatty liver models.

Methods: Obese mice, high fat diet-fed mice and free fatty acid-stimulated cells were used for GAS5 expression detection. GAS5 overexpression or knockdown models were established to elucidate the regulatory function of GAS5 in *de novo* lipogenesis (DNL) and mitochondrial function. Bioinformatic analyses and dual luciferase assays were used to investigate the interaction between GAS5, miR-26a-5p and phosphodiesterase (PDE) 4B. The involvement of the cyclic adenosine monophosphate (cAMP)/cAMP-response element-binding protein (CREB) pathway was evaluated using H89 and forskolin treatment.

Results: GAS5 was activated *in vitro* and *in vivo* fatty liver models. Knockdown of GAS5 reduced lipid droplet accumulation, DNL associated enzymes and preserved mitochondrial function, while GAS5 overexpression exacerbated hepatic lipid accumulation. Mechanistically, GAS5 sponged miR-26a-5p to increase PDE4B expression and subsequently modulated DNL and mitochondrial function *via* the cAMP/CREB pathway.

Conclusion: Downregulation of GAS5 can activate the cAMP/CREB pathway through miR-26a-5p/PDE4B axis to mitigate hepatic lipid accumulation. This study provides evidence that downregulation of GAS5 may be a potential therapeutic option for the treatment of NAFLD.

Keywords: non-alcoholic liver disease, hepatic lipid metabolism, GAS5, miR-26a-5p, phosphodiesterase (PDE) 4B, cAMP/CREB pathway

INTRODUCTION

Along with obesity and metabolic syndromes, non-alcoholic fatty liver disease (NAFLD) is among the most common chronic liver disease worldwide, with a global prevalence of approximately 25% (1, 2). NAFLD comprises a spectrum of fatty liver disorders, ranging from simple steatosis to non-alcoholic steatohepatitis (NASH), which can advance to liver cirrhosis and hepatocellular carcinoma (HCC) (3, 4). Abnormal hepatic lipid metabolism, especially excessive hepatic triglyceride (TG) accumulation, leads to NAFLD development (5, 6). Therefore, elucidating the cellular and molecular mechanism of hepatic lipid metabolism in fatty liver is crucial.

De novo lipogenesis (DNL), esterified free fatty acids (FFA) and excessive dietary intake contribute to the hepatic TG accumulation (7), and increased DNL plays a dominant role in NAFLD development (6). The catalysis of DNL-associated enzymes including adenosine triphosphate citrate lyase (ACLY), acetyl-coenzyme A carboxylase (ACC), and fatty acid synthase (FAS), leads to the conversion of citrate into fatty acid, which is eventually esterified to form TGs and other lipids (7). In addition to DNL, mitochondrial dysfunction is also involved in the pathogenesis of NAFLD; therefore, mitochondrial-related molecules could be used as potential targets for NAFLD treatment (8, 9). Peroxisome proliferator-activated receptor γ coactivator-1α (PGC-1α) plays an eventful role in the regulation of mitochondrial biogenesis and oxidative metabolism (10) and is highly expressed in mitochondrial-rich tissues, such as liver, brown fat and skeletal muscle (11). Moreover, owing to an upregulated lipogenic gene expression and a limited mitochondrial respiratory capacity, severe hepatic steatosis was observed in PGC-1α knockout mice (12).

Long non-coding RNA (lncRNA) is commonly defined as a class of transcript that has no protein coding capacity, with a length of over 200 nucleotides (13). Recently, lncRNAs have been increasingly reported to influence the development of various human diseases, including NAFLD. For example, lncRNA Gm15622 was confirmed to activate the hepatic DNL by sponging miR-742-3p and aggregated hepatic lipids accumulation (14). But fewer studies had linked lncRNAs to mitochondrial oxidative function in fatty liver compared to DNL. LncRNA growth arrests specific 5 (GAS5) was firstly isolated from the fibroblasts of a growth-arrested mouse, wherein the expression of GAS5 was significantly upregulated post-transcriptionally (15). Subsequently, GAS5 was identified as the 5'-terminal oligopyrimidine (5'TOP) class of genes that are clustered in messenger ribonucleoprotein (mRNP) particles when cell growth is arrested (16). Regarded as a tumor suppressor, GAS5 regulates cellular proliferation, invasion and metastasis in various types of human tumors (17, 18). Additionally, overexpressed GAS5 can reduce liver fibrosis by inhibiting the activation of stellate cells and reducing the accumulation of hepatic collagen (19). GAS5 has been recently reported to be upregulated in liver tissues and serum of patients with NAFLD (20); however, its function and underlying mechanism remain unclear.

MicroRNA (miRNA) is another group of non-coding RNAs, with 21–25 nucleotides, that work as post-transcriptional suppressors of targeted genes by facilitating mRNA degradation (21, 22). Functions of various miRNAs, including miR-26a, miR-34a and miR-214-3p, have been investigated in NAFLD (21–23). Overexpression of miR-26a has been reported to ameliorate hepatic steatosis by directly inducing eukaryotic initiation factor 2α (EIF2α) in mice fed with high-fat diet (23). Interestingly, the sponging of GAS5 with miR-26a-5p has been observed in degenerative nucleus pulposus cells, diabetic cardiomyopathy and laryngeal squamous cell carcinoma (24–26). Hence, the potential of GAS5 as a competing endogenous RNA (ceRNA) for miR-26a-5p in fatty liver is worth exploring.

PDE4B is a member of the Phosphodiesterase-4 (PDE4) family, whose inhibition regulates the cyclic adenosine monophosphate (cAMP) homeostasis and promotes the hepatic carnitine palmitoyl transferase 1α (CPT-1α) expression in alcohol-induced steatosis (ALD) (27). Given the similar pathophysiological changes between NAFLD and ALD, PDE4B/cAMP could be involved in the development of NAFLD.

This study verifies the expression of GAS5 in *in vivo* and *in vitro* fatty liver models and explores the function and mechanism of GAS5 in hepatic lipid metabolism.

METHODS AND MATERIALS

Materials and Reagents

High fat diet (HFD) with 60% kcal from fat and normal chow diet (ND) with 9.7% kcal from fat were purchased from Biotech HD Co., Ltd. (Beijing, China) and Future Biotech Co., Ltd. (Beijing, China), respectively. Oleic acid (OA), palmitic acid (PA), Dulbecco's Modified Eagle Medium (DMEM), bovine serum albumin (BSA), high-performance liquid chromatography (HPLC)-grade formic acid, HPLC-grade ammonium formate and ammonium acetate (NH_4AC) were purchased from Sigma-Aldrich (MO, USA). Foetal bovine serum (FBS) was obtained from Biological Industries (Israel). H89, forskolin, lipid peroxidation malondialdehyde (MDA) assay kit, superoxide dismutase (SOD) assay kit and ATP detection kit were purchased from Beyotime (Shanghai, China), whereas the triglyceride (TG) assay kit was purchased from Nanjing Jiancheng Institute of Biotechnology (Nanjing, China). Lipofectamine 3000, enhanced chemiluminescence (ECL) chromogenic reagent, mass spectrometry (MS)-grade methanol, MS-grade acetonitrile, HPLC-grade 2-propanol and ammonium hydroxide (NH_4OH) were purchased from Thermo Fisher Scientific (MA, USA). Acetonitrile was purchased from Merck (Darmstadt, Germany). Haematoxylin and eosin (HE), oil red O staining kits and DAPI were obtained from Service Biology (Wuhan, China). Phosphate buffered saline (PBS) and radioimmunoprecipitation assay (RIPA) lysis buffer were purchased from KeyGEN (Nanjing, China). An enzyme-linked immunosorbent assay (ELISA) kit for cAMP analysis was purchased from Chen Gong Biotechnology Co. Ltd. (Shanghai, China). RNA extraction kit was purchased from Yishan Biotech (Shanghai, China). The polymerase chain reaction (PCR) kit for mRNA detection and miRNA

detection were purchased from Takara (Takara Biotechnology, Dalian, China) and Sangon Biotech (Shanghai, China), respectively. Dual-luciferase kit was obtained from Yeasen (Shanghai, China).

Animals and Treatments

Seven-week-old male C57BL/6J mice and obese (ob/ob) mice with C57BL/6J genetic characteristics were purchased from Jiangsu GemPharmatech Co., Ltd. (Nanjing, China). The mice were kept under suitable temperature and humidity, with a 12 h light-dark cycle. After acclimation to the new environment for a week, the mice were divided into three groups: (1) ND group (n = 7): mice were fed with ND; (2) ob/ob group (n = 7): ob/ob mice were fed with ND; (3) HFD group (n = 7): mice were fed with HFD.

Body weights were recorded each day. The mice were group-housed and provided food and water ad libitum as a recent study described (28). After treatment with HFD or ND for 12 weeks, mice were anesthetized using an intraperitoneal injection of 1% pentobarbital sodium (50 mg/kg), and blood samples and liver tissues were collected.

Experimental protocols were approved by the Animal Care and Use Committee of Fudan University (Shanghai, China). Efforts were made to refine the welfare and reduce the suffering of the experimental mice. The animal studies are reported in compliance with the Animal Research: Reporting of Experiments guidelines (Kilkenny C, 2010).

Liver Specific GAS5 Overexpression

=AAV8-GAS5 plasmid and AAV8-GFP with virus titre more than 10^{13} vg/ml were constructed by Vigene (Jinan, China). Liver-specific GAS5 overexpression in C57BL/6J mice was established using an injection of AAV8-GAS5 plasmid. Briefly, after a week of acclimatation, seven-week-old male C57BL/6J mice were then divided into four groups (n=7): (1) older ND-fed group (OND), (2) older HFD-fed group (OHFD), (3) AAV8-GAS5 group and (4) AAV8-GFP group. Mice in AAV8-GAS5 group were injected intravenously with a mixture of 7 μl AVV8-GAS5 and 193 μl saline, while that of the AAV8-GFP group were injected with AAV8-GFP. Plasmid was stably expressed in mice 3 weeks after tail vein injection (29). During the 3 weeks, mice in all four group were fed with ND, and then mice of OND group were still fed with ND, while the other three groups were fed with HFD for the next 12 weeks.

In Vitro Models

Two normal human hepatocyte lines, HL-7702 (L-02; CVCL_6926) and QSG-7701 (7701; 3131C0001000200007) were purchased from Yuanchuang Biological Technology Co., Ltd. (Shanghai, China) and complied with the cell STR identification standards established by the International Committee for Cell Identification. Cells were cultured in DMEM containing 10% FBS and maintained in an incubator at 37°C with 5% CO_2. To establish *in vitro* models, L02 and 7701 cells were treated with a free fatty acid (FFA) mixture (1mM, OA:PA, 2:1 in DMEM with 10% FBS) for 24 h. H89 is a specific PKA inhibitor and forskolin is a cAMP activator (30). L02 and 7701 cells were cultured in DMEM containing 10% FBS and treated with 20 μM H89 or forskolin mixed with DMEM for 1 h before FFA stimulation.

Plasmid and Small Interfering RNA (siRNA) Transfection *In Vitro*

Full-length GAS5 sequence was cloned into the vector pcDNA3.1 (+) (GenePharma, Shanghai, China). Specific siRNAs for GAS5 and PDE4B as along with a mimic and an inhibitor of miR-26a-5p were designed and synthesised by GenePharma. Oligonucleotide sequences are shown in **Table 1**. Cells were seeded into six-well plates, and the transfection experiments were performed using Lipofectamine 3000, following the manufacturer's instructions.

Histological Analysis and Oil Red O Staining

Livers were collected and fixed in 4% paraformaldehyde for more than 24 h. Tissues were embedded with paraffin, and 5 μm sections were sliced for HE and oil red O staining. The oil red O staining was performed as previously described (31).

Biochemical Analysis of Tissues and Cells

Liver tissues and cell samples were homogenised using PBS or lysed using RIPA lysis buffer. Following this, TG, MDA and SOD levels were detected using the commercial test kits. cAMP levels in the liver tissues and cells were detected using an ELISA kit according to the manufacturer's protocol.

TABLE 1 | Small interfering RNAs (siRNAs) used in this study.

Name	Sense (5'-3')	Antisense (5'-3')
GAS5-1	GCUCUGGAUAGCACCUUAUTT	AUAAGGUGCUAUCCAGAGCTT
GAS5-2	GCAGACCUGUUAUCCUAAATT	UUUAGGAUAACAGGUCUGCTT
GAS5-3	GGACCAGCUUAAUGGUUCUTT	AGAACCAUUAAGCUGGUCCTT
PDE4B-1	GACGCUCAGACACCUAUUATT	UAAUAGGUGUCUGAGCGUCTT
PDE4B-2	CUGCCGAGUUCAUCUAUUATT	UAAUAGAUGAACUCGGCAGTT
PDE4B-3	CGGGAACAGAGAAUGUUUATT	UAAACAUUCUCUGUUCCCGTT
siRNA NC	UUCUCCGAACGUGUCACGUTT	ACGUGACACGUUCGGAGAATT
miR-26a-5p mimic	UUCAAGUAAUCCAGGAUAGGCU	–
miRNA mimic NC	UUGUACUACACAAAAGUACUG	–
miR-26a-5p inhibitor	AGCCUAUCCUGGAUUACUUGAA	–
miRNA inhibitor NC	CAGUACUUUUGUGUAGUACAA	–

RNA Extraction and Quantitative Real-Time PCR (RT-qPCR)

Total RNA was obtained from the liver tissues and cells using an RNA extraction kit and RT-qPCR was performed following the manufacturer's instructions using a QuantStudio 3 (Thermo Fisher Scientific) thermocycler. β-actin and U6 small nuclear RNA were used for the normalisation of mRNA and miRNA, respectively. Primers used for RT-qPCR in the study are presented in **Table 2**.

Western Blot

Total protein was extracted from the liver tissues or cell samples using RIPA lysis buffer. Antibodies including Adenosine triphosphate citrate lyase (ACLY, Cat No. 15421-1-AP), acetyl-coenzyme A carboxylase 1 (ACC1, Cat No. 21923-1-AP), fatty acid synthase (FAS, Cat No. 13098-1-AP), GAPDH (Cat No. 60004-1-Ig), peroxisome proliferator-activated receptor γ coactivator-1α (PGC-1α, Cat No. 66369-1-Ig) and cAMP-response element-binding protein (CREB, Cat No. 12208-1-AP) were purchased from Proteinech Group (IL, USA), while phosphodiesterase (PDE) 4B (Cat No. 72096) and phosphorylated CREB (p-CREB, Cat No. 9198) were purchased from Cell Signalling Technology (CST, MA, USA). The dilution of antibodies used in this study were as follows: ACLY (1:1000), ACC1 (1:1000), FAS (1:1000), GAPDH (1:5000), PGC-1α (1:1000), p-CREB (1:500), CREB (1:1000), and PDE4B (1:1000). Western blotting was performed according to the standard protocol and different bands were detected using ECL chromogenic reagent.

Immunofluorescence

L02 and 7701 cells were seeded on sterile glass coverslips and gently washed with PBS. Samples were fixed with 4% paraformaldehyde for 15 min and rinsed thrice for 5 min each. After 5 min of incubation with 0.2% Triton X, samples were immersed in 5% BSA for 1 h. Blocking buffer was then aspirated and coverslips were incubated with p-CREB (1:100, Cat No. 9198, CST, MA, USA) at room temperature for 2 h. The target antigen was visualised using a fluorescent microscope after incubation with an AlexaFluor488-labeled secondary antibody (Invitrogen, CA, USA) and 4', 6-diamidino-2-phenylindole (DAPI).

Luciferase Reporter Assay

The human embryonic kidney (HEK) 293T cell line was purchased from the Cell Bank of Type Culture Collection of the Chinese Academy of Sciences and cells were cultured in DMEM with 10% FBS. The binding sites of has-miR-26a-5p within GAS5 and PDE4B were predicted using ENCORI (https://starbase.sysu.edu.cn). The full-length of GAS5 and fragment of PDE4B 3′-UTR containing the predicted binding sites were amplified using PCR and cloned into a pmirGLO vector (AZENTA, Suzhou, China). The binding sites were mutated to establish the mutant (MUT) model. The reported plasmid and has-miR-26a-5p mimic or inhibitor were co-transfected into HEK 293T. Additionally, a commercial dual-luciferase kit was used to detect the luciferase assay after 36 h of transfection.

TABLE 2 | Primers used for qPCR in the study: For mice.

Gene name	Forward (5'-3')	Reverse (5'-3')	Gene ID
β-actin	GTGACGTTGACATCCGTAAAGA	GCCGGACTCATCGTACTCC	11461
SREBP-1c	TTGTGGAGCTCAAAGACCTG	TGCAAGAAGCGGATGTAGTC	20787
FAS	GCTGCGGAAACTTCAGGAAAT	AGAGACGTGTCACTCCTGGACTT	14104
ACC1	ATGCGATCTATCCGTCGGTG	AGCAGTTCTGGGAGTTTCGG	104371
ACLY	TTCGTCAAACAGCACTTCC	ATTTGGCTTCTTGGAGGTG	104112
DGAT1	GGAATATCCCCGTGCACAA	CATTTGCTGCTGCCATGTC	13350
CD36	ATGGGCTGTGATCGGAACTG	TTTGCCACGTCATCTGGGTTT	12491
GAS5	CTTGCCTGGACCAGCTTAAT	CAAGCCGACTCTCCATACCT	14455
miR-26a	AAGCTGAGTTCAAGTAATCCAGG	–	387218
PDE4B	GACCGGATACAGGTTCTTCG	CAGTGGATGGACAATGTAGTCA	18578
PGC-1α	TATGGAGTGACATAGAGTGTGCT	GTCGCTACACCACTTCAATCC	19017
CPT-1α	TGGCATCATCACTGGTGTGTT	GTCTAGGGTCCGATTGATCTTTG	25757
For human:			
Gene name	Forward (5'-3')	Reverse (5'-3')	Gene ID
β-actin	CTGGAACGGTGAAGGTGACA	AAGGGACTTCCTGTAACAATGCA	60
FAS	GGGATGAACCAGACTGCGTG	TCTGCACTTGGTATTCTGGGT	2194
ACC1	AATGTCCTTCTCCTCCAA	GAGTGAATGAGTTGTCCAA	31
GAS5	AGTAGCCGTCTCTGTGT	CTCCACGAACAGCTTCACAA	60674
miR-26a	TTCAAGTAATCCAGGATAGGCT	–	407015
PDE4B	CTATACCGATCGCATTCAGGTC	CTGTCCATTGCCGATACAATT	5142
PGC-1α	TCTGAGTCTGTATGGAGTGACAT	CCAAGTCGTTCACATCTAGTTCA	10891
CPT-1α	TCCAGTTGGCTTATCGTGGTG	TCCAGAGTCCGATTGATTTTTGC	1374
TFAM	ATAAAGAAGAGATAAGCAGATT	TGCCTATTAAGAGAAAACTAC	7019
NRF-1	GTACAAGAGCATGATCCTGGA	GCTCTTCTGTGCGGACATC	4899

A universal U6 reference forward primer, and universal PCR reverse primer were provided by the miRNA First Strand cDNA Synthesis kit.

Relative Quantitative Lipidome Analysis of Liver Tissues

Hepatic lipids were extracted with the methyl tert-butyl ether (MTBE) method. Briefly, 30 mg of the liver sample was mixed with 200 µl H_2O and vortexed for 30 s. Subsequently, 240 µl of precooling methanol was added to the mixture and vortexed for 30 s. Following this, 800 µl of MTBE was added to the mixture, which underwent ultrasound for 20 min at 4°C. The solution was centrifuged at 14000 g for 15 min at 10°C and the upper organic solvent layer was obtained and dried using nitrogen gas. The lipid extracts were re-dissolved in 200 µl 90% isopropanol/acetonitrile and centrifuged at 14000 g for 15 min, and the mass spectra was acquired using Q Exactive Plus system (Thermo Fisher).

Untargeted Metabolome Analysis of Liver Tissues

Livers were frozen in liquid nitrogen immediately after dissection. At least 80 mg tissues were cut and homogenised with 200 µl of H_2O and five ceramic beads. Then, 800 of µl methanol/acetonitrile (1:1, v/v) was added to the homogenised solution for metabolite extraction. The mixture was centrifuged for 15 min (14000 g, 4°C) and the supernatant dried in a vacuum centrifuge. For LC-MS analysis, the samples were re-dissolved in 100 µl acetonitrile/water (1:1, v/v) solvent. Samples were separated using an Agilent 1290 Infinity LC ultra-high performance liquid chromatography system (UHPLC, Agilent, CA, USA) and analysed using a Triple TOF 6600 mass spectrometer (AB SCIEX, CA, USA).

Statistical Analyses

All data are expressed as mean ± standard error of mean. Comparisons between groups were determined using unpair Student's t test or the Analysis of Variance (ANOVA). Statistical analyses were performed using GraphPad Prism 8 software (GraphPad Software, CA, USA). P value < 0.05 indicated significant difference. All data are available from the authors on reasonable request.

RESULTS

GAS5 Is Elevated in Ob/Ob Mice, HFD Fed Mice and FFA Stimulated Hepatocytes

The body weights of mice in different groups were recorded every week (**Figure 1A**). HFD mice grew significantly heavier than ND mice and there was significant difference from the 9th week. Importantly, HE and oil red O staining showed that ob/ob and HFD mice produced more lipid droplets in the hepatic intracellular vacuoles than the ND mice (**Figure 1B**). Correspondingly, the ratio of liver weight to body weight in the ob/ob and HFD mice was much higher than in the ND group (**Figure 1C**). Notably, the hepatic TG content was increased in the ob/ob and HFD mice (**Figure 1D**). Relative quantitative lipidome analyses of HFD and ND mice were conducted to determine lipid concentrations between the HFD and ND groups (**Figures S1, 2**). HFD fed mice had significantly higher levels of total lipids and TGs compared with that of the ND fed mice (**Figures 1E, F**).

DNL, lipid uptake and lipoprotein secretion contributed to hepatic lipid metabolism. As shown in **Figure 1G**, the expression of key genes associated with DNL, lipid uptake and lipoprotein secretion were significantly increased in ob/ob and HFD fed mice. Consistently, the protein levels of DNL-associated enzymes were also increased in the ob/ob and HFD mice (**Figure 1H**). Therefore, the NAFLD mice models were successfully established, and the expression of GAS5 was upregulated in the ob/ob and HFD mice (**Figure 1I**).

L02 and 7701 cells were used to establish the *in vitro* models. FFA caused an increase in the intracellular TG content (**Figure 1J**), which was evidenced by the increased lipid droplet production in the FFA-treated cells (**Figure 1K**). Moreover, GAS5 expression was higher in FFA treated cells than control cells (**Figure 1L**).

GAS5 Overexpression Aggravates Lipid Accumulation

Compared with the AAV8-GFP plus HFD groups, mice in the AAV8-GAS5 plus HFD group developed a significantly higher body weight and liver/body weight ratio (**Figures 2A, B**). Notably, increased lipid droplet accumulation in the hepatic intracellular vacuoles was observed in the GAS5 overexpressed group (**Figure 2C**). AVV8-GAS5 significantly increased the expression of GAS5 in liver tissues (**Figure 2D**). Changes in the biochemical parameters were observed, with increased hepatic TG levels in GAS5 overexpressed mice (**Figure 2E**).

Simultaneously, this study confirms that the expression of GAS5 in cells was upregulated with pcDNA-GAS5 transfection (described as GAS5 in Figures) (**Figure 2F**). Furthermore, GAS5 overexpression resulted in increased TG synthesis in FFA-stimulated cells (**Figure 2G**). Therefore, GAS5 overexpression is closely associated with hepatic and hepatocellular lipid accumulation.

GAS5 Knockdown Alleviates Hepatocellular DNL Lipogenesis

All three synthetic siRNA for GAS5 (siGAS5) significantly downregulated the intracellular GAS5 levels (**Figure 3A**). TG contents in the cells were also reduced after GAS5 knockdown (**Figure 3B**). Correspondingly, decreased lipid droplets were produced in the cells (**Figure 3C**). Moreover, the protein expression of DNL enzymes, ACC1 and FAS was downregulated in FFA-treated cells after GAS5 suppression (**Figure 3D**). Similar results were observed in the mRNA expression of ACC1 and FAS (**Figure 3E**). Considering that siGAS5-1 had the strongest inhibitory effect on GAS5 expression and had an obvious effect on inhibiting lipid droplet formation and reducing the expression of ACC1 and FAS in L02 and 7701 cells, we selected siGAS5-1 for subsequent experiments and described it as siGAS5.

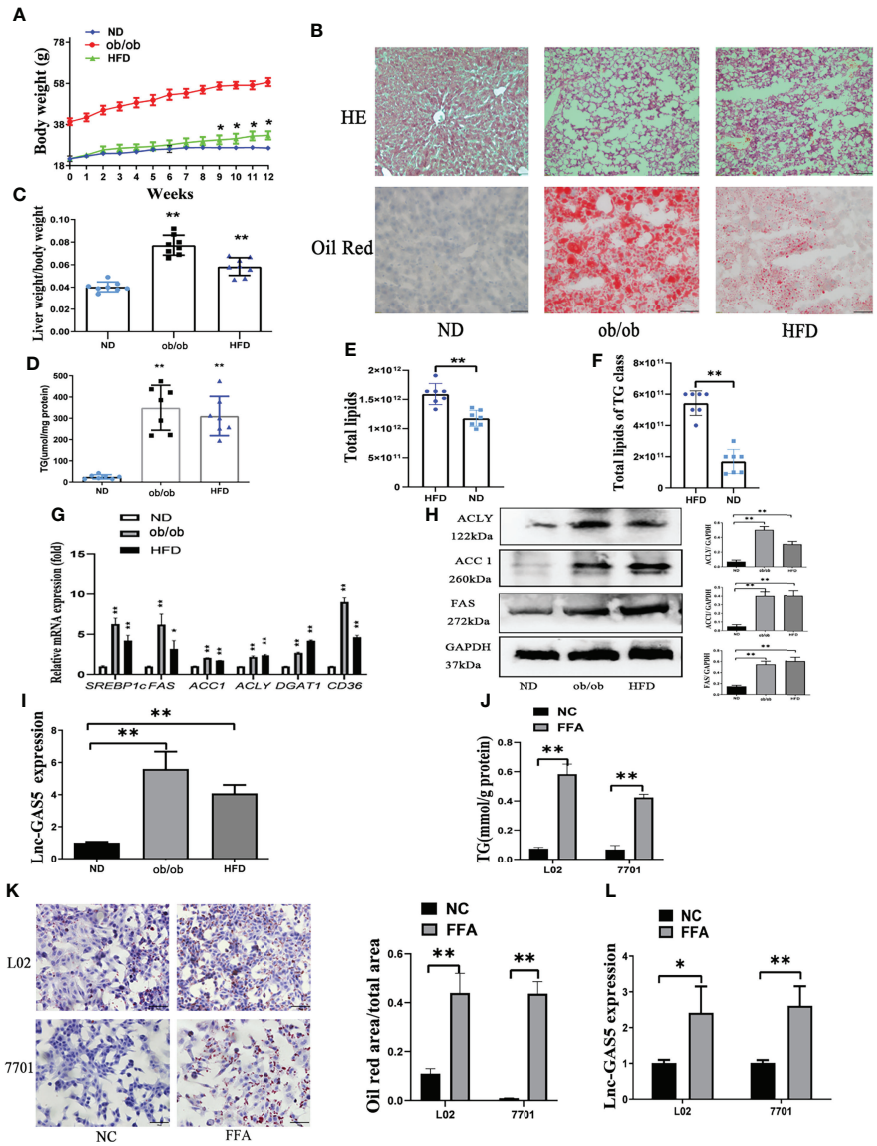

FIGURE 1 | The expression of long non-coding RNA growth arrest specific 5 (GAS5) in *in vivo* and *in vitro* non-alcoholic liver disease (NAFLD) models. The body weight of mice in normal chow diet (ND), obese (ob/ob) and high fat diet (HFD) groups were recorded **(A)**. After 12 weeks of HFD treatment, livers were collected for haematoxylin and eosin staining and oil red staining (Original magnification, ×200) **(B)**. The ratio of liver weight to body weight was calculated **(C)**. Levels of triglycerides (TGs) in the liver tissues were detected using commercial kits **(D)**. Total lipids in HFD and ND fed mice and TG concentration was detected using mass spectrometry **(E, F)**. The gene expression of SREBP-1c, FAS, ACC1, ACLY, DGAT1 and CD36 was detected using quantitative real-time polymerase chain reaction (RT-qPCR) **(G)**. Protein expression of ACLY, ACC1 and FAS was determined using western blotting **(H)**. Expression of GAS5 in ND, ob/ob and HFD mice were detected using RT-qPCR **(I)**. TG levels **(J)**, oil red staining (Original magnification, ×200) **(K)**, and lnc-GAS5 expression **(L)** of cells treated with FFA. Data are expressed as mean ± standard error of mean. $^{*}P < 0.05$ and $^{**}P < 0.01$; n = 7 in C-F and n = 3 in G-L.

GAS5 Knockdown Preserves Mitochondrial Function

MDA and SOD are oxidative stress markers, and the increased levels of MDA and decreased levels of SOD indicate that the mitochondrial function is suppressed in the ob/ob and HFD treated mice (**Figure 4A**). PGC-1α and CPT-1α play important roles in fatty acid oxidation and are key indicators of mitochondrial function, which were reduced in the ob/ob and HFD-fed mice (**Figures 4B, C**).

In L02 and 7701 cells, the levels of MDA were upregulated and SOD were downregulated in FFA-stimulated cells and the changes in MDA and SOD were reversed on GAS5 knockdown (**Figure 4D**). FFA treatment markedly decreased ATP production, but GAS5 knockdown could upregulate the ATP production in FFA-stimulated cells (**Figure 4E**). Furthermore, GAS5 knockdown increased the mRNA expression of TFAM and NRF-1 (**Figure 4F**). In **Figures 4G, H**, GAS5 knockdown helped cells maintain the

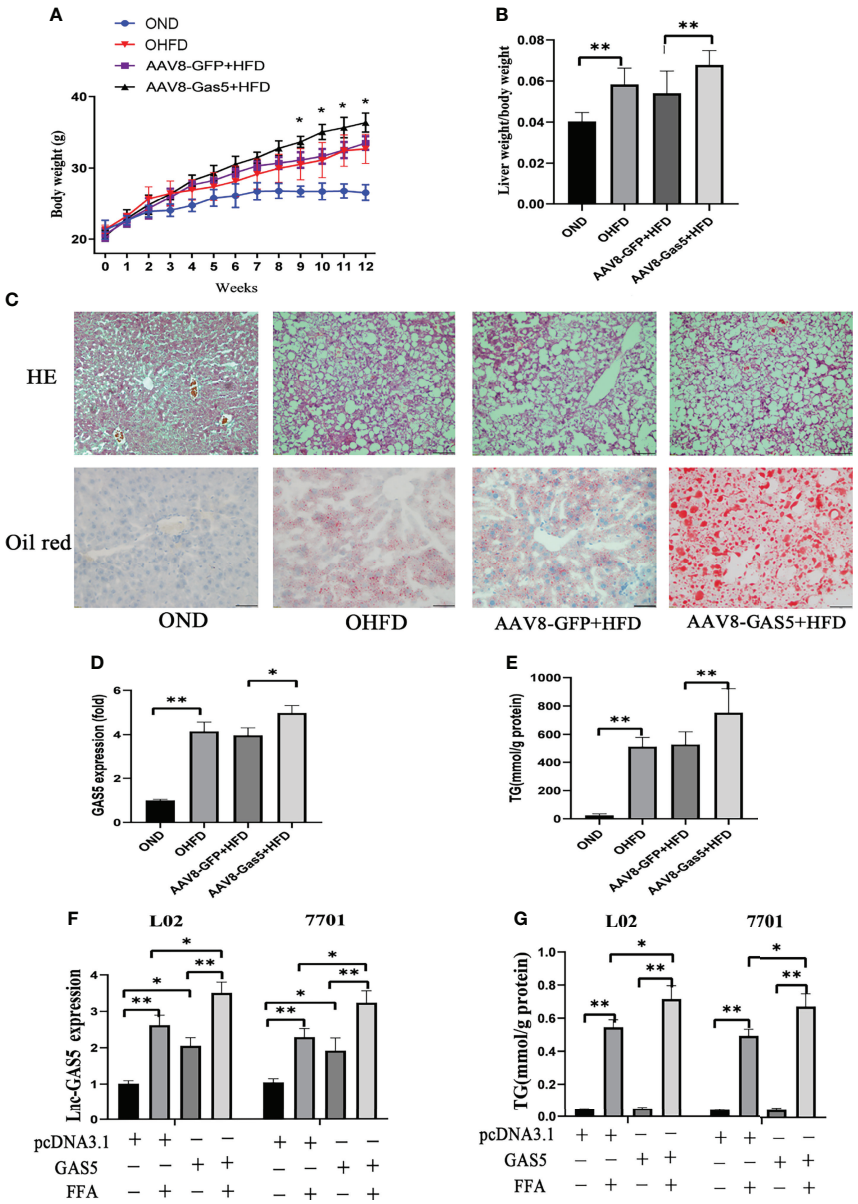

FIGURE 2 | Long non-coding RNA growth arrest specific 5 (GAS5) overexpression aggregates hepatic lipid accumulation. After mice were injected with AAV8-GAS5 or AAV8-GFP for 21 days, they were fed with high fat diet (HFD) or normal chow diet (ND). The body weight of mice in OND, OHFD, AAV8-GFP plus HFD and AAV8-GAS5 plus HFD group was recorded every week **(A)**, data are expressed as mean ± standard error of mean (SEM), $^{*}P < 0.05$, n = 7. The ratio of liver weight to body weight in different groups were calculated **(B)**, data are expressed as mean ± SEM, $^{**}P<0.01$, n = 7. The expression of GAS5 in different groups **(C)**, data are expressed as mean ± standard error of mean (SEM), $^{*}P<0.05$, $^{**}P<0.01$, n = 3. Haematoxylin and eosin staining and oil red staining of liver tissues in different groups (Original magnification, ×200) **(D)**. The detection of hepatic triglycerides (TGs) in different groups **(E)**, data are expressed as mean ± SEM, $^{**}P<0.01$, n = 7. Cells were transfected with pcDNA3.1-GAS5 (described as GAS5) or pcDNA3.1 vector and treated with free fatty acid. The quantitative real-time polymerase chain reaction analysis of GAS5 in different groups **(F)**, and the TG detection in different groups **(G)**; data are expressed as mean ± SEM, $^{*}P < 0.05$, $^{**}P < 0.01$, n = 3.

levels of PGC-1α and CPT-1α. Hence, GAS5 knockdown can protect the mitochondrial function.

GAS5 Modulates PDE4B Expression by Sponging With MiR-26a-5p

Sequencing analysis showed the potential binding sites between GAS5 and miR-26a-5p. Subsequently, the luciferase reporters were constructed, containing the wild-type GAS5 (GAS5 WT) or mutant GAS5 (GAS5 MUT). Compared with miRNA negative control (NC) or inhibitor NC, miR-26a-5p mimic or inhibitor suppressed or enhanced the luciferase reporter activities of GAS5 WT, but not those of GAS5 MUT (**Figure 5A**). Potential binding sites were also predicted between PDE4B and miR-26a-5p and further proved by luciferase reporters (**Figure 5B**). Therefore,

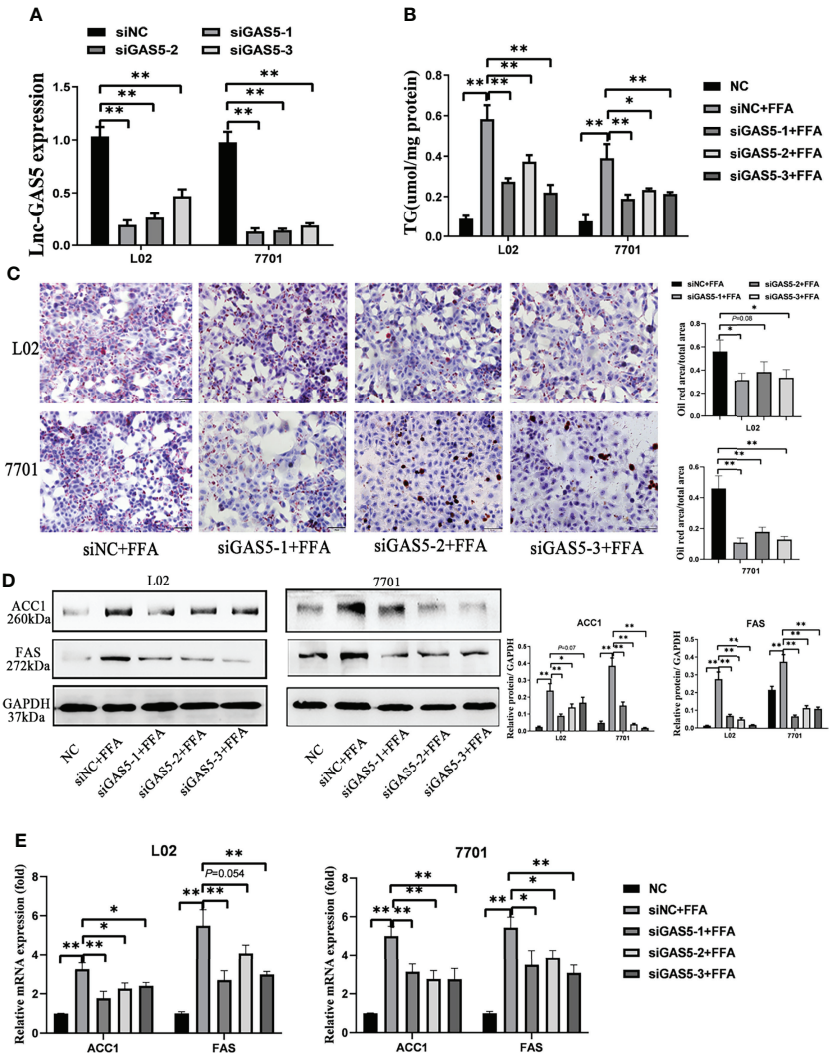

FIGURE 3 | Long non-coding RNA growth arrest specific 5 (GAS5) knockdown mitigates cellular *de novo* lipogenesis. After cells were transfected with three synthetic small interfering RNAs, the expression of lnc-GAS5 were determined using quantitative real-time polymerase chain reaction analysis (RT-qPCR) **(A)** and lipid accumulation in cells were assessed *via* oil red staining (Original magnification, ×200) **(B)**. The cellular triglyceride levels were detected using commercial kits **(C)**, and the protein and mRNA levels of ACC1 and FAS were measured *via* western blot and RT-qPCR, respectively **(D, E)**. Data are expressed as mean ± standard error of mean. **P*<0.05, and ***P*<0.01, n = 3.

GAS5 and PDE4B mRNA are physically associated with miR-26a-5p *via* these sites.

All three siRNA for PDE4B significantly reduced the expression of PDE4B in cells, and we chose siPDE4B-2 for subsequent experiments and described it as siPDE4B (**Figure S3**). GAS5 knockdown decreased PDE4B protein expression, whereas PDE4B expression was increased on miR-26a-5p inhibition. Decreased miR-26a-5p could promote PDE4B expression even when cells were treated with siPDE4B (**Figure 5C**). The overexpression of miR-26a-5p suppressed the levels of GAS5, while decreased miR-26a-5p upregulated the expression of GAS5. As a downstream molecule of miR-26a-5p, there exists an inverse correlation between PDE4B and miR-26a-5p (**Figure 5D**). GAS5 knockdown promoted the expression of miR-26a-5p in FFA-treated cells. Moreover, the decreased level of PDE4B also upregulated miR-26a-5p expression (**Figure 5E**). Hence, GAS5 sponges with miR-26a-5p and modulates PDE4B expression.

GAS5/MiR-26a-5p/PDE4B Axis Mediates FFA-Induced Hepatocellular Lipid Metabolism

When cells were transfected with siGAS5 and miR-26a-5p inhibitor, lipid accumulation and intracellular TG levels were increased compared to those treated with siGAS5 plus FFA (**Figures 6A, B**). Western blot and qRT-PCR results showed that

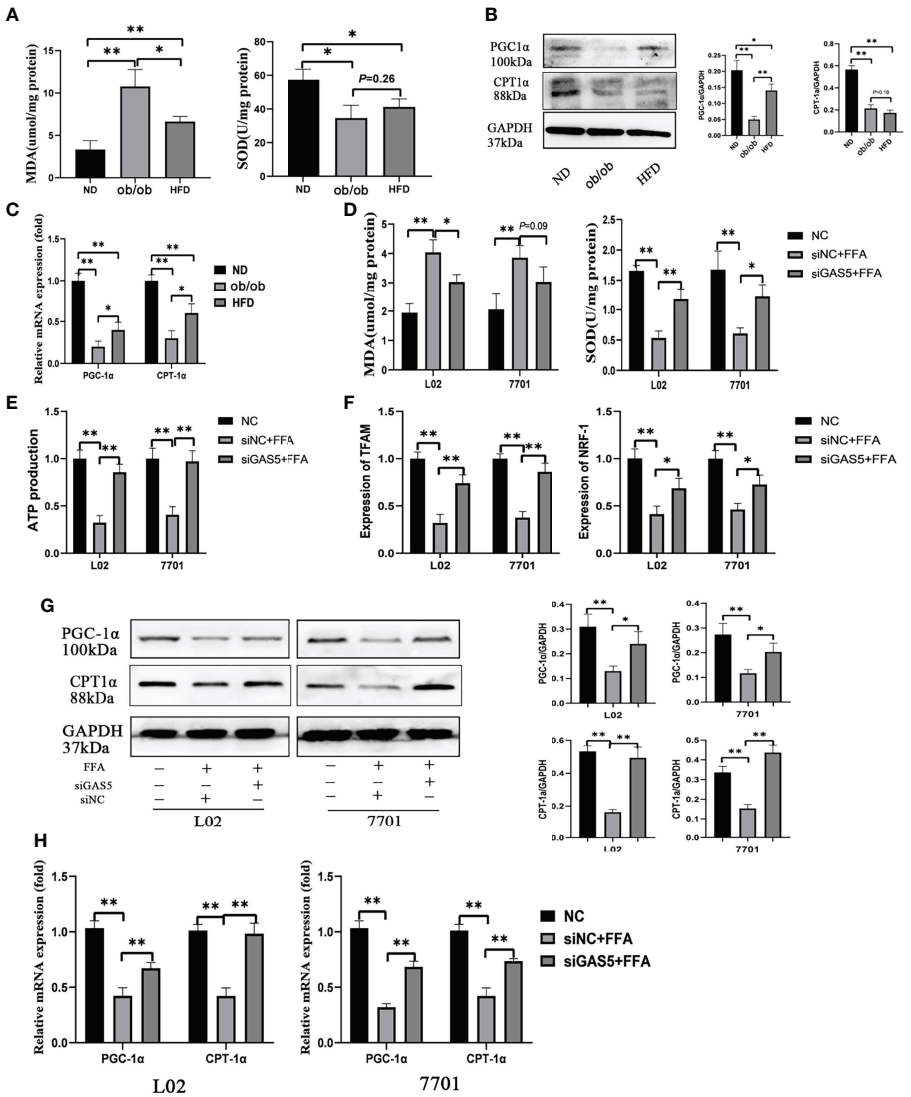

FIGURE 4 | Long non-coding RNA growth arrest specific 5 (GAS5) regulates mitochondrial function. The detection of hepatic malondialdehyde (MDA) and superoxide dismutase (SOD) levels in different groups of mice **(A)**. The protein and mRNA expression of PGC-1α and CPT-1α **(B, C)**. Cells were transfected with small interfering GAS5-1 (described as siGAS5 in subsequent experiments) and then treated with free fatty acid. The detection of cellular MDA and SOD levels **(D)**. The detection of ATP production in cells of FFA, siNC plus FFA and siGAS5 plus FFA groups **(E)**. The expression of mRNA levels of mitochondrial biogenesis including TFAM and NRF-1 in cells of FFA, siNC plus FFA and siGAS5 plus FFA groups **(F)**. The protein and mRNA expression of PGC-1α and CPT-1α in different groups of cells **(G, H)**. Data are expressed as mean ± standard error of mean. $^{*}P < 0.05$ and $^{**}P < 0.01$, n = 3.

GAS5 knockdown inhibited ACC1 expression and promoted PGC-1α expression, whereas these characteristics could be restricted on co-transfection with miR-26a-5p inhibitor (**Figures 6C, D**).

FFA-stimulated cellular lipid accumulation decreased with PDE4B downregulation, whereas it was increased with a miR-26a-5p inhibitor co-transfection (**Figure 6E**). Consistently, intracellular TG levels in PDE4B knockdown cells could be upregulated by a miR-26a-5p inhibitor (**Figure 6F**). In **Figure 6G**, the protein levels of ACC1 decreased when PDE4B was downregulated and this could be reversed by a miR-26a-5p inhibitor. As a protective molecule, changes in PGC-1α were contrasting to those in ACC1. Additionally, ACC1 and PGC-1α mRNA expression detection *via* RT-qPCR showed similar results (**Figure 6H**). Therefore, GAS5 regulates hepatocellular lipid accumulation *via* the miR-26a-5p/PDE4B axis.

Lnc-GAS5 Modulates cAMP/CREB Pathway

As a hepatic manifestation of metabolic syndromes, changes in hepatocellular metabolites can aid in elucidating the regulatory processes of NAFLD. The hepatic untargeted metabolomic analysis of HFD and ND mice were performed to demarcate the HFD and ND groups (**Figures S4, 5**). The concentration of 144 metabolites changed on comparing the HFD-fed and ND-fed mice

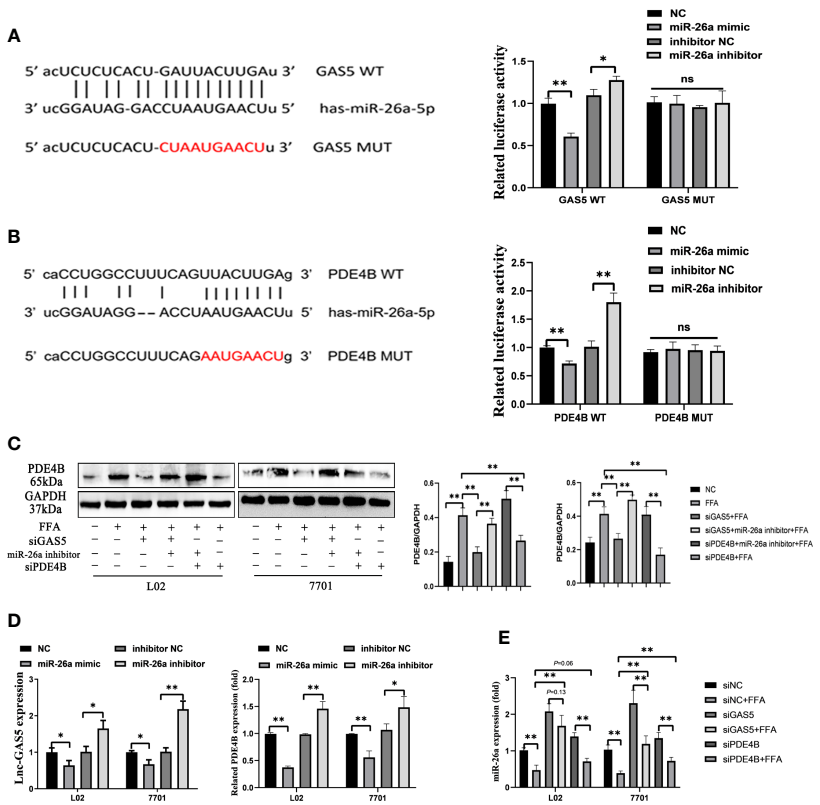

FIGURE 5 | Long non-coding RNA growth arrest specific 5 (GAS5) regulates phosphodiesterase-4D (PDE4B) by sponging miR-26a-5p. Bioinformatic predictions of the miR-26a-5p targeting GAS5 3′UTR through the binding sequence, and dual luciferase reporter detection of GAS5 and miR-26a-5p **(A)**. Bioinformatic predictions of the miR-26a-5p targeting PDE4B 3′UTR through the binding sequence, and dual luciferase reporter detection of PDE4B and miR-26a-5p **(B)**. The protein expression of PDE4B in different groups **(C)**. The expression of GAS5 and PDE4B of cells transfected with a miR-26a mimic or inhibitor **(D)**. The expression of miR-26a-5p in cells with GAS5 knockdown or PDE4B knockdown **(E)**. Data are expressed as mean ± standard error of mean. *$P < 0.05$ and **$P < 0.01$, n = 3. ns, not significant.

(**Figure S6A**), and different pattern of lipid and lipid like metabolites were shown in **Figure S6B**. The 20 most enriched Kyoto Encyclopaedia of Genes and Genomes pathways based on metabolite variations are shown in **Figure S6C**. Given the close association between PDE4B and cAMP, the changes and roles of the cAMP pathway were analysed in this study's models.

The variation of metabolites involved in the cAMP pathway were collected and significant differences between the HFD and ND groups were observed. The expression of 3-hydroxybutyrate and acetylcholine was downregulated in HFD-fed mice, whereas the hydrolysates of cAMP, adenosine 5'-monophosphate and adenosine were increased in HFD-fed mice (**Figure S6D**). Furthermore, HFD feeding decreased the levels of hepatic cAMP (**Figure 7A**). Similar results were detected in FFA-treated cells, whereas GAS5 knockdown increased the cAMP accumulation (**Figure 7B**). FFA treatment increased the expression of PDE4B and suppressed the expression of p-CREB and PGC-1α. Knockdown of GAS5 promoted CREB phosphorylation and reversed PGC-1α alteration. On the contrary, H89 dephosphorylated CREB and reduced PGC-1α expression (**Figure 7C**). Furthermore, H89 aggravated the accumulation of lipids in FFA-stimulated cells compared with those transfected with siGAS5 (**Figure 6D**). Although forskolin did not affect PDE4B expression, it notably promoted CREB phosphorylation and thereby suppressed ACC1 and FAS expression and increased PGC-1α expression (**Figure 7E**). Forskolin treatment reduced lipid droplet accumulation even when GAS5 was overexpressed (**Figure 7F**). Integrating the effects of H89 and forskolin on lipid accumulation, the cAMP/CREB pathway was involved in the regulation of GAS5 in hepatocellular lipid metabolism, which was confirmed by the p-CREB immunofluorescence in cells with different treatments. As shown in **Figure 7G**, p-CREB expression increased with siGAS5 transfection and forskolin treatment, but decreased with GAS5 overexpression and H89 treatment in cells, particularly in the nuclei.

DISCUSSION

The present study demonstrated that the expression of GAS5 was upregulated in fatty liver models *in vitro* and *in vivo*. Additionally, the function of the GAS5/miR-26a-5p/PDE4B and cAMP/CREB pathway in the regulation of hepatic lipid metabolism was investigated.

With various studies focusing on new targets for NAFLD diagnosis and treatment, lncRNAs has been reported as an increasingly promising candidate (32). Given its increased

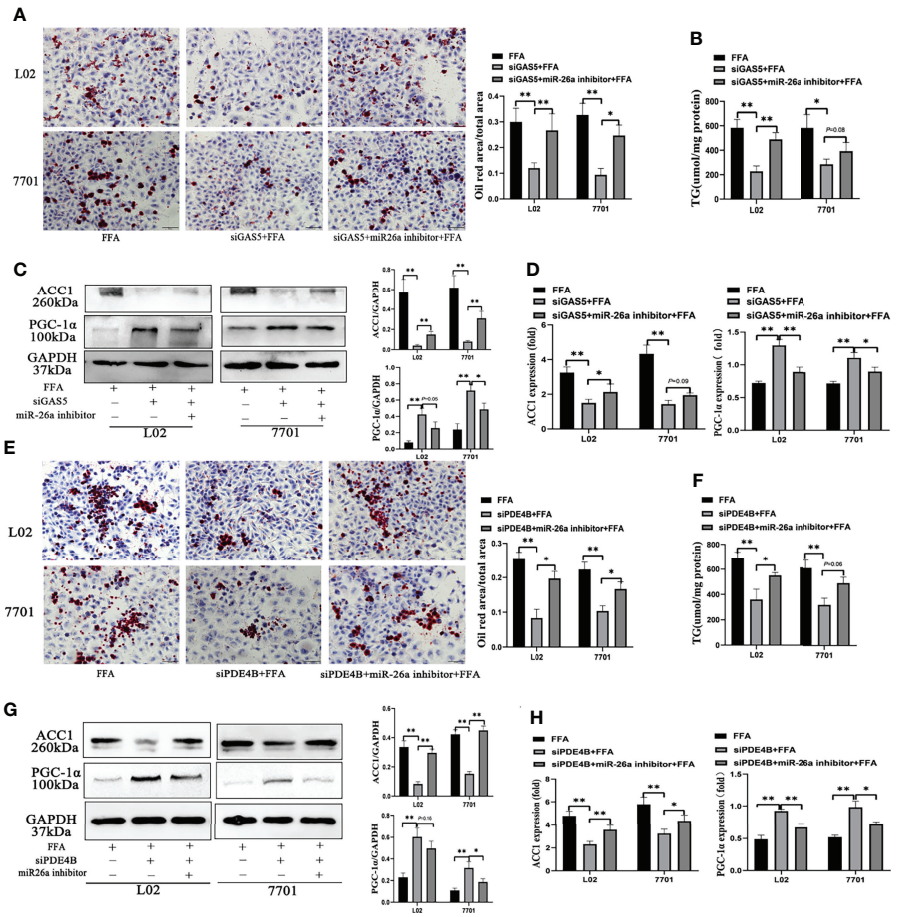

FIGURE 6 | The regulation of the long non-coding RNA growth arrest specific 5 (GAS5)/miR-26a-5p/phosphodiesterase-4D (PDE4B) axis in lipid metabolism. Cells were transfected with small interfering (si)GAS5 or siGAS5 plus miR-26a-5p inhibitor and stained with oil red (Original magnification, ×200) **(A)**. Triglyceride (TG) levels were detected using a commercial kit **(B)**, and the protein and mRNA expression of ACC1 and PGC-1α was detected *via* western blot and quantitative real-time polymerase chain reaction analysis (RT-qPCR), respectively **(C, D)**. Cells were stained with oil red after transfection with siPDE4B or siPDE4B plus a miR-26a-5p inhibitor, (Original magnification, ×400) **(E)**, TG levels detection **(F)**, and the protein and mRNA expression of ACC1 and PGC-1α was detected *via* western blot and RT-qPCR, respectively **(G, H)**. Data are expressed as mean ± standard error of mean. $^{*}P < 0.05$ and $^{**}P < 0.01$, n = 3.

expression in patients with NAFLD (20), GAS5 could have a role in regulating hepatic lipid metabolism. GAS5 was reported to have anti-tumour effects in many kinds of human tumours, however, Tao et al. demonstrated that GAS5 could be a proto-oncogene in HCC (33). That may partly be explained by the high tissue-specific feature of lncRNA, and therefore, the function of lncRNA in different tissues may be different (34). The single nucleotide polymorphism (SNP) detection and more *in vivo* studies will help us better understand the biological functions of lncRNAs (35, 36). This study confirmed that the expression of GAS5 was increased in leptin knockout mice, HFD fed mice and FFA stimulated cells. On elucidating the association between GAS5 and hepatic lipid metabolism, increased hepatic DNL was found to be a central metabolic indicator for NAFLD (6, 37, 38). When energy storage is sufficient, dietary lipids, carbohydrates and proteins act as substrates for DNL (39). The actions of regulatory enzymes, including ACLY, ACC and FAS, have been reported to play a role in the regulation of hepatic fatty acid synthesis (40–42). Increasing DNL is closely associated with iron overload and hepatic inflammation through bone morphogenetic protein (BMP6)/Sma- and Mad-related proteins (SMAD) pathway in NAFLD (43). A recent study showed that increased DNL in mice could reduce the expression of HMG-CoA reductase protein and the excretion of bile acids, and facilitated cholesterol uptake. In addition, DNL also led to the secretion of very low-density lipoproteintriglyceride, which was closely associated with hypertriglyceridemia (44). In NAFLD mice models, SREBP-1c, ACLY, ACC1, FAS, DGAT1 and CD36 were upregulated, with significant hepatic TG accumulation in the pathological sections. Lipidome detection is a novel method to study the pathogenesis of NAFLD or alcohol-induced fatty liver disease (45, 46), which detected both quality and quantity changes in lipids in the mice tissues. Liver-specific GAS5 overexpression in mice accelerated weight gain and TG accumulation, gradually developing severe hepatic steatosis and hepatocellular ballooning. Correspondingly, GAS5 knockdown alleviates the cellular lipid accumulation and

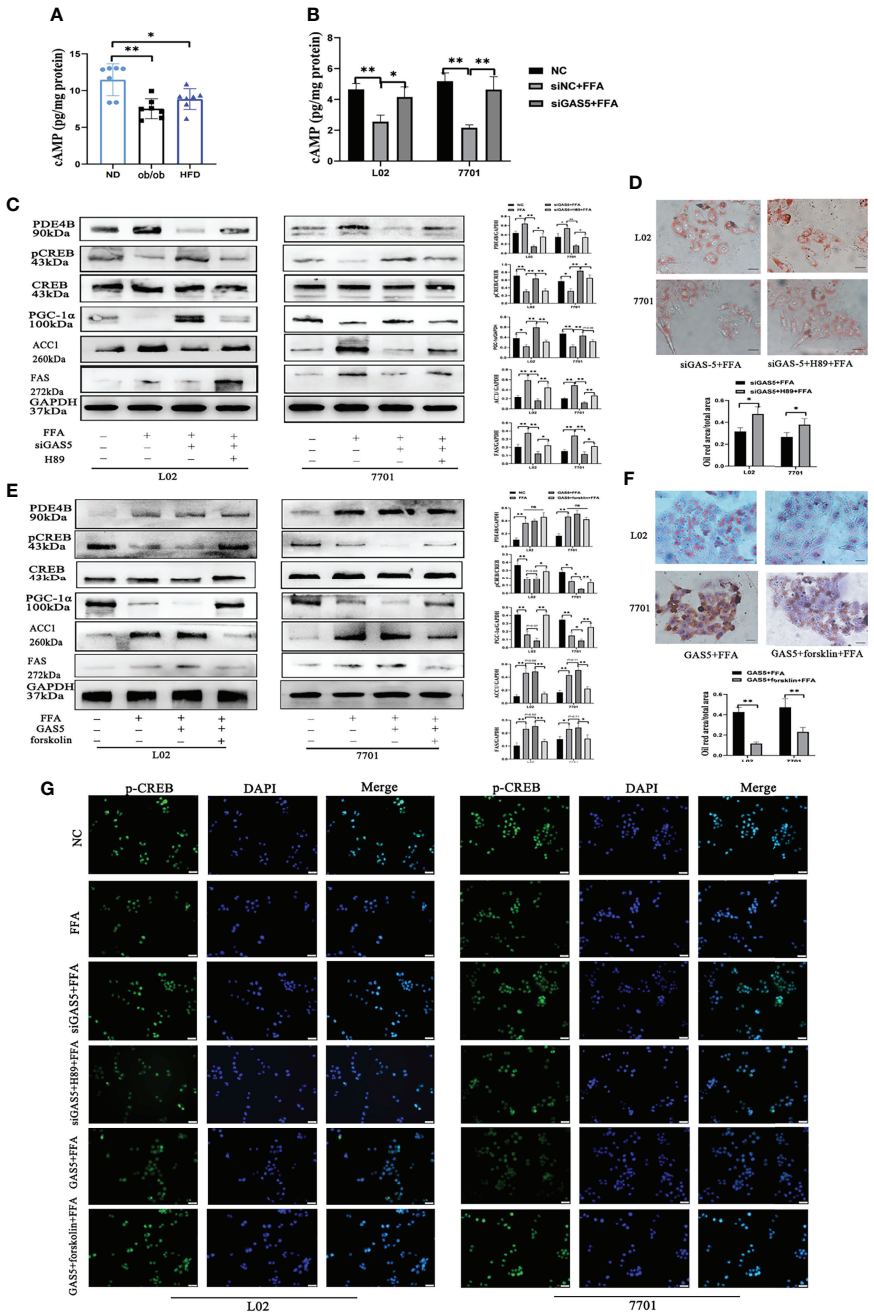

FIGURE 7 | Long non-coding RNA growth arrest specific 5 (GAS5) regulates cAMP/CREB pathway through phosphodiesterase-4B (PDE4B). The cAMP levels in liver tissues **(A)** and cells treated with free fatty acid (FFA) or siGAS5 plus FFA **(B)**. Protein expression of PDE4B, p-CREB, CREB, PGC-1α, ACC1 and FAS in cells treated with FFA after transfection with siGAS5 or siGAS5 plus H89 **(C)**. Oil red staining of cells transfected with siGAS5 or siGAS5 plus H89 followed by FFA treatment (Original magnification, ×400) **(D)**. Protein expression of PDE4B, p-CREB, CREB, PGC-1α, ACC1 and FAS in cells treated with FFA after transfection with GAS5 or GAS5 plus forskolin **(E)**. Oil red staining of cells transfected with GAS5 or GAS5 plus forskolin followed by FFA treatment (Original magnification, ×400) **(F)**. Immunofluorescence of p-CREB in cells with different treatment **(G)**. Data are expressed as mean ± standard error of mean. $^{*}P < 0.05$ and $^{**}P < 0.01$, n = 3.

downregulates DNL marker expressions, demonstrating that GAS5 is closely associated with the regulation of hepatic DNL.

LncRNAs regulate the expression of target genes by competing for shared microRNAs with mRNAs, which are known as ceRNAs (47). Bioinformatic analyses and luciferase reporter assay showed that GAS5 physically interacted with microRNA-26a-5p (miR-26a-5p) through their binding sites. The interaction between GAS5 and miR-26a-5p has been well demonstrated in this study, with GAS5 sponging with miR-26a-5p; furthermore, GAS5 knockdown upregulates miR-26a-5p (23). However, increased levels of miR-

26a have been demonstrated to mitigate NAFLD *in vivo* and *in vitro* (23, 48, 49). Ding et al. found that miR-26a could downregulate CD36, and thereby reducing the steatosis in HepG2 cells (50). Micewith miR-26a overexpression had significant lower liver weight and TG contents compared with that of the normal control mice (49). Conversely, overexpressed GAS5 notably reduced the expression of miR-26a-5p.

Recently, metabolomic analyses have provided novel insights into the pathophysiology of NAFLD (51, 52). Through the detection of hepatic metabolites, the protective cAMP response pathway was highlighted from the analysis of the KEGG signalling pathways. Known as a second messenger, cAMP can be synthesized by adenylyl cyclase from adenosine triphosphate and initiate downstream molecular interactions (53). In HFD-fed mice or FFA-treated cells, the expression of PDE4B was upregulated. Moreover, PDE4B, which is highly expressed in the liver, selectively hydrolyses cAMP (27). Low levels of cAMP lead to the reduction of mitochondrial function and oxygen consumption, thus promoting NAFLD and insulin resistance (54). Conversely, GAS5 knockdown elevated cAMP, which could be attributed to PDE4B inhibition. Increased cAMP phosphorylates CREB by activating protein kinase A and eventually promoting the induction of peroxisome proliferator-activated receptor (PPAR)-γ coactivator 1α (PGC-1α) (55). However, these changes could be reduced when GAS5 was upregulated. Reduced p-CREB expression exacerbates HFD-induced hepatic steatosis by downregulating PPARα (56), whereas activated p-CREB reduces PPAR-γ expression to regulate the hepatic DNL (57), which was confirmed by the downregulation of DNL-related ACC1 and FAS in GAS5 knockdown cells. However, GAS5 knockdown cells with H89 pre-treatment suppressed PGC-1α expression and increased ACC1 and FAS expression. Additionally, H89 reduced the expression of p-CREB by inhibiting the activity of PKA, and subsequently increasing the expression of SREBP-1c, ultimately leading to DNL (58). Conversely, forskolin pre-treatment increased the level of cAMP, upregulated the expression of PGC-1α and reduced the levels of ACC1 and FAS, without affecting PDE4B. Therefore, GAS5 regulates hepatic lipid metabolism *via* the cAMP response signalling pathway, at least partially.

A recent study identified GAS5 as a mitochondria-associated lncRNA, sustaining homeostasis by regulating mitochondrial metabolic enzymes in physiology and cancer (59). Mitochondria control energy metabolism in cells and pathways involved in the regulation of energy metabolism at least partially dependent on mitochondrial function (60). The PGC1 family, including PGC-1α, PGC-1β and PGC related coactivator (61), regulate the mitochondrial biogenesis by interacting with transcription factors or nuclear receptors (62). The expression of PGC-1α was downregulated in HFD treatment or FFA stimulation in this study, and reduced PGC-1α fails to maintain the content of mitochondrial-associated proteins (63). Moreover, GAS5 knockdown by siRNA significantly upregulated the levels of PGC-1α. Increased PGC-1α could promote the levels of lipin 1, subsequently activating PPARα to improve the mitochondrial fatty acid oxidation capacity and suppress DNL and lipid secretion (64). Carnitine palmitoyltransferase-1α (CPT-1α) is abundant in the liver and plays an important role in mitochondrial oxidation by converting fatty acyl-CoA to fatty acylcarnitine (65). In this study, impaired mitochondrial function after HFD or FFA treatment was indicated with increased MDA levels and decreased SOD levels. Consistent with a previous study, the increased expression of PGC-1α and CPT-1α ameliorated NAFLD by promoting mitochondrial function (31), with GAS5 knockdown increasing the expression of PGC-1α and CPT-1α.

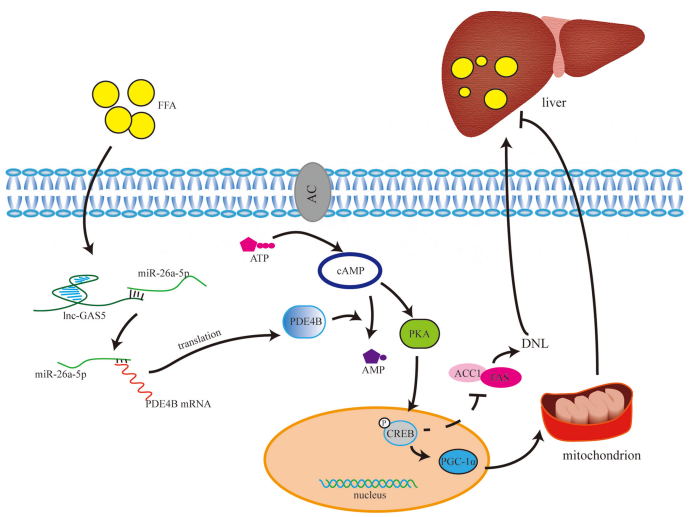

FIGURE 8 | The underlying mechanism of long non-coding RNA growth arrest specific 5 (GAS5) in regulating lipid metabolism. Under normal physiological conditions, cAMP is synthesised from ATP with the catalysis of adenylate cyclase. cAMP activates PKA to phosphorylate CREB, and phosphorylated CREB (p-CREB) upregulates PGC-1α and downregulates ACC1 and FAS expression. Therefore, through controlling the *de novo* lipogenesis (DNL) and mitochondrial function, high level of cAMP may reduce lipid accumulation in liver. cAMP is hydrolysed into AMP by phosphodiesterase, especially phosphodiesterase-4B in liver. GAS5 is upregulated in hepatocytes with high-fat treatment *via* the miR-26a-5p/PDE4B axis, which consumes cAMP, thereby promoting fat accumulation in the liver.

Furthermore, the overexpression of GAS5 suppresses the expression of PGC-1α and CPT-1α and aggravates hepatic lipid accumulation and liver damage.

In conclusion, the expression of GAS5 was increased in *in vivo* and *in vitro* fatty liver models. Moreover, GAS5 sponges with miR-26a-5p to upregulate PDE4B expression, thus modulating hepatic lipid metabolism *via* the cAMP/CREB pathway (**Figure 8**). This study provides a novel therapeutic strategy for downregulating GAS5 levels in fatty liver treatment.

DATA AVAILABILITY STATEMENT

The original contributions presented in the study are included in the article/**Supplementary Material**. Further inquiries can be directed to the corresponding authors.

ETHICS STATEMENT

The animal study was reviewed and approved by Animal Care and Use Committee of Fudan University.

AUTHOR CONTRIBUTIONS

XF, MJ, and SX contributed to conception and design of the study. YW and ZL analyzed the data. SX and XF wrote the first draft of the manuscript. MJ and QH wrote sections of the manuscript. All authors contributed to manuscript revision, read, and approved the submitted version.

FUNDING

The study was supported by Shanghai Science and Technology Committee (No. 15411969800) and Construction Project of Backup Discipline Platform of Jinshan Hospital Affiliated to Fudan University (No. HBXK-2021-2).

ACKNOWLEDGMENTS

We thank the help from the staff of the Laboratory Animal Department of Shanghai Public Health Clinical Center in animal experiments and Bullet Edits (www.bulletedits.cn) for editing, proofreading services.

SUPPLEMENTARY MATERIAL

The Supplementary Material for this article can be found online at: https://www.frontiersin.org/articles/10.3389/fendo.2022.889858/full#supplementary-material

REFERENCES

1. Younossi ZM, Koenig AB, Abdelatif D, Fazel Y, Henry L, Wymer M. Global Epidemiology of Nonalcoholic Fatty Liver Disease-Meta-Analytic Assessment of Prevalence, Incidence, and Outcomes. *Hepatology* (2016) 64(1):73–84. doi: 10.1002/hep.28431
2. Younossi Z, Tacke F, Arrese M, Chander Sharma B, Mostafa I, Bugianesi E, et al. Global Perspectives on Nonalcoholic Fatty Liver Disease and Nonalcoholic Steatohepatitis. *Hepatology* (2019) 69(6):2672–82. doi: 10.1002/hep.30251
3. Farrell GC, Larter CZ. Nonalcoholic Fatty Liver Disease: From Steatosis to Cirrhosis. *Hepatology* (2006) 43(2 Suppl 1):S99–S112. doi: 10.1002/hep.20973
4. Starley BQ, Calcagno CJ, Harrison SA. Nonalcoholic Fatty Liver Disease and Hepatocellular Carcinoma: A Weighty Connection. *Hepatology* (2010) 51 (5):1820–32. doi: 10.1002/hep.23594
5. Hall Z, Bond NJ, Ashmore T, Sanders F, Ament Z, Wang X, et al. Lipid Zonation and Phospholipid Remodeling in Nonalcoholic Fatty Liver Disease. *Hepatology* (2017) 65(4):1165–80. doi: 10.1002/hep.28953
6. Lambert JE, Ramos-Roman MA, Browning JD, Parks EJ. Increased *De Novo* Lipogenesis is a Distinct Characteristic of Individuals With Nonalcoholic Fatty Liver Disease. *Gastroenterology* (2014) 146(3):726–35. doi: 10.1053/j.gastro.2013.11.049
7. Softic S, Cohen DE, Kahn CR. Role of Dietary Fructose and Hepatic *De Novo* Lipogenesis in Fatty Liver Disease. *Dig Dis Sci* (2016) 61(5):1282–93. doi: 10.1007/s10620-016-4054-0
8. Begriche K, Igoudjil A, Pessayre D, Fromenty B. Mitochondrial Dysfunction in NASH: Causes, Consequences and Possible Means to Prevent it. *Mitochondrion* (2006) 6(1):1–28. doi: 10.1016/j.mito.2005.10.004
9. Paradies G, Paradies V, Ruggiero FM, Petrosillo G. Oxidative Stress, Cardiolipin and Mitochondrial Dysfunction in Nonalcoholic Fatty Liver Disease. *World J Gastroenterol* (2014) 20(39):14205–18. doi: 10.3748/wjg.v20.i39.14205
10. Iwabu M, Yamauchi T, Okada-Iwabu M, Sato K, Nakagawa T, Funata M, et al. Adiponectin and AdipoR1 Regulate PGC-1alpha and Mitochondria by Ca(2+) and AMPK/Sirt1. *Nature* (2010) 464(7293):1313–9. doi: 10.1038/nature08991
11. Puigserver P, Wu Z, Park CW, Graves R, Wright M, Spiegelman BM. A Cold-Inducible Coactivator of Nuclear Receptors Linked to Adaptive Thermogenesis. *Cell* (1998) 92(6):829–39. doi: 10.1016/s0092-8674(00)81410-5
12. Leone TC, Lehman JJ, Finck BN, Schaeffer PJ, Wende AR, Boudina S, et al. PGC-1alpha Deficiency Causes Multi-System Energy Metabolic Derangements: Muscle Dysfunction, Abnormal Weight Control and Hepatic Steatosis. *PLoS Biol* (2005) 3(4):e101. doi: 10.1371/journal.pbio.0030101
13. Hombach S, Kretz M. Non-Coding RNAs: Classification, Biology and Functioning. *Adv Exp Med Biol* (2016) 937:3–17. doi: 10.1007/978-3-319-42059-2_1
14. Ma M, Duan R, Shen L, Liu M, Ji Y, Zhou H, et al. The lncRNA Gm15622 Stimulates SREBP-1c Expression and Hepatic Lipid Accumulation by Sponging the miR-742-3p in Mice. *J Lipid Res* (2020) 61(7):1052–64. doi: 10.1194/jlr.RA120000664
15. Coccia EM, Cicala C, Charlesworth A, Ciccarelli C, Rossi GB, Philipson L, et al. Regulation and Expression of a Growth Arrest-Specific Gene (Gas5) During Growth, Differentiation, and Development. *Mol Cell Biol* (1992) 12 (8):3514–21. doi: 10.1128/mcb.12.8.3514-3521.1992
16. Smith CM, Steitz JA. Classification of Gas5 as a Multi-Small-Nucleolar-RNA (snoRNA) Host Gene and a Member of the 5'-Terminal Oligopyrimidine Gene Family Reveals Common Features of snoRNA Host Genes. *Mol Cell Biol* (1998) 18(12):6897–909. doi: 10.1128/MCB.18.12.6897
17. Gasic V, Stankovic B, Zukic B, Janic D, Dokmanovic L, Krstovski N, et al. Expression Pattern of Long Non-Coding RNA Growth Arrest-Specific 5 in the Remission Induction Therapy in Childhood Acute Lymphoblastic Leukemia. *J Med Biochem* (2019) 38(3):292–8. doi: 10.2478/jomb-2018-0038
18. Mourtada-Maarabouni M, Hasan AM, Farzaneh F, Williams GT. Inhibition of Human T-Cell Proliferation by Mammalian Target of Rapamycin (mTOR)

Antagonists Requires Noncoding RNA Growth-Arrest-Specific Transcript 5 (GAS5). *Mol Pharmacol* (2010) 78(1):19–28. doi: 10.1124/mol.110.064055
19. Yu F, Zheng J, Mao Y, Dong P, Lu Z, Li G, et al. Long Non-Coding RNA Growth Arrest-Specific Transcript 5 (GAS5) Inhibits Liver Fibrogenesis Through a Mechanism of Competing Endogenous RNA. *J Biol Chem* (2015) 290(47):28286–98. doi: 10.1074/jbc.M115.683813
20. Han MH, Lee JH, Kim G, Lee E, Lee YR, Jang SY, et al. Expression of the Long Noncoding RNA GAS5 Correlates With Liver Fibrosis in Patients With Nonalcoholic Fatty Liver Disease. *Genes (Basel)* (2020) 11(5):545. doi: 10.3390/genes11050545
21. Alshehri AS, El-Kott AF, El-Kenawy AE, Khalifa HS, AlRamlawy AM. Cadmium Chloride Induces non-Alcoholic Fatty Liver Disease in Rats by Stimulating miR-34a/SIRT1/FXR/p53 Axis. *Sci Total Environ* (2021) 784:147182. doi: 10.1016/j.scitotenv.2021.147182
22. Lee DH, Park SH, Ahn J, Hong SP, Lee E, Jang YJ, et al. Mir214-3p and Hnf4a/Hnf4alpha Reciprocally Regulate Ulk1 Expression and Autophagy in Nonalcoholic Hepatic Steatosis. *Autophagy* (2021) 17(9):2415–31. doi: 10.1080/15548627.2020.1827779
23. Xu H, Tian Y, Tang D, Zou S, Liu G, Song J, et al. An Endoplasmic Reticulum Stress-MicroRNA-26a Feedback Circuit in NAFLD. *Hepatology* (2021) 73 (4):1327–45. doi: 10.1002/hep.31428
24. Tan L, Xie Y, Yuan Y, Hu K. LncRNA GAS5 as miR-26a-5p Sponge Regulates the PTEN/PI3K/Akt Axis and Affects Extracellular Matrix Synthesis in Degenerative Nucleus Pulposus Cells. *Vitro Front Neurol* (2021) 12:653341. doi: 10.3389/fneur.2021.653341
25. Zhu C, Zhang H, Wei D, Sun Z. Silencing lncRNA GAS5 Alleviates Apoptosis and Fibrosis in Diabetic Cardiomyopathy by Targeting miR-26a/B-5p. *Acta Diabetol* (2021) 58(11):1491–501. doi: 10.1007/s00592-021-01745-3
26. Wang J, Zhu Y, Ni S, Liu S. LncRNA GAS5 Suppressed Proliferation and Promoted Apoptosis in Laryngeal Squamous Cell Carcinoma by Targeting MiR-26a-5p and Modifying Ulk2. *Cancer Manag Res* (2021) 13:871–87. doi: 10.2147/CMAR.S250778
27. Avila DV, Barker DF, Zhang J, McClain CJ, Barve S, Gobejishvili L. Dysregulation of Hepatic cAMP Levels *via* Altered Pde4b Expression Plays a Critical Role in Alcohol-Induced Steatosis. *J Pathol* (2016) 240(1):96–107. doi: 10.1002/path.4760
28. Guzman S, Dragan M, Kwon H, de Oliveira V, Rao S, Bhatt V, et al. Targeting Hepatic Kisspeptin Receptor Ameliorates Nonalcoholic Fatty Liver Disease in a Mouse Model. *J Clin Invest* (2022) 132(10):e145889. doi: 10.1172/JCI145889
29. Kota J, Chivukula RR, O'Donnell KA, Wentzel EA, Montgomery CL, Hwang HW, et al. Therapeutic microRNA Delivery Suppresses Tumorigenesis in a Murine Liver Cancer Model. *Cell* (2009) 137(6):1005–17. doi: 10.1016/j.cell.2009.04.021
30. Yan F, Wang Q, Lu M, Chen W, Song Y, Jing F, et al. Thyrotropin Increases Hepatic Triglyceride Content Through Upregulation of SREBP-1c Activity. *J Hepatol* (2014) 61(6):1358–64. doi: 10.1016/j.jhep.2014.06.037
31. Wu L, Mo W, Feng J, Li J, Yu Q, Li S, et al. Astaxanthin Attenuates Hepatic Damage and Mitochondrial Dysfunction in non-Alcoholic Fatty Liver Disease by Up-Regulating the FGF21/PGC-1alpha Pathway. *Br J Pharmacol* (2020) 177(16):3760–77. doi: 10.1111/bph.15099
32. De Vincentis A, Rahmani Z, Muley M, Vespasiani-Gentilucci U, Ruggiero S, Zamani P, et al. Long Noncoding RNAs in Nonalcoholic Fatty Liver Disease and Liver Fibrosis: State-of-the-Art and Perspectives in Diagnosis and Treatment. *Drug Discovery Today* (2020) 25(7):1277–86. doi: 10.1016/j.drudis.2020.05.009
33. Tao R, Hu S, Wang S, Zhou X, Zhang Q, Wang C, et al. Association Between Indel Polymorphism in the Promoter Region of lncRNA GAS5 and the Risk of Hepatocellular Carcinoma. *Carcinogenesis* (2015) 36(10):1136–43. doi: 10.1093/carcin/bgv099
34. DiStefano JK, Gerhard GS. Long Noncoding RNAs and Human Liver Disease. *Annu Rev Pathol* (2022) 17:1–21. doi: 10.1146/annurev-pathol-042320-115255
35. Lu S, Su Z, Fu W, Cui Z, Jiang X, Tai S. Altered Expression of Long non-Coding RNA GAS5 in Digestive Tumors. *Biosci Rep* (2019) 39(1): BSR20180789. doi: 10.1042/BSR20180789
36. Ruan X, Li P, Ma Y, Jiang CF, Chen Y, Shi Y, et al. Identification of Human Long Noncoding RNAs Associated With Nonalcoholic Fatty Liver Disease and Metabolic Homeostasis. *J Clin Invest* (2021) 131(1):e136336. doi: 10.1172/JCI136336
37. Diraison F, Moulin P, Beylot M. Contribution of Hepatic *De Novo* Lipogenesis and Reesterification of Plasma non Esterified Fatty Acids to Plasma Triglyceride Synthesis During Non-Alcoholic Fatty Liver Disease. *Diabetes Metab* (2003) 29(5):478–85. doi: 10.1016/s1262-3636(07)70061-7
38. Cohen CC, Li KW, Alazraki AL, Beysen C, Carrier CA, Cleeton RL, et al. Dietary Sugar Restriction Reduces Hepatic *De Novo* Lipogenesis in Adolescent Boys With Fatty Liver Disease. *J Clin Invest* (2021) 131(24):e150996. doi: 10.1172/JCI150996
39. Moore JB, Gunn PJ, Fielding BA. The Role of Dietary Sugars and *De Novo* Lipogenesis in non-Alcoholic Fatty Liver Disease. *Nutrients* (2014) 6 (12):5679–703. doi: 10.3390/nu6125679
40. Wang Q, Li S, Jiang L, Zhou Y, Li Z, Shao M, et al. Deficiency in Hepatic ATP-Citrate Lyase Affects VLDL-Triglyceride Mobilization and Liver Fatty Acid Composition in Mice. *J Lipid Res* (2010) 51(9):2516–26. doi: 10.1194/jlr.M003335
41. Mao J, DeMayo FJ, Li H, Abu-Elheiga L, Gu Z, Shaikenov TE, et al. Liver-Specific Deletion of Acetyl-CoA Carboxylase 1 Reduces Hepatic Triglyceride Accumulation Without Affecting Glucose Homeostasis. *Proc Natl Acad Sci U.S.A.* (2006) 103(22):8552–7. doi: 10.1073/pnas.0603115103
42. Chirala SS, Chang H, Matzuk M, Abu-Elheiga L, Mao J, Mahon K, et al. Fatty Acid Synthesis is Essential in Embryonic Development: Fatty Acid Synthase Null Mutants and Most of the Heterozygotes Die. *Utero Proc Natl Acad Sci U.S.A.* (2003) 100(11):6358–63. doi: 10.1073/pnas.0931394100
43. Zhu M, Chen H, Zhou S, Zheng L, Li X, Chu R, et al. Iron Oxide Nanoparticles Aggravate Hepatic Steatosis and Liver Injury in Nonalcoholic Fatty Liver Disease Through BMP-SMAD-Mediated Hepatic Iron Overload. *Nanotoxicology* (2021) 15(6):761–78. doi: 10.1080/17435390.2021.1919329
44. Berger JM, Moon YA. Increased Hepatic Lipogenesis Elevates Liver Cholesterol Content. *Mol Cells* (2021) 44(2):116–25. doi: 10.14348/molcells.2021.2147
45. Kartsoli S, Kostara CE, Tsimihodimos V, Bairaktari ET, Christodoulou DK. Lipidomics in non-Alcoholic Fatty Liver Disease. *World J Hepatol* (2020) 12 (8):436–50. doi: 10.4254/wjh.v12.i8.436
46. Clugston RD, Gao MA, Blaner WS. The Hepatic Lipidome: A Gateway to Understanding the Pathogenes is of Alcohol-Induced Fatty Liver. *Curr Mol Pharmacol* (2017) 10(3):195–206. doi: 10.2174/1874467208666150817111419
47. Cesana M, Cacchiarelli D, Legnini I, Santini T, Sthandier O, Chinappi M, et al. A Long Noncoding RNA Controls Muscle Differentiation by Functioning as a Competing Endogenous RNA. *Cell* (2011) 147(2):358–69. doi: 10.1016/j.cell.2011.09.028
48. Ali O, Darwish HA, Eldeib KM, Abdel Azim SA. miR-26a Potentially Contributes to the Regulation of Fatty Acid and Sterol Metabolism *In Vitro* Human HepG2 Cell Model of Nonalcoholic Fatty Liver Disease. *Oxid Med Cell Longev* (2018) 2018:8515343. doi: 10.1155/2018/8515343
49. He Q, Li F, Li J, Li R, Zhan G, Li G, et al. MicroRNA-26a-Interleukin (IL)-6-IL-17 Axis Regulates the Development of non-Alcoholic Fatty Liver Disease in a Murine Model. *Clin Exp Immunol* (2017) 187(1):174–84. doi: 10.1111/cei.12838
50. Ding D, Ye G, Lin Y, Lu Y, Zhang H, Zhang X, et al. MicroRNA-26a-CD36 Signaling Pathway: Pivotal Role in Lipid Accumulation in Hepatocytes Induced by PM2.5 Liposoluble Extracts. *Environ pollut* (2019) 248:269–78. doi: 10.1016/j.envpol.2019.01.112
51. Di Sessa A, Riccio S, Pirozzi E, Verde M, Passaro AP, Umano GR, et al. Advances in Paediatric Nonalcoholic Fatty Liver Disease: Role of Lipidomics. *World J Gastroenterol* (2021) 27(25):3815–24. doi: 10.3748/wjg.v27.i25.3815
52. Luukkonen PK, Qadri S, Ahlholm N, Porthan K, Mannisto V, Sammalkorpi H, et al. Distinct Contributions of Metabolic Dysfunction and Genetic Risk Factors in the Pathogenesis of Non-Alcoholic Fatty Liver Disease. *J Hepatol* (2021) 76(3):526–535. doi: 10.1016/j.jhep.2021.10.013
53. Kleinboelting S, van den Heuvel J, Steegborn C. Structural Analysis of Human Soluble Adenylyl Cyclase and Crystal Structures of its Nucleotide Complexes-Implications for Cyclase Catalysis and Evolution. *FEBS J* (2014) 281 (18):4151–64. doi: 10.1111/febs.12913
54. Wang B, Tsakiridis EE, Zhang S, Llanos A, Desjardins EM, Yabut JM, et al. The Pesticide Chlorpyrifos Promotes Obesity by Inhibiting Diet-Induced

Thermogenesis in Brown Adipose Tissue. *Nat Commun* (2021) 12(1):5163. doi: 10.1038/s41467-021-25384-y
55. Zhang WS, Pan A, Zhang X, Ying A, Ma G, Liu BL, et al. Inactivation of NF-Kappab2 (P52) Restrains Hepatic Glucagon Response *via* Preserving PDE4B Induction. *Nat Commun* (2019) 10(1):4303. doi: 10.1038/s41467-019-12351-x
56. Zhang K, Kim H, Fu Z, Qiu Y, Yang Z, Wang J, et al. Deficiency of the Mitochondrial NAD Kinase Causes Stress-Induced Hepatic Steatosis in Mice. *Gastroenterology* (2018) 154(1):224–37. doi: 10.1053/j.gastro.2017.09.010
57. Herzig S, Hedrick S, Morantte I, Koo SH, Galimi F, Montminy M. CREB Controls Hepatic Lipid Metabolism Through Nuclear Hormone Receptor PPAR-Gamma. *Nature* (2003) 426(6963):190–3. doi: 10.1038/nature02110
58. Tai CC, Chen CY, Lee HS, Wang YC, Li TK, Mersamm HJ, et al. Docosahexaenoic Acid Enhances Hepatic Serum Amyloid A Expression *via* Protein Kinase A-Dependent Mechanism. *J Biol Chem* (2009) 284(47):32239–47. doi: 10.1074/jbc.M109.024661
59. Sang L, Ju HQ, Yang Z, Ge Q, Zhang Z, Liu F, et al. Mitochondrial Long non-Coding RNA GAS5 Tunes TCA Metabolism in Response to Nutrient Stress. *Nat Metab* (2021) 3(1):90–106. doi: 10.1038/s42255-020-00325-z
60. Piccinin E, Villani G, Moschetta A. Metabolic Aspects in NAFLD, NASH and Hepatocellular Carcinoma: The Role of PGC1 Coactivators. *Nat Rev Gastroenterol Hepatol* (2019) 16(3):160–74. doi: 10.1038/s41575-018-0089-3
61. Lin J, Handschin C, Spiegelman BM. Metabolic Control Through the PGC-1 Family of Transcription Coactivators. *Cell Metab* (2005) 1(6):361–70. doi: 10.1016/j.cmet.2005.05.004
62. Spiegelman BM, Heinrich R. Biological Control Through Regulated Transcriptional Coactivators. *Cell* (2004) 119(2):157–67. doi: 10.1016/j.cell.2004.09.037
63. Aharoni-Simon M, Hann-Obercyger M, Pen S, Madar Z, Tirosh O. Fatty Liver Is Associated With Impaired Activity of PPARgamma-Coactivator 1alpha (PGC1alpha) and Mitochondrial Biogenesis in Mice. *Lab Invest* (2011) 91 (7):1018–28. doi: 10.1038/labinvest.2011.55
64. Finck BN, Gropler MC, Chen Z, Leone TC, Croce MA, Harris TE, et al. Lipin 1 is an Inducible Amplifier of the Hepatic PGC-1alpha/PPARalpha Regulatory Pathway. *Cell Metab* (2006) 4(3):199–210. doi: 10.1016/j.cmet.2006.08.005
65. Song S, Attia RR, Connaughton S, Niesen MI, Ness GC, Elam MB, et al. Peroxisome Proliferator Activated Receptor Alpha (PPARalpha) and PPAR Gamma Coactivator (PGC-1alpha) Induce Carnitine Palmitoyltransferase IA (CPT-1a) *via* independent gene elements. *Mol Cell Endocrinol* (2010) 325(1-2):54–63. doi: 10.1016/j.mce.2010.05.019

Conflict of Interest: The authors declare that the research was conducted in the absence of any commercial or financial relationships that could be construed as a potential conflict of interest.

frontiers | Frontiers in Endocrinology

TYPE Original Research
PUBLISHED 09 August 2022
DOI 10.3389/fendo.2022.917041

OPEN ACCESS

EDITED BY
Julang Li,
University of Guelph, Canada

REVIEWED BY
Jacopo Sabbatinelli,
Università Politecnica delle Marche, Italy
Georgios K. Dimitriadis,
King's College Hospital NHS Foundation Trust, United Kingdom

*CORRESPONDENCE
Alexandra E. Butler
aeb91011@gmail.com

†These authors share senior authorship

SPECIALTY SECTION
This article was submitted to Diabetes: Molecular Mechanisms, a section of the journal Frontiers in Endocrinology

RECEIVED 10 April 2022
ACCEPTED 21 July 2022
PUBLISHED 09 August 2022

CITATION
Ramanjaneya M, Priyanka R, Bensila M, Jerobin J, Pawar K, Sathyapalan T, Abou-Samra AB, Halabi NM, Moin ASM, Atkin SL and Butler AE (2022) MiRNA and associated inflammatory changes from baseline to hypoglycemia in type 2 diabetes. *Front. Endocrinol.* 13:917041. doi: 10.3389/fendo.2022.917041

MiRNA and associated inflammatory changes from baseline to hypoglycemia in type 2 diabetes

Manjunath Ramanjaneya[1,2], Ruth Priyanka[1,2], Milin Bensila[1,2], Jayakumar Jerobin[1,2], Krunal Pawar[3], Thozhukat Sathyapalan[4], Abdul Badi Abou-Samra[2], Najeeb M. Halabi[5], Abu Saleh Md Moin[6], Stephen L. Atkin[6†] and Alexandra E. Butler[6*†]

[1]Qatar Metabolic Institute, Hamad Medical Corporation, Doha, Qatar, [2]Translational Research Institute, Hamad Medical Corporation, Doha, Qatar, [3]Amity Institute of Biotechnology, Amity University, Jaipur, India, [4]Academic Endocrinology, Diabetes and Metabolism, Hull York Medical School, Hull, United Kingdom, [5]Weill Cornell Medicine in Qatar, Education City, Qatar Foundation, Doha, Qatar, [6]Research Department, Royal College of Surgeons in Ireland Bahrain, Adliya, Bahrain

Objective: Hypoglycemia in type 2 diabetes (T2D) increases morbidity and mortality but the underlying physiological response is still not fully understood, though physiological changes are still apparent 24 hours after the event. Small noncoding microRNA (miRNA) have multiple downstream biological effects that may respond rapidly to stress. We hypothesized that hypoglycemia would induce rapid miRNA changes; therefore, this pilot exploratory study was undertaken.

Methods: A pilot prospective, parallel study in T2D (n=23) and controls (n=23). Insulin-induced hypoglycemia (2mmol/l: 36mg/dl) was induced and blood sampling performed at baseline and hypoglycemia. Initial profiling of miRNA was undertaken on pooled samples identified 96 miRNA that were differentially regulated, followed by validation on a custom designed 112 miRNA panel.

Results: Nine miRNAs differed from baseline to hypoglycemia in control subjects; eight were upregulated: miR-1303, miR-let-7e-5p, miR-1267, miR-30a-5p, miR-571, miR-661, miR-770-5p, miR-892b and one was downregulated: miR-652-3p. None of the miRNAs differed from baseline in T2D subjects.

Conclusion: A rapid miRNA response reflecting protective pathways was seen in control subjects that appeared to be lost in T2D, suggesting that mitigating responses to hypoglycemia with blunting of the counter-regulatory response in T2D occurs even in patients with short duration of disease.

Clinical trial registration: https://clinicaltrials.gov/ct2/show/NCT03102801?term=NCT03102801&draw=2&rank=1, identifier NCT03102801.

KEYWORDS
Type 2 diabetes, hypoglycemia, miRNA, metabolic pathways, proteomics

Introduction

Severe hypoglycemia in type 2 diabetes (T2D) is associated with cardiovascular-related events that are a risk for increased mortality (1–6), observations that have been reflected in the reports from both retrospective and longitudinal cohort studies (7–10). Causative factors underlying the clinical observations resulting from hypoglycemia include endothelial and thrombotic dysfunction (11–13), oxidative and inflammatory stress (14, 15) and the heat shock protein response (16), but the diverse range of underlying mechanistic dysfunctions resulting from hypoglycemia have not been completely clarified.

MicroRNAs (miRNAs) are non-coding RNAs of ~22 nucleotides in length that function post-transcriptionally as regulators of gene expression; their inhibitory actions lead to mRNA cleavage, repression of translation and mRNA decay (17–20). Each miRNA may impact expression of multiple target mRNAs, thus affecting an array of cellular and biologic pathways. MiRNAs are thought to play a role in many disease states including diabetes and its associated co-morbidities (21, 22). A growing body of evidence shows the critical role of miRNAs in cellular stress responses (23), such as in diabetes, where, for example, miR-126 is involved in vascular repair (24), miR-146 is associated with proinflammatory factors and oxidative stress (25) and knockdown of miR-185 may increase oxidative stress (26, 27). What is also apparent is that the miRNA response can be relatively rapid and may occur within one hour of a stress event (23, 28, 29).

Changes in glucose may modulate miRNA changes with diminished expression of miR-215-5p miR-296-5p and miR-497-3p levels in response to high glucose in the human myometrium (30), and miRNA-375 (miR-375), miRNA-155 (miR-155), miRNA- 21 (miR-21), miRNA-33 (miR-33), the let-7 family have been highlighted to be related to and glucometabolic regulation (31).

In vitro, the low glucose condition decreased the expression of miRNA-17-5p and miRNA-20a-5p in hepatoma cells (32), whilst several miRNA were modulated by low glucose in embryonal mouse hypothalamus cells (33). In animal models, hypoglycemia resulted in ventromedial hypothalamus downregulation of miR7a-5p that, when targeted overexpression was used, the epinephrine response to hypoglycemia was restored (34). In a study restricted to 14 patients with type 2 diabetes alone who underwent a hypoglycemic challenge, selective miRNA analysis restricted to those associated with platelet expression was undertaken on hsa-miR-106a.5p, hsa-miR-126-3p, hsa-miR-126-5p, hsa-miR-15a-5p, hsa-miR-15b-3p, has-miR-15b-5p, hsa-miR-16-5p, hsa-miR-223-3p, hsa-miR-223-5p, hsa-miR-129-2-3p. The results focused on longer term changes of 1 day and 7 days after the hypoglycemic episode but showed that miR-106a-5p, miR-15b, miR-15a, miR-16-5p, miR-223 and miR-126 were increased (35). However, the miRNA response and the rapidity of the response to the development of hypoglycemia in humans remains unknown, but hypothetically the rapid modulation of miRNA may drive subsequent pathophysiological changes; therefore, this pilot exploratory study was undertaken.

Methods

Study design

This pilot prospective parallel study was performed in 46 Caucasian subjects (age range 40–70 years), T2D (n = 23) and control (n = 23), at the Diabetes Centre at Hull Royal Infirmary (36). All T2D patients had diabetes duration <10 years and treatment with a stable dose of medication (metformin, angiotensin converting enzyme inhibitor/angiotensin receptor blocker and/or statin) over the 3-month period prior to participation in the study. For anti-diabetic therapy in the T2D group, only metformin was allowed and HbA1c was required to be <10% (86 mmol/mol), with no hypoglycemic unawareness/hypoglycemia within the 3-month period prior to participation, and no diabetes related complications. For control subjects, an oral glucose tolerance test (OGTT) was used to exclude diabetes. All participants had body mass index (BMI) of 18-49kg/m^2, normal screening blood biochemistry, no cancer history or contraindication to undertake insulin infusion to hypoglycemia.

Study participants

A medical history with clinical examination, routine blood tests plus an electrocardiogram was performed on all participants. Hypoglycemia was induced by a continuous insulin infusion, as previously detailed (11), with blood samples taken at baseline and hypoglycemia. The infusion from baseline to severe hypoglycemia

was over a 1-hour timeframe with blood glucose dropping from 3.5 to 2 mmol/l over an approximately 25-minute period.

Each participant provided written and signed informed consent, and the trial conducted per the Declaration of Helsinki. Approval for the trial was granted by the North West-Greater Manchester East Research Ethics Committee (REC number:16/NW/0518); trial registration at www.clinicaltrials.gov (NCT03102801) on 06/04/2017.

Insulin infusion

The insulin infusion was performed as previously detailed (11). "Following an overnight fast, 30–60 min prior to the commencement of the test (0830 h), bilateral ante-cubital fossa indwelling cannulas were inserted. To induce hypoglycemia, soluble intravenous insulin (Humulin S, Lilly, UK) was given in a pump starting at a dose of 2.5 mU/kg body weight/min with an increment of 2.5 mU/kg body weight/min every 15 min by hypoglycemic clamp, until two readings of capillary blood glucose measured by a glucose analyser (HemoCue glucose 201 +) ≤ 2.2 mmol/L (< 40 mg/dl) or a reading of ≤ 2.0 mmol/L (36 mg/dl) was achieved. Initially, patients with T2D were clamped to euglycemia (5mmol/l; 90mg/dl), then subsequently to hypoglycemia. The blood sample schedule was timed subsequently in respect to the time point that hypoglycemia occurred. Following the identification of hypoglycemia, intravenous glucose was given in the form of 150 ml of 10% dextrose and a repeat blood glucose check was performed after 5 min if blood glucose was still < 4.0 mmol/L".

Biochemical markers

As previously described (36), "blood samples were separated immediately by centrifugation at 2000 g for 15 min at 4°C, and the aliquots were stored at -80°C, within 30-min of blood collection, until batch analysis. Fasting plasma glucose (FPG), total cholesterol, triglycerides, and high-density lipoprotein (HDL) cholesterol levels were measured enzymatically using a Beckman AU 5800 analyser (Beckman-Coulter, High Wycombe, UK)".

RNA extraction from human plasma

Total RNA was extracted using the MagMAX™ mirVana™ RNA Isolation Kit (Thermo Fischer Scientific, Waltham, MA, USA) on an automated KingFisher instrument (Thermo Fischer Scientific, Waltham, MA, USA). The MagMAX™ mirVana™ RNA isolation kit is a magnetic bead-based kit that uses MagMAX magnetic-bead technology for efficient isolation of total RNA from plasma samples from 100 µl of human plasma.

Expression analysis of microRNA by taqman openarray human advanced microRNA panel

2 µl of the extracted total RNA was used for cDNA conversion using TaqMan™ Advanced miRNA cDNA Synthesis Kit as per manufacturer's recommended protocol. Given the low abundance of miRNA in plasma samples, cDNA was preamplified prior to the final real-time PCR step. 1:20 diluted cDNA was mixed with 2X TaqMan OpenArray Real-Time Master Mix solution to perform real-time PCR on the OpenArray plate. 5 µL sample of PCR reactions was pipetted into each well of a 384-well plate and samples with the master mix were loaded from the 384-well sample plate onto the OpenArray plate using the OpenArrayAccuFill System. The PCR was performed on the QuantStudio 12K Flex Real-Time PCR System (Thermo Fischer Scientific, Waltham, MA, USA). The miRNA measurements were done in two phases. 1) profiling and 2) validation. Initially profiling was done using pooled samples (4 in each group) obtained from 12 subjects in both control and diabetes group at baseline and at hypoglycemia. Profiling for miRNA was performed using standard The TaqMan® OpenArray® Human MicroRNA Panel, QuantStudio™ 12K Flex panel which is a fixed content panel that contains 754 well-characterized human miRNA sequences. Profiling was done to identify lead targets for validation according to the manufacturer's recommended protocol. Profiling experiments were done in a set of pooled samples taken from both the baseline and hypoglycemia timepoints and using default miRNA panels which consisted of 754 miRNAs. From this pooled sample data analysis, 96 miRNA that were differentially regulated were selected for the validation phase. Validation was done on custom designed 112 miRNA panel which included 96 miRNAs identified from the profiling phase, internal controls and other miRNAs that were published in the literature to be differentially expressed in patients with diabetes-related complications. The miRNA validation was done on diabetic and control subject samples, n=23 per group, at baseline and at hypoglycemia. The miRNA expressions were quantified using ExpressionSuite Software (Thermo Fischer Scientific, Waltham, MA, USA) data-analysis tool that utilizes the comparative Cτ (ΔΔCτ) method to accurately quantify relative miRNA expressions. ExpressionSuite generates the results in the form of Rq values, which are equivalent to the log2 scale, therefore any changes indicate a log2 fold change.

Ingenuity Pathway Analysis (IPA) software (Qiagen, Germantown, Maryland, USA) allows for data analysis together with integration of data derived from an array of experimental datasets, including gene expression and miRNA. Here, we performed IPA to illustrate the canonical pathways related to the top 10 altered miRNAs in control and T2D subjects highlighted in this study.

Statistics

There was no information regarding changes in miRNA on which to base a sample size calculation. For such pilot studies, Birkett and Day (37) suggest a minimum of 20 degrees of freedom to estimate variance from which a larger trial could be powered, hence 23 subjects in each group were recruited. SPSS (v22, Chicago, Illinois) was used for statistical analysis. Descriptive data is presented as mean ± SD for continuous data and n (%) for categorical data. T-tests or Mann Whitney tests were used to compare means/medians as appropriate. Mean normalization was performed before analysis using the global mean of each miRNA. Normalization was performed using GenEx software (provided with the Bioanalyzer) to achieve a global mean of all miRNAs with Ct <35. An unpaired t-test was used to test paired changes between T2D and controls in miRNA levels.

Results

Demographic and clinical characteristics of the study participants are shown in Table 1. Those subjects with T2D were of relatively short 4.5-year disease duration (38), were free of microvascular and macrovascular complications, had an increased BMI, and with lower total cholesterol and HDL compared to controls.

All subjects experienced neuroglycopenic symptoms, feeling tremulous and sweating, as blood glucose was lowered, though this was transient and reversed quickly as soon as the hypoglycemic target was reached which was immediately reversed with dextrose.

There were no differences in miRNAs between T2D and controls at baseline, as shown in Supplementary Table 1, or at hypoglycemia. The top 10 miRNA with the greatest changes from baseline to hypoglycemia are shown in Table 2, in which it can be seen that 9 of the miRNAs differed significantly in controls (eight were upregulated: miR-1303, miR-let-7e-5p, miR-1267, miR-30a-5p, miR-571, miR-661, miR-770-5p and miR-892b, whilst one was downregulated: miR-652-3p); mean Relative Quantification (RQ) fold changes for these top 10 miRNAs are shown in Figure 1. Notably, no miRNAs differed significantly from baseline to hypoglycemia in T2D subjects, though mean RQ fold changes for the top 10 miRNAs that showed differing expression are shown in Figure 2.

All of the 112 miRNA that were measured in this customized panel in the validation phase of this study are shown in Supplementary Table 2.

Ingenuity Pathway Analysis (IPA) was performed on the top 10 altered miRNAs in control (Figure 3) and T2D (Figure 4) subjects. Specifically focusing on the top 10 miRNAs found in T2D (as shown in Table 2), nine of these miRNAs were associated with neurological disease giving a score of $p<0.04–p<4^{14}$ (the score calculates the likelihood that the network eligible molecules are found as part of the network by random chance alone; mathematically the score is the negative exponent of the right-tailed Fisher's exact test). In addition, nine of these miRNAs were associated with organismal injury and abnormalities that are associated with diabetes complications, with a score of $p<0.05–p<4^{14}$.

Discussion

The novelty of this study was the demonstration that miRNAs are both up-regulated and down-regulated at hypoglycemia, an insult that occurred within 1-hour of initiating the insulin infusion, and that these changes were only seen in controls and not in T2D. There have been no human studies in the literature detailing early miRNAs changes

TABLE 1 Demographic and clinical characteristics of the study participants.

Baseline	Type 2 Diabetes (n=23)	Controls (n=23)	p-value
Age (years)	64 ± 8	60 ± 10	0.15
Sex (M/F)	12/11	11/12	0.77
Weight (kg)	90.9 ± 11.1	79.5 ± 8.8	<0.0001
Height (cm)	167 ± 14	169 ± 5	0.64
BMI (kg/m^2)	32 ± 4	28 ± 3	<0.0001
Duration of diabetes (years)	4.5 ± 2.2	N/A	
HbA1c (mmol/mol)	51.2 ± 11.4	37.2 ± 2.2	<0.0001
HbA1c (%)	6.8 ± 1.0	5.6 ± 0.2	<0.0001
Total cholesterol (mmol/l)	4.2 ± 1.0	4.8 ± 0.8	0.014
Triglyceride (mmol/l)	1.7 ± 0.7	1.3 ± 0.6	0.06
HDL-cholesterol (mmol/l)	1.1 ± 0.3	1.5 ± 0.4	0.001
LDL-cholesterol (mmol/l)	2.2 ± 0.8	2.7 ± 0.9	0.05
CRP (mg/l)	3.1 ± 2.9	5.3 ± 0.3	0.66

BMI, Body mass index; BP, Blood pressure; HDL-cholesterol, High density lipoprotein cholesterol; LDL-cholesterol, Low density lipoprotein cholesterol; CRP, C-reactive protein; HbA1c, Hemoglobin A1c.

10.3389/fendo.2022.917041

TABLE 2 Top 10 miRNAs that changed from baseline to hypoglycemia in T2D and control subjects in the validation experiment.

CONTROLS Target Name	Rq	P-Value	T2D Target Name	Rq	P-Value
hsa-miR-1303_478698_mir	2.26	0.01	hsa-miR-106b-5p_478412_mir	4.60	0.06
hsa-miR-652-3p_478189_mir	0.77	0.02	hsa-miR-194-5p_477956_mir	0.70	0.11
hsa-let-7e-5p_478579_mir	1.93	0.03	hsa-let-7g-5p_478580_mir	1.19	0.14
hsa-miR-1267_478672_mir	1.93	0.03	hsa-let-7d-3p_477848_mir	2.61	0.15
hsa-miR-30a-5p_479448_mir	1.93	0.03	hsa-miR-181b-5p_478583_mir	1.32	0.17
hsa-miR-571_479054_mir	1.93	0.03	hsa-miR-152-3p_477921_mir	1.88	0.17
hsa-miR-661_479144_mir	1.93	0.03	hsa-miR-195-5p_477957_mir	0.79	0.17
hsa-miR-770-5p_479178_mir	1.93	0.03	hsa-miR-181a-5p_477857_mir	1.36	0.18
hsa-miR-892b_479198_mir	1.93	0.03	hsa-miR-222-3p_477982_mir	1.14	0.19
hsa-miR-423-5p_478090_mir	0.81	0.07	hsa-miR-342-3p_478043_mir	1.32	0.21

Rq, relative level of miRNA expression.

in response to modulation of blood glucose to hypoglycemia with which to compare, and therefore future studies will be needed to confirm these findings. In a study restricted to 14 patients with type 2 diabetes who underwent a hypoglycemic challenge but without a control population, selective miRNA analysis derived from platelet expression showed that upregulation of the miRNA was seen at 1 day and 7 days but no miRNA analysis was reported in the first 24 hours (35). The control population in this study were diabetes free and represented an optimal response to hypoglycemia and showed that the miRNA changes seen were marked and differed significantly from the T2D subjects, suggesting that even in patients with a short duration of diabetes (i.e. less than 10 years after which hypoglycemic unawareness may develop, the

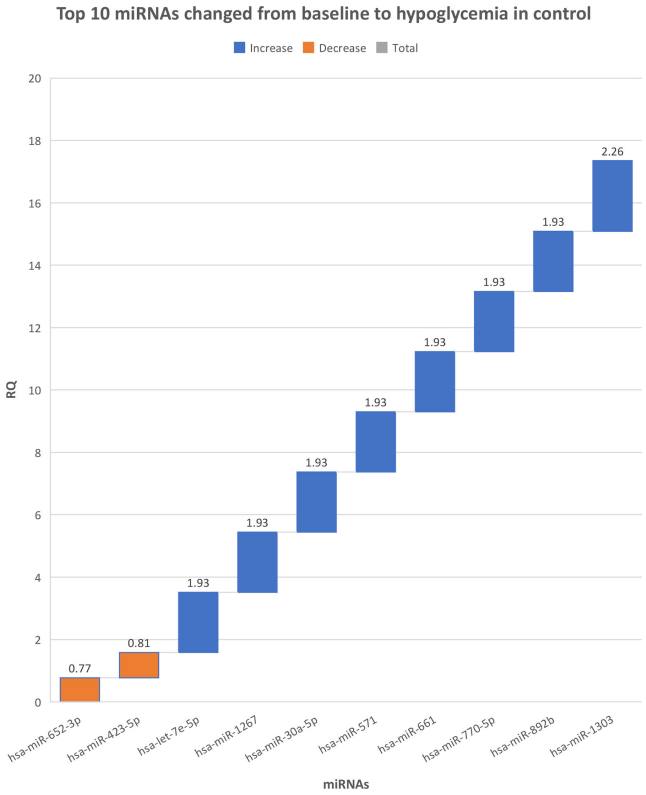

FIGURE 1
The top 10 miRNAs that changed from baseline to hypoglycemia in control subjects. RQ, mean relative quantification.

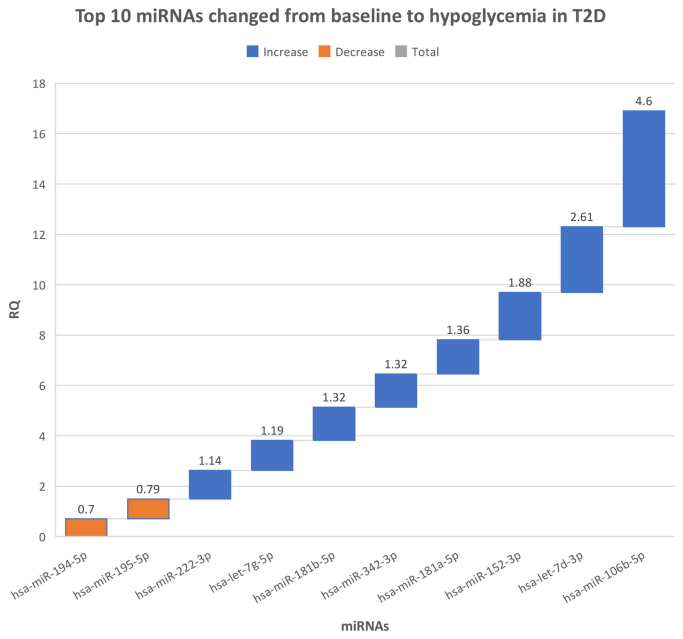

FIGURE 2
The top 10 miRNAs that changed from baseline to hypoglycemia in type 2 diabetes subjects. RQ, mean relative quantification.

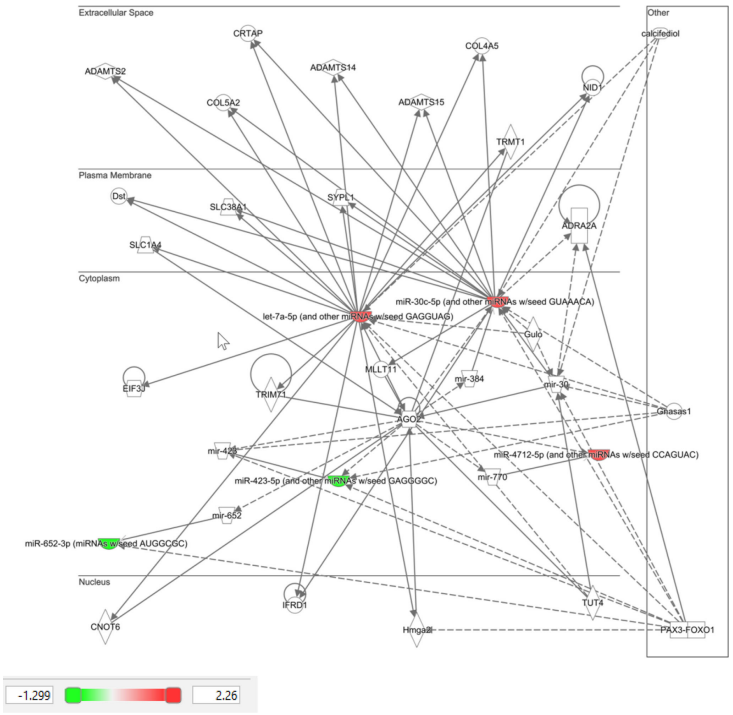

FIGURE 3
Ingenuity pathway analysis of top 10 miRNA that showed differential expression in control subjects in response to hypoglycemia.

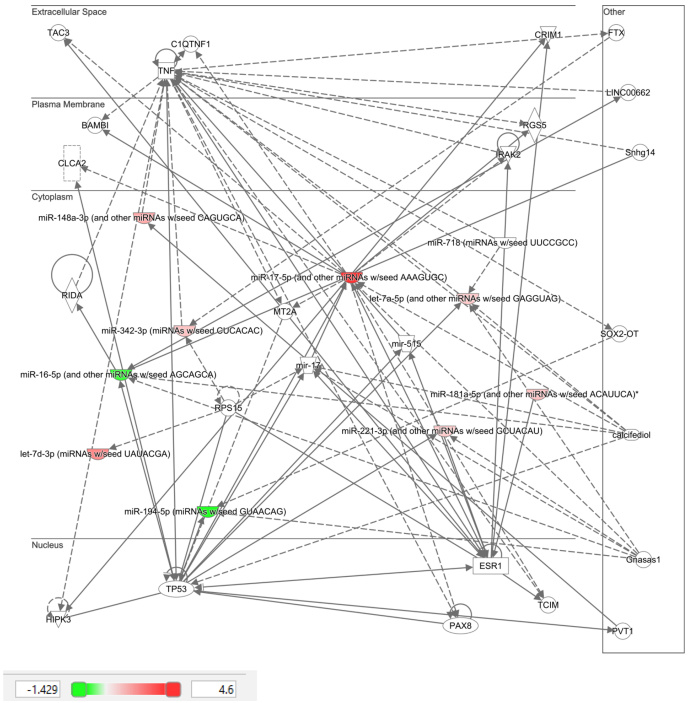

FIGURE 4
Ingenuity pathway analysis of top 10 miRNA that showed differential expression in type 2 diabetic subjects in response to hypoglycemia.

physiological response to hypoglycemia is altered and perhaps blunted, a phenomenon better recognised in patients with T2D of longer duration (39, 40). In animal models, experimentally induced recurrent hypoglycemia resulted in ventromedial hypothalamus downregulation of miR7a-5p that, when targeted overexpression was used, the epinephrine response to hypoglycemia was restored (34). Overall, many of the miRNAs that were significantly different in controls have been associated with potential beneficial actions, suggesting that their changes may be protective, and that this protection is lost, or potentially delayed, in T2D. Previously, we have looked at metadrenaline and nor-metadrenaline in a hypoglycemic study in a separate cohort that showed differences at 24-hours but not at the point of hypoglycemia (15) and therefore these were not measured in this study. It is well described in the literature that the growth hormone and cortisol responses occur following the onset of hypoglycemia and, as the samples for miRNA measurement were taken at the exact timepoint of hypoglycemia, they would not be expected to be elevated as indicated by prolactin levels that did not differ either between or within groups (data not shown).

IPA clearly showed that the top 10 miRNAs in T2D are likely to be part of specific disease pathways; the neurological disease pathway encompasses Alzheimer's disease that is associated with type 2 diabetes (41) and the organismal injury and abnormalities pathway that is associated with diabetes complications. While no individual miRNA was significant in T2D due to patient variability, the top 10 most significant miRNAs were significantly associated with specific diseases that may be diabetes related.

MiR-1303 was upregulated by hypoglycemia and has been associated with T2D, particularly in patients with complications (42); however, its exact role in diabetes is unclear. Within tumor biology, miR-1303 is regulated by the long non coding RNA BCRT1, and the increase in miR-1303 was associated with decreased cellular proliferation that may be of importance in microvascular complication development and therefore may be protective in this case.

MiR-let-7e-5p was also upregulated by hypoglycemia and has been shown to be upregulated by exercise (43), suggesting that stimulus-driven higher levels may be of benefit. MiR-let-7e-5p is down-regulated in DVT patients and overexpression of miR-let-7e-5p enhances the ability for thrombus revascularization in a rat model of venous thrombosis (44), suggesting a beneficial effect on thrombosis; however, its role in diabetes is unclear at present.

MiR-1267 was upregulated by low glucose and has been noted to be upregulated in podocytes (45), suggestive of a possible role in diabetic nephropathy, though this is speculative.

MiR-30a-5p was upregulated and has been reported to be a potential biomarker for T2D (46). In tumor biology and other models, upregulation is associated with a reduction of cellular growth (47) and a reduction of oxidative stress (48), and its upregulation may be nephroprotective against high glucose (49).

MiR-571 was upregulated by hypoglycemia and, together with miR-1303, it has been associated with T2D, particularly in patients with complications (42), most particularly microvascular complications (50). Similarly, miR-661 was upregulated and, together with miR-1303 and miR-571, it has been related to the development of microvascular complications (50), including nephropathy (42).

MiR-770-5p was upregulated in low glucose and its expression has been associated with podocyte inflammation and apoptosis (51, 52) and, together with miR-661 and miR-571, it was associated with diabetes microvascular complications (50).

MiR-892 was upregulated and has been shown to activate NF-kB, with a reduction in cellular proliferation in tumour models (53), and may have an effect on angiogenesis but its role in the development or protection against diabetes related complications needs clarification.

MiR-652-3p was downregulated by hypoglycemia, and, in a meta-analysis, its reduction was associated with T2D (54); its downregulation by statins has a protective effect on the endothelium (55) and perhaps its downregulation here is a reflection of a protective effect.

A study strength is that the T2D participants had short disease duration and relative treatment naïvete. Limitations include small study numbers, as a larger population may have shown additional miRNA changes. Additionally, the time course was limited to baseline to the point of hypoglycemia, though marked changes in miRNA levels in controls were apparent during that timeframe. The increased BMI of the T2D participants should not have altered the hypoglycemia-induced miRNA changes. As participants were Caucasian, these results may not be generalizable to other ethnicities. In future studies, it would be of interest to perform a time course to determine resolution of the miRNA levels in controls and whether miRNA changes showed a lag in T2D, occurring at a later time point. It is possible that the fundamental differences in the miRNA response between T2D and controls seen here could be due to a delayed response in T2D, an important point that should be addressed in future studies. Alternatively, it is important to bear in mind that hypoglycemia does not occur in normal controls and, in the face of this abnormal stimulus, then the response may be an abreaction. Of note, serum measurement of the individual miRNAs may not reflect cellular levels or activity. Assessment of the changes in miRNA at the tissue level are critical to determine the significance of the circulatory changes and their clinical application; whilst this was beyond the scope of our study, future studies should be undertaken to address this.

In conclusion, this study has shown, for the first time, rapid miRNA responses to hypoglycemia, of protective mechanisms in control subjects that appeared to be lost in T2D. Taken together, this suggests that mitigating responses to hypoglycemia with blunting of the counter-regulatory response in T2D occurs even in T2D with a short duration of disease.

Data availability statement

The original contributions presented in the study are included in the article/Supplementary Material. Further inquiries can be directed to the corresponding author.

Ethics statement

This study was reviewed and approved by the Yorkshire and the Humber Research Ethics Committee. The patients/participants provided their written informed consent to participate in this study.

Author contributions

MR, RP, MB, JJ and KP performed miRNA measurements. TS performed clinical studies and edited the manuscript. AA-S supervised miRNA laboratory work. SA contributed to study design, data interpretation and the writing of the manuscript. NH performed the Ingenuity Pathway Analysis. AM and AB analyzed the data and wrote the manuscript. All authors reviewed and approved the final version of the manuscript. AB is the guarantor of this work. All authors contributed to the article and approved the submitted version.

Conflict of interest

Authors MR, RP, MB,JJ and AA-S were employed by Hamad Medical Corporation

The remaining authors declare that the research was conducted in the absence of any commercial or financial relationships that could be construed as a potential conflict of interest.

Publisher's note

All claims expressed in this article are solely those of the authors and do not necessarily represent those of their affiliated organizations, or those of the publisher, the editors and the reviewers. Any product that may be evaluated in this article, or claim that may be made by its manufacturer, is not guaranteed or endorsed by the publisher.

Supplementary material

The Supplementary Material for this article can be found online at: https://www.frontiersin.org/articles/10.3389/fendo.2022.917041/full#supplementary-material

References

1. Action to Control Cardiovascular Risk in Diabetes Study G, Gerstein HC, Miller ME, Byington RP, Goff DCJr., Bigger JT, et al. Effects of intensive glucose lowering in type 2 diabetes. *N Engl J Med* (2008) 358(24):2545–59. doi: 10.1056/NEJMoa0802743

2. Group AC, Patel A, MacMahon S, Chalmers J, Neal B, Billot L, et al. Intensive blood glucose control and vascular outcomes in patients with type 2 diabetes. *N Engl J Med* (2008) 358(24):2560–72. doi: 10.1056/NEJMoa0802987

3. Miller ME, Bonds DE, Gerstein HC, Seaquist ER, Bergenstal RM, Calles-Escandon J, et al. The effects of baseline characteristics, glycaemia treatment approach, and glycated haemoglobin concentration on the risk of severe hypoglycaemia: post hoc epidemiological analysis of the ACCORD study. *BMJ* (2010) 340:b5444. doi: 10.1136/bmj.b5444

4. Bonds DE, Miller ME, Bergenstal RM, Buse JB, Byington RP, Cutler JA, et al. The association between symptomatic, severe hypoglycaemia and mortality in type 2 diabetes: retrospective epidemiological analysis of the ACCORD study. *BMJ* (2010) 340:b4909. doi: 10.1136/bmj.b4909

5. Investigators OT, Mellbin LG, Ryden L, Riddle MC, Probstfield J, Rosenstock J, et al. Does hypoglycaemia increase the risk of cardiovascular events? a report from the ORIGIN trial. *Eur Heart J* (2013) 34(40):3137–44. doi: 10.1093/eurheartj/eht332

6. Investigators N-SS, Finfer S, Chittock DR, Su SY, Blair D, Foster D, et al. Intensive versus conventional glucose control in critically ill patients. *N Engl J Med* (2009) 360(13):1283–97. doi: 10.1056/NEJMoa0810625

7. Bedenis R, Price AH, Robertson CM, Morling JR, Frier BM, Strachan MW, et al. Association between severe hypoglycemia, adverse macrovascular events, and inflammation in the Edinburgh type 2 diabetes study. *Diabetes Care* (2014) 37 (12):3301–8. doi: 10.2337/dc14-0908

8. Kosiborod M, Inzucchi SE, Goyal A, Krumholz HM, Masoudi FA, Xiao L, et al. Relationship between spontaneous and iatrogenic hypoglycemia and mortality in patients hospitalized with acute myocardial infarction. *JAMA* (2009) 301(15):1556–64. doi: 10.1001/jama.2009.496

9. Goto A, Arah OA, Goto M, Terauchi Y, Noda M. Severe hypoglycaemia and cardiovascular disease: systematic review and meta-analysis with bias analysis. *BMJ* (2013) 347:f4533. doi: 10.1136/bmj.f4533

10. Davis SN, Duckworth W, Emanuele N, Hayward RA, Wiitala WL, Thottapurathu L, et al. Effects of severe hypoglycemia on cardiovascular outcomes and death in the veterans affairs diabetes trial. *Diabetes Care* (2019) 42 (1):157–63. doi: 10.2337/dc18-1144

11. Al-Qaissi A, Papageorgiou M, Deshmukh H, Madden LA, Rigby A, Kilpatrick ES, et al. Effects of acute insulin-induced hypoglycaemia on endothelial microparticles in adults with and without type 2 diabetes. *Diabetes Obes Metab* (2019) 21(3):533–40. doi: 10.1111/dom.13548

12. Kahal H, Aburima A, Spurgeon B, Wraith KS, Rigby AS, Sathyapalan T, et al. Platelet function following induced hypoglycaemia in type 2 diabetes. *Diabetes Metab* (2018) 44:431–6. doi: 10.1016/j.diabet.2018.04.004

13. Atkin AS, Moin ASM, Nandakumar M, Al-Qaissi A, Sathyapalan T, Atkin SL, et al. Impact of severe hypoglycemia on the heat shock and related protein response. *Sci Rep* (2021) 11(1):17057. doi: 10.1038/s41598-021-96642-8

14. Halama A, Kahal H, Bhagwat AM, Zierer J, Sathyapalan T, Graumann J, et al. Metabolic and proteomic signatures of hypoglycaemia in type 2 diabetes. *Diabetes Obes Metab* (2019) 21(4):909–19. doi: 10.1111/dom.13602

15. Kahal H, Halama A, Aburima A, Bhagwat AM, Butler AE, Graumann J, et al. Effect of induced hypoglycemia on inflammation and oxidative stress in type 2 diabetes and control subjects. *Sci Rep* (2020) 10(1):4750. doi: 10.1038/s41598-020-61531-z

16. Atkin AS, Moin ASM, Al-Qaissi A, Sathyapalan T, Atkin SL, Butler AE. Plasma heat shock protein response to euglycemia in type 2 diabetes. *BMJ Open Diabetes Res Care* (2021) 9(1):e002057. doi: 10.1136/bmjdrc-2020-002057

17. Lee Y, Kim M, Han J, Yeom KH, Lee S, Baek SH, et al. MicroRNA genes are transcribed by RNA polymerase II. *EMBO J* (2004) 23(20):4051–60. doi: 10.1038/sj.emboj.7600385

18. Bartel DP. MicroRNAs: genomics, biogenesis, mechanism, and function. *Cell* (2004) 116(2):281–97. doi: 10.1016/S0092-8674(04)00045-5

19. Kim VN, Han J, Siomi MC. Biogenesis of small RNAs in animals. *Nat Rev Mol Cell Biol* (2009) 10(2):126–39. doi: 10.1038/nrm2632

20. Krol J, Loedige I, Filipowicz W. The widespread regulation of microRNA biogenesis, function and decay. *Nat Rev Genet* (2010) 11(9):597–610. doi: 10.1038/nrg2843

21. Ortega FJ, Mercader JM, Catalan V, Moreno-Navarrete JM, Pueyo N, Sabater M, et al. Targeting the circulating microRNA signature of obesity. *Clin Chem* (2013) 59(5):781–92. doi: 10.1373/clinchem.2012.195776

22. Atkin SL, Ramachandran V, Yousri NA, Benurwar M, Simper SC, McKinlay R, et al. Changes in blood microRNA expression and early metabolic responsiveness 21 days following bariatric surgery. *Front Endocrinol* (2018) 9:773. doi: 10.3389/fendo.2018.00773

23. Leung AK, Sharp PA. MicroRNA functions in stress responses. *Mol Cell* (2010) 40(2):205–15. doi: 10.1016/j.molcel.2010.09.027

24. Witkowski M, Weithauser A, Tabaraie T, Steffens D, Kränkel N, Witkowski M, et al. Micro-RNA-126 reduces the blood thrombogenicity in diabetes mellitus *via* targeting of tissue factor. *Arterioscler Thromb Vasc Biol* (2016) 36(6):1263–71. doi: 10.1161/ATVBAHA.115.306094

25. Fulzele S, El-Sherbini A, Ahmad S, Sangani R, Matragoon S, El-Remessy A, et al. MicroRNA-146b-3p regulates retinal inflammation by suppressing adenosine deaminase-2 in diabetes. *BioMed Res Int* (2015) 2015:846501. doi: 10.1155/2015/846501

26. La Sala L, Cattaneo M, De Nigris V, Pujadas G, Testa R, Bonfigli AR, et al. Oscillating glucose induces microRNA-185 and impairs an efficient antioxidant response in human endothelial cells. *Cardiovasc Diabetol* (2016) 15:71. doi: 10.1186/s12933-016-0390-9

27. Caporali A, Meloni M, Völlenkle C, Bonci D, Sala-Newby GB, Addis R, et al. Deregulation of microRNA-503 contributes to diabetes mellitus-induced impairment of endothelial function and reparative angiogenesis after limb ischemia. *Circulation* (2011) 123(3):282–91. doi: 10.1161/CIRCULATIONAHA.110.952325

28. Simone NL, Soule BP, Ly D, Saleh AD, Savage JE, Degraff W, et al. Ionizing radiation-induced oxidative stress alters miRNA expression. *PLoS One* (2009) 4(7): e6377. doi: 10.1371/journal.pone.0006377

29. Cui S, Sun B, Yin X, Guo X, Chao D, Zhang C, et al. Time-course responses of circulating microRNAs to three resistance training protocols in healthy young men. *Sci Rep* (2017) 7(1):2203. doi: 10.1038/s41598-017-02294-y

30. Favaro RR, Morales-Prieto DM, Herrmann J, Sonnemann J, Schleussner E, Markert UR, et al. Influence of high glucose in the expression of miRNAs and IGF1R signaling pathway in human myometrial explants. *Arch Gynecol Obstet* (2021) 303(6):1513–22. doi: 10.1007/s00404-020-05940-5

31. Zhang B-h, Shen C-a, Zhu B-w, An H-y, Zheng B, Xu S-b, et al. Insight into miRNAs related with glucometabolic disorder. *Biomed Pharmacother* (2019) 111:657–65. doi: 10.1016/j.biopha.2018.12.123

32. Ueki S, Murakami Y, Yamada S, Kimura M, Saito Y, Saito H. microRNA-mediated resistance to hypoglycemia in the HepG2 human hepatoma cell line. *BMC Cancer* (2016) 16(1):1–13. doi: 10.1186/s12885-016-2762-7

33. Mussa BM, Taneera J, Mohammed AK, Srivastava A, Mukhopadhyay D, Sulaiman N. Potential role of hypothalamic microRNAs in regulation of FOS and FTO expression in response to hypoglycemia. *J Physiol Sci* (2019) 69(6):981–91. doi: 10.1007/s12576-019-00718-0

34. Agrawal R, Durupt G, Verma D, Montgomery M, Vieira-de Abreu A, Taylor C, et al. MicroRNA-7a overexpression in VMH restores the sympathoadrenal response to hypoglycemia. *JCI Insight* (2019) 4(20):e130521. doi: 10.1172/jci.insight.130521

35. Eyileten C, Wicik Z, Keshwani D, Aziz F, Aberer F, Pferschy PN, et al. Alteration of circulating platelet-related and diabetes-related microRNAs in individuals with type 2 diabetes mellitus: a stepwise hypoglycaemic clamp study. *Cardiovasc Diabetol* (2022) 21(1):1–12. doi: 10.1186/s12933-022-01517-5

36. Moin ASM, Al-Qaissi A, Sathyapalan T, Atkin SL, Butler AE. Hypoglycaemia in type 2 diabetes exacerbates amyloid-related proteins associated with dementia. *Diabetes Obes Metab* (2021) 23(2):338–49. doi: 10.1111/dom.14220

37. Birkett MA, Day SJ. Internal pilot studies for estimating sample size. *Stat Med* (1994) 13(23-24):2455–63. doi: 10.1002/sim.4780132309

38. U.K. prospective diabetes study 16. overview of 6 years' therapy of type II diabetes: a progressive disease. U.K. prospective diabetes study group. *Diabetes* (1995) 44(11):1249–58.

39. Sprague JE, Arbeláez AM. Glucose counterregulatory responses to hypoglycemia. *Pediatr Endocrinol Rev PER* (2011) 9(1):463–75.

40. Davis SN, Mann S, Briscoe VJ, Ertl AC, Tate DB. Effects of intensive therapy and antecedent hypoglycemia on counterregulatory responses to hypoglycemia in type 2 diabetes. *Diabetes* (2009) 58(3):701–9. doi: 10.2337/db08-1230

41. Chatterjee S, Mudher A. Alzheimer's disease and type 2 diabetes: A critical assessment of the shared pathological traits. *Front Neurosci* (2018) 12:383. doi: 10.3389/fnins.2018.00383

42. Wang C, Wan S, Yang T, Niu D, Zhang A, Yang C, et al. Increased serum microRNAs are closely associated with the presence of microvascular complications in type 2 diabetes mellitus. *Sci Rep* (2016) 6:20032. doi: 10.1038/srep20032

43. Mayr B, Müller EE, Schäfer C, Droese S, Schönfelder M, Niebauer J. Exercise-induced changes in miRNA expression in coronary artery disease. *Clin Chem Lab Med CCLM / FESCC* (2021) 59(10):1719–27. doi: 10.1515/cclm-2021-0164

44. Kong L, Du X, Hu N, Li W, Wang W, Wei S, et al. Downregulation of let-7e-5p contributes to endothelial progenitor cell dysfunction in deep vein thrombosis *via* targeting FASLG. *Thromb Res* (2016) 138:30–6. doi: 10.1016/j.thromres.2015.12.020

45. Müller-Deile J, Dannenberg J, Liu P, Lorenzen J, Nyström J, Thum T, et al. Identification of cell and disease specific microRNAs in glomerular pathologies. *J Cell Mol Med* (2019) 23(6):3927–39. doi: 10.1111/jcmm.14270

46. Pordzik J, Jakubik D, Jarosz-Popek J, Wicik Z, Eyileten C, De Rosa S, et al. Significance of circulating microRNAs in diabetes mellitus type 2 and platelet reactivity: bioinformatic analysis and review. *Cardiovasc Diabetol* (2019) 18(1):113. doi: 10.1186/s12933-019-0918-x

47. Cheng CC, Yang BL, Chen WC, Ho AS, Sie ZL, Lin HC, et al. STAT3 mediated miR-30a-5p inhibition enhances proliferation and inhibits apoptosis in colorectal cancer cells. *Int J Mol Sci* (2020) 21(19):7315. doi: 10.3390/ijms21197315

48. He Y, Lang X, Cheng D, Zhang T, Yang Z, Xiong R. miR−30a−5p inhibits hypoxia/reoxygenation−induced oxidative stress and apoptosis in HK−2 renal tubular epithelial cells by targeting glutamate dehydrogenase 1 (GLUD1). *Oncol Rep* (2020) 44(4):1539–49. doi: 10.3892/or.2020.7718

49. Yang X, Yang M, Chen Y, Qian Y, Fei X, Gong C, et al. miR-30a-5p targets Becn1 to ameliorate high-glucose-induced glomerular podocyte injury in immortalized rat podocyte cell line. *Am J Transl Res* (2021) 13(3):1516–25.

50. VatanIman R, Malekpour SH, Afshari A, Zare M. MiR-770-5p, miR-661 and miR-571 expression level in serum and tissue samples of foot ulcer caused by diabetes mellitus type II in Iranian population. *Mol Biol Rep* (2021) 48(12):7811–8. doi: 10.1007/s11033-021-06798-9

51. Wang L, Li H. MiR-770-5p facilitates podocyte apoptosis and inflammation in diabetic nephropathy by targeting TIMP3. *Biosci Rep* (2020) 40(4): BSR20193653. doi: 10.1042/BSR20193653

52. Zhang J, Song L, Ma Y, Yin Y, Liu X, Luo X, et al. lncRNA MEG8 upregulates miR-770-5p through methylation and promotes cell apoptosis in diabetic nephropathy. *Diabetes Metab Syndr Obes: Targets Ther* (2020) 13:2477. doi: 10.2147/DMSO.S255183

53. Jiang L, Yu L, Zhang X, Lei F, Wang L, Liu X, et al. miR-892b silencing activates NF-κB and promotes aggressiveness in breast cancer. *Cancer Res* (2016) 76(5):1101–11. doi: 10.1158/0008-5472.CAN-15-1770

54. Villard A, Marchand L, Thivolet C, Rome S. Diagnostic value of cell-free circulating microRNAs for obesity and type 2 diabetes: a meta-analysis. *J Mol Biomarkers Diagn* (2015) 6(6):251. doi: 10.4172/2155-9929.1000251

55. Liang L, Su W, Zhou L, Cao Y, Zhou X, Liu S, et al. Statin downregulation of miR-652-3p protects endothelium from dyslipidemia by promoting ISL1 expression. *Metabol: Clin Exp* (2020) 107:154226. doi: 10.1016/j.metabol.2020.154226

Frontiers in Endocrinology

Explores the endocrine system to find new therapies for key health issues

The second most-cited endocrinology and metabolism journal, which advances our understanding of the endocrine system. It uncovers new therapies for prevalent health issues such as obesity, diabetes, reproduction, and aging.

Discover the latest Research Topics

See more →

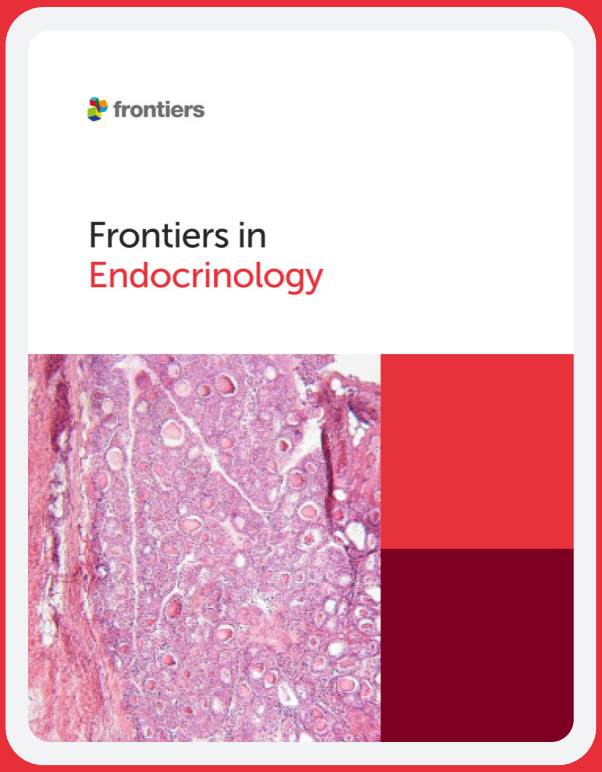

Frontiers

Avenue du Tribunal-Fédéral 34
1005 Lausanne, Switzerland
frontiersin.org

Contact us

+41 (0)21 510 17 00
frontiersin.org/about/contact